

AD-A054 154

LOCKHEED-CALIFORNIA CO BURBANK

F/G 1/3

FULL SCALE CRASH TEST EXPERIMENTAL VERIFICATION OF A METHOD OF --ETC(U)

FEB 78 G WITTLIN, M A GAMON, W L LABARGE

DOT-FA75WA-3707

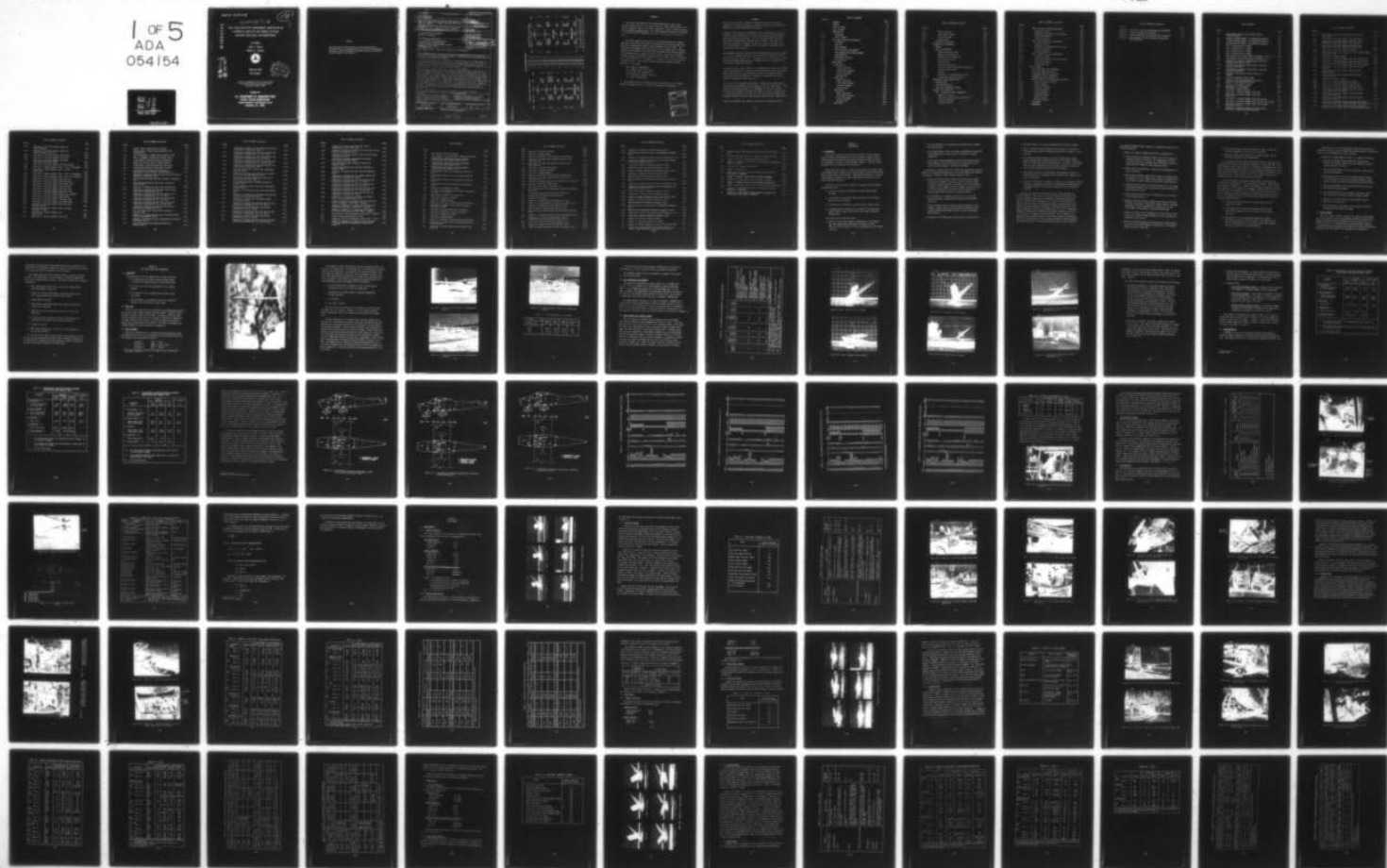
UNCLASSIFIED

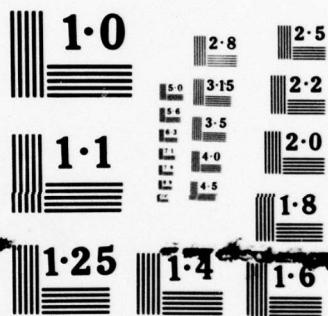
LR-28306

FAA-RD-77-188

NL

1 OF 5
ADA
054154





NATIONAL BUREAU OF STANDARDS
MICROCOPY RESOLUTION TEST CHART

Report No: FAA-RD-77-188

FOR FURTHER TRAN

AD A054154

FULL SCALE CRASH TEST EXPERIMENTAL VERIFICATION OF
A METHOD OF ANALYSIS FOR GENERAL AVIATION
AIRPLANE STRUCTURAL CRASHWORTHINESS

Gil Wittlin

Max A. Gamon

William L. LaBarge



February 1978

Final Report



AD No. ~~1~~
DDC FILE COPY

Document is available to the U.S. public through
the National Technical Information Service,
Springfield, Virginia 22161.

Prepared for

U.S. DEPARTMENT OF TRANSPORTATION
FEDERAL AVIATION ADMINISTRATION
Systems Research & Development Service
Washington, D.C. 20590

NOTICE

This document is disseminated under the sponsorship of the Department of Transportation in the interest of information exchange. The United States government assumes no liability for its contents or use thereof.

Technical Report Documentation Page

1. Report No. 78 FAA-RD-77-188	2. Government Accession No.	3. Recipient's Catalog No.	
4. Title and Subtitle 6 Full Scale Crash Test Experimental Verification of a Method of Analysis for General Aviation Structural Crashworthiness.	5. Report Date 11 Feb 1978	6. Performing Organization Code L 12 424e	
7. Author(s) 10 Gil Wittlin, Max A. / Gamon, William L. / LaBarge	8. Performing Organization Report No. 14 LR-28306	9. Work Unit No. (TRAIS)	
9. Performing Organization Name and Address Lockheed-California Company Burbank, California	11. Contract or Grant No. 15 DOT-FA75WA-3707	13. Type of Report and Period Covered 9 Final rept. June 1976 to Dec 77	
12. Sponsoring Agency Name and Address U.S. Department of Transportation Federal Aviation Administration Systems Research and Development Service Washington, D.C. 20590	14. Sponsoring Agency Code Federal Aviation Administration ARO-520		
15. Supplementary Notes The Cessna Aircraft Company participated as a subcontractor			
16. Abstract The results of the Task II effort to experimentally verify a method of analysis of the structural dynamics response of general aviation airplanes subjected to a crash environment are presented. Included in this report is a description of the preparation for the performance of four instrumented full-scale crash tests involving a single-engine, high wing type airplane. All crash testing was performed at the NASA Langley Impact Dynamics Research Facility (IDRF). The crash tests involved a wide range of impact attitudes and included one impact into a soil covered terrain. Program KRASH, refined for general aviation airplane application during TASK I, is used to mathematically model the single-engine, high-wing type airplane for each of the crash tests. An analysis of each crash condition is performed and the results with regard to post-crash sequence, cg velocity, energy distribution, cabin deformation, member deflections, structure failures, and floor, occupant and engine mass accelerations are presented. Correlation between analysis and test results is presented for each crash test. Comparisons of analytical and test results are presented for the composite of all four crash tests. The analytical results are shown to be in agreement with test results. Conclusions are presented following the summary of results. Appendices A, B, C and D are included and contain soil test data, literature survey and evaluation results, test data, and structural model data, respectively. A three volume KRASH User's Manual is described in a separate document.			
17. Key Words Crashworthiness, Structural Dynamics, Light Fixed-Wing Aircraft, Mathematical Models, Large Deformations, Crushing, Energy Absorption, Full-Scale Crash Test, Correlation		18. Distribution Statement Document is available to the public through the National Technical Information Service, Springfield, VA 22151	
19. Security Classif. (of this report) Unclassified	20. Security Classif. (of this page) Unclassified	21. No. of Pages 392	22. Price

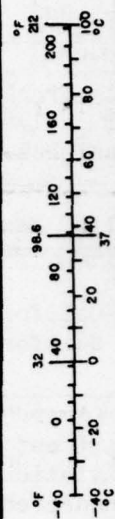
METRIC CONVERSION FACTORS

Approximate Conversions to Metric Measures

Symbol	When You Know	Multiply by	To Find	Symbol
LENGTH				
in	inches	2.5	centimeters	cm
ft	feet	30	meters	m
yd	yards	0.9	kilometers	km
mi	miles	1.6		
AREA				
in ²	square inches	6.5	square centimeters	cm ²
ft ²	square feet	0.09	square meters	m ²
yd ²	square yards	0.8	square meters	m ²
mi ²	square miles	2.6	square kilometers	km ²
	acres	0.4	hectares	ha
MASS (weight)				
oz	ounces	28	grams	g
lb	pounds	0.45	kilograms	kg
	short tons (2000 lb)	0.9	tonnes	t
VOLUME				
tsp	teaspoons	5	milliliters	ml
Tbsp	tablespoons	15	milliliters	ml
fl oz	fluid ounces	30	milliliters	ml
c	cups	0.24	liters	l
pt	pints	0.47	liters	l
qt	quarts	0.95	liters	l
gal	gallons	3.8	liters	l
ft ³	cubic feet	0.03	cubic meters	m ³
yd ³	cubic yards	0.76	cubic meters	m ³
TEMPERATURE (exact)				
°F	Fahrenheit temperature	5/9 (after subtracting 32)	Celsius temperature	°C

Approximate Conversions from Metric Measures

Symbol	When You Know	Multiply by	To Find	Symbol
LENGTH				
mm	millimeters	0.04	inches	in
cm	centimeters	0.4	inches	in
m	meters	3.3	feet	ft
km	kilometers	1.1	yards	yd
		0.6	miles	mi
AREA				
cm ²	square centimeters	0.16	square inches	in ²
m ²	square meters	1.2	square yards	yd ²
ha	hectares (10,000 m ²)	0.4	square miles	mi ²
		2.5	acres	
MASS (weight)				
g	grams	0.035	ounces	oz
kg	kilograms	2.2	pounds	lb
t	tonnes (1000 kg)	1.1	short tons	
VOLUME				
ml	milliliters	0.03	fluid ounces	fl oz
l	liters	2.1	pints	pt
l	liters	1.06	quarts	qt
m ³	cubic meters	0.26	gallons	gal
m ³	cubic meters	35	cubic feet	ft ³
m ³	cubic meters	1.3	cubic yards	yd ³
TEMPERATURE (exact)				
°C	Celsius temperature	9/5 (then add 32)	Fahrenheit temperature	°F



*1 in = 2.54 (exact). For other exact conversions and more detailed tables, see NBS Misc. Publ. 286, Units of Weights and Measures, Price \$2.25, SO Catalog No. C13.10-286.

FOREWORD

This report was prepared by the Lockheed-California Company under Contract DOT-FA75-WA-3707. The report contains a partial description of the effort performed as Task II of a three task effort. Task II covers the period from July 1976 to December 1977. The work was administered under the direction of the Federal Aviation Administration with H. Spicer acting as Technical Monitor.

The project leader was Gil Wittlin of the Lockheed-California Company. Important contributions were made to the program by the Cessna Aircraft Company and the NASA Langley Impact Dynamics Research Facility (IDRF). The Cessna Aircraft Company, under the direction of D.J. Ahrens and W.B. Bloedel prepared the airplanes for the crash tests, performed data reduction and provided valuable data with regard to general aviation structure and designs. The NASA Langley Impact Dynamics Research Facility (IDRF), under the direction of Dr. R.A. Thomson and V.L. Vaughan, Jr., conducted all the crash tests and recorded the data. The following Lockheed-California Company personnel assisted in the program:

- M.A. Gamon (Program KRASH)
- W.L. LaBarge (Literature Survey)
- W.M. Crooks (Test preparation)
- H.P. Weinberger (Computer services)
- P.C. Durup (Consultation)

The Lockheed effort was performed under the supervision of J.E. Wignot, (dynamic loads group) and R.F. O'Connell (Aeromechanics Department).

ACCESSION for	
NTIS	White Section <input checked="" type="checkbox"/>
DDC	Buff Section <input type="checkbox"/>
UNANNOUNCED	<input type="checkbox"/>
JUSTIFICATION	
BY	
DISTRIBUTION/AVAILABILITY CODES	
Dist.	SP. CIAL
A	

SUMMARY

The results of the Task II effort to experimentally verify a method of analysis of the structural dynamics response of general aviation airplanes subjected to a crash environment are presented.

Included in this report is a description of the preparation for the performance of four instrumented full-scale crash tests involving a single-engine, high wing type airplane. All crash testing was performed at the NASA Langley Impact Dynamics Research Facility (IDRF). The crash tests involved a wide range of impact attitudes and included one impact into a soil covered terrain. In support of the soil impact a literature survey and evaluation was performed.

Program KRASH, refined for general aviation airplane application during Task I, is used to mathematically model the single-engine, high-wing type airplane for each of the crash tests. Descriptions of the math models, as well as additional KRASH modifications, to further enhance its capability and facilitate its usage, are provided.

An analysis of each crash condition is performed and the results with regard to post-crash sequence, cg velocity, energy distribution, cabin deformation, member deflections, structure failures, and floor, occupant and engine mass accelerations are presented. Correlation between analysis and test results is presented for each crash test.

The results of the program are summarized. Comparisons of analytical and test results are presented for the composite of all four crash tests. The analytical results are shown to be in agreement with the test results. Conclusions are presented following the summary of results. Appendices A, B, C and D are included and contain soil test data, literature survey and evaluation results, test data, and structural and model data, respectively.

A three volume KRASH User's Manual is described in a separate document.

TABLE OF CONTENTS

Section		Page
	FOREWORD	iii
	SUMMARY	iv
	LIST OF FIGURES	ix
	LIST OF TABLES	xv
1	INTRODUCTION	1-1
1.1	BACKGROUND	1-1
1.2	TASK II EFFORT	1-6
2	FULL SCALE CRASH TEST PREPARATION	2-1
2.1	OBJECTIVES	2-1
2.2	TEST SITE	2-1
2.3	TEST SPECIMENS	2-1
2.4	TEST CONDITIONS AND SEQUENCE	2-6
2.5	SWING HARNESS AND PULLBACK SYSTEMS	2-6
2.6	INSTRUMENTATION	2-12
2.7	PHOTOGRAPHIC COVERAGE	2-25
2.8	DATA REDUCTION	2-25
3	TEST RESULTS	3-1
3.1.	CRASH TEST 1	3-1
3.1.1	Impact Conditions	3-1
3.1.2	Crash Impact Sequence	3-1
3.1.3	Structural Damage	3-3
3.1.4	Response Data	3-10
3.2	CRASH TEST 2	3-17
3.2.1	Impact Conditions	3-17
3.2.2	Crash Impact Sequence	3-18
3.2.3	Structural Damage	3-18
3.2.4	Response Data	3-20
3.3	CRASH TEST 3	3-29
3.3.1	Impact Conditions	3-29
3.3.2	Crash Impact Sequence	3-29
3.3.3	Structural Damage	3-32
3.3.4	Response Data	3-32
3.4	CRASH TEST 4	3-47

TABLE OF CONTENTS (Continued)

Section		Page
3.4.1	Impact Conditions	3-47
3.4.2	Crash Impact Sequence	3-48
3.4.3	Structural Damage	3-48
3.4.4	Response Data	3-62
3.5	RESTRAINT SYSTEM LOADS	3-70
4	PROGRAM KRASH REFINEMENTS	4-1
4.1	GENERAL	4-1
4.2	TASK II REFINEMENTS	4-2
4.2.1	Symmetrical Model Coding	4-2
4.2.2	Massless Node Capability	4-4
4.2.3	Summary and Plot Capability	4-8
4.2.4	Force Failure Coding	4-8
4.2.5	Material Code	4-8
4.2.6	Filtered Acceleration	4-10
4.2.7	Revised Stiffness and Damping Formulation	4-11
4.2.8	Flexible Ground Coding	4-12
4.2.9	Restart	4-13
4.2.10	Unsymmetrical Load-Deflection Curves	4-13
4.2.11	Pinned-Fixed Beam End Conditions	4-13
5	MATHEMATICAL MODEL DESCRIPTIONS	5-1
5.1	PROGRAM KRASH	5-1
5.2	AIRPLANE DESCRIPTION	5-1
5.3	CRASH TEST MATHEMATICAL MODELS	5-3
6	ANALYSIS AND CORRELATION	6-1
6.1	TEST 1 ANALYSIS AND TEST COMPARISONS	6-1
6.1.1	Sequence of Events	6-1
6.1.2	Deflections, Deformations and Failures	6-7
6.1.3	Structure Responses	6-9
6.1.4	Occupant Response	6-19

TABLE OF CONTENTS (Continued)

Section		Page
6.2	TEST 2 ANALYSIS AND TEST COMPARISONS	6-24
6.2.1	Sequence of Events	6-24
6.2.2	Deflections, Deformations and Failures	6-28
6.2.3	Structure Responses	6-31
6.2.4	Occupant Response	6-31
6.3	TEST 3 ANALYSIS AND TEST COMPARISONS	6-43
6.3.1	Sequence of Events	6-43
6.3.2	Deflections, Deformations and Failures	6-48
6.3.3	Structure Responses	6-53
6.3.4	Occupant Response	6-64
6.4	TEST 4 ANALYSIS AND TEST COMPARISONS	6-70
6.4.1	Sequence of Events	6-70
6.4.2	Deflections, Deformations, and Failures	6-74
6.4.3	Structure Responses	6-77
6.4.4	Occupant Response	6-87
7	TASK II RESULTS	7-1
7.1	FULL SCALE CRASH TEST PREPARATION	7-1
7.2	FULL SCALE CRASH TEST RESULTS	7-1
7.3	LITERATURE SURVEY AND EVALUATION	7-11
7.4	MATHEMATICAL MODEL DESCRIPTION	7-12
7.5	ANALYSIS RESULTS AND CORRELATION WITH TESTS	7-14
7.5.1	Energy, Velocity and Events	7-14
7.5.2	Seat Leg Damage	7-16
7.5.3	Structure Failures	7-16
7.5.4	Structure Response	7-21
7.5.5	Cabin Deformation	7-26
7.5.6	Occupant Response	7-28
7.5.7	Impact into Soil	7-30
7.5.8	Severity Ranking	7-34
8	CONCLUSIONS	8-1
9	REFERENCES	9-1

TABLE OF CONTENTS (Continued)

Section	Page
APPENDIX A CRASH TEST 4 SOIL BED MAINTENANCE AND MEASUREMENT	A-1
APPENDIX B SURVEY OF TECHNICAL PUBLICATIONS	B-1
APPENDIX C MEASURED RESPONSE TIME HISTORIES TESTS 1 THROUGH 4	C-1
APPENDIX D SINGLE-ENGINE, HIGH-WING AIRPLANE STRUCTURE AND MATH MODEL DATA	D-1

LIST OF FIGURES

Figure		Page
2-1	NASA-Langley Research Center Impact Dynamics Research Facility	2-2
2-2	Airplane Specimen Number 1 in As-Received Condition	2-4
2-3	Airplane Specimen Number 2 in As-Received Condition	2-4
2-4	Airplane Specimen Number 3 in As-Received Condition	2-5
2-5	Test 1 Airplane Prior to Impact	2-8
2-6	Test 2 Airplane Prior to Impact	2-8
2-7	Test 3 Airplane Prior to Impact	2-9
2-8	Test 4 Airplane Prior to Impact	2-9
2-9	Swing Harness and Pullback System Arrangement, Tests 1, 2, 4	2-10
2-10	Swing Harness and Pullback System Arrangement, Test 3	2-10
2-11	Accelerometer Locations, Single-Engine, High-Wing Airplane, Crash Tests 1 and 2	2-17
2-12	Accelerometer Locations, Single-Engine, High-Wing Airplane, Crash Test 3	2-18
2-13	Accelerometer Locations, Single-Engine, High-Wing Airplane, Crash Test 4	2-19
2-14	Occupants and Restraint Systems Installed in Airplane	2-24
2-15	Location of Forward Onboard Camera	2-27
2-16	Location of Aft Onboard Camera, Battery Box, Junction Box and Pyrotechnic Timer	2-27
2-17	Location of Wing Mounted Camera	2-28
2-18	Photographic Coverage Layout	2-28
3-1	Crash Test 1, Impact Sequence	3-2
3-2	Crash Test 1, Post-Test Damage, Front View	3-6
3-3	Crash Test 1, Post-Test Damage, Left Front Quarter View	3-6
3-4	Crash Test 1, Post-Test Damage, Right Rear Quarter	3-7
3-5	Crash Test 1, Post-Test Damage, Seat and Lower Cabin Region	3-7
3-6	Crash Test 1, Post-Test Damage, Engine and Fuselage Underside Structure	3-8
3-7	Crash Test 1, Post-Test Damage, Side View Showing Underside of Forward and Mid Cabin Region	3-8

LIST OF FIGURES (Continued)

Figure		Page
3-8	Crash Test 1, Post-Test Damage, Seats and Forward Floor Region	3-9
3-9	Crash Test 1, Post-Test Damage, Seat Leg Failures	3-9
3-10	Crash Test 1, Post-Test Damage, Instrument Panel, Rudder Pedals and Floor Structure, Pilot Side	3-11
3-11	Crash Test 1, Post-Test Damage, Instrument Panel, Rudder Pedals and Floor Structure, Copilot Side	3-11
3-12	Crash Test 1, Post-Test Damage, Left Wing	3-12
3-13	Crash Test 1, Post-Test Damage, Top View of Engine, Engine Mount and Firewall	3-12
3-14	Crash Test 2, Impact Sequence	3-19
3-15	Crash Test 2, Post-Test Damage, Left Front Quarter View	3-22
3-16	Crash Test 2, Post-Test Damage, Right Rear Quarter View	3-22
3-17	Crash Test 2, Post-Test Damage, Front View (Cowl Removed)	3-23
3-18	Crash Test 2, Post-Test Damage, Nose Gear and Lower Fuselage	3-23
3-19	Crash Test 2, Post-Test Damage, Nose Gear Lower Support Failure	3-24
3-20	Crash Test 2, Post-Test Damage, Forward Fuselage Floor and Tunnel	3-24
3-21	Crash Test 3, Impact Sequence	3-31
3-22	Crash Test 3, Post-Test Damage, Front View	3-39
3-23	Crash Test 3, Post-Test Damage, Left Side View	3-39
3-24	Crash Test 3, Post-Test Damage, Right Side View	3-40
3-25	Crash Test 3, Post-Test Damage, Right Main Landing Gear and Right Door Distortion	3-40
3-26	Crash Test 3, Post-Test Damage, Left Main Landing Gear and Aft Door Post	3-41
3-27	Crash Test 3, Post-Test Damage, Main Landing Gear Bulkhead Deformation	3-41
3-28	Crash Test 3, Post-Test Damage, Passenger Compartment Interior Showing Copilot, Restraint System and Buckled Floor	3-42
3-29	Crash Test 3, Post-Test Damage, Passenger Compartment Showing Door Post, Upper Cabin, Pilot and Restraint System	3-42

LIST OF FIGURES (Continued)

Figure		Page
3-30	Crash Test 3, Post-Test Damage, Engine and Forward Fuselage	3-43
3-31	Crash Test 3, Post-Test Damage, Engine and Forward Fuselage Side View	3-43
3-32	Crash Test 3, Post-Test Damage, Copilot Seat	3-44
3-33	Crash Test 3, Post-Test Damage, Pilot Seat	3-44
3-34	Crash Test 3, Post-Test Damage, Instrument Panel and Rudder Pedal Region	3-45
3-35	Crash Test 3, Post-Test Damage, Left Wing Failure	3-45
3-36	Crash Test 4, Impact Sequence, Time = 0.0 to .250 Seconds	3-49
3-37	Crash Test 4, Impact Sequence, Time = .300 to .550 Seconds	3-50
3-38	Crash Test 4, Impact Sequence, Time = .600 to .850 Seconds	3-51
3-39	Crash Test 4, Impact Sequence, Time = .900 to 1.15 Seconds	3-52
3-40	Crash Test 4, Post-Test Damage, Left Side View	3-56
3-41	Crash Test 4, Post-Test Damage, Right Side View	3-56
3-42	Crash Test 4, Post-Test Damage, Rear Quarter View	3-57
3-43	Crash Test 4, Post-Test Damage, Cabin Top View	3-57
3-44	Crash Test 4, Post-Test Damage, Left Front View	3-58
3-45	Crash Test 4, Post-Test Damage, Right Front View	3-58
3-46	Crash Test 4, Post-Test Damage, Right Front, Firewall	3-59
3-47	Crash Test 4, Post-Test Damage, Engine Mounts	3-59
3-48	Crash Test 4, Post-Test Damage, Instrument Panel	3-60
3-49	Crash Test 4, Post-Test Damage, Cabin Right Side	3-60
3-50	Crash Test 4, Post-Test Damage, Cabin Left Side, Occupants Removed	3-61
3-51	Crash Test 4, Post-Test Damage, Cabin Left Side, Occupants In Place	3-61
3-52	Crash Test 4, Post-Test Damage, Pilot Legs and Feet	3-63
3-53	Crash Test 4, Post-Test Damage, Pilot Torso	3-63

LIST OF FIGURES (Continued)

Figure		Page
4-1	Typical Tubular Engine Mount Arrangement	4-6
4-2	Typical Pilot or Copilot Power Adjustable Seat Configuration	4-7
4-3	Model Arrangement in KRASH Without Massless Nodes	4-7
4-4	Model Arrangement in KRASH With Massless Nodes	4-9
5-1	Single-Engine, High-Wing Airplane Configuration	5-2
5-2	Weight and Center-of-Gravity Flight Envelope	5-3
5-3	Single-Engine, High-Wing Symmetrical Math Model	5-5
5-4	Occupant-Seat-Restraint System Model in KRASH	5-10
5-5	Relationship of Airfield Cone Penetration Resistance to CBR on Buckshot Clay (Reference 9)	5-12
6-1	Comparison of Analysis and Test Longitudinal and Vertical Velocities Versus Time, Test 1	6-3
6-2	Total Energy and Energy Components Obtained by Analysis, Test 1	6-4
6-3	Strain Energy Distribution Histories, Obtained by Analysis, Test 1	6-6
6-4	Comparison of Analysis and Test Cabin Deformations	6-11
6-5	Comparison of Analysis and Test Engine Vertical and Longitudinal Accelerations, Test 1	6-13
6-6	Comparison of Analysis and Test Floor Vertical and Longitudinal Accelerations, F.S. 27, Test 1	6-14
6-7	Comparison of Analysis and Test Floor Vertical and Longitudinal Accelerations, F.S. 60, Test 1	6-15
6-8	Comparison of Analysis and Test Floor Vertical and Longitudinal Accelerations, F.S. 90-108, Test 1	6-16
6-9	Comparison of Analysis and Test Wing Vertical and Longitudinal Accelerations, Test 1	6-17
6-10	Pilot and Copilot DRI's Versus Time, Obtained by Analysis, Test 1	6-20
6-11	Comparison of Analysis and Test Pilot and Copilot Pelvic Vertical Accelerations, Test 1	6-21
6-12	Comparison of Analysis and Test Longitudinal and Vertical Velocities, Test 2	6-26
6-13	Total Energy and Energy Components Obtained by Analysis, Test 2	6-27

LIST OF FIGURES (Continued)

Figure		Page
6-14	Comparison of Analysis and Test Engine Vertical and Longitudinal Accelerations, Test 2	6-32
6-15	Comparison of Analysis and Test Floor Vertical and Longitudinal Accelerations, F.S. 27, Test 2	6-33
6-16	Comparison of Analysis and Test Floor Vertical and Longitudinal Accelerations, F.S. 60, Test 2	6-34
6-17	Comparison of Analysis and Test Floor Vertical and Longitudinal Accelerations, F.S. 90-108, Test 2	6-35
6-18	Comparison of Analysis and Test Wing Vertical and Longitudinal Accelerations, Test 2	6-36
6-19	Pilot and Copilot DRI's versus Time, Obtained by Analysis, Test 2	6-38
6-20	Comparison of Analysis and Test Pilot and Copilot Pelvic Vertical Accelerations, Test 2	6-40
6-21	Analytically Obtained Longitudinal and Vertical Velocities versus Time, Test 3	6-45
6-22	Total Energy and Energy Components Obtained by Analysis, Test 3	6-46
6-23	Strain Energy Distribution Histories, Obtained by Analysis, Test 3	6-49
6-24	Comparison of Analysis and Test Cabin Deformations, Test 3	6-51
6-25	Comparison of Analysis and Test Engine Vertical and Longitudinal Accelerations, Test 3	6-54
6-26	Comparison of Analysis and Test Engine Lateral Accelerations, Test 3	6-55
6-27	Comparison of Analysis and Test Floor Vertical and Longitudinal Accelerations, F.S. 27, Test 3	6-56
6-28	Comparison of Analysis and Test Floor Lateral Accelerations, F.S. 27, Test 3	6-57
6-29	Comparison of Analysis and Test Floor Vertical and Longitudinal Accelerations, F.S. 60, Test 3	6-58
6-30	Comparison of Analysis and Test Floor Lateral Accelerations, F.S. 60, Test 3	6-59
6-31	Comparison of Analysis and Test Floor Vertical and Longitudinal Accelerations, F.S. 90-108, Test 3	6-60

LIST OF FIGURES (Continued)

Figure		Page
6-32	Comparison of Analysis and Test Floor Lateral Accelerations, F.S. 90-108, Test 3	6-61
6-33	Comparison of Analysis and Test Pilot and Copilot Pelvic Vertical Accelerations, Test 3	6-66
6-34	Comparison of Analysis and Test Copilot Pelvic Lateral Accelerations, Test 3	6-67
6-35	Analytically Obtained Longitudinal and Vertical Velocities Versus Time, Test 4	6-72
6-36	Total Energy and Energy Components Obtained by Analysis, Test 4	6-73
6-37	Strain Energy Distribution Histories Obtained by Analysis, Test 4	6-75
6-38	Comparison of Analysis and Test Cabin Deformations, Test 4	6-79
6-39	Comparison of Analysis and Test Engine Vertical and Longitudinal Accelerations, Test 4	6-81
6-40	Comparison of Analysis and Test Floor Vertical and Longitudinal Accelerations, F.S. 27, Test 4	6-82
6-41	Comparison of Analysis and Test Floor Vertical and Longitudinal Accelerations, F.S. 60, Test 4	6-83
6-42	Comparison of Analysis and Test Floor Vertical and Longitudinal Accelerations, F.S. 90-108, Test 4	6-84
6-43	Comparison of Analysis and Test Wing Vertical and Longitudinal Accelerations, Test 4	6-85
6-44	Comparison of Analysis and Test Pilot and Copilot Pelvic Vertical Accelerations, Test 4	6-88
7-1	Summary of Comparison of Analysis and Test Structure Vertical Responses, Crash Tests 1 through 4	7-22
7-2	Summary of Comparison of Analysis and Test Structure Longitudinal Responses, Crash Tests 1 through 4	7-23
7-3	Summary of Comparison of Analysis and Test Times of Occurrence of Peak Values, Crash Tests 1 through 4	7-24
7-4	Distribution of Time Differences, Crash Tests 1 through 4	7-25
7-5	External Spring Load-Deflection Curve	7-26
7-6	Comparison of Cabin Deformations, Crash Tests 1, 3 and 4	7-27
7-7	Summary of Comparison of Analysis and Test Occupant Lower Torso Vertical Accelerations, Crash Tests 1 through 4	7-29

LIST OF TABLES

Table		Page
2-1	Test Weights and C.G. Locations	2-5
2-2	Test Sequence for Single-Engine, High-Wing Airplanes	2-7
2-3	Single-Engine, High-Wing Airplane Attachment Locations and Cable Lengths, Tests 1 and 4	2-13
2-4	Single-Engine, High-Wing Airplane Attachment Locations and Cable Lengths, Test 2	2-14
2-5	Single-Engine, High-Wing Airplane Attachment Location and Cable Lengths, Test 3	2-15
2-6	Accelerometer Locations and Response Settings for Test 1	2-20
2-7	Accelerometer Locations and Response Settings for Test 2	2-21
2-8	Accelerometer Locations and Response Settings for Test 3	2-22
2-9	Accelerometer Locations and Response Settings for Test 4	2-23
2-10	Available Accelerometers for Tests	2-24
2-11	Load Cell and Displacement Measurement Installations for Tests 1, 2, 3, and 4	2-26
2-12	Camera Type, Location and Coverage Data	2-29
3-1	Crash Test 1 Sequence of Events	3-4
3-2	Crash Test 1 Damage Summary	3-5
3-3	Summary of Crash Test 1 Peak Airplane Accelerations	3-13
3-4	Crash Test 1 Occupant Pelvis Peak Accelerations and Pulse Durations	3-15
3-5	Crash Test 1 Occupant Head Peak Accelerations	3-16
3-6	Tolerance Acceleration Levels for Occupants	3-17
3-7	Crash Test 2 Sequence of Events	3-18
3-8	Crash Test 2 Damage Summary	3-21
3-9	Summary of Crash Test 2 Peak Airplane Accelerations	3-25
3-10	Crash Test 2 Occupant Pelvis Peak Accelerations and Pulse Durations	3-27
3-11	Crash Test 2 Occupant Head Peak Accelerations and Durations	3-28

LIST OF TABLES (Continued)

Table		Page
3-12	Crash Test 3 Sequence of Events	3-30
3-13	Crash Test 3 Damage Summary	3-33
3-14	Summary of Crash Test 3 Peak Airplane Accelerations	3-34
3-15	Crash Test 3 Occupant Pelvis Peak Accelerations and Pulse Durations	3-37
3-16	Crash Test 3 Occupant Head Peak Accelerations and Pulse Durations	3-38
3-17	Crash Test 3 Severity Index Results	3-47
3-18	Crash Test 4 Sequence of Events	3-53
3-19	Crash Test 4 Damage Summary	3-55
3-20	Summary of Crash Test 4 Peak Airplane Accelerations	3-64
3-21	Crash Test 4 Occupant Pelvis Peak Accelerations and Pulse Durations	3-67
3-22	Crash Test 4 Occupant Head Peak Accelerations and Durations	3-68
3-23	Crash Test 4 Severity Index Results	3-69
3-24	Restraint System Loads, Crash Tests 1-4	3-70
5-1	Mass Identification for Single-Engine, High-Wing Airplane, Left Side	5-6
5-2	Corresponding Mass Identification for Right Side	5-6
5-3	Massless Node Locations and Representations	5-7
5-4	Summary of Math Models	5-13
6-1	Comparison of Analysis and Test Sequences, Test 1	6-2
6-2	Summary of Energy Components Obtained by Analysis, Test 1	6-5
6-3	Comparison of Analysis and Test Failures, Test 1	6-8
6-4	Member Deflections Obtained by Analysis, Test 1	6-10
6-5	Maximum External Spring Deflections Obtained by Analysis, Test 1	6-12
6-6	Comparison of Analysis and Test Structure Responses, Test 1	6-18
6-7	Comparison of Pilot and Copilot Pelvic Vertical Accelerations for Analysis Versus Test, Test 1	6-22
6-8	Stress Ratio Results Obtained by Analysis, Test 1	6-23
6-9	Comparison of Analysis and Test Sequences, Test 2	6-25
6-10	Summary of Energy Components Obtained by Analysis, Test 2	6-28

LIST OF TABLES (Continued)

Table		Page
6-11	Comparison of Analysis and Test Failures, Test 2	6-29
6-12	Maximum External Spring Deflections Obtained by Analysis, Test 2	6-30
6-13	Comparison of Analysis and Test Structure Responses, Test 2	6-37
6-14	Comparison of Analysis and Test Pilot and Copilot Pelvic Vertical Accelerations, Test 2	6-41
6-15	Stress Ratio Results Obtained by Analysis, Test 2	6-42
6-16	Comparison of Test and Analysis Sequences, Test 3	6-44
6-17	Summary of Energy Components Obtained by Analysis, Test 3	6-47
6-18	Comparison of Analysis and Test Failures, Test 3	6-50
6-19	Member Deflections Obtained by Analysis, Test 3	6-52
6-20	Maximum External Spring Deflections Obtained by Analysis, Test 3	6-53
6-21	Comparison of Analysis and Test Structure Responses, Test 3	6-62
6-22	Comparison of Pilot and Copilot Pelvic Accelerations for Analysis Versus Test, Test 3	6-68
6-23	Stress Ratio Results Obtained by Analysis, Test 3	6-69
6-24	Comparison of Analysis and Test Sequences, Test 4	6-71
6-25	Summary of Energy Components Obtained by Analysis, Test 4	6-74
6-26	Comparison of Analysis and Test Failures, Test 4	6-76
6-27	Member Deflections Obtained by Analysis, Test 4	6-78
6-28	Maximum External Spring Deflections Obtained by Analysis, Test 4	6-80
6-29	Maximum Ground Deflections Obtained by Analysis, Test 4	6-80
6-30	Comparison of Analysis and Test Structure Responses, Test 4	6-86
6-31	Stress Ratio Results Obtained by Analysis, Test 4	6-89
7-1	Summary of Crash Test Impact Conditions	7-2
7-2	Summary of Crash Tests Sequence of Events	7-4
7-3	Summary of Airframe Damage as a Result of the Crash Tests	7-5
7-4	Summary of Occupant-Seat-Restraint System Failures and Occupant Impacts Experienced During the Crash Tests	7-6

LIST OF TABLES (Continued)

Table		Page
7-5	Summary of Wing Damage Experienced as a Result of the Crash Tests	7-7
7-6	Nose and Main Gear Failures as a Result of the Crash Tests	7-8
7-7	Summary of Severity Index Results, Tests 3 and 4	7-9
7-8	Summary of Occupant Pelvis Vertical and Longitudinal Responses, Tests 1 through 4	7-10
7-9	Assessment of Occupant Survivability	7-11
7-10	Summary of Math Models	7-13
7-11	Comparison of Analytically Obtained Energy Distributions, Crash Tests 1 through 4	7-15
7-12	Summary of Analysis versus Crash Test Seat Leg Damage	7-17
7-13	Summary of Seat Leg Stress Ratios Obtained by Analysis	7-18
7-14	Summary of Analysis versus Crash Test Structure Failures	7-19
7-15	Summary of Analytical Results for Different Ground Flexibilities	7-31
7-16	Comparison of Energy Distribution as a Function of Ground Flexibility, Crash Test 4	7-33
7-17	Comparison of Test Severity Ranking Based on Analysis and Test Results, Crash Tests 1 through 4	7-35

SECTION I

INTRODUCTION

1.1 BACKGROUND

This report contains the results of the second of three technical tasks to develop an experimentally verified method of analysis for the crashworthiness of general aviation airplane structures and facilitate the development of improved crashworthiness designs. The first technical task effort was reported on in Reference 1.

During the Task 1 effort a review and evaluation of 61 light fixed-wing airplane models, produced by the major domestic general aviation airplane manufacturers, was performed. The evaluation takes into consideration airplane configuration, usage, operational characteristics, and structural characteristics.

Included in the review and evaluation of general aviation airplane characteristics are:

- A matrix of airplane configuration, maximum takeoff weight and usage
- A description of structural design characteristics of current general aviation airplanes
- A description of the various general aviation airplane types
- A categorization of airplanes as a function of configuration, maximum takeoff weight, stall speed, cruise speed, usage and accommodations.

The results of the study show that:

- There are three basic airplane configurations; single-engine low-wing, single-engine high-wing, twin-engine low-wing. There is a limited number of a fourth configuration; twin-engine, high-wing.

- With the exception of the agricultural airplane most airplanes have multiple uses.
- The airplanes tend, insofar as usage, accommodations, weight and speed characteristics are involved, to group into distinct categories.
- While there are many manufacturers and airplane models and the design details of the structure may vary, there are only two basic structural designs: monocoque and tubular.

During Task I, accident data from the FAA Civil Aeromedical Institute (CAMI) and the National Transportation Safety Board (NTSB) were reviewed and evaluated. Included in this accident evaluation were:

- Results of 18 CAMI accident records showing (a) the frequency of occurrence by phase of operation, type of accident, angle of impact, roll/yaw attitude, and terrain, (b) the distribution by degree of cabin damage, structural damage, and injury types and (c) the occurrence of seat and seat belt failures and occupant impact with controls and instrument panels
- The development of a computer program to sort and process selected pertinent crashworthiness accident data from NTSB data tapes
- Results obtained from the accident computer program for each airplane category using the 1971 through 1973 National Transportation Safety Board (NTSB) accident records encompassing 8491 accidents.

The findings of the NTSB accident data evaluation indicate that:

- The impact angle in a crash is predominantly less than 45 degrees.
- Stall, collisions with ground/water and collisions with obstacles are the prevalent types of accidents which result in serious or fatal injuries.
- In accidents wherein injuries are involved, light weight single-engine airplanes have a greater number of stall accidents than accidents involving collision with ground/water or obstacles. Conversely, heavier weight single-engine and twin-engine airplanes experienced more accidents involving collisions with the ground.
- The personnel involved in agricultural type airplane accidents, in which injuries occur, experienced less fatalities per occupant in all types of accidents.
- The ratio of fatalities to number of occupants, for accidents involving injuries, is generally lower for the single-engine airplane than the corresponding ratio for twin-engine airplanes for the same type of accident.

Based on the evaluation of general aviation airplane designs and accident statistics and a review of general aviation manufacturers computer and manpower capability, the mathematical modeling requirements were set forth in Task I (Reference 1). The review and evaluation of general aviation airplane configurations, usages, operational and structural design characteristics, accidents, industry design practices and industry computer capabilities, indicated that the use of a computerized analytical technique for performing crash analysis would be an asset to the industry if it contained certain features. The development of a general aviation airplane industry crash analysis computer program must take into consideration the need to analyze reasonably complex airframes and crash conditions, yet not impose unrealistic and costly investments

in specialized manpower and/or equipment to facilitate improved future crashworthy designs.

Ideally, the computer program should have the capability to:

- Provide sufficient information which can be used to assess an occupant's chance for survival. As a minimum this information should consist of defining floor acceleration pulses and evaluating cabin damage and cabin geometry change.
- Define forces, accelerations, velocities and displacements in three directions.
- Treat multidirectional impact forces, angles and angular rates representative of the probable crash conditions associated with the different airplane usages and operational characteristics.
- Represent various types of structural behavior for a wide range of structural element types, particularly wherein post-failure large deflections occur.
- Treat structural failures and the consequences of the failures on surrounding structure.
- Represent different airplane configurations such as high-wing, low-wing, single-engine, twin-engine, tandem engines, individual and multiple seating accommodations, weights up to at least 12,500 pounds, and retracted or extended landing gear.
- Provide the means to treat differences in terrain (level, hilly, water, dirt, concrete) using available data for describing the properties of the terrain.
- Treat the significant phases of multiple impact crashes wherein the effect of an initial impact is accounted for in subsequent impacts during the same crash.

- Utilize crash input acceleration magnitude, shape, duration and direction information as an input to the airplane.
- Facilitate usage and understanding of standard values, English symbols and simplified input requirements.

It is desirable that the computer program be written in Fortran IV and be applicable for use on the large size computers (i.e. IBM 360, IBM 370, CDC 6600) having at least 375,000 bytes of core storage. Furthermore, as a minimum the documentation should consist of a User's Manual describing the theory, input-output requirements, a sample illustrative problem, techniques for representing structure, instructions on how to utilize specialized features, program limitations, and structural design guidelines.

To meet these basic requirements, program KRASH, developed earlier (Reference 2), was modified to include additional features. These features are described in Reference 1. Having refined KRASH to facilitate its usage by the general aviation industry, the program's capability was then assessed with the use of two different sets of limited controlled crash test data for two different airplane configurations (single engine high-wing and low-wing). The comparison of test and analysis was performed for the following three impact conditions:

- (a) 45 feet per second longitudinal velocity impact into a 45 degree dirt barrier
- (b) cg velocity of 1.6 feet per second (down) and 21.6 feet per second (forward) and a pitch attitude of 38.5 degrees (nose down)
- (c) cg velocity of 0.5 feet per second (down) and 3.8 feet per second (forward), a pitch attitude of 19.6 degrees (nose down in inverted position), and a pitch rate of 89.4 degrees per second (nose down in inverted position)

Condition (a) is a test representing a stall spin accident while conditions (b) and (c) are the primary and secondary impacts, respectively, during a test representing an overturn accident.

During Task I Program KRASH was shown to be capable of defining:

- Spatial and temporal energy distribution including mass kinetic and potential, member strain and damping, structural crushing and ground friction;
- Large nonlinear behavior into the post-failure region including cabin deformation;
- Acceleration pulses at the floor in regions where occupants are located for the purpose of determining occupant response using an available occupant-seat-restraint system math model;
- Forces, accelerations, velocities and deflections resulting from multidirectional impacts;
- Structural behavior for a wide range of structural element types associated with general aviation airplane design;
- Large motion rigid-body behavior wherein ground contact forces can be defined; and
- Mathematical model requirements for two different airplane configurations (high-wing, low-wing).

1.2 TASK II EFFORT

While the results of Task I indicate that computer program KRASH is a potentially valid tool for performing structural crashworthiness analysis of general aviation airplanes, they also indicate that the effectiveness of it as an analytical tool could be further enhanced. A systematic approach employing several highly instrumented flightworthy airplanes along with complete film coverage and a comprehensive

correlation study between test and analytical data will contribute to the verification of the program's capability, define its limitations and provide additional input data for inclusion in a User's Manual.

The primary objective of this portion of Task II, which is reported herein, is the verification of the mathematical simulation (KRASH) with full-scale controlled crash test data. This report contains the following information:

- Test preparations for four fully instrumented single-engine, high-wing airplane crash tests
- Results of the four single-engine, high-wing airplane crash tests including pertinent recorded data and film
- Program KRASH refinements
- Single-engine, high-wing airplane math models representative of crash test conditions
- Comparison of test and analytical results for each of the crash tests
- Literature survey, evaluation and matrix categorization for structure/soil interaction data and related subjects
- A summary of results
- Conclusions formulated as a result of the work performed in this portion of Task II.

The results of this effort and the previous task (Reference 1) will be used to help develop potential design crash environment criteria and the formulation of methods for showing compliance during the completion of Task II which will be reported at a later date.

SECTION 2

FULL SCALE CRASH TEST PREPARATION

2.1 OBJECTIVES

The objectives of the test program are to provide test data

- for correlation with digital computer program KRASH as modified for general aviation airplane application
- to be used as a basis for improvement of the computer program
- for subsequent use in occupant-seat-restraint system math models
- for development of improvements for future crashworthy airframe and seat-restraint system design.

2.2 TEST SITE

All full scale crash tests were performed at the NASA-Langley Research Center (LRC) Impact Dynamics Research Facility (IDRF). Figure 2-1 shows the basic structure (gantry) of the IDRF. The gantry is 241 feet high, 403 feet long and 270 feet wide at the ground. Aircraft are crashed into the impact surface as free bodies by use of a pendulum swing method to obtain desired flight paths and velocities. The crash test facility and testing technique are fully described in Reference 3.

2.3 TEST SPECIMENS

Three used flightworthy and structurally sound single-engine, high-wing airplanes were used in the performance of the full-scale crash tests. The vintage of the test airplanes used are:

Specimen 1,	1967 - Test 1
Specimen 2,	1964* - Tests 2 and 4
Specimen 3,	1966 - Test 3

* The Test 2 airplane sustained minor damage and was repaired and used again in Test 4.

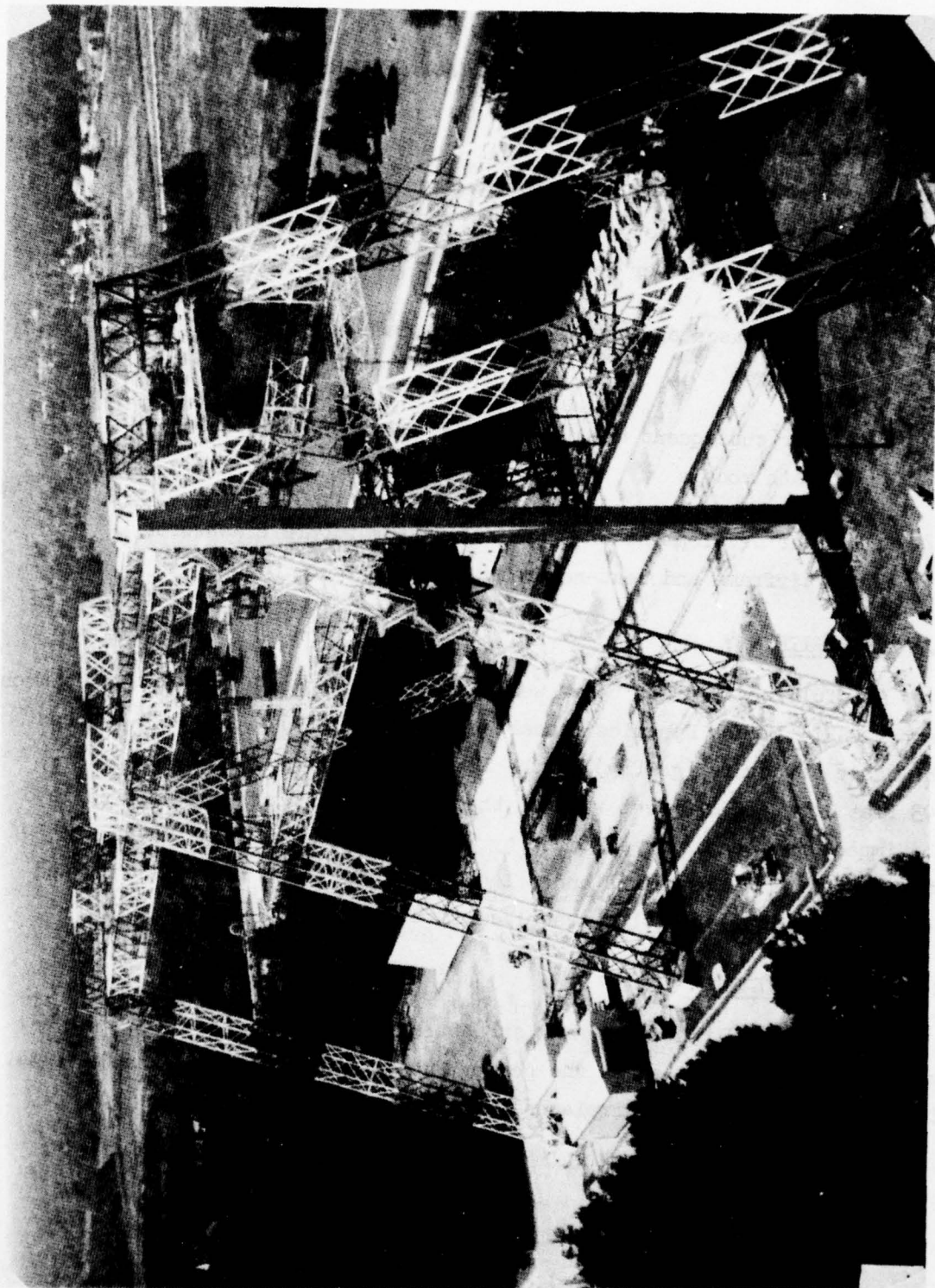


Figure 2-1. NASA-Langley Research Center Impact Dynamics Research Facility

The airplanes in their as-received condition are shown in Figure 2-2, 2-3, and 2-4, respectively. The airplanes are of the same basic structural design and specifications. In preparation for the tests, the fuel tanks were purged and upholstery, rear seats, wheel fairings, left door, tail section and miscellaneous equipment such as radios were removed from each of the airplanes. In addition, the airplanes were painted yellow with identifying black stripes and markers located as follows:

- two-inch black stripe to identify O.O B.L. on the top and bottom and O.O W.L. on the left and right side
- three-quarter inch black stripe to identify bulkhead and stringer locations.
- c.g. location
- test target alignment.

The tail section was represented by a substitute structure having the proper mass and location. Removal of the tail surface minimizes adverse aerodynamic effects and simplifies the pullback cable arrangement.

Initial preparation of the airplanes also included installation of wing spoilers, installation of cameras, lights and accelerometer mounting brackets, and structural modification to the airplane to accept harness and pullback attachments. This work was performed at the Cessna Aircraft Company, Pawnee Division facility in Wichita, Kansas. After initial preparation, the swing system was installed to insure proper fit. Thereafter, the swing system was detached and along with the disassembled airplane trucked to NASA's IDRF where the airplanes were reassembled. Final installation of accelerometers, cameras and pre-test checkout took place at the IDRF. The weight and c.g. location, including instrumentation, water in the tanks to simulate fuel, and ballast for each of the test specimens are given in Table 2-1. In each of the tests, the wing flaps were set in the up position.



Figure 2-2. Airplane Specimen Number 1 in As-Received Condition



Figure 2-3. Airplane Specimen Number 2 in As-Received Condition



Figure 2-4. Airplane Specimen Number 3 in As-Received Condition

TABLE 2-1. TEST WEIGHTS AND C.G. LOCATIONS

Test	1	2	3	4
Weight (lb)	2336	2390	2371	2375
C.G. Location (in.)				
F.S.	43.9	47.14	43.9	43.9
W.L.	6.9	6.9	6.9	6.9
B.L.	0.0	0.0	0.0	0.0

The water in each fuel tank was dyed a different color so that fuel tank damage, if it occurs during the tests, can readily be detected.

The alignment target used on each airplane is located at F.S. 16.66, W.L. -16.5 and LBL 19.45.

2.4 TEST CONDITIONS AND SEQUENCE

The impact test conditions are noted in Table 2-2. The NASA notation ($\theta = \gamma + \alpha$) is adhered to in establishing the impact conditions, where γ is the flight path angle, θ is the pitch angle, and α is the angle of attack. The nomenclature and expressions described in Reference 3 are followed. The planned impact position for each of the tests is shown in Figures 2-5, 2-6, 2-7 and 2-8, for Tests 1 through 4, respectively.

The impact surface for Tests 1, 2, and 3 is concrete. Compacted soil representing a lightly plowed field is used as an impact surface in Test 4. Details of the soil characteristics used in the test are given in Appendix A, while the soil literature survey, evaluation and matrix categorization for structure/soil interaction data, and related subjects are presented in Appendix B.

2.5 SWING HARNESS AND PULLBACK SYSTEMS

Figure 2-9 shows the airplane with its swing, pitch, and pullback system and the umbilical cable arrangement for Tests 1, 2 and 4. The pullback system is a four point release (2 at the landing gear and 2 at the wing aft spar). The swing harness is also a four point release (forward pitch cable, aft pitch cable and 2 swing cable attach points). Pullback, swing and pitch cable separation is accomplished through the use of pyrotechnics provided and operated by NASA. For Test 3 a slight variation in the location of the swing cable and pitch cable attachments is necessary to achieve the desired 20 degree roll angle and allow the line of action to pass through the airplane c.g. Figure 2-10 shows the Test 3 airplane with the swing, pitch and pullback systems installed. The location of the swing

TABLE 2-2. TEST SEQUENCE FOR SINGLE-ENGINE, HIGH-WING AIRPLANES

Condition Number	Flight Path Angle Deg.	θ Pitch Angle Deg.	α Angle of Attack Deg.	Flight Path Impact Velocity mph	ϕ Roll Angle Deg.	ψ Yaw Angle Deg.	Comments
1	-30	-30	0	55 \pm 5	0	0	<ul style="list-style-type: none"> • Similar to twin-engine, low-wing air-plane test (Ref. 3) • Represent a probable accident condition. • CAMI data shows 60 percent of accidents occur with an impact angle \leq 30 degrees. • Nose down impact.
2	-15	+10	+25	55 \pm 5	0	0	<ul style="list-style-type: none"> • Similar to twin-engine, low-wing air-plane test (Ref. 3) • Variation in accident type. • Mid cabin impact followed by possible secondary impact at forward structure. • Nose up impact
3	-34	-34	0	55 \pm 5	20	0	<ul style="list-style-type: none"> • Unsymmetrical impact condition. • Increased impact angle. • Represents more severe impact condition than Tests 1 or 2.
4	-30	-30	0	55 \pm 5	0	0	<ul style="list-style-type: none"> • Same as Test 1 above, except impact onto soil terrain
<p>(a) $\theta = \gamma + \alpha$ (follows NASA notation), is negative in dive, θ positive nose up relative to ground, α is positive nose up relative to flight path.</p> <p>(b) Stall speed = 50 mph (flaps down), 57 mph (flaps up).</p> <p>(c) Ground contact surface is concrete for tests 1, 2 and 3. The soil ground surface used for Test 4 is described in Appendix A.</p> <p>(d) Positive roll angle is right wing down, positive yaw angle is tail left.</p> <p>(e) The angles and velocity shown are nominal values. Final impact conditions can vary slightly due to wind conditions during the test.</p>							

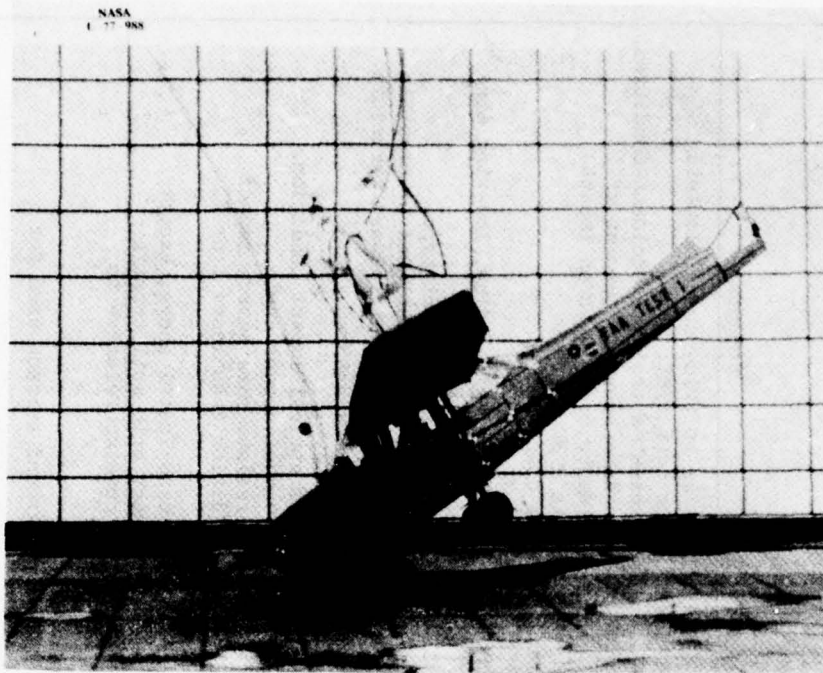


Figure 2-5. Test 1 Airplane Prior to Impact

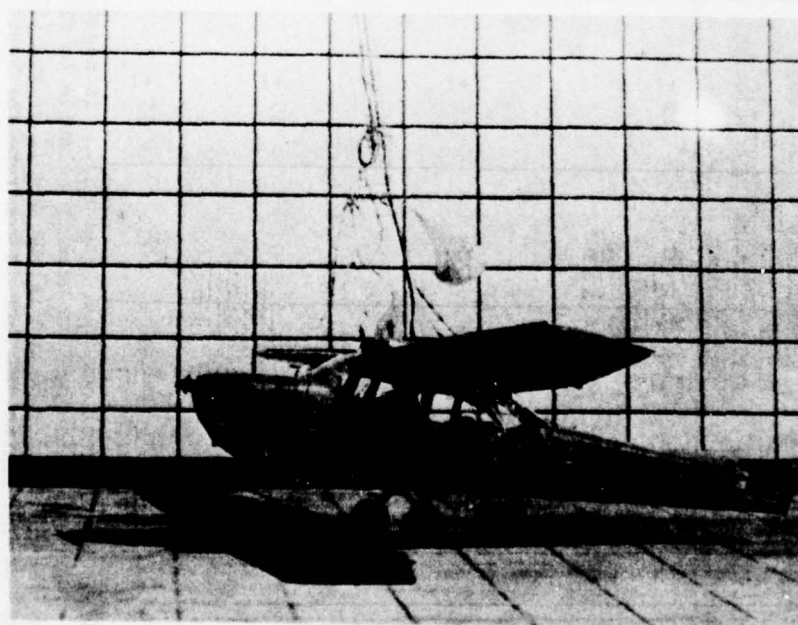


Figure 2-6. Test 2 Airplane Prior to Impact



Figure 2-7. Test 3 Airplane Prior to Impact

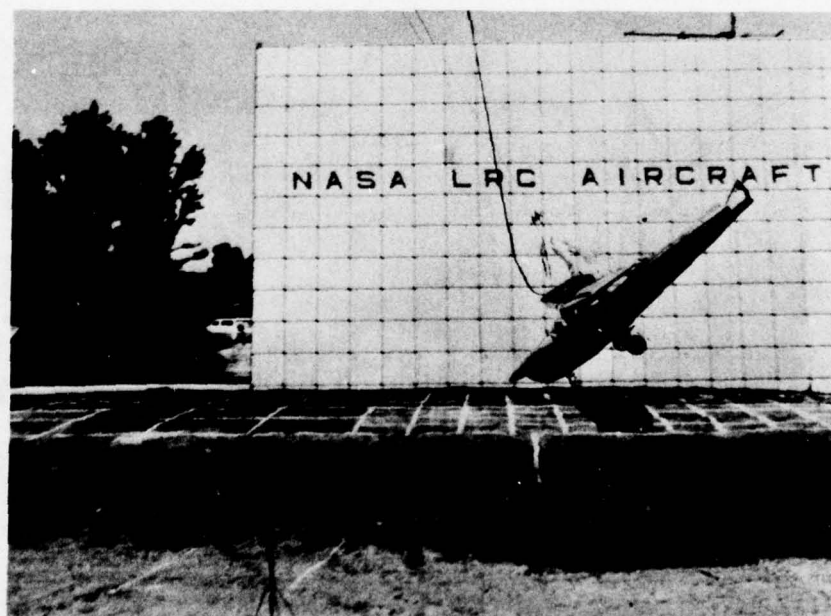


Figure 2-8. Test 4 Airplane Prior to Impact

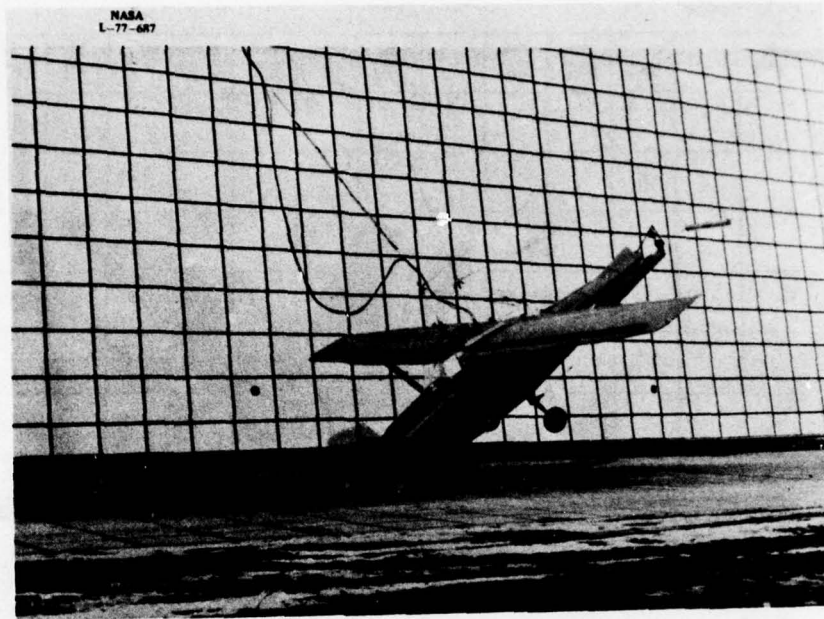


Figure 2-9. Swing Harness and Pullback System Arrangement, Tests 1, 2, 4

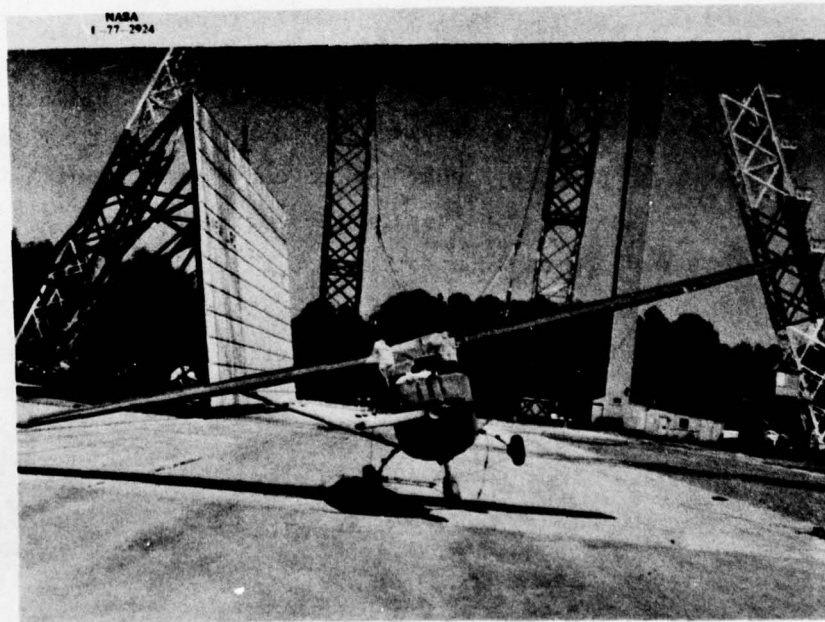


Figure 2-10. Swing Harness and Pullback System Arrangement, Test 3

attachment on the left wing and the slight offset at where the forward pitch cables attach to the firewall is shown. The location of the aft pitch cable attachment and the umbilical cable, both not shown, is also offset slightly.

The swing system hardware design details consist of the following:

- **Swing Cable Attachment:** A wing spar bracket was designed and fabricated to use for attachment of the swing cables. The forward and aft wing spars are modified to include a special fitting to accomplish this attachment. For Tests 1, 2, and 4 the attachment hardware is located outboard of the carry-thru spar, which allows for a lateral distance between attachments of approximately 43 inches. For Test 3 the attachment hardware is located outboard of the right wing carry-thru spar and at B.L. 49.66 on the left wing (Figure 2-10) which provides a lateral distance between attachments of approximately 71 inches. The swing cable line of action passes through the airplane c.g. in each of the tests.
- **Pitch Cable Attachment:** Pitch cable brackets are located at the 0.0 B.L. The forward pitch cable attachment is through a cable system from the top of the engine firewall (F.S. 3.4) to the lower engine mount attach points. The aft pitch cable bracket is attached to the tailcone at bulkhead (F.S. 114.0). The pitch cable line of action passes through the airplane c.g. in each test.

- **Pullback Cable Attachment:** The upper pullback cable attaches to the aft wing spar at the swing cable bracket. The lower pullback cable attaches to the landing gear. The pullback cable line of action passes through the airplane c.g. in each test.
- **Design Criteria:**
 - Pitch Cable Attachment Brackets - The pitch cable attachments are designed to a minimum strength of 1000* pounds each.
 - Swing Cable Attachment - The Aircraft is expected to encounter a 1g centrifugal force load in addition to the 1g gravitation force during swing down. Each bracket (2) is designed for a minimum of 2 g's* (total of 4 g's*).
 - Pullback Cable Attachment Structure - The lower attachment structure for the pullback cable and also the upper cable attachment are designed for a total of 3.0 g's.*

The planned test and sequence are shown in Table 2-2. In order to achieve the impact conditions noted in Table 2-2, the cable lengths and airplane attach points are changed. A summary of attach point locations and true length dimensions is shown in Table 2-3 (Tests 1 and 4), Table 2-4 (Test 2) and Table 2-5 (Test 3).

2.6 INSTRUMENTATION

A minimum of forty-four accelerometer channels were employed to record the dynamic response of the structure and occupant(s) during each test. The signals are fed into a junction box on board the airplane. The

*Design Loads

TABLE 2-3. SINGLE-ENGINE, HIGH-WING AIRPLANE ATTACHMENT
LOCATIONS AND CABLE LENGTHS, TESTS 1 AND 4

Attachment (a)	Location			True Length (b) (in.)
	F.S. (in.)	W.L. (in.)	B.L. (in.)	
<u>Pitch Harness</u> (c)				
Forward attach point	3.4	17.15	0.0	76.3
Aft attach point	114.0	22.75	0.0	88.2
<u>Pullback Harness</u> (c)				
Upper attach point	66.57	33.1	21.3	215.0
Lower attach point	65.0	-19.1	21.0	216.6
<u>Swing Cable</u> (c)				
Attach point	47.14	42.0	21.75	32.2
<u>Pullback Bar</u> (c)				
Cable attach point	280.0	6.96	18.0	-
<u>"D" Ring Locations</u> (c)	47.14	73.7	26.57	-
<p>(a) All attach points except the pullback bar and "D" ring are on the airplane fuselage.</p> <p>(b) True lengths are measured from attach point to swing cable interface point ("D" ring)</p> <p>(c) Left and right sides</p>				

TABLE 2-4. SINGLE-ENGINE, HIGH-WING AIRPLANE ATTACHMENT
LOCATIONS AND CABLE LENGTHS, TEST 2

Attachment (a)	Location			True Length (b) (in.)
	F.S. (in.)	W.L. (in.)	B.L. (in.)	
<u>Pitch Harness</u> (c)				
Forward attach point	3.4	17.15	0.0	61.5
Aft attach point	114.0	22.75	0.0	111.3
<u>Pullback Harness</u> (c)				
Upper attach point	66.57	33.1	21.3	204.7
Lower attach point	65.0	-19.1	21.0	229.8
<u>Swing Cable</u> (c)				
Attach point	30.67	42.0	21.75	32.2
<u>Pullback Bar</u> (c)				
Cable attach point	258.1	105.37	22.0	-
<u>"D" Ring Location</u> (c)	17.25	70.85	26.57	-
<p>(a) All attach points except the pullback bar and "D" ring are on the airplane fuselage.</p> <p>(b) True lengths are measured from attach point to swing cable interface point ("D" ring)</p> <p>(c) Left and right sides</p>				

TABLE 2-5. SINGLE-ENGINE, HIGH-WING AIRPLANE ATTACHMENT
LOCATION AND CABLE LENGTHS, TEST 3

Attachment (a)	Location			True Length (b) (in.)
	F.S. (in.)	W.L. (in.)	B.L. (in.)	
Pitch Harness (c)				
Forward attach point	3.4	17.15	3.0	96.2
Aft attach point	114.0	22.75	5.55	104.6
Pullback Harness (c)				
Upper attach point	66.57	33.1	21.3	215.0
Lower attach point	65.0	-19.1	21.0	216.6
Swing Cable				
Attach point, left	47.14	43.72	21.75	36.0
Attach point, right	47.14	42.00	21.75	61.9
Pullback Bar (c)				
Cable attach point	280.0	6.96	22.0	- -
"D" Ring Location (c)	47.14	87.22	38.79	- -
<p>(a) All attach points except the pullback bar and "D" ring are on the airplane fuselage.</p> <p>(b) True lengths are measured from attach point to swing cable interface point ("D" ring).</p> <p>(c) Left and right side.</p>				

junction box centroid is located at F.S. 77.3, W.L. 5.5, L.B.L. 20.0. Layouts showing the locations of the accelerometers are presented in Figures 2-11 through 2-13 for the planned symmetrical and unsymmetrical tests. Tests 1, 2 and 4 involve symmetrical impact and only accelerations in the airplane longitudinal and vertical directions were measured. With the exception of the accelerometers located on the nose and main gears for Test 4, the accelerometer locations for Tests 1, 2 and 4 were identical. In Test 3 the impact was unsymmetrical and accelerations were measured in the airplane vertical, longitudinal and lateral directions. Tables 2-6 and 2-7 depict the accelerometer number, location, type, axis, tape and channel number, peak G setting, and polarity response settings for each accelerometer used for Tests 1 and 2, respectively. Tables 2-8 and 2-9 describes the accelerometer setup for Tests 3 and 4, respectively. The total number of each type accelerometer available for the test program, along with their respective capabilities, is given in Table 2-10. Positive polarity for all tests is up, aft and right.

For each test there were two instrumented dummies (Tables 2-6 through 2-9) located in the pilot and copilot seats. The pilot is 95th percentile anthropomorphic dummy weighing 224 pounds.* The anthropometric dummy, representing the copilot, weighs 202 pounds, (approximately 80th percentile by weight). The 95th percentile dummy has two restraint system transducers (load cells one each for the lap belt and shoulder harness and one chest deflection measurement whose responses are recorded on dc channels. The dummy representing the copilot has two restraint system transducer signals (lap belt and shoulder harness) recorded on dc channels. The dummies with their restraint systems and load cells are shown seated in an airplane in Figure 2-14. Also, some of the target markers and stripes on the airplane are shown. The markers along with the black stripes are used to help determine approximate structural deformation encountered during the tests.

*Weight includes clothes and shoes.

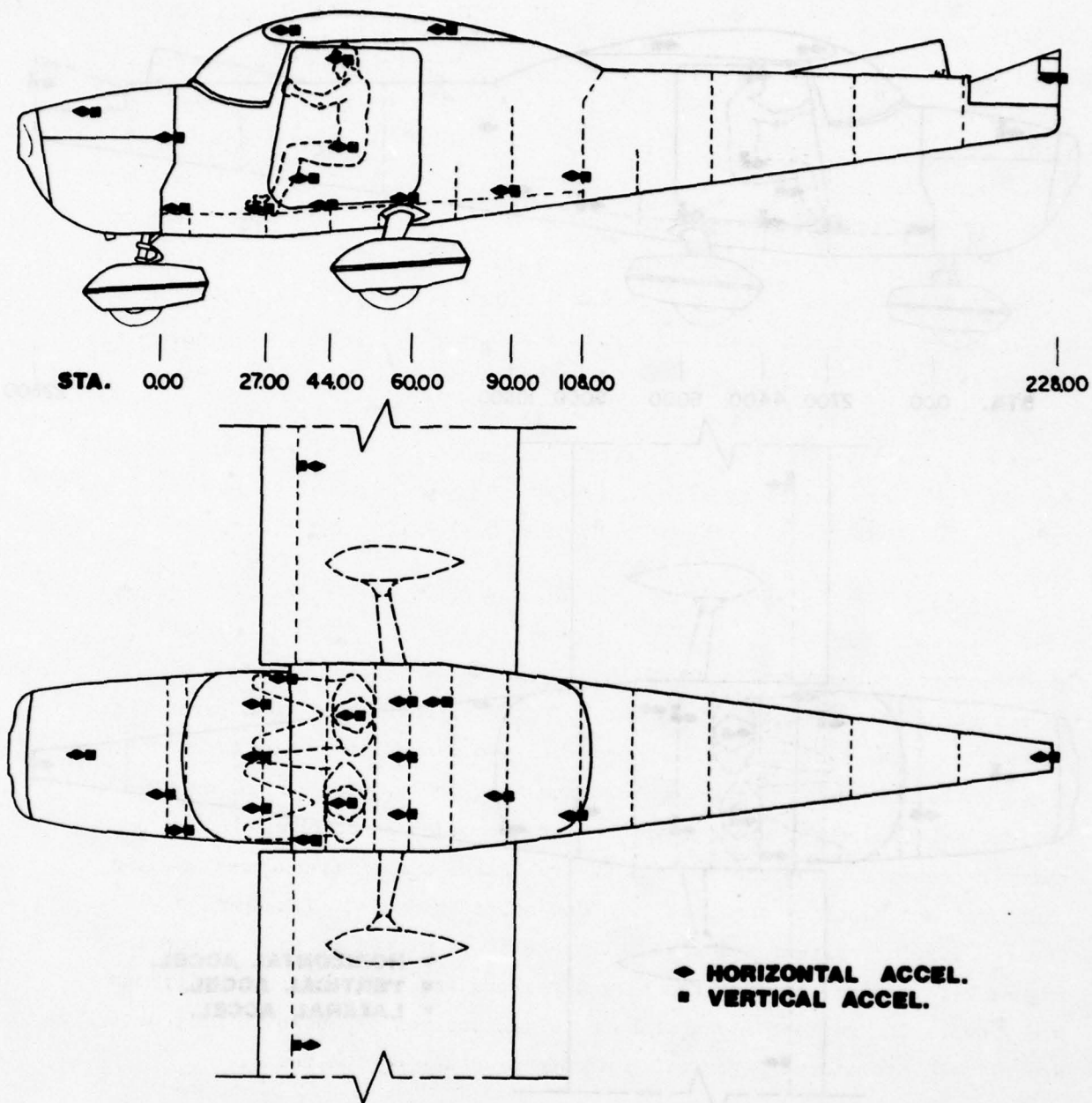


Figure 2-11. Accelerometer Locations, Single-Engine, High-Wing Airplane, Crash Tests 1 and 2

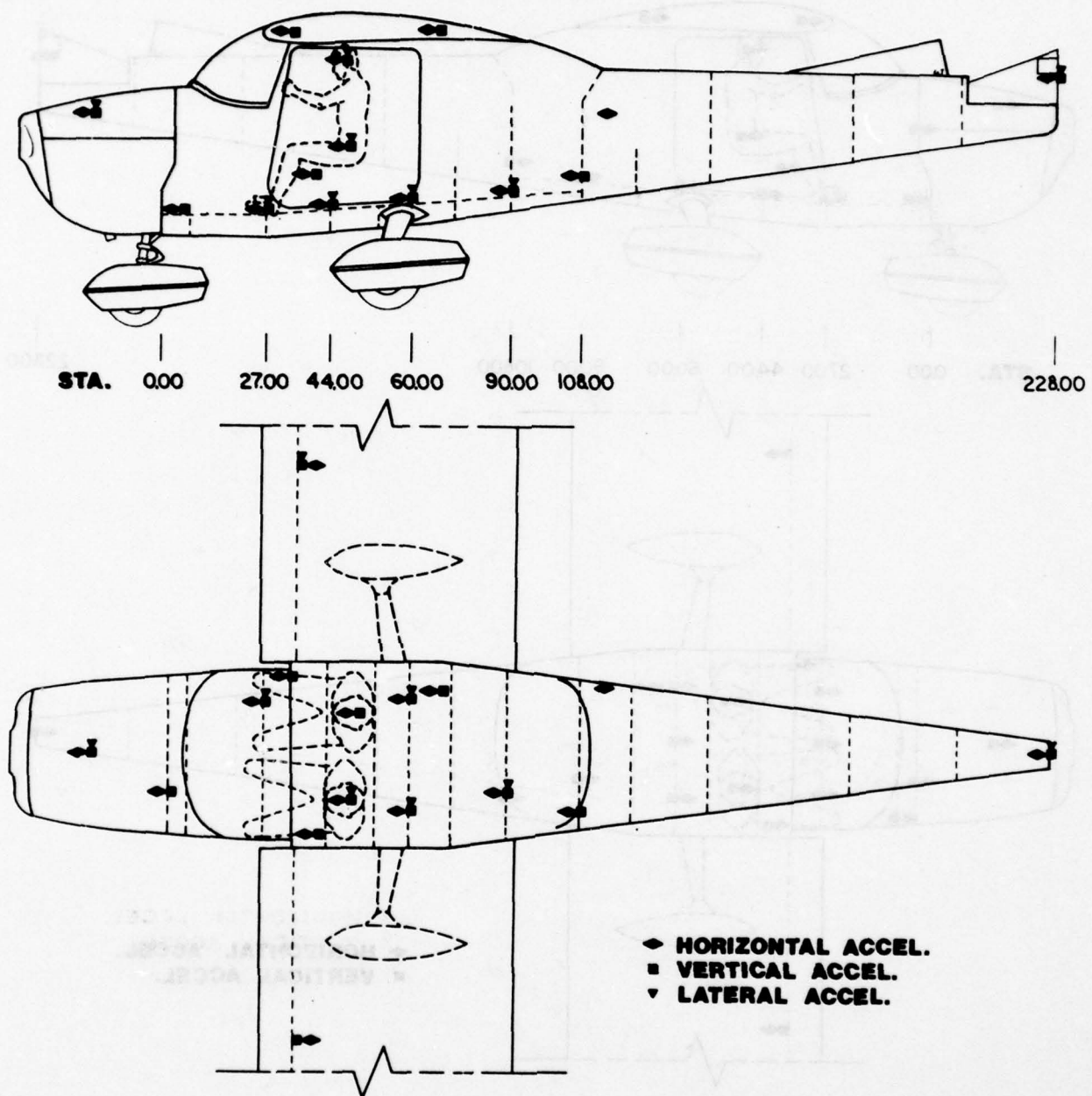


Figure 2-12. Accelerometer Locations, Single-Engine, High-Wing Airplane, Crash Test 3

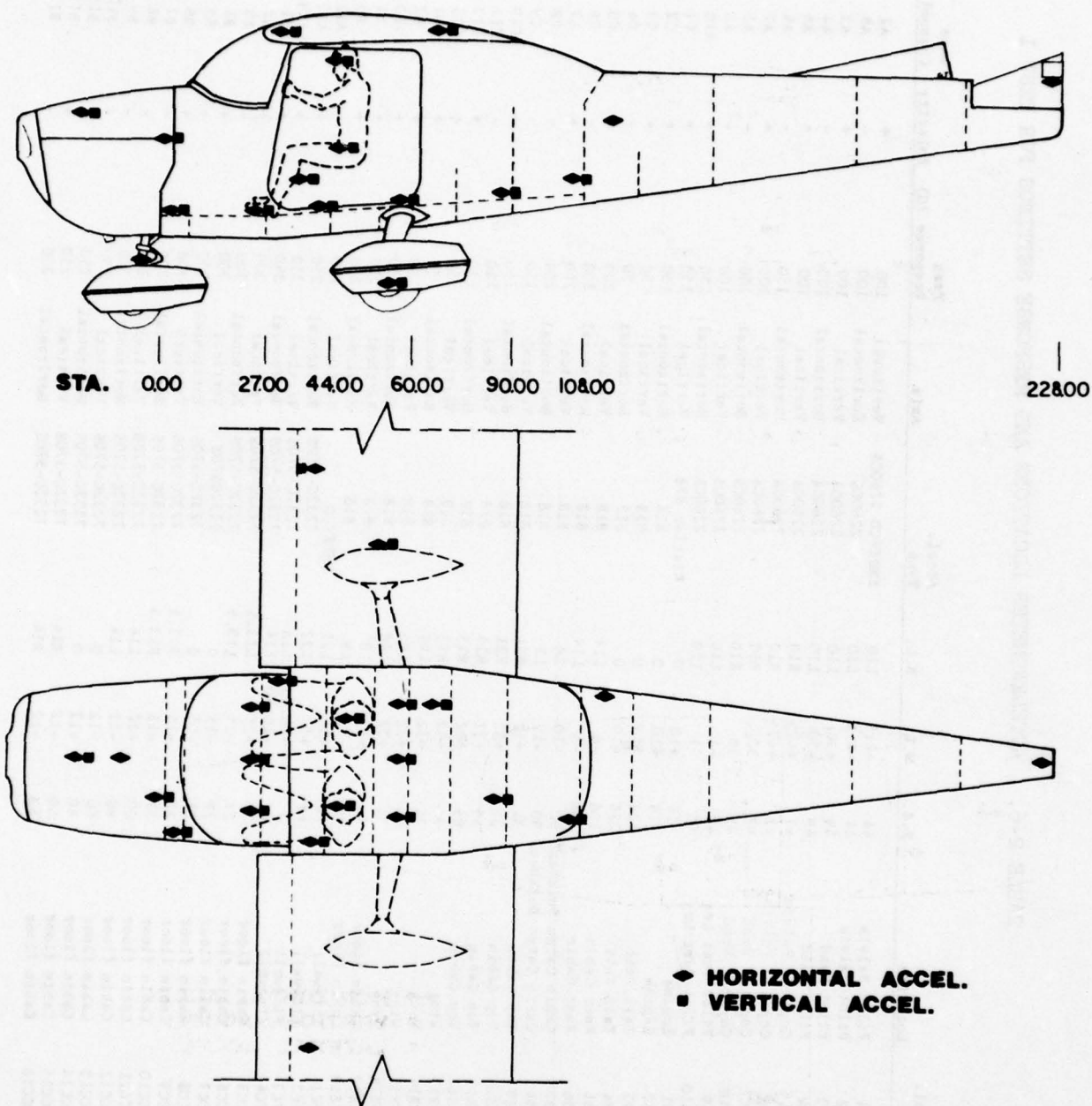


Figure 2-13. Accelerometer Locations, Single-Engine, High-Wing Airplane, Crash Test 4

TABLE 2-6. ACCELEROMETER LOCATIONS AND RESPONSE SETTINGS FOR TEST 1

Accel. No.	Location	P.S.	W.L.	B.L.	Accel. Type	Axis	Peak Response (G)	Polarity	Tape Channel
VP1	Pilot Pelvis	44	+4.5	L10	ENDEVCO 2260CA	Vertical	100	+	A2
VP2	Pilot Pelvis	44	+4.5	L10	2260CA	Horizontal	100	-	A8
VP3	Pilot Head	49	+30	L10	2260CA	Vertical	100	+	A3
VP4	Pilot Head	49	+30	L10	2260CA	Horizontal	100	-	A4
VCA5	Copilot Pelvis	42	+4.5	R10	2260CA	Vertical	100	+	A6
HCA6	Copilot Pelvis	42	+4.5	R10	2260CA	Horizontal	150	-	A9
VCA7	Copilot Head	47	30	R10	2260CA	Vertical	100	+	A7
HCA8	Copilot Head	47	30	R10	2260CA	Horizontal	100	-	A1
VSA9	Pilot Seat Leg	40	-1	L10	2260CA	Vertical	100	-	A5
MSA10	Pilot Seat Leg	40	-1	L10	2260CA	Horizontal	150	+	A10
VEB1	Engine	-18	+10	0	Kistler 818	Vertical	150	+	C1
HE32	Engine	-18	+10	0	818	Horizontal	150	+	C2
VTB3	Tail Unit	228	+10	0	818	Vertical	50	-	C3
HTB4	Tail Unit	228	+10	0	818	Horizontal	50	+	C4
VCB5	Rear Cabin	108	-6	L14	818	Vertical	200	+	C5
VCB6	Rear Cabin	108	-6	L14	818	Horizontal	200	-	C6
VCB7	Cabin Cargo Bulkhead	90	-10	L8	818	Vertical	200	+	C7
VCB8	Cabin Cargo Bulkhead	90	-10	L8	818	Horizontal	200	-	C8
VCB9	Top Cabin	34	+32	R21	818	Vertical	150	-	C9
VCB10	Top Cabin	34	+32	R21	818	Horizontal	150	+	C10
VCB11	Top Cabin	65	+32	R15	818	Vertical	150	-	C11
VCB12	Top Cabin	65	+32	R15	818	Horizontal	150	+	C12
VCB13	Wing	34	+32	R98	818	Vertical	50	+	C13
VCB14	Wing	34	+32	R98	818	Horizontal	50	+	D1
VCB15	Wing	34	+32	R98	818	Vertical	50	+	D2
VCB16	Wing	34	+32	R98	818	Horizontal	50	+	D3
VCB17	Cabin Floor	44	-13	L8	818	Vertical	250	+	D4
VCB18	Cabin Floor	44	-13	L8	818	Horizontal	250	+	D5
VFC1	Firewall	+8	+5	L22	ENDEVCO	Vertical	250	-	A11
HFC2	Firewall	+8	+5	L22	7232C-570S	Horizontal	250	+	A12
VFC3	Firewall	0	-16.80	L1A	7232C-570S	Vertical	350	+	A13
HFC4	Firewall	0	-16.80	L1A	7232C-570S	Horizontal	350	+	B1
VCC5	Cabin floor	27	-15	L13.5	7232C-570S	Vertical	300	+	B2
VCC6	Cabin floor	27	-15	L13.5	7232C-570S	Horizontal	300	+	B3
VCC7	Cabin floor	27	-15	0	7232C570S	Vertical	300	+	B4
VCC8	Cabin floor	27	-15	0	7232C-570S	Horizontal	300	+	B5
VCC9	Cabin floor	27	-15	R13.5	7232C-570S	Vertical	300	+	B6
VCC10	Cabin floor	27	-15	R13.5	7232C-570S	Horizontal	300	+	B7
VCC11	Cabin floor	60	-12	L14	7232C-570S	Vertical	250	+	B8
VCC12	Cabin floor	60	-12	L14	7232C-570S	Horizontal	250	+	B9
VCC13	Cabin floor	60	-12	0	7232C-570S	Vertical	250	+	B10
VCC14	Cabin floor	60	-12	0	7232C-570S	Horizontal	250	+	B11
VCC15	Cabin floor	60	-12	R14	7232C-570S	Vertical	250	+	B12
VCC16	Cabin floor	60	-12	R14	7232C-570S	Horizontal	250	+	B13

TABLE 2-7. ACCELEROMETER LOCATIONS AND RESPONSE SETTINGS FOR TEST 2

Accel. No.	Location	F.S.	W.L.	B.L.	Accel. Type	Axis	Peak Response (G)	Polarity	Tape Channel
VP11	Pilot Pelvis	44	+4.5	L10	ENDEVCO 2260CA	Vertical	100	+	A2
HPA2	Pilot Pelvis	44	+4.5	L10	2260CA	Horizontal	100	-	A8
VP13	Pilot Head	49	+30	L10	2260CA	Vertical	100	+	A3
HPA4	Pilot Head	49	+30	L10	2260CA	Horizontal	100	-	A4
VCA5	Copilot Pelvis	42	+4.5	R10	2260CA	Vertical	100	+	A6
HCA6	Copilot Pelvis	42	+4.5	R10	2260CA	Horizontal	100	-	A9
VCA7	Copilot Head	47	30	R10	2260CA	Vertical	100	+	A7
HCA8	Copilot Head	47	30	R10	2260CA	Horizontal	100	-	A1
VSA9	Pilot Seat Leg	40	-1	L10	2260CA	Vertical	150	-	A5
NSA10	Pilot Seat Leg	40	-1	L10	2260CA	Horizontal	150	+	A10
VEB1	Engine	-18	+10	0	Kistler 818	Vertical	150	+	C1
HEB2	Engine	-18	+10	0	818	Horizontal	150	+	C2
VTB3	Tail Unit	228	+10	0	818	Vertical	75	-	C3
MTB4	Tail Unit	228	+10	0	818	Horizontal	75	+	C4
VCB5	Rear Cabin	108	-6	L14	818	Vertical	250	+	C5
MCB6	Rear Cabin	108	-6	L14	818	Horizontal	250	-	C6
VCB7	Cabin Cargo Bulkhead	90	-10	L8	818	Vertical	250	+	C7
MCB8	Cabin Cargo Bulkhead	90	-10	L8	818	Horizontal	250	-	C8
VCB9	Top Cabin	34	+32	R21	818	Vertical	200	-	C9
MCB10	Top Cabin	34	+32	R21	818	Horizontal	200	+	C10
VCB11	Top Cabin	65	+32	R15	818	Vertical	200	-	C11
MCB12	Top Cabin	65	+32	R15	818	Horizontal	200	+	C12
VWB13	Wing	34	+32	R98	818	Vertical	100	+	C13
HWB14	Wing	34	+32	R98	818	Horizontal	100	+	D1
VWB15	Wing	34	+32	L98	818	Vertical	100	+	D2
HWB16	Wing	34	+32	L98	818	Horizontal	100	+	D3
VCB17	Cabin Floor	44	-13	L8	818	Vertical	350	+	D4
MCB18	Cabin Floor	44	-13	L8	818	Horizontal	350	+	D5
VFC1	Firewall	+8	+5	L22	ENDEVCO	Vertical	250	-	A11
WFC2	Firewall	+8	+5	L22	7232C-5705	Horizontal	250	+	A12
VFC3	Firewall	0	-16.80	L1A	7232C-5705	Vertical	350	+	A13
WFC4	Firewall	0	-16.80	L1A	7232C-5705	Horizontal	350	+	B1
VCC5	Cabin floor	27	-15	L13.5	7232C-5705	Vertical	350	+	B2
WCC6	Cabin floor	27	-15	L13.5	7232C-5705	Horizontal	350	+	B3
VCC7	Cabin floor	27	-15	0	7232C5705	Vertical	350	+	B4
WCC8	Cabin floor	27	-15	0	7232C-5705	Horizontal	350	+	B5
VCC9	Cabin floor	27	-15	R13.5	7232C-5705	Vertical	350	+	B6
WCC10	Cabin floor	27	-15	R13.5	7232C-5705	Horizontal	350	+	B7
VCC11	Cabin floor	60	-12	L14	7232C-5705	Vertical	350	+	B8
WCC12	Cabin floor	60	-12	L14	7232C-5705	Horizontal	350	+	B9
VCC13	Cabin floor	60	-12	0	7232C-5705	Vertical	350	+	B10
WCC14	Cabin floor	60	-12	0	7232C-5705	Horizontal	350	+	B11
VCC15	Cabin floor	60	-12	R14	7232C-5705	Vertical	350	+	B12
WCC16	Cabin floor	60	-12	R14	7232C-5705	Horizontal	350	+	B13

TABLE 2-8. ACCELEROMETER LOCATIONS AND RESPONSE SETTINGS FOR TEST 3

Accel. No.	Location	F.S.	W.L.	B.L.	Accel. Type	Axis	Peak Response(G)	Polarity	Tape Channel
VP1	Pilot Pelvis	44	+4.5	L10	ENDEVCO 2260CA	Vertical	100	+	A1
HPA2	Pilot Pelvis	44	+4.5	L10	2260CA	Horizontal	100	-	A2
LPA3	Pilot Pelvis	44	+4.5	L10	2260CA	Lateral	100	-	A3
HPA4	Pilot Head	49	+30	L10	2260CA	Vertical	100	+	A4
HPA5	Pilot Head	49	+30	L10	2260CA	Horizontal	100	+	A5
LPA6	Pilot Head	49	+30	L10	2260CA	Lateral	100	+	A6
VCA7	Copilot Pelvis	42	+4.5	R10	2260CA	Vertical	100	+	A7
WC8	Copilot Pelvis	42	+4.5	R10	2260CA	Horizontal	100	-	A8
LCA9	Copilot Pelvis	42	+4.5	R10	2260CA	Lateral	100	-	A9
VCA10	Pilot seat leg	40	-1	L10	ENDEVCO 7232C-570S	Vertical	150	-	A10
VEB1	Engine	-18	+10	0	Kistler 818	Vertical	150	+	C1
NEB2	Engine	-18	+10	0	818	Horizontal	150	+	C2
LEB3	Engine	-18	+10	0	818	Lateral	150	+	C3
VTB4	Tail Unit	228	+10	0	818	Vertical	100	-	C4
RTB5	Tail Unit	228	+10	0	818	Horizontal	100	-	C5
LTB6	Tail Unit	228	+10	0	818	Lateral	100	+	C6
VCB7	Rear Cabin	108	-6	L14	818	Vertical	250	+	C7
WCB8	Rear Cabin	108	-6	L14	818	Horizontal	250	-	C8
VCB9	Cabin Cargo Bulkhead	90	-10	L8	818	Vertical	250	+	C9
WCB10	Cabin Cargo Bulkhead	90	-10	L8	818	Horizontal	250	+	C10
LCB11	Cabin Cargo Bulkhead	90	-10	L8	818	Lateral	250	+	C11
VCB12	Top Cabin Fwd.	34	+32	R21	818	Vertical	200	+	C12
WCB13	Top Cabin Fwd.	34	+32	R21	818	Horizontal	200	+	C13
VCB14	Top Cabin Rear	65	+32	R15	818	Vertical	200	-	D1
WCB15	Top Cabin Rear	65	+32	R15	818	Horizontal	200	+	D2
VNB16	Wing Right	34	+32	R98	818	Vertical	100	+	D3
WNB17	Wing Right	34	+32	R98	818	Horizontal	100	+	D4
LNB18	Wing Right	34	+32	R98	818	Lateral	100	+	D5
VNB19	Wing, left	34	+32	L98	818	Vertical	100	+	D6
WNB20	Wing, left	34	+32	L98	818	Horizontal	100	+	D7
VFC21	Firewall	0	-16.8	L14	ENDEVCO 7232C-750S	Vertical	350	+	A11
HFC22	Firewall	0	-16.8	L14	7232C-750S	Horizontal	350	+	A12
VCC3	Cabin Floor	27	-15	R13.5	7232C-750S	Vertical	350	+	A13
HCC4	Cabin Floor	27	-15	R13.5	7232C-750S	Horizontal	350	+	B1
LCC5	Cabin Floor	27	-15	R13.5	7232C-750S	Lateral	350	+	B2
VCC6	Cabin Floor	44	-13	R8	7232C-750S	Vertical	350	+	B3
HCC7	Cabin Floor	44	-13	R8	7232C-750S	Horizontal	350	+	B4
LCC8	Cabin Floor	44	-13	R8	7232C-750S	Lateral	350	+	B5
VCC9	Cabin Floor	60	-12	L14	7232C-750S	Vertical	300	+	B6
HCC10	Cabin Floor	60	-12	L14	7232C-750S	Horizontal	300	+	B7
LCC11	Cabin Floor	60	-12	L14	7232C-750S	Lateral	300	+	B8
VCC12	Cabin Floor	60	-12	R14	7232C-750S	Vertical	350	+	B9
HCC13	Cabin Floor	60	-12	R14	7232C-750S	Horizontal	350	+	B10
LCC14	Cabin Floor	60	-12	R14	7232C-750S	Lateral	350	+	B11
HCC15	Co-Pilot Head	47	30	R10	7232C-750S	Vertical	100	+	B12
LCC16	Co-Pilot Head	47	30	R10	7232C-750S	Horizontal	100	+	B13
HCC17	Pilot Seat Leg	40	-1	L10	7232C-750S	Lateral	150	+	D8
***	Elt Bracket	115	+10	R14	ENDEVCO 2260C	Horizontal	100	-	

***This accelerometer was added at the request of the FAA and the output was recorded on an oscillograph through J-Box channel 32

TABLE 2-9. ACCELEROMETER LOCATIONS AND RESPONSE SETTINGS FOR TEST 4

Accel. No.	Location	F.S.	V.L.	B.L.	Accel. Type	Axis	Peak Response(G)	Polarity	Tape Channel
VP41	Pilot Pelvis	44	+4.5	L10	ENDEVCO	Vertical	100	+	A1
HPA2	Pilot Pelvis	44	+4.5	L10	2260CA	Horizontal	100	-	A2
VP43	Pilot Head	49	+30	L10	2260CA	Vertical	100	+	A3
HPA4	Pilot Head	49	+30	L10	2260CA	Horizontal	100	-	A4
VCA5	Copilot Pelvis	42	+4.5	R10	2260CA	Vertical	100	+	A5
HCA6	Copilot Pelvis	42	+4.5	R10	2260CA	Horizontal	100	-	A6
VCA7	Copilot Head	47	30	R10	2260CA	Vertical	100	+	A7
HCA8	Copilot Head	47	30	R10	2260CA	Horizontal	100	-	A8
VSA9	Pilot Seat Leg	40	-1	L10	2260CA	Vertical	150	-	A9
HSAL0	Pilot Seat Leg	40	-1	L10	2260CA	Horizontal	150	+	A10
VEB1	Engine	-18	+10	0	Kistler	Vertical	150	+	C1
HEB2	Engine	-18	+10	0	818	Horizontal	150	+	C2
VTB3	Tail Unit	228	+10	0	818	Vertical	75	+	C3
VNC4	Nose Gear	-6.7	+10	0	818	Vertical	75	+	C4
VCB5	Rear Cabin	108	-6	L14	818	Vertical	250	+	C5
NCB6	Rear Cabin	108	-6	L14	818	Horizontal	250	-	C6
VCB7	Cabin Cargo Bulkhead	90	-10	L8	818	Vertical	250	+	C7
NCB8	Cabin Cargo Bulkhead	90	-10	L8	818	Horizontal	250	-	C8
VCB9	Top Cabin	34	+32	R21	818	Vertical	200	-	C9
NCB10	Top Cabin	34	+32	R21	818	Horizontal	200	+	C10
VCB11	Top Cabin	65	+32	R15	818	Vertical	200	+	C11
NCB12	Top Cabin	65	+32	R15	818	Horizontal	200	-	C12
VWB13	Wing	34	+32	R98	818	Vertical	100	+	C13
NWB14	Wing	34	+32	R98	818	Horizontal	100	+	D1
WMB15	Wing	34	+32	L98	818	Vertical	100	+	D2
HRB16	Right Main Gear	60	-31.7	R48.8	818	Horizontal	100	+	D3
VCB17	Cabin Floor	44	-13	L8	818	Vertical	350	+	D4
NCB18	Cabin Floor	44	-13	L8	818	Horizontal	350	+	D5
VRB19	Right Main Gear	60	-31.7	R48.8	818	Vertical	50	+	D6
HEB20	Elc Bracket	115	+10	R14	818	Horizontal	100	-	D7
VFC1	Firewall	+3	+5	L22	ENDEVCO	Vertical	250	+	A11
HFC2	Firewall	+3	+5	L22	7232C-750S	Horizontal	250	+	A12
VFC3	Firewall	0	-16.80	L14	7232C-750S	Vertical	350	+	A13
HFC4	Firewall	0	-16.80	L14	7232C-750S	Horizontal	450	+	B1
VCC5	Cabin Floor	27	-15	L13.5	7232C-750S	Vertical	350	+	B2
HCC6	Cabin Floor	27	-15	L13.5	7232C-750S	Horizontal	400	+	B3
VCC7	Cabin Floor	27	-15	0	7232C-750S	Vertical	350	+	B4
HCC8	Cabin Floor	27	-15	0	7232C-750S	Horizontal	400	+	B5
VCC9	Cabin Floor	27	-15	R13.5	7232C-750S	Vertical	350	+	B6
HCC10	Cabin Floor	27	-15	R13.5	7232C-750S	Horizontal	400	+	B7
VCC11	Cabin Floor	60	-12	L14	7232C-750S	Vertical	350	+	B8
HCC12	Cabin Floor	60	-12	L14	7232C-750S	Horizontal	350	+	B9
VCC13	Cabin Floor	60	-12	0	7232C-750S	Vertical	350	+	B10
HCC14	Cabin Floor	60	-12	0	7232C-750S	Horizontal	350	+	B11
VCC15	Cabin Floor	60	-12	R14	7232C-750S	Vertical	350	+	B12
HCC16	Cabin Floor	60	-12	R14	7232C-750S	Horizontal	350	+	B13

TABLE 2-10. AVAILABLE ACCELEROMETERS FOR TESTS

Accelerometer	Type	Acceleration Range (g's)	Shock Capability (g's)	Freq. Range (Hz)	Number Available
Endevco 2260CA	dc	250	750	0-2000	12
Endevco 7232-7505	dc	750	2500	0-2000	18
Kistler 818	ac	250	2000	2-5000	20

In Tests 1 and 2 two displacement rods (at F.S. 27 and F.S. 63) and two linear motion potentiometers (requiring dc channels) were installed in the airplane for the purpose of recording cabin deformation. The results of Tests 1 and 2 indicated that the two linear potentiometers should be replaced by accelerometers to improve the coverage of the unsymmetrical crash condition of Test 3 in view of the limited number of available dc channels. In addition the potentiometers are prone to failure under combined loads before large displacements are reached. The vertical displacement rod and potentiometer are shown in Figure 2-14 on the vehicle right side near the aft door post.



Figure 2-14. Occupants and Restraint Systems Installed in Airplane

All data were recorded by NASA using the existing IDRF recording system. A total of 52 channels of data plus timing and radar to determine velocity were recorded in each test. Each tape of recorded data has an IRIG "A" time code (except Test 2 in which an IRIG "B" was used) so that all the signals can be synchronized. Starting with the second test, NASA introduced a filter in their recording system which is 3 dB down at 1000 Hz. IRIG "B" is compatible with frequencies at or below 1000 Hz. However, radar resolution is ± 0.1 mph with IRIG "A" and ± 0.8 mph with IRIB "B". The setup for the load cells and displacement measurements are shown in Table 2-11.

2.7 PHOTOGRAPHIC COVERAGE

Up to 17 high-speed cameras and 3 normal speed documentary cameras were used to record the trajectory of the airplanes and the action during impact. Three of the high-speed cameras were located onboard the airplanes. One camera was mounted in the center of the instrument panel facing rearward. The front onboard camera was located in the open position between the control wheels, see Figure 2-15. A second onboard camera was mounted in the rear luggage compartment facing forward, see Figure 2-16.

Figure 2-16 also shows the locations of a) the battery box (white box in front of camera bracket), b) the platform for pyrotechnics (forward of the battery box) c) aft mounted onboard cameras and d) the junction box (not shown) which is forward of the luggage door and on the wall between F.S. 65 and F.S. 90. The third onboard camera is located on the left wing facing inboard (Figure 2-17). The location of all the cameras and descriptions, including speeds, lenses and coverage are given in Figure 2-18 and Table 2-12, respectively. Camera numbers 19 and 20 were used on Test 3 only. In addition to the film coverage, pretest and post-test still photographs of the test setup and crash related damage were also obtained. All films have a timing code.

2.8 DATA REDUCTION

The histories of all accelerometer, load cell and position transducer responses are recorded on magnetic tape with a frequency capability of up to 1000 Hz.* The tapes are digitized and history plots obtained. The digitized data is filtered, using 100 and 300 Hz cutoff frequencies. Selected digitized

*Down 3 dB at 1000 Hz.

TABLE 2-11. LOAD CELL AND DISPLACEMENT MEASUREMENT INSTALLATIONS FOR TESTS 1, 2, 3, AND 4

Data Channel	Location	Peak Setting	Polarity	Tape and Channel			
				Test 1	Test 2	Test 3	Test 4
PS1	Pilot Shoulder Strap	+1150 (a)	+ Tension	D-6	D-6	D-9	D-9
CPS1	Copilot Shoulder Strap	+1150 (a)	+ Tension	D-7	D-7	D-10	D-10
PL1	Pilot Lap Belt	+1150 (a)	+ Tension	D-8	D-8	D-11	D-11
CPL1	Copilot Lap Belt	+1113 (a)	+ Tension	D-9	D-9	D-12	D-12
PCD1	Pilot Chest Deflection	+2.5 (b)	+ Tension	D-12	D-12	(c)	D-8
CLD1	Cabin Longitudinal Displacement	+3 (b)	+ Tension	D-10	D-10	(c)	(c)
CVD1	Cabin Vertical Displacement	+3 (b)	+ Tension	D-11	D-11	(c)	(c)
<p>(a) Force in Pounds</p> <p>(b) Deflection in Inches</p> <p>(c) Not Installed</p>							

NASA
L-77-1564



Figure 2-15. Location of Forward Onboard Camera

NASA
L-77-1570

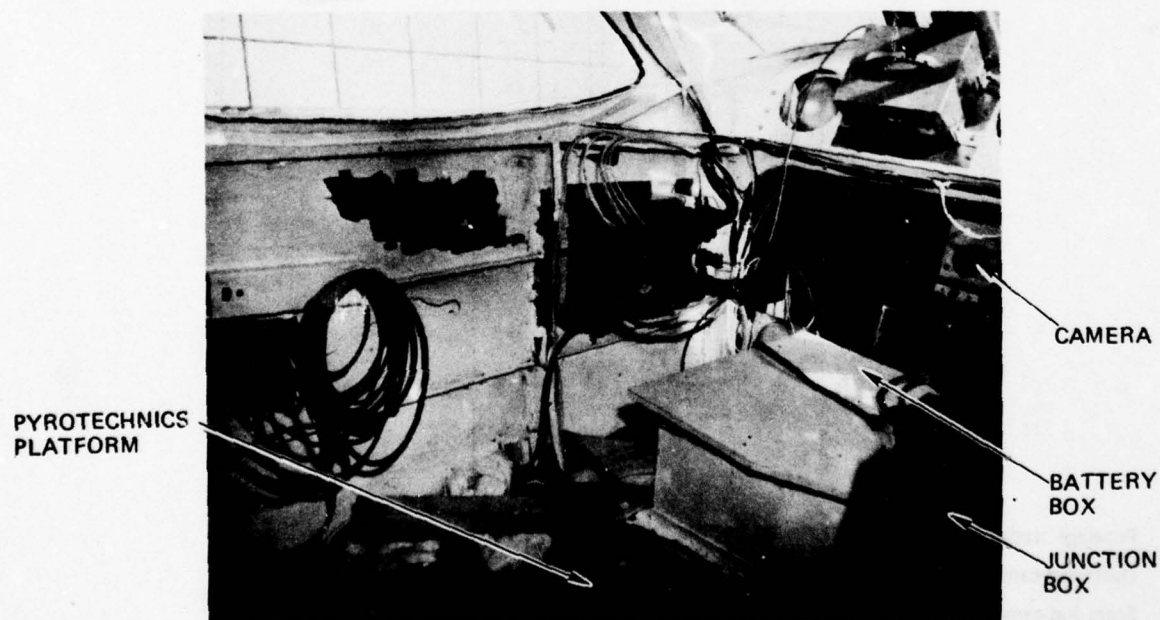


Figure 2-16. Location of Aft Onboard Camera, Battery Box, Junction Box and Pyrotechnic Timer

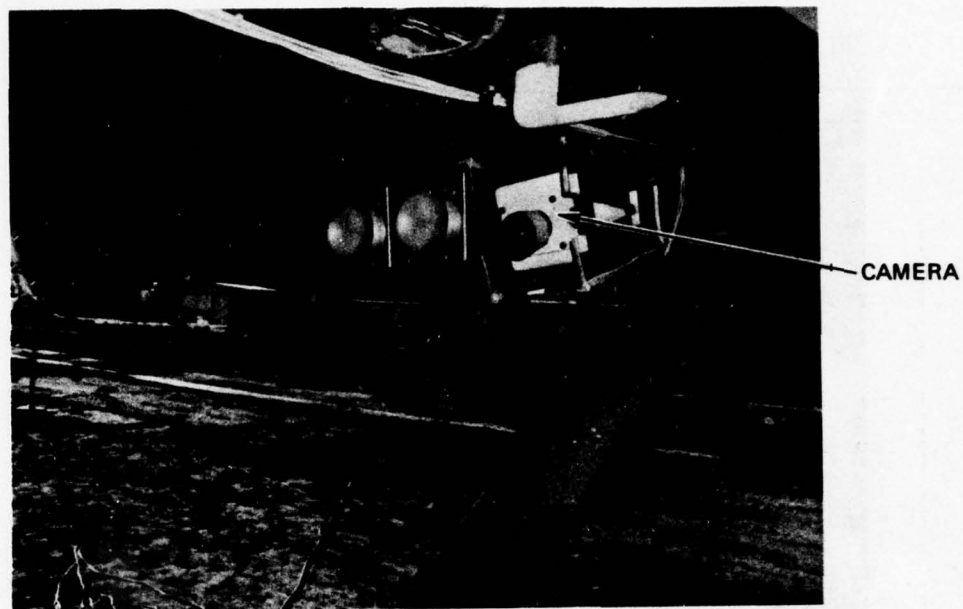


Figure 2-17. Location of Wing Mounted Camera

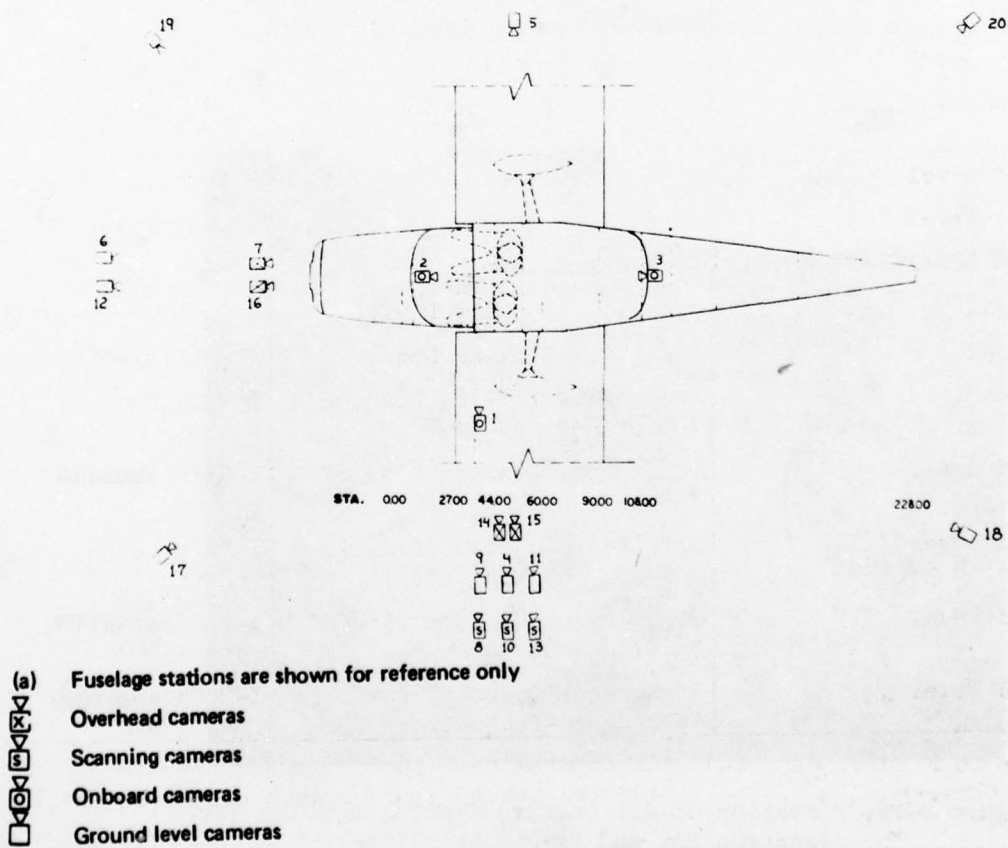


Figure 2-18. Photographic Coverage Layout
2-28

TABLE 2-12. CAMERA TYPE, LOCATION AND COVERAGE DATA^{(a)(d)}

No.	Location	Coverage	Lens
1.	Wing Mounted ^(b) F.S.35.0,W.L.11.0,LBL 75	Left Side View of Occupants, Seats and Cabin	10 mm
2.	Front Onboard ^(b) F.S.16.6,W.L.15.8,RBL 2.3	View Looking at Occupants from the Front	Fish-eye
3.	Rear Onboard ^(b) F.S.118,W.L.5.0,B.L. 0.0	View Looking at Occupants, Seats and Side Structure from the Rear	10 mm
4.	Ground Level	c.g. and General Data	2 Fuselage Lengths
5.	Ground Level	Right Side View of Forward Fuselage and Cabin	1 Fuselage Length
6.	Ground Level	Overall Front View of Fuselage Impact Region	1-1/2 Wing Spans
7.	Overhead	Front View Looking Down on Impact Region	1-2 Wing Spans
8.	Ground Level ^(c)	Documentary Scan of Crash Sequence	Zoom
9.	Ground Level ^(c)	Fixed Wide Angle	9 Fuselage Lengths
10.	Ground Level ^(e)	Scan of Crash for Sequence Photos	Zoom
11.	Ground Level	Large Field Side View	4 Fuselage Lengths
12.	Ground Level	Front View of Fuselage Impact	1 Wing Span
13.	Ground Level	High Speed Scan	Zoom
14.	Overhead	Side View Looking Down	4 Fuselage Lengths
15.	Overhead	Side View Looking Down	4 Fuselage Lengths
16.	Overhead	Front View Looking Down on Impact Region	1 Wing Span
17.	Ground Level	Left Front Quarter View of Fuselage and Cabin	1-2 Fuselage Lengths
18.	Ground Level	Left Rear Quarter of Cabin and Aft Section	1-2 Fuselage Lengths
19.	Ground Level	Right Front Quarter View of Fuselage and Cabin	1-2 Fuselage Lengths
20.	Ground Level	Right Rear Quarter View of Cabin and Aft Section	1-2 Fuselage Lengths
<p>(a) Refer to Figure 2-18. (d) All cameras have 16mm film and operate at 400 (b) 50-g Cameras pictures/second (pps) unless otherwise noted (c) 24 pps (e) 70mm, 20 pps</p>			

acceleration data are numerically integrated to obtain velocities. A sampling rate of 5000 samples per second is used in digitizing the data and the filter characteristics are such that the terminal frequency is twice that of the cutoff frequency.

No presampling filter of the analog data was required since the recording equipment electronically filters frequencies above 750 Hz*. The 300 Hz low-pass filtering expression for the number of weights (N_w) is:

$$N_w = \frac{4f_s}{f_r} - 1$$

where f_s = sampling rate (5000 samples/second)

$$f_r = f_t - f_c = 600 - 300 = 300 \text{ Hz}$$

$$N_w = 67.7 \text{ (67 or 69 is used)}$$

The 100 Hz low-pass filter characteristics are:

$$f_r = 200 - 100 = 100 \text{ Hz}$$

$$f_s = 500 \text{ Hz}$$

$$N_w = 201 \text{ Hz}$$

Appraisal of injury potential of a head impact, where appropriate, is described in Reference 4 which uses the Weighted Impulse Criterion (Gadd Severity Index). The Severity Index (SI) expression is:

$$SI = \int_0^t a^n dt$$

a = acceleration

n = 2.5

t = time

*Down 3 dB at 1000 Hz.

This application of the Weighted Impulse Criterion is directed only to the occupant head acceleration measurements.

In addition to the recorded test data analysis, the high speed film was reviewed and data pertinent to sequence of events, impact conditions, airplane post-crash behavior, structural failures and deformation has been evaluated and summarized.

SECTION 3
TEST RESULTS

3.1 CRASH TEST 1

3.1.1 Impact Conditions

The impact conditions for crash Test 1 as obtained from radar, high speed film analysis and a review of photographs are:

Velocities (mph)

along flight path	55.5
longitudinal	47.4
vertical	28.7

Angles (degrees)

flight path (γ)	-30.72
impact (θ)	-30.17
attack (α)	.55
roll (ϕ)	4.13
yaw (ψ)	-3.27

Rotational Velocities (degrees per second)

pitch ($\dot{\theta}$)	46.4
roll ($\dot{\phi}$)	negligible
yaw ($\dot{\psi}$)	negligible

where; γ is negative in dive,

$\theta, \dot{\theta}$ are positive nose up relative to ground

α is positive nose up relative to flight path

$\phi, \dot{\phi}$ are positive right wing down

$\psi, \dot{\psi}$ are positive tail left

and $\theta = \gamma + \alpha$

3.1.2 Crash Impact Sequence

The crash sequence for Test 1 is shown in Figure 3-1 at impact and every 30 milliseconds thereafter (up to 150 milliseconds). Analysis of

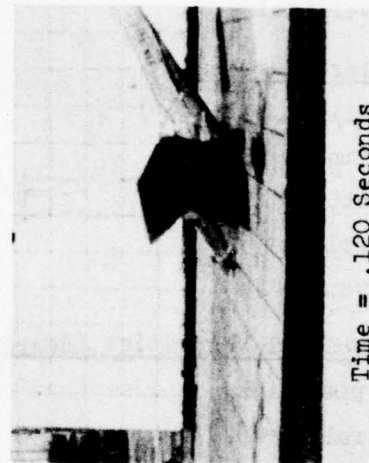
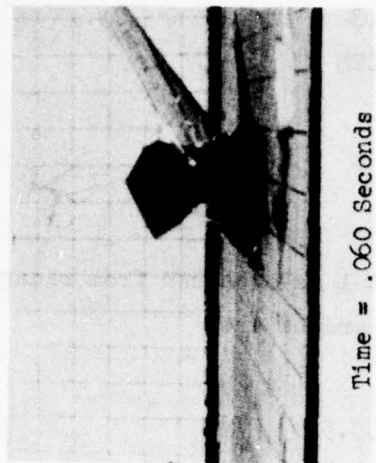
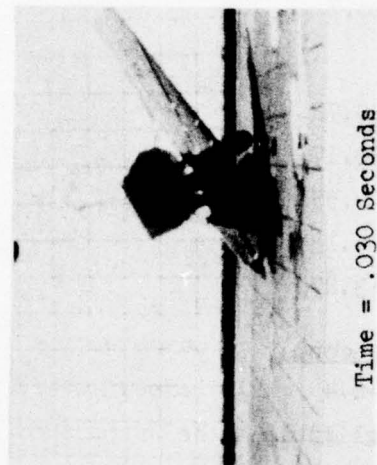
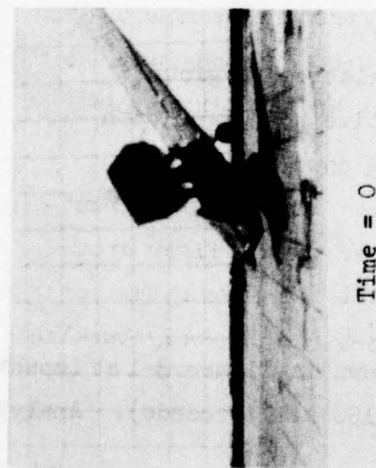


Figure 3-1. Crash Test 1, Impact Sequence

the high speed film provides the sequence of events following impact given in Table 3-1.

3.1.3 Structural Damage

A review of the post-test condition of the airplane, the high speed films and the post-test photographs showed that the airplane sustained substantial forward fuselage damage, loss of nose gear, failure of engine mounts, moderate cabin damage, extensive deformation of the floor near the occupant leg positions (F.S. 27) and at the landing gear bulkhead (F.S. 60), sheared front seat legs (pilot and copilot), and only minor damage to the wings (left wing torsion failure), the wing attachments to the fuselage, the aft cabin (F.S. 60-108) and the tail section. Table 3-2 presents a summary of the Test 1 damage.

Figures 3-2 through 3-13 depict the post-test condition of the airplane used in Test 1. Figures 3-2 and 3-3 show a front and left front-quarter view, respectively, of the airplane. Figures 3-4 and 3-5 illustrate the right side damage. The damage to the lower fuselage at the landing gear attach point can be seen in Figure 3-5 along with a close-up of the right side cabin region. The floor damage near the landing gear bulkhead is partially in view. Also, the rear seat legs which were pulled out of their tracks can be observed. Figures 3-6 and 3-7 are views of the airplane underside after the cowl was removed. Without the support of the ground, the engine tilts down on its buckled mounts. These two figures illustrate the degree of damage experienced by the engine mounts, the firewall, the nose gear, the lower fuselage structure, and the fuselage underside in the region of the cabin and as far back as the landing gear bulkhead.

Figures 3-8 and 3-9 illustrate the seat leg damage. The front legs of both the pilot and copilot seats separated above the floor attach fitting. Examination of failures indicated that the rivets that attach the fittings to the legs sheared. In Figure 3-8 the severely buckled floor

TABLE 3-1. CRASH TEST 1 SEQUENCE OF EVENTS

Event	Time in Seconds After Initial Impact
Nose Gear Tire Impact	0
Nose Gear Support Failure	.012
Engine Lower Structure Impact	.034
Engine Spinner Impact	.046
Lower Firewall Impact	.050
Right Main Gear Tire Impact	.060
Left Main Gear Tire Impact	.080
Right Main Gear Bulkhead Failure	.082
Pilot Seat Forward Leg Failure	.095
Maximum Left Main Landing Gear Tire Deflection	.100
Tail Cone Buckles	.108

TABLE 3-2. CRASH TEST 1 DAMAGE SUMMARY

Location	Type of Damage	Applicable Figures
Engine and Firewall	Engine mounts severely buckled. Firewall severely buckled.	3-6, 3-13
Forward Fuselage	Lower fuselage crushed several inches.	3-2, 3-6, 3-7
Cabin	Moderate deformation of lower structure from wing strut attachment (F.S. 27) to aft door bulkhead (F.S. 65).	3-2, 3-3, 3-4
	Floor buckled severely below pilot seat and at aft bulkhead. Minor damage (tears) to upper cabin structure.	3-8, 3-10, 3-11
Wings	Left wing torsion failure. No strut or attachment failures. No fuel tank rupture or fuel spillage.	3-12
Seats and Restraint System	Pilot and copilot front seat legs sheared. Pilot and copilot aft seat legs pulled loose from tracks. No seat belt or harness failure. No contact of structure by occupant.	3-8, 3-9
Tail Section	Slight buckle aft of rear baggage door (F.S. 108)	3-2
Nose Gear	Failed lower support structure in compression. Upper support structure pulled away from firewall. Nose gear and tire moved aft.	3-6, 3-7
Main Gear	Inboard bolt failure on right side. No apparent permanent deformation of landing gear.	3-4, 3-5, 3-6, 3-7

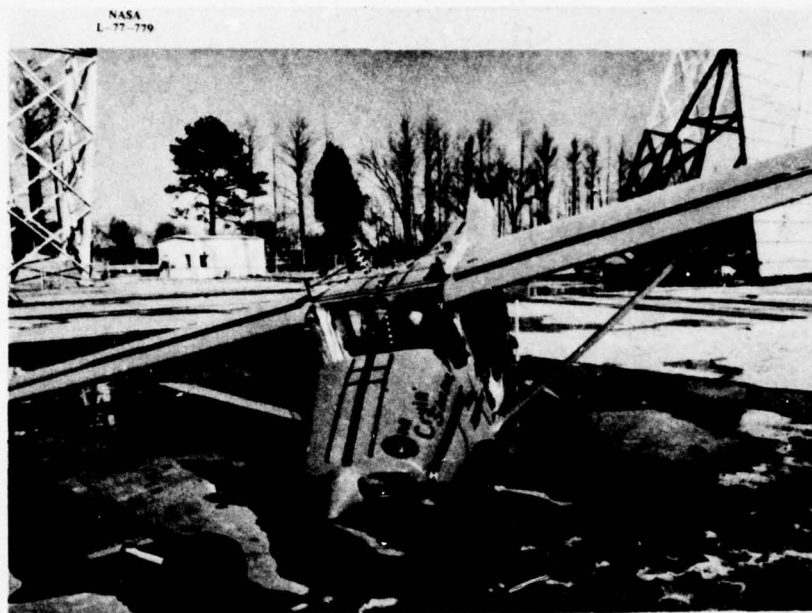


Figure 3-2. Crash Test 1, Post-Test Damage, Front View



Figure 3-3. Crash Test 1, Post-Test Damage, Left Front Quarter View

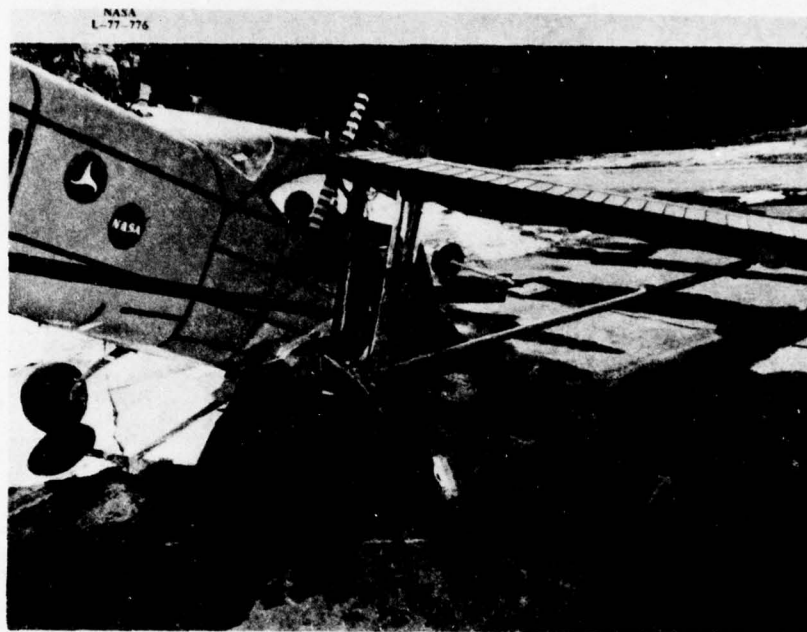


Figure 3-4 Crash Test 1, Post-Test Damage, Right Rear Quarter



Figure 3-5. Crash Test 1, Post-Test Damage, Seat and Lower Cabin Region

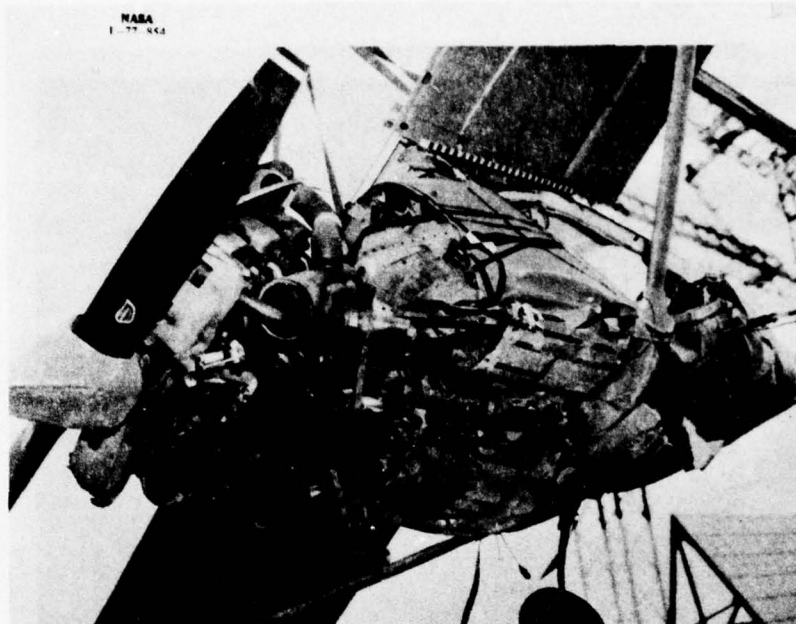


Figure 3-6. Crash Test 1, Post-Test Damage, Engine and Fuselage Underside Structure

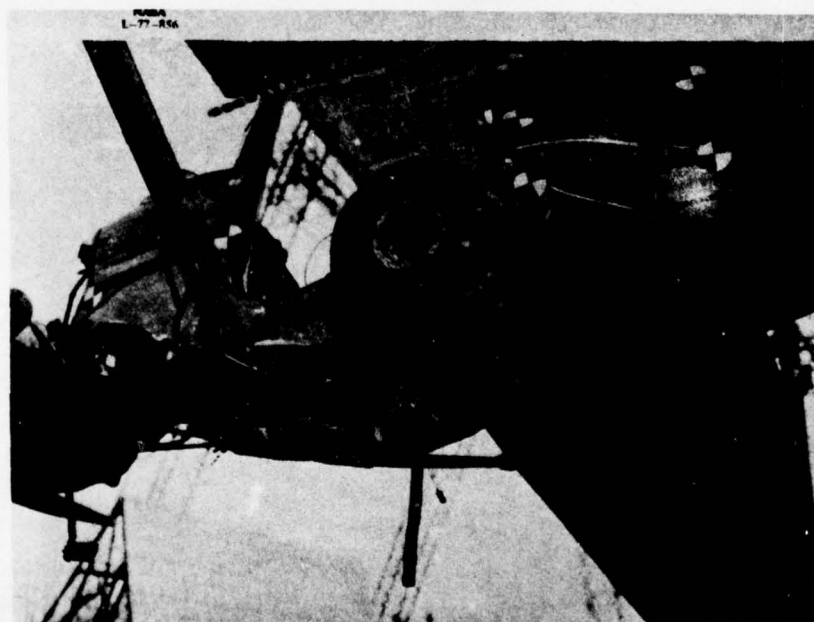


Figure 3-7. Crash Test 1, Post-Test Damage, Side View Showing Underside of Forward and Mid Cabin Region

NASA
1-77-871

Separated
Seat Leg

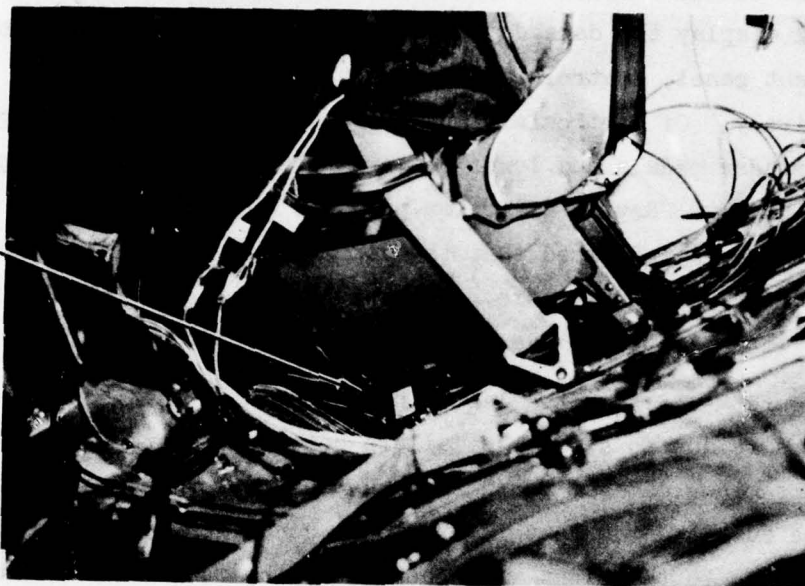


Figure 3-8. Crash Test 1, Post-Test Damage, Seats and Forward Floor Region

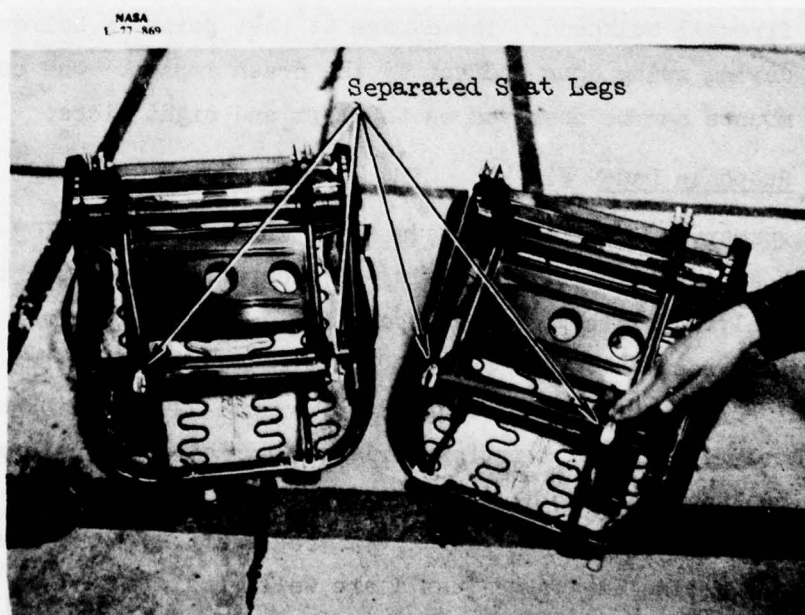


Figure 3-9. Crash Test 1, Post-Test Damage, Seat Leg Failures

structure at and forward of the front seat legs is evident. Figures 3-10 and 3-11 display the damage to the front interior, including the lower instrument panel, controls and floor in the pilot and copilot region, respectively. Of particular importance is the extent of damage to the floor, rudder pedals and lower center console because of the potential for leg injury. Review of motion pictures and examination of the instrument panel area indicated that the dummies, representing the pilot and copilot, did not contact the panels with a force sufficient to cause damage, if contact was made at all.

Figure 3-12 shows the left wing and strut attachment. The wrinkled structure is due to a torsion failure between the front and mid spar. Other than this minor damage, the wings and their attachments to the strut and fuselage survived the test in excellent condition. Although there was some minor damage to the right wing fuel tank, the tank's did not rupture and the fuel was retained.

Figure 3-13 shows a top view of the engine and its mounts after removal of the cowl. The pitch harness cable was attached at the top center of the firewall bulkhead. The damage at that point is believed to have been caused during swing down and not by the crash impact. The buckled top engine mounts can be observed on the left and right sides.

3.1.4 Response Data

A summary of Test 1 responses is given in Tables 3-3, 3-4 and 3-5 for the peak airplane, occupant pelvis and occupant head accelerations, respectively. Initial time of impact for each test is given in Appendix C. Table 3-3 presents 100 Hz. and 300 Hz. filtered data showing airplane peak load, direction and time of occurrence. Table 3-4 contains occupant pelvis peak accelerations and durations oriented normal to and along the occupant's backbone for 750 Hz., 300 Hz and 100 Hz frequencies. Similarly, Table 3-5 presents occupant head peak accelerations. The head peak accelerations experienced during Test 1 are well within tolerable levels

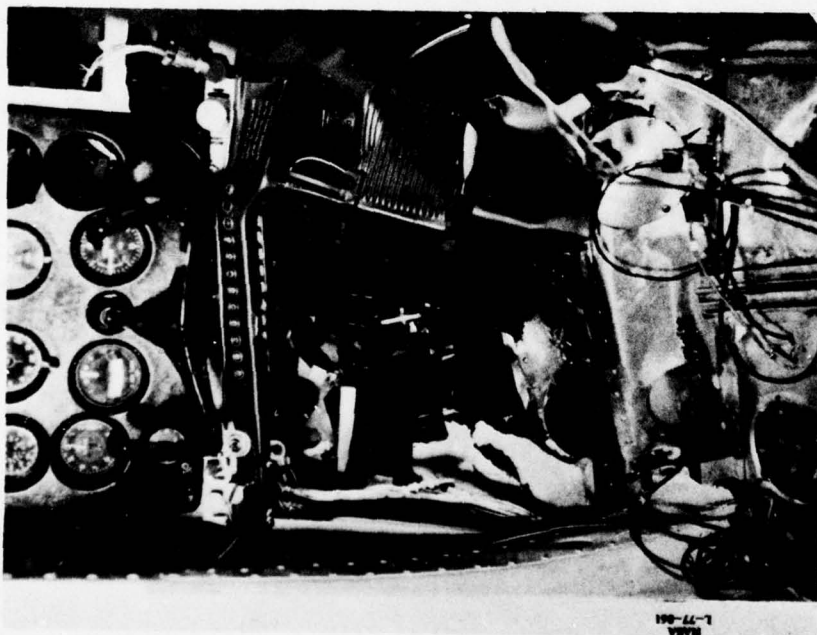


Figure 3-10. Crash Test 1, Post-Test Damage, Instrument Panel, Rudder Pedals and Floor Structure, Pilot Side

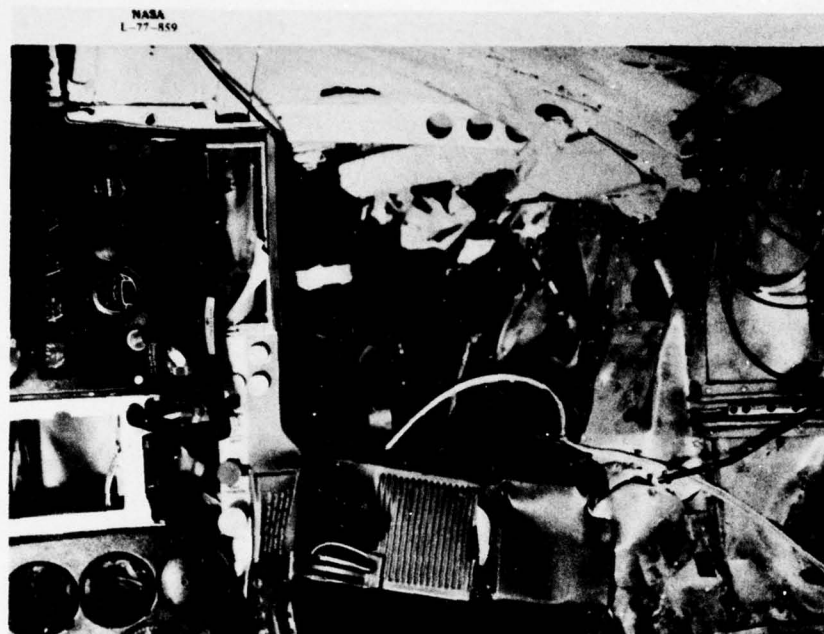
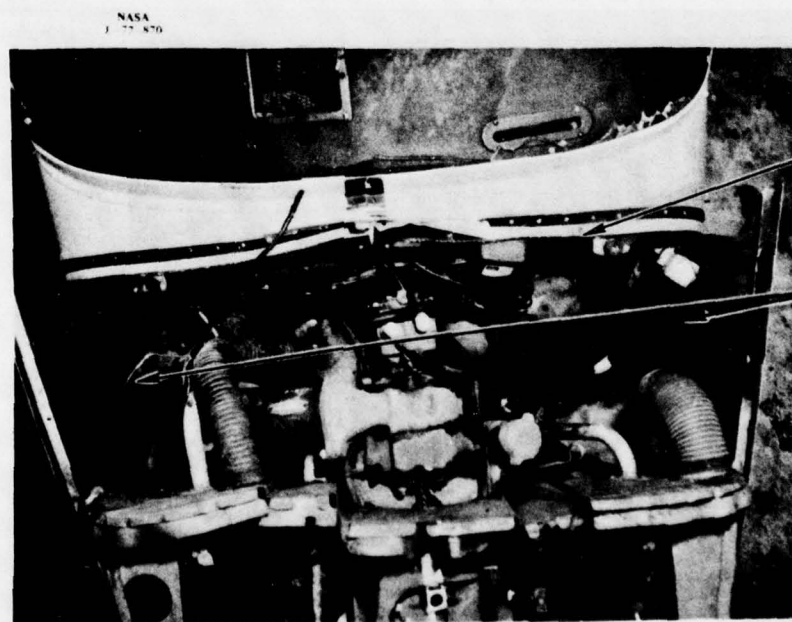


Figure 3-11. Crash Test 1, Post-Test Damage, Instrument Panel, Rudder Pedals and Floor Structure, Copilot Side



Figure 3-12. Crash Test 1, Post-Test Damage, Left Wing



Firewall

Upper
Engine
Mounts

Figure 3-13. Crash Test 1, Post-Test Damage, Top View of Engine, Engine Mount and Firewall

TABLE 3-3. SUMMARY OF CRASH TEST 1 PEAK AIRPLANE ACCELERATIONS

Location (a)		Direction	100 Hz. Data		300 Hz. Data	
			Peak g	Time (c)	Peak g	Time (c)
<u>Engine</u>						
BL 0.0	VEC1, C-1 ^(b)	Up	39	.055	40/58	.053/.064
		Down	26	.044	40	.093
	HEB2, C-2	Fwd	27	.075	30/35	.073/.093
		Aft	52	.058	60	.060
<u>Firewall Lwr.</u>						
LBL 14.0	VFC3, A-13	Up	130	.073	250	.073
		Down	140	.047	300	.048
	HFC4, B-1	Fwd	153	.042	300	.043
		Aft	96	.074	230	.072
<u>Cabin Floor Fwd. F.S. 27</u>						
LBL 13.5	VCC5, B-1	Up	46	.097	120	.097
		Down	25	.043	80/115	.041/.103
	HCC6, B-3	Fwd	15/21	.095/.111	100/140	.042/.118
		Aft	19/64	.041/.099	140/180	.040/.106
BL 0.0	VCC7, B-4	Up	80	.093	200	.083
		Down	110	.122	120	.122
	HCC8, B-5	Fwd	70	.103	240	.103
		Aft	153	.098	300	.098
RBL 13.5	VCC9, B-6	Up	79	.091	220	.091
		Down	23/15	.024/.088	60	.088
	HCC10, B-7	Fwd	70	.11	200	.088/.113
		Aft	90	.099	260	.090
<u>Cabin Floor Mid. F.S. 44</u>						
LBL 8.0	VCB17, D-4	Up	19/37	.081/.19	60/70	.083/.092
		Down	100/145	.088/.111	180/240	.086/.112
	HCB18, D-5	Fwd	150	.111	170	.111
		Aft	15	.045	100	.118
<u>Aft Cabin Floor F.S. 90</u>						
LBL 8.0	VCB7, C-7	Up	15/28	.050/.117	52/50	.085/.117
		Down	17/17	.045/.143	55/50	.086/.112
	HCB8, C-8	Fwd	42	.046	80	.046
		Aft	40/38	.041/.116	44/52	.042/.116
<u>Top Cabin, F.S. 65</u>						
RBL 15.0	VCB11, C-11	Up	25/70	.078/.105	50/130	.088/.105
		Down	13	.083	60	.09
	HCB12, C-12	Fwd	33	.105	70	.105
		Aft	13	.077	30	.085

TABLE 3-3. (Cont.)

Location (a)		Direction	100 Hz. Data		300 Hz. Data	
			Peak g	Time (c)	Peak g	Time (c)
<u>Cabin Floor, FS 108</u>						
LBL 14.0	VCB5, C-5 ^(b)	Up	31	.093	50	.080
		Down	47	.088	100	.088
	HCB6, C-6	Fwd	16/22	.105/.138	60	.085
		Aft	30	.093	80	.092
<u>Landing Gear Floor Region, F.S. 60</u>						
LBL 14.0	VCC11, B-8	Up	45	.115	45	.115
		Down	9	.102	10	.103
	HCC12, B-9	Fwd	17/14	.025/.045	17/14	.025/.045
		Aft	20/24	.078/.106	21/25	.078/.106
BL 0.0	VCC13, B-10	Up	34/37	.09/.111	34/36	.09/.111
		Down	6	.086	6	.086
	HCC14, B-11	Fwd	16/13	.026/.046	16/13	.026/.046
		Aft	27/29	.10/.112	27/30	.10/.112
RBL 14	VCC15, B-12	Up	34/50	.100/.112	34/50	.099/.112
		Down	17/12	.026/.046	18/12	.026/.046
	HCC16, B-13	Fwd	13	.079	24	.078
		Aft	58	.090	60	.091
<u>Wing</u>						
RBL 98.0	VWB13, C-13	Up	25/33	.088/.101	74	.086
		Down	28/13	.026/.078	38/36	.028/.076
	HWB14, D-1	Fwd	27	.092	100	.093
		Aft	11/10	.068/.126	60	.095
LBL 98.0	VWB15, D-2	Up	25	.108	44	.108/.115
		Down	20/10	.024/.082	37	.086
	HWB16, D-3	Fwd	6/8	.099/.118	36/42	.093/.123
		Aft	9	.083	30/35	.086/.123
<u>Tail Mass</u>						
BL 0.0	VTB3, C-3	Up	11	.086	12	.085
		Down	7	.058	8	.058
	HTB4, C-4	Fwd	22/26	.075/.116	25/25	.073/.116
		Aft	40	.068	40	.068
<u>Top Cabin, FS 32</u>						
RBL 21.0	VCB9, C-9	Up	75	.105	90	.103
		Down	80	.093	150	.094
	HCB10, C-10	Fwd	35	.100	87	.101
		Aft	34	.105	60	.105

(a) LBL, RBL denote left and right butt line, respectively. F.S. denotes fuselage station.

(b) Accelerometer number, Tape and channel number, respectively.

(c) Time in seconds after impact.

TABLE 3-4. CRASH TEST 1 OCCUPANT PELVIS PEAK ACCELERATIONS AND PULSE DURATIONS

Location	Up Direction		Down Direction		Forward Direction		Aft Direction	
	Peak g at Time	Avg. g, Duration	Peak g at Time	Avg. g, Duration	Peak g at Time	Avg. g, Duration	Peak g at Time	Avg. g, Duration
Pilot Pelvis (A-2, A-8)(a)								
100 Hz	64 @.124	40 .0075 20 .015	2 @.094	-	23 @.092	20 .003 10 .030	12 @.086	10 .015
300 Hz	66 @.124	60 .002 20 .012	5 @.088	-	31 @.092	30 .003 20 .004	13 @.11	10 .015
750 Hz	78 @.124	60 .002 50 .005	25 @.078	-	80 @.093	-	@.078	-
Copilot Pelvis (A-6, A-9)(a)								
100 Hz	50 @.119	45 .008 30 .020	4 @.067	-	17 @.100	15 .002	13 @.094	12 .015
300 Hz	56 @.126	50 .005 40 .015 30 .035	5 @.067	-	23 @.100	20 .002	16 @.095	8 .015
750 Hz	66 @.126	50 .005 .059	5 @.067	-	35 @.100	15 .004	20 @.094	-
(a) Tape and channel numbers for vertical and longitudinal responses, respectively. Times and durations are in seconds.								

TABLE 3-5. CRASH TEST 1 OCCUPANT HEAD PEAK ACCELERATIONS

Location	Up Direction		Down Direction		Forward Direction		Aft Direction	
	Peak g at Time	Avg. g, Duration	Peak g at Time	Avg. g, Duration	Peak g at Time	Avg. g, Duration	Peak g at Time	Avg. g, Duration
Pilot Head (A-3, A-4)(a)								
100 Hz	10 @.098	5, .008	10 @.123 37 @.144	5, .008	5 @.135	-	38 @.141	10, .013
300 Hz	10 @.098 20 @.141	5, .008	10 @.123 75 @.143	-	5 @.135	-	18 @.124 56 @.141	10, .012
750 Hz	56 @.141	-	12 @.123 100 @.143	-	5 @.130	-	30 @.124 80 @.141	-
Copilot Head (A-7, A-1)(a)								
100 Hz	30 @.118	20, .008	60 @.143	-	-	-	20 @.138	10, .077
300 Hz	48 @.118	20, .008	4 @.085 60 @.143	-	-	-	20 @.143	10, .007
750 Hz	48 @.11	-	10 @.085 62 @.143	-	-	-	20 @.143	-

(a) Tape and channel numbers for vertical and longitudinal responses, respectively.
Times and durations are in seconds.

(Reference 4) for impact situations, thus further confirming that the occupants' heads most likely did not impact the structure.

The tolerable occupant pelvis responses in four directions relative to the spine are given in Table 3-6. A comparison of the test results in Table 3-4 with the data contained in Table 3-6 indicates that the acceleration levels experienced by the dummies during Test 1 were not of a severity to cause serious injury. However, the damage to the lower forward fuselage structure most likely would have caused severe leg injuries.

TABLE 3-6. TOLERANCE ACCELERATION LEVELS FOR OCCUPANTS (REFERENCE 5)

Direction	Voluntary Exposure		Severe Injury		
	Peak g	τ	Peak g	Duration sec	Peak g @ $\tau = .004$ sec
Forward	35	.1	55/40	.02/.1	90
Aft	45	.04	75/44	.02/.1	160
Up	16	.04	42	.007-.050	80
Down	10	.01	50	.02 -.160	70
τ = Duration in Seconds					

Typical data histories from Test 1, including filter accelerations and restraint system loads, are presented in Appendix C.

3.2 CRASH TEST 2

3.2.1 Impact Conditions

The impact conditions for Test 2 as obtained from radar, high speed film analysis and a review of photographs are:

Velocities (mph)

along flight path	50.8
longitudinal	48.6
vertical	14.8

Angles (degrees)

flight path (γ)	-17.0
impact (θ)	+13.5

attack (α)	+30.5
roll (ϕ)	+ 3.25
yaw (ψ)	-11.25

Rotational Velocities (degrees per second)

pitch ($\dot{\theta}$)	6.9
roll ($\dot{\phi}$)	negligible
yaw ($\dot{\psi}$)	negligible

The nomenclature and definition of positive directions are the same as noted in section 3.1.1.

3.2.2 Crash Impact Sequence

The crash sequence for Test 2 is shown in Figure 3-14 at impact and every 50 milliseconds thereafter (up to 250 milliseconds). Analysis of the high speed film provides the sequence of events following impact given in Table 3-7.

3.2.3 Structural Damage

A review of the post-test condition of the airplane, the high speed films and the post-test photographs showed that the airplane sustained damage to the aft tail section (F.S. 205-F.S. 228), failure of the nose gear lower support structure (nose gear pulled forward), slight structural

TABLE 3-7. CRASH TEST 2 SEQUENCE OF EVENTS

Event	Time In Seconds After Initial Impact
Right Main Gear Tire Impact	0
Left Main Gear Tire Impact	.023
Tail Impact	.033
Nose Gear Tire Impact	.046
Tail Lifts off Ground	.125
Maximum Left Main Gear Deflection	.150

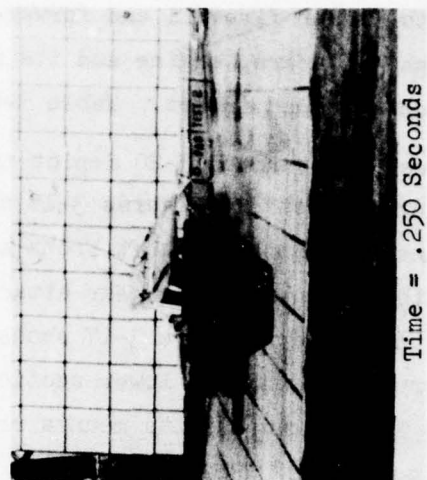
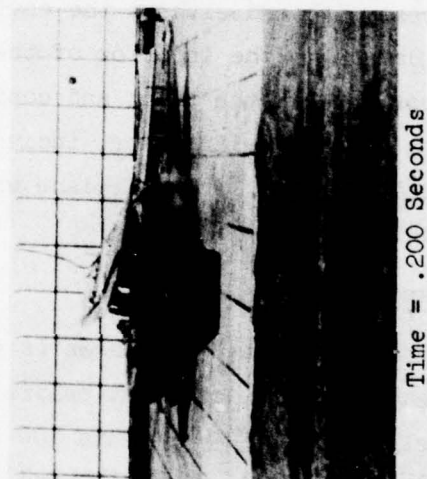
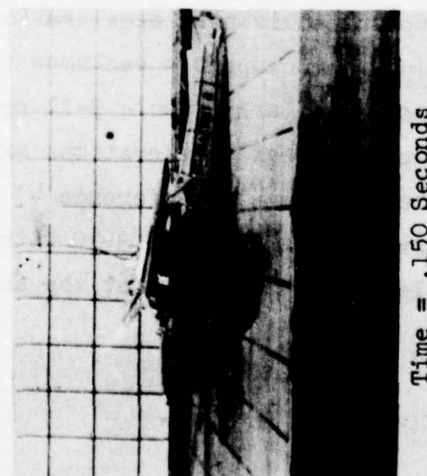
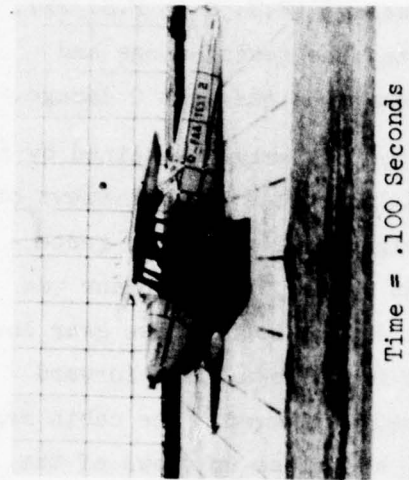
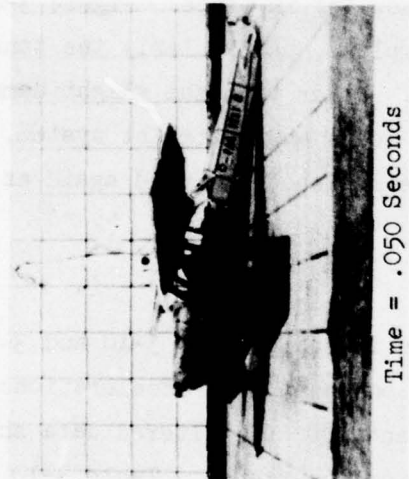
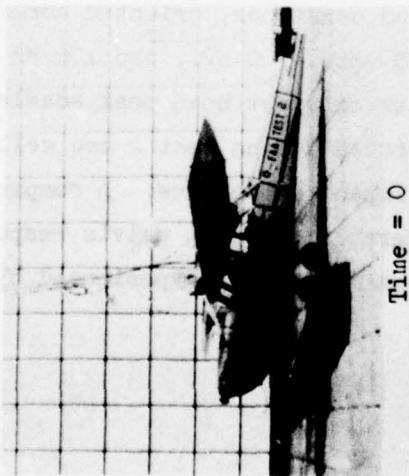


Figure 3-14. Crash Test 2, Impact Sequence

damage to the lower firewall and forward fuselage (F.S. 0 to F.S. 27). The main landing gears, engine and its mounts, the seats, wings and cabin region remained intact. Table 3-8 summarizes the Test 2 damage.

Figures 3-15 through 3-20 depict the type of damage sustained by the airplane during Test 2. Figures 3-15 and 3-16 provide general views of the airplane from both the left front and right rear quarters, respectively. Other than the nose gear attachment region, the airplane was virtually undamaged. Figure 3-17 shows the damage to the nose gear lower support structure, and the lower section of the firewall and forward fuselage. The engine and its mounts remained undamaged. The cabin region sustained no damage. Figures 3-18 and 3-19 are close-up views of the damaged areas with and without the engine cowling in place. Figure 3-20 shows the damage to the interior of the airplane, particularly the tunnel at the floor between the pilot and copilot. Other than the slight damage to the area shown, the interior, including seats and restraint system, is in good condition. This airplane was refurbished and used again as the vehicle for Test 4.

3.2.4 Response Data

A summary of Test 2 responses is given in Tables 3-9, 3-10 and 3-11 for the peak airplane, occupant pelvis and occupant head accelerations, respectively. Table 3-9 presents 100 Hz. and 300 Hz. filtered data showing airplane peak load, direction and time of occurrence. Table 3-10 contains occupant pelvis peak accelerations and durations, oriented normal to and along the occupant's backbone for 750 Hz., 300 Hz., and 100 Hz frequencies. Similarly, Table 3-11 presents occupant head peak accelerations. The head peak accelerations experienced during Test 2 are well within tolerable levels (Reference 4) for impact situations. A comparison of the test results in Table 3-10 with tolerable occupant pelvis response data (Table 3-6) indicates that the acceleration levels experienced by the

TABLE 3-8. CRASH TEST 2 DAMAGE SUMMARY

Location	Type of Damage	Applicable Figures
Engine and Firewall	Firewall buckled in lower region	3-17, 3-19
Forward Fuselage	Slight damage to underside structure aft of firewall	3-18
Cabin	No structural damage	3-15, 3-16, 3-20.
Wings	No structural damage No fuel spillage	3-15, 3-16
Seat and Restraint System	Seat and restraint system remain undamaged	3-15, 3-16
Tailcone	Buckled structure between F.S. 205-228 sustained during tail impact	3-15, 3-16
Nose Gear	Failed lower support structure in tension. Nose gear and tire moved forward.	3-17, 3-18, 3-19.
Main Gears	No damage	3-15, 3-16

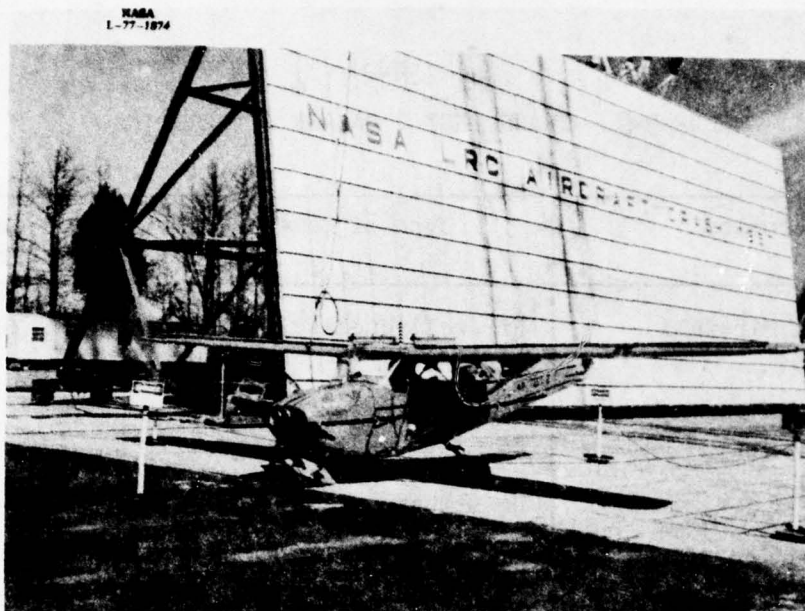


Figure 3-15. Crash Test 2, Post-Test Damage, Left Front Quarter View



Figure 3-16. Crash Test 2, Post-Test Damage, Right Rear Quarter View

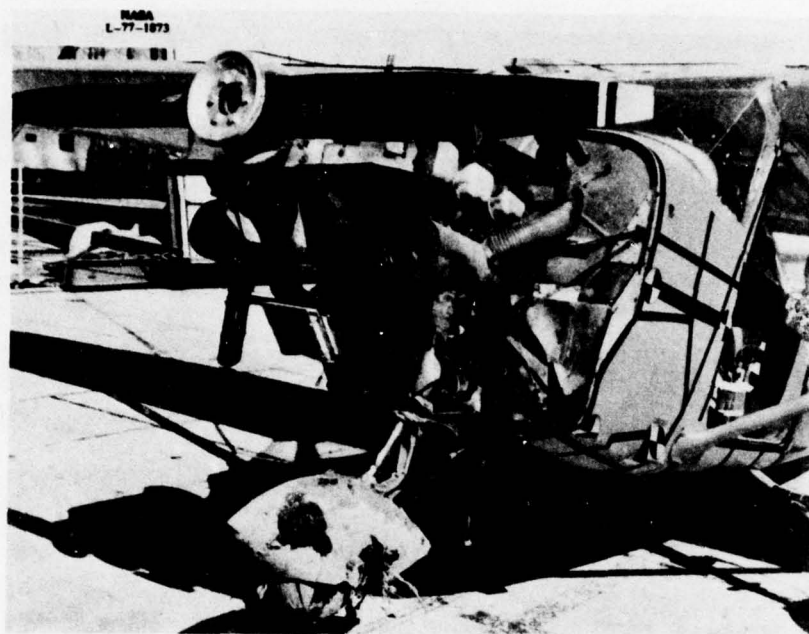


Figure 3-17. Crash Test 2, Post-Test Damage, Front View
(Cowl Removed)

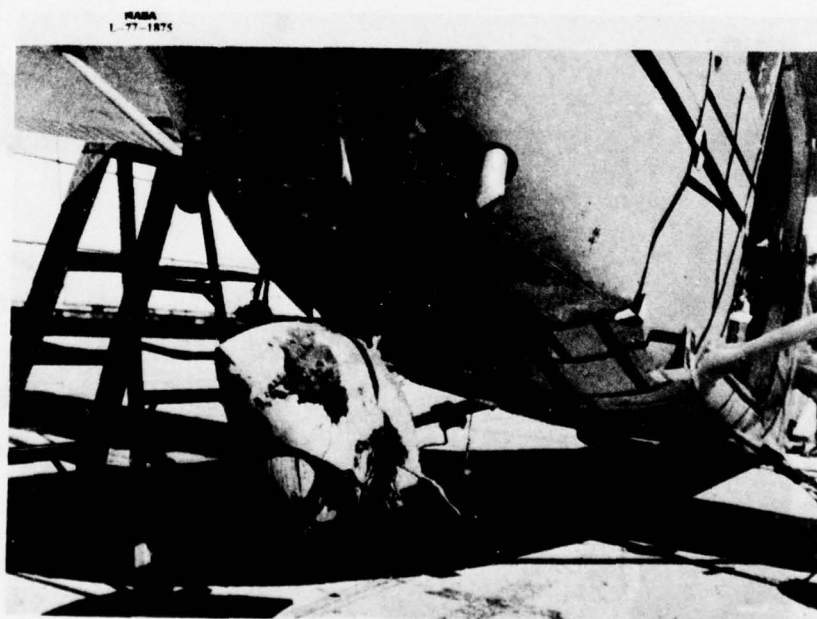


Figure 3-18. Crash Test 2, Post-Test Damage, Nose Gear and
Lower Fuselage



Figure 3-19. Crash Test 2, Post-Test Damage, Nose Gear Lower Support Failure

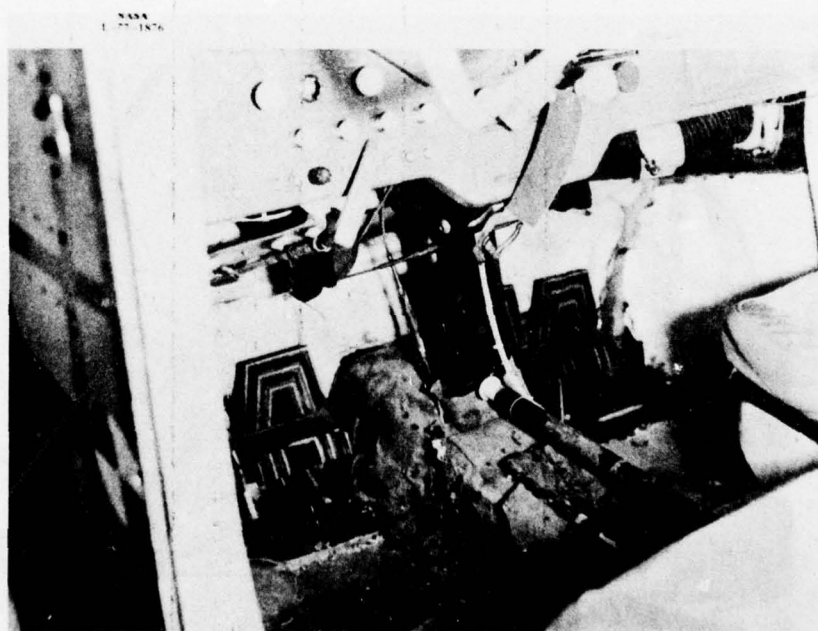


Figure 3-20. Crash Test 2, Post-Test Damage, Forward Fuselage Floor and Tunnel

TABLE 3-9. SUMMARY OF CRASH TEST 2 PEAK AIRPLANE ACCELERATIONS

Location ^(a)	Direction	100 Hz. Data		300 Hz. Data	
		Peak g	Time ^(c)	Peak g	Time ^(c)
Engine					
VEC1, C-1 ^(b)	Up	9	.085	9	.064
	Down	5	.135	5	.113
BL					
O.O HEB2, C-2	Fwd	6	.085	6	.065
	Aft	9	.135	10	.115
Firewall Lwr.					
VFC3, A-13	Up	56	.087	88	.088
	Down	68	.092	110	.092
LBL					
14.0 HFC4, B-1	Fwd	20	.08	60/40	.055/.080
	Aft	13	.06	30	.068/.086
Cabin Floor Fwd. F.S. 27					
VCC5, B-2	Up	16/14	.095/.06	25/16	.05/.095
	Down	5	.088	8	.054/.086
LBL					
13.5 HCC6, B-3	Fwd	7	.063	17	.073
	Aft	7	.114	16	.03
VCC7, B-1	Up	15	.05	36	.05
	Down	6	.055	14	.054
BL					
O.O HCC8, B-5	Fwd	6	.048	25	.114
	Aft	4	.06/.09	25	.117
VCC9, B-6	Up	14	.05	35	.05
	Down	8	.055	20	.054
RBL					
13.5 HCC10, B-7	Fwd	6	.010	32/7	.048/.010
	Aft	7	.022	30/11	.05/.024
Cabin Floor Mid. F.S. 44					
VCB17, D-4	Up	6	.02/.06	17/16	.02/.052
	Down	5	.055	17/15	.036/.05
LBL					
8.0 HCB18, D-5	Fwd	11	.055	26/16	.034/.055
	Aft	24	.05	44	.05
Aft Cabin Floor F.S. 90					
VCB7, C-7	Up	36	.058	46	.058/.072
	Down	31	.064	60	.07
LBL					
8.0 HCB8, C-8	Fwd	10	.036	26/28	.034/.08
	Aft	10	.031	28/25	.032/.07
Top Cabin, F.S. 65					
VCB11, C-11	Up	24	.048	24	.03/.04/.065
	Down	14	.060	17	.06
RBL					
15.0 HCB12, C-12	Fwd	10	.034	15	.034
	Aft	6	.063	13/8	.038/.113

TABLE 3-9. (Cont.)

Location (a)	Direction	100 Hz. Data		300 Hz. Data	
		Peak g	Time (c)	Peak g	Time (c)
Cabin Floor, F.S. 108					
VCB5, C-5 ^(b)	Up	25	.028	30	.028
LBL	Down	26	.068	33	.068
14.0					
HCB6, C-6	Fwd	25	.128	30	.118/.122
	Aft	70	.122	100	.122
Landing Gear Floor Region, F.S. 60					
VCC11, B-8	Up	30	.052	40	.032/.052/.07
LBL	Down	8	.066	20/16	.034/.067
14.0					
HCC12, B-9 ^(d)	Fwd	-	-	-	-
	Aft	-	-	-	-
VCC13, B-10	Up	22	.052	33	.052
BL	Down	10	.058	21/15	.035/.06
0.0					
HCC14, B-11	Fwd	6	.057	18	.027
	Aft	6	.022/.03/.064	24/22/19	.022/.025/.03
VCC15, B-12	Up	21	.064	27	.064
RBL	Down	20	.058	30	.012/.060
14.0					
HCC16, B-13	Fwd	-	-	18	.067
	Aft	8	.02/.052	20	.060
Wing					
VWB13, C-13	Up	12	.050	16/15	.082/.05
RBL	Down	8	.140	12/15	.08/.13
98.0					
HWB14, D-1	Fwd	6/4	.025/.09	10	.055
	Aft	7	.075	16	.065
VWB15, D-2	Up	14	.070	21	.062
LBL	Down	6	.080	32	.068
98.0					
HWB16, D-3	Fwd	6/3	.036/.15	17	.05
	Aft	5	.08	17	.072
Tail Mass					
VTB3, C-3	Up	180	.022	190	.022
BL	Down	50	.035	50	.035
0.0					
HTB4, C-4	Fwd	105	.025	160	.025
	Aft	30	.053	45/40	.022/.055
Top Cabin, F.S. 32					
VCB9, C-9	Up	14	.065	26	.054
RBL	Down	13	.060	28	.052
21.0					
HCB10, C-10	Fwd	10	.045	13	.056
	Aft	6	.075	9	.065
(a) LBL, RBL denote left and right butt line, respectively. F.S. denotes fuselage station.					
(b) Accelerometer number, tape and channel number, respectively.					
(c) Time in seconds after impact.					
(d) Data not available.					

TABLE 3-10. CRASH TEST 2 OCCUPANT PELVIS PEAK ACCELERATIONS AND PULSE DURATIONS

Location	Up Direction		Down Direction		Forward Direction		Aft Direction	
	Peak g at Time	Avg g, Duration	Peak g at Time	Avg g, Duration	Peak g at Time	Avg g, Duration	Peak g at Time	Avg g, Duration
Pilot Pelvis (A-2,A-8)								
100 Hz	10 @ .09	10, .008 6, .038	-	-	8.5 @ .11	8, .010	-	-
300 Hz	11 @ .09	10, .008 6, .038	-	-	9 @ .108	8, .010	-	-
750 Hz	11 @ .09	-	-	-	10 @ .06 10 @ .11	-	-	-
Copilot Pelvis (A-6,A-9)								
100 Hz	12.5 @ .11	10, .005 7.5, .037	1.5 @ .165	-	3.5 @ .150	3, .020	-	-
300 Hz	15 @ .11	8, .020	3 @ .165	-	3.5 @ .150	3, .015	-	-
750 Hz	18 @ .11	-	-	-	4 @ .150	-	-	-
(a) Tape and channel numbers for vertical and longitudinal responses, respectively. Times and durations are in seconds.								

TABLE 3-11. CRASH TEST 2 OCCUPANT HEAD PEAK ACCELERATIONS AND DURATIONS

Location	Up Direction		Down Direction		Forward Direction		Aft Direction	
	Peak g at Time	Avg g, Duration	Peak g at Time	Avg g, Duration	Peak g at Time	Avg g, Duration	Peak g at Time	Avg g, Duration
Pilot Head (A-3,A-4) (a)								
100 Hz	12 @ .09 12 @ .11	10, .030 5, .060	-	-	-	-	3.3 @ .155	3, .018
300 Hz	12.5 @ .090	11, .025 5, .060	-	-	-	-	3.5 @ .152	3, .015
750 Hz	12.5 @ .10	-	-	-	-	-	4 @ .15	-
Copilot Head (A-7,A-1) (a)								
100 Hz	22 @ .167	20, .004 16, .012 8, .018	-	-	11.5 @ .105	10, .015 6, .055	-	-
300 Hz	25 @ .166	20, .004 15, .015 5, .022	-	-	12.5 @ .112	10, .020 5, .067	-	-
750 Hz	25 @ .165	-	-	-	18 @ .108 28 @ .176	-	20 @ .177	-
(a) Tape and channel numbers for vertical and longitudinal responses, respectively. Times and durations are in seconds.								

dummies during Test 2 were not sufficiently severe to cause serious injury. Based on the minor damage sustained by the airplane during Test 2, the lack of occupant injury is realistic.

Typical data histories from Test 2, including filtered accelerations and restraint system loads, are presented in Appendix C.

3.3 CRASH TEST 3

3.3.1 Impact Conditions

The impact conditions for Test 3 as obtained from film analysis and a review of photographs are:

Velocities (mph)

along flight path	58.1 mph
longitudinal	47.6 mph
vertical	33.2 mph

Angles (degrees)

flight path (γ)	-34.86
impact (θ)	-39.4
attack (α)	-4.54
roll (ϕ)	18.75
yaw (ψ)	-7.9

Rotational Velocities (degrees per second)

pitch ($\dot{\theta}$)	14.3
roll ($\dot{\phi}$)	negligible
yaw ($\dot{\psi}$)	negligible

The nomenclature and definition of positive directions are the same as noted in Section 3.1.1

3.3.2 Crash Impact Sequence

The crash sequence for Test 3 is shown in Figure 3-21 at impact and every 50 milliseconds thereafter (up to 250 milliseconds). Analysis of the high speed film provides the sequence of events following impact given in Table 3-12.

TABLE 3-12. CRASH TEST 3 SEQUENCE OF EVENTS

Event	Time in Seconds After Initial Impact
Nose Gear Tire Impact	0
Nose Gear Support Failure	.012
Engine Lower Structure Impact	.024
Propellor Impact	.032
Right Wing Impact	.038
Lower Firewall and Forward Fuselage Impact	.048
Right Main Gear Tire Impact	.062
Tail Cone Failure	.075
Left Wing Strut Column Failure	.085
Copilot Seat Aft Leg Departs Rail	.090
Pilot Head Impact with Instrument Panel	.092
Copilot Head Impact with Instrument Panel	.121
Left Main Gear Tire Impact	.135
Peak Right Main Gear Deflection	.150
Left Wing Rear Spar Failure	.160

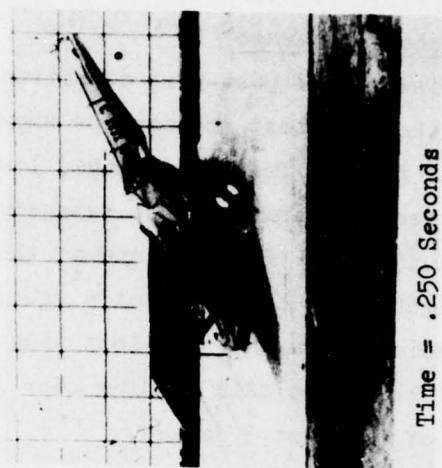
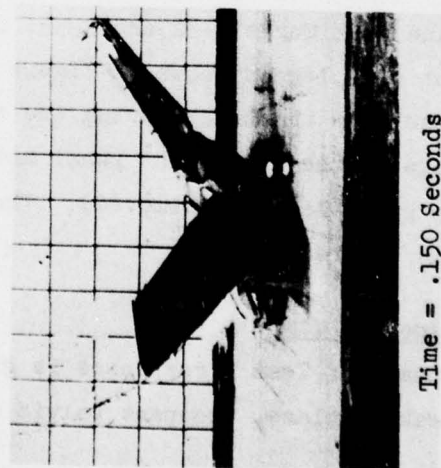
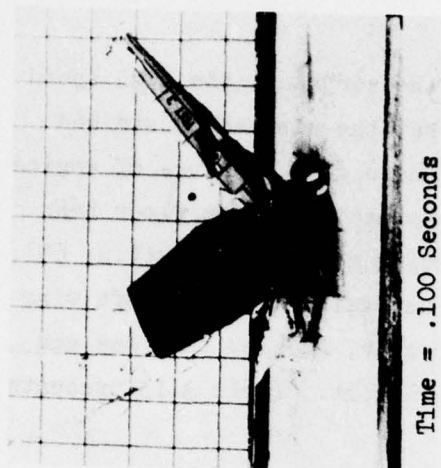
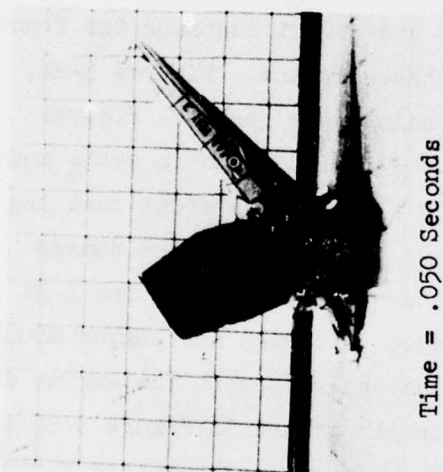
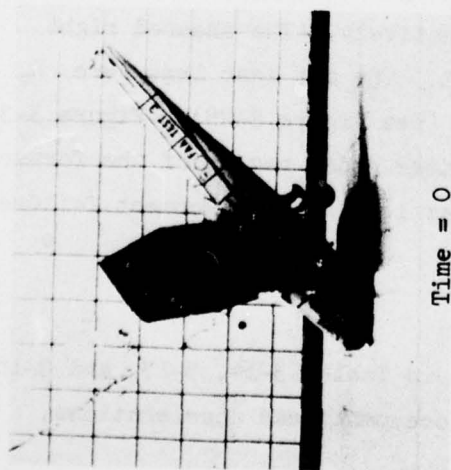


Figure 3-21. Crash Test 3, Impact Sequence

3.3.3 Structural Damage

A review of the post-test condition of the airplane, the high speed films and the post-test photographs showed that the airplane sustained substantial forward fuselage damage, loss of nose gear, failure of engine mounts, extensive cabin damage, extensive deformation of the floor near the occupant's legs (F.S. 27) and at the landing gear bulkhead (F.S. 60), sheared right front leg of pilot's seat, column failure of the left wing strut, tension failure of the left wing rear spar, buckled tailcone and failure of the right main landing gear inboard bolt. Table 3-13 presents a summary of the Test 3 damage.

Figures 3-22 through 3-35 depict the post-crash test condition of the airplane used in Test 3. Figures 3-22, 3-23 and 3-24 illustrate the front, left and right side views, respectively, of the airplane. Figures 3-25, 3-26 and 3-27 show the damage in the main landing gear region. Figures 3-28 and 3-29 depict the condition of the copilot's and pilot's seats and restraint systems, respectively. The buckled floor at the front seat leg can be seen in Figure 3-28. Figure 3-29 shows the extent of the damage to the left front door and upper cabin structure. Figures 3-30 and 3-31 display the engine and forward fuselage damage. Although the engine mounts were buckled sufficient residual strength remained such that the engine did not separate from the airplane. The fluid on the ground in Figure 3-31 is residual oil that leaked from the engine. No fuel spillage or tank rupture was experienced in the test. The copilot and pilot seats were removed from the airplane in Figures 3-32 and 3-33, respectively. The sheared right front pilot seat leg is shown in Figure 3-33. The aft seat legs were pulled loose from the track during the test (see Figure 3-28). Figure 3-34 shows damage to the instrument panel and rudder pedal region of the forward cabin (the pilot has been removed). The rear left spar attachment failure is shown in Figure 3-35.

3.3.4 Response Data

A summary of Test 3 responses is given in Tables 3-14, 3-15, and 3-16 for the peak airplane, occupant pelvis and occupant head accelerations,

TABLE 3-13. CRASH TEST 3 DAMAGE SUMMARY

Location	Type of Damage	Applicable Figures
Engine and Firewall	Engine mounts severely buckled. Engine shoved back into firewall.	3-30, 3-31
Forward Fuselage	Lower fuselage crushed.	3-22, 3-23, 3-24
Cabin	Left front door post buckled forward at midpoint. Right front door post buckled forward and outboard.	3-28, 3-29
	Floor at base of instrument panel severely buckled.	3-34
Wings	Left wing strut column failure. Left wing rear spar tension failure. Right wing failed approximately 40 inches inboard of tip. Right wing fuel tank lower skin buckled. No fuel tank rupture or leakage.	3-35
Seats and Restraint system	Copilot seat pulled loose from floor. Pilot right front seat leg failed. No seat belt or harness failure. Impact by pilot and copilot heads on instrument panel.	3-28, 3-29 3-32, 3-33
Tail Section	Buckled approximately 12 inches aft of rear baggage door (F.S. 108).	3-22, 3-23, 3-24
Nose Gear	Failed aft (similar to Test 1).	3-25, 3-26
Main Gear	Inboard bolt failure on right side. Right wheel displaced aft approximately 12 inches as a result of bulkhead failure.	3-25, 3-26, 3-27

TABLE 3-14. SUMMARY OF CRASH TEST 3 PEAK AIRPLANE ACCELERATIONS

Location (a)	Direction	100 Hz. Data		300 Hz. Data	
		Peak g	Time (c)	Peak g	Time (c)
<u>Engine</u>					
VECL, C-1 (b)	Down	20	.046, .067	40	.046
	Up	80	.041	112	.041
BL 0.0	Fwd	40	.045-.060	120	.048
	Aft	200	.040	260	.040
LEB3, C-3	Right	45	.040	70	.041
	Left	16	.052	35/38	.046/.053
<u>Firewall Lwr.</u>					
VFC1, A-11	Down	60	.032	200	.034, .045
	Up	100	.062, .113	200	.025, .048, .062
LBL 14.	Fwd	125	.118	200	.030-.040
	Aft	200	.110	620	.072
<u>Cabin Floor Fwd. FS 27</u>					
VCC3, A-13	Down	45	.112	65	.051
	Up	76	.088	100	.090
RBL 13.5	Fwd	120	.105	180	.105
	Aft	110/160	.097/.111	400	.111
HCC4, B-1	Right	33/20	.088/.098	100	.097
	Left	10	.093, .103	65	.095
<u>Cabin Floor Mid, FS 44</u>					
VCC6, B-3	Down	10/20	.028/.110	55	.102
	Up	20/30/34	.084/.108/.107	60	.087, .103, .110
RBL 8.0	Fwd	16/12	.03/.100	20/30	.028, .104
	Aft	22/35	.054/.015	74	.086
HCC7, B-4	Right	17/26	.098, .103/.142	50	.086
	Left	10/11/15	.095/.108/.117	31/44	.054/.117
<u>Aft Cabin Floor, FS 90</u>					
VCB9, C-9	Down	12/15	.075/.038/.12	38	.087
	Up	14	.060, .07, .08	35	.085
LBL 8.0	Fwd	30	.047, .058	40	.028, .049, .057
	Aft	46/52	.062/.053	45	.052, .062, .092
HCB10, C-10	Right	25	.078	60	.085
	Left	10	.059	60/30	.082/.058
LCB11, C-11					

(a) LBL, RBL denote left and right butt line, respectively. F.S. denotes fuselage Station.
(b) Accelerometer number, Tape and channel number, respectively.
(c) Time in seconds after impact.

TABLE 3-14. (Cont.)

Location (a)	Direction	100 Hz. Data		300 Hz. Data	
		Peak g	Time (c)	Peak g	Time (c)
<u>Top Cabin, FS 65</u>					
VCB14, D-1	Down	5/10	.035, .045/.125	-	-
	Up	90	.084	230	.142
RBL					
15	Fwd	50	.085	60	.083
	Aft	10	.043, .055	20	.083
<u>Cabin Floor FS 108</u>					
VCB7, C-7 (b)	Down	24/56	.058/.090	120	.088
	Up	36/56	.054/.086	160	.086
LBL					
14	Fwd	15-20	.05, .06, .09	70	.082
	Aft	34	.062, .085	120	.084
<u>Landing Gear Floor Region, FS 60</u>					
VCC9, B-6	Down	8/11	.028/.112	30	.087
	Up	8/12/18	.102/.108/.117	40	.085
LBL					
14	Fwd	15/16	.030/.113	36	.084
	Aft	23/28/30	.054/.096, .086	76	.086
HCC10, B-7					
LCC11, B-8	Right	14/19	.086/.078	36	.079
	Left	4	.095, .087	20	.082
VCC12, B-9	Down	50	.087	80	.085
	Up	22/24	.077/.087	50	.079, .087
RBL					
14	Fwd	12	.10	64	.083
	Aft	36/38	.107/.132	105	.084
HCC13, B-10					
LCC14, B-11	Right	20/15	.078, .100/.112	66	.098
	Left	6/10	.105/.140	38	.117
<u>Wing</u>					
VWB16, D-3	Down	30	.118	120	.114
	Up	30	.085	120	.112
RBL					
98	Fwd	10/14	.077/.105	80	.110
	Aft	15	.075	80	.108
HWB17, D-4					
LWB18, D-5	Right	6	.044	30	.076
	Left	7	.116	30	.077
VWB19, D-6	Down	20/40	.033	100	.113
	Up	20	.06, .103	90/80	.085/.121
(a) LBL, RBL denote left and right butt line, respectively. F.S. denote fuselage Station. (b) Accelerometer number, Tape and channel number, respectively. (c) Time in seconds after impact.					

TABLE 3-14. (Cont.)

Location (a)		Direction	100 Hz. Data		300 Hz. Data	
			Peak g	Time (c)	Peak g	Time (c)
LBL 98	HWB20, D-7	Fwd Aft	12 10	.10,.113 .095	40 60	.087,.097 .125
<u>Tail Mass</u>						
	VTB4, C-4	Down Up	10 10	.03-.14 .03-.04	- -	- -
BL 0.0	HTB5, C-5	Fwd Aft	120 10	.150 .130	- -	- -
	LTB6, C-6	Right Left	20 16	.044 .036	20 36	.045 .035
<u>Top Cabin FS 34</u>						
	VCB12, C-12	Down Up	108 36	.099 .080	200 70	.108 .082
RBL 21	HCB13, C-13	Fwd Aft	80 14/10	.098 .054/.066	140 20	.108 .055,.065

(a) LBL, RBL denote left and right butt line, respectively. F.S. denotes fuselage Station.

(b) Accelerometer number, Tape and channel number, respectively.

(c) Time in seconds after impact.

TABLE 3-15. CRASH TEST 3 OCCUPANT PELVIS PEAK ACCELERATIONS AND PULSE DURATIONS

Location	Down Direction		Up Direction		Forward Direction		Aft Direction		Right Direction		Left Direction	
	Peak g at Time	Avg g, Duration	Peak g at Time	Avg g, Duration	Peak g at Time	Avg g, Duration	Peak g at Time	Avg g, Duration	Peak g at Time	Avg g, Duration	Peak g at Time	Avg g, Duration
Pilot Pelvis (A-1,A-2,A-3)												
100 Hz	8 @ .07		60 @ .120	40, .010 30, .020	4 @ .077		24 @ .122 16 @ .083	12, .020	150 @ .069	120, .005 80, .008	30 @ .124	10, .035
300 Hz	20 @ .072		52 @ .112 60 @ .120	40, .010 20, .025	6 @ .078		35 @ .112	10, .040	170 @ .078	80, .008	30 @ .125	20, .015
750 Hz	60 @ .07		70 @ .120		15 @ .072 15 @ .128		38 @ .072 40 @ .112 44 @ .128		180 @ .077		30 @ .124	
Copilot Pelvis (A-7,A-8,A-9)												
100 Hz		(b)	(b)	(b)	16 @ .125	10, .010	30 @ .12	20, .013	23 @ .11 23 @ .122	20, .006	4 @ .112	
300 Hz					25 @ .124	10, .010	48 @ .119	40, .002 26, .005	30 @ .108 30 @ .117	20, .005	14 @ .104	10, .002
750 Hz					30 @ .140 30 @ .125		50 @ .117		40 @ .108		15 @ .104	

(a) Tape and Channel numbers for vertical, longitudinal and lateral responses, respectively.

(b) Trace lost during the impact.

Times and Durations are in seconds.

TABLE 3-16. CRASH TEST 3 OCCUPANT HEAD PEAK ACCELERATIONS AND PULSE DURATIONS

Location	Down Direction		Up Direction		Forward Direction		Aft Direction		Right Direction		Left Direction	
	Peak g at Time	Avg g, Duration	Peak g at Time	Avg g, Duration	Peak g at Time	Avg g, Duration	Peak g at Time	Avg g, Duration	Peak g at Time	Avg g, Duration	Peak g at Time	Avg g, Duration
Pilot Head (A-4, A-5, A-6) (a)												
100 Hz	40 @ .107 40 @ .127	20, .018	52 @ .131	40, .006	160 @ .107	80, .008 40, .015	25 @ .102		90 @ .107	60, .004	20 @ .142	10, .030
300 Hz	87 @ .107	25, .006	50 @ .13	25, .010	190 @ .107		30 @ .124		190 @ .107	40, .003	21 @ .142	20, .010
750 Hz	140 @ .117		50 @ .13		200 @ .107		30 @ .132		220 @ .107		20 @ .14	
Copilot Head (B12, B13) (c)												
100 Hz	(b)	(b)	(b)	(b)	(c)	(c)	(c)		12 @ .114 50 @ .10	10, .005 40, .014	20 @ .127	
300 Hz									22 @ .115 50 @ .18	40, .014	26 @ .129	
750 Hz									37 @ .114 50 @ .18		28 @ .128	

(a) Tape and Channel numbers for vertical, longitudinal and lateral responses, respectively.

(b) Not recorded.

(c) Trace lost during the impact.

Times and duration are in seconds.

AD-A054 154

LOCKHEED-CALIFORNIA CO BURBANK

F/G 1/3

FULL SCALE CRASH TEST EXPERIMENTAL VERIFICATION OF A METHOD OF --ETC(U)

FEB 78 G WITTLIN, M A GAMON, W L LABARGE

DOT-FA75WA-3707

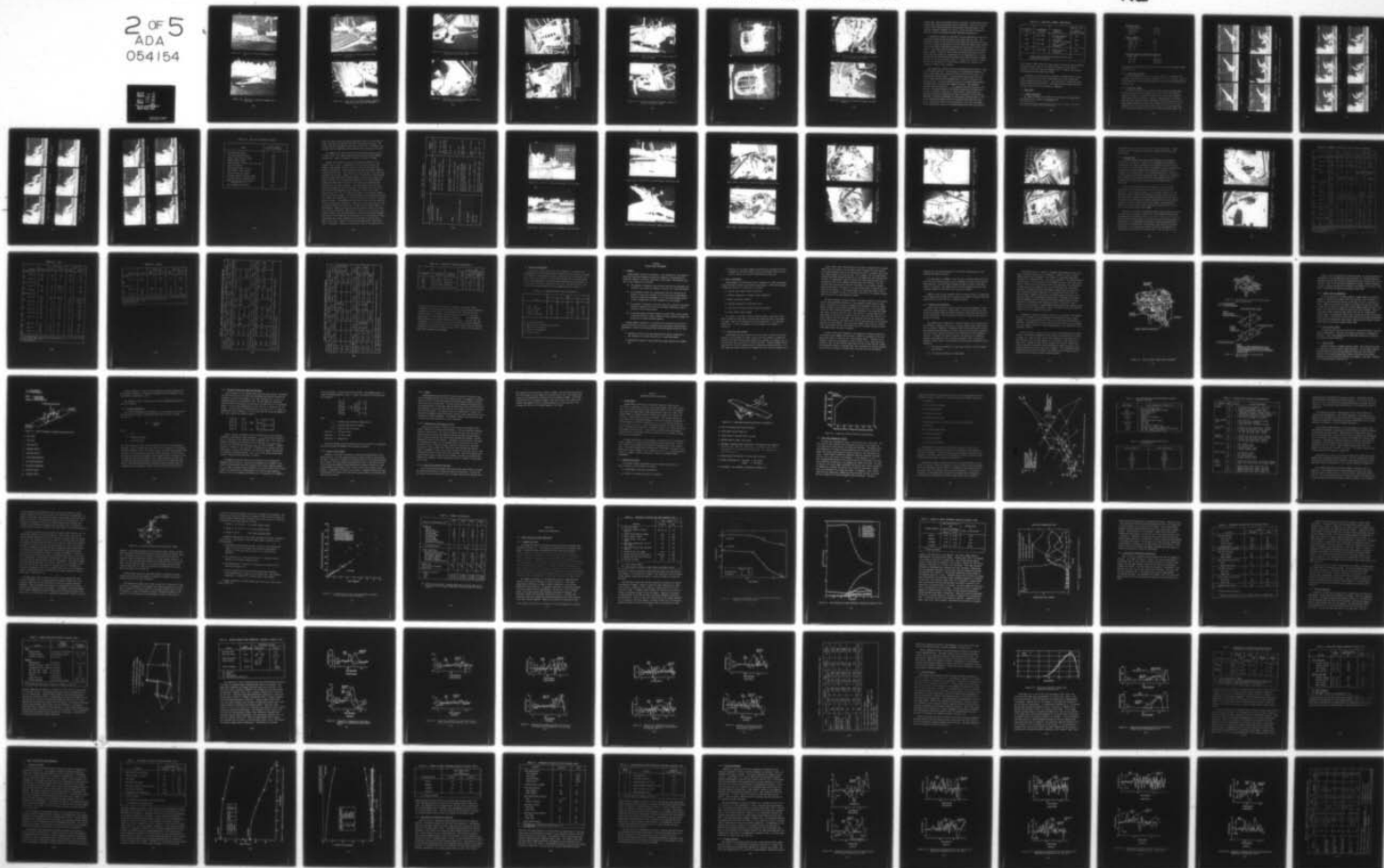
UNCLASSIFIED

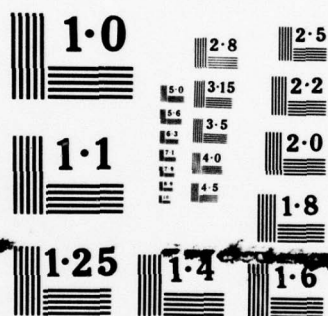
LR-28306

FAA-RD-77-188

NL

2 OF 5
ADA
054154





NATIONAL BUREAU OF STANDARDS
MICROCOPY RESOLUTION TEST CHART

NASA
L-77-3212

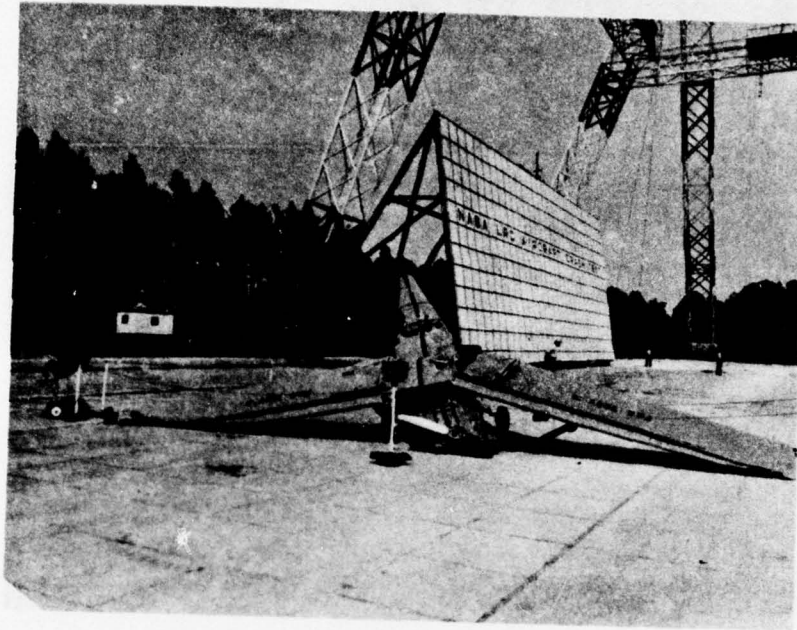


Figure 3-22. Crash Test 3, Post-Test Damage, Front View

NASA
L-77-3211

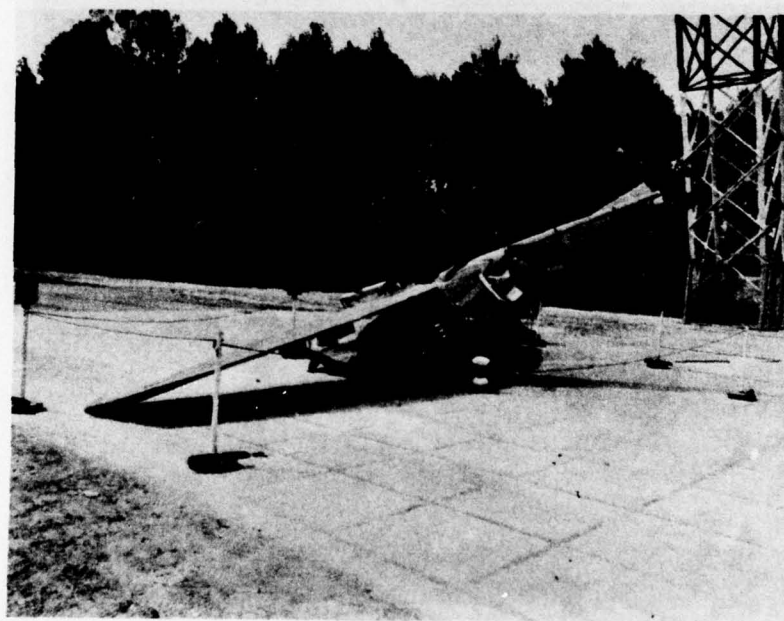


Figure 3-23. Crash Test 3, Post-Test Damage, Left Side View



Figure 3-24. Crash Test 3, Post-Test Damage, Right Side View

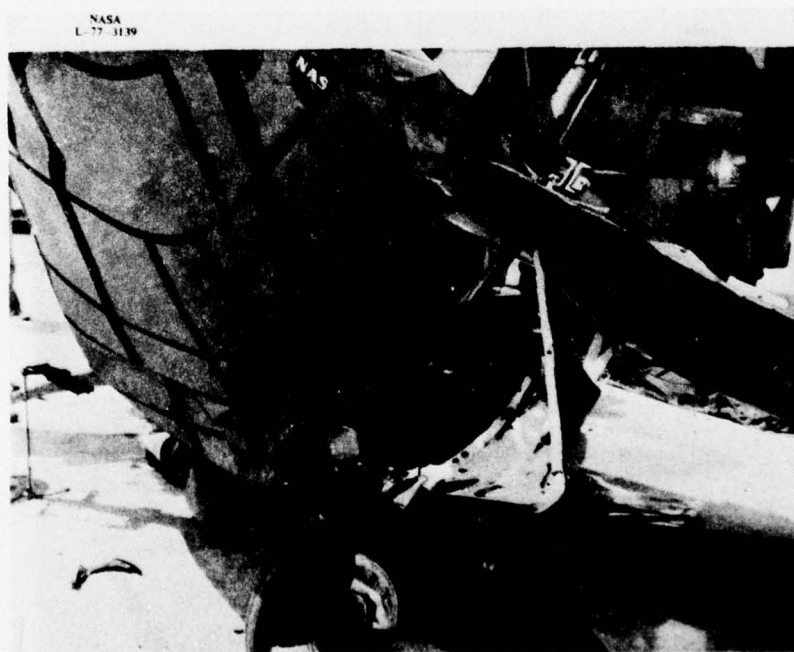


Figure 3-25. Crash Test 3, Post-Test Damage, Right Main Landing Gear and Right Door Distortion

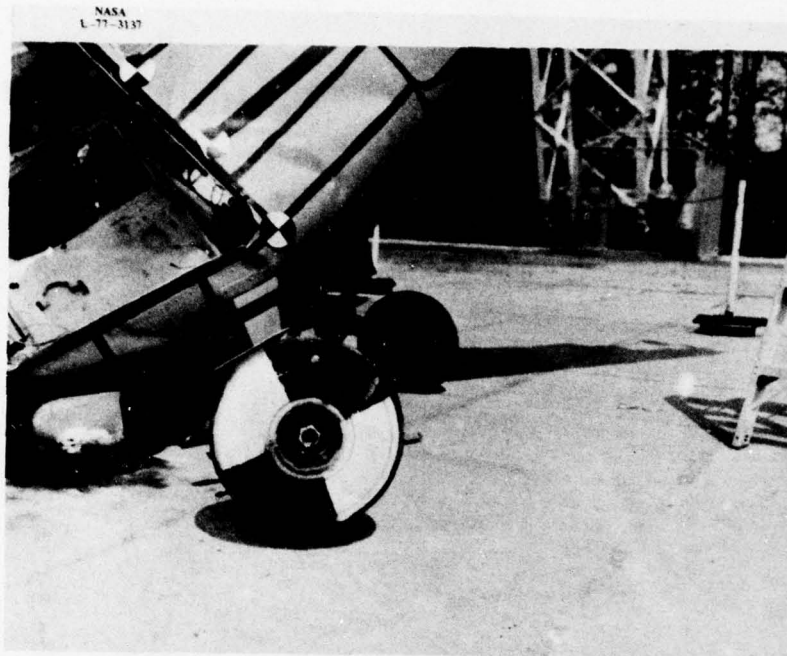


Figure 3-26 Crash Test 3, Post-Test Damage, Left Main Landing Gear and Aft Door Post

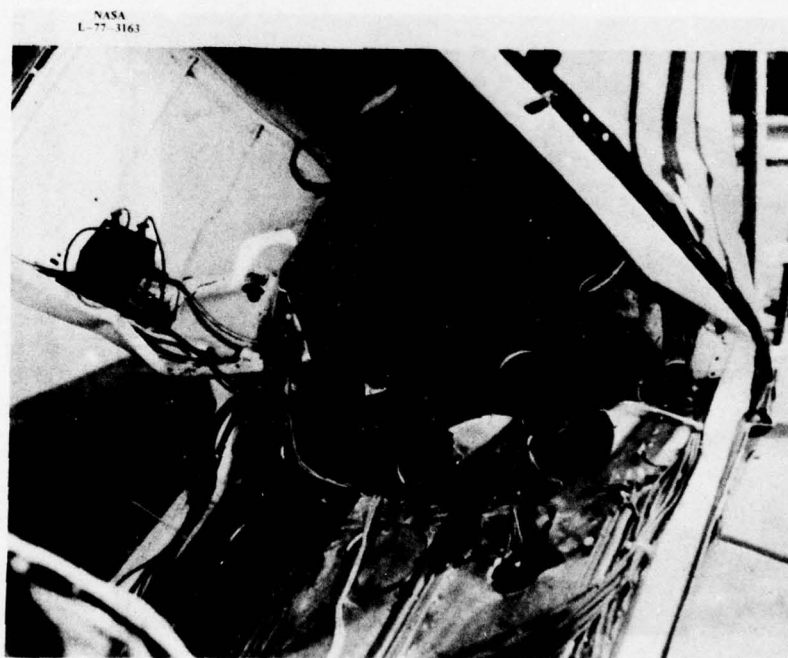


Figure 3-27. Crash Test 3, Post-Test Damage, Main Landing Gear Bulkhead Deformation

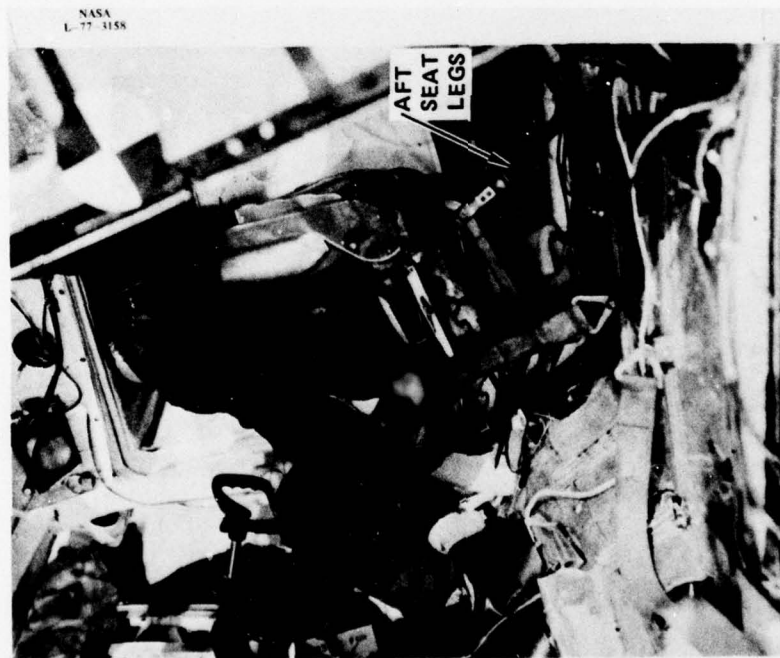


Figure 3-28. Crash Test 3, Post-Test Damage, Passenger Compartment Interior Showing Copilot, Restraint System and Buckled Floor

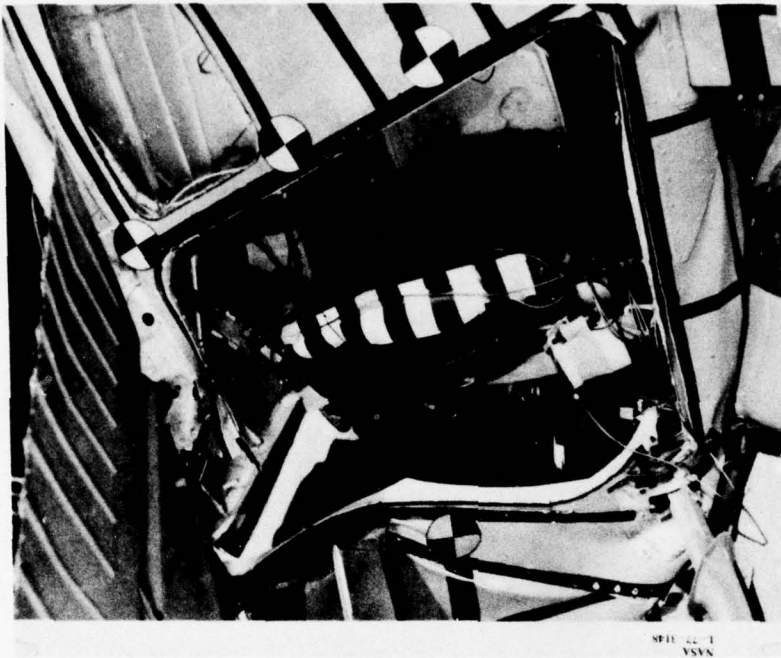


Figure 3-29. Crash Test 3, Post-Test Damage, Passenger Compartment Showing Door Post, Upper Cabin, Pilot and Restraint System

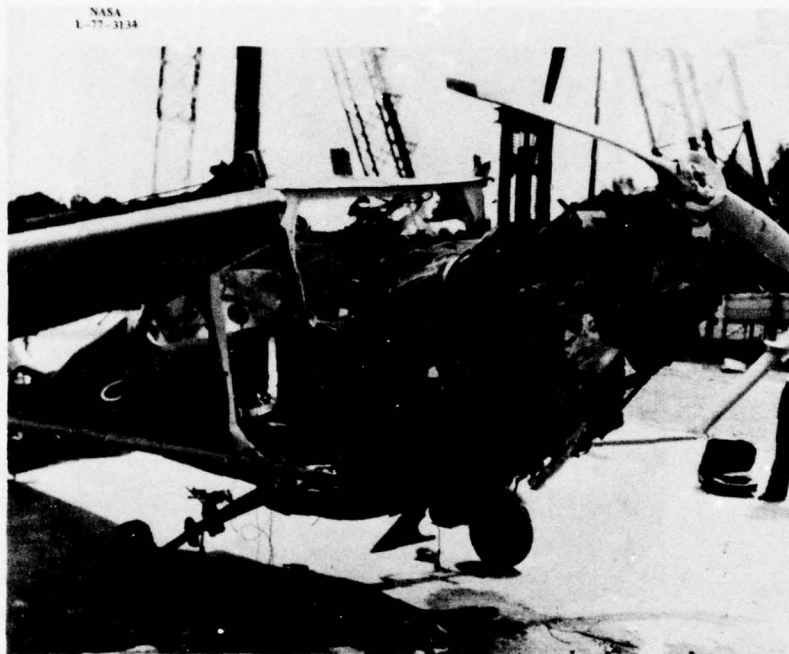


Figure 3-30. Crash Test 3, Post-Test Damage, Engine and Forward Fuselage

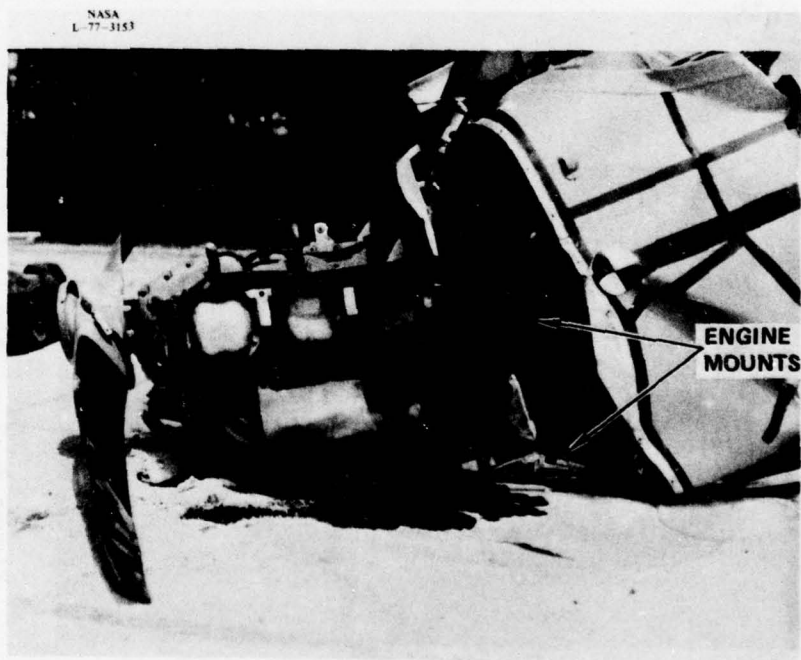


Figure 3-31. Crash Test 3, Post-Test Damage, Engine and Forward Fuselage Side View

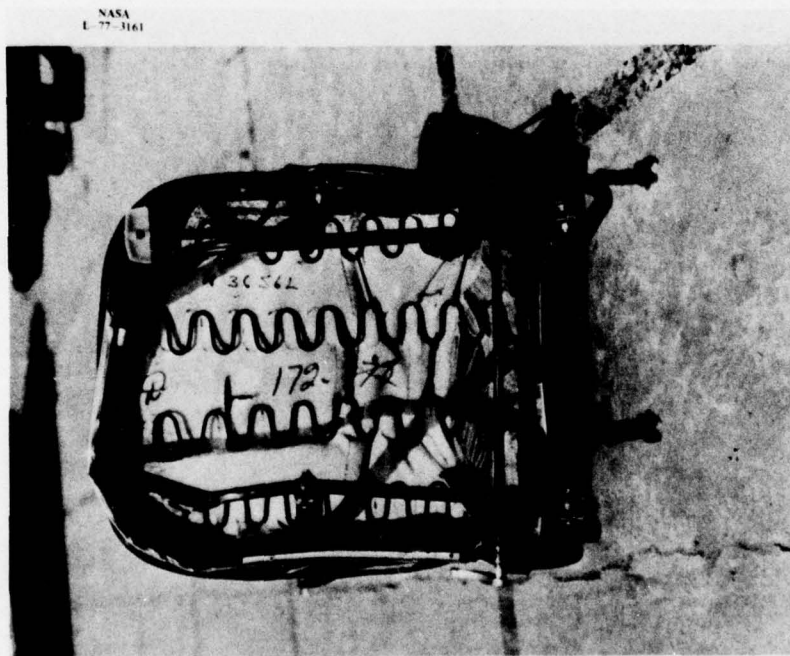


Figure 3-32. Crash Test 3, Post-Test
Damage, Copilot Seat

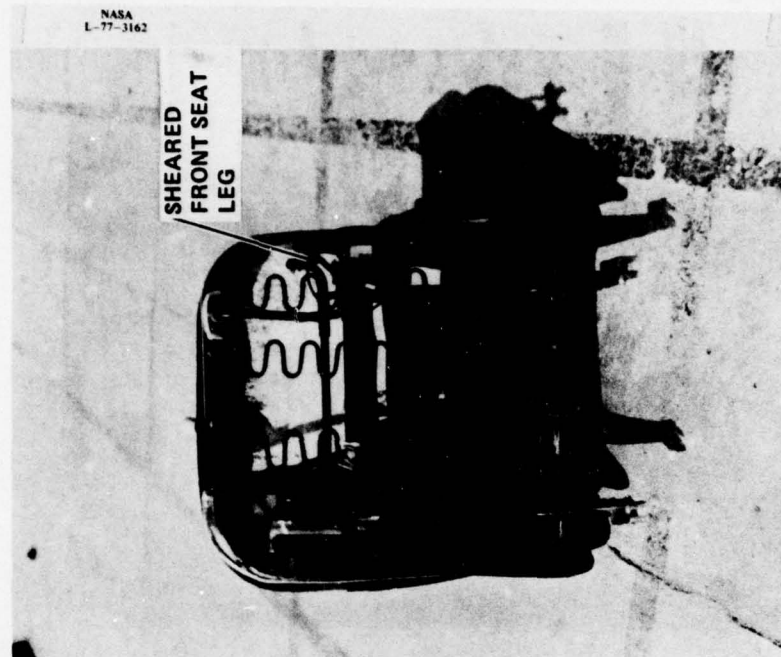


Figure 3-33. Crash Test 3, Post-Test
Damage, Pilot Seat

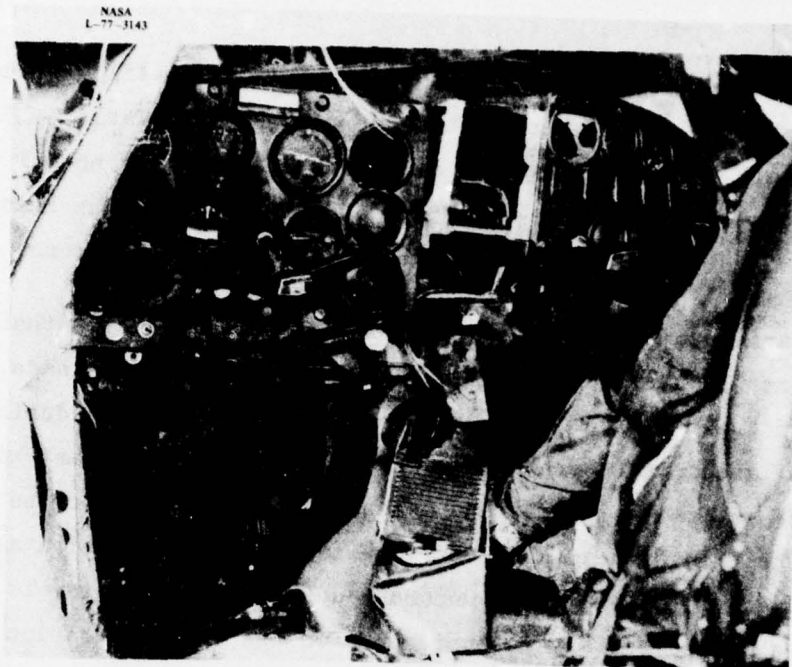


Figure 3-34. Crash Test 3, Post-Test Damage, Instrument Panel and Rudder Pedal Region



Figure 3-35. Crash Test 3, Post-Test Damage, Left Wing Failure

respectively. Table 3-14 presents 100 Hz. and 300 Hz. filtered data showing airplane peak load, direction and time of occurrence. Table 3-15 contains occupant pelvis peak accelerations and durations oriented normal to and along the occupant's backbone for 750 Hz., 300 Hz and 100 Hz frequencies. Similarly, Table 3-16 presents occupant head peak accelerations.

A comparison of Table 3-15 and Table 3-6 data indicates that the crash could have resulted in serious injury to the pilot from up loads. The acceleration trace for the copilot's pelvic region was lost during the test. The pilot's lateral acceleration in the left direction appears high compared to the other lateral accelerations measured at the pelvis of the pilot and copilot. The pilot's head acceleration in the right direction also appears high. However, a review of the recorded data sensitivity levels and calibration does not reveal any inconsistency in the instrumentation. Unlike the fore aft and vertical directions there are no Eiband curves for lateral responses in the pelvic region by which to evaluate the severity of injury. However, for the lateral 'g' levels shown in Table 3-15, injury to the occupant is likely to have occurred.

Peak response in excess of 100 g's was experienced by the pilot's head in the forward direction. From the data in the SAE Handbook (Reference 4) serious skull damage most likely could have occurred if the cause of the accelerations was from impact. The high speed films indicate that the pilot's head contacted the instrument panel or corner of the door post during the test. The only operative trace for the copilot head acceleration shows 50 g's or less in the lateral direction. Film analysis indicates that the copilot's head also impacted structure during the test. Analysis to determine severity index values associated with head impacts for Test 3 is given in Table 3-17. These severity index values were obtained following the procedures set forth in Section 2.8 entitled DATA REDUCTION. The data in Reference (4) shows that a severity index of 1000 is the threshold of danger to life for internal head injury in frontal blows. The severity index value corresponding to the pilot head impact in the longitudinal direction is substantially greater than the threshold

TABLE 3-17. CRASH TEST 3 SEVERITY INDEX RESULTS

Accelerometer No.	Accelerometer Location	Direction of Response	Severity Index 750 Hz Unfiltered Data
VPA4	Pilot Head	Vertical (parallel to backbone)	136
HPA5	Pilot Head	Longitudinal (normal to backbone)	1785
LPA6	Pilot Head	Lateral (normal to backbone)	482
LCC16	Copilot Head	Lateral (normal to backbone)	2337
Copilot head vertical and longitudinal traces were unavailable for analysis			

value of 1000. Thus a serious or fatal injury to the pilot can be expected. The severity index value for the copilot head impact in the lateral direction is also well above the threshold value. However, the criteria for side blows are not explicitly stated.

In addition to head and pelvic responses, consideration must also be given to the fact that the lower cabin region aft of the firewall was greatly compressed during the test. This could lead to severe leg injury. Typical data histories from Test 3, including filtered accelerations and restraint system loads, are presented in Appendix C.

3.4 CRASH TEST 4

3.4.1 Impact Conditions*

The impact conditions for crash test 4 as obtained from high speed film analysis and a review of photographs are:

*For Crash Test 4 the airplane impacted onto a soil terrain. All other tests were performed on a concrete surface.

Velocities (mph)

along flight path	55.9 mph
longitudinal	48.4 mph
vertical	31.9 mph

Angles (degrees)

flight path (γ)	-32.0
impact (θ)	-34.8
attack (α)	-2.8
roll (ϕ)	<1.0
yaw (ψ)	<1.0

Rotational Velocities (degrees per second)

pitch ($\dot{\theta}$)	18.2
roll ($\dot{\phi}$)	negligible
yaw ($\dot{\psi}$)	negligible

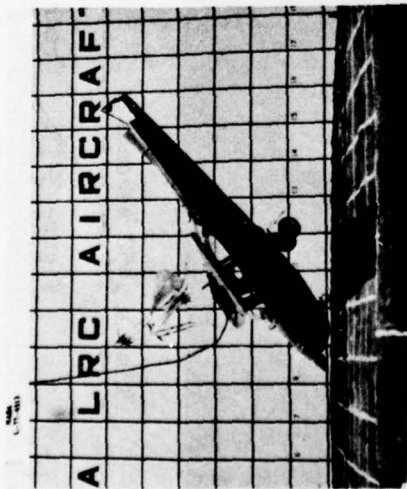
The nomenclature and definition of positive directions are the same as noted in Section 3.1.1.

3.4.2 Crash Impact Sequence

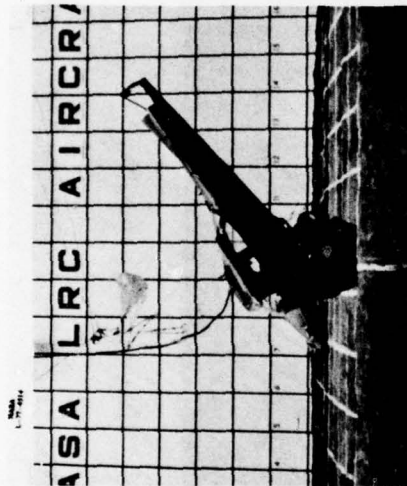
The crash sequence for Test 4 is shown in Figures 3-36 through 3-39 at impact and every 50 milliseconds thereafter (up to 1.15 seconds). Analysis of the high speed film provides the sequence of events following impact given in Table 3-18.

3.4.3 Structural Damage

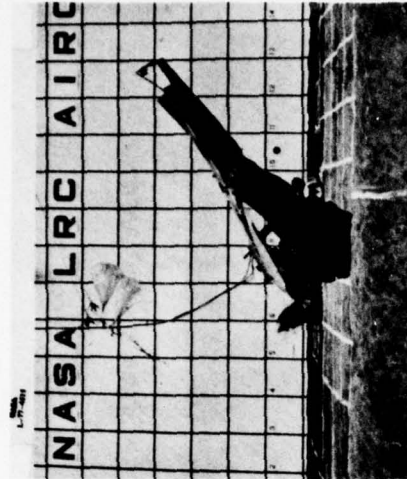
A review of the post-test condition of the airplane, the high speed films and the post-test photographs showed that the airplane sustained complete crushing of the forward fuselage as far back as the occupant's cabin region, loss of nose gear, failure of engine mounts to the extent that the engine separated from the airframe, extensive deformation of the cabin geometry and the floor near the occupant leg positions (F.S. 27), crushing of the aft cabin region, tension failure of the left wing rear spar, a severely buckled tail cone, and a mangled instrument panel. The



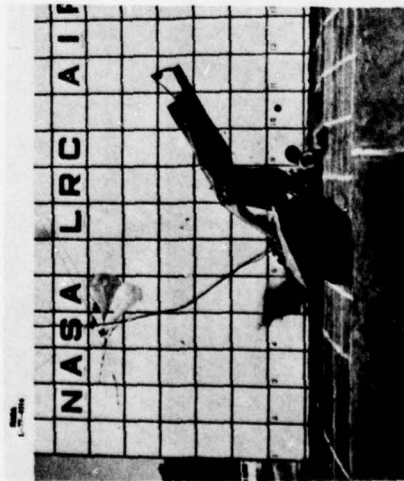
Time = 0



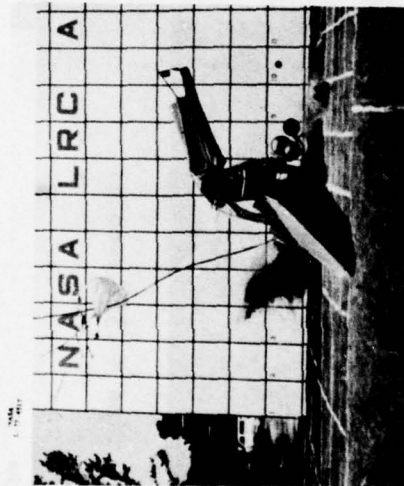
Time = .050 seconds



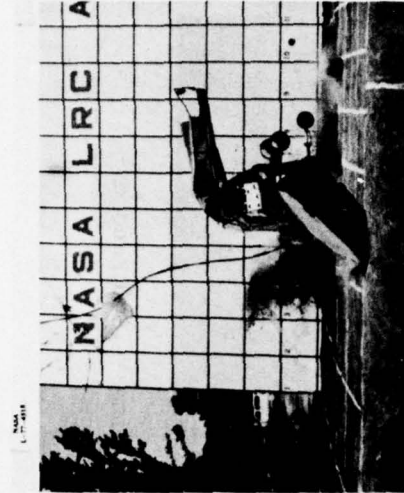
Time = .100 seconds



Time = .150 seconds



Time = .200 seconds



Time = .250 seconds

Figure 3-36. Crash Test 4, Impact Sequence, Time = 0.0 to .250 Seconds



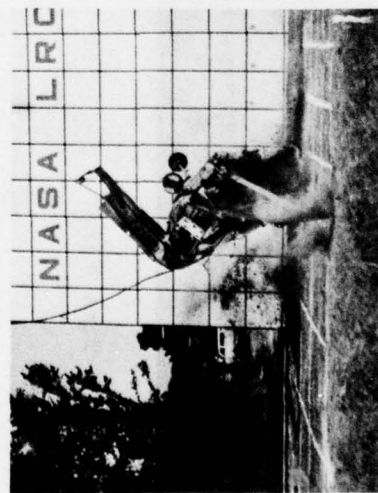
Time = .300 seconds



Time = .350 seconds



Time = .400 seconds



Time = .450 seconds



Time = .500 seconds

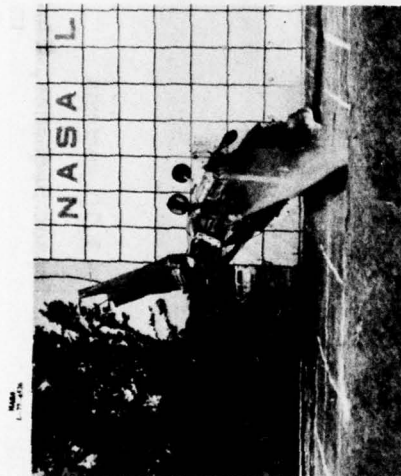


Time = .550 seconds

Figure 3-37. Crash Test 4, Impact Sequence, Time = .300 to .550 Seconds



Time = .600 seconds



Time = .650 seconds



Time = .700 seconds



Time = .750 seconds



Time = .800 seconds



Time = .850 seconds

Figure 3-38. Crash Test 4, Impact Sequence, Time = .600 to .850 Seconds



Time = .900 seconds



Time = .950 seconds



Time = 1.00 seconds



Time = 1.05 seconds



Time = 1.10 seconds



Time = 1.15 seconds

Figure 3-39. Crash Test 4, Impact Sequence, Time = .900 to 1.15 Seconds

TABLE 3-18. CRASH TEST 4 SEQUENCE OF EVENTS

Event	Time in Seconds After Initial Impact
Nose Gear Tire Impact	0
Nose Gear Support Failure	.024
Engine Lower Structure Impact	.030
Engine Spinner Impact	.034
Engine Spinner completely under the soil	.052
Tail Cone Buckles	.076
Engine Buried under the soil	.078
Pilot Impacts Control Wheel	.078
Left Main Gear Tire Impact	.088
Occupant Contacts Instrument Panel	.096
Left Main Gear Tire Leaves Ground	.114
Engine Shoved Back Into Forward Fuselage (F.S. 27)	.138
Left Wing Rear Spar Failure	.250

pilot and copilot front seat rails pulled away from the floor during the crash. The rear seat legs and rails were intact after the crash. The copilot seat belt attachment pulled away from the floor. Otherwise, the occupant seat and restraint systems remained intact throughout the crash.

The damage to the cabin floor near the main landing gear was minor. In Tests 1 and 3 this region experienced extensive and moderate damage, respectively. Table 3-19 presents a summary of the Test 4 damage.

Figures 3-40 through 3-53 depict the post-test condition of the airplane used in Test 4. Figures 3-40, 3-41 and 3-42 illustrate the damage to the airplane from the left side, right side and right rear quarter, respectively. Figure 3-43 shows the cabin top damage (airplane hoisted after the test). The separation of the left wing at the rear spar attachment can be seen. Figures 3-44, 3-45, 3-46 and 3-47 show the engine mounts, firewall and forward fuselage damage. Shortly after impact the engine dug into the soil, developing high forces in the drag direction. Because the engine dug into the soil, the airplane was prevented from sliding and as a result overturned. The engine mounts failed and the engine block separated from the airframe. The engine came to rest about five feet from the remainder of the airplane at the end of the test. Figures 3-44, 3-45, 3-46, 3-47 depict the damage to the firewall, engine mount and forward fuselage. The forward fuselage was completely demolished. The firewall was crushed back to the front door posts a distance of approximately 27 inches. The wings and wing struts are intact with the exception of the left wing rear spar failure. There was no fuel tank rupture or fuel spillage encountered as a result of the impact or post-impact behavior of the airframe. Figures 3-48 and 3-49 show the copilot's side of the cabin with and without occupants, respectively. Because of the crushing of the forward fuselage, the instrument panel and floor were extensively damaged. The position of the dummy and the compression of the forward part of cabin surrounding the occupant indicates that an occupant would have little chance of survival. Figures 3-50 and 3-51 show the pilot's side of the cabin. The damage is similar to the copilot's side of the cabin and it is

TABLE 3-19. CRASH TEST 4 DAMAGE SUMMARY

Location	Type of Damage	Applicable Figures
Engine and Firewall	Engine mounts severely buckled. Engine separated from airframe.	3-40, 3-44, 3-45
Forward Fuselage	Lower fuselage completely crushed.	3-45, 3-46, 3-47
Cabin	Both front door posts severely buckled.	3-40, 3-41, 3-44, 3-46, 3-49, 3-50, 3-51
	Floor at base of instrument panel completely crushed.	3-48, 3-50
Wings	Left wing rear spar tension failure.	3-43,
	No fuel tank rupture or leakage.	3-40, 3-41
Seats and Restraint Systems	Pilot and copilot front seat rails pulled loose from floor. Copilot seat belt attachment to the floor pulled loose.	3-49, 3-50, 3-51, 3-52, 3-53
Tail Section	Severely buckled at rear bulkhead F.S. 108.	3-40, 3-41, 3-42, 3-43
Nose Gear	Failed aft (similar to Tests 1 and 3).	3-41, 3-42
Main Gear	Relatively little damage. Main tires contacted the ground for only a short time period.	3-40, 3-41, 3-42, 3-43

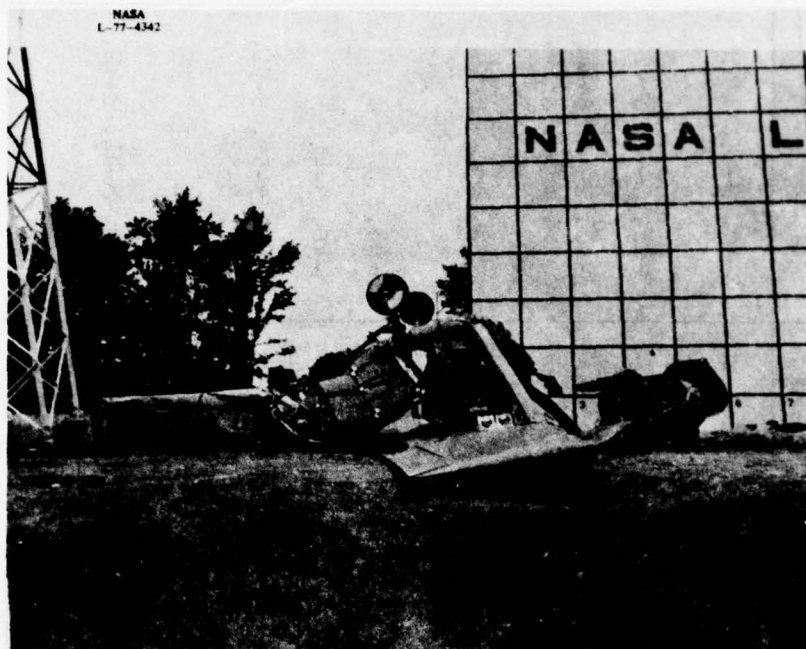


Figure 3-40. Crash Test 4, Post-Test Damage, Left Side View



Figure 3-41. Crash Test 4, Post-Test Damage, Right Side View

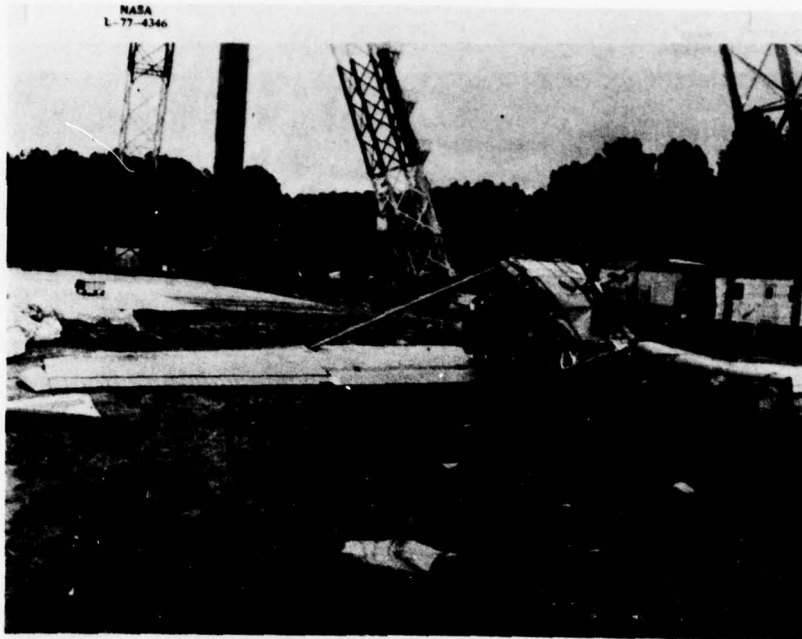


Figure 3-42. Crash Test 4, Post-Test Damage, Rear Quarter View



Figure 3-43. Crash Test 4, Post-Test Damage, Cabin Top View

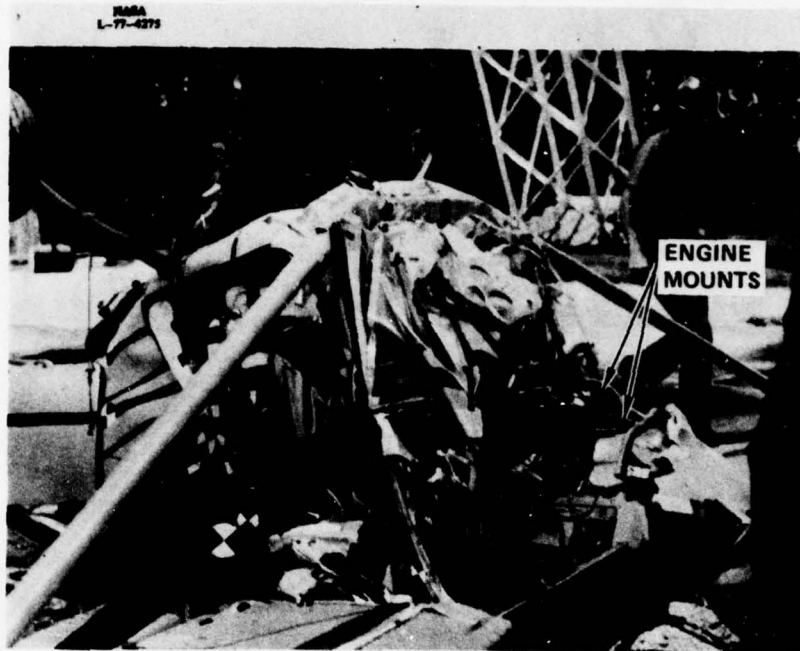


Figure 3-44. Crash Test 4, Post-Test Damage, Left Front View



Figure 3-45. Crash Test 4. Post-Test Damage, Right Front View

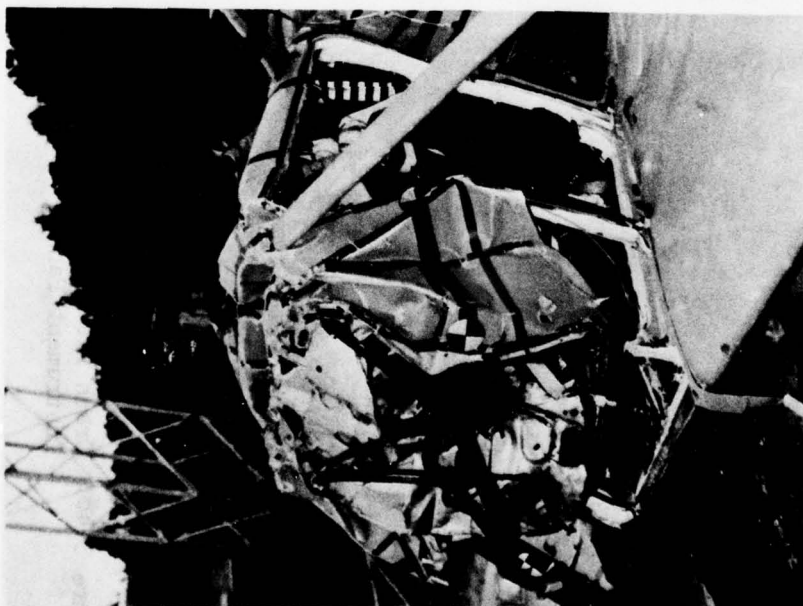


Figure 3-46. Crash Test 4, Post-Test
Damage, Right Front, Firewall

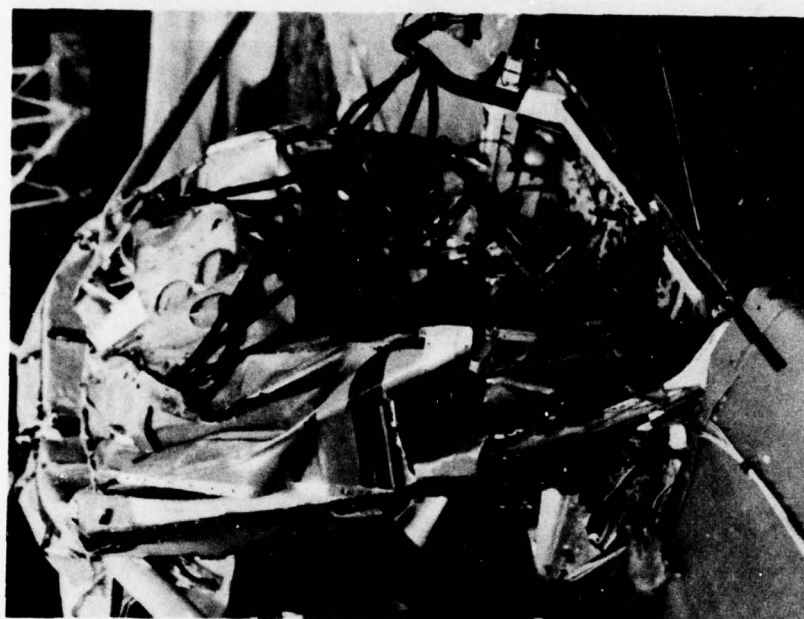


Figure 3-47. Crash Test 4, Post-Test Damage,
Engine Mounts

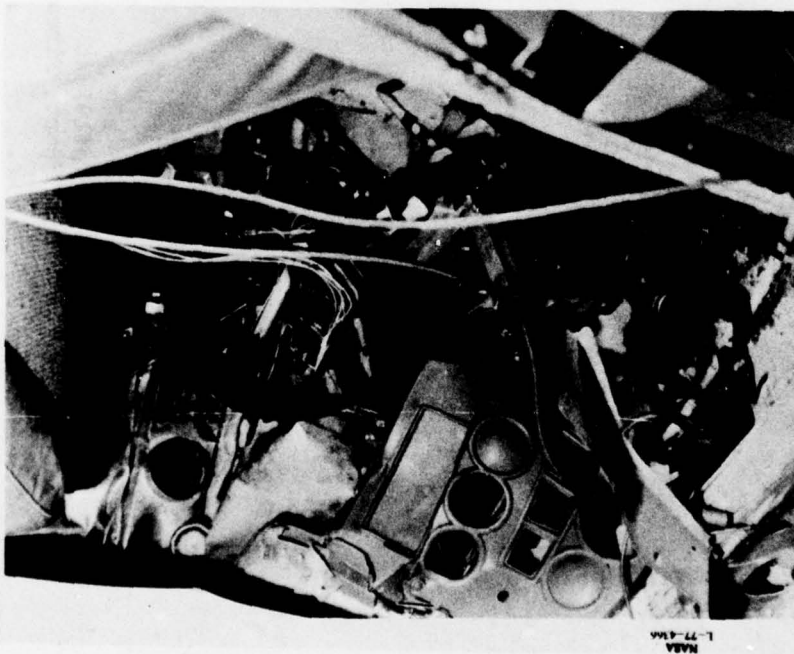


Figure 3-48. Crash Test 4, Post-Test Damage,
Instrument Panel

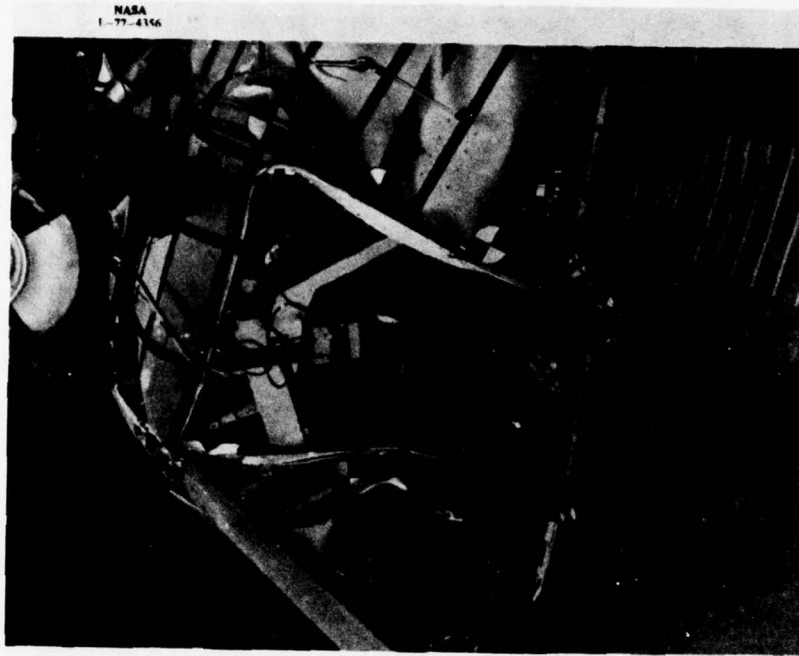


Figure 3-49. Crash Test 4, Post-Test Damage,
Cabin Right Side

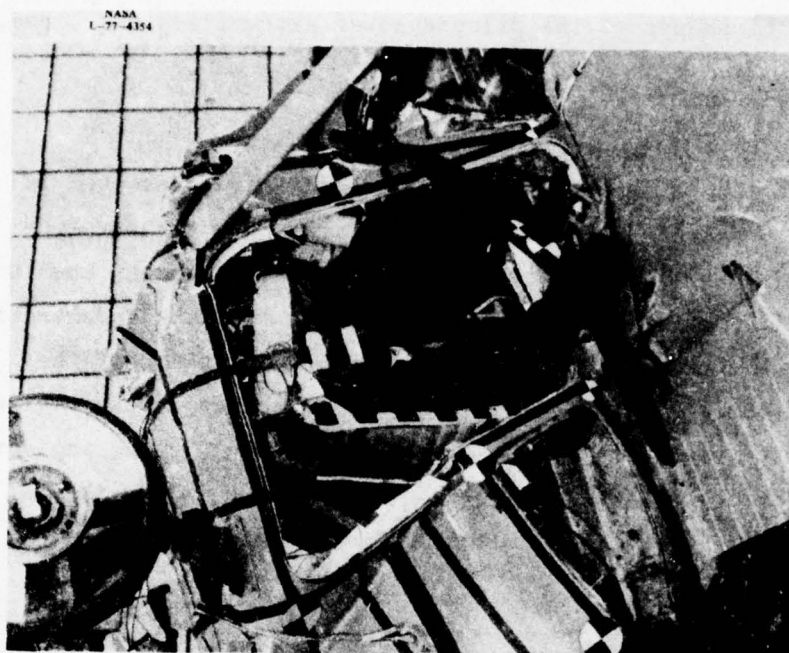


Figure 3-51. Crash Test 4, Post-Test Damage,
Cabin Left Side, Occupants
In Place

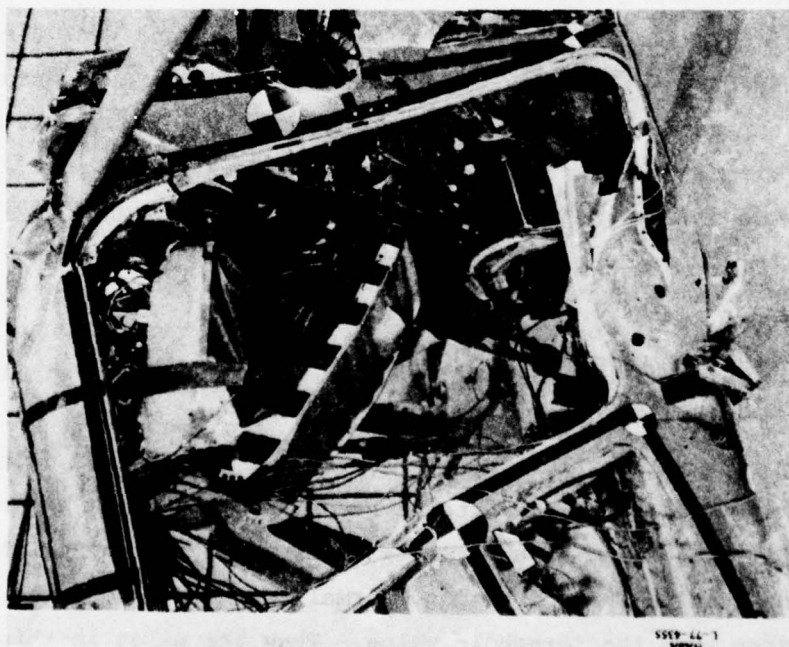


Figure 3-50. Crash Test 4, Post-Test Damage,
Cabin Left Side, Occupants
Removed

anticipated that a pilot would have little chance for survival. Figures 3-52 and 3-53 are close-ups of the pilot's lower extremities and torso, respectively.

3.4.4 Response Data

The results obtained from Test 4 data reduction are presented in Tables 3-20, 3-21 and 3-22. Table 3-20 is a summary of peak airplane accelerations and time of occurrence of the accelerations using the 100 Hz. and 300 Hz. filtered data. Table 3-21 presents the peak accelerations, the time of occurrence and duration experienced in the region of the occupant's pelvis during Test 4. The tolerable responses in the region of the occupant's pelvis were given previously in Table 3-6 and indicates, when compared with the data in Table 3-21, that serious injury to the occupants in both the up and down directions most likely would be encountered.

Table 3-22 shows that peak head accelerations of 250 g's were experienced by the dummy representing the pilot in the down and aft directions. These responses appear to be the result of impact with the instrument panel. Film analysis indicates that pilot contact with the instrument panel occurred at around 100-milliseconds after crash impact. The copilot also experienced 100 g head accelerations in the down and aft directions at about 100-milliseconds after impact. From Reference 4, impacts with objects which result in peak head accelerations of 100 g's or more can produce serious skull damage.

The results of analysis to determine severity index values associated with head impacts are given in Table 3-23. The recorded unfiltered data is normally used to obtain severity index values. However, for comparative purposes severity index values for the 300 Hz and 100 Hz filtered data are also presented. As expected, the unfiltered recorded data yields higher values than the filtered data. The severity index value for the pilot's head impact in the longitudinal direction (normal to the backbone) is substantially higher than the threshold value. Thus the pilot in this



Figure 3-52. Crash Test 4, Post-Test Damage,
Pilot Legs and Feet



Figure 3-53. Crash Test 4, Post-Test Damage,
Pilot Torso

TABLE 3-20. SUMMARY OF CRASH TEST 4 PEAK AIRPLANE ACCELERATIONS

Location (a)	Direction	100 Hz. Data		300 Hz. Data	
		Peak g	Time (c)	Peak g	Time (c)
Engine					
VE1, C-1 (b)	Up	40	.050	48	.055
	Down	20	.077	30/46	.065/.165
BL					
0.0	HEB2, C-2	Fwd	36/65	40	.090
		Aft	90/115	100/300	.050/.155
Firewall Lwr.					
VFC3, A-13	Up	80	.11	(d)	.030-.090/.145
	Down	-	-	100-125,750 125-200,750	.030-.090,.113/ .110
LBL					
14.	Fwd	120/800 (d)	.05/.095	- (d)	.055/.080
	Aft	100/1200 (d)	.025/.090	-	.068/.086
Cabin Floor Fwd. FS 27					
VCC5, B-1	Up	30/34	.070/.100	112	.078
	Down	32	.075	135	.08
LBL					
13.5	HCC6, B-3	Fwd	60	60	.077
		Aft	100	72	.080
BL					
0.0	VCC7, B-4	Up	75/750 (d)	185/750 (d)	.077/.080
		Down	125	350/500 (d)	.075
	HCC8, B-5	Fwd	250/500 (d)	160 (d)	.060/.075
		Aft	240/1000 (d)	160 (d)	.065/.075
	VCC9, B-6	Up	44/60/95	175	.15
		Down	32/31	120	.067
RBL					
13.5	HCC10, B-7	Fwd	100	180	.080
		Aft	25	220	.078
Cabin Floor Mid, FS 44					
VCB17, D-4	Up	16/120	.11/.21	120	.108
	Down	108	.08	200	.08
LBL					
8.0	HCB18, D-5	Fwd	106	270	.102
		Aft	30	50	.08
Aft Cabin Floor, FS 90					
VCB7, C-7	Up	28/30	.060/.120	60	.097
	Down	28	.065	110	.118
LBL					
8.0	HCB8, C-8	Fwd	74	(d)	(d)
		Aft	70/68	(d)	(d)

(a) LBL, RBL denote left and right butt line, respectively. F.S. denotes fuselage station.
 (b) Accelerometer number, tape and channel number, respectively.
 (c) Time in seconds after impact.
 (d) Questionable data.

TABLE 3-20. (Cont.)

Location (a)	Direction	100 Hz. Data		300 Hz. Data	
		Peak g	Time (c)	Peak g	Time (c)
Top Cabin, FS 65					
VCB11, -C-11	Up	170	.15	400	.15
	Down	60	.165	100	.175
RBL					
15 HCB12, C-12	Fwd	70	.21	110	.17
	Aft	112	.157	260	.168
Cabin Floor, FS 108					
VCB5, C-5 (b)	Up	35	.060/.105	60	.105
	Down	30	.055/.105	54	.125
LBL					
14 HCB6, C-6	Fwd	54	.065	55	.075
	Aft	74	.070	85	.060
Landing Gear, FS 60					
VCC11, B-8	Up	20/24	.105/.118	36	.115
	Down	12/10	.06/.130	17/20	.03,.06,.11,.19
LBL					
14 HCC12, B-9	Fwd	8	.050	16/18	.077/.120
	Aft	80	.105	94	.105
VCC13, B-10	Up	28	.115	88	.102
	Down	7	.100	40	.105
B.L.					
0.0 HCC14, B-11	Fwd	14/70	.05/.22	40/70	.120/.22
	Aft	75	.100	130	.100
VCC15, B-12	Up	55	.110	88	.102
	Down	10	.098	22	.100,.105
RBL					
14 HCC16, B-13	Fwd	26	.110	50	.120
	Aft	56	.100	100	.100
Wing					
VWB13, C-13	Up	30	.105	65	.105
	Down	20	.085	92	.087
RBL					
98 HWB14, D-1	Fwd	16	.19	50	.087
	Aft	40	.11	46	.09
VWB15, D-2	Up	26	.11	44	.11
LBL	Down	28	.09	74	.09
98					
(a) LBL, RBL denote left and right butt line, respectively. F.S. denotes fuselage station.					
(b) Accelerometer number, tape and channel number, respectively.					
(c) Time in seconds after impact.					
(d) Questionable data.					

TABLE 3-20. (Cont.)

Location (a)	Direction	100 Hz. Data		300 Hz. Data	
		Peak g	Time (c)	Peak g	Time (c)
Tail Mass					
VTB3, C-3	Up	12	.062	14	.050
	Down	7	.110	8	.110
BL 0.0					
Top Cabin FS 32					
VCB9, C-9	Up	20/40	.15/.2	64	.150
	Down	56	.100	110	.100
RBL					
21	Fwd	85	.135	200	.145
HCB10, C-10	Aft	95	.210	270	.21
(a) LBL, RBL denote left and right butt line, respectively. F.S. denotes fuselage station. (b) Accelerometer number, tape and channel number, respectively. (c) Time in seconds after impact. (d) Questionable data.					

TABLE 3-21. CRASH TEST 4 OCCUPANT PELVIS PEAK ACCELERATIONS AND PULSE DURATIONS

Location	Up Direction		Down Direction		Forward Direction		Aft Direction	
	Peak g at Time	Avg g, Duration	Peak g at Time	Avg g, Duration	Peak g at Time	Avg g, Duration	Peak g at Time	Avg g, Duration
Pilot Pelvis (A-1,A-2) (a)								
100 Hz	100 @ .172	60, .015	80 @ .125	80, .005 40, .014	64 @ .115	40, .015 20, .040	10 @ .130	10, .017
300 Hz	145 @ .172	80, .003 40, .010	80 @ .125	80, .005 40, .022	110 @ .135 60 @ .115	40, .018	50 @ .155	-
750 Hz	140 @ .172	-	100 @ .125	-	100 @ .115 180 @ .133	-	80 @ .15 40 @ .115	-
Copilot Pelvis (A-5,A-6) (a)								
100 Hz	90 @ .105	80, .002	30 @ .085	20, .003	80 @ .100	60, .006 40, .018	20 @ .070	10, .007
300 Hz	95 @ .105	75, .004	60 @ .085	-	106 @ .100	60, .004 40, .014	20 @ .070	20, .004 10, .007
750 Hz	150 @ .105	-	100 @ .08- .09	-	170 @ .100	-	-	-
(a) Tape and channel numbers for vertical and longitudinal responses, respectively.								
(b) Times and durations are in seconds								

TABLE 3-22. CRASH TEST 4 OCCUPANT HEAD PEAK ACCELERATIONS AND DURATIONS

Location	Up Direction		Down Direction		Forward Direction		Aft Direction	
	Peak g at Time	Avg g, Duration	Peak g at Time	Avg g, Duration	Peak g at Time	Avg g, Duration	Peak g at Time	Avg g, Duration
Pilot Head (A-3,A-4) (a)								
100 Hz			110 @ .118	100, .002 40, .008			200 @ .115	160, .005 80, .010
300 Hz			180 @ .118	40, .008			230 @ .115	160, .007 80, .010
750 Hz			250 @ .118				250 @ .115	
Copilot Head (A-7,A-8) (a)								
100 Hz	110 @ .120	100, .003 50, .015	50 @ .172	25, .005	15 @ .075	10, .005	50 @ .108	40, .013
300 Hz	140 @ .120	80, .006 40, .016	80 @ .172	40, .003 20, .005	18 @ .075	10, .005	60 @ .108	40, .009 30, .018
750 Hz	170 @ .120		100 @ .11 85 @ .172		100 @ .105		100 @ .108 35 @ .075	

(a) Tape and channel numbers for vertical and longitudinal responses, respectively.

(b) Times and durations are in seconds.

TABLE 3-23. CRASH TEST 4 SEVERITY INDEX RESULTS

Accelerometer No.	Accelerometer Location	Direction of Response	Severity Index		
			750 Hz Raw Data	300 Hz Filtered Data	100 Hz Filtered Data
VPA3	Pilot Head	Vertical	1055	814	543
HPA4	Pilot Head	Longitudinal	4056	3976	3691
VCA7	Copilot Head	Vertical	1368	1016	945
HCA8	Copilot Head	Longitudinal	373	230	207

case most likely would have sustained a serious or fatal head injury. Conversely, the copilot's severity index value in the longitudinal direction is below the threshold value. The high speed films indicated that the copilot moved in an outboard direction during the crash test. This may explain the low frontal impact values. Because no lateral accelerometers were installed on the dummies representing the occupants in this test, the consequence of the lateral motion can not be determined using the severity index method. Both the pilot and copilot severity index values for vertical (parallel to the backbone) impact are above 1000. However, the criteria for this type of impact are not defined.

3.5 RESTRAINT SYSTEM LOADS

In Section 2.0 "Full Scale Crash Test Preparation" the dummies were instrumented with lap belt and shoulder harness load cells which were recorded on dc channels. The restraint system is compatible with the airplanes that were used for test vehicles. The restraint systems did not include inertia reels. The performance of the lap belt and shoulder harness attachments to the structure are noted in Tables 3-2, 3-8, 3-13, 3-19 and Table 7-4. The lap belt and shoulder harness loads are summarized below in Table 3-24.

TABLE 3-24. RESTRAINT SYSTEM LOADS, CRASH TESTS 1-4

Location	Test			
	1	2	3	4
Pilot - Lap	860	(d)	1,350	1,200
Pilot - Shoulder	510		680	(e)
Copilot - Lap	300		1,040	800
Copilot - Shoulder	440		910	(e)

(a) All loads are tension.

(b) Based on 300 Hz low-pass filtered data.

(c) Loads are in pound units.

(d) No belt loads measured.

(e) Data trace lost.

SECTION 4
PROGRAM KRASH REFINEMENTS

4.1 GENERAL

Program KRASH, described in Reference 1, was developed for the purpose of providing a practical engineering analytical approach for determining the structural response of vehicles subjected to crash loads. The essential features of the program are as follows:

- (a) The program is designed to provide data from which an assessment can be made of the occupant's chances of survival in a crash environment.
- (b) The formulation takes into consideration that the load-deflection behavior (linear and nonlinear) of a structure can be approximated using good engineering judgement so as to provide responses with an accuracy commensurate with the intended use of the program.
- (c) The analysis is premised on the fact that only a portion of the major structural elements (and these can be readily identified) need be modeled in the nonlinear region.
- (d) The program employs stiffness reduction factors (KR's) which provide a method by which the linear stiffness of each structural element can be modified to treat nonlinear behavior.

Program KRASH's formulation is consistent with the amount and quality of detailed structural data that is available during preliminary design studies. Furthermore, analyses using program KRASH during preliminary design can serve to:

- ascertain critical structural design regions wherein alterations to the response will be most beneficial in a crash environment.
- determine the extent to which additional energy absorption is needed, and

- determine the structural element load-deflection characteristics and, consequently, structural design and size requirements that are needed to meet a specified or desired crashworthiness capability.

4.2 TASK II REFINEMENTS

Program KRASH, as refined during Task I (Reference 1), meets the general aviation airplane industry crash analysis requirements. The previous changes to KRASH are described in Reference 1 and include:

- Inclined rigid impact surface capability
- Internal computation of element linear stiffnesses
- Member directional stresses
- Internal computation of nonlinear curves
- Provisions for modeling earth scooping and plowing
- Input, output format changes.

As a result of the Task II effort, reported herein, additional refinements to KRASH have been made to provide more versatility and to facilitate its usage. Some of the refinements are briefly described in the following subsections. A detail description of all refinements is contained in Reference 6.

4.2.1 Symmetrical Model Coding

Program KRASH has been recoded to allow the input of model data for only one-half of the airplane for cases in which both the airplane is symmetrical (normally the case) and the impact condition is symmetric (no lateral, roll or yaw velocities and no initial roll or yaw attitude). Previously KRASH required input data for the full airplane, even for symmetrical impact conditions. For the symmetrical impact condition the program uses only the half airplane model.

Thus, either a more detailed model can be used as compared with a complete model within the limits of the allowable number of masses and beam elements, or the same modeling detail can be maintained as used in a complete model which will reduce computer run time and cost. As an example, for the single-engine high-wing airplanes modeled during Task II, the symmetrical half airplane model involved in a symmetrical impact can achieve the same modeling detail with 30 masses as that of the complete airplane model with 48 masses. The half airplane model requires more than half the masses of the complete airplane model because some of the masses are on the airplane plane of symmetry and are common to both models. In the above example, the symmetrical model yields a reduction in computer run time of 38 percent from that of the complete airplane model involved in the same symmetrical impact.

The basic program calculation scheme is the same as before, with the addition of certain boundary conditions if the symmetrical model option is exercised. The masses in the plane of symmetry are constrained to have no unsymmetrical motions (zero lateral displacement, yaw and roll). All other masses retain the full 6 degrees-of-freedom. The deflections of the transverse beams that connect a mass on the left side of the vehicle to an equal mass on the right side, are calculated by assuming that the right side mass behaves as the mirror image of the left side mass. The equations of motion are solved only for the left side mass; the state vector for the right side mass is then deduced from the left side results. Note that these "dummy" right side mass calculations are required only for those masses that are connected directly by transverse beams across the plane of symmetry.

In order to take full advantage of the symmetrical modeling capabilities, a subroutine called GENMOD has been added to KRASH that generates a full airplane model from the input data for a half-airplane model. Therefore, if an analysis is made of an unsymmetrical impact condition (e.g., yawed and rolled airplane), only the half airplane model data set need be input and the program will internally compute an expanded model that represents the complete airplane. The data for this complete airplane model is printed out, and the program

analyzes the time history response of the complete airplane model to the unsymmetrical impact condition.

The significance of GENMOD is that the user can always operate with the input for a half airplane model, even if unsymmetrical impact conditions are being analyzed. Thus, when model changes are made, only half of the data needs to be revised. Any changes made to the half airplane model are automatically changed on both sides of the airplane by GENMOD.

GENMOD is coded on the assumption that the airplane itself is symmetrical. If an unsymmetrical airplane must be analyzed (an unusual situation), then the program user must input data for a complete airplane.

4.2.2 Massless Node Capability

KRASH allows the user to define node points which are massless. These points are rigidly connected to mass points. With this capability the user can attach internal beams and external springs at points other than the c.g. of each lumped mass. This feature can be helpful in modeling seats and an engine on its mount.

While KRASH has the capability to model 80 masses, mass locations cannot be arbitrarily assigned, particularly in regions wherein light weight structure is located. Experience in modeling light fixed-wing airplane structure has indicated that reasonable care must be taken in selecting mass locations such that element response frequencies are compatible with the integration interval. The higher the element frequency, the smaller the integration interval (and higher the cost to perform an analysis) that is required to maintain a stable system. Two areas that are particularly vulnerable in this regard are:

- (1) The rigorous modeling of a finite mass (engine) which has several attach points
- (2) The rigorous modeling of a seat system.

Both systems involve a network of extremely light members (struts, seat legs) if all node points are to be presented. Figure 4-1 shows a typical tubular engine mount arrangement. The engine is a relatively large mass, attached to its mounting bed at 1 and 2 (one side shown). The tubular supporting structure, in turn, attaches to the firewall at points A and B (one side shown). Without the use of massless nodes, the engine has to be idealized as a lumped mass with the weight at its c.g., and the upper and lower mounts each must be modeled as internal beam members (dashed lines in Figure 4-1) which represent stiffness properties in six directions for more than one tubular member. However, with the use of massless nodes, each mount can be modeled directly at its appropriate attach point. For example, the engine mount arrangement can now be modeled with flexible members having the area properties of individual tubes connecting point A to 2 and B to 1 and 2 (Figure 4-1) for each side. Program KRASH contains rigid body equations which relate the motions of these nodes to those of the mass to which the nodes are attached (at c.g. of engine in this case).

In addition, nodes can be added at any point on the engine. For example, node point 3 (Figure 4-1) could represent an accelerometer location whose response is being monitored during a test or for which previous test data is available. Similarly nodes can be specified at points A and B on the firewall which are rigidly connected to a mass representation of the firewall at a more convenient location.

Figure 4-2 shows a typical pilot or copilot power adjustable seat configuration. The modeling arrangement without benefit of massless nodes is shown in Figure 4-3. Since the seat pan and floor structure in the region of the seat legs are relatively light weight, it is difficult to model them with much detail. Ideally 4 masses should represent the seat pan. However this causes a potential integration related instability problem requiring a compromise representing the seat legs with one member. This compromise requires representing the property of several floor members with one beam as well as idealizing the seat legs as another individual member.

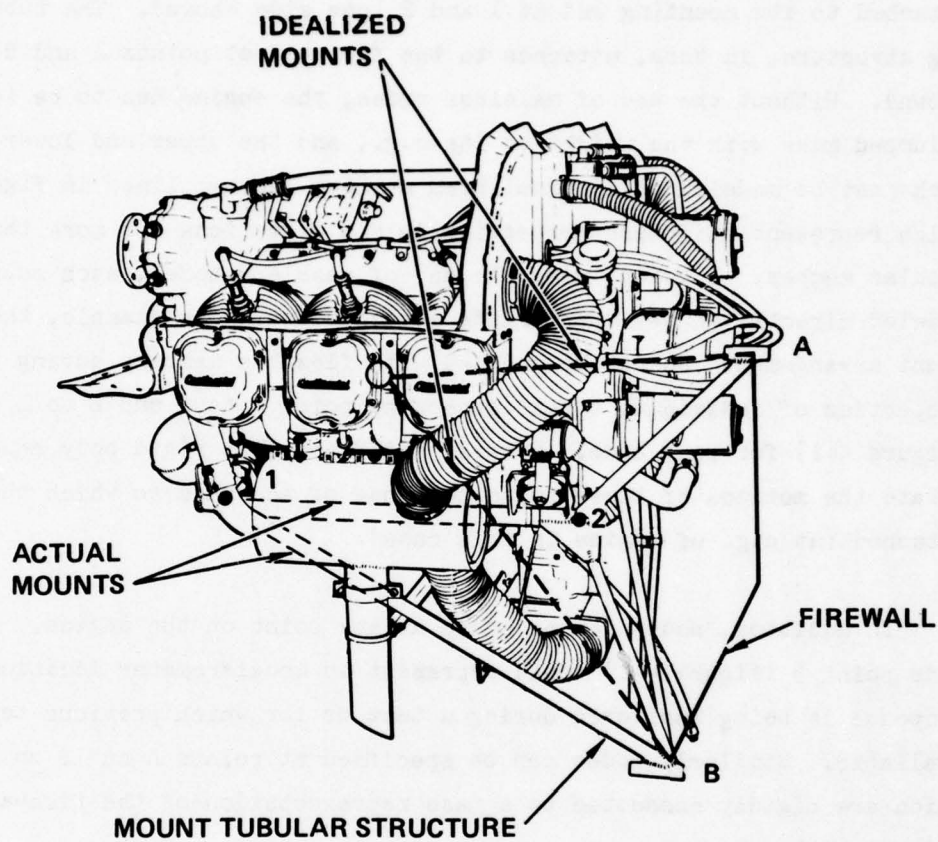


Figure 4-1. Typical Tubular Engine Mount Arrangement

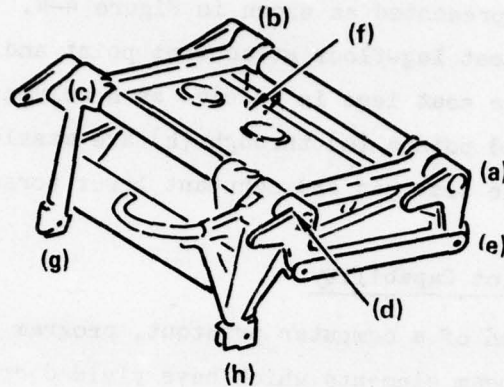


Figure 4-2. Typical Pilot or Copilot Power Adjustable Seat Configuration

— RIGID MEMBER
 - - - FLEXIBLE MEMBER

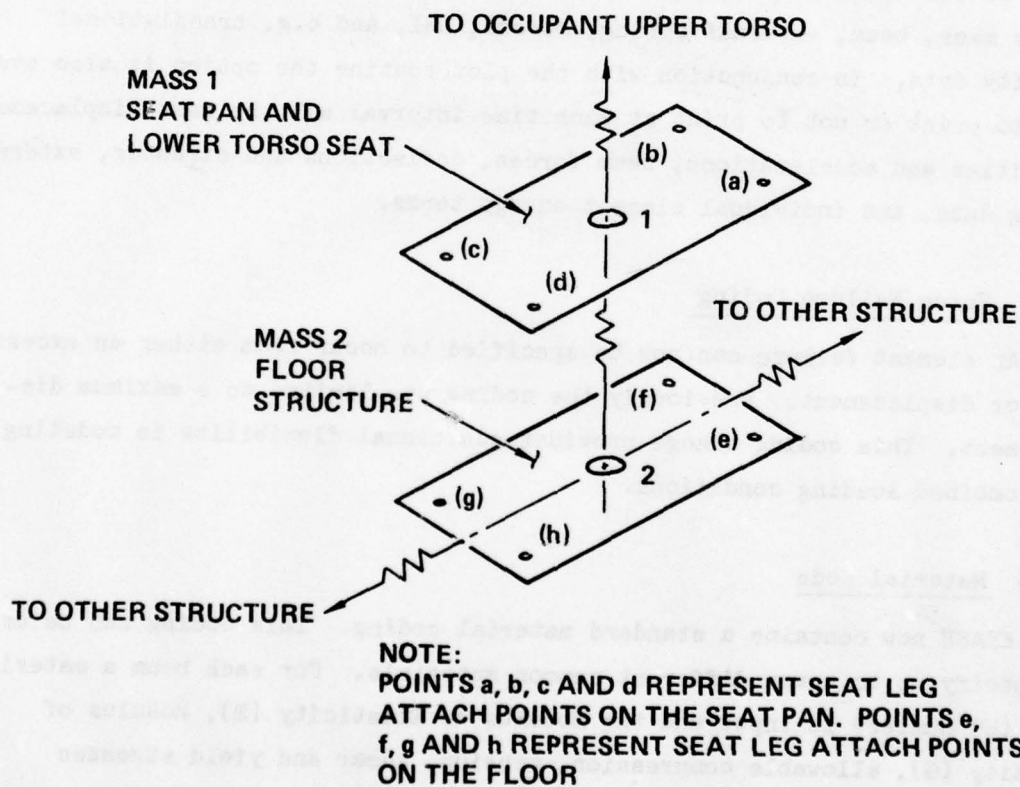


Figure 4-3. Model Arrangement in KRASH Without Massless Nodes

However, with the application of massless nodes, the occupant-seat-floor arrangement can be represented as shown in Figure 4-4. Massless nodes are established at each seat leg-floor attachment point and at each corner of the seat pan. Each of the seat legs is modeled as a column. Points 2 through 5 are mass locations and points (a) through (h) are massless node points. Mass point 1 represents the seat pan and occupant lower torso.

4.2.3 Summary and Plot Capability

At the conclusion of a computer printout, program KRASH now provides a summary of internal beam elements which have yielded or have ruptured. In addition to the element and direction of failure, the time of occurrence is noted. KRASH still provides the summary of energies as a function of time. In addition, the option is available to obtain summary prints and plots (3 per page) of the data that is normally printed at each time interval. This includes mass, beam, external spring, stress, DRI, and c.g. translational velocity data. In conjunction with the plot routine the option is also available to print or not to print at each time interval all the mass displacements, velocities and accelerations, beam forces, deflections and stresses, external spring data, and individual element energy terms.

4.2.4 Force Failure Coding

An element failure can now be specified to occur from either an excessive load or displacement. Previously the coding was limited to a maximum displacement. This coding change provides additional flexibility in modeling for combined loading conditions.

4.2.5 Material Code

KRASH now contains a standard material coding. This coding can be used to specify up to seven different common materials. For each beam a material code (MC number) is input and the Modulus of Elasticity (E), Modulus of Rigidity (G), allowable compression, tension, shear and yield stresses associated with the particular material are assigned to that beam. Currently the following material selections are:

— RIGID MEMBER
 ~ FLEXIBLE MEMBER

MASS 1 — SEAT PAN AND
 LOWER TORSO
 MASSES 2-4 — FLOOR STRUCTURE

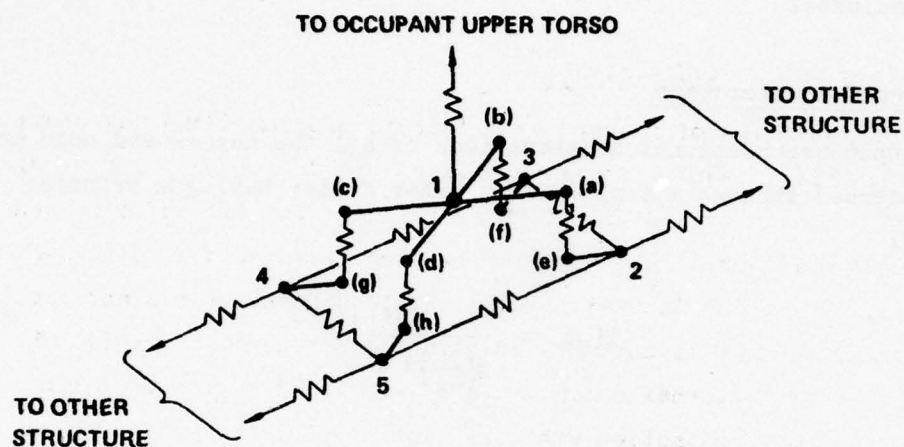


Figure 4-4. Model Arrangement in KRASH with Massless Nodes

1. 4130 Steel
2. 6150 Steel
3. Stainless 300
4. Aluminum 2024-T3
5. Aluminum 6061-T3
6. Cast Aluminum B195-T4
7. Low Modulus Material
8. Zero-Torsion Material
9. DRI-Spine (man)
10. DRI-Spine (DRI)

Material Numbers 7 through 10 do not represent particular materials but add modeling flexibility. A discussion regarding the use of material codes is available in References 6 and 7.

The program is coded so that the user can input additional materials not currently included.

4.2.6 Filtered Acceleration

The output translational accelerations of all the masses and node points are now processed through a simple first order filter having a transfer function of:

$$T(\omega) = \frac{1}{j\left(\frac{\omega}{\omega_c}\right) + 1}$$

where

$$j = \sqrt{-1}$$

$$\omega = \text{Response Frequency}$$

$$\omega_c = \text{Cutoff Frequency}$$

The cutoff frequency ($\omega_c/2\pi$) for this low pass filter is an input parameter. Generally a cutoff frequency less than 200 Hz will be specified. The analytical filter normally is not a first order filter, but rather a much higher order having 20 - 30 dB/octave slope above the cutoff frequency. For this reason, correlation with test data program cutoff frequency should be between 0.5 and 0.8 times the test filter frequency. Thus, KRASH output now includes both filtered and unfiltered acceleration time histories of the masses and node points. The filtered accelerations are employed only for output data; the integration of the equations of motion uses the unfiltered data as before.

4.2.7 Revised Stiffness and Damping Formulation

The calculation of the internal beam forces has been revised. Previously, the forces at one end of the beam were calculated utilizing the relative deflections of one end with respect to the other ($\Delta X_j - \Delta X_i$, etc.), and a 6 x 6 stiffness matrix for a cantilevered beam. Now the forces are calculated using the absolute deflections of each end of the beam and a 12 x 12 stiffness matrix. In the actual computations, the full 12 x 12 k matrix is not employed. If the coupled z- θ bending portion of the full 12 x 12 k matrix is expanded and terms recombined, it can be shown that the forces and moments at the i and j ends of the beam are given by

$$\begin{Bmatrix} \Delta F_{zi} \\ \Delta M_i \\ \Delta F_{zj} \\ \Delta M_j \end{Bmatrix} = \begin{bmatrix} -k_z & & -k_{z\theta} \\ k_{z\theta} & -k_{\theta/4} & 3k_{z\theta/4} \\ k_z & & k_{z\theta} \\ k_{z\theta} & k_{z\theta} & 3k_{\theta/4} \end{bmatrix} \begin{Bmatrix} \Delta z_j - \Delta z_i \\ \Delta \theta_j - \Delta \theta_i \\ \Delta \theta_j + \Delta \theta_i \end{Bmatrix}$$

The Δ 's indicate incremental forces and deflections for the numerical integration time interval being considered. k_z , $k_{z\theta}$ and k_{θ} are the terms of the 6 x 6 cantilever beam stiffness matrix originally used. Notice that the relative deflections and rotations are still used ($\Delta z_j - \Delta z_i$, $\Delta \theta_j - \Delta \theta_i$), but that the rotational sum terms ($\Delta \theta_j + \Delta \theta_i$) are also included. A similar equation is written for the coupled y - ψ bending, while the axial and torsional modes (x and ϕ) are uncoupled. All forces and moments are expressed in a beam axis coordinate system. This is now a time varying system whose x axis is always pointing from mass i to mass j.

The damping forces were previously calculated using a diagonalized damping coefficient matrix. They are now calculated as the product of the coupled stiffness matrix times the velocity vector times a damping constant $2\zeta / \omega_n$, where a separate natural frequency ω_n is used for each of the 6 directions. This model yields an approximation of structural type damping as opposed to the viscous damping previously used. The expression for damping

forces and moments is shown below for the couplex z and θ damping forces. A similar expression applies to the y, ψ terms. The axial and torsional terms are uncoupled.

$$\begin{Bmatrix} F'_{zDi} \\ M_{\theta Di} \\ F_{zDj} \\ M_{\theta Dj} \end{Bmatrix} = 2 \frac{\zeta_{ij}}{\omega_n} \begin{bmatrix} k \end{bmatrix} \begin{Bmatrix} \dot{z}_j - \dot{z}_i \\ \theta_j - \theta_i \\ \theta_j + \theta_i \end{Bmatrix}$$

where

ζ_{ij} = internal beam structural damping factor

ω_n = internal beam natural frequency

$\dot{z}, \dot{\theta}$ = beam end point velocities

subscript i = i^{th} end of beam

subscript j = j^{th} end of beam

subscript D = damping term

Strain and damping energy calculations have been revised to be consistent with the new strain and damping force calculation schemes.

4.2.8 Flexible Ground Coding

Provision is now made for modeling a simplified representation of soil characteristics. For each external spring, an elastic model of the soil surface may be specified. Separate soil characteristics for each external spring may be input. The linear ground load-deflection model is combined in series with the nonlinear external spring load-deflection model to arrive at a combined nonlinear characteristic curve. This is then used as before in the analysis. Unloading of the soil is not allowed. A separate plowing force may be specified in the input; this force acts in the direction of the ground drag force due to friction.

4.2.9 Restart

Program KRASH has been revised to allow the option of starting a case from an intermediate time cut from a previous case. For example, an analysis may be run from 0 to 150 milliseconds, and then restarted from the 50 millisecond point with revised data. The type of data changed would generally be the characteristics of nonlinear beam load-deflection curves that have not yet gone nonlinear, so that the early portion of the analysis would be valid even for the revised data. This feature allows the program user to explore the influence of parameter variations without having to rerun long sections of the analysis that remain unchanged. Considerable computer run time and cost may be saved with proper application of this capability.

4.2.10 Unsymmetrical Load-Deflection Curves

Coding has been added to KRASH to model internal beam elements which behave differently in tension and compression. Only the beam axial loads are treated in this fashion. The types of elements for which this provision is useful include seat belts and diagonal elements representing shear panels. Both of these are modeled with tension-only unsymmetrical elements in which compressive forces are not allowed. A deadband is also provided in the model for unsymmetrical beams. In the deadband region, the beam has zero load. This can be used to represent contact between two surfaces not originally touching, but which contact each other after large deformations during a crash. An example of this is the contact between the nose wheel and the lower fuselage after impact and failure of the nose gear. This can be modeled with a beam between the nose wheel and the fuselage, utilizing a compression-only element with deadband. Another application would be occupant to cabin structure contact.

4.2.11 Pinned-Fixed Beam End Conditions

The internal beam force/moment calculations have been extended to include all possible combinations of pinned and fixed end conditions. If both ends are pinned, both the lateral force and the moment about the pin axis are zero.

This capability was previously included in KRASH. With one beam end fixed and the other pinned, only the moment at the pinned end is zero. The proper equations for this pinned-fixed situation are now included in KRASH. In the analytical model for a high-wing airplane, this type of beam can be used for the inboard wing segment, which is normally pinned at the wing junction to the fuselage and fixed to the outboard segment of the wing.

SECTION 5

MATHEMATICAL MODEL DESCRIPTIONS

5.1 PROGRAM KRASH

Program KRASH, developed for helicopters under U.S. Army Contract (Reference 2), expanded to include fixed wing aircraft during Task I (Reference 1) and further refined during this Task II effort, is used to mathematically model the single-engine, high-wing airplanes used in the crash tests. Program KRASH is a digital computer program which predicts the response of vehicles to multidirectional crash environments. The program computes the time history of N interconnected masses. Each mass is allowed six degrees of freedom defined by inertial coordinates x_i, y_i, z_i , and Eulerian angles ϕ_i, θ_i, ψ_i , where $i = 1, 2, \dots, N$. Euler's equations of motion are written for each mass. The equations of motion are integrated numerically to obtain velocities, displacements and rotations. Gravity forces, internal forces and moments, external forces, and energies (kinetic, potential, strain, damping, crushing, and friction) are computed.

For small deflections a linear analysis is followed and for large deflections, a technique is used that allows general plastic deformation. The program provides for unloading and subsequent reloading along a linear elastic line. The current program and its application is described, in detail, in the KRASH User's Manual Volumes I and II (References 6 and 7). A brief description of Task II changes to KRASH is presented in Section 4, PROGRAM 'KRASH' REFINEMENTS.

5.2 AIRPLANE DESCRIPTION

The airplane modeled using KRASH and crash tested during Task II is shown in Figure 5-1 and described as follows:

- Single-engine, high-wing configuration
- Two sets of side-by-side seats (4 occupants)

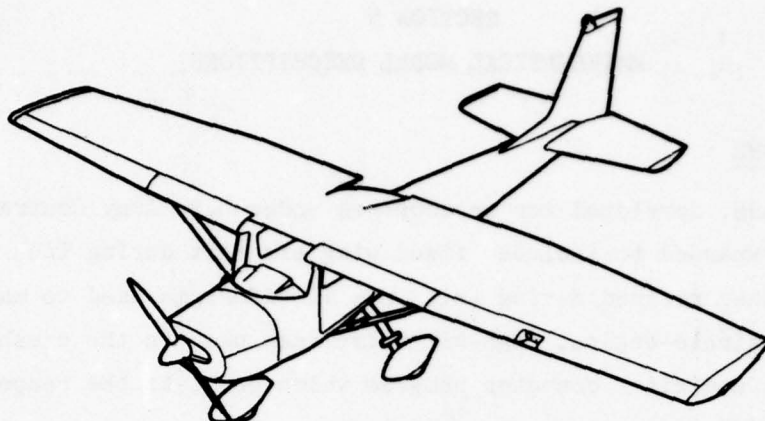


Figure 5-1. Single-Engine, High-Wing Airplane Configuration

- Used for training and business purposes
- Stall speed <57 mph (flaps up)
- Cruise speed (75 percent power), 125 mph
- Maximum takeoff weight, 2300 pounds
- Fuselage is semimonocoque construction. The wing is a box structure having two main spars and is braced with two midspan struts. The landing gear is a nonretractable tricycle type. The empennage is a cantilever design.
- Flight design load factors of +3.8 g's and -1.52 g's.
- Overall dimensions are: wing span = 434 inches
length = 323 inches
- The weight - c.g. envelope is presented in Figure 5-2.

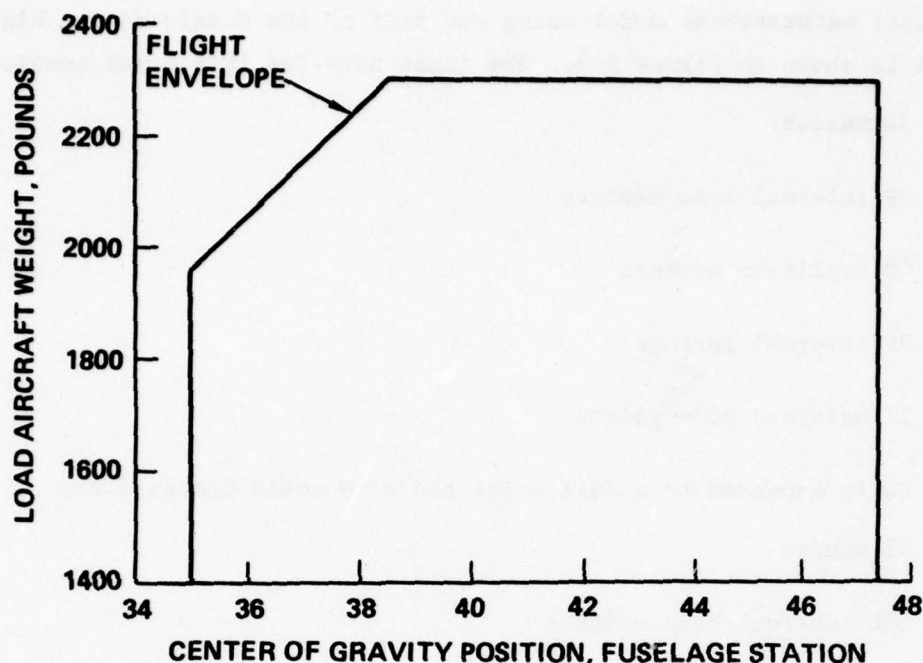


Figure 5-2. Weight and Center-of-Gravity Flight Envelope

5.3 CRASH TEST MATHEMATICAL MODELS

The same basic mathematical model is used for all four crash tests. The input data for the different test conditions varies due to test weight and c.g. position and initial impact velocities and attitudes. The member stiffness properties, the external spring properties, and the member load deformation and failure characteristics remain the same for each analytical test model. Program KRASH's symmetrical modeling capability permitted inputting data for only a half model of the airplane. In the analysis of Tests 1, 2 and 3 program KRASH generated a full model from the one half model input data which permitted accounting for the unsymmetrical impact conditions. As noted in Section 3 the actual impact conditions for Tests 1 and 2, while intended to be symmetrical, included roll and yaw due to the wind conditions. However Test 3 was performed with a large roll angle (~19 degrees). Test 4 impact conditions were essentially symmetrical which permitted the use of the symmetrical capability for both the geometry and the analysis. The basic

symmetrical mathematical model using one half of the single-engine high-wing airplane is shown in Figure 5-3. The input data for this model consists of:

- 30 masses
- 59 internal beam members
- 68 nonlinear members
- 22 external springs
- 17 massless node points

If fully expanded to a full model the size would increase to:

- 48 masses
- 100 internal beam members
- 118 nonlinear members
- 32 external springs
- 32 massless node points

Mass identification used in the math model is given in Table 5-1.

Table 5-2 presents the mass numbers and their counterparts on the opposite side of this airplane. (Masses located along the airplane centerline are not presented.) Massless node points are identified in Table 5-3 and the theory regarding massless nodes is provided in Reference 6.

The external springs represent the location at which structure or tires contact the ground. While an allowance of 32 such contact points is provided for in the math model shown in Figure 5-3, depending on the airplane attitude at impact, some of the springs will not contact the ground. The external spring data is obtained and/or developed from available data including tire and landing gear load-deflection curves, engine contact point stiffness

TABLE 5-1. MASS IDENTIFICATION FOR SINGLE-ENGINE, HIGH-WING AIRPLANE, LEFT SIDE

Mass Number	Masses Represented (Figure 5-3)
1	Nose Gear Unsprung Mass
2,3	Main Landing Gear Unsprung Region
23,5,7	Mid Fuselage Cabin
18,27,19,23,28,6	Floor Region
9,10	Firewall
25,11,12	Fuselage Aft Bulkhead
13	Engine
14	Nose Landing Gear Trunnion
8,15,17,16,5	Left Wing
3,24,30	Tail Unit
20	Seat (Shown in Figure 5-4)
21,22	Occupant, DRI (Shown in Figure 5-4)
26,29	Nose Gear Support Attachments at the Firewall
4	Main Gear Fuselage Attach Point

TABLE 5-2. CORRESPONDING MASS IDENTIFICATION FOR RIGHT SIDE

Left Side Mass No.	Right Side Mass No.
2	31
4,5	32,33
6,7	34,35
8,9	36,37
10,11,12	38,39,40
15,16,17	41,42,43
20	44
21,22	45,46
23	47
28	48

TABLE 5-3. MASSLESS NODE LOCATIONS AND REPRESENTATIONS

Location	Mass	Node	Location Represented
Engine	13	1	Forward mount attachment - left side
	13	2	Aft mount attachment - left side
	13	3	Engine accelerometer mount location
	13	4	Approximate location of engine contract point for forward rotation of failed nose gear
	13	5	Forward mount attachment - right side
	13	6	Aft mount attachment - right side
Main Landing Gear	4	1	Left main gear - bulkhead attachment
	19		Center Bulkhead attachment
	32	1	Right main gear - bulkhead attachment
Pilot Seat-Floor	6	1	Forward seat leg attach point, outboard
	18	1	Forward seat leg attach point, inboard
	28	1	Aft seat leg attach point, outboard
	27	1	Aft seat leg attach point, inboard
Copilot Seat-Floor	18	2	Forward seat leg attach point, inboard
	34	1	Forward seat leg attach point, outboard
	27	2	Aft seat leg attach point, inboard
	48	1	Aft seat leg attach point, outboard
Pilot Seat	20	1	Aft outboard corner
	20	2	Aft inboard corner
	20	3	Forward outboard corner
	20	4	Forward inboard corner
Copilot Seat	44	1	Aft outboard corner
	44	2	Aft inboard corner
	44	3	Forward outboard corner
	44	4	Forward inboard corner
Pilot	21	1	Upper torso attach point for shoulder harness
Copilot	45	1	Upper torso attach point for shoulder harness
Firewall	9	1	Engine attach point, lower, left side
	10	1	Engine attach point, upper, left side
	37	1	Engine attach point, lower, right side
	38	1	Engine attach point, upper, right side

characteristics, and substructure analysis and test. The external spring contact points for the model are located at masses 1, 2, 9, 29, 6, 18, 28, 27, 23, 19, 11, 25, 3, 30, 17 and the corresponding masses on the right side (see Table 5-2). The load-deflection characteristics of the springs are shown in Appendix D.

The internal beam elastic characteristics of the beam elements are obtained from representative cross section properties. The proper section area inertias are computed so that overall axial bending and torsional stiffnesses are represented. Discussions on typical representations of the cross sections are provided in the User's Manual (Reference 7).

The nonlinear characteristics of the beam elements are obtained from preliminary calculations of uncoupled loads and deflections which are modified to incorporate coupled behavior. KRASH prints the uncoupled data which is used as an initial input. Results from the initial computer runs representing Test 2 showed that the deflection at yield can be higher when coupled forces are present. Consequently, nonlinear deflection values have been revised in accordance with data obtained from the comparison of results from Test 2 analysis and the test itself. These nonlinear characteristics are now employed for the analysis of Tests 1, 2, 3 and 4. The member linear and nonlinear properties are presented in Appendix D.

Nonlinearities, as well as failures, are monitored in KRASH using stress, maximum force and maximum deflection checks. The data supporting this monitoring effort are obtained from information from design and criteria for the particular airplane being modeled. These data are contained in Appendix D.

The occupant-seat-restraint system is modeled in KRASH as shown in Figure 5-4. The occupant weight is divided between the upper torso, lower torso and floor in the ratio of 44, 44 and 12 percent, respectively (Reference 8). The floor mass including the occupants 12 percent contribution, half of the seat mass and the floor structure within the region of the occupant is

divided among four mass locations 6, 18, 27 and 28 (see Figure 5-3) which connect to nodes 6-1, 18-1, 27-1 and 28-1 (see Figure 5-4), respectively. In Figure 5-4 the lower torso weight and half the seat weight are included in the mass at location 20. The upper torso weight is placed at location 21. The properties for members 20-21 and 20-22 are selected to best represent the occupant. The frequency and damping ratio for member 20-21 is intended to properly model the dynamic response of the upper torso to the seat's excitation.

The mass at location 22 is the same as the upper torso (mass 21), but the damping and stiffness are slightly different. This is done to obtain the Dynamic Response Index (DRI) for mass 22 that will correlate well with statistical data. The important point is that mass 22 is driven by mass 20, but the interconnecting forces only drive mass 22, not mass 20. There is no feedback from mass 22 to mass 20, thus the DRI does not alter the rest of the system. The DRI is a measure of potential vertebrae compression injury and as such is a limited tool, particularly where other than vertical loads are involved. The theory for DRI modeling in KRASH is contained in Reference 6. Massless nodes 20-1, 20-2, 20-3 and 20-4 connect to massless nodes 28-1, 27-1, 6-1 and 18-1, respectively. The structural characteristics of the seat legs are contained in the data which describes each of these members. The seat is treated as a rigid body in that mass 20 is linked to each of its 4 node points (20-1, 20-2, 20-3 and 20-4) by rigid members. Massless node 21-1 in Figure 5-4 represents the contact point on the occupant's upper torso for the restraint harness. The harness in turn is connected to the upper structure of the airplane, node 5 (see Figure 5-3).

The math model shown in Figure 5-3 contains three unsymmetrical load-deflection elements. Two of the unsymmetrical elements connect each of the occupants' upper torso to the upper cabin structure to represent shoulder harnesses. These two members connect mass 21 to massless node 21-1 (pilot) and mass 45 to massless node 45-1 (copilot). Both members are tension members only. Another unsymmetrical element connects the nose gear lower mass to the engine underside structure and is a compression member which includes a 12 inch

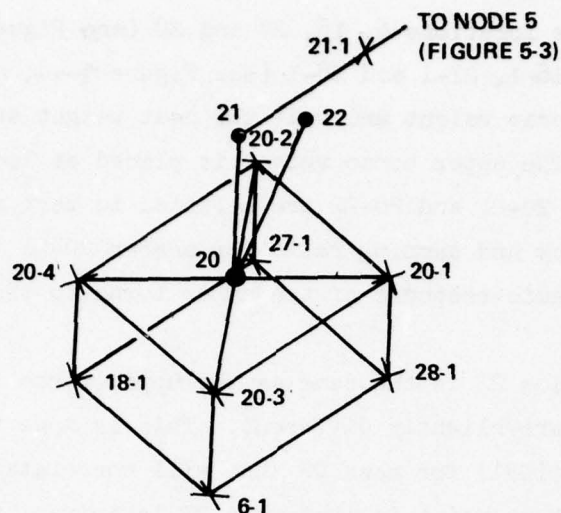


Figure 5-4. Occupant-Seat-Restraint System Model in KRASH

deadband. This member represents the post-failure contact between the nose gear and engine structure after failure of the nose gear lower support structure. The member will only be activated in cases like Test 2 where the nose gear rotates forward after failure of its lower support structure. In Tests 1, 3 and 4 the nose gear rotates aft and under the floor of the cabin area. The post-failure contact in this case is extended external spring acting at mass point 18. Thus, the post-failure interference of the nose gear after failure is accounted for.

The math model contains pin-pin beam elements to represent the wing column struts and pin-fixed elements to elements to represent the wing to fuselage front and rear spar attachments.

The high angle of attack used in Test 2 along with a velocity of 50 mph resulted in an aerodynamic lift component which was not present in the other tests. Because of the spoiler mounted on the upper surface, total lift was not attained. In order to represent the Test 2 conditions properly in the analysis, a lift term based on the aerodynamics involved in the test (a

velocity of 50 mph and an angle of attack of 25 degrees) was determined. The resulting lift force which was used in analysis of Test 2 was 0.65 times the airplane weight acting at about 15 percent of the wing chord (F.S. 38.15) and distributed at each wing location as follows:

- Masses 5, 16, 36 and 42 - 0.03 times airplane weight
- Masses 8, 15, 33 and 41 - 0.11 times airplane weight
- Masses 17 and 43 - 0.045 times airplane weight

Unlike the previous three crash tests, Crash Test 4 involved an impact on a soil terrain. The behavior of the soil under impact is modeled in the following manner:

- The pressure acting on the airplane is related to the average CBR value of the soil in the impact area using the curve shown in Figure 5-5. The curve shown in Figure 5-5 is obtained from Reference 9.
- The maximum area of structure penetration is estimated from the geometry of the forward fuselage region.
- The average force is obtained by multiplying the pressure by the area and dividing by two.
- The soil flexibility is then obtained by dividing the measured ground penetration (18 inches) by the average force. The resultant flexibility of .00036 in/lb is then an input to the program.

A summary comparison of the math models used for the four crash tests is shown in Table 5-4.

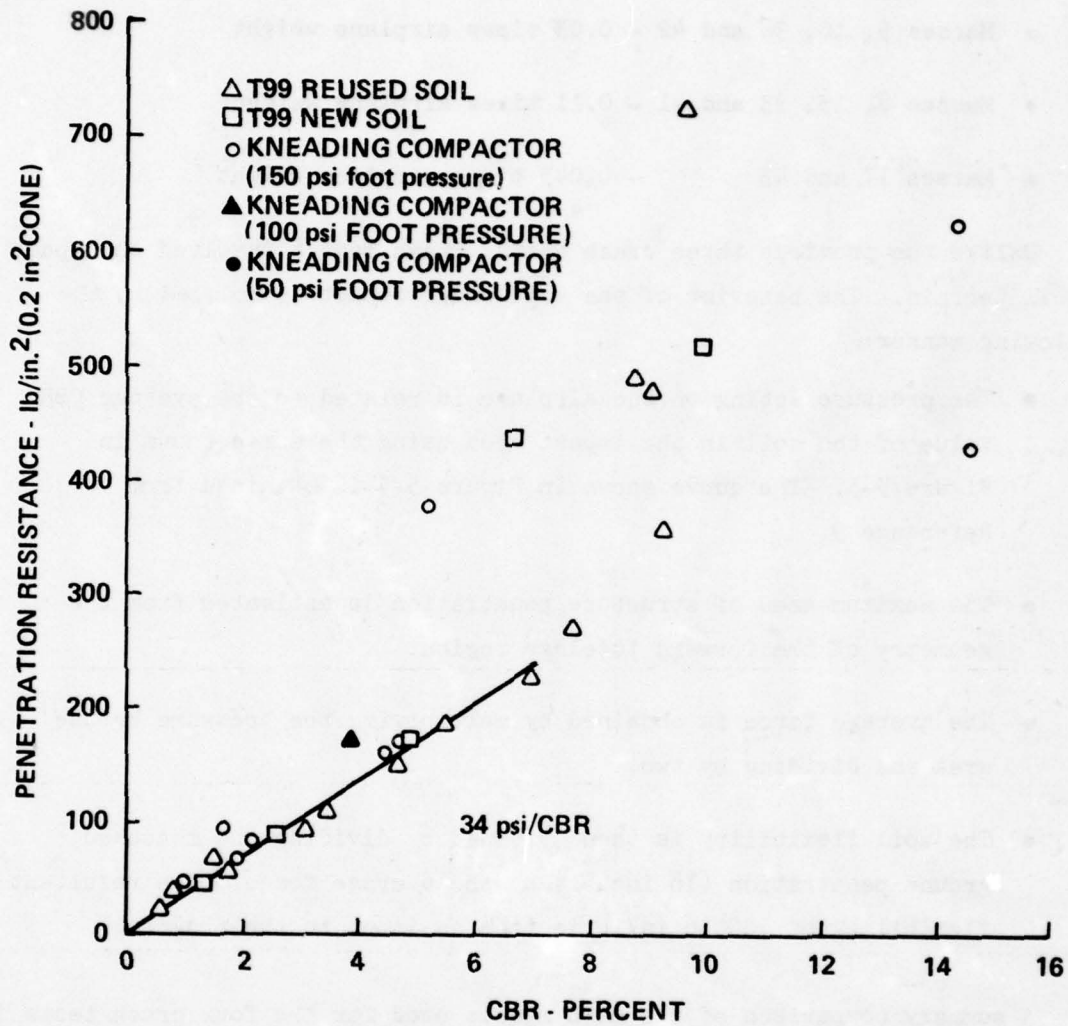


Figure 5-5. Relationship of Airfield Cone Penetration Resistance to CBR on Buckshot Clay (Reference 9)

TABLE 5-4. SUMMARY OF MATH MODELS

Full (F) or Half-Model (H) ^(a)	TEST 1 F	TEST 2 F	TEST 3 F	TEST 4 H
Number of:				
Masses	48	48	48	30
Node Points	32	32	32	17
External Springs	32	32	32	22
Linear Beams	100	100	100	59
Nonlinear Beams	118	118	118	68
DRI Elements	2	2	2	1
Pin-Pin Beams	2	2	2	1
Pin-Fixed Beams	4	4	4	2
Unsymmetrical Elements	7	7	7	4
Lift/Weight Ratio	0	.65	0	0
Impact Conditions:				
Vertical Velocity (fps)	42.3	21.8	48.7	43.4
Longitudinal Velocity (fps)	68.9	71.3	70.	69.6
Pitch Angle (degrees)	-30.	13.5	-39.4	-34.8
Roll Angle (degrees)	4.1	3.3	18.7	0.
Yaw Angle (degrees)	-3.3	-11.5	-7.9	0.
Pitch Rate (degrees/second)	46.4	6.9	14.3	18.2
Weight (lb)	2370	2390	2370	2370
C.G. Position (Fuselage Station-in)	44.1	47.2	44.1	44.1
Inertias (lb-in-sec ²)				
Roll	1.84 E04	1.84 E04	1.84 E04	1.84 E04
Pitch	1.77 E04	2.10 E04	1.77 E04	1.77 E04
Yaw	2.96 E04	3.25 E04	2.96 E04	2.96 E04

(a) Refers to the analysis. Airplane data input as a half model in all four cases with the program computing full airplane data for Tests 1, 2 and 3.

SECTION 6

ANALYSIS AND CORRELATION

6.1 ^{*} TEST 1 ANALYSIS AND TEST COMPARISONS

6.1.1 Sequence of Events

The analytical results are obtained using the 48 mass 100 member model described in Section 5.1. The analysis was performed for .120 seconds beyond impact. During this time the significant crash events have occurred. In addition, beyond .120 second after impact the drifting of data channels makes the validity of many of the test traces questionable. The sequence of events as obtained by analysis versus that obtained from film analysis is shown in Table 6-1. From Table 6-1 it can be seen that the time of occurrence of events obtained by analysis generally compares favorable with the test results obtained from film analysis. The analysis indicates a buckling of the wing column struts which is not evident in the films of the test nor in the post test observations of the structure. The analysis shows a nose gear support failure, a right main landing gear bulkhead failure and a buckling of the tail-cone, all within 13 milliseconds of their noted occurrences during the test.

The change in airplane c.g. translational velocity, longitudinal and vertical, as obtained by analysis is shown in Figure 6-1. The camera angles make it difficult to obtain a direct comparison of the test and analysis velocity histories. The analysis shows that the vertical component of velocity reaches zero at approximately .120 seconds. This is approximately .020 seconds earlier than estimated from the film analysis. For reference, several film estimated velocities are noted. In general the analytical trend shows energy being absorbed somewhat earlier than indicated in the test velocity changes. However, the trends are consistent in that

* For brevity crash tests are referred to as tests throughout this section.

TABLE 6-1. COMPARISON OF ANALYSIS AND TEST SEQUENCES, TEST 1

Sequence	Time - Seconds (a)	
	Analysis	Test
• Nose Gear Impact	0	0
• Nose Gear Support Structure Failure	.08-.011 (b)	.012
• Engine Lower Structure Impact	.051	.034
• Engine Spinner Impact	.057	.046
• Lower Firewall (left side) Impact	.054	.050
• Right Main Landing Gear (M.L.G.) Tire Impact	.066	.060
• Right Main Landing Gear Bulkhead Failure	.095	.082
• Left Main Gear Tire Impact	.075	.080
• Forward Seat Leg Failure (Pilot)	.086-.090	.095
• Maximum Left MLG Tire Deflection	.090	.100
• Tailcone Yielding	.102	.108
(a) After initial impact		
(b) Lower support followed by upper support attachment failure		

the vertical velocity undergoes a large magnitude change from approximately .060 seconds to .120 seconds after impact. The longitudinal velocity change is more gradual, reflecting the effect of friction between the ground and structure.

The analytical results provide data regarding the temporal and spatial distribution of energy. Figure 6-2 shows the total energy and its components (kinetic, potential, strain, damping, crushing and friction) as a function of time. At impact, kinetic energy (94.3 percent) and potential energy (5.7 percent) account for all the energy. Thereafter the energy is redistributed in the form of strain, structural damping, crushing and ground friction. Table 6-2 shows the distribution of the energy components as a percentage of the total energy. Included in Table 6-2 is the maximum percent value and its time of occurrence as well as the percent of total

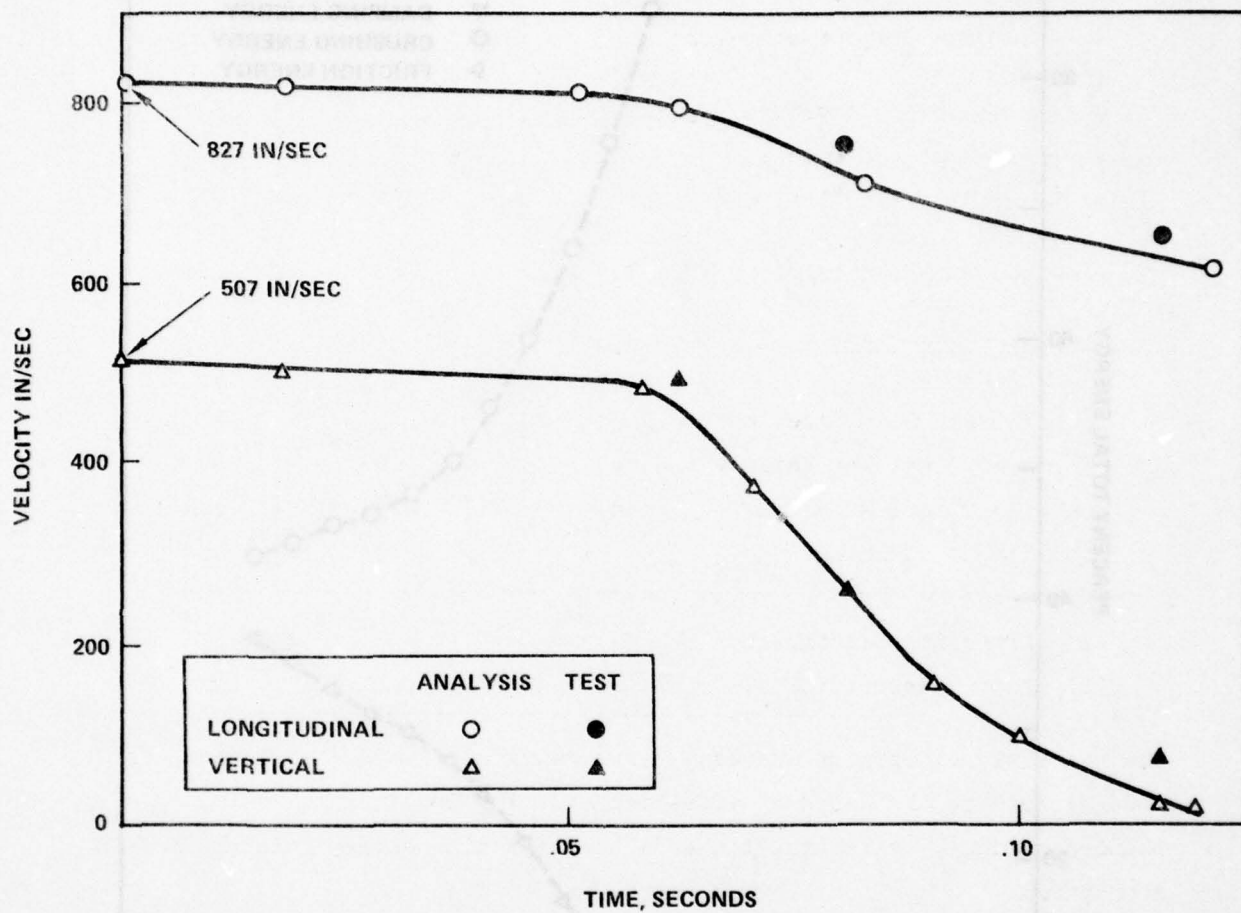


Figure 6-1. Comparison of Analysis and Test Longitudinal and Vertical Velocities Versus Time, Test 1.

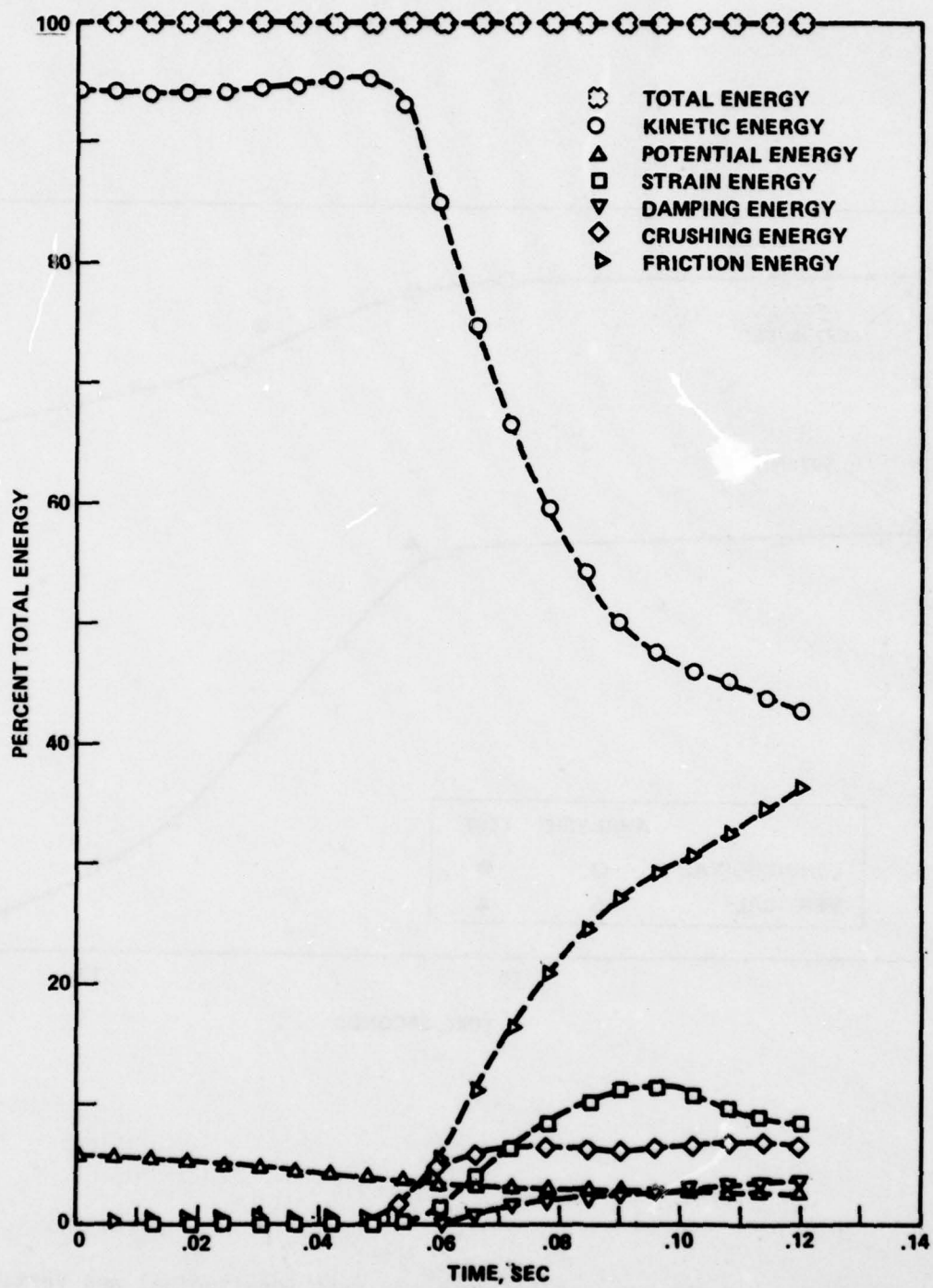


Figure 6-2. Total Energy and Energy Components Obtained by Analysis, Test 1

TABLE 6-2. SUMMARY OF ENERGY COMPONENTS OBTAINED BY ANALYSIS, TEST 1

Energy Component	Peak Percent Value and Time of Occurrence		Percent Value at Time = 0.120 Seconds
	Percent	Time ^(a)	
Strain	11.42	0.093	8.37
Damping	3.74	0.120	3.74
Crushing	6.96	0.114	6.25
Friction	36.08	0.120	36.08
(a) Time in seconds.			

energy at the conclusion of the analysis. The strain energy peaks at approximately .093 seconds after impact. However, from .078 to .120 seconds it is within 27 percent of its peak value. The crushing energy remains nearly constant from .063 seconds to .120 seconds. During this time various regions of structure are in contact with the ground. While some crushable structure is unloading other structures are still deforming. Damping and friction energies continually increase since they are dissipative processes and therefore not reversible. These energy percentages would increase as the airplane slides out to rest. Potential energy, which reflects the height above the ground of the individual masses, decreases slightly to 2.6 percent of the total. The potential energy would not be expected to change further since the airplane is sliding and maintains its position relative to the ground until its forward motion is arrested. The total energy at the conclusion of the analysis is 100.11 percent. A deviation of only .11 percent in energy has occurred through .120 seconds of crash analysis indicating a relatively stable math model is being used. Figure 6-3 shows the percentage distribution of strain energy as a function of location in the airplane and time. In addition the total strain energy is depicted. Immediately after impact, what little strain energy is absorbed by the structure is primarily

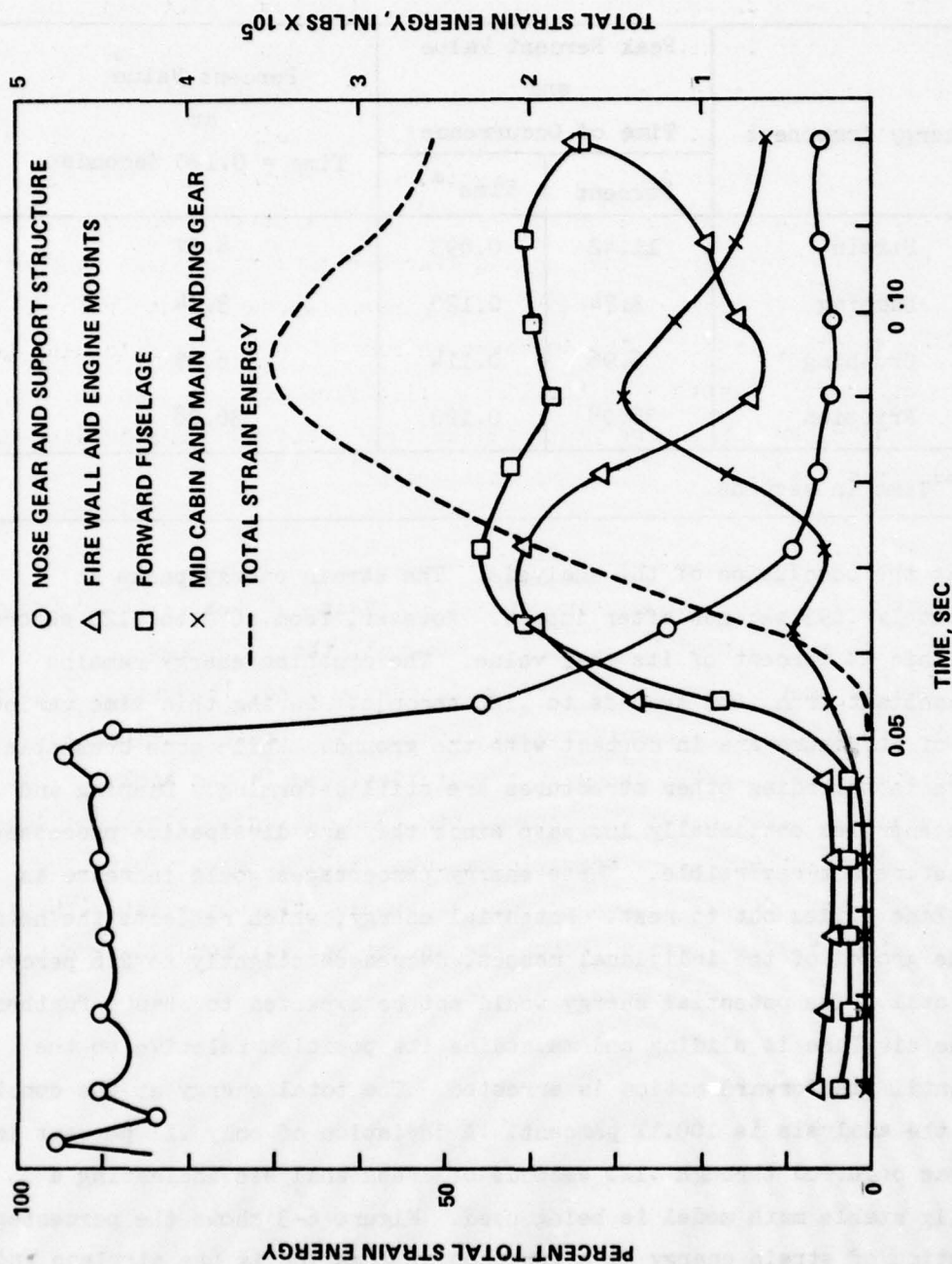


Figure 6-3. Strain Energy Distribution Histories Obtained by Analysis, Text 1

taken out by the nose gear and its supporting structure. Between .012 and .040 seconds after impact the nose gear support structure has ruptured and no other structure is in contact with the ground. As the lower forward fuselage structure contacts the ground the total strain energy increases rapidly. The deformations of the firewall, engine mounts and forward fuselage structure start to account for most of the strain energy at time = .060 and on. Thereafter, the landing gear contacts the ground and the strain energy continues to increase until a peak is reached at approximately .093 seconds after impact. The increase in mid cabin and main landing gear strain energy is noticeable in the time period from .070 seconds on. The events as noted by the energy plots appear consistent with the results as obtained from analysis of films and photographs.

6.1.2 Deflections, Deformations and Failures

Table 6-3 shows a comparison between analysis and test with regard to failures. As a result of the Test 1 impact, all the seat legs sheared or pulled away from the floor rails, the tailcone buckled, the engine mounts buckled, the nose gear supports failed and the right main landing gear bulkhead bolt failed. All these events are depicted in the analysis. The analysis also shows the two wing column struts buckling. This event does not occur during the test. The engine mounts yield at approximately .061 seconds and after. No comparison can be made of this event with film analysis since the cowl was covering the engine and its mount during the test.

TABLE 6-3. COMPARISON OF ANALYSIS AND TEST FAILURES, TEST 1

Location	Test 1	
	Analysis	Test
Seat Leg Failures		
Pilot Forward	Yes	Yes
Pilot Rear	Yes ^(b)	Yes
Copilot Forward	Yes	Yes
Copilot Rear	Yes ^(b)	Yes ^(a)
Tailcone Yield or Failure	Yes	Yes
Nose Gear Failures		
Lower Support	Yes	Yes
Upper Support	Yes	Yes
Main Landing Gear Failures		
Gear	No	No
Support Structure	Yes	Yes
Wing Spar Failures		
Left Wing	No	No
Right Wing	No	No
Wing Column Strut Failures		
Left Wing	Yes	No
Right Wing	Yes	No
Engine Mounts Buckle	Yes	Yes
<p>(a) Pulls loose from track.</p> <p>(b) Based on stress ratio ≥ 1.25 for either inboard or outboard leg.</p>		

Table 6-4 shows the analysis results with regard to internal member deflections. The analysis shows that the engine mounts deflect axially between 2 and 3 inches. A deflection of 4 inches or more is required before contact is made between the engine housing and firewall. Observations of the vehicle after the test indicated that no contact between the engine structure and the firewall occurred. The forward fuselage compression represented by member 7-9 (Figure 5-3) shows a peak axial deflection of 5.2 inches. An axial deflection of 4.7 inches (vertical compression of member 9-10) is reached at the firewall. Deflections at the landing gear are consistent with the deflections observed from film analysis. However, the deflections at the door posts are generally lower than observed for the test. Figure 6-4 shows a comparison of the forward fuselage and occupant cabin regions as obtained by analysis and estimated from test data for the airplane in its post crash position. For reference the pretest position of the cabin regions is also shown in Figure 6-4. The analysis depicts the deformation in the forward region but underpredicts the damage in the mid cabin region, particularly at the rear door post.

Table 6-5 shows the results of the analysis with regard to maximum deflections experienced by the external springs. The springs represent areas which can contact the ground. Analytically obtained tire deflections compare favorably with test results. However, estimates of deflections in or near the region represented by the structure are more difficult, due to the nature of the distortion that takes place. Also in a dynamic situation the structure springs back after reaching a peak deflection. No film analysis could be made of the peak deflections, only estimates from the post crash condition.

6.1.3 Structure Responses

Figures 6-5 through 6-9 show comparisons of analysis and test structure responses at various locations throughout the airplane. Table 6-6 summarizes the results. The engine responses are compared in Figure 6-5. Typically the test and analysis data both show one major response. The analysis response shape is more broadband than the test response. The analysis peak values are approximately 27 to 32 percent higher than the test values and occur from .016 to .020 seconds later than noted in the test data. The floor

TABLE 6-4. MEMBER DEFLECTIONS OBTAINED BY ANALYSIS, TEST 1

Location	Element Node Points i-j(a)	Deflection, Inches
<u>Axial</u>		
Engine Mounts	9-13,10-13,13-37,13-38	2.0 - 3.2
Forward Fuselage	6-9,7-9,34-37,35-37	3.1 - 5.2
Firewall (Vertical)	9-10,37-38	4.7
<u>Bending</u>		
Landing Gears	2-4,31-32	4.3 - 8.4
Forward Door Post - Lower	6-7,34-35	5.7
Forward Door Post - Upper	7-8,35-36	3.3
Rear Door Post - Lower	4-23,32-47	2.0
Rear Door Post - Upper	5-23,33-47	5.6
Firewall	9-10,37-38	9.1
Tunnel Structure	18-26,18-29	12.8 - 13.1
Forward Fuselage	6-9,7-10,34-37,35-37	10.0 - 13.0
(a) See Math Model Description, Figure 5-3. Tables 5-1 and 5-2.		

response comparisons are taken at a forward (F.S. 127), mid (F.S. 60) and aft (F.S. 90-108) location. The response histories are shown in Figures 6-6, 6-7 and 6-8, respectively. Unlike the engine response the floor accelerations exhibit more oscillatory motion. Disregarding one sharp pulse observed in the test data at F.S. 27 and a relatively high analytical peak at F.S. 60, the analysis and test peak values agree within ± 22 percent. The times of occurrence of peak values generally agree within a few milliseconds to .025 seconds. Figure 6-9 shows a comparison of wing responses. In the vertical direction the data agrees within 8 percent and from .013 to .022 seconds. In the longitudinal direction the data agrees within 46 percent and .015 seconds. However, the test data polarity may be opposite that shown.

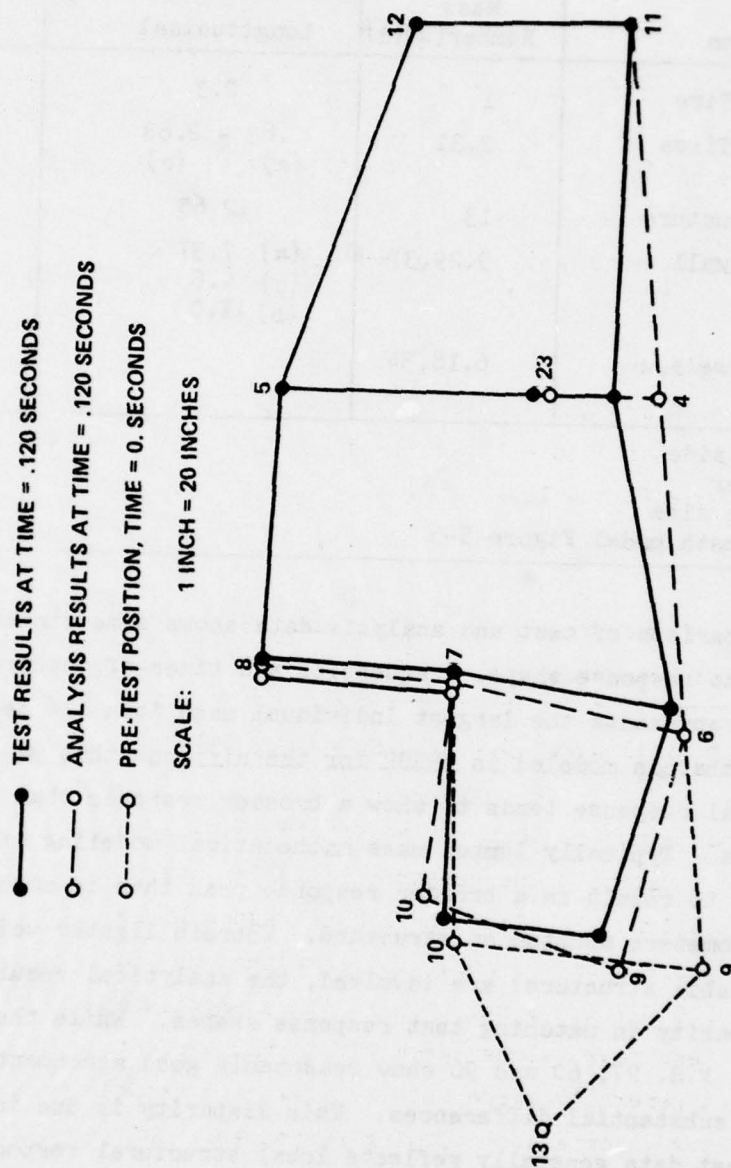


Figure 6-4. Comparison of Analysis and Test Cabin Deformations

TABLE 6-5. MAXIMUM EXTERNAL SPRING DEFLECTIONS OBTAINED BY ANALYSIS, TEST 1

Location	Mass Number(s)(d)	Deflection, Inches	
		Longitudinal	Vertical
Nose Gear Tire	1	2.3	3.87
Main Gear Tires	2,31	.83 - 2.83 (a) (c)	4.73 (a) (c)
Engine Structure	13	12.65	7.93
Lower Firewall	9,29,37	(a) 7.37 (c) 9.6 (b) 11.0	1.8 2.8 5.4
Forward Fuselage	6,18,34		5.26(b) 1.98(c)
(a) Left side (b) Center (c) Right side (d) See math model Figure 5-3			

The comparison of test and analysis data shows some striking similarities with regard to response shape, frequencies and times of occurrences. The engine mass represents the largest individual mass item (16 percent of the total mass) that is modeled in KRASH for the airplane that was crash tested. The analytical response tends to show a broader response than is evident in the test data. Typically lumped mass mathematical modeling of a distributed system tends to result in a broader response peak than is normally obtained from accelerometers mounted on structure. Wherein lighter weight items (floor and cabin structure) are involved, the analytical results tend to show greater disparity in matching test response shapes. While the overall responses at F.S. 27, 60 and 90 show reasonably good agreement, their response shapes show substantial differences. This disparity is due in part to the fact that test data generally reflects local structural responses which inherently exhibit higher frequencies. The longitudinal response at F.S. 90 may best illustrate this point. While the peak response values compare very favorably and the times of occurrence agree within .005 to .025 seconds, the response shapes differ substantially. The analysis is wide band

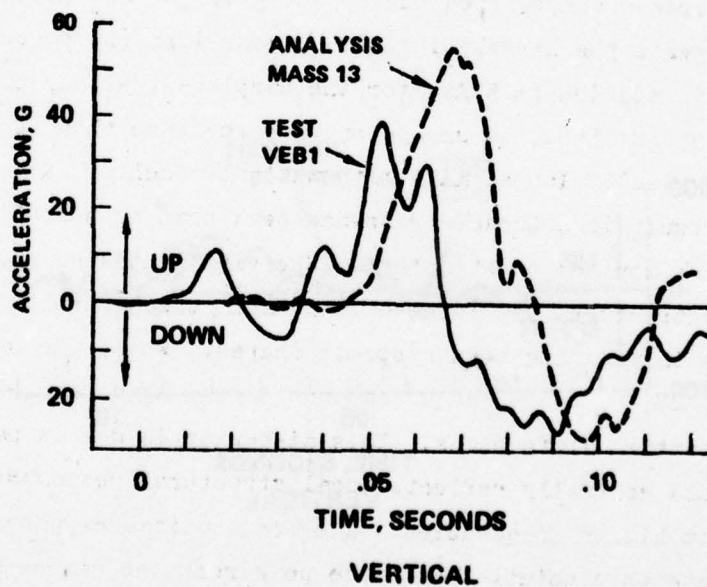
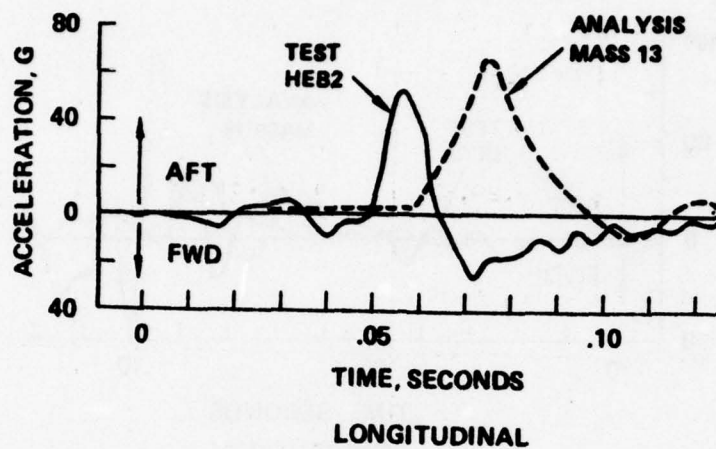


Figure 6-5. Comparison of Analysis and Test Engine Vertical and Longitudinal Accelerations, Test 1

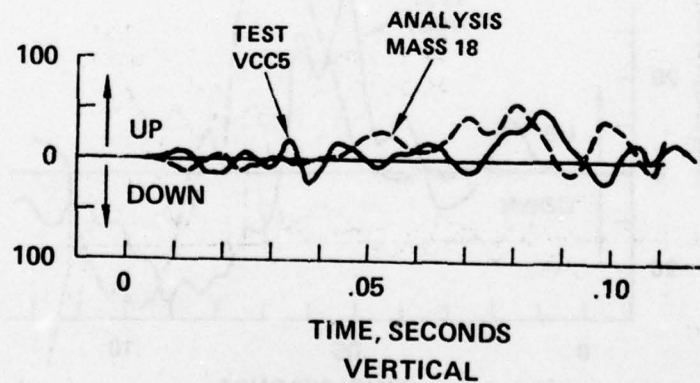
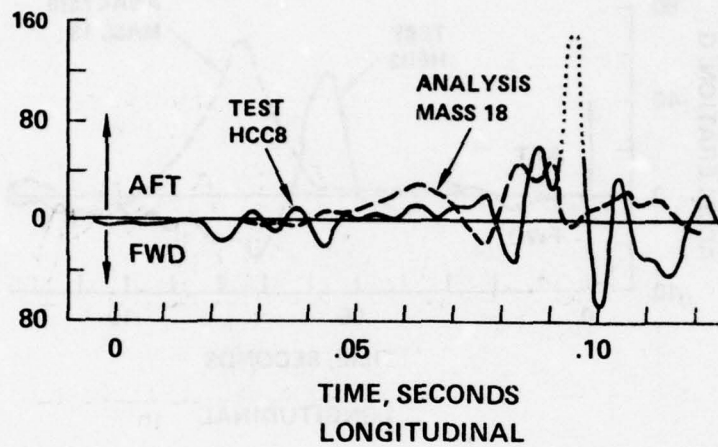


Figure 6-6. Comparison of Analysis and Test Floor Vertical and Longitudinal Accelerations, F.S. 27, Test 1

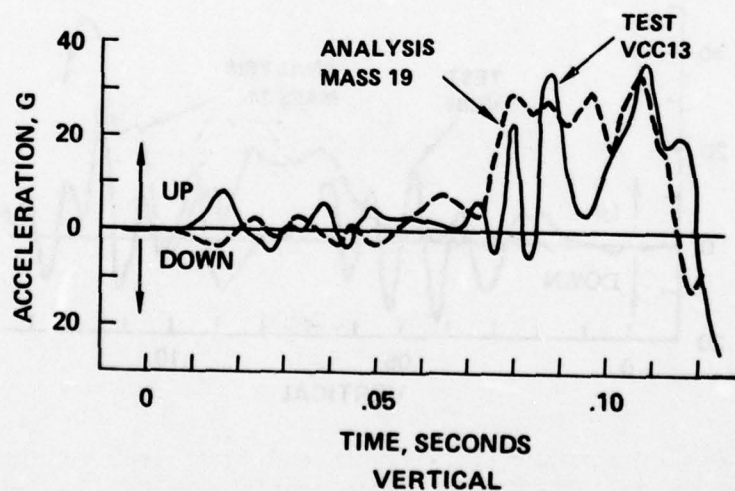
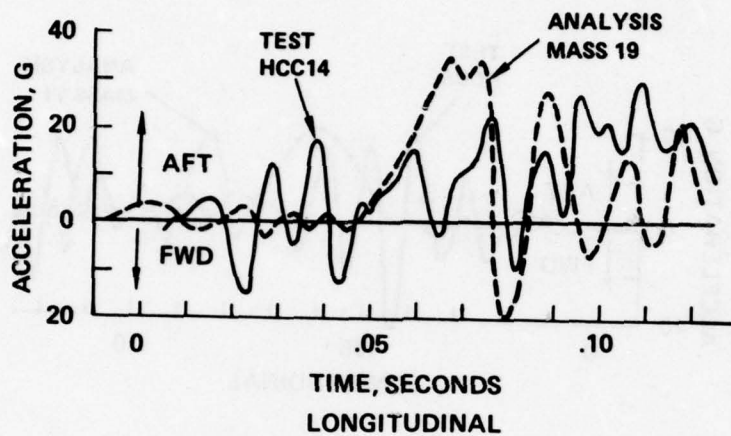


Figure 6-7. Comparison of Analysis and Test Floor Vertical and Longitudinal Accelerations. F.S. 60, Test 1

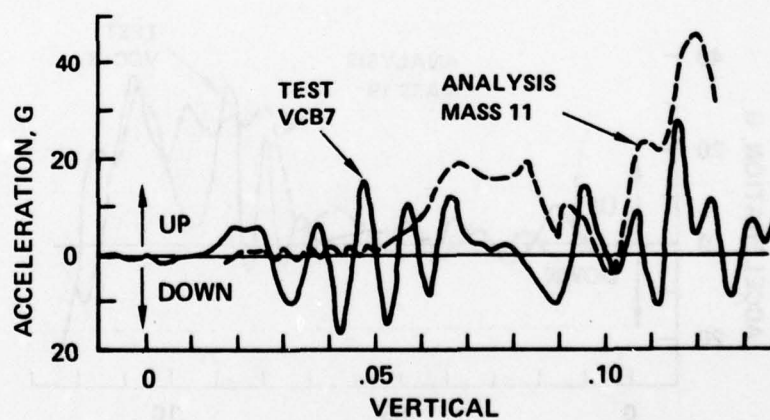
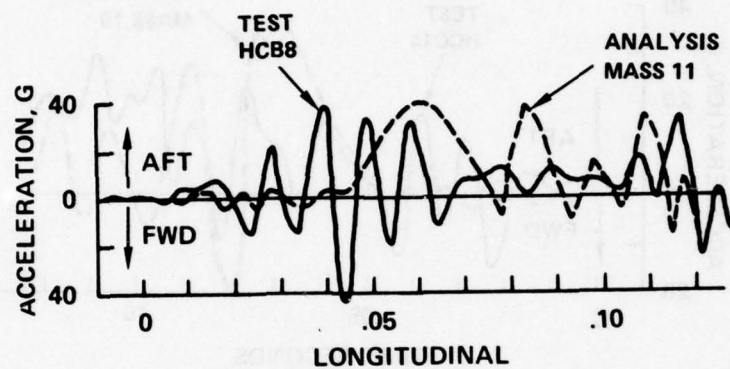


Figure 6-8. Comparison of Analysis and Test Floor Vertical and Longitudinal Accelerations, F.S. 90-108, Test 1

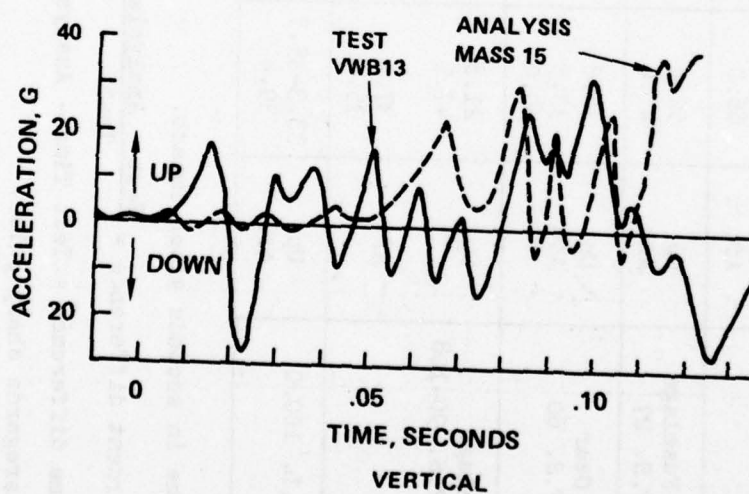
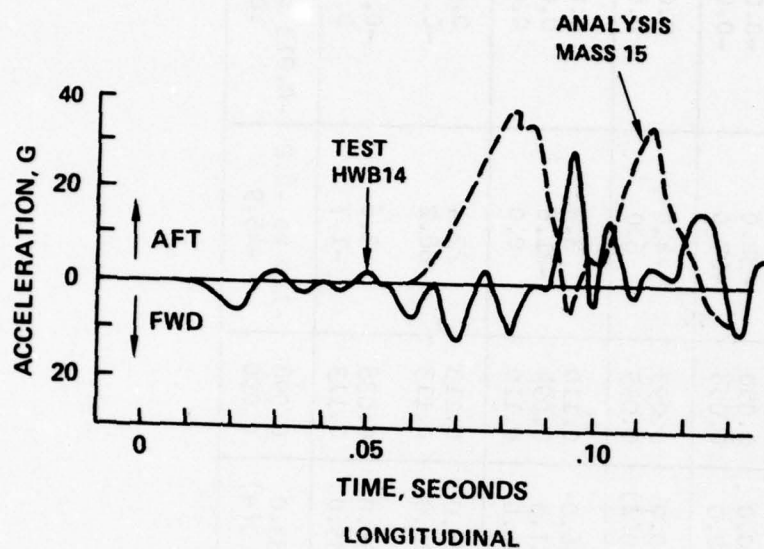


Figure 6-9. Comparison of Analysis and Test Wing Vertical and Longitudinal Accelerations. Test 1

TABLE 6-6. COMPARISON OF ANALYSIS AND TEST STRUCTURE RESPONSES, TEST 1

Location	Direction	Analysis		Test		Percent Difference (b)	Time Difference (c)
		G-Peak	Time (a)	G-Peak	Time (a)		
Engine	Up	52.8	0.066	40.0	0.050	-32.0	-0.016
	Aft	66.0	0.078	52.0	0.058	-27.0	-0.020
Forward Fuselage Floor, F.S. 27	Up	52.0	0.087	50.0	0.095	-4.0	0.008
	Aft	47.0	0.090	50.0(d)	0.095	6.0	0.005
Landing Gear Floor, F.S. 60	Up	34.8	0.108	36.0	0.110	3.3	0.002
	Aft	33.5	0.066	27.5	0.094	-21.8	0.028
		30.0	0.084	30.0	0.110	0.0	0.026
Aft Fuselage Floor, F.S. 90-108	Up	21.8	0.108	28.0	0.113	22.4	0.005
	Aft	47.1	0.114	28.0	0.113	-68.2	-0.001
Wing. B.L. 100.0	Up	37.3	0.067	36.0	0.038	-3.6	-0.025
		35.6	0.108	35.0	0.113	-1.7	0.005
	Up	33.3-35.7	0.111-0.120	33.0	0.098	-1.0 to -8.2	-0.013 to -0.022
	Aft	39.4	0.075	27.0(e)	0.090	-45.9	.015

(a) Time in seconds after impact.

(b) Percent difference = $\frac{\text{Test} - \text{Analysis}}{\text{Test}} \times 100$

(c) Time difference = Test Time - Analysis Time

(d) Disregards sharp pulse.

(e) Polarity may be reversed.

exhibiting a frequency response of approximately 20 Hz, while the test data is more oscillatory showing a frequency response of around 100 Hz.

Another difference between the test and analysis results is the type of filters employed by both. The analysis uses a 70 Hz low pass filter which is down 3 db at 70 Hz and has a slope of 6 DB/octave above this point. The test data is reduced with a 100 Hz filter with a slope of 20-30 DB/octave above 100 Hz. While the analysis attempts to compensate for the differences in filter high frequency rejection by using a lower cutoff frequency, the two filters are sufficiently different to distort the history comparisons involving high frequency response components.

6.1.4 Occupant Response

The occupant-seat-restraint system is modeled in KRASH as described in Section 5.1 and is shown in Figure 5-4. The modeling in KRASH is not intended to be as elaborate or detailed as the modeling of an occupant-seat-restraint system such as that described in Reference 8. However, KRASH does provide data which can be useful in the evaluation of the occupants' potential for survival during a crash condition. Included in the available data are floor responses, DRI responses, member rupture information, energy absorption distribution, cabin deformations and stress monitoring. Figure 6-10 shows the DRI responses for the pilot and copilot. The DRI's have maximum values of 8.8 and 9.9 for the pilot and copilot, respectively. The peak values occur approximately .102 seconds after impact. Based on data presented in Reference 11, there is little or no probability that a spinal vertebrae compression injury would occur with the type of airplane and crash impact conditions involved. The low DRI values indicating little likelihood of a spinal compression injury agrees in general with the measured acceleration responses which are substantially below the threshold of tolerance for occupants as noted in Section 3.1.4.

Figure 6-11 shows the pilot and copilot lower torso vertical acceleration responses obtained from the analysis as well as the pilot and copilot pelvic vertical acceleration responses measured during the test. The peak values and times of occurrence are noted in Table 6-7.

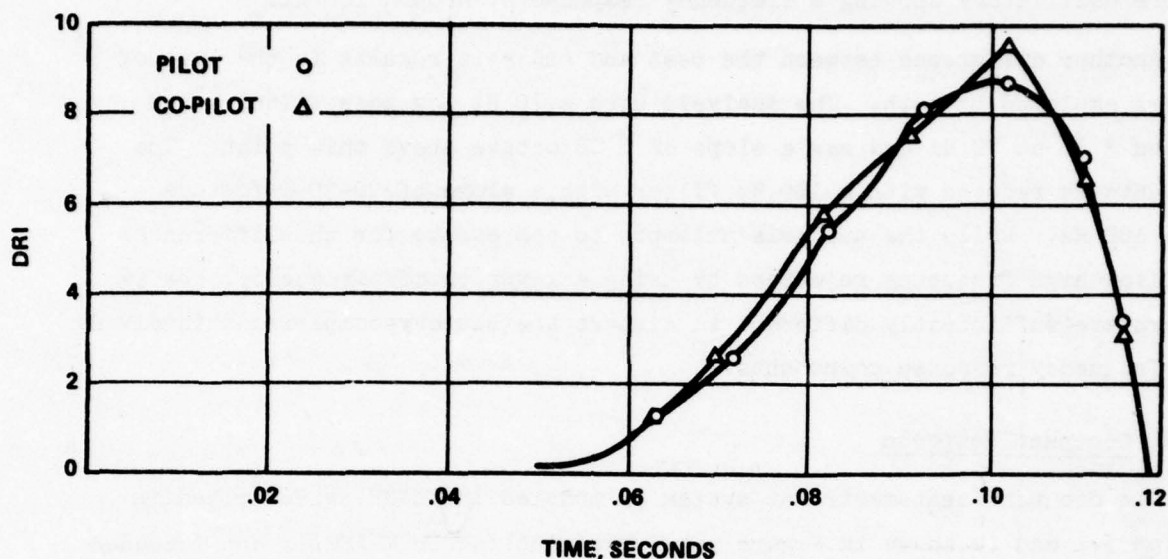


Figure 6-10. Pilot and Copilot DRI's Versus Time, Obtained by Analysis, Test 1

From Figure 6-11 it can be seen that the analysis data follows very closely the test data until approximately .110 seconds after impact. Both the pilot and copilot vertical responses reach higher peaks at approximately .120 seconds. However, this is in a region of time where many channels of the test data are questionable. In comparing the responses up to .110 seconds, the test peak values vary between +5.0 and -40 percent as compared to the analysis and are within .003 to .014 seconds of each other. If the higher copilot test peak value is included the difference is 20.8 and not 5 percent. If the higher pilot vertical peak response at .125 seconds were included the discrepancy would be +41 percent instead of -40 percent. In the longitudinal direction there is a large discrepancy between the test and analysis peak values and their time of occurrence. The analytical peaks are between 40 and 50 g's versus 10 to 15 g's noted in the test traces. In the analysis the occupant lower torso and seat masses are lumped together and the occupant is restrained by a tension-only member connecting to the occupant's upper torso

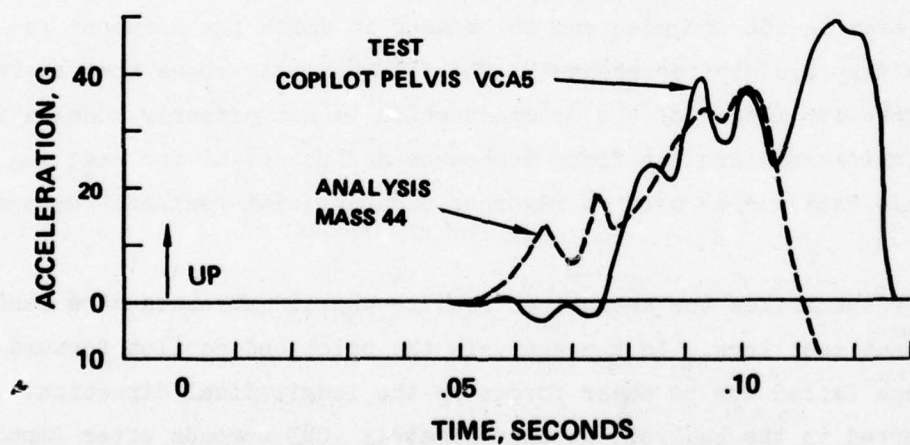
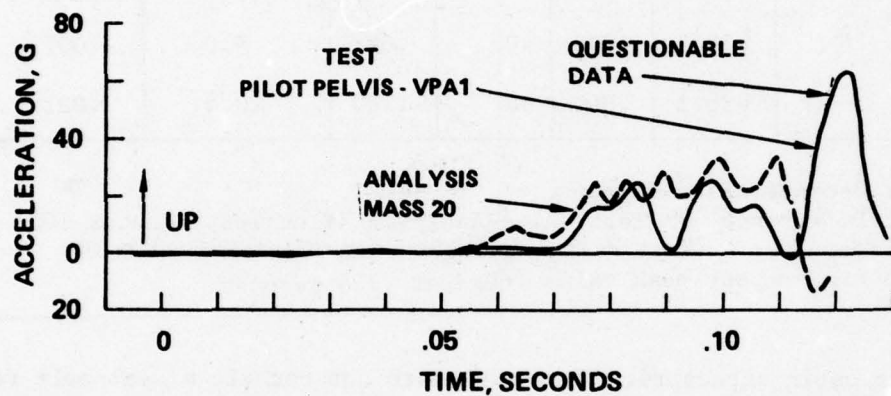


Figure 6-11. Comparison of Analysis and Test Pilot and Copilot Pelvic Vertical Accelerations, Test 1

TABLE 6-7. COMPARISON OF PILOT AND COPILOT PELVIC VERTICAL ACCELERATIONS FOR ANALYSIS VERSUS TEST, TEST 1

Location	Direction	Analysis		Test		Percent Difference (b)	Time Difference (c)
		G _{Peak}	Time (a)	G _{Peak}	Time (a)		
Pilot Pelvis	Up	{ 35.0 35.4	.099 .110	25 (d)	.096	-40.	-.003 to -0.014
Copilot Pelvis	Up	{ 38.1 38.1	.099 .099	40 48	.092 .120	5.0 20.8	-.007 .021
(a) Time in Seconds after Impact (b) Percent Difference = Test Value-Analysis Value/Test Value x 100 (c) Time Difference = (Test Value-Analysis Value/Test Value) x 100 (d) Ignores higher test peak value (60g) at .125 seconds.							

from the upper cabin structure. The model does not contain a seat belt representation. This is not a rigorous model in that flexibility between the occupant and seat is not included and the manner in which the occupant is restrained is very crudely represented. The film analysis shows that there is significant fore-aft motion of the occupant which is not properly modeled in KRASH. Of significance are the floor responses and potential for seat leg failures. This data can be used in rigorous occupant-seat-restraint system models.

Table 6-8 summarizes the analytical results wherein stresses were monitored for the occupant seat legs. In the analysis the pilot and copilot forward inboard seat legs failed due to shear forces in the longitudinal direction. These failures occurred in the analysis at approximately .083 seconds after impact. In the test, failure of the pilot front seat legs was observed from film analysis to occur at approximately .095 seconds after impact. The analysis results (Table 6-8) based on the maximum shear stress theory indicate that the shear yield is exceeded at each of the legs except for the copilot rear inboard seat leg between .075 and .099 seconds after impact. Maximum stress ratio values of 1.00 to 1.76 are experienced. The actual stress ratio is not

TABLE 6-8. STRESS RATIO RESULTS OBTAINED BY ANALYSIS, TEST 1

Location	(c) Member i - j	Time at Which Stress Ratio > 1.0 (a)	Maximum Stress Ratio Value
<u>Pilot Seat Legs</u>			
Forward Outboard	6 - 20	.078	1.27
Forward Inboard	18 - 20	.081	1.31 (b)
Rear Inboard	20 - 27	.075	1.00
Rear Outboard	40 - 28	.075	1.76
<u>Copilot Seat Legs</u>			
Forward Outboard	34 - 44	.087	1.41
Forward Inboard	18 - 44	.089	1.73 (b)
Rear Inboard	27 - 44	-	.91
Rear Outboard	44 - 48	.099	1.25
(a) Time in Seconds (b) Seat leg fails (c) See Table 5-1 and 5-2, and Figures 5-3, 5-4			

as significant as the fact that stress ratios between 1.0 and 1.5 are achieved indicating a high potential for seat shear failures to occur. The stress ratios are not accurate as an absolute measure of predicting failure but they do provide the user with a relative means of assessing potential failures.

6.2 TEST 2 ANALYSIS AND TEST COMPARISONS

6.2.1 Sequence of Events

The analytical results were obtained using the 48 mass, 100 member model described in Section 5.1. The sequence of events as obtained by analysis versus that obtained from film analysis is shown in Table 6-9. The analysis was run for a crash duration of .144 seconds. From Table 6-9 it can be seen that all significant events occur within .144 seconds. For the analysis, the occurrence of the maximum main gear deflection is estimated from the available computer data. The analysis agrees with the test data within .015 seconds. Both the analysis and test results show a lack of structural damage except for some buckling of the tail section and the lower forward fuselage and firewall regions. The change in airplane cg translational velocity, longitudinal and vertical, obtained by analysis is shown in Figure 6-12. For reference, several test points estimated from the film analysis are also shown in Figure 6-12. The test results indicate that the airplane vertical component of velocity reaches zero in approximately .150 seconds after impact. The analysis indicates that the vertical component of velocity will be reduced to zero by approximately .160 seconds. The change in velocity components obtained by analysis agrees with the test data.

As is observed in the high speed films, the crash sequence (Figure 3-14), and the post-crash airplane condition (Figures 3-15 through 3-20), the airplane rebounds off the main gears onto the nose gear which fails at its lower support. Thereafter, the airplane moves down the runway in a nose down attitude, finally coming to rest on the damaged nose gear and undamaged main gears. The velocity plots shown in Figure 6-12 illustrate this motion up until the initial rebound. However, the significant events have occurred during this time interval.

The analytical data regarding the temporal and spatial distribution of energy are shown in Figure 6-13. Included in the plot is the total energy and its components (kinetic, potential, strain, damping, crushing and friction) as a function of time. As can be expected, at the initiation of the crash impact the kinetic energy ($\approx 95\%$) and the potential energy ($\approx 5\%$) account for all the energy. Thereafter, the energy is redistributed in the form of strain, friction,

TABLE 6-9. COMPARISON OF ANALYSIS AND TEST SEQUENCES, TEST 2

Sequence	Time-Seconds (a)	
	Analysis	Test
Right Main Gear Tire Impact	0	0
Left Main Gear Tire Impact	.021	.023
Tail Impact	.033	.033
Nose Gear Tire Impact	.051	.046
Nose Gear Support Structure Failure	.064	.070
Tail Contact Relieved	.099	.108
Maximum Main Gear Deflection	.159 ^(c)	.144 ^(b)
(a) After Impact		
(b) Estimated from airplane cg velocity history		
(c) Estimated from analysis data		

structural damping and crushing. Table 6-10 shows the distribution of energy components as a percentage of the total energy. The peak values occur at the conclusion of the analysis. Compared to the first test results the magnitude of the energy components are very small. Kinetic energy has decreased to 75 percent of the total from 95 percent at time zero. The strain energy peak is only 3.7 percent of the total. The crushing is just under 3 percent. Damping and friction energies, which will continue to rise until the airplane comes to rest, are .7 and 15.5 percent, respectively. The potential energy is reduced to 2.5 percent, and while it will fluctuate somewhat as the airplane pitches, its magnitude will not change significantly. The distribution of energies appears consistent with the test results in that little deformation occurs during the crash test. The strain energy distribution from the analysis shows a heavy contribution from the main landing gears and the supporting structure initially after impact. Thereafter the contribution from the forward fuselage structure to the strain energy increases. The crushing energy

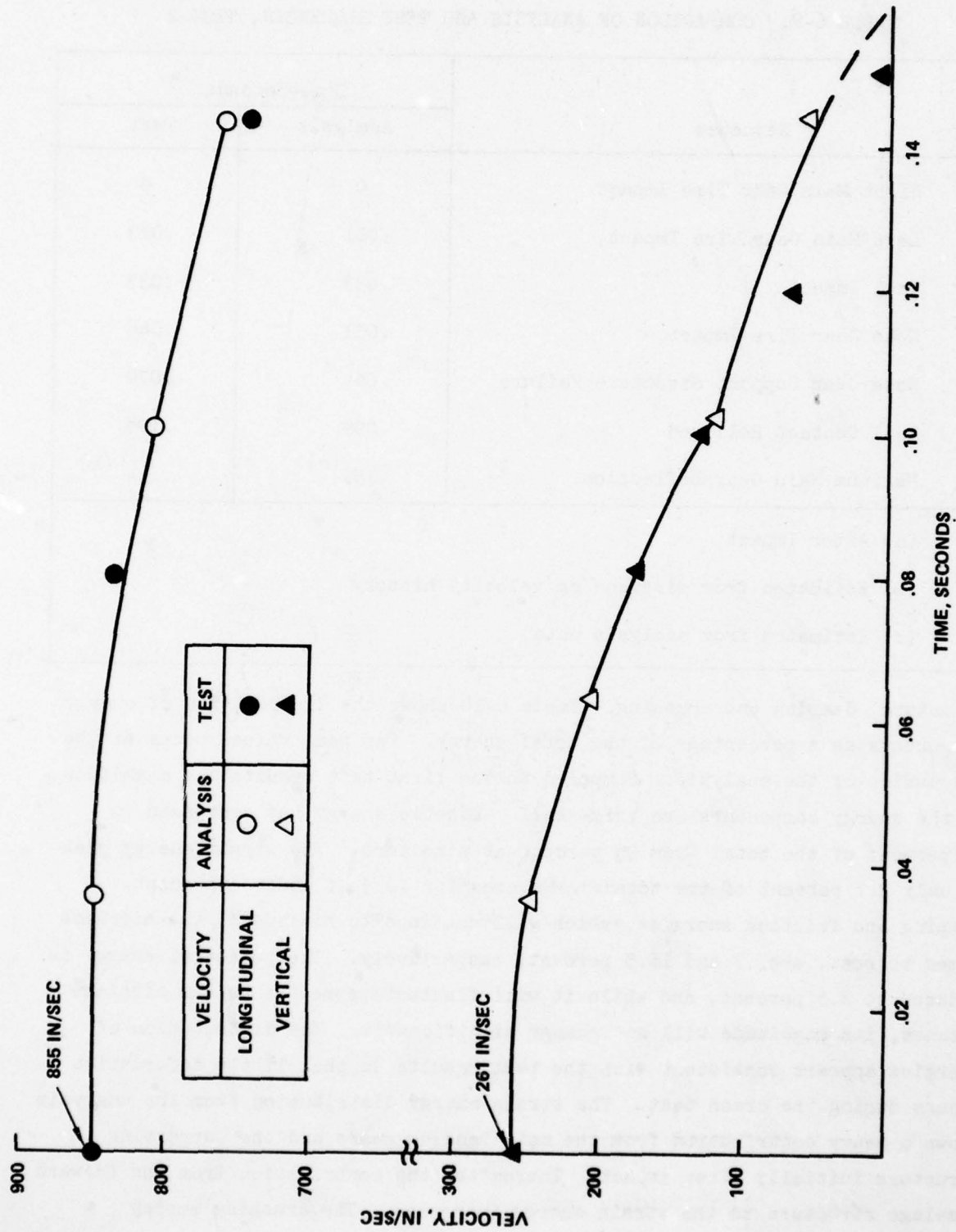


Figure 6-12. Comparison of Analysis and Test Longitudinal and Vertical Velocities, Test 2

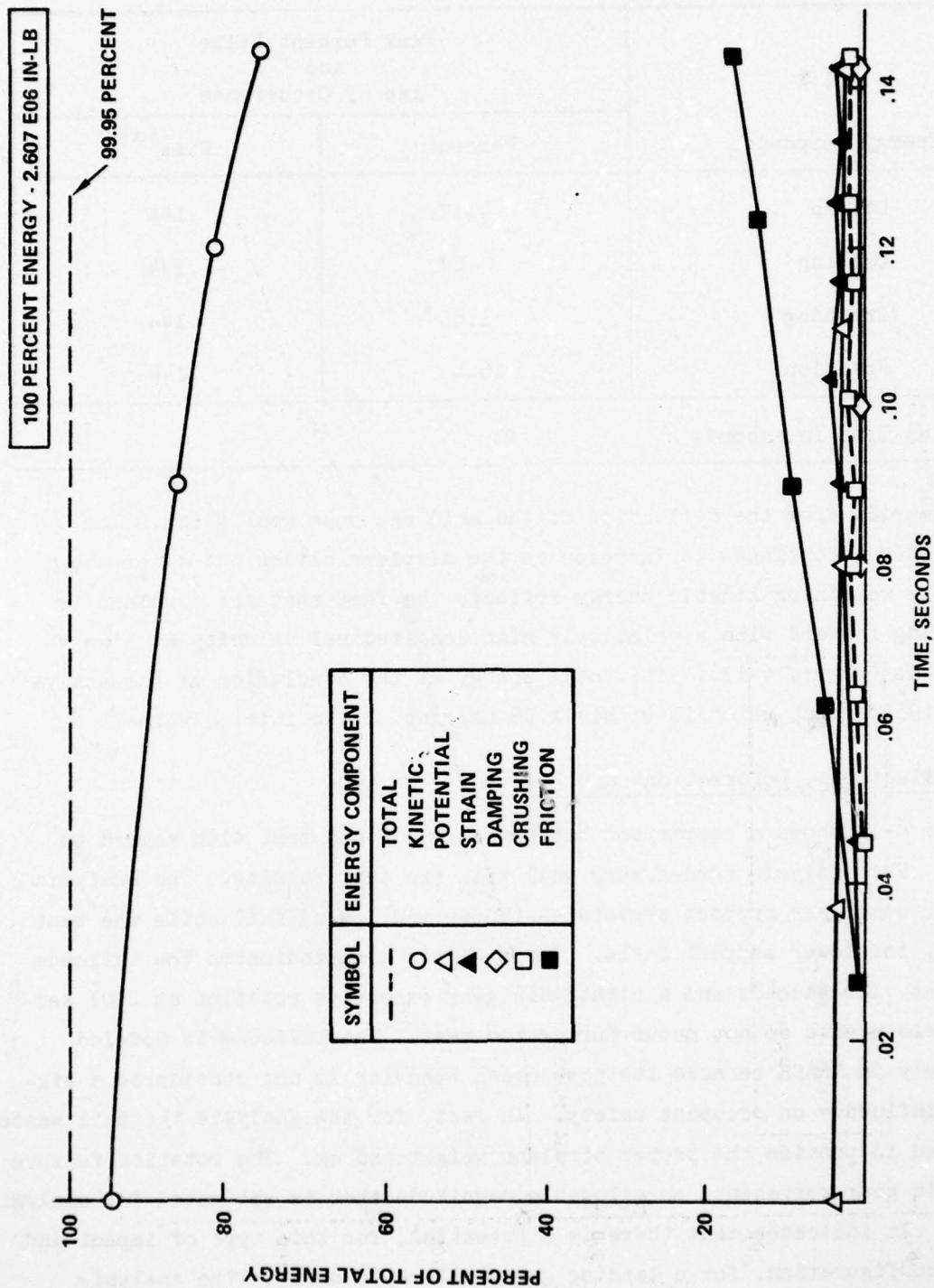


Figure 6-13. Total Energy and Energy Components Obtained by Analysis, Test 2

TABLE 6-10. SUMMARY OF ENERGY COMPONENTS OBTAINED BY ANALYSIS, TEST 2

Energy Component	Peak Percent Value and Time of Occurrence	
	Percent	Time ^(a)
Strain	4.17	.144
Damping	.68	.144
Crushing	1.85	.144
Friction	16.4	.144
(a) Time in seconds		

comes primarily from the deflection of the main and nose gear tires. The friction energy continues to increase as the airplane slides out after the crash. The remaining kinetic energy reflects the fact that the airplane is still moving forward with a relatively high longitudinal velocity at time = .144 seconds (Figure 6-13). The total energy at the conclusion of the analysis is 99.95 percent which is within ± 0.05 percent of the initial value.

6.2.2 Deflections, Deformations and Failures

Table 6-11 shows a comparison between analysis and test with regard to failures. The analysis agrees very well with the test results. The analysis shows both nose gear support structures (upper and lower) fail while the test shows only the lower support fails. The analysis also indicates the tailcone yielding at .126 seconds and a right main gear excessive rotation at .107 seconds. These events do not occur during the test. The tailcone is modeled very crudely in KRASH because its post crash behavior is not considered a significant influence on occupant safety. In fact, for the analysis the tail masses are altered to provide the proper airplane weight and cg. The rotation failure of the main gear represents an allowable magnitude that is estimated for analysis purposes. It indicates that there is a potential, for this type of impact and airplane configuration, for a landing gear failure to occur. The analysis

TABLE 6-11. COMPARISON OF ANALYSIS AND TEST FAILURES, TEST 2

Location	Analysis	Test
Seat Leg Failures		
Pilot Forward	No	No ^(a)
Pilot Rear	No	No ^(a)
Copilot Forward	No	No ^(a)
Copilot Rear	No	No ^(a)
Tailcone Yield or Buckle	Yes	No
Nose Gear Failures		
Lower Support	Yes	Yes
Upper Support	Yes	No
Main Landing Gear Failures		
Gear	Yes ^(b)	No
Support Structure	No	No
Wing Spar Failures		
Left Wing	No	No
Right Wing	No	No
Wing Column Strut Failures		
Left Wing	No	No
Right Wing	No	No
Engine Mounts Buckle	No	No
(a) Based on no failures and stress ratio < 1.0		
(b) Right gear		

shows that the engine mounts do not yield which also agrees with the test data. While there is some yielding of structure in the analytical results, the associated deflections are very small. The analysis of Test 1 showed these same elements compressing and/or bending several inches. The analysis shows that the cabin region remains essentially unchanged as would be expected from an evaluation of the test results. The maximum deflections of the external springs are shown in Table 6-12. The tire and tail structure deformations appear

TABLE 6-12. MAXIMUM EXTERNAL SPRING DEFLECTIONS OBTAINED BY ANALYSIS, TEST 2

Mass No. (a)	Location	Maximum Deflection, Inches
1	Nose Gear Tire	3.8
2	Left Main Gear Tire	5.9
3	Tail Structure, F.S. 205	2.23
29	Lower Finewall (Center) F.S. 0.0	1.8
30	Tail Structure, F.S. 228	2.5
31	Right Main Gear Tire	5.9
(a) See Figure 5-3, Tables 5-1 and 5-2		

reasonable when compared to the test results. The analysis shows some slight contact between the lower firewall and forward fuselage regions with the ground after .135 seconds. In the test no such contact was noted. However, this contact is slight and causes a deflection of .9 to 1.8 inches. The analysis shows that there was no contact with the ground of the midcabin lower fuselage. During the test the main landing gear deflected substantially but the fuselage underside barely missed touching the ground. Analytically, the main landing gears deflect approximately 16.4 and 14 inches for the right and left side, respectively. The test shows a peak deflection of approximately 16 inches. In both the analysis and the test there is no contact between the cabin fuselage underside and the ground.

The fact that Test 2 experienced virtually no internal structure deformation provided valuable inputs with which to evaluate the proper selection of deflection values at which nonlinearities occur. As noted earlier in Section 5 "Math Model Descriptions", program KRASH computes preliminary loads and deflections which can be used as a guideline as to the magnitude of initial nonlinear deflection values to input into KRASH.

6.2.3 Structure Responses

Figures 6-14 through 6-18 show the comparison of analysis and test structure responses at various locations throughout the airplane. Table 6-13 summarizes both sets of results. The engine responses are compared in Figure 6-14. From Figure 6-14 it can be seen that the analytically obtained response shape appears to lag the test response curve by .015 to .030 seconds. While the peak values differ substantially the actual difference is in the order of 3.6 to 8.0 g's in the vertical and longitudinal directions. In the down direction there is a transient 16.2 g response which occurs after the nose gear support structure fails. When elements rupture in the program a momentary force discontinuity sometimes occurs. This response reflects that discontinuity. In Test 2 there is no contact between the engine and the ground. Thus the engine response reflects load paths from the nose gear via the firewall and cabin structure.

The floor responses are shown in Figures 6-15, 6-16 and 6-17 for F.S. 27, F.S. 60 and F.S. 90-108, respectively. Overall the peak values agree within -10 to +20 percent and their times of occurrence agree within .004 to .033 seconds. The test data appears more oscillatory than the analysis data, particularly in the vertical direction. However, in the longitudinal direction the analysis data exhibits about the same frequency characteristics as the test data. The wing responses are compared in Figure 6-18. The differences between the analysis and test are in the order of 3 to 40 percent and .006 to .032 seconds for peak value and time of occurrence comparisons. An examination of the response curves shown in Figures 6-15 through 6-18 shows the test data to exhibit more oscillatory motion, as can be expected, than the analysis data. While in some instances the differences appear to be large percentage-wise, the responses are relatively low in magnitude as compared to Test 1, and the actual difference is usually less than a few g's.

6.2.4 Occupant Response

The analysis was performed using the same occupant-seat-restraint system modeled for Test 1. The math model is described in Section 5.1. Figure 6-19 shows the analytically obtained DRI responses for the pilot and copilot. The DRI's reach maximum values of 9.1 and 8.5 at approximately .099 and .102 seconds

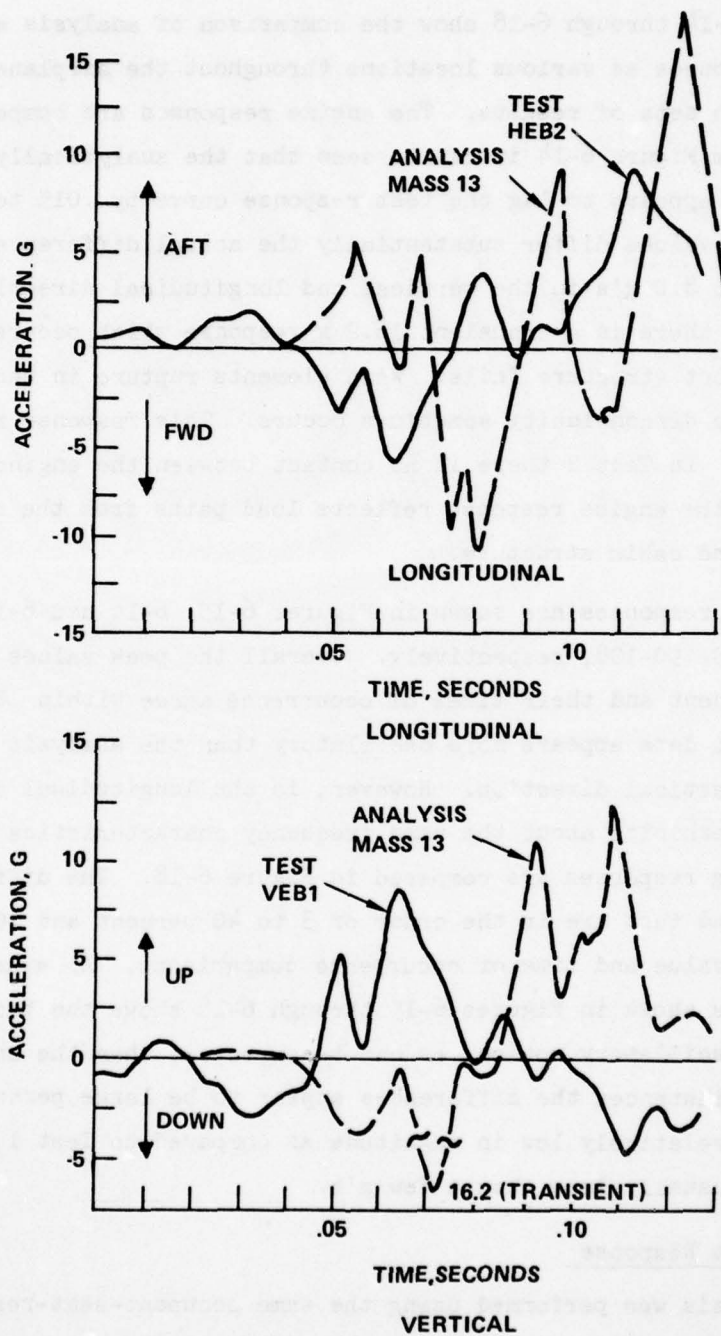


Figure 6-14. Comparison of Analysis and Test Engine Vertical and Longitudinal Accelerations, Test 2

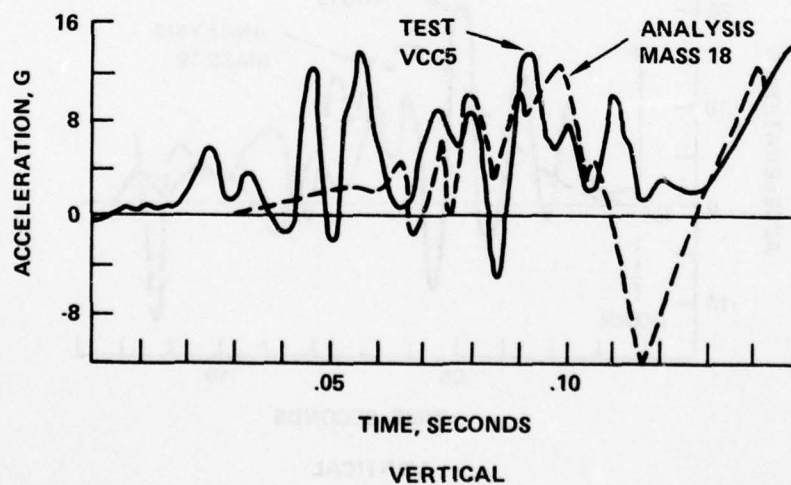
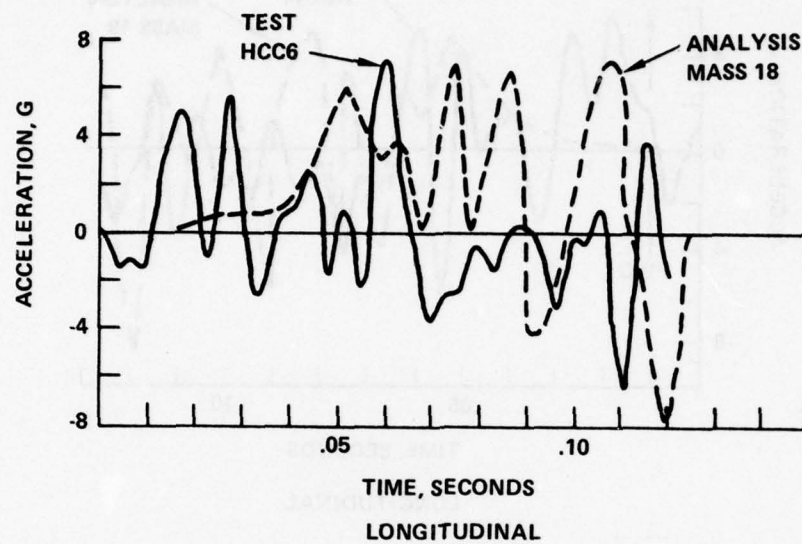


Figure 6-15. Comparison of Analysis and Test Floor Vertical and Longitudinal Accelerations, F.S. 27, Test 2

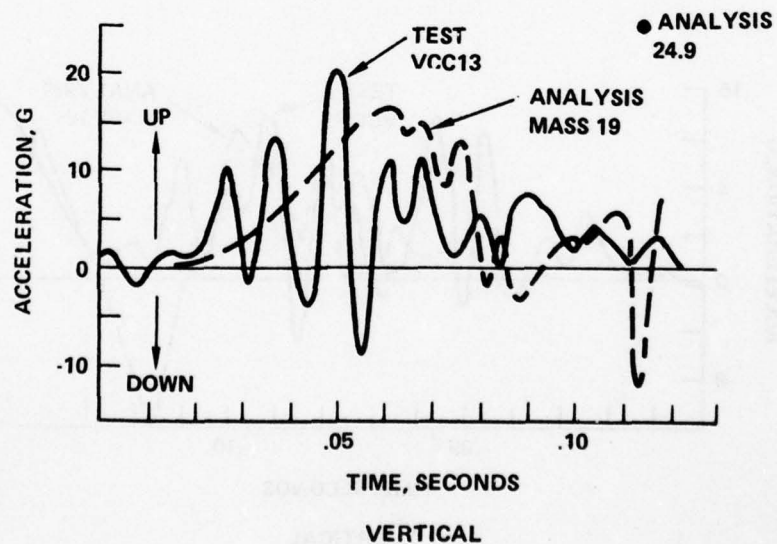
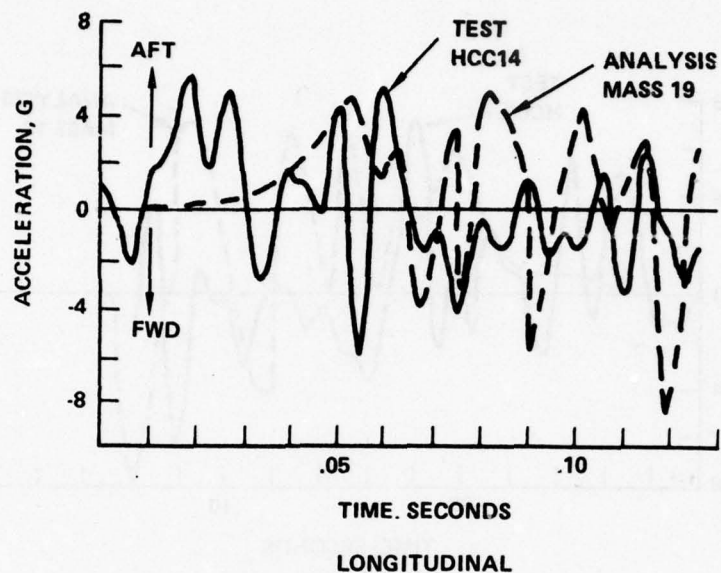


Figure 6-16. Comparison of Analysis and Test Floor Vertical and Longitudinal Accelerations, F.S. 60, Test 2

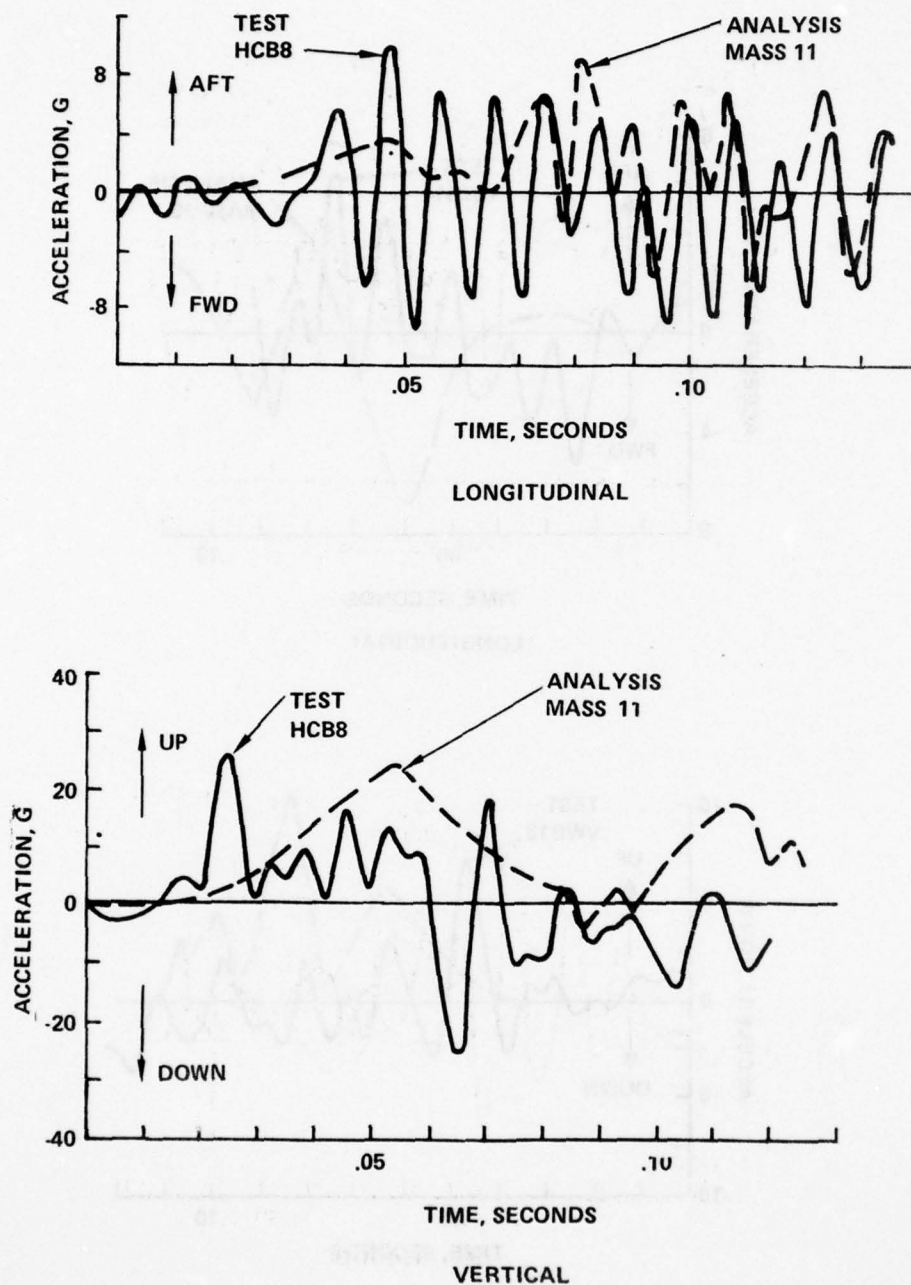


Figure 6-17. Comparison of Analysis and Test Floor Vertical and Longitudinal Accelerations, F.S. 90-108, Test 2

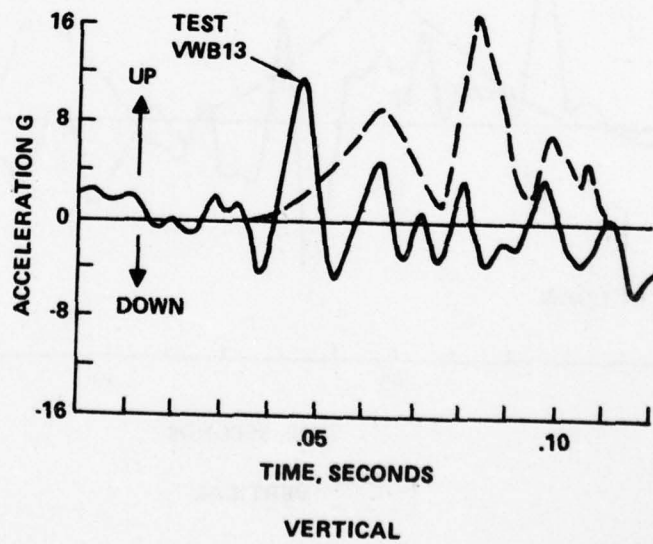
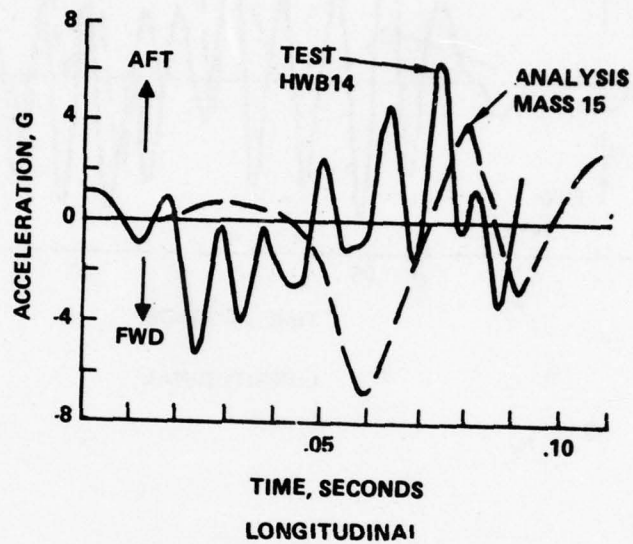


Figure 6-18. Comparison of Analysis and Test Wing Vertical and Longitudinal Accelerations, Test 2

TABLE 6-13. COMPARISON OF ANALYSIS AND TEST STRUCTURE RESPONSES, TEST 2

Location	Direction	Analysis		Test		Percent Difference (b)	Time Difference (c)
		G _{peak}	Time (a)	G _{peak}	Time		
Engine	Up	12.6	.108	9	.117	-40 (d)	.009
	Aft	{ 9.1 17.3	{ .096 .123	9.3	.135	{ 2.2 -86.0 (e)	{ .039 .016
Forward Fuselage Floor, F.S. 27	Up	{ 13.2 12.9	{ .096 .141	{ 14 15	{ .110 .145	{ 5.7 14.	{ .014 .004
	Aft	6.8	.075	7	.060	2.8	-.015
Landing Gear Floor, F.S. 60	Up	16 (g)	.063	20.0	.050	+20.0	-.013
	Aft	{ 5.4 4.3	{ .051 .102	{ 5.6 5.2	{ .070 .113	{ 3.5 17.3	{ .019 .011
Aft Fuselage Floor,	Up	22	.057	{ 26 20	{ .028 .070	{ 15.4 -10.0	{ -.029 .013
	Aft	8.3	.081	10	.048	17.0	.033
Wing B.L. 100	Up	{ -16.8 -11.6	{ .084 .132	12	.100	{ -40. 3.3	{ .016 -.032
	Aft	4.8	.081	6.3	.075	38.3 (f)	-.006
(a) Time in seconds after impact (b) Percent difference = $\left(\frac{\text{test value} - \text{analysis value}}{\text{test value}} \right) \times 100$ (c) Time difference = test time - analysis time (d) Difference of 3.6 g's (e) Difference of 8 g's (f) Difference of 3.0 g's (g) Transient peak of 24.9 g's disregarded							

AD-A054 154

LOCKHEED-CALIFORNIA CO BURBANK

F/G 1/3

FULL SCALE CRASH TEST EXPERIMENTAL VERIFICATION OF A METHOD OF --ETC(U)

FEB 78 G WITTLIN, M A GAMON, W L LABARGE

DOT-FA75WA-3707

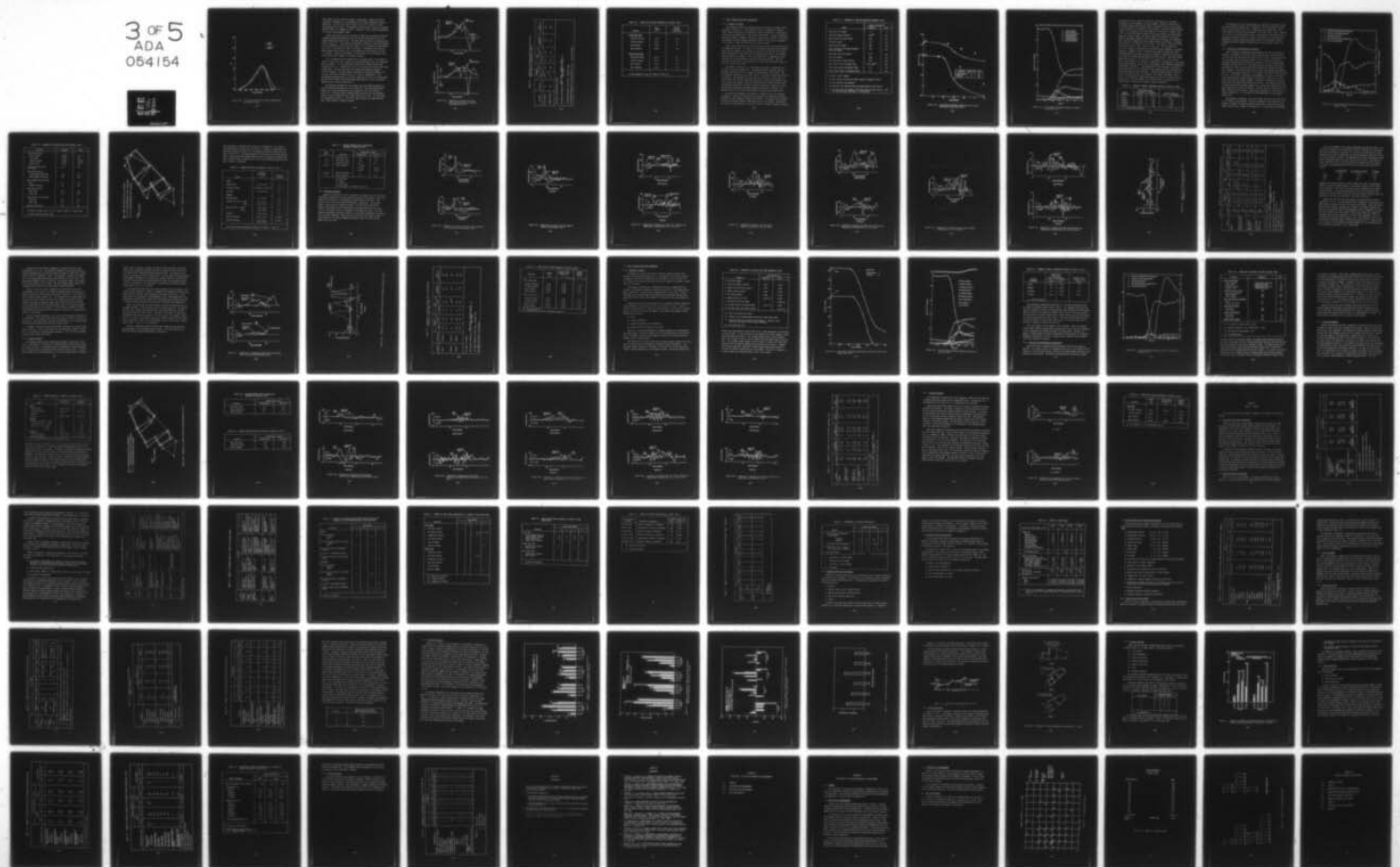
UNCLASSIFIED

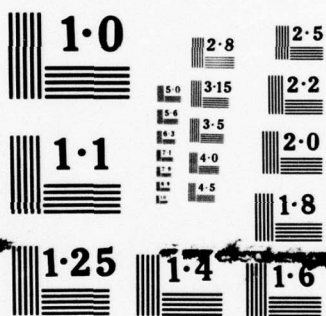
LR-28306

FAA-RD-77-188

NL

3 OF 5
ADA
054154





NATIONAL BUREAU OF STANDARDS
MICROCOPY RESOLUTION TEST CHART

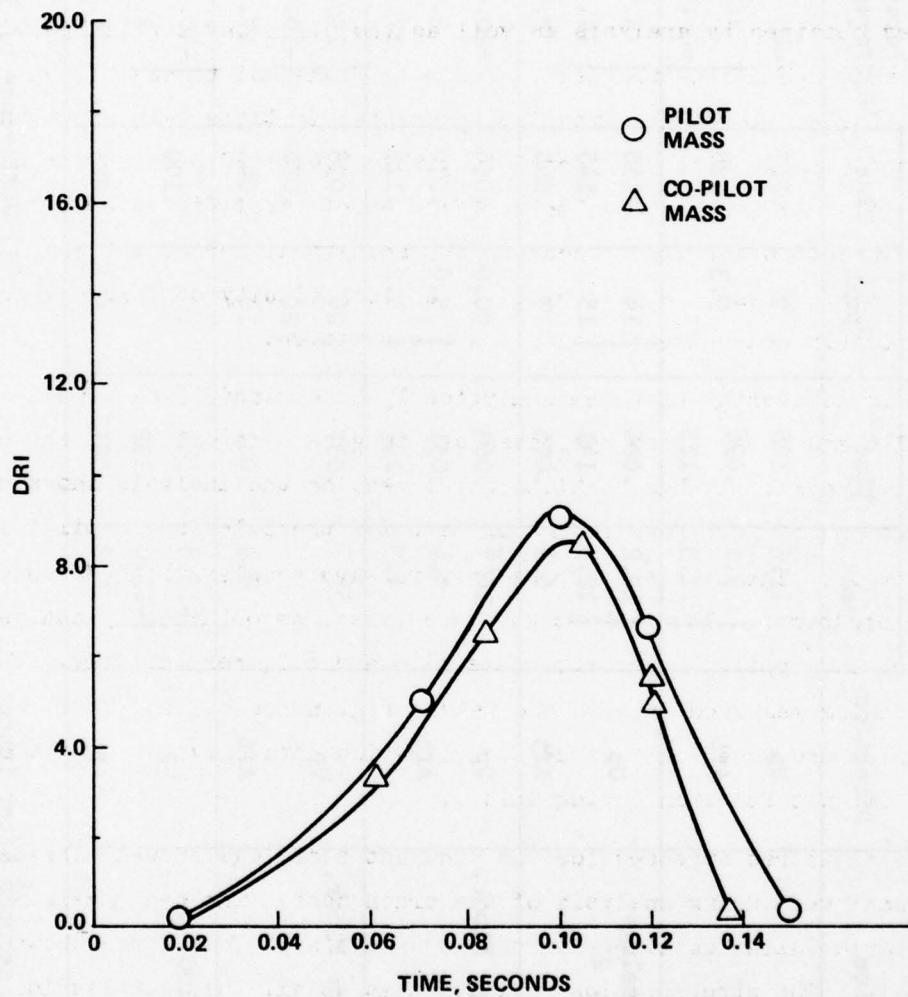


Figure 6-19. Pilot and Copilot DRI's versus Time, Obtained by Analysis, Test 2

after impact, for the pilot and copilot, respectively. Based on the data presented in Reference 11, the probability of a spinal compression injury is negligible. The DRI would have to reach a value of 18 to give a 10 percent probability of injury. The potential for this type of injury is slightly higher in Test 1 as compared to Test 2. However, in both tests the possibility of a spinal injury appears remote.

Figure 6-20 shows the pilot and copilot lower torso vertical acceleration responses obtained by analysis as well as the pilot and copilot pelvic responses measured during the test. The peak loads and times of occurrences are noted in Table 6-14. The comparison presented in Table 6-14 shows the analysis to be in agreement with the test data within 8.6 to 20 percent for peak values and .014 to .015 seconds in time of occurrence. From Figure 6-20 there are sharp downward pulses which occur in the analytical curves between .114 and .117 seconds. These are attributed to a discontinuity of forces which occur after the main gear exceeds its allowable rotation.

It is noteworthy that the analytically determined times of occurrence of peak DRI's and lower torso responses are in good agreement with the corresponding test signals. In the longitudinal direction the analysis shows peak accelerations of 10.7 forward and 8.1 aft for the pilot and copilot lower torso, respectively. The test data shows only forward acceleration responses for the occupants. The peak forward accelerations obtained by analysis for the pilot and copilot lower torso are 11.4 and 8.1, respectively. The corresponding measured data in the pelvic region are 8.0 and 7.0, respectively. The results are based on recorded acceleration data only, since the onboard cameras did not function during Test 2.

The monitored stresses for the occupant seat legs showed extremely low values achieved during analysis of the crash test. The peak maximum shear stress ratio values obtained during the analysis of Test 2 are shown in Table 6-15. The stress ratios indicate that at all the seat leg locations there is little probability that a shear failure will occur. All the ratios are substantially below 1.0. The stress ratio results are consistent with Test 2 data and Test 1 analysis results.

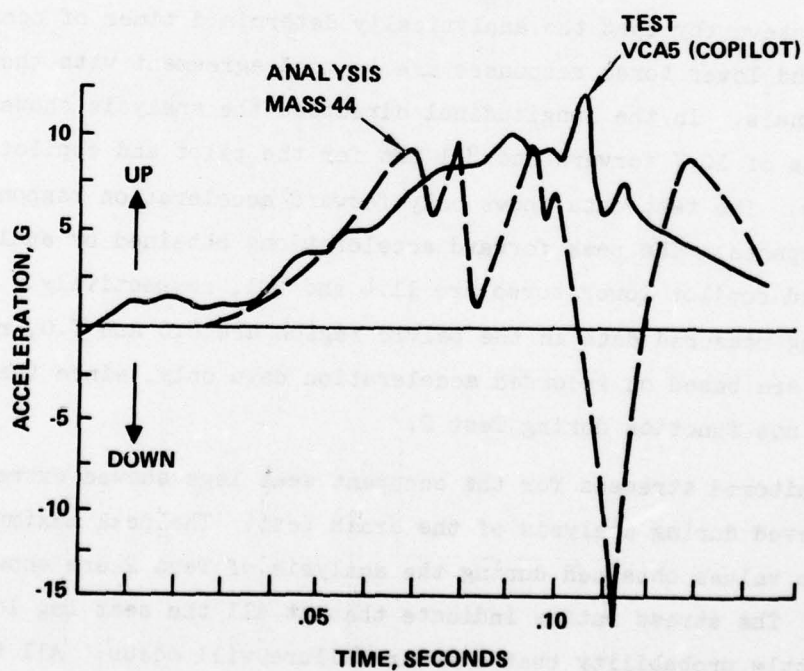
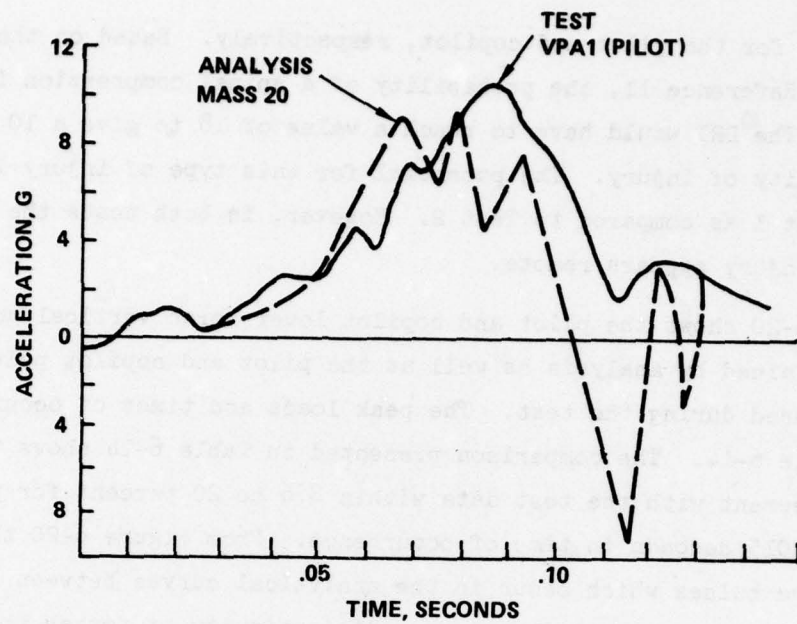


Figure 6-20. Comparison of Analysis and Test Pilot and Copilot Pelvic Vertical Accelerations, Test 2

TABLE 6-14. COMPARISON OF ANALYSIS AND TEST PILOT AND COPILOT
PELVIC VERTICAL ACCELERATIONS, TEST 2

Location	Direction	Analysis		Test		Percent (b) Difference	Time (c) Difference
		G _{peak}	Time (a)	G _{peak}	Time (a)		
Pilot pelvis	Up	9.6 ^(d)	.075	10.5	.090	8.6	.015
Copilot pelvis	Up	10. ^(d)	.096	12.5	.110	20.0	.014
(a) Time in seconds after impact							
(b) Percent difference = $\left(\frac{\text{test value} - \text{analysis value}}{\text{test value}} \right) \times 100$							
(c) Time difference = test time - analysis time							
(d) Transient responses in down direction @ .114 - .117 not included.							

TABLE 6-15. STRESS RATIO RESULTS OBTAINED BY ANALYSIS, TEST 2

Location	Member i-j ^(a)	Maximum Stress Ratio Value
<u>Pilot Seat Legs</u>		
Forward Outboard	6-20	.86
Forward Inboard	18-20	.82
Rear Inboard	20-27	.71
Rear Outboard	20-28	.83
<u>Copilot Seat Legs</u>		
Forward Outboard	34-44	.64
Forward Inboard	18-44	.74
Rear Inboard	27-44	.64
Rear Outboard	44-48	.77
(a) See Figures 5-3 and 5-4, Tables 5-1 and 5-2		

6.3 TEST 3 ANALYSIS AND TEST COMPARISONS

6.3.1 Sequence of Events

The analytical results are obtained using the 48 mass, 100 member model described in Section 5.1. The sequence of events as obtained by analysis versus that obtained from film analysis is shown in Table 6-16. The analysis and test include events up to .120 seconds after impact. The most significant events with regard to damage, failures and responses occur within .120 seconds. The sequence of events compares favorably except for the times of occurrence of the wing tip impact and the wing strut column failure.

Some of the events obtained from film analysis cannot be ascertained from the analytical results. The impact of the occupants heads with the instrument panel and the departure of the copilot's rear seat leg from the floor guide track were obtained from analysis of the onboard camera films. The analysis does not model the occupant in detail and, therefore, no comparison is made with the test results insofar as occupant motion is concerned. Based on analytical stress ratios, the potential for a rear seat leg failure exists at .087-.090 seconds after impact.

The change in airplane c.g. translational velocities, longitudinal and vertical, is shown in Figure 6-21. The analysis results indicate that the airplane vertical velocity is arrested in approximately .072 seconds. The film analysis indicates a much longer period (.135 seconds) before the velocity is arrested. The estimate of the cg velocity is difficult because the airplane rotates onto the left main gear tire which is not fully compressed until .162 seconds after impact. Both the analysis and test results indicate that the airplane longitudinal velocity is slowly arrested as a result of friction between the structure and the ground during its slide-out. However, the analysis tends to show a more rapid change in velocity than does the test.

The spatial and temporal distribution of energy for Test 3 is obtained by analysis. Figure 6-22 shows the total energy and its components (kinetic, potential, strain, damping, crushing and friction). At impact, kinetic energy (94.8%) and potential energy (5.2%) account for all the energy. Thereafter, the energy is redistributed in the form of strain, structural damping, crushing

TABLE 6-16. COMPARISON OF TEST AND ANALYSIS SEQUENCES, TEST 3

Event	Time in Seconds ^(a)	
	Analysis	Test
Nose Gear Tire Impact	0	0
Nose Gear Support Failure	.007 ^(b)	.012
Engine Lower Structure Impact	.033	.024
Propeller Impact	.027	.032
Right Wing Tip Impact	.063	.038
Lower Firewall and Forward Fuselage Left Side Impact	.045	.048
Right Main Gear Tire Impact	.060	.062
Tail Cone Buckle	.099	.075
Left Wing Strut Column Failure	.049	.085
Copilot Seat Aft Leg Departs Rail	.087-.090 ^(d)	.090
Pilot Head Impacts Instrument Panel	(c)	.092
Copilot Head Impacts Instrument Panel	(c)	.120
<p>(a) After initial impact</p> <p>(b) Lower support followed by upper support attachment failure</p> <p>(c) Not available from analysis</p> <p>(d) Potential seat failure based on maximum shear stress theory</p> <p>(e) Left main gear tire impact (.135) and left rear spar failure (.160) not included since time (max) = .120 seconds.</p>		

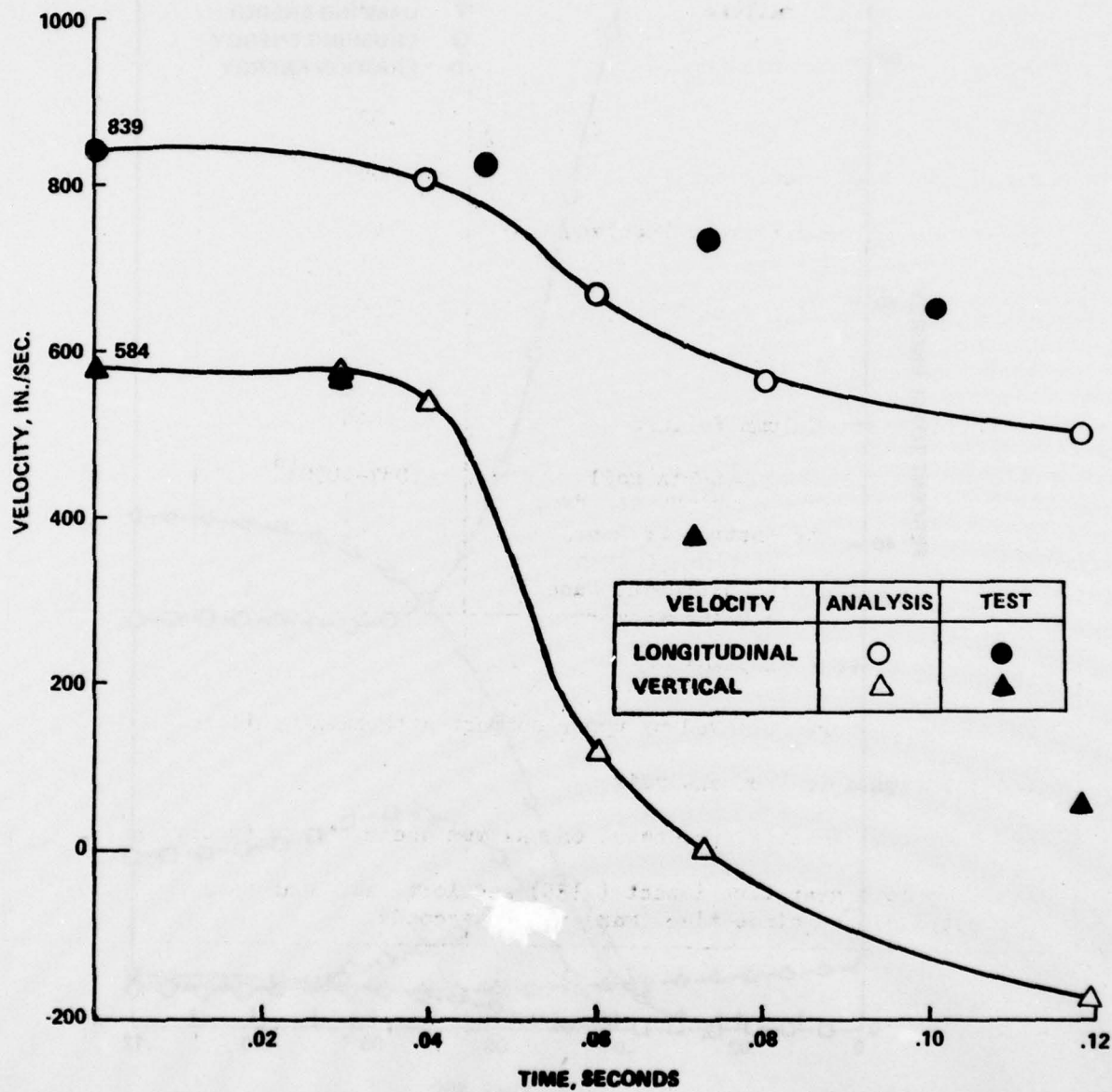


Figure 6-21. Analytically Obtained Longitudinal and Vertical Velocities versus Time, Test 3

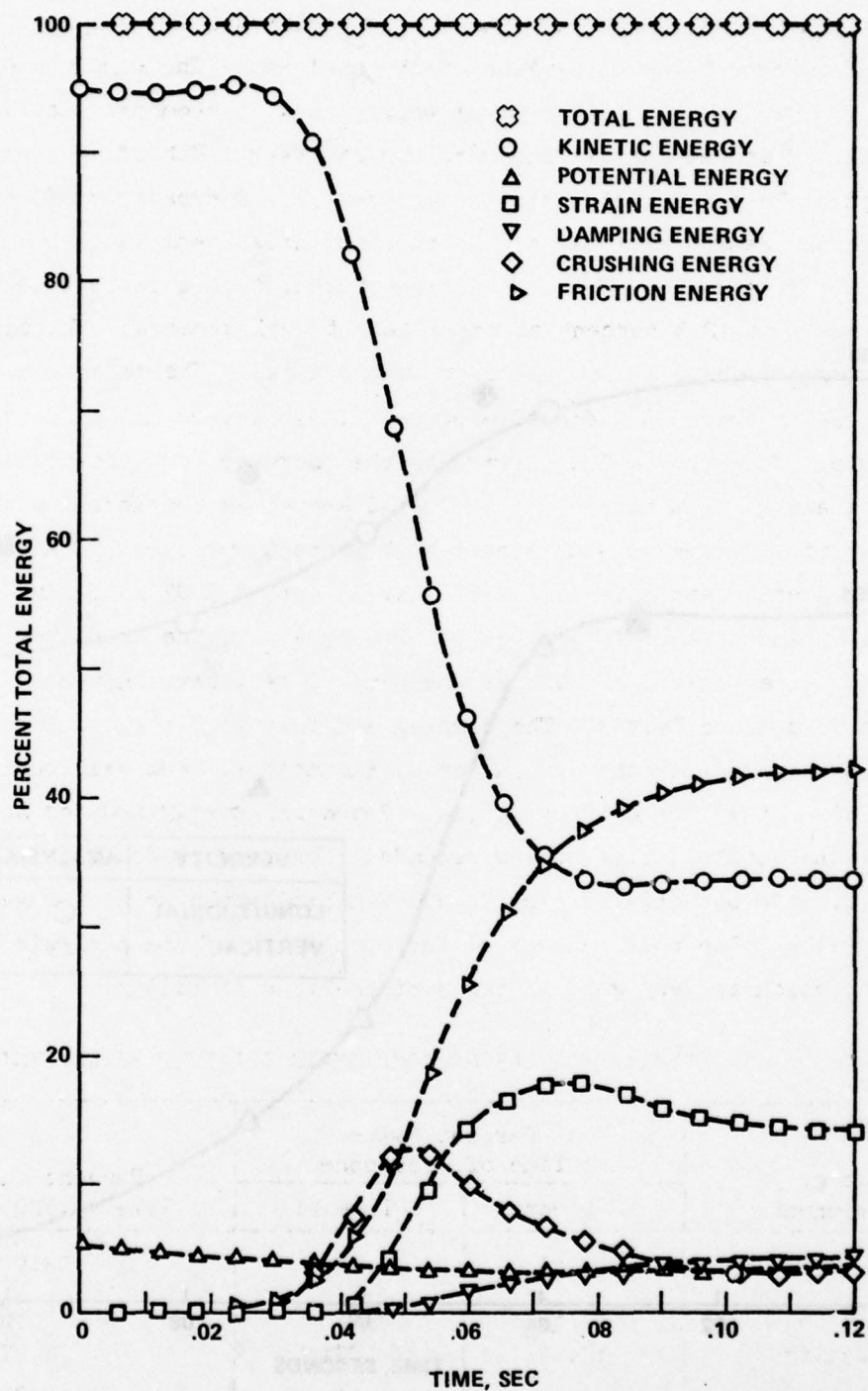


Figure 6-22. Total Energy and Energy Components Obtained by Analysis, Test 3

and ground friction. Table 6-17 shows the distribution of the energy components as a percentage of the total energy. Included in Table 6-16 is the maximum percent value and its time of occurrence as well as the percent of total energy at the conclusion of the analysis. The strain energy reaches a peak of 17.8 percent of the total energy at .075 seconds. However, from .057 to .120 seconds strain accounts for at least 1/8th of the total energy. Compared to Test 1 results, the strain energy is increased by 56 percent. Based on the damage observed in the two post-crash vehicles, the comparative Test 1 and Test 3 analytical strain energy results are realistic. Crushing energy peaks at 12.5 percent of the total at .051 seconds. Thereafter crushing energy reduces to only 3 percent of the total. The reduction from 12.5 to 3.0 percent is indicative of relatively severe unloading of crushable structure. Compared to Test 1 results the increase (80 percent) in peak crushing energy as a percent of the total energy is consistent with the relative severity of damage experienced by both test vehicles. The total energy associated with Test 3 is 3.39×10^6 in.-lb versus 3.07×10^6 in.-lb for Test 1, an increase of 10.4 percent. Consequently, the magnitude of the strain and crushing energies, as well as the percentages, have increased substantially between Test 1 and Test 3. The damping and friction energies, as expected, are at peak values at the conclusion of the analysis and will continue to increase since they are not reversible. Potential energy reduces to 3.62 percent of the total at time = .120 seconds. For reasons described in Section 6.1.1 the potential energy should exhibit little or no change from this latter value. The total energy at the conclusion of the analysis is 100.1 percent, which is very good in terms of analysis stability.

TABLE 6-17. SUMMARY OF ENERGY COMPONENTS OBTAINED BY ANALYSIS, TEST 3

Energy Component	Peak Percent Value and Time of Occurrence		Percent Value at Time = .120 Seconds
	Percent	Time (a)	
Strain	17.81	.075	13.9
Damping	4.28	.120	4.28
Crushing	12.54	.051	2.97
Friction	41.83	.120	41.83
(a) Seconds after impact			

The distribution of the strain energy as a function of airplane location and time is shown in Figure 6-23. In addition to the percentages, the total strain energy history is presented. Immediately after impact very little strain energy is absorbed by the structure. As in the case of Test 1 (Section 6.1.1) most of the strain energy up until .040 seconds is associated with the nose gear and support structure. However, the magnitude is extremely small. Thereafter the strain energy distribution shifts to the firewall, forward fuselage and midcabin regions, respectively, as these regions contact the ground.

6.3.2 Deflections, Deformations and Failures

Table 6-18 shows a comparison between analysis and test with regard to failures. During Test 3 the pilot's front seat legs fail and the copilot's front and rear seat legs pull loose from the floor tracks. The analysis does not show shear failure occurring, however, it does show the potential for exceeding the shear stress capability at several of the seat leg attachment locations (see Section 6.3.4). The analysis depicts tailcone buckling, nose gear support failures, wing spar and strut failures and substantial engine mount buckling. The analysis shows that the right main landing gear bulkhead load in the longitudinal direction is 70 percent of the failure load and rising at time = .120 seconds. The extent of the damage as a result of the failure of the right main gear support structure during Test 3 appeared to be less severe when compared to Test 1 damage. Furthermore, film analysis could not detect when the bulkhead failure may have occurred. The analysis shows that the upper engine mounts deflect axially over 4 inches which indicates that the engine housing can contact the firewall. The test results indicate that the engine did contact the firewall. The overall deformation of the structure is shown in Figure 6-24. For reference the undeformed cabin is also shown in Figure 6-24.

The extensive deformation of the cabin region observed in the test films is not evident in the analysis. The major difference is the failure of the analysis to predict the large vertical discontinuity in the cabin roof area (above the left door, element 5-8, Figure 5-3). If this region were modeled

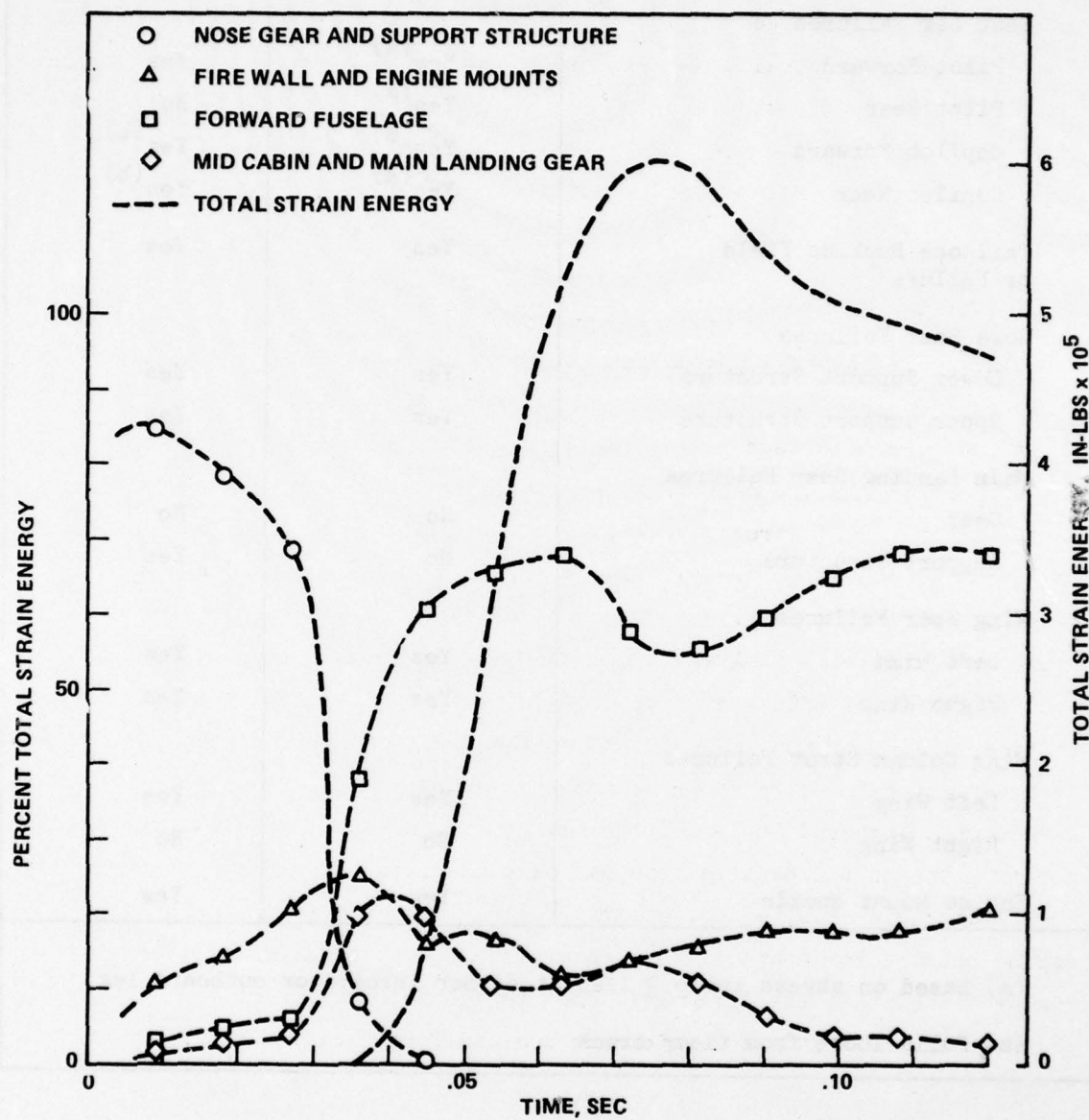


Figure 6-23. Strain Energy Distribution Histories Obtained by Analysis, Test 3

TABLE 6-18. COMPARISON OF ANALYSIS AND TEST FAILURES, TEST 3

Location	Analyses	Test
Seat Leg Failures		
Pilot Forward	Yes ^(a)	Yes
Pilot Rear	Yes ^(a)	No
Copilot Forward	Yes ^(a)	Yes ^(b)
Copilot Rear	Yes ^(a)	Yes ^(b)
Tailcone Buckles Yield or Failure	Yes	Yes
Nose Gear Failures		
Lower Support Structure	Yes	Yes
Upper Support Structure	Yes	Yes
Main Landing Gear Failures		
Gear	No	No
Support Structure	No	Yes
Wing Spar Failures		
Left Wing	Yes	Yes
Right Wing	Yes	Yes
Wing Column Strut Failures		
Left Wing	Yes	Yes
Right Wing	No	No
Engine Mount Buckle	Yes	Yes
(a) Based on stress ratio ≥ 1.25 at either inboard or outboard leg.		
(b) Pulls loose from floor track		

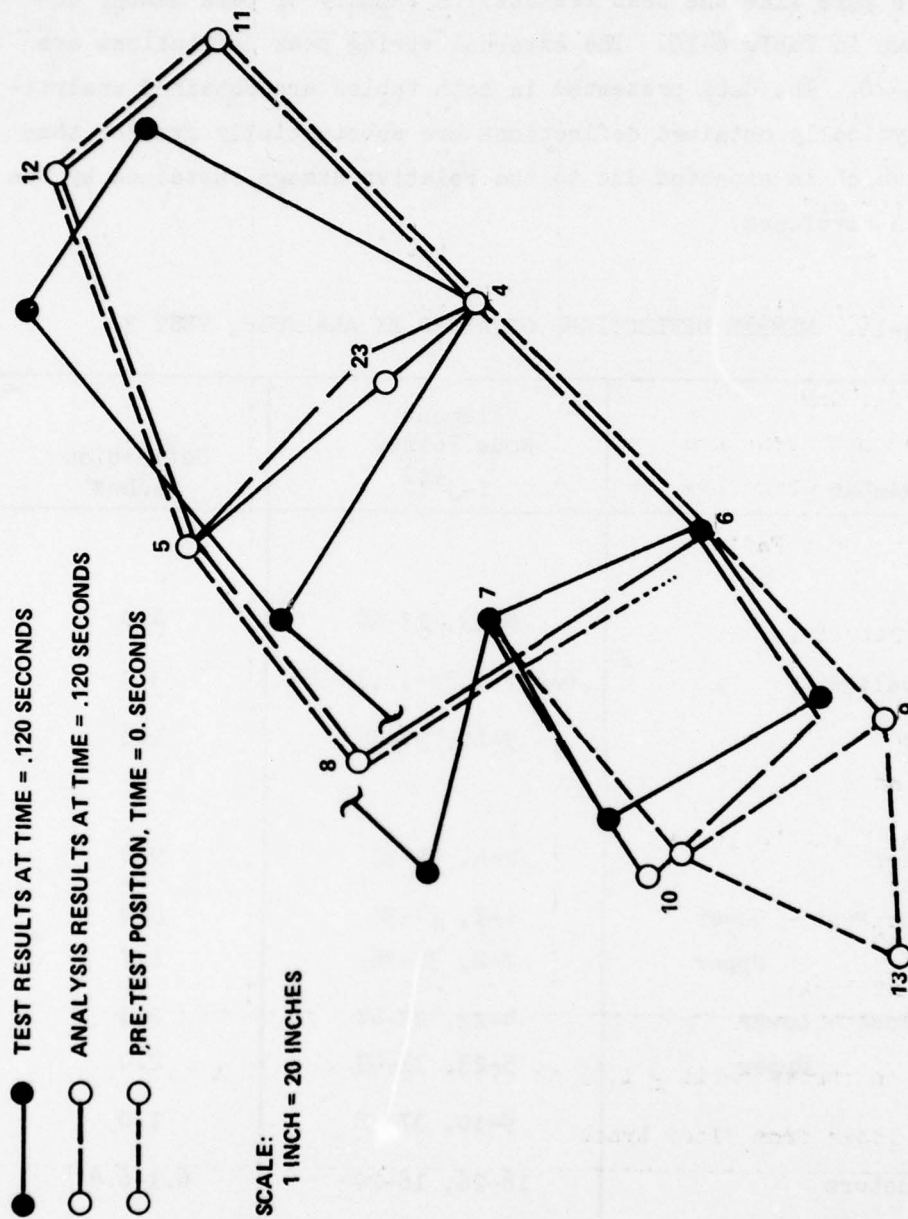


Figure 6-24. Comparison of Analysis and Test Cabin Deformations, Test 3

more accurately to reproduce this failure, the remainder of the structure would then behave more like the test results. A summary of peak member deflections is shown in Table 6-19. The external spring peak deflections are shown in Table 6-20. The data presented in both tables are obtained analytically. The analytically obtained deflections are substantially greater than Test 1 results, which is expected due to the relative damage sustained by the Test 1 and Test 3 airplanes.

TABLE 6-19. MEMBER DEFLECTIONS OBTAINED BY ANALYSIS, TEST 3

Member	Element Node Points i-j ^(a)	Deflection inches
<u>Axial</u>		
Engine Mount	9-13, 13-38	4.0
Forward Fuselage	6-9, 7-9, 34-37, 35-37	3.0
Firewall	9-10, 37-38	1.6
<u>Bending</u>		
Landing Gears	2-4, 31-32	9.2
Forward Door Post - Lower	6-7, 34-35	5.0
Upper	7-8, 35-36	1.7
Rear Door Post - Lower	4-23, 23-47	2.3
Upper	5-23, 33-47	2.0
Firewall	9-10, 37-38	1.0
Tunnel Structure	18-26, 18-29	6.1-6.8
Forward Fuselage	6-9, 34-37 7-10, 35-38	6.6-7.1
(a) See Math Model Description, Figure 5-3, Tables 5-1 and 5-2		

TABLE 6-20. MAXIMUM EXTERNAL SPRING DEFLECTIONS
OBTAINED BY ANALYSIS, TEST 3

Mass No. ^(d)	Location	Deflection, Inches	
		Longitudinal	Vertical
1	Nose Gear Tire	3.73	3.98
2,31	Main Gear Tires	1.42	3.34
13	Engine Structure	18.2	10.9
9,29,37	Lower Firewall	4.23 ^(a)	-
		10.6 ^(b)	5.6 ^(b)
		13.0 ^(c)	4.65 ^(c)
6,18,34	Forward Fuselage	-	-
43	Right Wing Tip	2.0	1.79
(a) Left side (b) Center (c) Right Side (d) See Figure 5-3, Tables 5-1 and 5-2			

6.3.3 Structure Responses

Figures 6-25 through 6-32 show a comparison of analyses and test structure acceleration responses at various locations throughout the airplane. Table 6-21 summarizes the results of the comparison between analysis and test. Figures 6-25 and 6-26 show the engine acceleration comparisons. The response shapes in each direction compare favorably. The test peak responses are sharper, particularly in the longitudinal and lateral directions, and occur .008 to .017 seconds earlier as compared to the analytical values. The test measured longitudinal response of 200 g's is obviously a measurement reflecting local structure response. Otherwise 200 g's acting on 383 pounds of engine mass would drive the engine through the firewall, which of course did not happen during the test.

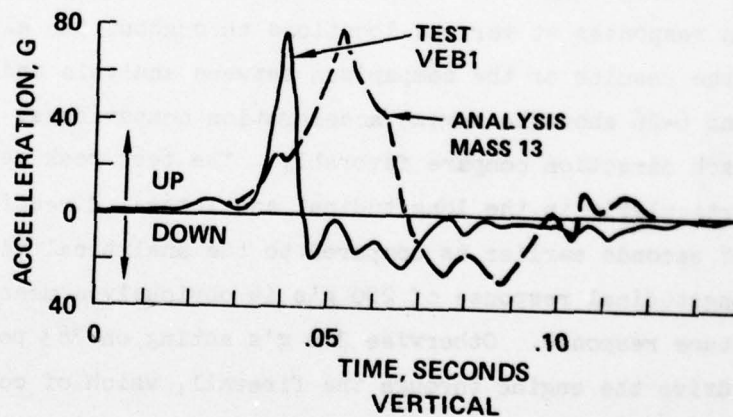
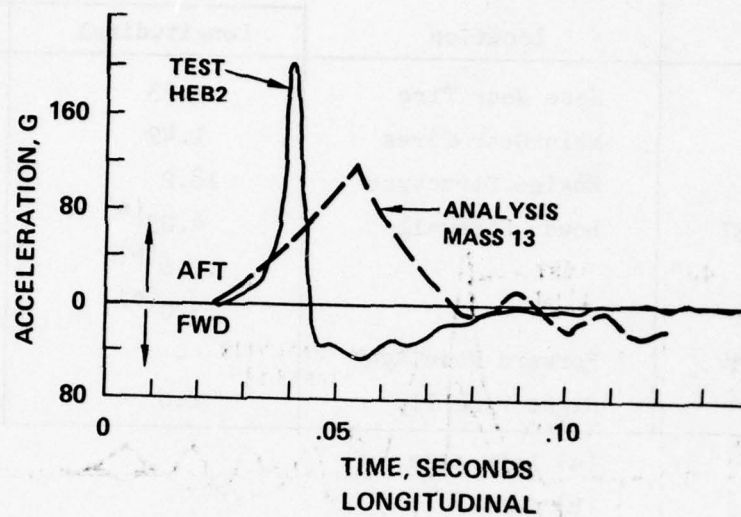


Figure 6-25. Comparison of Analysis and Test Engine Vertical and Longitudinal Accelerations, Test 3

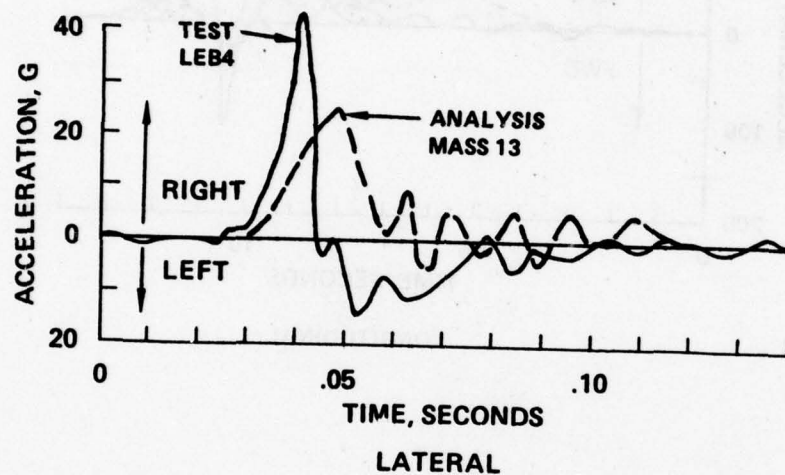


Figure 6-26. Comparison of Analysis and Test Engine Lateral Accelerations, Test 3

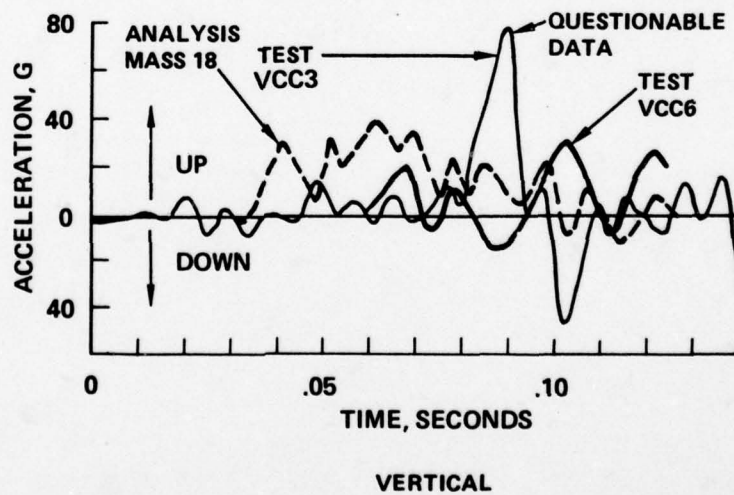
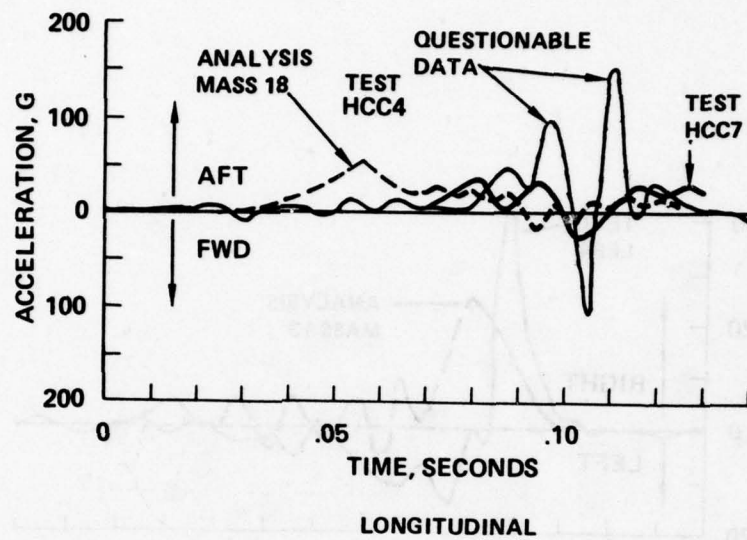


Figure 6-27. Comparison of Analysis and Test Floor Vertical and Longitudinal Accelerations, F.S. 27, Test 3

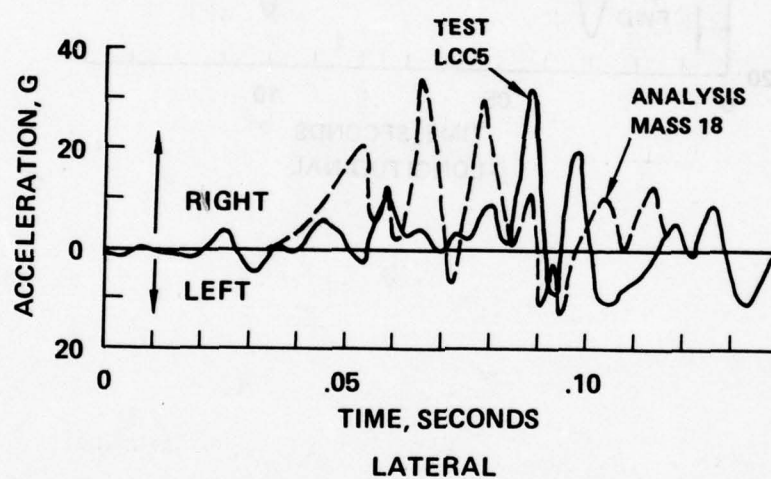


Figure 6-28. Comparison of Analysis and Test Floor Lateral Accelerations, F.S. 27, Test 3

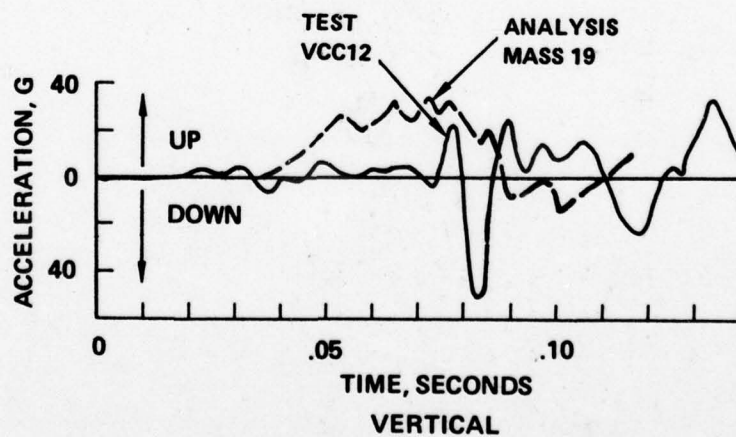
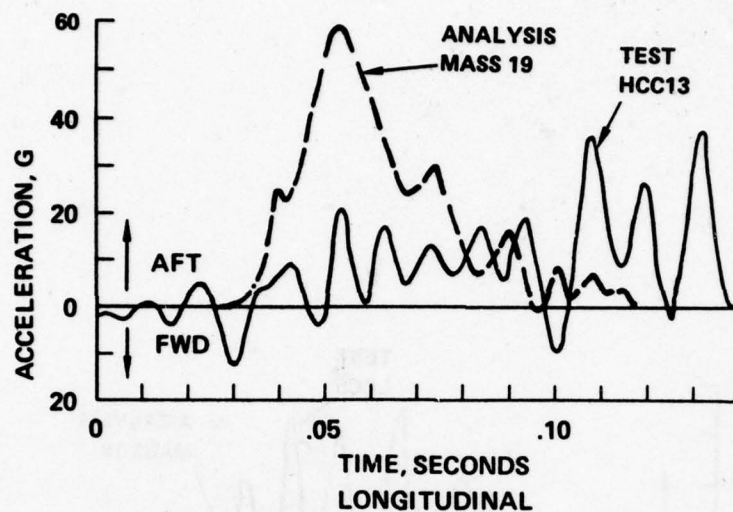


Figure 6-29. Comparison of Analysis and Test Floor Vertical and Longitudinal Accelerations, F.S. 60, Test 3

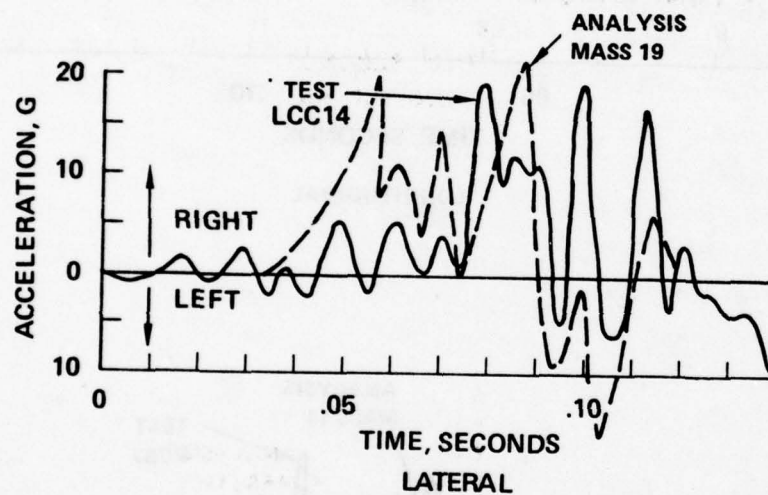


Figure 6-30. Comparison of Analysis and Test Floor Lateral Accelerations, F. S. 60, Test 3

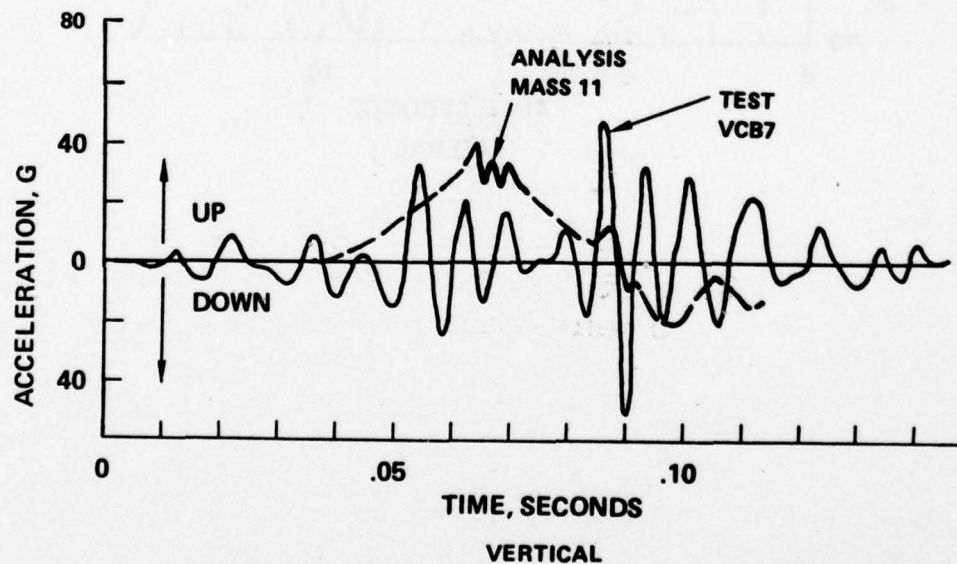
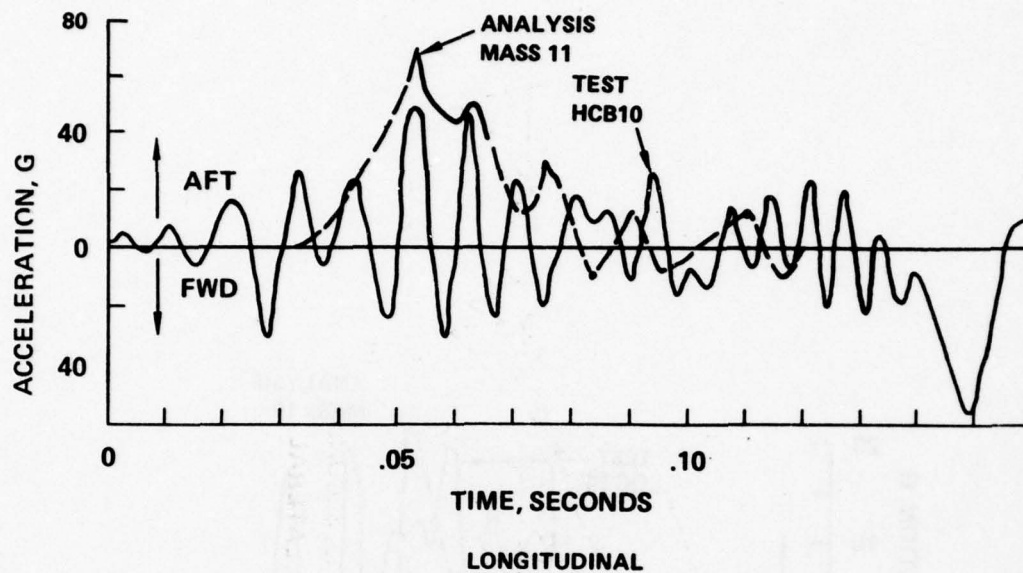


Figure 6-31. Comparison of Analysis and Test Floor Vertical and Longitudinal Accelerations, F.S. 90-108, Test 3

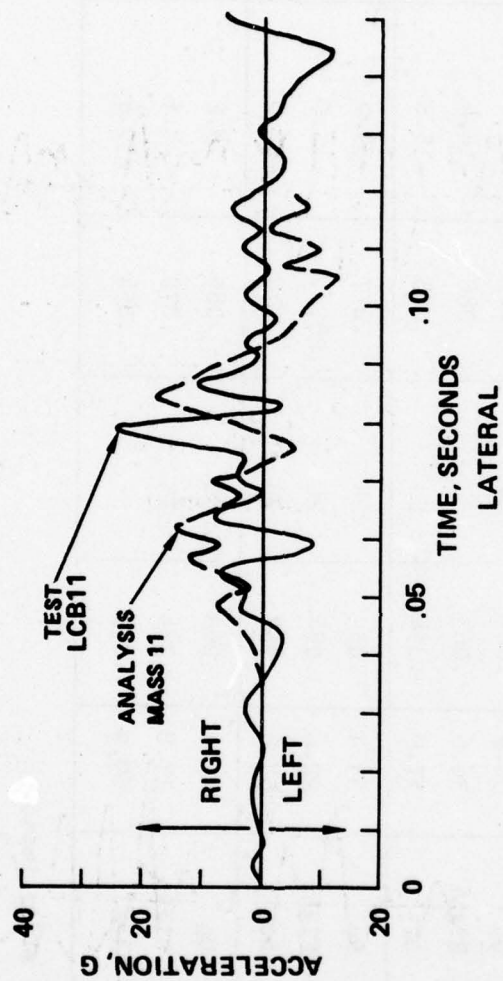


Figure 6-32. Comparison of Analysis and Test Floor Lateral Accelerations, F. S. 90-108, Test 3

TABLE 6-21. COMPARISON OF ANALYSIS AND TEST STRUCTURE RESPONSES, TEST 3

Location	Direction	Analysis		Test		Percent (b) Difference	Time (c) Difference
		G _{peak}	Time (a)	G _{peak}	Time (a)		
Engine	Up	75	.057	75	.040	0	-.017
	Right	23.6	.048	42/30 (d)	.040	25.2 (d)	-.008
	Aft	104	.057	200/124 (d)	.040	16.1 (d)	-.017
Forward Fuselage Floor, F.S. 27	Up	38.9	.063	30	.100 (f)	-30	.037
	Right	36.6	.063	32	.088	-14.4	.025
	Aft	57.9	.054	50 (e)	.088	-15.8	.034
Main Landing Gear Floor, F.S. 60	Up	33.4	.05	24	.077	-39.2	.027
	Right	22.6	.084	20	.08, .100	-13.0	-.004 to .016
	Aft	58.6	.057	36	.110	-62.8	.053
Aft Fuselage Floor, F.S. 90-108	Up	40.4	.063	50	.085	19.2	.022
	Right	17.8	.084	25	.079	28.8	-.005
	Aft	69.9	.051	50	.054	-39.8	.003

(a) Time in seconds after impact

(b) Percent difference = $\left(\frac{\text{Test Value} - \text{Analysis Value}}{\text{Test Value}} \right) \times 100$

(c) Time difference = test time - analysis time

(d) Based on 50 Hz low-pass filter

(e) Disregards sharp pulses

(f) Based on VCC6 location test data

Due to the sharpness of the engine longitudinal and lateral pulses, 50 Hz low-pass filtering of the test data was utilized to determine how the comparisons would be affected. From Table 6-21 it can be seen that with the lower frequency filter the test magnitudes are reduced and agree within 16 to 25 percent of the analytical values. The comparison of the test and analysis engine vertical responses agrees very well with the 100 Hz filter. The engine response analytical results are less affected by filtering than test results. For example unfiltered analytical results for the three directions are as follows:

	<u>g, Unfiltered</u>	<u>g, Filtered (100 Hz)</u>	<u>% Change</u>
Up	82.8	75.0	+10.4
Right	27.8	23.6	+17.8
Aft	104	104	-0-

Compared to the results based on 100 Hz filtered test data, the unfiltered analytical results correlate better in the lateral direction; show slightly more discrepancy in the vertical direction and are unchanged in the longitudinal direction. Lowering the analytical filter cutoff frequency (not attempted) would most likely affect the vertical response (sharpest analytical peak pulse) more than the longitudinal and lateral directions.

Figures 6-27 and 6-28 show the comparison of analyses and test floor responses at F.S. 27. The test measured floor responses at this location show sharp pulses at between .085 and .110 seconds after impact. While the pulses show that this region is experiencing an impact, the extreme sharpness and shape of the pulse indicate that the magnitudes may be misleading. The sharp aft load followed by an equally sharp forward load (Figure 6-27) appear to represent local structure responses. For this reason responses at F.S. 44 (VCC6 and HCC7) are also shown in Figure 6-27. The responses at F.S. 44 do not exhibit the extreme change in directions noted at F.S. 27. Based on both F.S. 27 and F.S. 44 test data, the analysis agrees with the test data within 14 to 30 percent and within .025 to .037 seconds.

Figures 6-29 and 6-30 show a comparison of analysis and test floor accelerations at F.S. 60. The analytical response in the lateral direction matches reasonably well with the test data with regard to peak value (13 percent) and time of occurrence (-.004 to .016 seconds). However, the comparisons in the longitudinal and vertical directions do not fare as well. The peak values disagree by 39 to 63 percent. The analysis peaks occur substantially earlier than the test values. The test response shapes exhibit more oscillatory motion than do the analytically obtained responses.

Figures 6-31 and 6-32 show a comparison of analyses and test floor accelerations at F.S. 90-108. The lateral responses compare favorably with regard to peak value (28.8 percent) and time of occurrence (-.005 seconds) as well as response shape (Figure 6-32). The responses in the longitudinal and vertical directions (Figure 6-31) also show similarities between test and analysis with regard to response shape, peak value and time of occurrence. In the longitudinal direction the data agrees within .003 seconds, although the peak values differ by 40 percent. In the vertical direction the peak values agree within 19 percent and the times of occurrence of the peak values differ by .022 seconds.

The wing response comparisons (not shown) show substantial difference in all directions. The analysis peak values are as much as twice as high as the test values. The high analysis values are attributed in part to corresponding discontinuities resulting when wing spar failures occur.

In general, the analytically obtained floor responses occur earlier than noted in the test. This is consistent with the observation, based on evaluation of film analysis, regarding energy absorption. The floor peak responses generally agree within ± 30 percent.

6.3.4 Occupant Response

The occupant seat-restraint system model in KRASH is described in Section 5.1 and Figure 5-4. The DRI's in the math model for Test 3 show a negative value from time = .054 seconds and on, indicating the occupant spine may be in tension and not compression as was the case in Tests 1 and 2. The DRI, being a measure of spinal compression, is not a valid indication of potential

spinal injury in tension. Figures 6-33 and 6-34 show the pilot and copilot lower torso acceleration responses obtained by analysis as well as the pilot and copilot pelvic responses measured during the test. The peak loads and times of occurrence are noted in Table 6-22. As in the case of floor acceleration response comparisons, the analytically obtained times of occurrence for the peak values precede the corresponding test points by substantial margins (.037 to .053 seconds). The comparison of peak vertical and lateral values fares better (-6.8 to +22.5 percent).

The analytically obtained pilot lateral responses are very similar to the copilot lateral responses. However, no comparison is presented with test data which shows an extremely large unexplained 150 g peak to the left. In the right direction the response is approximately 30 g's. The comparisons in the longitudinal directions (not shown) have discrepancies which reflect the lack of restraint system modeling, as was the case in previous test comparisons.

Table 6-23 summarizes the results wherein stresses are monitored for the occupant seat legs. In the analysis none of the seat legs fail. In the test the pilot front inboard seat leg failed and the copilot and pilot aft seat legs pulled loose from their tracks. The time of occurrence of these events is estimated from the film analysis to be .090 seconds. The analysis results (Table 6-21) based on the maximum shear stress theory indicate that the shear yield is exceeded at each of the legs between .063 and .096 seconds. Maximum stress ratios of 1.02 to 1.57 are achieved.

The Test 3 analytical results indicate that insofar as seat failure is concerned there is less potential than for Test 1. The test results show more seat failures occurred during Test 1 than Test 3.

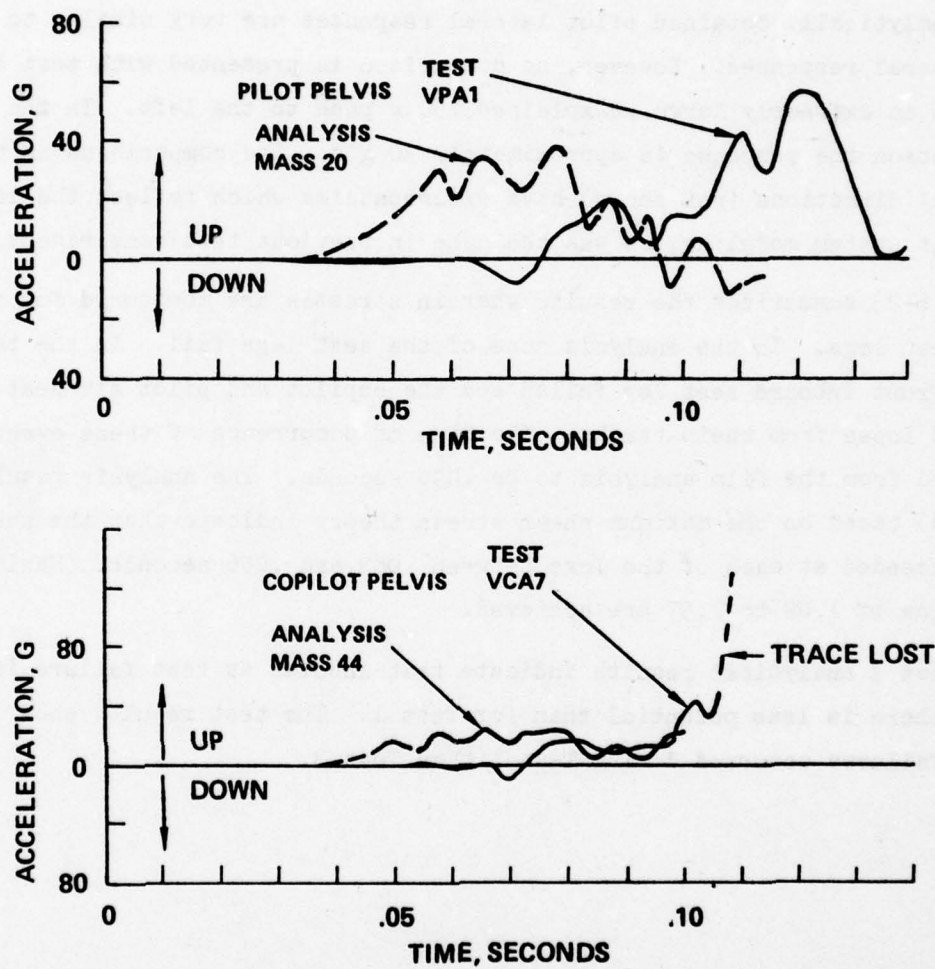


Figure 6-33. Comparison of Analysis and Test Pilot and Copilot Pelvic Vertical Accelerations, Test 3

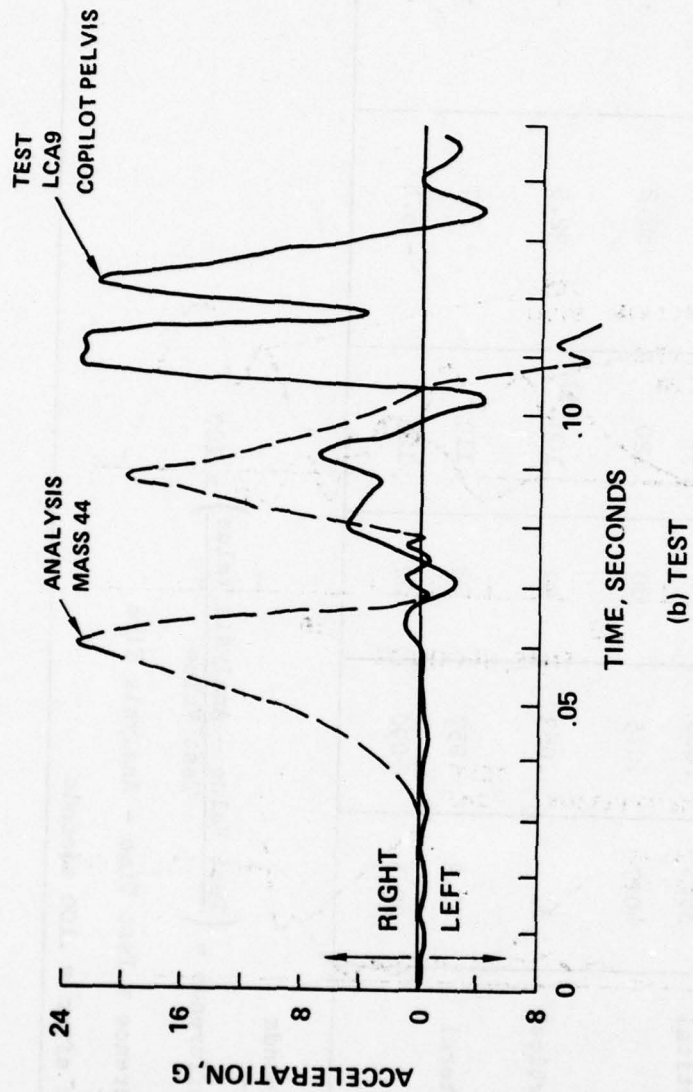


Figure 6-34. Comparison of Analysis and Test Copilot Pelvic Lateral Acceleration, Test 3

TABLE 6-22. COMPARISON OF PILOT AND COPILOT PELVIC ACCELERATIONS
FOR ANALYSIS VERSUS TEST, TEST 3

Location	Direction	Analysis		Test		Percent (b) Difference	Time (c) Difference
		G _{peak}	Time (a)	G _{peak}	Time (a)		
Pilot	Vertical	35.5	.066	44	.110	19.3	.044
		40.7	.075	60	.120	32.2	.045
Copilot	Vertical	31	.063	40	.100 ^(d)	22.5	.037
Copilot	Lateral	23.4	.057	23	.110	- 1.7	.053
		20.5	.090	22	.125	- 6.8	.035
(a) Time in seconds							
(b) Percent difference = $\left(\frac{\text{Test Value} - \text{Analysis Value}}{\text{Test Value}} \right) \times 100$							
(c) Time difference = Test Time - Analysis Time							
(d) Trace lost after $\approx .100$ seconds							

TABLE 6-23. STRESS RATIO RESULTS OBTAINED BY ANALYSIS, TEST 3

LOCATION	MEMBER i - j (b)	TIME AT WHICH STRESS RATIO > 1.0 (a)	MAXIMUM STRESS RATIO
Pilot Seat Logs			
Forward Outboard	6-20	0.063	1.02
Forward Inboard	18-20	0.054	1.34
Rear Inboard	20-27	0.096	1.52
Rear Outboard	20-28	0.063	1.57
Copilot Seat Logs			
Forward Outboard	34-44	0.051	1.37
Forward Inboard	18-44	0.114	1.15
Rear Inboard	27-44	0.087	1.33
Rear Outboard	44-48	0.063	1.26
(a) Time in Seconds			
(b) See Figures 5-3 and 5-4, Tables 5-1 and 5-2.			

6.4 TEST 4 ANALYSIS AND TEST COMPARISONS

6.4.1 Sequence of Events

The analytical results are obtained using the 30 mass 59 member half-airplane model described in Section 5.1. The sequence of events as obtained by analysis versus that obtained from film analysis is shown in Table 6-24. The comparison of analytical and test results with regard to sequence of events shows good agreement.

The change in airplane c.g. translational velocity, longitudinal and vertical, as obtained by analysis is shown in Figure 6-35. The camera angles make it difficult to obtain a direct comparison of cg velocities. However, estimates from the high speed film and post-crash photographs indicate that the analysis shows a more rapid decrease in velocities than occurs during the test.

Figure 6-36 shows the total energy and its components (kinetic, potential, strain, damping, crushing and friction) as a function of time. As can be observed in Figure 6-36, at impact the kinetic energy (94.3%) and the potential energy (5.7%) account for all the energy. After impact the energy is redistributed in the form of:

- strain
- structural damping
- crushing (including soil deformation)
- ground friction (including soil plowing)

Table 6-25 shows the distribution of energy components as a percentage of the total energy. Included in Table 6-25 is the maximum percent value and the time of occurrence as well as the percent of total at the conclusion of the analysis (time = 0.120 seconds).

From Figure 6-36 it can be seen that the kinetic energy reduces to 13.5 percent of the total by 0.090 seconds and increases slightly thereafter. The potential energy reduces to 2.8 percent of the total by 0.090 seconds and increases slightly thereafter as the airplane rebounds. The strain energy rises

TABLE 6-24. COMPARISON OF ANALYSIS AND TEST SEQUENCES, TEST 4

Sequence	Time-Seconds (a)	
	Analysis	Test
● Nose Gear Impact	0	0
● Nose Gear Support Failure	0.018	0.024
● Engine Lower Structure Impact	0.042	0.032
● Engine Spinner Impact	0.042	0.034
● Tail Cone Buckles	0.098	0.076
● Engine Buried into Soil	0.081 (b)	0.078
● Left Main Gear Tire Impact		0.088 (d)
● Occupant Impacts Instrument Panel	0.090 (c)	0.096
● Left Main Gear Tire Leaves Ground		0.114 (d)
(a) Time in seconds after impact (b) Analysis shows maximum ground deflection under engine mass (c) Occupant motion not available from analysis. Analysis shows front seat leg shear stress failure potential. (d) Tire skims the soil		

sharply from approximately 0.060 seconds until a peak percentage of 29.9 percent at 0.090 seconds. At the conclusion of the analysis the strain energy is still relatively high (25 percent). The crushing energy starts rising rapidly at about 0.042 seconds, at which time the engine structure makes contact with the soil. The crushing energy reaches a peak of nearly 17 percent at 0.084 which coincides with the time the maximum soil penetration has occurred. Damping and friction energy are continually rising, having reached peak values of 7.2 and 35.8 percent respectively at 0.120 seconds. The rate of increase in friction energy has slowed perceptibly after 0.090 seconds.

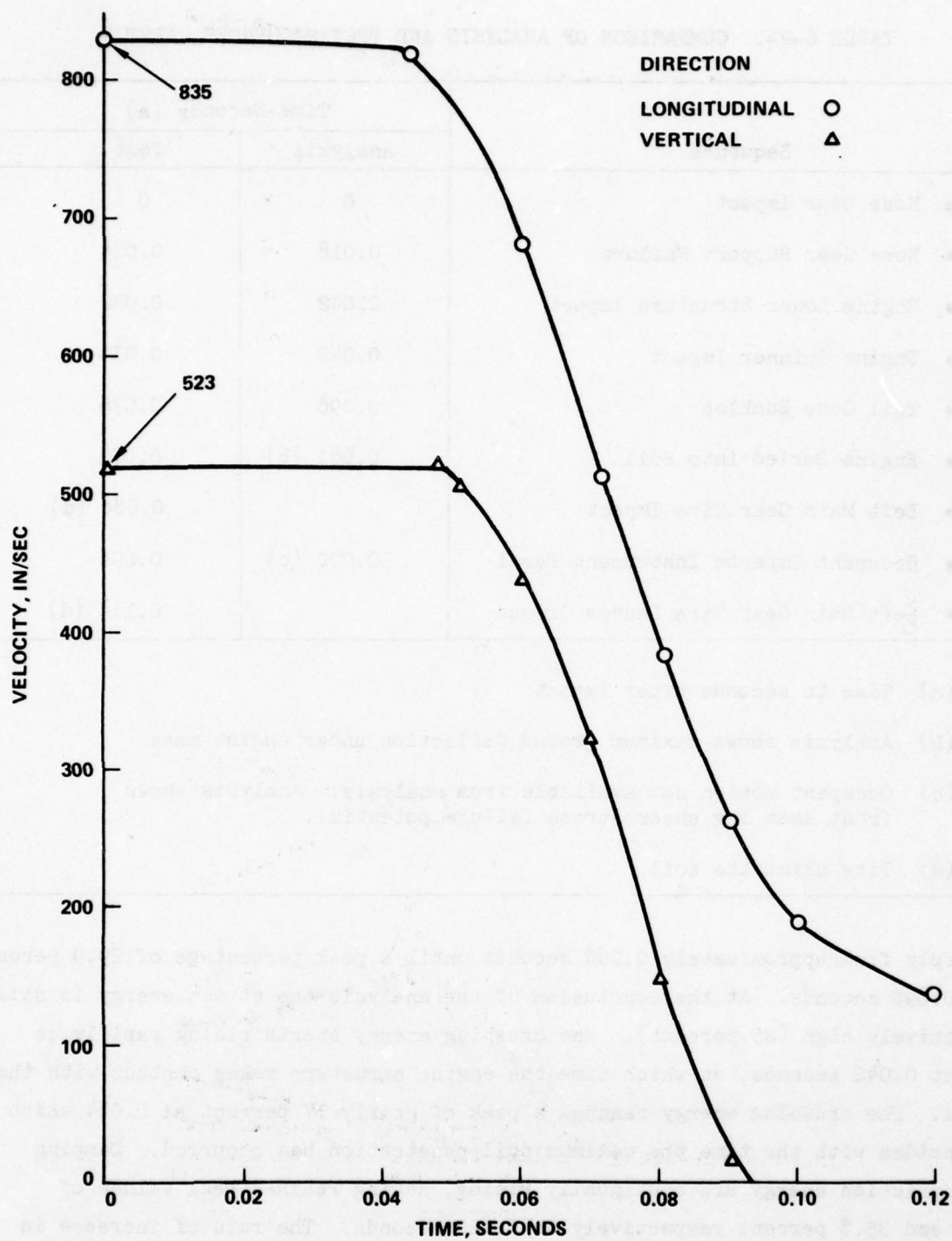


Figure 6-35. Analytically Obtained Longitudinal and Vertical Velocities Versus Time, Test 4

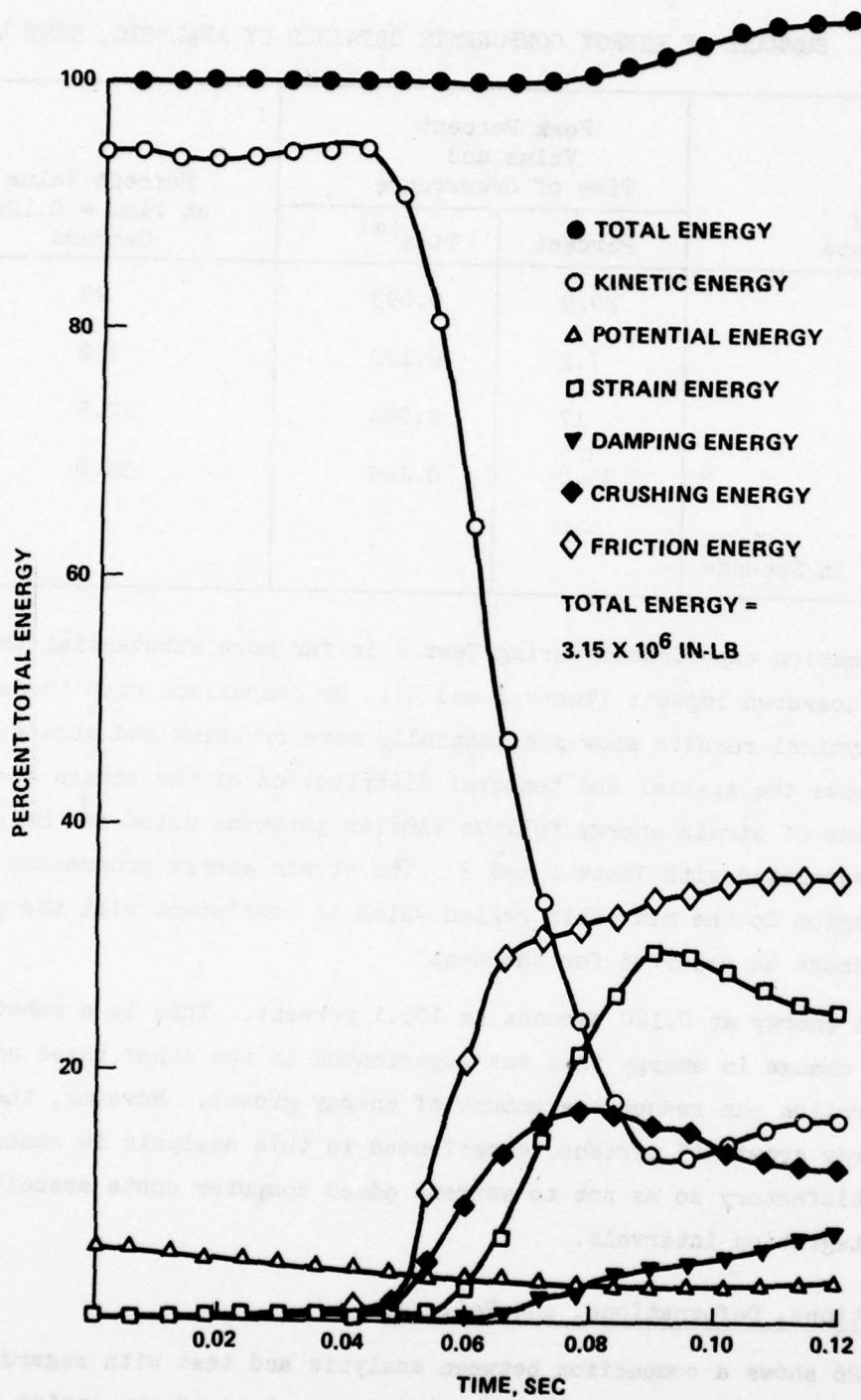


Figure 6-36. Total Energy and Energy Components Obtained by Analysis, Test 4

TABLE 6-25. SUMMARY OF ENERGY COMPONENTS OBTAINED BY ANALYSIS, TEST 4

Energy Components	Peak Percent Value and Time of Occurrence		Percent Value at Time = 0.120 Seconds
	Percent	Time ^(a)	
Strain	29.9	0.093	25
Damping	7.2	0.120	7.2
Crushing	17	0.084	12.5
Friction	35.8	0.120	35.8
(a) Time in Seconds			

The deformation experienced during Test 4 is far more substantial than the other two nosedown impacts (Tests 1 and 3). By comparison with these two tests the analytical results show substantially more crushing and strain energy. Figure 6-37 shows the spatial and temporal distribution of the strain energy. The distribution of strain energy follows similar patterns noted in the analytical results associated with Tests 1 and 3. The strain energy progresses from the forward region to the mid cabin region which is consistent with the progression of damage as observed for the test.

The total energy at 0.120 seconds is 105.1 percent. This is a substantially higher change in energy than was experienced in the other three analyses. A finer integration can reduce the amount of energy growth. However, the degree of energy growth (5 percent) experienced in this analysis is considered marginally satisfactory so as not to warrant added computer costs associated with finer integration intervals.

6.4.2 Deflections, Deformations, and Failures

Table 6-26 shows a comparison between analysis and test with regard to failures. As a result of Test 4 the airplane incurs loss of the engine from its supports, a wing rear spar failure, failure of nose gear support structure, and buckling of the tailcone. The analysis indicates that the nose gear support

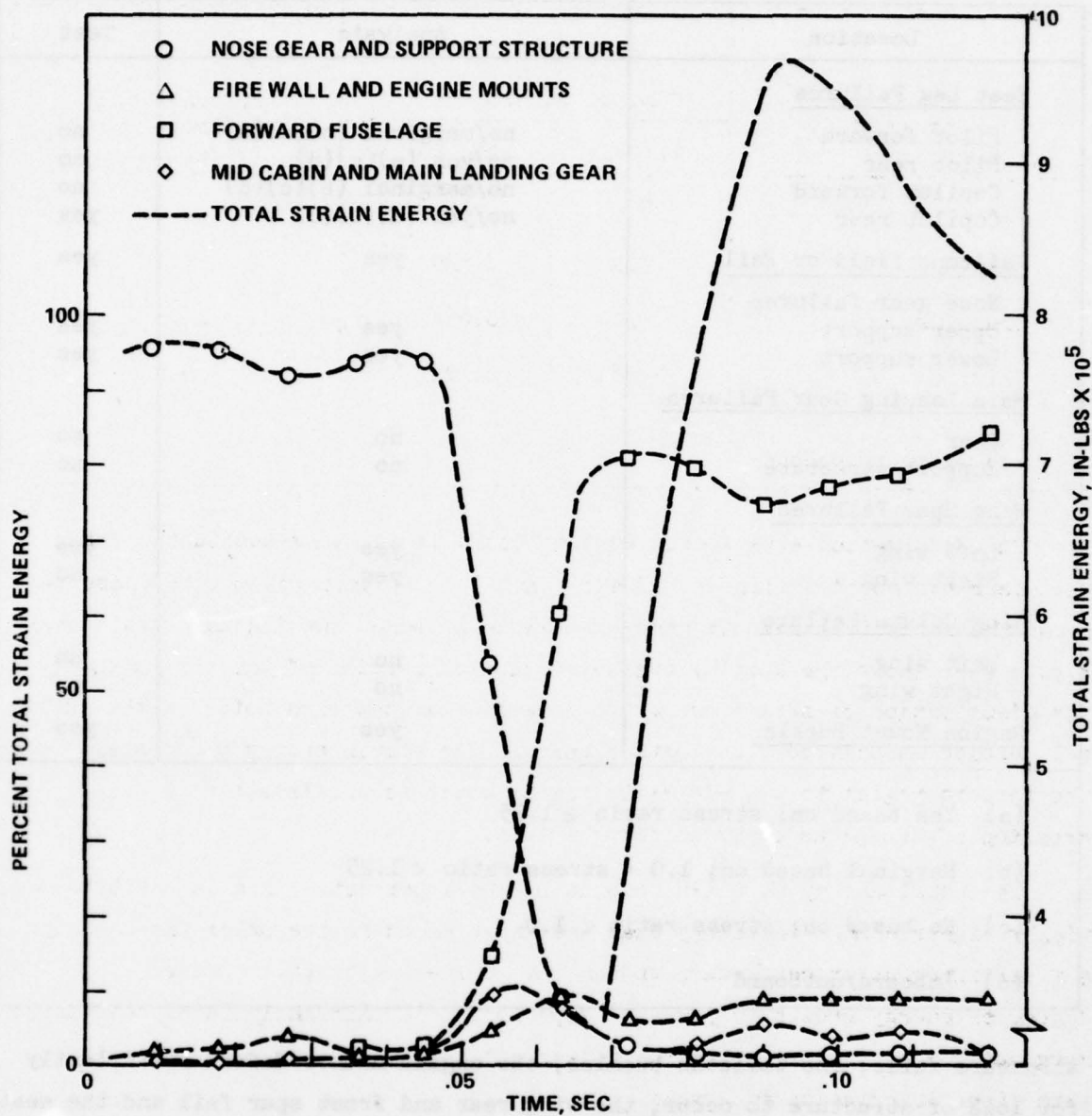


Figure 6-37. Strain Energy Distribution Histories Obtained by Analysis, Test 4

TABLE 6-26. COMPARISON OF ANALYSIS AND TEST FAILURES, TEST 4

Location	Analysis	Test
<u>Seat Leg Failures</u>		
Pilot forward	no/marginal (b)(c)(d)	no
Pilot rear	no/yes (a)(c)(d)	no
Copilot forward	no/marginal (b)(c)(d)	no
Copilot rear	no/yes (a)(c)(d)	yes
<u>Tailcone Yield or Fail</u>	yes	yes
Nose gear failures		
Upper support	yes	yes
Lower support	yes	yes
<u>Main Landing Gear Failures</u>		
Gear	no	no
Support structure	no	no
<u>Wing Spar Failures</u>		
Left wing	yes	yes
Right wing	yes	no
<u>Wing Column Failure</u>		
Left wing	no	no
Right wing	no	no
<u>Engine Mount Buckle</u>	yes	yes
<p>(a) Yes based on; stress ratio ≥ 1.25</p> <p>(b) Marginal based on; $1.0 < \text{stress ratio} < 1.25$</p> <p>(c) No based on; stress ratio < 1.0</p> <p>(d) Inboard/outboard</p>		

structure fails, the tailcone buckles, the engine mounts deform sufficiently for loss of structure to occur, the wing rear and front spar fail and the seats show the potential to fail due to excessive stress. The engine mounts yield after approximately 0.065 seconds and deflect axially over 4 inches which indicates that the engine moves aft into the firewall. Of course, the analysis cannot show loss of engine unless the engine mounts were treated as members that rupture (due to excessive force or deflection) instead of members which

are allowed to restiffen. The forward fuselage panels deform axially nearly 10 inches which is substantially more than in any of the previous test analyses. This large deformation is consistent with the test results which show severe crushing of the forward fuselage. A summary of axial and bending deflections is presented in Table 6-27. From Table 6-27 it can be seen that the member deflections are higher overall than obtained in any of the previous analyses. Figure 6-38 shows a comparison of cabin deformations obtained from analysis versus test at approximately 0.120 seconds after impact. For reference the undeformed cabin is also shown in Figure 6-38. The results compare very favorably in the forward fuselage section, wherein the firewall has been pushed nearly back to F.S. 27. The analysis does not depict the yielding at the rear door post as pronounced as in the estimate of the post test condition.

Tables 6-28 and 6-29 show the maximum deflections experienced by the external springs representing the structure and the soil, respectively, at various locations. The ground deflection due to engine penetration (engine longitudinal) was measured after the test to be approximately 18 inches. The analysis shows a deflection of 12.7 inches at this location.

6.4.3 Structure Responses

Figures 6-39 through 6-43 show a comparison of analysis and test structure responses at various locations throughout the airplane. Table 6-30 summarizes the results of the comparison. The analytically obtained engine response peaks (Figure 6-39) show agreement within 2.2 to 34 percent with test data. However, the response shapes of the analytically obtained data differ substantially from the corresponding test data. In the test the engine is torn loose from its mounts and at the conclusion of the test it is several feet away from the remaining airplane structure. In the analysis the engine mounts are represented by load-deflection curves which allow for restiffening after an initial loss of load carrying capability (post-buckle condition). In using the restiffening curve the engine mount is not allowed to rupture and separate from the airplane. This factor plus the difficulty in realistically representing time varying soil forces prevents a good comparison of engine response results. The floor

TABLE 6-27. MEMBER DEFLECTIONS OBTAINED BY ANALYSIS, TEST 4

Member	Element Nodes i-j (a)	Deflection Inches
<u>Axial</u>		
Engine Mount	9-13, 10-13	4.2
Forward Fuselage	6-9, 7-9	8.4 - 9.8
Firewall	9-10	-
Tunnel	18-26, 18-29	7.8 - 8.6
<u>Bending</u>		
Forward Door Post - Lower	6-7	6.5
Forward Door Post - Upper	7-8	3.1
Rear Door Post - Lower	4-23	3.5
- Upper	5-23	5.14
<u>Firewall</u>		
	9-10	11.5
Tunnel Structure	18-26, 18-29	1.2 - 3.6
Forward Fuselage	6-9, 7-10	2.7 - 6.0
(a) See Math Model Figure 5-3, Tables 5-1, 5-2.		

responses are shown in Figures 6-40, 6-41 and 6-42 for F.S. 27, F.S. 60, and F.S. 90-108, respectively. The peak responses show agreement within a few percent to as much as 30 percent. The times of occurrence of the peak responses agree within 0.001 to 0.022 seconds. The response shapes are generally in agreement. The analytical results tend to show less oscillatory motion than observed in the test data. Figure 6-43 shows a comparison of wing responses. While the analysis results in the vertical direction show agreement within 2.5 percent and 0.004 seconds, the response shapes show more oscillatory motion than noted in the test results. In the longitudinal direction the analysis and test results differ substantially.

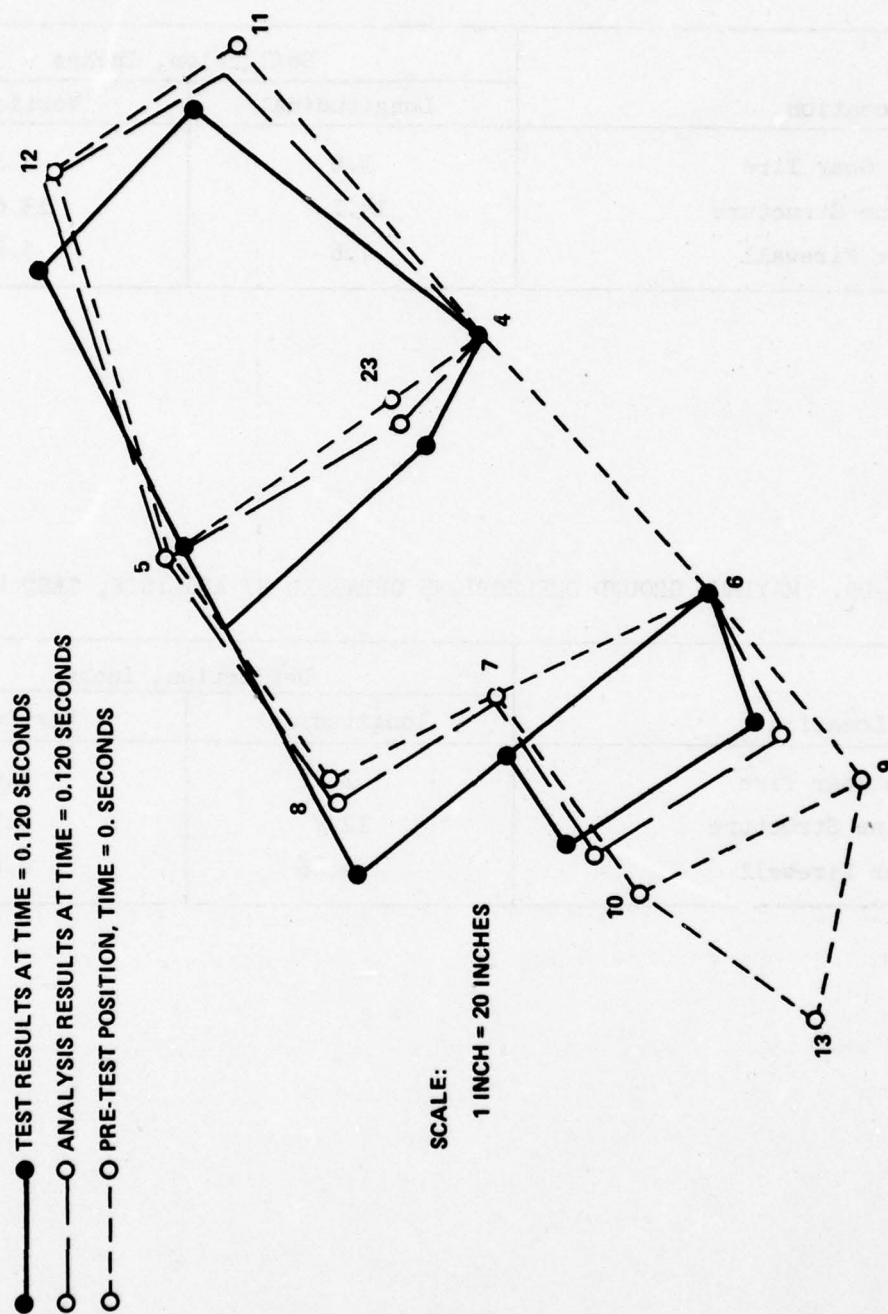


Figure 6-38. Comparison of Analysis and Test Cabin Deformations, Test 4

TABLE 6-28. MAXIMUM EXTERNAL SPRING DEFLECTIONS
OBTAINED BY ANALYSIS, TEST 4

Location	Deflection, Inches	
	Longitudinal	Vertical
Nose Gear Tire	3.2	3.3
Engine Structure	14.1	13.6
Lower Firewall	7.6	5.4

TABLE 6-29. MAXIMUM GROUND DEFLECTIONS OBTAINED BY ANALYSIS, TEST 4

Location	Deflection, Inches	
	Longitudinal	Vertical
Nose Gear Tire	1.72	1.68
Engine Structure	12.7	5.54
Lower Firewall	9.86	6.46

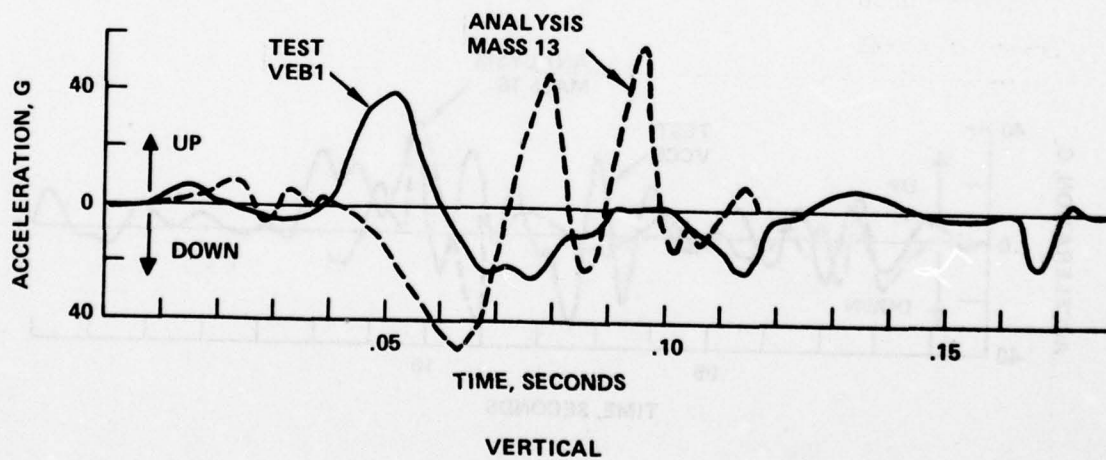
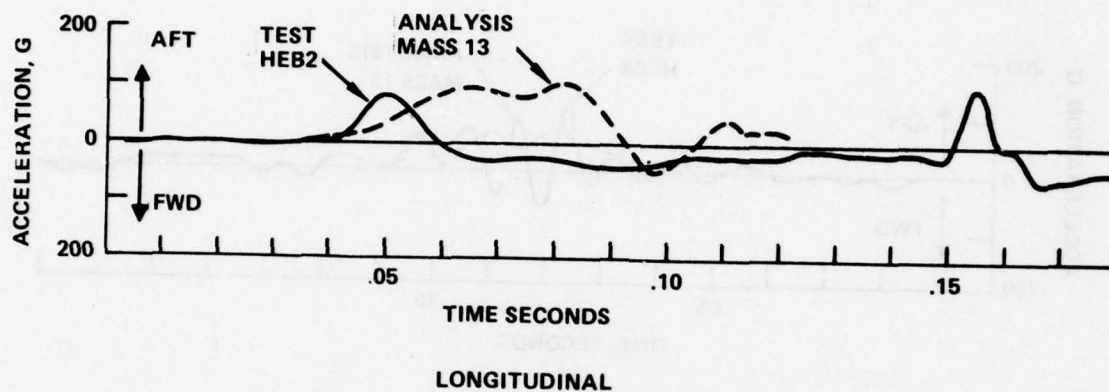


Figure 6-39. Comparison of Analysis and Test Engine Vertical and Longitudinal Accelerations, Test 4

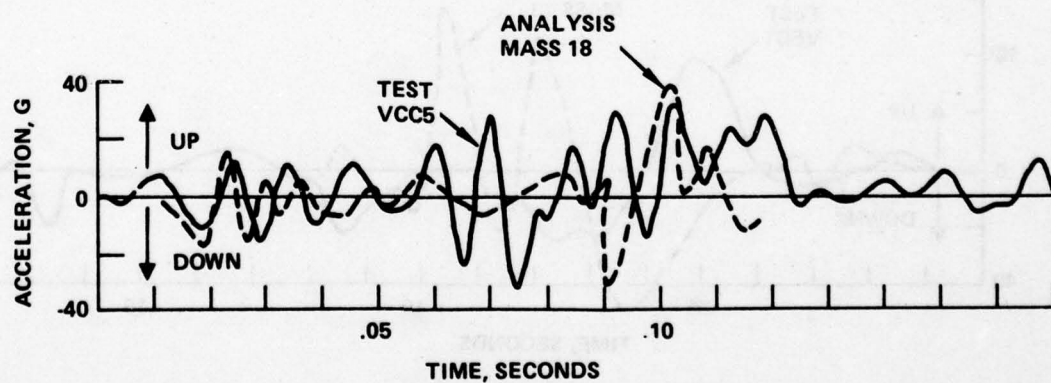
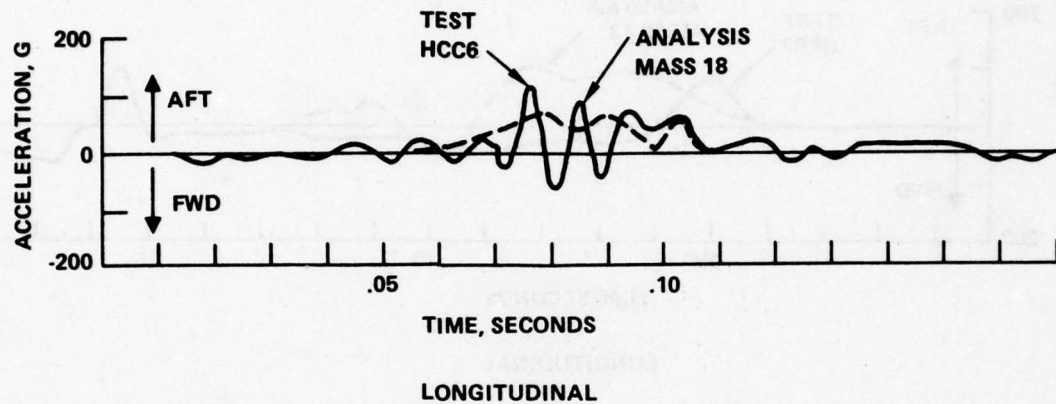


Figure 6-40. Comparison of Analysis and Test Floor
Vertical and Longitudinal Accelerations, F.S. 27,
Test 4

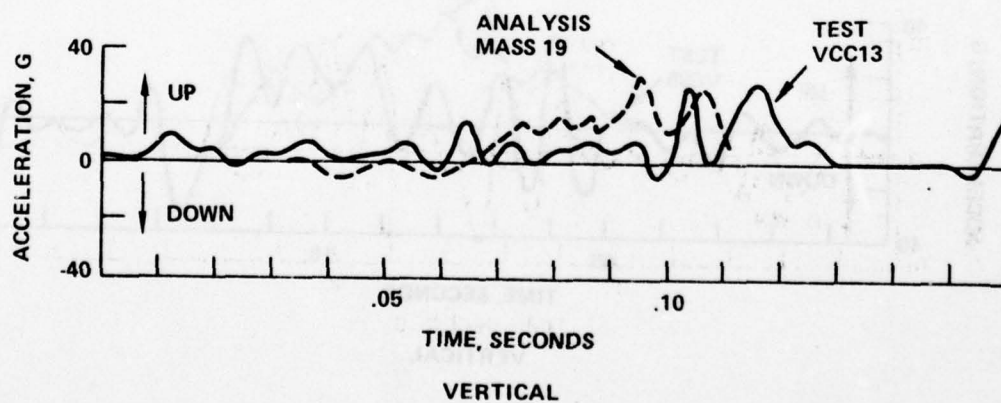
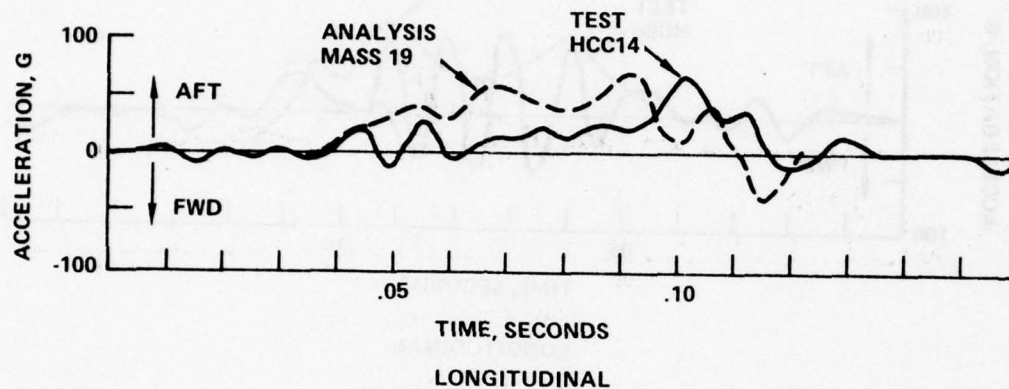


Figure 6-41. Comparison of Analysis and Test Floor Vertical and Longitudinal Accelerations, F.S. 60, Test 4

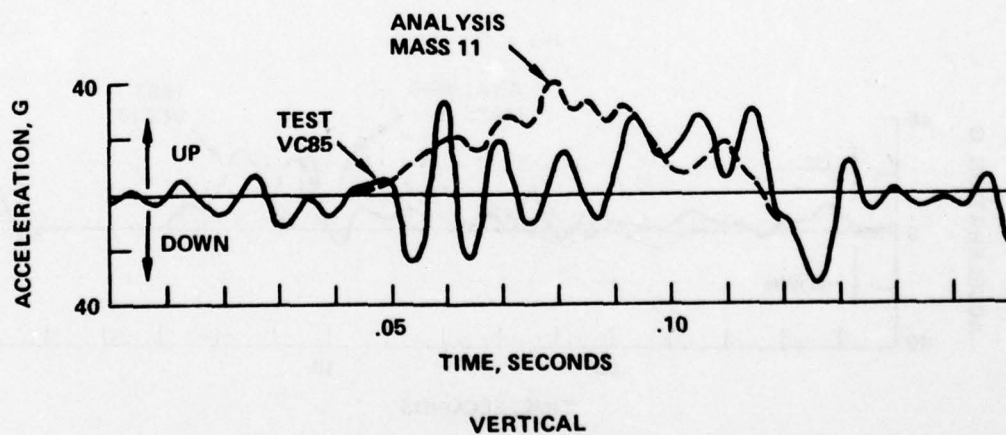
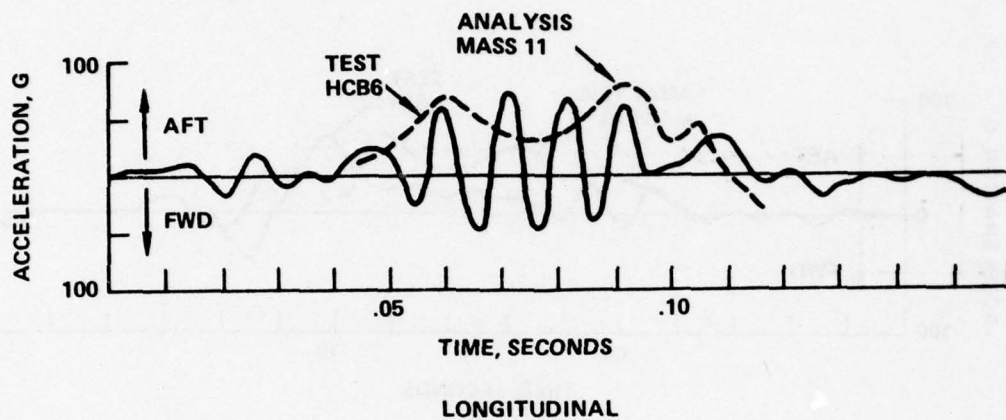


Figure 6-42. Comparison of Analysis and Test Floor Vertical and Longitudinal Accelerations, F.S. 90-108, Test 4

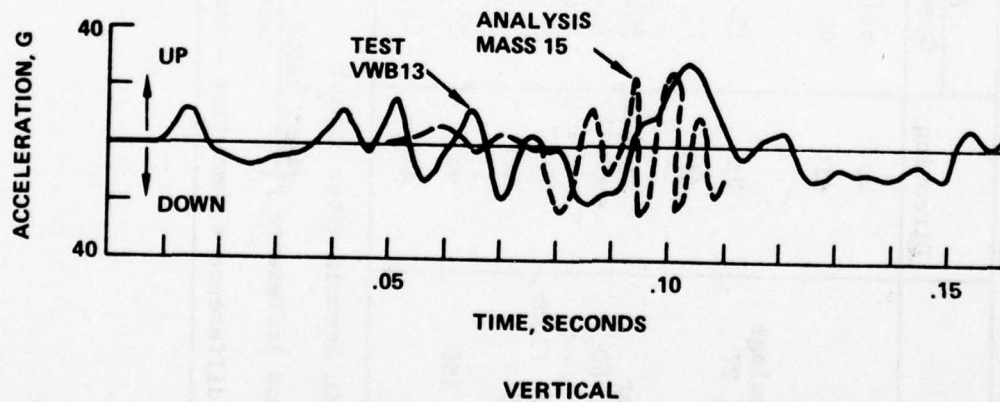
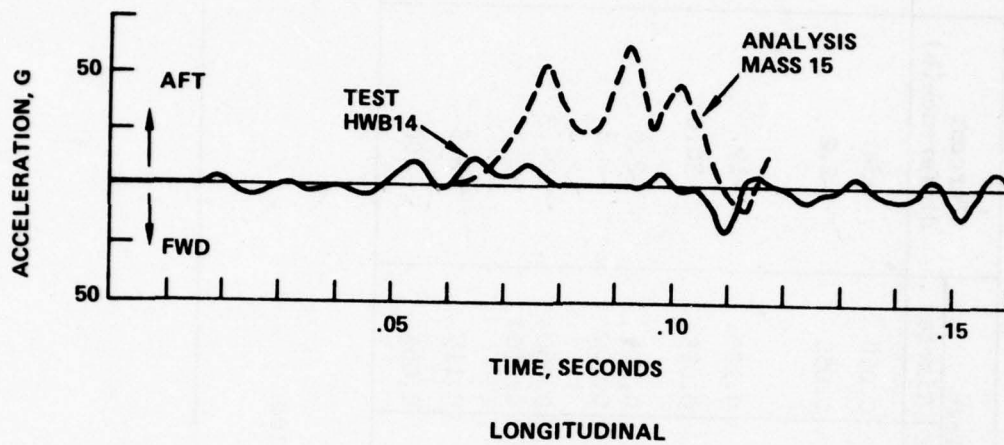


Figure 6-43. Comparison of Analysis and Test Wing Vertical and Longitudinal Accelerations, Test 4

TABLE 6-30. COMPARISON OF ANALYSIS AND TEST STRUCTURE RESPONSES, TEST 4

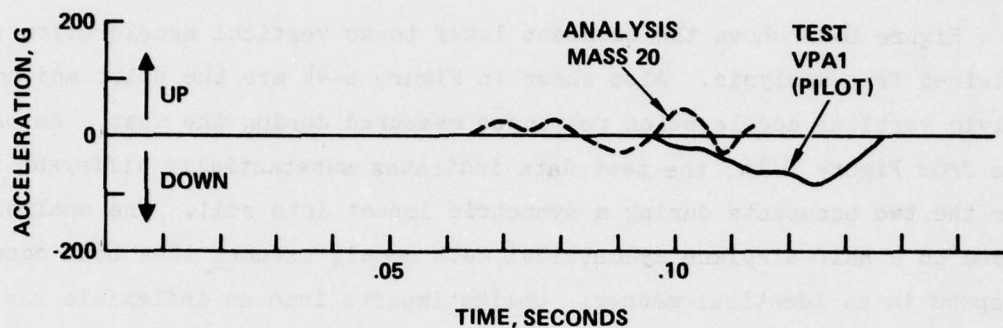
Location	Direction	Analysis		Test		Percent Difference(b)	Time Difference(c)
		Gpeak	Time(a)	Gpeak	Time(a)		
Engine	Up	53.6	0.096	40	0.050	-34.	-.046
	Aft	92	0.069	90	0.050	-2.2	-.019
Forward Fuselage Floor, F.S. 27	Up	35.7	0.099	30	0.100	-19.	-.001
	Aft	70	0.072	100	0.075	30.0	.003
Landing Gear Floor, F.S. 60	Up	30.6	0.093	30	0.115	-2.0	.022
	Aft	71.6	0.090	70	0.100	-2.3	.010
Aft Fuselage Floor, F.S. 90-108	Up	39.8	0.078	32	0.060	-24.3	-.018
	Aft	82.	0.078	80	0.070	-2.5	-.008
Wing B. L. 100	Up	27.3	0.111	28	0.115	+2.5	.004
	Aft	63.	0.093	25	0.065	> -100	-.028
(a) Time in Seconds After Impact							
(b) Percent difference = $\left(\frac{\text{test value} - \text{analysis value}}{\text{test value}} \right) \times 100$							
(c) Time difference = test time - analysis time							

6.4.4 Occupant Response

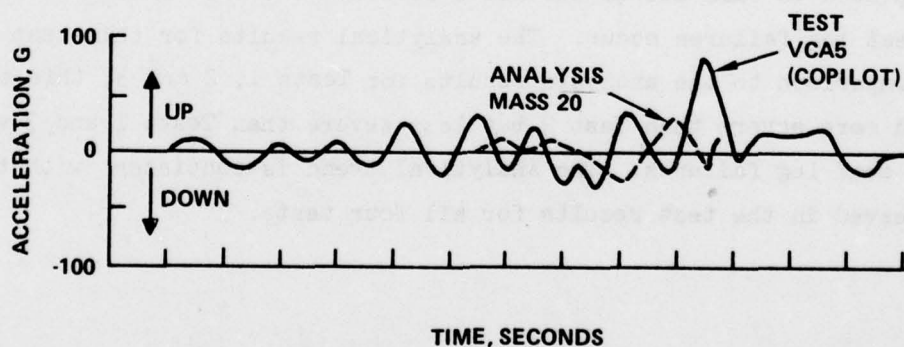
The analytically obtained DRI's record negative values which indicate the occupants experience tensile and not compressive loads. Consequently, the interpretation of DRI values is of no significance for this test.

Figure 6-44 shows the occupant lower torso vertical acceleration response obtained from analysis. Also shown in Figure 6-44 are the pilot and copilot pelvic vertical acceleration responses measured during the test. As one can see from Figure 6-44, the test data indicates substantially different motion for the two occupants during a symmetric impact into soil. The analysis, based on a half-airplane symmetrical math model, assumes that both occupants respond in an identical manner. Unlike impacts into an inflexible surface (concrete), the post-crash behavior of an airplane in soil develops forces which can complicate an analysis.

Table 6-31 summarizes the analytical results wherein stresses are monitored for the occupant seat legs. Since the math model is a half-airplane representation of a symmetrical impact condition, the responses for only one occupant (pilot-left side) are provided. The right side (copilot) responses are taken to be identical to the left side responses. From Table 6-31 it can be seen that for only one of the four seat legs does the monitored stress ratio exceed a value of 1.25. This indicates the possibility that only one of the four legs may be expected to fail due to excessive stress. The test results indicate that no seat leg failures occur. The analytical results for this test indicate that in comparison to the analysis results for Tests 1, 2 and 3, this test is considered more severe than Test 2 but less severe than Tests 1 and 3 with regard to seat leg failures. The analytical trend is consistent with the trend observed in the test results for all four tests.



(a) PILOT



(b) COPILOT

Figure 6-44. Comparison of Analysis and Test Pilot and Copilot Pelvic Vertical Accelerations, Test 4

TABLE 6-31. STRESS RATIO RESULTS OBTAINED BY ANALYSIS, TEST 4

Location	Member i-j (a)	Time at Which Stress Ratio >1.0	Maximum Stress Ratio
<u>Seat Legs</u>			
Forward Outboard	6-20	0.090	1.207
Forward Inboard	18-20	-	0.961
Rear Inboard	20-27	-	0.897
Rear Outboard	20-28	0.072	1.714
(a) See Figures 5-3, 5-4 and Tables 5-2, 5-3.			

SECTION 7

TASK II RESULTS

The following discussion presents a summary of the results of the Task II effort.

7.1 FULL SCALE CRASH TEST PREPARATION

Three light high-wing, single-engine airplanes were prepared for crash testing at the NASA-Langley Impact Dynamics Research Facility (IDRF). In preparation for the tests the airplanes had their fuel tanks purged, their upholstery, rear seats, wheel fairings, left door, tail section and radios removed. The airplanes were painted yellow and the cg, the O.O. B.L., the O.O. W.L. and the bulkhead and stringer locations identified by black tape. For each airplane the tail section was represented by a substitute structure having the proper mass and location. The fuel tanks were filled with dyed water. The airplanes weighed between 2330 and 2390 pounds. The cg position varied from F.S. 43.9 (tests 1, 3 and 4) to F.S. 47.1 (Test 2).

A minimum of 44 accelerometer channels were used to record the dynamic response of the structure and occupants during each test. A 95th percentile dummy and a 80th percentile dummy were installed in the front seats. Occupant accelerations were obtained from accelerometers installed in the occupant heads and pelvises. In addition, occupant seat belt and shoulder harness loads were recorded, structural deflections were measured, the crash sequence was recorded on film and photographs of the post-crash condition of the airplanes were taken. A total of 17 high speed cameras including three onboard the airplane were utilized for each test.

7.2 FULL SCALE CRASH TEST RESULTS

Four crash tests were performed. The impact conditions are noted in Table 7-1. For each crash test the crash sequence was filmed and composite

TABLE 7-1. SUMMARY OF CRASH TEST IMPACT CONDITIONS

	Test Number			
	1	2	3	4
Impact Velocities (MPH) along flight path longitudinal vertical	55.5 47.4 28.7	50.8 48.6 14.8	58.1 47.6 33.2	55.9 48.4 31.9
Angles (degrees) flight path (γ) impact (θ) attack (α) roll (ϕ) yaw (ψ)	-30.72 -30.17 .57 + 4.13 - 3.27	-17 +13.5 +30.5 + 3.25 -11.5	-34.86 -39.4 - 4.54 +18.75 - 7.9	-32. -34.8 - 2.8 < 1.0 < 1.0
Rotational Velocities (deg/sec) pitch (θ) roll (ϕ) yaw (ψ)	46.4 negligible negligible	6.9 negligible negligible	14.3 negligible negligible	18.2 negligible negligible
<p>γ is negative in dive</p> <p>θ are positive nose up relative to ground</p> <p>α is positive nose up relative to flight path</p> <p>ϕ are positive right wing down</p> <p>ψ are positive tail left</p> <p>and $\theta = \gamma + \alpha$</p> <p>ft/sec = 1.467 x MPH</p>				

prints showing the crash sequences are presented in Section 3.0. In addition, post-crash photographs depicting the damage to the airplanes are also provided.

A summary of the sequence of events for all the crash tests is presented in Table 7-2. Summaries of damage and failures sustained by each of the airplanes are presented in Tables 7-3 through Table 7-6 for the airframe, the occupant-seat-restraint system, the wing and fuel tanks, and the nose and main gears, respectively. From Table 7-4 it can be seen that, with the exception of one lap belt attachment failure during crash test 4, the restraint systems remained intact. From Table 7-5 it can be seen that none of the four crash tests did a fuel tank rupture or fuel spill, thus indicating little hazard from a post-crash fire.

Tables 7-7 and 7-8 present a summary of seventy index results and occupant pelvis vertical and longitudinal responses, respectively. The results shown in Table 7-7 indicate that severe head injury would result to both occupants for Tests 3 and 4.

Table 7-9 summarizes a qualitative assessment of the chances of occupant survivability during each of the crash tests. Four hazards are assessed including:

- accelerations experienced by occupants in the fore-aft and up-down directions. An assessment for the lateral direction is not presented because of the lack of available applicable tolerance data.
- Occupiable cabin deformation.
- Lethal blows, impact of occupant with structure or object and vice versa.
- Post-crash fire potential.

From Table 7-9 it can be seen that the results of Tests 1 and 2 indicate relatively low accelerations experienced by the occupants, little occupiable cabin damage, no impact of the occupants with structure or objects and no danger of a post-crash fire. An assessment of Test 3 results indicates moderate to high acceleration forces, moderate to severe occupiable cabin deformation, possible danger from impact between occupant and structure and no danger from a post-crash fire. An assessment of Test 4 shows potential for moderate to high acceleration levels, severe occupiable cabin deformation, a relatively high probability of a lethal blow and no danger from a post-crash fire.

TABLE 7-2. SUMMARY OF CRASH TESTS SEQUENCE OF EVENTS

(a) Time Period	Test Number			
	1	2	3	4
0	Nose Gear Tire Impact	Right Main Gear (RMG) Tire Impact	Nose Gear Tire Impact	Nose Gear Tire Impact
.001-.020	Nose Gear Support Structure Fails-.012		Nose Gear Support Structure Fails-.012	
.021-.040	Engine Lower Structure Impact-.034	LMG Tire Impact-.023 Tail Impacts-.033	Engine Lower Structure Impact-.024 Right Wing Tip Impact-.038	Nose Gear Support Structure Fails-.024 Engine Lower Structure Impact-.030 Engine Spinner Impact-.034
.041-.060	Engine Spinner Impact-.046 Lower Firewall Impact-.050 Right Main Gear (RMG)-.060 Tire	Nose Gear Tire Impact-.046	Lower Firewall and Forward Fuselage Impact-.048	Engine Spinner Buried in Soil-.052 Left Main Gear Tire Impact-.074
.061-.080	Left Main Gear (LMG) Tire Impact-.080		Right Main Gear Impact-.062 Tail Cone Buckles-.075 Pilot Head Impacts Instrument Panel-.080	Tail Cone Buckles-.076 Engine Buried in Soil-.078 Pilot Impacts Control Wheel-.078
.081-.100	RMG Bulkhead Failure-.082		Left Wing Strut Column Fails-.085 Co-Pilot Seat, Departs Rail-.090 Pilot Head Impacts Instrument Panel-.092	Right Main Gear Tire Impact-.082 Left Main Gear Tire Impact-.088 Pilot Contacts Instrument Panel-.096
.100-	Tail Cone Buckles-.108	Tail Lifts Off Ground-.125 Max. LMG Deflection-.150	Co-Pilot Head Impacts Instrument Panel-.121 Left Main Gear Tire-.135 Impact Max. LMG Deflection-.150 Left Wing Rear Spar Failure-.160	Left Main Gear Tire Leaves Ground-.114 Engine Shoved into Forward-.138 Fuselage Left Wing Spar Failure-.250 -.300
(a) Time in seconds after impact				

TABLE 7-3. SUMMARY OF AIRFRAME DAMAGE AS A RESULT OF THE CRASH TESTS

Location	Test Number			
	1	2	3	4
Engine and Firevall	Mounts buckled Firevall buckled (Figures 3-6, 3-13)	Firevall Buckled in Lower Region (Figures 3-17, 3-19)	Severe buckling, engine shoved back into firevall (Figures 3-30, 3-31)	Engine Torn Loose From Mounts - (Figures 3-40, 3-44, 3-45)
Forward Fuselage	Lower Fuselage Crushed several inches (Figures 3-2, 3-6, 3-7)	Slight damage to underside aft of firevall (Figures 3-18)	Severe crushing of lower fuselage (Figures 3-22 to 3-24)	Lower fuselage completely crushed (Figures 3-45 to 3-47)
Passenger Cabin Compartment	Moderate Deformation (Figures 3-2, 3-3, 3-4)	No damage (Figures 3-15, 3-16, 3-20)	Left and right front door posts buckled forward and outboard. Substantial deformation of cabin area Cabin top structure ruptured (Figures 3-28, 3-29)	Door posts severed. Cabin volume substantially compressed (Figures 3-40, 3-41, 3-44, 3-46, 3-49, 3-50, 3-51)
Floor	Severely buckled at F.S. 27 and F.S. 65 (Figures 3-8, 3-10, 3-11)	No damage (Figures 3-15, 3-16)	Severely buckled at base of floorboard. Moderate buckling near landing gear bulkhead (Figure 3-34)	Base of instrument panel completely crushed (Figure 3-48)
Tail Section	Slight buckle aft of F.S. 108 (Figure 3-2)	Buckled between F.S. 205-208 (Figures 3-15, 3-16)	Moderate buckling aft of F.S. 108 (Figures 3-22 to 3-24)	Severely buckled aft of F.S. 108 (Figures 3-40 to 3-43)

TABLE 7-4. SUMMARY OF OCCUPANT-SEAT-RESTRAINT SYSTEM FAILURES AND
OCCUPANT IMPACTS EXPERIENCED DURING THE CRASH TESTS

Location	Test Number			
	1	2	3	4
<u>Pilot</u>				
Seat leg failure forward	X		X	
rear				
Seat leg pulled from floor tracks forward			X	X
rear	X			
Shoulder harness or attachment failure				
Lap belt or attachment failure				
Occupant contact with Instrument Panel			X	X
<u>Co-Pilot</u>				
Seat leg failure forward	X			
rear				
Seat leg pulled from floor tracks forward			X	X
rear	X		X	
Shoulder harness or attachment failure				
Lap belt or attachment failure				X
Occupant contact with Instrument Panel			X	X
X Denotes occurrence				

TABLE 7-5. SUMMARY OF WING DAMAGE EXPERIENCED AS A RESULT OF THE CRASH TESTS

Location	Test Number			
	1	2	3	4
<u>Left Wing</u>				
torsional failure	X			
rear spar failure			X (b)	X (b)
column strut buckle			X	
fuel tank rupture				
fuel spillage				
wing tip damage				X
<u>Right Wing</u>				
torsional failure				
rear spar failure			X (c)	
column strut buckle				
fuel tank rupture				
fuel spillage				
wing tip damage			X	X
(a) X denotes occurrence (b) tension failure (c) compression failure				

TABLE 7-6. NOSE AND MAIN GEAR FAILURES AS A RESULT OF THE
CRASH TESTS

Location	Crash Test Number			
	1	2	3	4
Nose Gear				
Lower Support Failure	X	X	X	X
Upper Support Failure	X		X	X
Gears Failed Aft	X		X	X
Gears Failed Forward		X		
Right Main Gear				
Inboard Bolt Failure	X		X	
Gear Failure				
Left Main Gear				
Inboard Bolt Failure				
Gear Failure				
X denotes occurrence				

TABLE 7-7. SUMMARY OF SEVERITY INDEX RESULTS, TESTS 3 AND 4

Accelerometer Location	Direction of Response	Severity Index (a)	
		Test 3	Test 4
Pilot Head	Vertical (parallel to backbone)	136	1055
Pilot Head	Longitudinal (normal to backbone)	1785	4056
Pilot Head	Lateral (normal to backbone)	482	(b)
Copilot Head	Vertical (parallel to backbone)	(b)	1368
Copilot Head	Longitudinal (normal to backbone)	(b)	373
Copilot Head	Lateral (normal to backbone)	2337	(b)
(a) Based on 750Hz Data			
(b) Data unavailable			

TABLE 7-8. SUMMARY OF OCCUPANT PELVIS VERTICAL AND LONGITUDINAL RESPONSES, TESTS 1 THROUGH 4

Location	Direction	Test Number							
		1		2		3		4	
		Acceleration (a)	Duration (b)	Acceleration (a)	Duration (b)	Acceleration (a)	Duration (b)	Acceleration (a)	Duration (b)
Pilot	Up	40	.007	10	.008	40	.010	60	.015
	Down	(d)	(d)	(d)	(d)	(d)	(d)	80	.005
	Forward	20	.003	8	.010	(d)	(d)	40	.015
	Aft	10	.015	(d)	(d)	12	.020	10	.017
Copilot	Up	45	.008	10	.005	(c)	(c)	80	.002
	Down	(d)	(d)	(d)	(d)	(c)	(c)	20	.003
	Forward	15	.002	3	.020	10	.010	60	.006
	Aft	12	.015	(d)	(d)	20	.013	10	.007
(a) g's (b) seconds (c) not recorded (d) low value									

TABLE 7-9. ASSESSMENT OF OCCUPANT SURVIVABILITY

Hazard	Crash Test Number			
	1	2	3	4
1. Accelerations experienced by occupants				
Fore-Aft	L	L	M	M
Up-Down	L	L	H	H
2. Occupiable Cabin Deformation	L	L	M-H	H
3. Lethal Blow (Due to Impact with Structure or Object)	L	L	M	H
4. Post-Crash Fire	N		N	N
<p>H High level or severe damage</p> <p>M Moderate level or damage</p> <p>L Low level or little damage</p> <p>N No danger</p>				

7.3 LITERATURE SURVEY AND EVALUATION

Twenty-six technical publications are reviewed and their contents categorized to assist in future programs. The literature is reviewed with regard to airplane structure/flexible ground interaction. In particular the emphasis is placed in the following areas

- Analysis
- Landing Surface (Soil) Characteristics
- Landing Surface/Gear Interaction Tests
- Full Scale Aircraft Crash Tests
- Design

In each of the above noted subject areas an evaluation is performed which identifies the literature applicable to the particular subject. A composite

summary of the pertinent aspects of the literature with regard to structural crashworthiness analysis is presented. For each report included in the survey and evaluation, an abstract is presented. In addition, a literature survey subject index matrix and a soil/interaction test parameter index are provided. The literature survey data is presented in Appendix B.

7.4 MATHEMATICAL MODEL DESCRIPTION

The high-wing single-engine airplane type analyzed during Task II is modeled using digital computer program KRASH, as modified during Task II. Airplane math model size data are shown in Table 7-10. Details of the modeling is presented in Section 5 and Appendix D.

The analysis for crash tests 1, 2 and 3 was performed using a full airplane representation. The analysis for crash test 4 was performed using a half-airplane representation. The impact conditions are noted in Table 7-1. For test 4 a symmetrical impact condition ($\phi = 0, \psi = 0$) was used. The math models used for each of the four tests were identical except for:

- weight and cg representation
- initial impact conditions
- Post-failure representation of aft failed nose gear structure
- lift considerations for test 2
- soil representation for test 4

TABLE 7-10. SUMMARY OF MATH MODELS

Full (F) or Half-Model (H) ^(a)	TEST 1 F	TEST 2 F	TEST 3 F	TEST 4 H
Number of:				
Masses	48	48	48	30
Node Points	32	32	32	17
External Springs	32	32	32	22
Linear Beams	100	100	100	59
Nonlinear Beams	118	118	118	68
DRI Elements	2	2	2	1
Pin-Pin Beams	2	2	2	1
Pin-Fixed Beams	4	4	4	2
Unsymmetrical Elements	7	7	7	4
Lift/Weight Ratio	0	.65	0	0
Impact Conditions:				
Vertical Velocity (fps)	42.3	21.8	48.7	43.4
Longitudinal Velocity (fps)	68.9	71.3	70.	69.6
Pitch Angle (degrees)	-30.	13.5	-39.4	-34.8
Roll Angle (degrees)	4.1	3.3	18.7	0.
Yaw Angle (degrees)	-3.3	-11.5	-7.9	0.
Pitch Rate (degrees/second)	46.4	6.9	14.3	18.2
Weight (lb)	2370	2390	2370	2370
C.G. Position (Fuselage Station-in)	44.1	47.2	44.1	44.1
Inertias (lb-in-sec ²)				
Roll	1.84 E04	1.84 E04	1.84 E04	1.84 E04
Pitch	1.77 E04	2.10 E04	1.77 E04	1.77 E04
Yaw	2.96 E04	3.25 E04	2.96 E04	2.96 E04
(a) Refers to the analysis. Airplane data input as a half model in all four cases with the program computing full airplane data for Tests 1, 2 and 3.				

7.5 ANALYSIS RESULTS AND CORRELATION WITH TESTS

The following range of impact conditions for the four crash tests performed during the task described in this report are analyzed with program KRASH:

● Flight path velocity	74.5 to 85.2 ft./sec.
● Longitudinal velocity	69.5 to 71.3 ft./sec.
● Vertical Velocity	21.8 to 48.7 ft./sec.
● Flight path angle	-17 to -34.9 degrees
● Impact angle	13.5 to -39.4 degrees
● Attack angle	.5 to 30.5 degrees
● Roll angle	0. to 18.7 degrees
● Yaw angle	0. to 11.3 degrees

For the four crash tests the following analytical results are presented:

- Time history of energy components.
- Sequence of post-impact events
- cg vertical and longitudinal velocity histories.
- Spatial and temporal distribution of strain energy.
- Occupant seat leg stress ratios.
- Summaries of internal member failures and deflections
- Acceleration response histories for the engine, the floor at F.S.27, F.S.60, and F.S.90-108, the wing, and the occupants.
- Cabin deformation.
- External structure (springs) crushing.
- Occupant responses; accelerations and DRI's.

7.5.1 Energy, Velocity and Events

Table 7-11 shows a comparison of analytically obtained energy distributions. Based on the amount of energy absorbed via crushing and strain the most severe

TABLE 7-11. COMPARISON OF ANALYTICALLY OBTAINED ENERGY DISTRIBUTIONS, CRASH TESTS 1 THROUGH 4

	Test No.			
	1	2	3	4
Total Energy, in-lb	3.073×10^6	2.6×10^6	3.212×10^6	2.97×10^6
Maximum Value (a)				
Strain	11.4	4.2	17.81	29.9
Damping	3.74	.79	4.28	7.2
Crushing	6.47	1.85	12.54	17.0
Friction	36.08	16.4	41.83	35.8
Final Value (a)				
Kinetic	42.94	74.2	33.39	16.4
Potential	2.63	2.5	3.62	3.11
Strain	8.37	4.19	13.90	25.02
Damping	3.74	.79	4.28	7.19
Crushing	6.25	1.85	2.97	12.51
Friction	36.08	16.42	41.83	35.77
Energy Percent Change (b)	+11	-.05	+10	+5.01
Maximum Time of Analysis, seconds	.120	.144	.120	.12
(a) Percent of total				
(b) $\left(\frac{\text{Final Total}-\text{Initial Total}}{\text{Initial Total}} \right) \times 100$				

crash condition analyzed is Test 4, followed by Test 3, Test 1 and Test 2, respectively. The test results, based on structural damage sustained by the airplane, the acceleration levels recorded and the potential for occupant injury indicate the same order of test severity as noted by the interpretation of data contained in Table 7-11.

The analytically obtained cg translational longitudinal and vertical velocity histories are presented in Section 6 (Figures 6-1, 6-12, 6-21, and 6-35), along with test data points. The sequence of events obtained by analyses are compared to the test event times in Section 6 (Tables 6-1, 6-8, 6-15, and 6-23). Also included in Section 6 are analytically obtained plots of the strain energy spatial and temporal distributions (Figures 6-3, 6-23, and 6-37) for Tests 1, 3 and 4, respectively.

7.5.2 Seat Leg Damage

Table 7-12 presents a comparison of analytical and test results with regard to occupant seat leg damage (failure or derailment). While the analysis does not show agreement with the test data at all locations for each test, it does show agreement with the trend indicated by the test results. The test results show that the most severe test insofar as seat leg failures are concerned is Test 1, followed by Tests 3, 4 and 2, respectively. Table 7-13 presents data which further substantiates that the analytical trends are in agreement with the observed test trends. The higher stress ratios are associated with Tests 1 and 3. The lower stress ratios are associated with 2 and 4. At none of the seat leg locations do the Test 2 stress ratios reach a value of 1.0.

7.5.3 Structure Failures

Table 7-14 presents a summary of structure failures obtained in the analysis and observed from the tests. Overall, there is excellent agreement between the analysis and the tests. However the analysis results show the occurrence of several events which are not evident in the test results. For example, the Test 2 analysis indicates that the tailcone yields, the upper nose gear support fails and the right main gear rotation exceeds the programmed allowable value.

TABLE 7-12. SUMMARY OF ANALYSIS VERSUS CRASH TEST SEAT LEG DAMAGE

Location	Test Number							
	1		2		3		4	
	Analysis	Test	Analysis	Test	Analysis	Test	Analysis	Test
Pilot Forward	Yes	Yes	No	No	Marginal/yes (d)	Yes	No/marginal (d)	No
Rear	Marginal/yes (d)	Yes	No	No	Yes	No	No/yes (d)	No
Co-pilot Forward	Yes	Yes	No	No	Marginal/yes (d)	Yes	No/marginal (d)	No
Rear	Marginal/yes (d)	Yes	No	No	Yes	Yes	No/yes (d)	No
<p>(a) "<u>Yes</u>" indicates failure or derailment for tests, failure or stress ratio >1.25 for analysis</p> <p>(b) "<u>Marginal</u>" indicates analysis stress ratio between 1.0 and 1.25</p> <p>(c) "<u>No</u>" indicates no failure or derailment for tests, stress ratio <1.0 for analysis</p> <p>(d) Inboard/Outboard</p>								

TABLE 7-13. SUMMARY OF SEAT LEG STRESS RATIOS
OBTAINED BY ANALYSIS

Location	(a) Maximum Stress Ratio for			
	Test 1	Test 2	Test 3	Test 4
Pilot				
Forward Outboard	1.27	.86	1.02	1.207
Forward Inboard	1.31 (b)	.82	1.34	.961
Rear Inboard	1.0	.71	1.52	.897
Rear Outboard	1.76	.83	1.57	1.714
Copilot				
Forward Outboard	1.41	.64	1.37	1.207
Forward Inboard	1.73 (b)	.74	1.15	.961
Rear Inboard	.91	.64	1.33	.897
Rear Outboard	1.25	.77	1.26	1.714
Overall Average	1.33	.75	1.32	1.19
(a) Stress Ratio = $\frac{\text{Shear stress}}{\text{allowable yield stress}}$				
(b) Seat Leg Fails				

TABLE 7-14. SUMMARY OF ANALYSIS VERSUS CRASH TEST STRUCTURE FAILURES

Location	Test Number							
	1		2		3		4	
	Analysis	Test	Analysis	Test	Analysis	Test	Analysis	Test
<u>Nose Gear Failure</u>								
Lower Support	•	•	•	•	•	•	•	•
Upper Support	•	•	•	•	•	•	•	•
<u>Main Landing Gear Failure</u>								
Gear			•					
Support Structure	•	•				•		
<u>Wing Rear Spar Failure</u>								
Left Wing					•	•	•	•
Right Wing					•	•	•	
<u>Wing Column Strut Failure</u>								
Left Wing	•				•	•		
Right Wing	•							
<u>Engine Mount Buckle</u>	•	•			•	•	•	•
<u>Tailcone Yield or Failure</u>	•	•	•		•	•	•	•
• Denotes occurrence								

The Test 1 analysis shows wing column strut buckling, and the Test 4 analysis shows a right wing spar failure. These differences between the test and the analysis results are directly related to the selection of program input data, particularly the selection of section properties, nonlinearities and failure criteria. Generally, except for the main gear rotation, the discrepancies involve areas wherein post-failure behavior does not influence occupant safety. In the situation wherein the right main gear fails (Test 2) the analysis is simply indicating a high potential for failure. While the failure may not have actually occurred during that particular test, the review of the high speed films indicates the airplane did indeed come very close to bottoming out the main landing gear and crushing the mid cabin fuselage underside. In one instance the analysis does not indicate a failure (Test 3, right main landing gear bulkhead support) which is surmised to have occurred during the test. This type of failure was also noted in Test 1. Actually, judging from the relative deformation of the floor structure near the landing gear bulkhead region, the consequence of this failure was more damaging for Test 1 than Test 3. No such landing gear bulkhead failure occurred during Test 2 or Test 4. The analysis shows that the load required to fail the bulkhead is reached during Test 1. For Test 3 the load reaches 72 percent of the required failure load. However, this peak load occurs at the conclusion of the analysis and is rising sharply. The bulkhead support structure could conceivably attain a failure load with additional computing time. There is no determination of when this failure occurs during the test. However, once again, the analytical trend agrees with the test trend when the load level at the bulkhead for all four tests are considered. The analysis shows the following:

Test No	Percent Failure Load at Main Landing Gear Bulkhead
1	≥100
3	72
4	63
2	33

7.5.4 Structure Response

Figures 7-1, 7-2 and 7-3 show summaries of the composite comparison of analysis and test structure response results at several locations for all four tests. Figure 7-1 shows the comparisons for the peak accelerations in the vertical direction. The percentage differences are shown in parentheses. In some individual comparisons, a substantial percentage difference exists. However, the overall trend of the analysis considering all four conditions is in agreement with the trend exhibited by the four crash test results. From Figure 7-1 it can be seen that the predominant response at all locations is not always associated with the same test. Similarly, Figure 7-2 shows a composite comparison for responses in the longitudinal direction. Once again the trend shown in the analysis results for all the tests is in agreement with the test data. Figure 7-3 shows the summary for the composite comparison of all analysis and test results with regard to the time of occurrence of the peak accelerations. The variation in time between analysis and test results shows differences from as little as .001 seconds to as much as .052 seconds. Figure 7-4 shows the distribution of time differences associated with the comparison of all the analyses and tests. In 75 percent of the comparisons the difference is $\pm .020$ seconds or less. In half the comparisons the difference is .015 seconds or less.

The largest discrepancies are associated with the engine vertical comparison for Test 4 (soil) and the F.S.27 and F.S.60 floor comparisons for Test 3. For the Test 4 case the differences in analysis and test for engine responses have been discussed in Section 6.4.3. The Test 3 analysis peak responses occur much earlier than the corresponding test peaks. The difference in time of occurrence of peak responses is consistent with the plot of cg translational velocities (Figure 6-21). In Table 7-11 a summary of energy components is listed. From this table it can be seen that the crushing energy for Test 3 reduces from a peak of 12.5 percent of the total energy to less than 3 percent of the total energy at the conclusion of the analysis. This trend indicates that, perhaps, the external springs used in the model do not allow for sufficient energy absorption prior to bottoming.

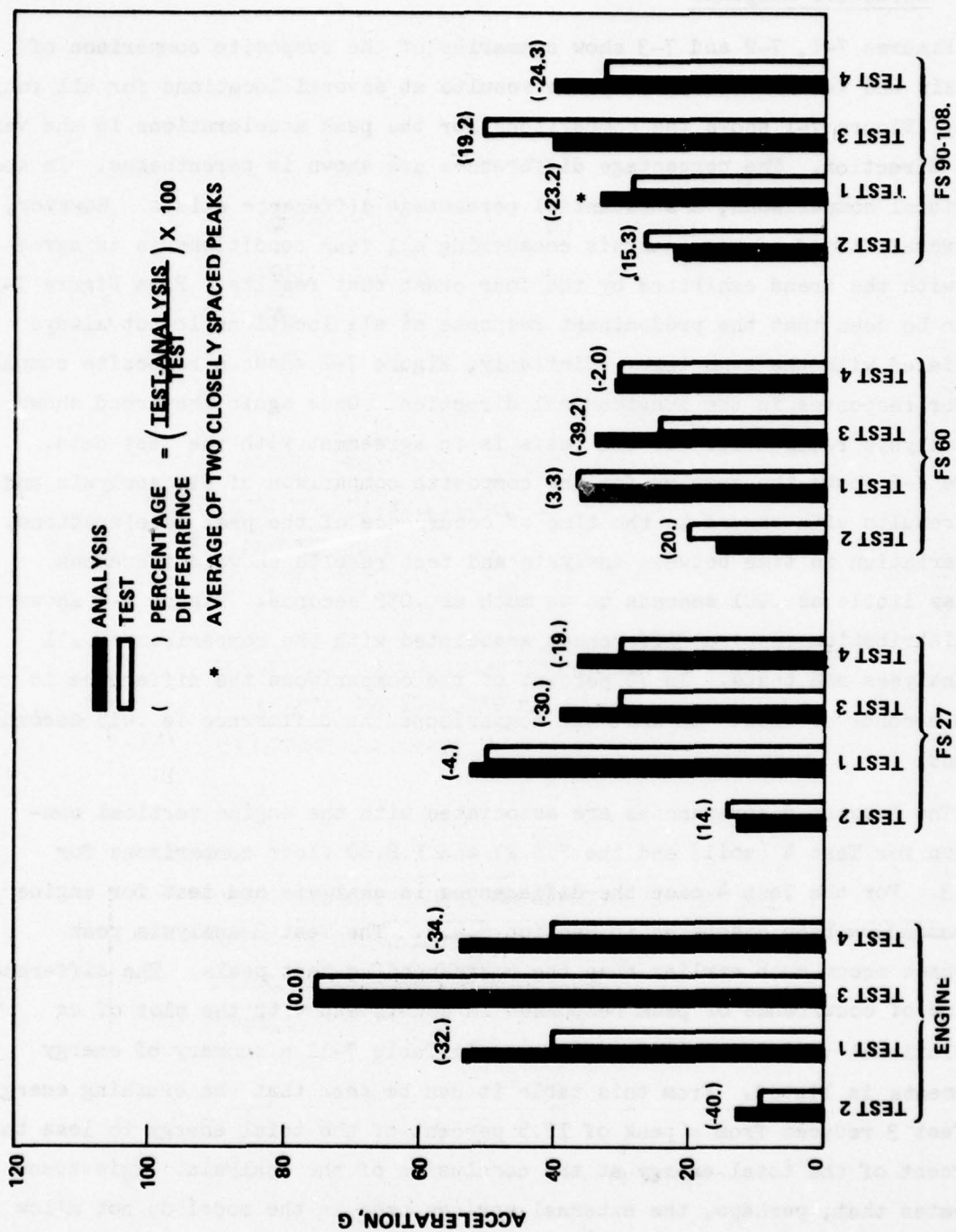


Figure 7-1. Summary of Comparison of Analysis and Test Structure Vertical Responses, Crash Tests 1 through 4

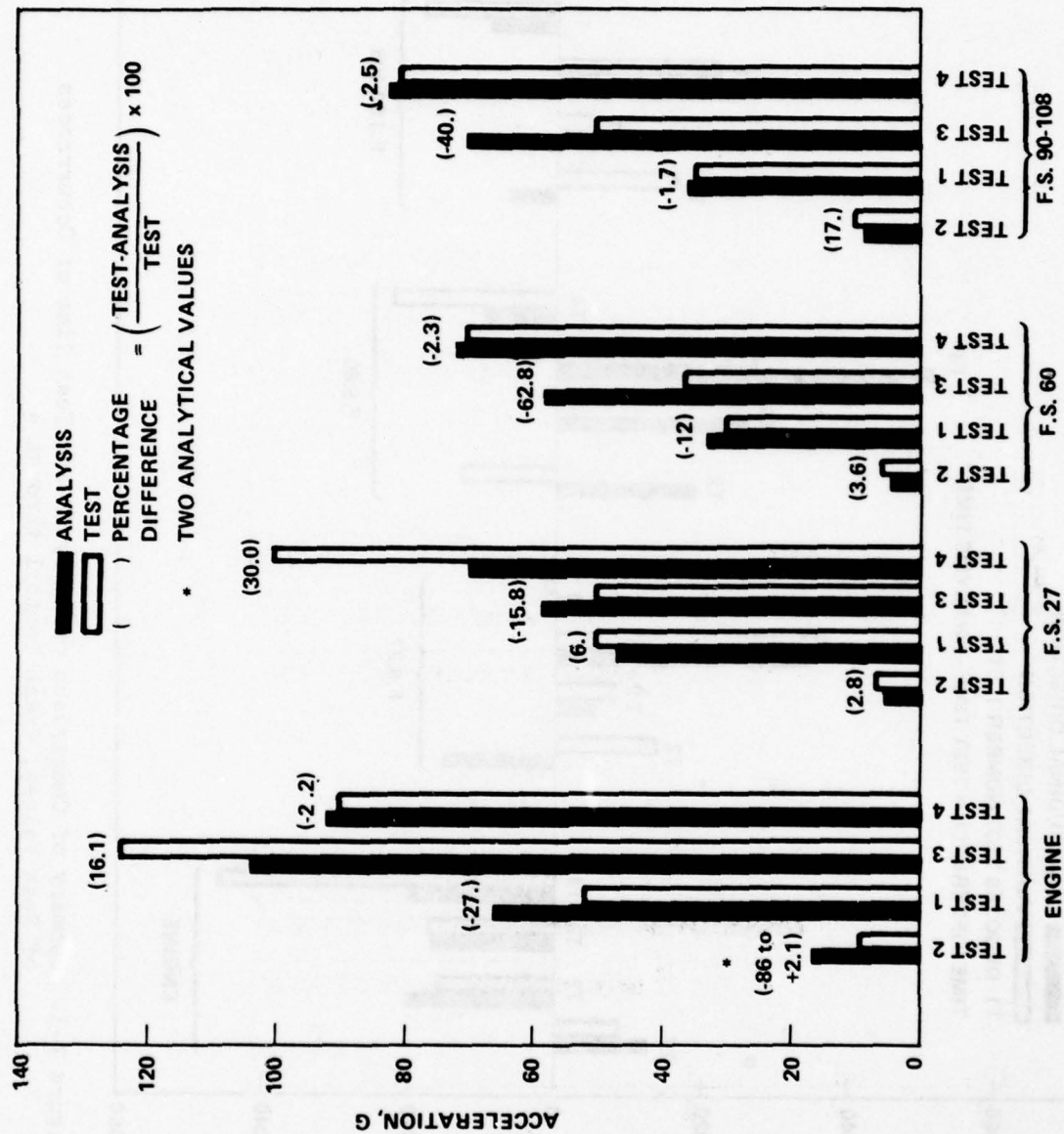


Figure 7-2. Summary of Comparison of Analysis and Test Structure Longitudinal Responses, Crash Tests 1 through 4

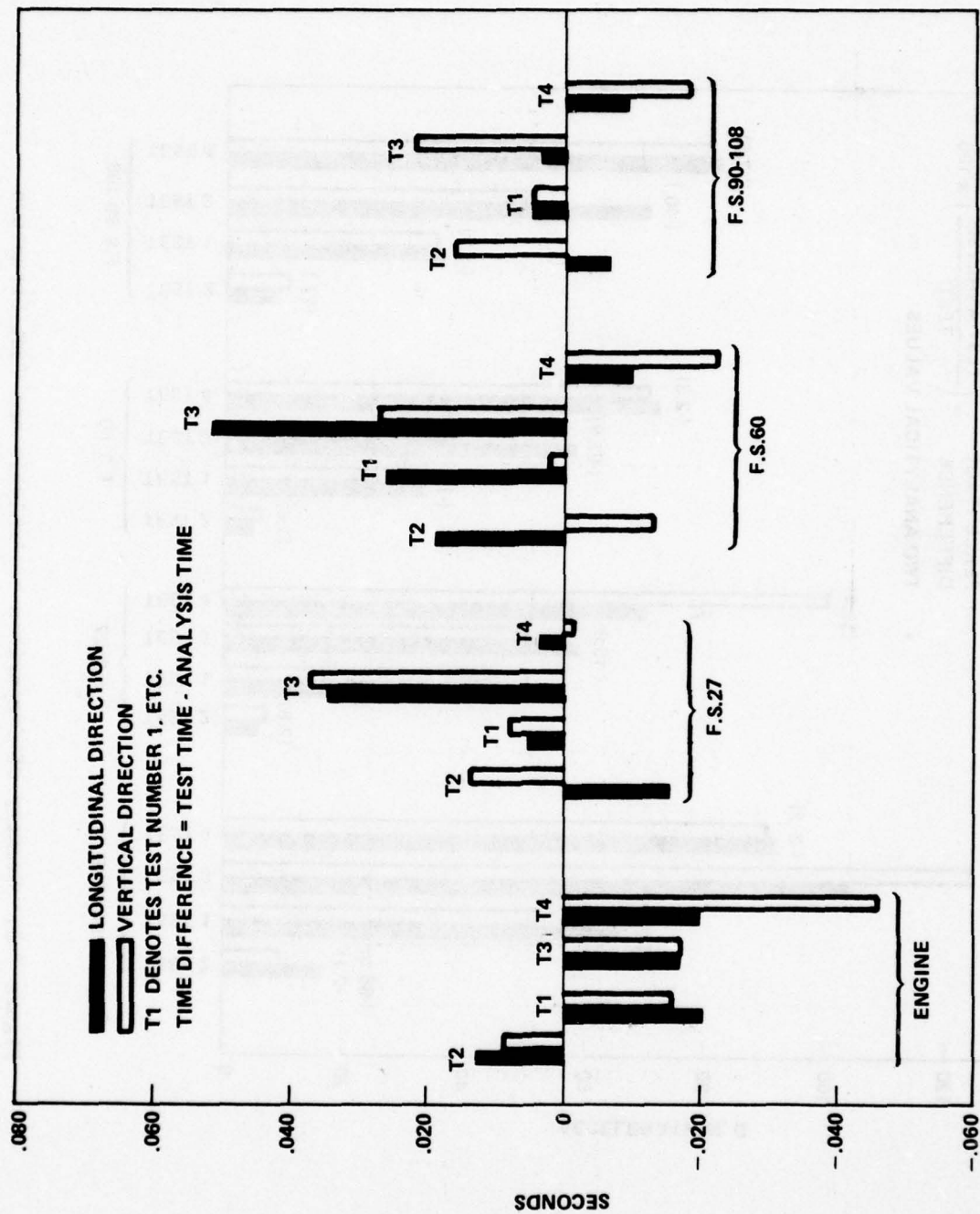


Figure 7-3. Summary of Comparison of Analysis and Test Time of Occurrences of Peak Values, Crash Tests 1 through 4

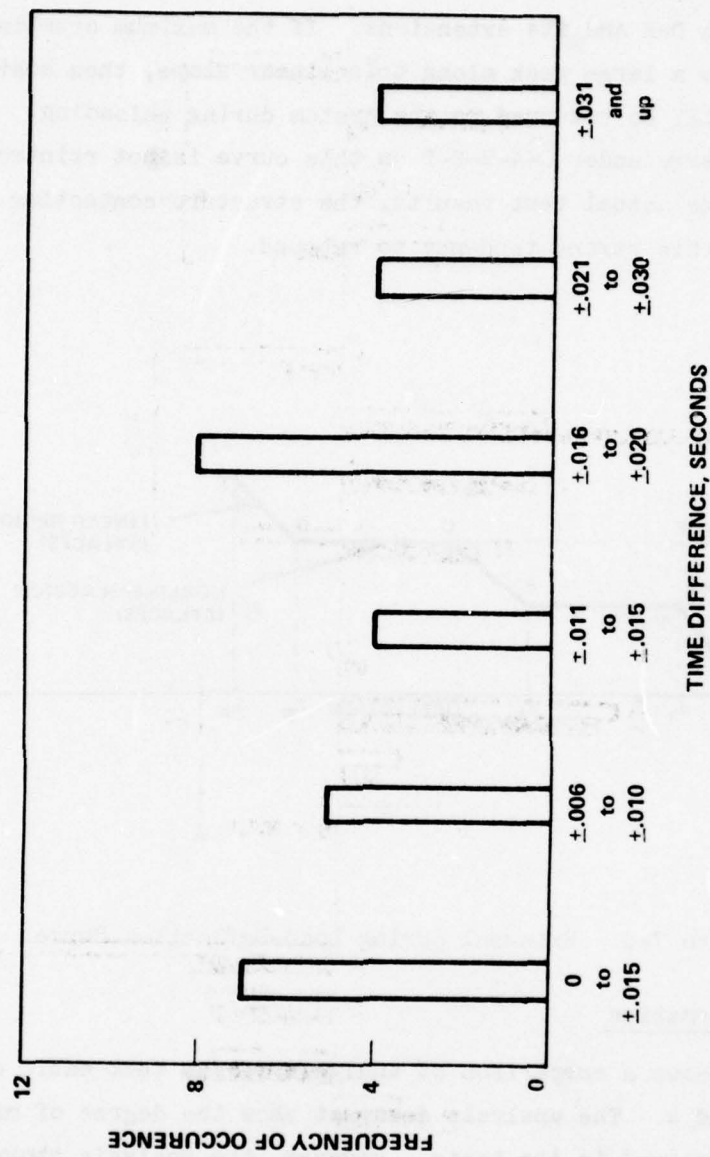


Figure 7-4. Distribution of Time Differences, Crash Tests 1 through 4

Figure 7-5 is used to illustrate this point. The spring, which is used to represent structure crushing, bottoms when point D (Figure 7-5) is reached.

After bottoming, subsequent loading and unloading proceeds in a linear fashion along line D-E and its extensions. If the maximum crushing energy is associated with a large peak along this linear slope, then most of this crushing energy will be returned to the system during unloading. Only that portion of the energy under O-A-B-C-D on this curve is not reintroduced into the system. In the actual test results, the structure contacting the ground does not exhibit this strong tendency to rebound.

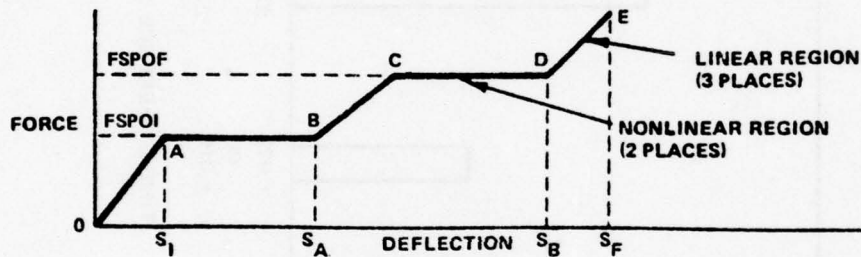
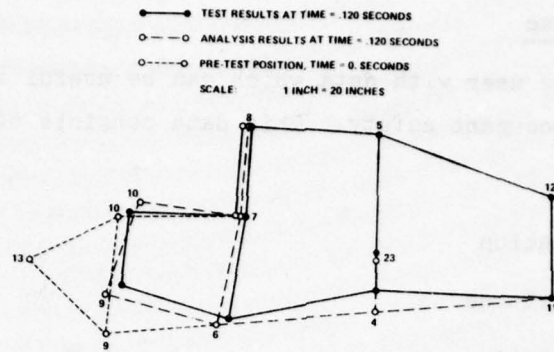


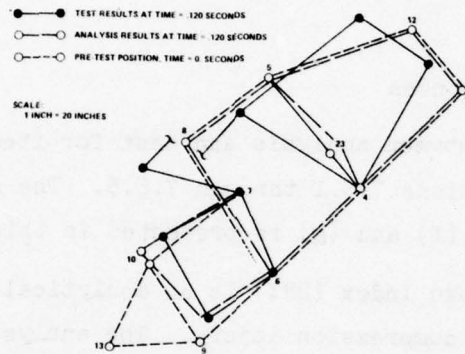
Figure 7-5. External Spring Load-Deflection Curve

7.5.5 Cabin Deformation

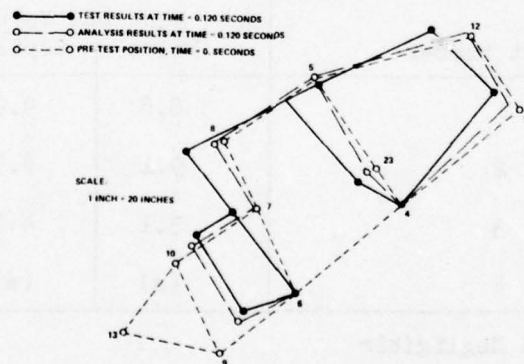
Figure 7-6 shows a comparison of analysis versus test cabin deformations for Tests 1, 3 and 4. The analysis does not show the degree of midcabin deformation that is observed in the tests. However, the analysis shows a trend to more deformation, particularly in the forward fuselage, as we progress from Test 1 to Test 3 to Test 4. The differences between the analysis and test are related to the selection of input data parameters, primarily internal beam non-linear characteristics.



TEST 1



TEST 3



TEST 4

Figure 7-6. Comparison of Cabin Deformations, Crash Tests 1, 3 and 4

7.5.6 Occupant Response

KRASH provides the user with data which can be useful in evaluating potential dangers to occupant safety. This data consists of:

- (a) Floor pulses
- (b) Cabin deformation
- (c) Structure failures
- (d) Element deflections
- (e) Energy distribution
- (f) DRI's
- (g) Occupant responses

The comparisons between analysis and test for items (a) through (e) have been summarized in Sections 7.5.1 through 7.5.5. The summary of analysis and test results for items (f) and (g) is presented in this section.

The Dynamic Response Index (DRI) is an analytical measure of potential for an occupant spinal compression injury. The analysis of each of the four crash test conditions indicates little or no probability of such an injury to the pilot or copilot. The peak DRI values are shown below:

Test Number	Peak DRI Value	
	Pilot	Copilot
1	8.8	9.9
2	9.1	8.5
3	3.1	4.2
4	(a)	(a)
(a) Negligible		

The occupant lower torso accelerations are obtained analytically and compared to the measured pelvic responses. Figure 7-7 presents a summary of the vertical responses. From Figure 7-7 it can be seen that:

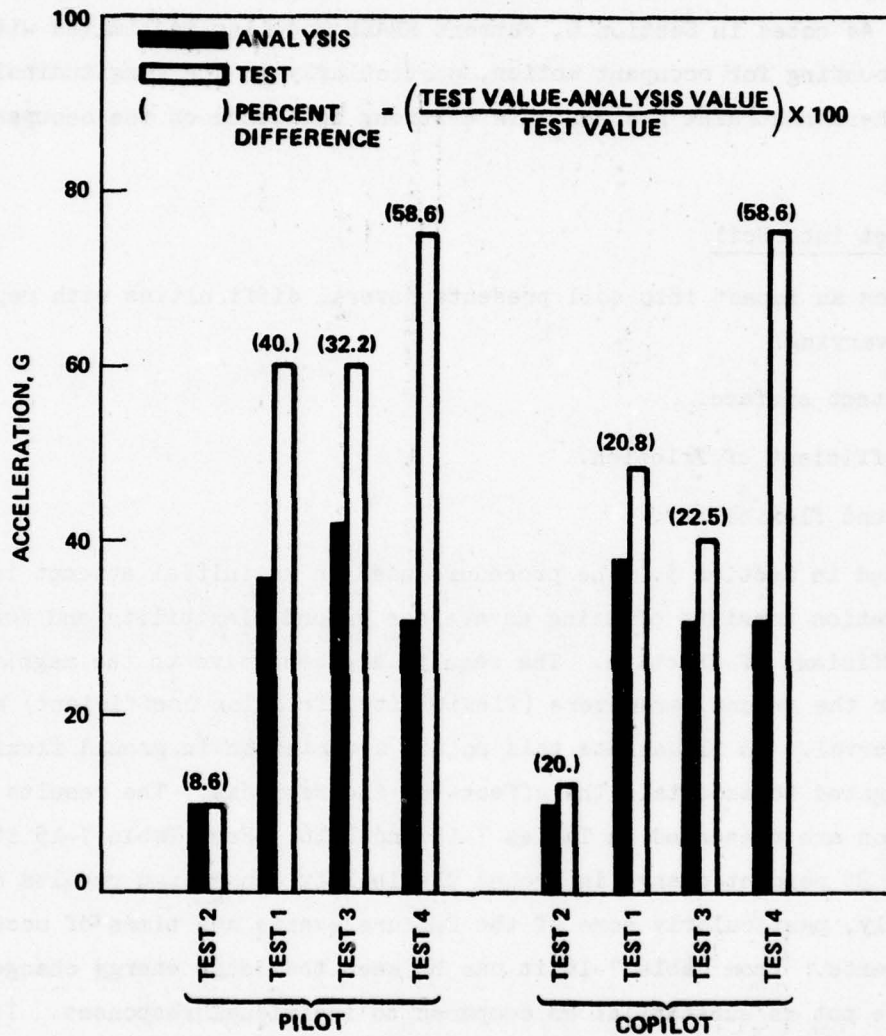


Figure 7-7. Summary of Comparison of Analysis and Test Occupant Lower Torso Vertical Accelerations, Crash Tests 1 through 4

- The analytical peak values are generally lower than the corresponding test values.
- The analysis trend is similar to the test trend except for Test 4 (impact into soil).

The comparison of occupant responses in the longitudinal direction is not presented. As noted in Section 6, current KRASH modeling is limited with regard to accounting for occupant motion, particularly in the longitudinal direction where restraint systems have a strong influence on the occupants behavior.

7.5.7 Impact into Soil

Modeling an impact into soil presents several difficulties with representing a time varying:

- Contact surface.
- Coefficient of friction.
- Ground flexibility.

As noted in Section 5.0 the procedure used in an initial attempt to model soil penetration consists of using an average ground flexibility and constant ground coefficient of friction. The results are sensitive to the magnitude selected for the ground parameters (flexibility, friction coefficient) and integration interval. To illustrate this point, a variation in ground flexibility was investigated to ascertain the effects on the response. The results of this investigation are presented in Tables 7-15 and 7-16. From Table 7-15 it can be seen that a 25 percent change in ground flexibility can change results quite significantly, particularly some of the failure events and times of occurrence of other events. From Table 7-16 it can be seen that some energy changes occur, but they are not as substantial as compared to individual responses. It is interesting to note that the higher ground flexibility analysis was run to 0.160 seconds (versus 0.120 seconds for 0.0036 ground flexibility) and that

TABLE 7-15. SUMMARY OF ANALYTICAL RESULTS FOR DIFFERENT GROUND FLEXIBILITIES

Location and/or Event	Ground Flexibility - In/Lb				Test Results	
	.00036		.00045			
	G Peak	Time (a)	G Peak	Time (a)	G Peak	Time (a)
<u>Engine Acceleration</u>						
Vertical	53.6	.096	43.7	.081	40	.040
Longitudinal	92	.069	102	.087	90	.040
<u>Floor Acceleration at F.S.27</u>						
Vertical	35.7	.099	36.8	.078	30	.100
Longitudinal	70	.072	65.7	.069	100	.075
<u>Floor Acceleration at F.S.60</u>						
Vertical	30.6	.093	29.1	.120	30	.115
Longitudinal	71.6	.090	71.4	.075	70	.100
<u>Floor Acceleration at F.S.90-108</u>						
Vertical	40	.078	36.8	.078	32	.060
Longitudinal	82	.090	65.7	.069	80	.070
(a) Time in seconds after impact						

TABLE 7-15. SUMMARY OF ANALYTICAL RESULTS FOR DIFFERENT GROUND FLEXIBILITIES (CONT.)

Location and/or Event	Ground Flexibility - In/Lb				Test Results	
	.00036		.00045			
	G Peak	Time (a)	G Peak	Time (a)	G Peak	Time (a)
<u>Wing, B.L.100</u>						
Vertical	27.3	.111	28.8	.141	28	.115
Longitudinal	63	.093	61	.111	25	.065
<u>Nose Gear Failure</u>	-	.017	-	.018	-	.024
<u>Tail Buckle</u>	-	.098	-	.098	-	.076
<u>Engine Buckle</u>	-	.065	-	.065	-	(b)
<u>Front Spar Failure</u>	-	.084	-	(c)	-	(c)
<u>Rear Spar Failure</u>	-	.103	-	.106	-	.250
<u>Landing Gear Bulkhead Failure</u>	-	(c)	-	.147	-	(c)
<u>Pilot Seat Leg Forward Inboard Failure</u>	-	(c)	-	.122	-	(c)
Soil Deformation	12.5 inches		14.4 inches		18 inches	
(a) Time in seconds after impact						
(b) Times unavailable						
(c) Did not occur						

TABLE 7-16. COMPARISON OF ENERGY DISTRIBUTION AS A FUNCTION OF
GROUND FLEXIBILITY, CRASH TEST 4

ENERGY COMPONENT	GROUND FLEXIBILITY		
	.00036	.00045	
Time of Analysis (T_F), Seconds	.120	.120	.160
Peak Energy (a)			
Strain	29.9	27.8	27.8
Damping	7.19	5.08	7.63
Crushing	17.0	18.1	18.1
Friction	35.8	36.34	36.59
Energy at T_F (a)			
Kinetic	16.4	16.47	16.09
Potential	3.11	3.03	3.72
Strain	25.02	24.53	21.36
Damping	7.19	5.08	7.63
Crushing	12.51	14.55	14.62
Friction	35.8	36.34	36.59
Percent Energy Change (b)	+ 5.01	+ 5.26	+ 5.32
(a) Percent of total energy			
(b) $\left(\frac{\text{Final Total} - \text{Initial Total}}{\text{Initial Total}} \right) \times 100$			

practically no additional energy growth occurred in the analytical results during the extended time. This suggests that the modeling of the soil has an influence on the computation of energy.

7.5.8 Severity Ranking

The analysis results are compared to the test results on the basis of how they would rank tests with regard to severity. Table 7-17 presents the results of this comparison. The comparison takes into consideration energy, structure damage, failures, cabin deformation, occupant response and structure response. Consistently the analyses and test results are in agreement with regard to the severity rank that should be applied to the test conditions.

TABLE 7-17. COMPARISON OF TEST SEVERITY RANKING BASED ON ANALYSIS AND TEST RESULTS, CRASH TESTS 1 THROUGH 4

Consideration	Test Numbers							
	1		2		3		4	
	Analysis	Test	Analysis	Test	Analysis	Test	Analysis	Test
Energy; Strain and Crushing	3	3	4	4	2	2	1	1
Member Deflections	2	3	4	4	3	2	1	1
Cabin Deformation	3	3	4	4	2	2	1	1
Seat Leg Damage	1	1	4	4	2	2	3	3
Structure Failures	1	2	4	4	1	1	3	2
Occupant Response (including Severity Index)	2,3	3	4	4	2,3	2	1	1
Structure Response								
Engine	3	3	4	4	1	1	2	2
F.S. 27	3	3	4	4	2	2	1	1
F.S. 60	3	3	4	4	2	2	1	1
F.S. 90-108	3	3	4	4	2	2	1	1
Landing Gear Bulkhead Damage	1	1	4	4	2	2	3	3
Landing Gear Failure Potential	2	2	1	1	3	3	4	4

Ranking: 1. most severe
 2. 2nd most severe
 3. 3rd most severe
 4. least severe

SECTION 8

CONCLUSIONS

1. Four full scale crash tests of a light, single-engine, high wing airplane configuration encompassing a wide range of impact conditions were successfully performed.
2. Program KRASH's capability:
 - To perform satisfactory structural crashworthiness analysis for general aviation airplanes has been successfully verified with experimental data from four full scale crash tests.
 - Has been expanded and its usage facilitated with modifications incorporated during Task II.
3. Math modeling of airplane crashes into soil requires additional analytical refinements and data substantiation.
4. KRASH is not used to model detailed occupant-restraint-seat system interaction. KRASH obtained data provides input parameters for more complete occupant-restraint-seat math models.

SECTION 9

REFERENCES

1. Wittlin, G., Gamon, M.A., A METHOD OF ANALYSIS FOR GENERAL AVIATION AIRPLANE STRUCTURAL CRASHWORTHINESS, Lockheed-California Company, FAA-RD-76-123, U.S. Dept. of Transportation, Federal Aviation Administration, Systems Research and Development Service, Wash. D.C., Sept. 1976
2. Wittlin, G., Gamon, M.A., EXPERIMENTAL PROGRAM FOR THE DEVELOPMENT OF IMPROVED HELICOPTER STRUCTURAL CRASHWORTHINESS ANALYTICAL AND DESIGN TECHNIQUES, Lockheed-California Company, USAAMRDL TR 72-72A, B, U.S. Army Air Mobility Research and Development Laboratory, Ft. Eustis, Va., May 1973.
3. Vaughan, V., Jr., Alfaro, Bou E., IMPACT DYNAMICS RESEARCH FACILITY FOR FULL-SCALE AIRCRAFT CRASH TESTING, NASA TN D-8179, April 1976.
4. SAE Handbook, Standards, Information Reports, and Recommended Practices, 1971.
5. Eiband, M.A., HUMAN TOLERANCE TO RAPIDLY APPLIED ACCELERATIONS: A SUMMARY OF LITERATURE, NASA MEMO 5-19-59E, 1959.
6. Gamon, M.A., GENERAL AVIATION AIRPLANE STRUCTURAL CRASHWORTHINESS - USER'S MANUAL, VOLUME I, PROGRAM "KRASH" THEORY, Lockheed-California Company, FAA-RD-77-189I, Federal Aviation Administration, Wash. D.C., Feb. 1978.
7. Gamon, M.A., Wittlin, G., LaBarge, W.L., GENERAL AVIATION AIRPLANE STRUCTURAL CRASHWORTHINESS - USER'S MANUAL, VOLUME II, INPUT/OUTPUT, TECHNIQUES AND APPLICATIONS, Lockheed-California Company, FAA-RD-77-189II, Federal Aviation Administration, Wash. D.C., Feb. 1978.
8. Dr. Laananen, D.H., DEVELOPMENT OF A SCIENTIFIC BASIS FOR ANALYSIS OF AIRCRAFT SEATING SYSTEMS, FAA-RD-74-130, U.S. Dept. of Transportation, Federal Aviation Administration, Systems Research and Development Service, Wash. D.C., January 1975
9. Crenshaw, B.M., et al, AIRCRAFT LANDING GEAR DYNAMIC LOADS FROM OPERATIONS ON CLAY AND SANDY SOIL, AFFDL-TR-69-51, Air Force Flight Dynamics Laboratory, Dayton, Ohio, Feb. 1971.
10. Park, K.C., Wittlin, G., DEVELOPMENT AND EXPERIMENTAL VERIFICATION OF PROCEDURES TO DETERMINE NONLINEAR LOAD DEFLECTION CHARACTERISTICS OF HELICOPTER SUBSTRUCTURES SUBJECTED TO CRASH FORCES, USAAMRDL TR 74-12A, B, U.S. Army Air Mobility Research and Development Laboratory, Ft. Eustis, Va., May 1974.
11. Turnbow, J.W., et al, CRASH SURVIVAL DESIGN GUIDE, USAAMRDL-TR-71-22, Eustis Directorate, U.S. Army Air Mobility and Research Laboratory, Ft. Eustis, Va., Oct. 1971.

APPENDIX A

CRASH TEST 4 SOIL BED MAINTENANCE AND MEASUREMENT

- A.1 GENERAL
- A.2 PRE-TEST SOIL MEASUREMENTS
- A.3 POST-TEST SOIL MEASUREMENTS
- A.4 SOIL TEST RESULTS

APPENDIX A

CRASH TEST 4 SOIL BED MAINTENANCE AND MEASUREMENT

A.1 GENERAL

For Crash Test 4 a soil bed was installed. Preparation of the soil for this test consisted of pre-test, post-test and laboratory tests to ascertain soil properties. The following subsections describe briefly the maintenance and preparation of the soil bed for Crash Test 4.

A.2 PRE-TEST SOIL MEASUREMENTS

The soil bed was installed several days prior to the test. Pre-test penetration measurements indicated significant drying of the soil and some strength increases from initial measurements. To increase the soil moisture, approximately 750 gallons of water were added and the soil covers replaced.

On the day prior to the test, surface CBR measurements were made using a NASA supplied crane as a reaction load for the CBR jack. Limits on accessibility restricted the location at which measurements could be made. Time during which the crane was available also limited the number of measurements. After CBR tests were completed, airfield penetrometer measurements were also made to obtain a profile of soil strength with depth. In many cases, penetrometer tests had to be repeated because buried tree roots were encountered. At the end of the work day the soil surface was sprinkled by water hose and covered to retard evaporation.

The soil bed was uncovered for grid marking just prior to the crash test. Access to the test bed surface was limited beyond approximately 9:30 a.m. Consequently, there was some surface drying prior to the 1:30 p.m. test but was not of a sufficient amount to significantly affect the soil bed strength.

A.3 POST-TEST SOIL MEASUREMENTS

Access to the soil after the crash area was delayed approximately 45 minutes for safety reasons. Initial probes of the soil around the impact area indicated little change in the average soil strength. Airfield index measurements indicated that loose soil had refilled an impact crater left by the aircraft engine.

It was planned to excavate the loose material and attempt to measure the true impact crater on the day after the test, but heavy rains throughout the day prevented excavation. This work was performed the following day.

A.4 SOIL TEST RESULTS

Field and laboratory soil tests were performed under the direction of Dr. B. Cheng of Old Dominion University. Figures A-1, A-2, and A-3 show the soil surface grid pattern, the summary of CBR measurements and the summary of penetrometer measurements, respectively.

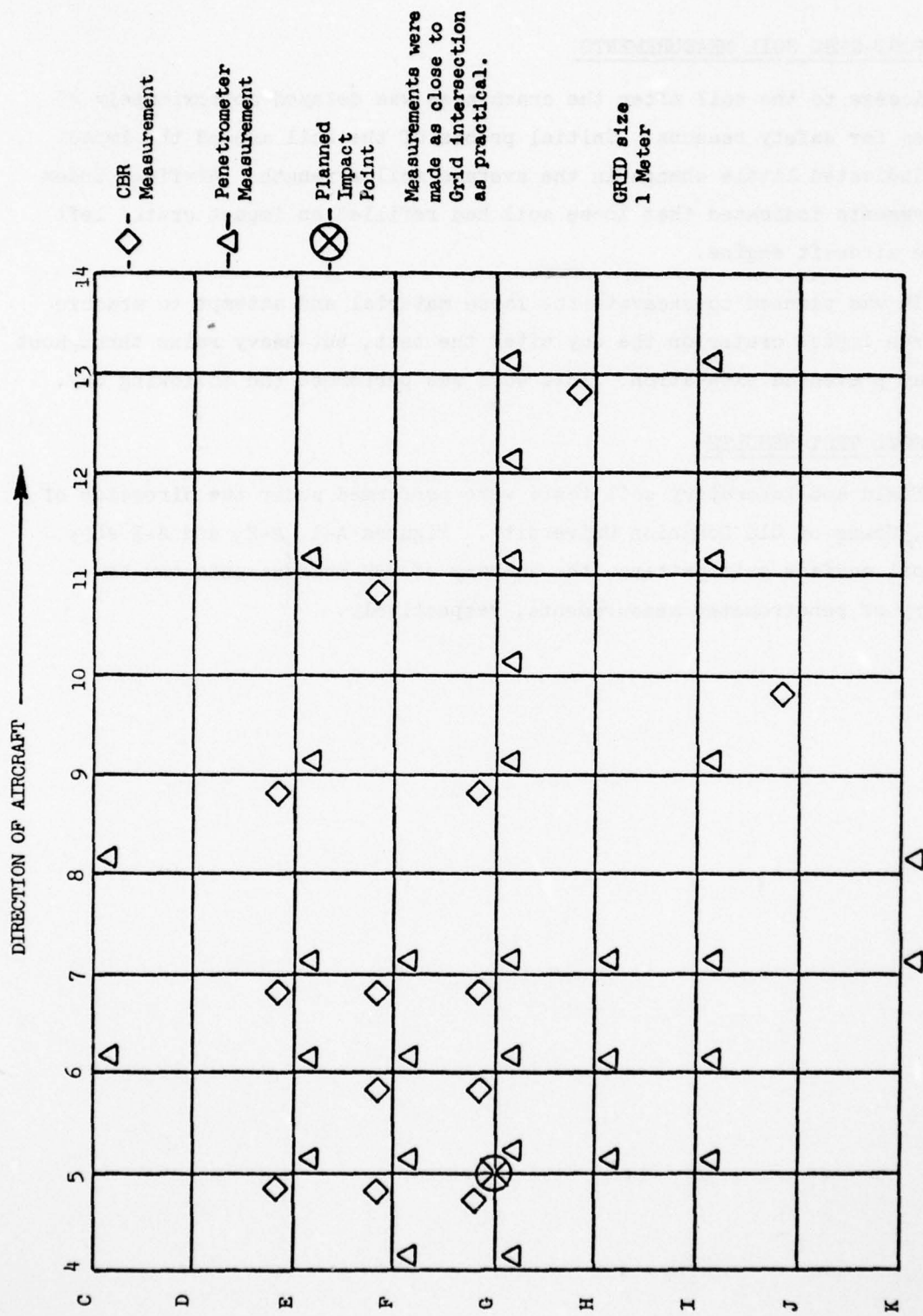


Figure A-1. Soil Surface Grid Pattern

CBR MEASUREMENTS
(Surface Only)

GRID Location	CBR
E5	10.0
E7	3.6
E9	0.8
F5	3.5
F6	5.0
F7	5.0
F11	2.7
G5	4.0
G6	6.2
G7	2.9
G9	0.9
H13	6.3
J10	4.1
<hr/>	
Total 13 Points	Average CBR 4.23

Figure A-2. Summary of CBR Measurements

APPENDIX B
SURVEY OF TECHNICAL PUBLICATIONS

- B.1 GENERAL DISCUSSION
- B.2 ANALYSIS
- B.3 LANDING SURFACE (SOIL) CHARACTERISTICS
- B.4 LANDING SURFACE/GEAR INTERACTION TESTS
- B.5 FULL SCALE AIRCRAFT CRASH TESTS
- B.6 DESIGN PROCEDURES AND CRITERIA
- B.7 SUMMARY
- B.8 LITERATURE MATRIX CATEGORIZATION
- B.9 ABSTRACTS

AD-A054 154

LOCKHEED-CALIFORNIA CO BURBANK

F/G 1/3

FULL SCALE CRASH TEST EXPERIMENTAL VERIFICATION OF A METHOD OF --ETC(U)

FEB 78 G WITTLIN, M A GAMON, W L LABARGE

DOT-FA75WA-3707

UNCLASSIFIED

LR-28306

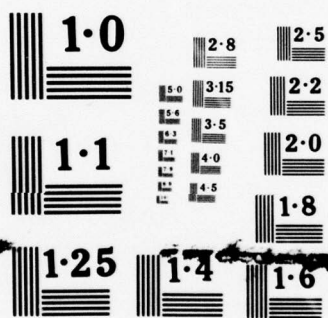
FAA-RD-77-188

NL

4 OF 5
ADA
054154

1/1





NATIONAL BUREAU OF STANDARDS
MICROCOPY RESOLUTION TEST CHART

APPENDIX B

SURVEY AND EVALUATION OF TECHNICAL PUBLICATIONS

B.1 GENERAL DISCUSSION

During the program, technical publications were reviewed and their contents categorized to assist in future studies as noted, in accordance with the various aspects of developing improved structural crashworthiness designs for general aviation airplanes. A review and evaluation of 26 publications are presented herein. The literature is reviewed with regards to aircraft structure/flexible ground interaction. In particular, the emphasis is placed in the following areas:

- Analysis

Analytical Model, Data Correlation, Parametric Studies

- Landing Surface (Soil) Characteristics

Material Properties, Roughness Properties, Performance Coefficients

- Landing Surface/Gear Interaction Tests

Test Procedures, Data Analysis

- Full Scale Aircraft Crash Tests

Test Procedures, Data Analysis, Empirical Criteria

- Design

Procedure, Criteria, Design Analysis Tools
(nomographs, computer programs)

For each of the subject areas listed above, an evaluation is performed which identifies the literature applicable to that particular subject and the contribution of each report. A composite summary of the pertinent

aspects of the literature with regard to structural crashworthiness analysis is also presented.

In addition to the literature survey and evaluation, a summary or abstract of each report, a literature survey subject index and a soil/interaction test parameter index are included. Both of the indices contain a matrix categorization of the contents of the reports and area of application or test parameter. The report reference numbers listed in the indices are applicable to this Appendix only.

B.2 ANALYSIS

The bulk of mathematical modeling of flexible ground/aircraft structure deals with tire/wheel/landing gear representations. Reference (2) describes the results of a study to investigate the interaction between the landing gear of the OV-10A airplane (Gross Weight = 9755-10547 pounds) and soft soil for landings ranging in sink speed from 8 to 18 ft/sec. An analytical model of the pneumatic tire on soft soil was developed. No correlation between analysis and test was performed. References (3), (4) and (5) describe a series of programs sponsored by the Air Force Flight Dynamics Laboratories (AFFDL) which were conducted primarily to develop methods for evaluating techniques for determining aircraft take-off performance, loads and capabilities. Reference (4) describes computer programs which were developed for calculating loads and dynamic response of aircraft operating on unpaved surfaces. Reference (3) describes a computer program which incorporates the soil/wheel interaction model with a simulation of the C-130 during taxi and takeoff. Reference (5) describes an analog computer program developed to incorporate the high speed effects found during testing into a soil-gear interaction model.

References (8), (10) and (11) describe additional AFFDL sponsored efforts involving landing gear-soils interaction. Reference (8) describes

the variables which significantly influence aircraft performance when operating on soil runways. At the time of the referenced report, sinkage analysis accuracy was considered to be between $\pm 50\%$ and $\pm 100\%$. Reference (10) describes efforts aimed at defining landing-gear soil interaction and developing flotation criteria to be used in comparative evaluation of the relative merits of various landing gear configurations. Empirical sinkage prediction equations were developed for cohesive and cohesionless soils. Reference (11) describes the third phase of a study to analytically define landing gear-soil interaction. The three studies, References (8), (10), (11), cover single and multiple wheel gears operating on clay, sand and mixed soils. Reference (15) describes a study which includes the development of a mathematical model to study tire-soil interaction. Empirical expressions were developed which relate soil sinkage and rolling resistance to soil strength, tire vertical force, tire characteristics and taxi velocity. Reference (16) presents a prediction method for estimating wheel sinkage, landing gear drag, and aircraft take-off performance on clay and sand airfields of various bearing strengths. The method is based on using modified mobility numbers developed by the U.S. Army Waterways Experimental Station (WES). Reference (19) presents a statistical analysis technique for the classification of virgin terrestrial and extraterrestrial surface roughness. Semi-empirical relationships are presented in Reference (1) to relate shearing resistance and rate of shear deformation. The data presented in this study are based on laboratory tests in which the strain rate varies up to 13.3 rad/sec. Correlation between analysis and test is presented in References (3), (5), (15) and (16). Figures B-1 and B-2, obtained from Reference (3), present a comparison between analysis and test results for CBR 1.5 Clay.

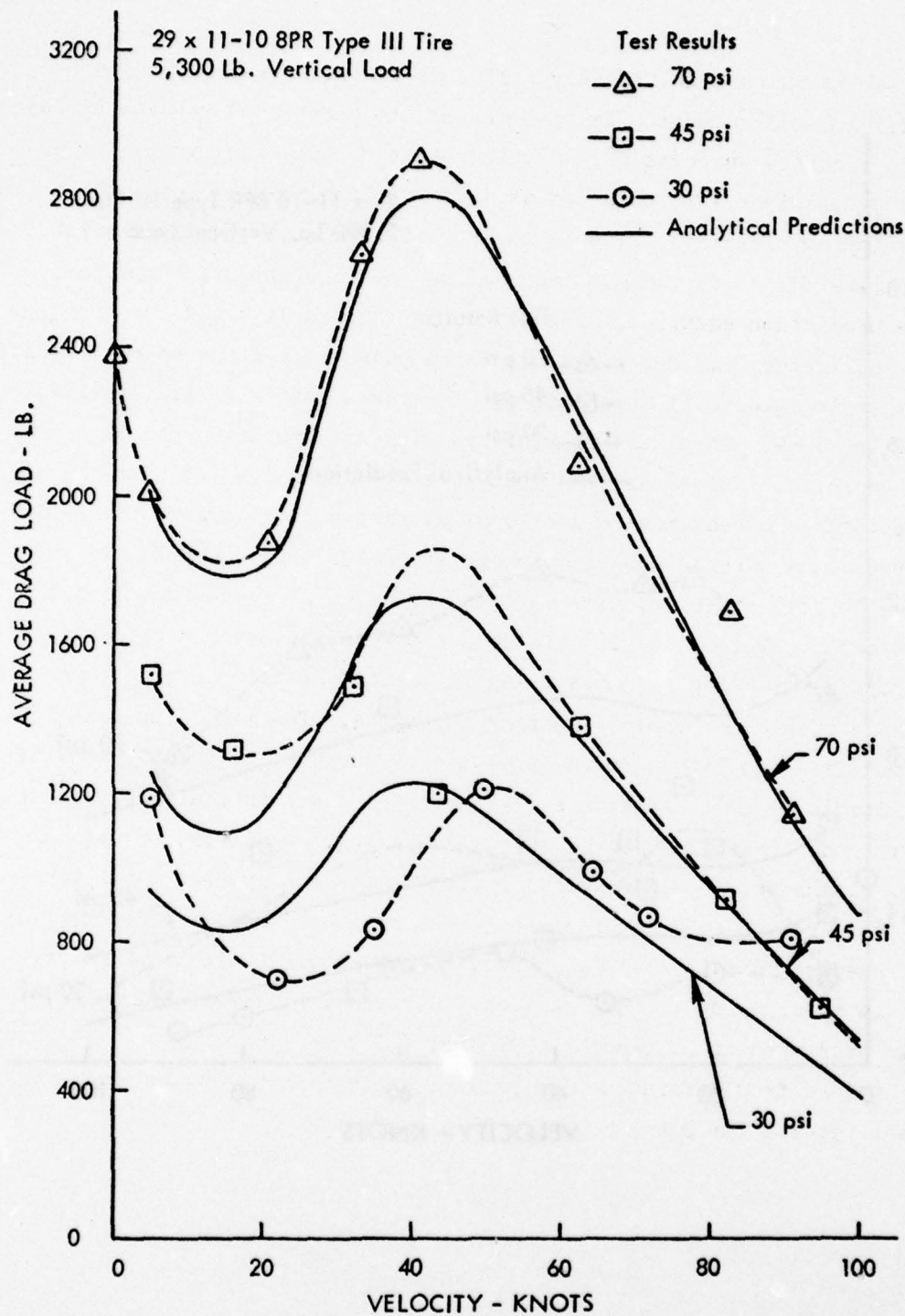


Figure B-1. Comparison of Analytical and Test Drag Loads for CBR 1.5 Clay (Reference 3)

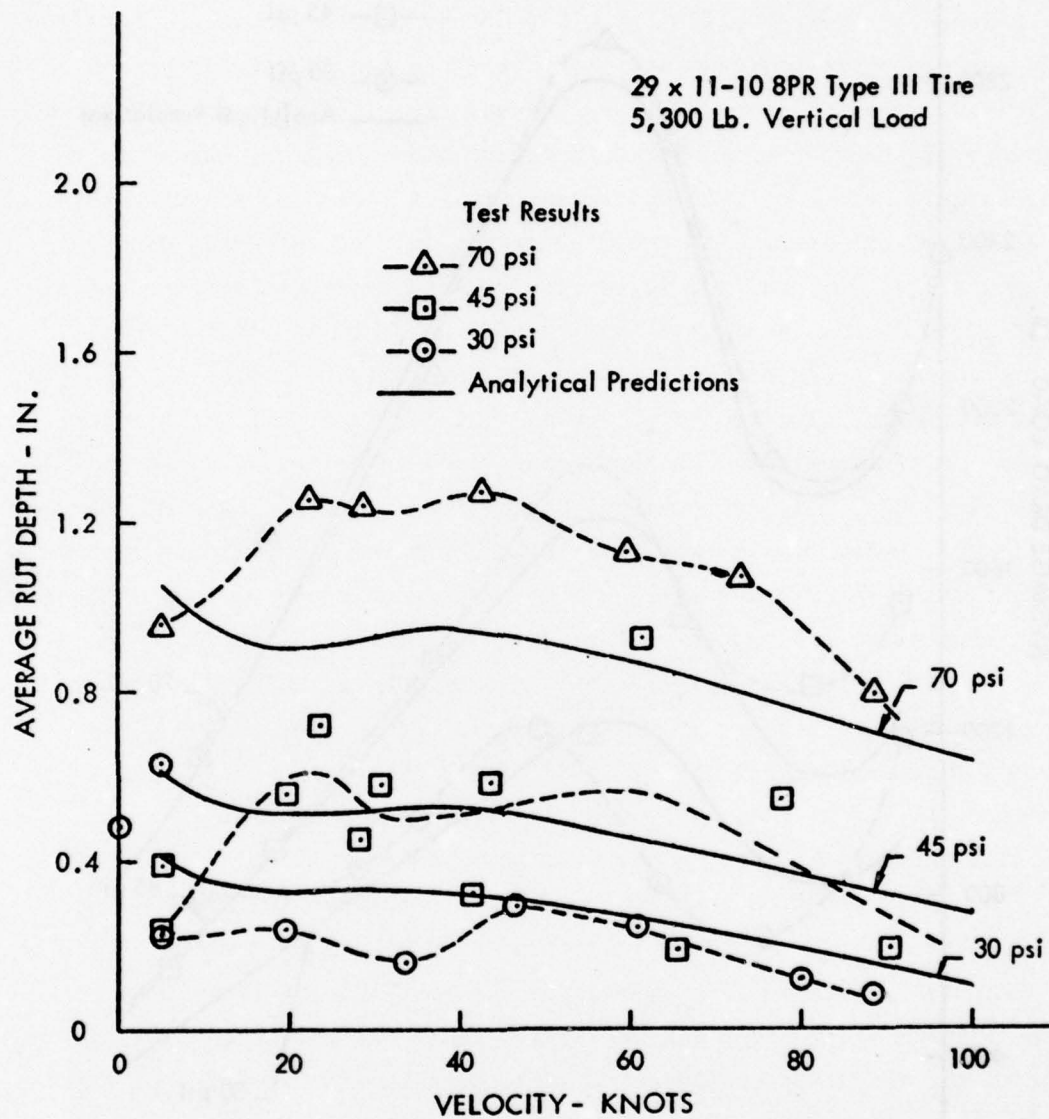


Figure B-2. Comparison of Analytical and Test Rut Depths for CBR 2.3 Clay (Reference 3)

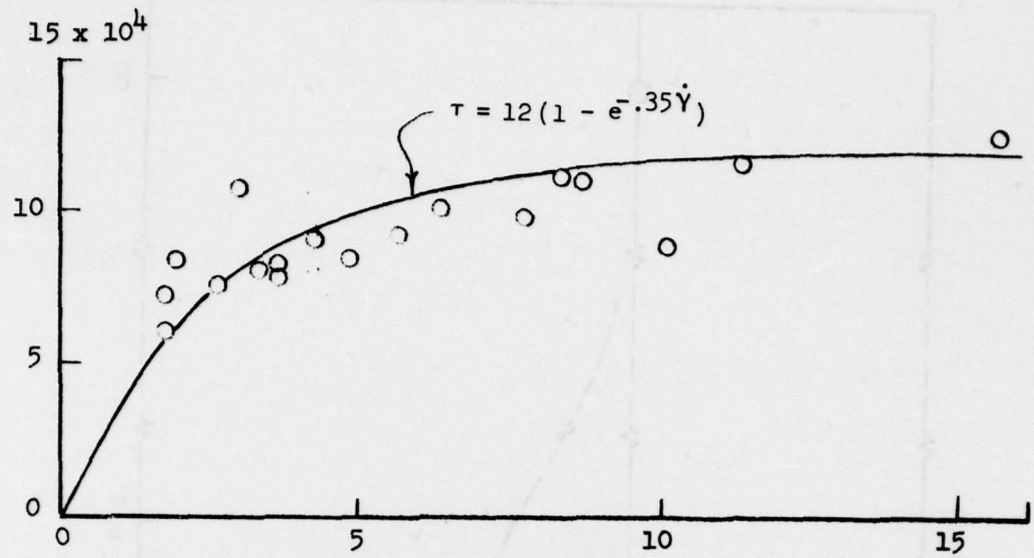
B-3 LANDING SURFACE (SOIL) CHARACTERISTICS

References (3), (6), (10), (14), (16), and (21) discuss programs in which the properties of sand and clay soils are considered. Clay soil properties are also discussed in References (1), (4), (5), and (17). Reference (7) provides soil strength performance data for coarse grained sandy soils. Reference (26) describes triaxial tests for investigating the effect of strain-rate on the strength of dry and saturated sands. References (3), (4) and (5), while involving soil materials, were performed primarily to develop analytical methods for determining landing gear dynamic loads. An investigation of different soils at different strength levels under very slow (≤ 1 mph) moving vehicles is described in Reference (6). Reference (10) considers clay, sand and mixed soils for use in the development of sinkage prediction equations. The soil was assumed an elastic, perfectly plastic material in this program. A preliminary Single Wheel Relative Merit Index (RMI) was developed during this program to permit a comparative evaluation of the flotation characteristics of aircraft tires on soil. Reference (13) describes a program in which a series of traffic tests were performed on mat-surfaced and unsurfaced subgrades. Numerous wheel configurations, loads and tire pressures were included. In Reference (14), four clay test beds of different moisture content and one sand bed were used to explore the effects on axle drag loads developed during operation at different tire inflation pressures in free rolling, locked wheel braking and yawed (cornering) modes, all at forward speeds up to 95 knots. Reference (15) summarizes the results of a five-phase program. Phase II included a site selection and field measurement program to obtain field roughness profiles and soil strength information from fields typical of those expected to be found in remote theaters of operation. The sites selected represented various degrees of preparation, from semi-prepared to unprepared and included a variety of soil types. Reference (17) contains a description of the construction and maintenance of the buckshot clay test bed used for tandem and single wheel, high speed landing gear

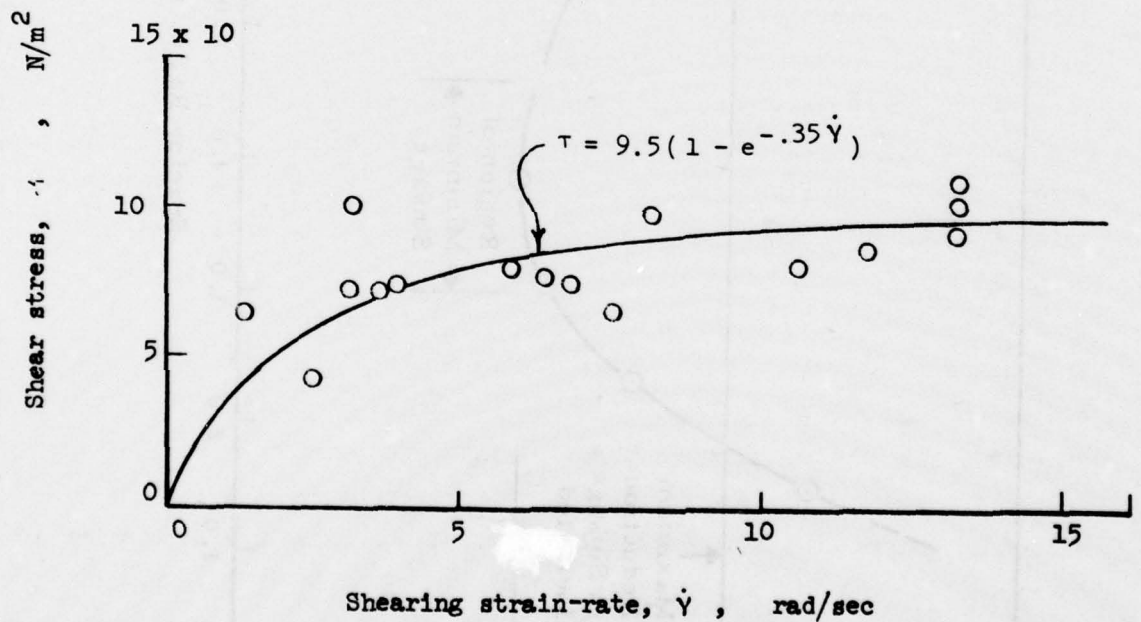
tests conducted at the NASA Landing Loads Track. Reference (21) describes a program to determine the effect of aircraft dynamic wheel loads on airport pavements. Appendices C and F of Reference (11) contain data with regard to soil laboratory tests and wave propagation velocities for paving materials, respectively. Landing surface roughness characteristics are discussed in References (2), (3), (4), (15), (19), and (21).

B.4 LANDING SURFACE/GEAR INTERACTION TESTS

References (1), (3), (5), (6), (11), (14), (17) and (18) describe laboratory tests to define material behavior, facilitate the development of analytical models, define parameter relationships or further the development of criteria. With the exception of References (1) and (11), the references relate landing gear and/or wheel performance to soil strength and/or behavior. Reference (1) describes tests to determine shearing resistance of cohesive soils subject to shear strains applied at various rates. The relationship between shearing resistance and rate of shear deformation was established for various soil densities expressed in terms of initial void ratio or water content (see Figure B-3). Reference (11) presents the results of twinplate vertical load tests to determine sinkage interaction effects produced by adjacent dynamic plate loads (see Figure B-4). Soil and/or landing surface field tests are described in References (2) and (13). The data from Reference (2) are used to form a representation of soil static and dynamic properties. Figures B-5 and B-6, obtained from Reference (2), illustrate the type of curves that are generated from the test data. The results of laboratory soil and scaled pavement tests are presented in Reference (21). Soil characteristics such as California Bearing Rates (CBR), moisture content, grain size distribution and damping characteristics were determined. Concrete and asphaltic-concrete slab characteristics were also determined. Typical CBR, dry density, moisture content and subsoil modulus relationships are shown in Figures B-7 and B-8. Empirical criteria are presented in References (7), (11) and (13). In Reference (7) independent tire soil and system parameters are related to



(a) mean water content = 30.5%



(b) mean water content = 31.5%

Figure B-3. Plot of Shearing Stress vs. Strain Rate (Reference 1)

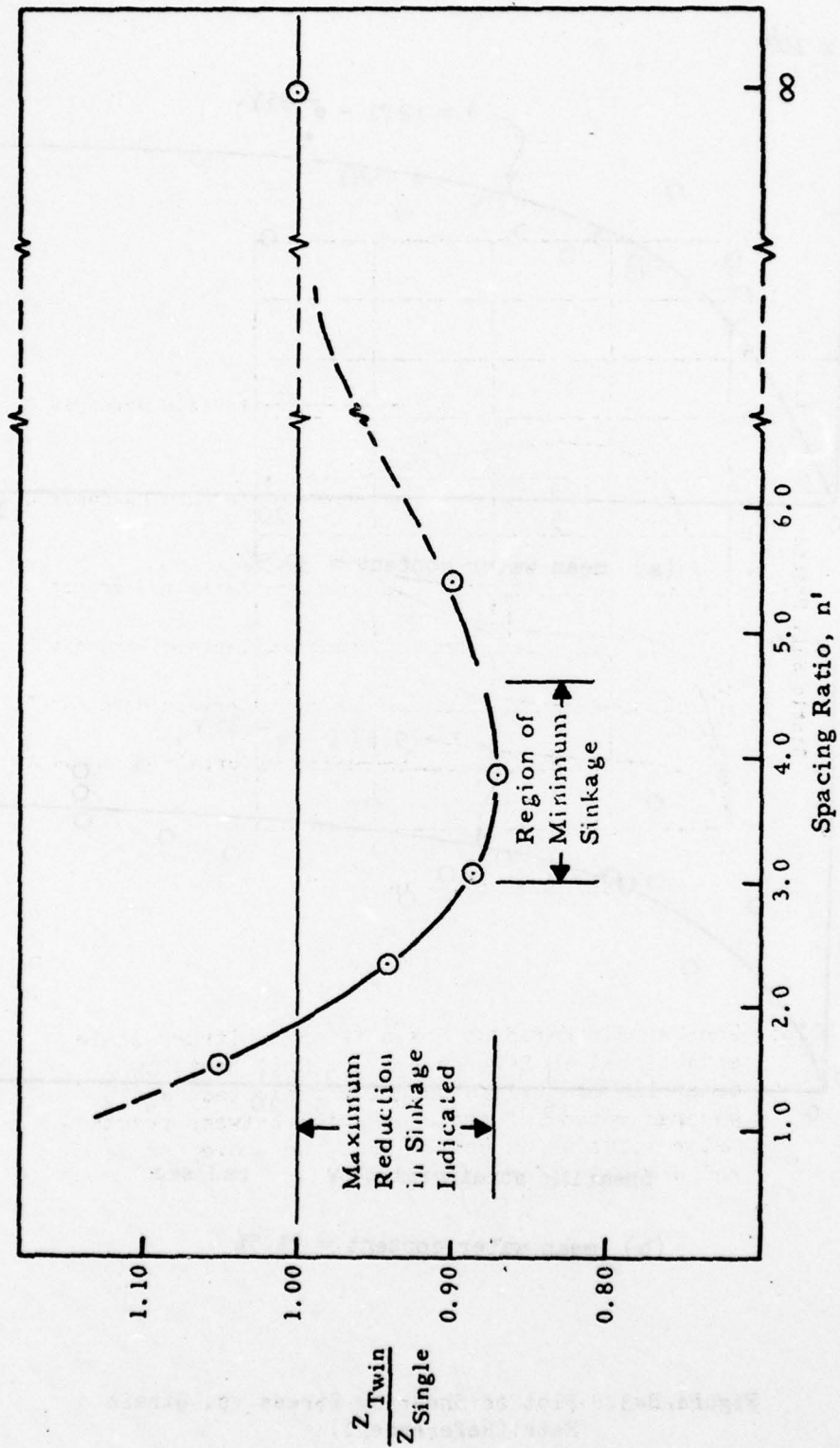
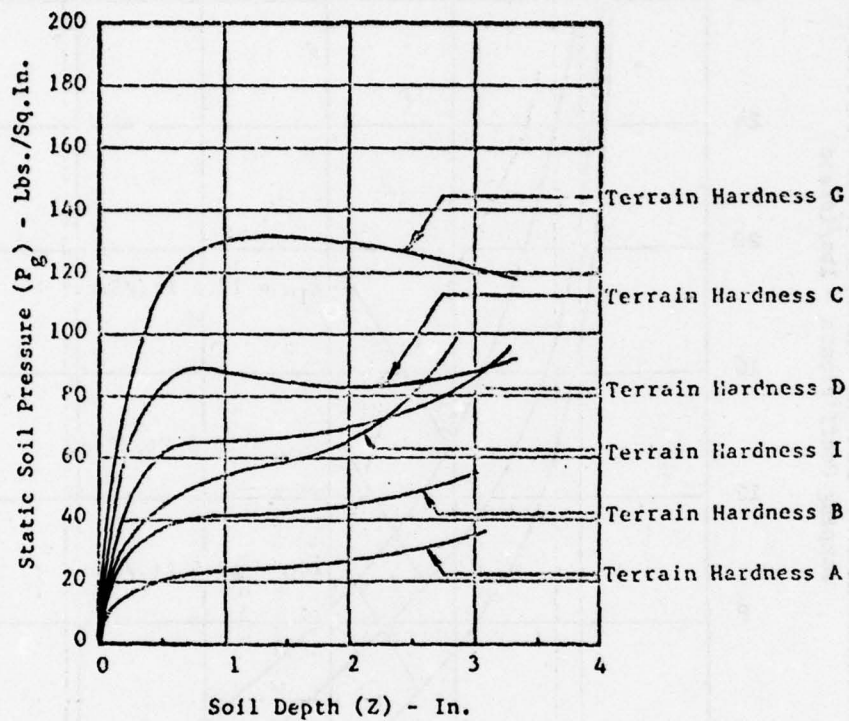


Figure B-4. Z_{Twin}/Z_{Single} vs. Wheel Spacing, Clay Soil (Reference 11)



NOTE: The Terrain Hardness Scale is an arbitrary scale established in Reference (2). Soil tests to determine CBR values were not conducted, and a general method of transformation between penetrometer value which established the above curves and CBR units does not exist.

Figure B-5. Static Soil Pressure Curves
(Reference 2)

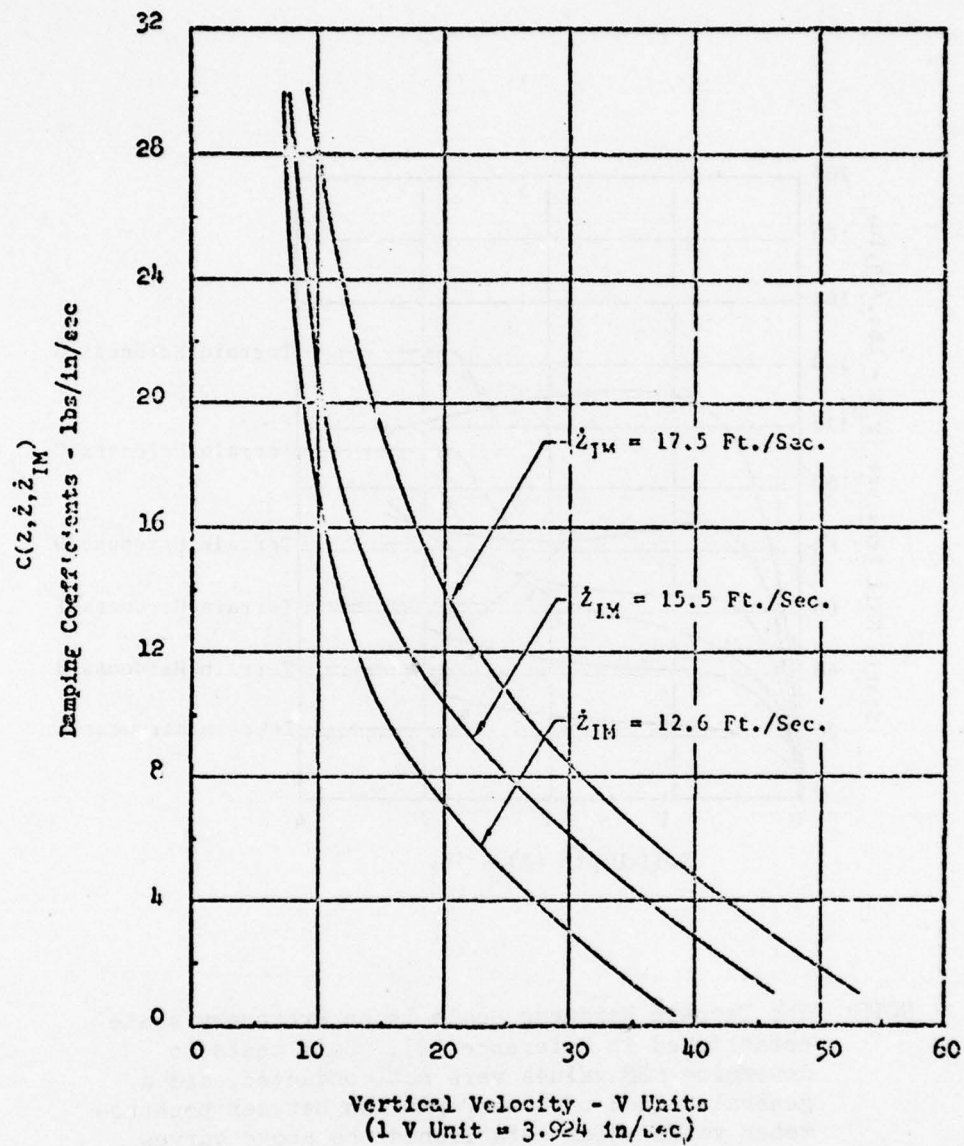


Figure B-6. Soil Dynamic Damping Coefficients for Terrain Hardness B (Reference 2)

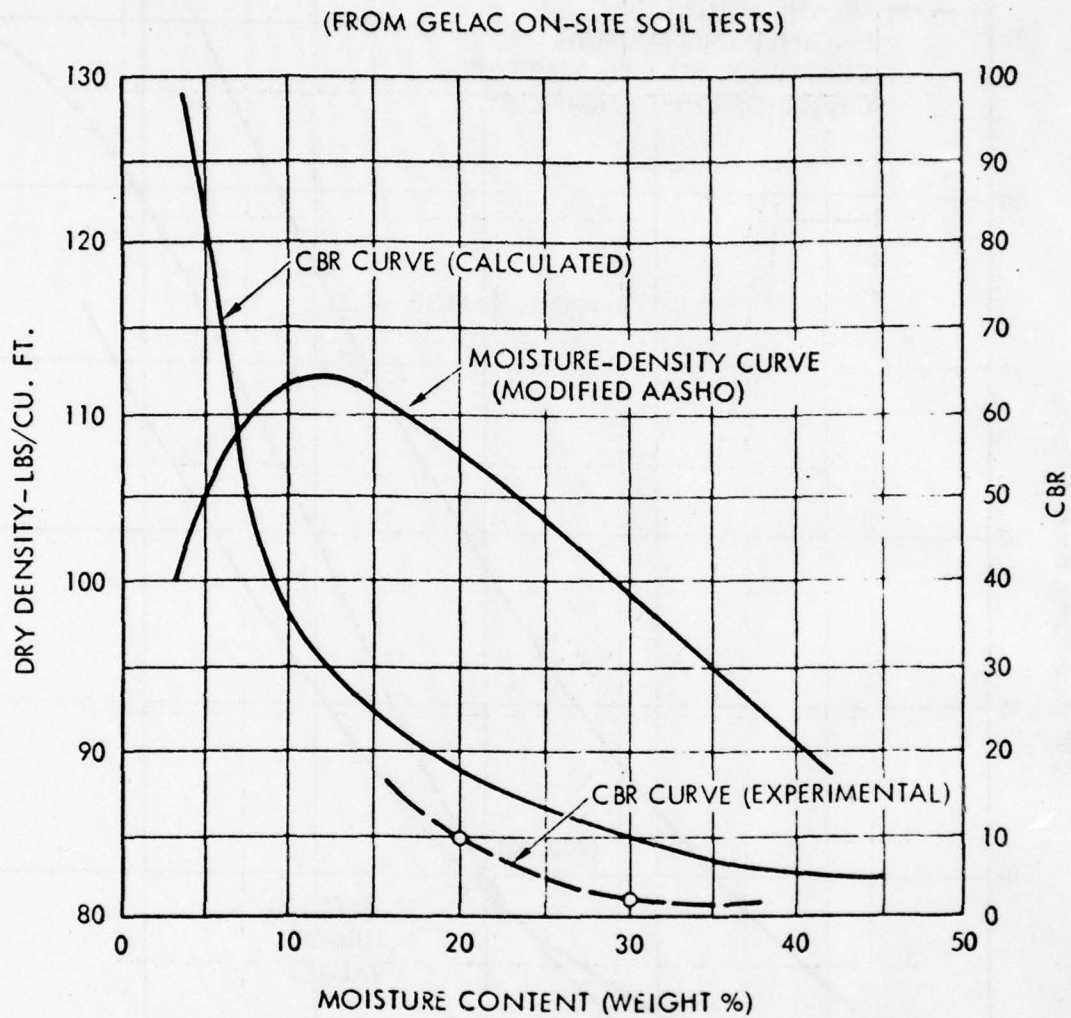


Figure B-7. Subsoil Properties - CBR and Dry Density vs Moisture Content (Reference 27)

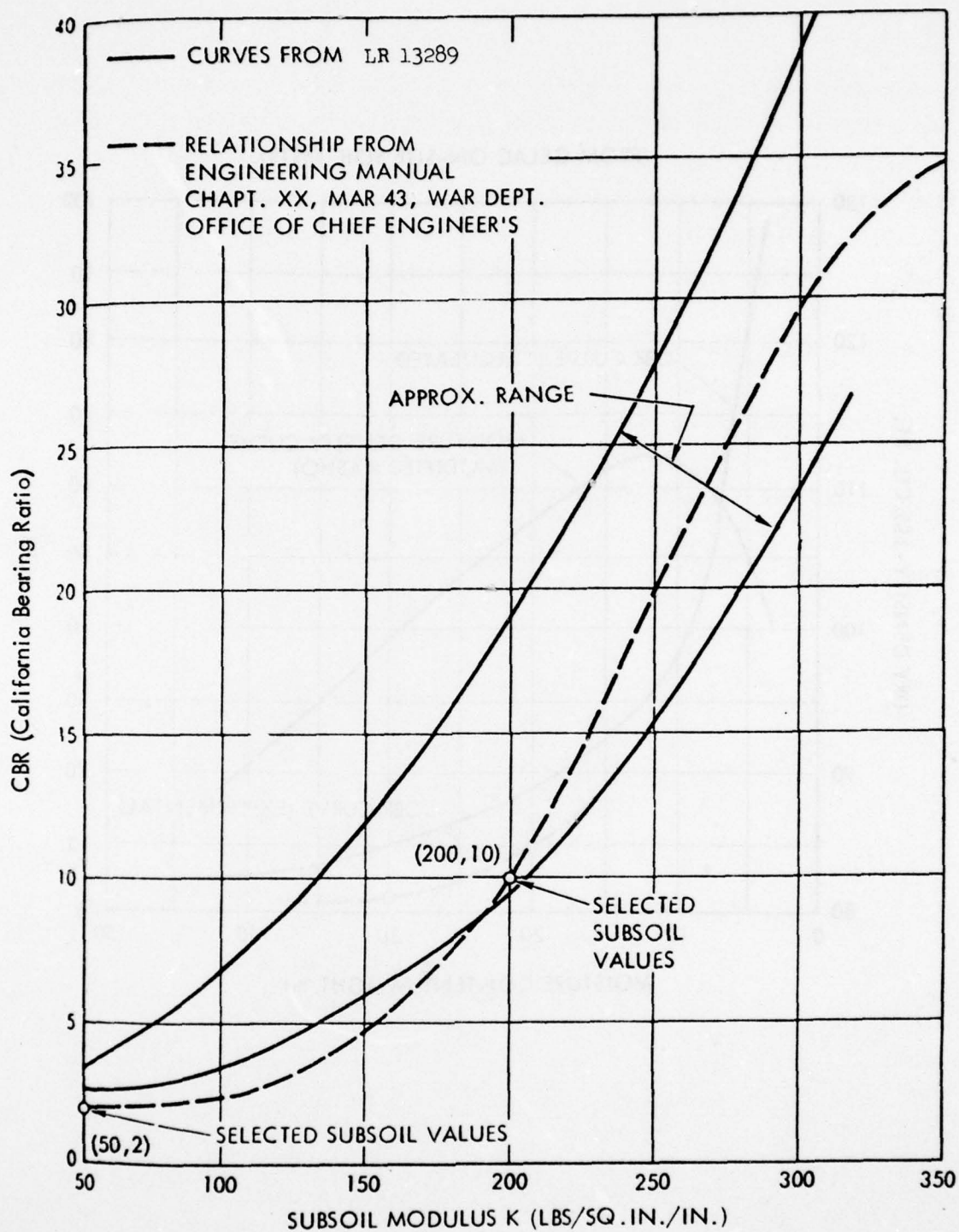


Figure B-8. CBR and Subsoil Modulus Relationship (Reference 27)

performance coefficients. A combination of independent parameters called mobility numbers were developed which account for the combined effects of soil strength, tire section width and diameter, wheel load and tire deflection on wheel performance as measured by performance coefficients. The mobility numbers developed in this report are applicable to single wheel landing gears operating on sand at speeds common to surface vehicles. Reference (11) provides criteria applicable to multiwheel landing gears which permit the evaluation of aircraft flotation performances rather than single tire performance. The criteria also permits designers to determine optimum landing gear configurations for aircraft leading to drag minimization. Reference (13) presents single wheel criteria for the efficient design of aircraft landing gears based on testing involving different wheel configurations (1 to 12 wheels), loads (1000 to 273000 pounds), and tire pressures (10 to 250 psi).

B.5 FULL SCALE AIRCRAFT CRASH TESTS

Full scale aircraft crash tests in which a flexible ground surface is included are described in References (20), (22), (23) and (24). Reference (20) describes the results of crash tests of light-airplanes (1200 pounds) into an earthen barrier. Impact speeds of 42, 47 and 60 mph were investigated. To simulate accidents in which the airplane stalls and strikes the ground as it enters a spin, the earthen barrier was shaped and located relative to a guide rail along which the airplane traveled such that the engine, left landing gear and left wing tip struck the barrier simultaneously. The airplanes used were a steel tube, fabric covered, tandem, two-seat type. The report concludes that the occupants of airplanes of the type used in the investigation would not be endangered by deforming cabin structure unless crash impact speeds exceeded 42 mph. Inwardly collapsing cabin structure, however, is a potential hazard in the higher-speed crashes. Reference (22) presents results of a program involving full-scale transport airplanes simulating takeoff and landing accidents for pressurized low-wing, unpressurized low-wing and unpressurized high wing aircraft. The resultant damage was from moderate to severe. The unmanned airplanes were guided along a runway under their own power into a set of obstacles designed to produce a series of crash events. The impact angles varied from 4 to 29 degrees and the impact velocity ranged from 63 to 109 mph. Figure B-9, obtained from Reference (22), shows plots of variation of maximum normal acceleration as a function of impact angle and distance from impact point. The crash site for the tests described in Reference (22) was predominantly clay. The sliding coefficient for aluminum was taken as equal to 0.30. This report contains a discussion in which the relationship between crumpling, plowing and friction forces are treated. The kinetic-energy loss is equated to the work done in collapsing the fuselage structure and compressing the soil. Utilizing the test data obtained during the effort, a general relationship between maximum acceleration and impact angle was developed (Figure B-10). How-

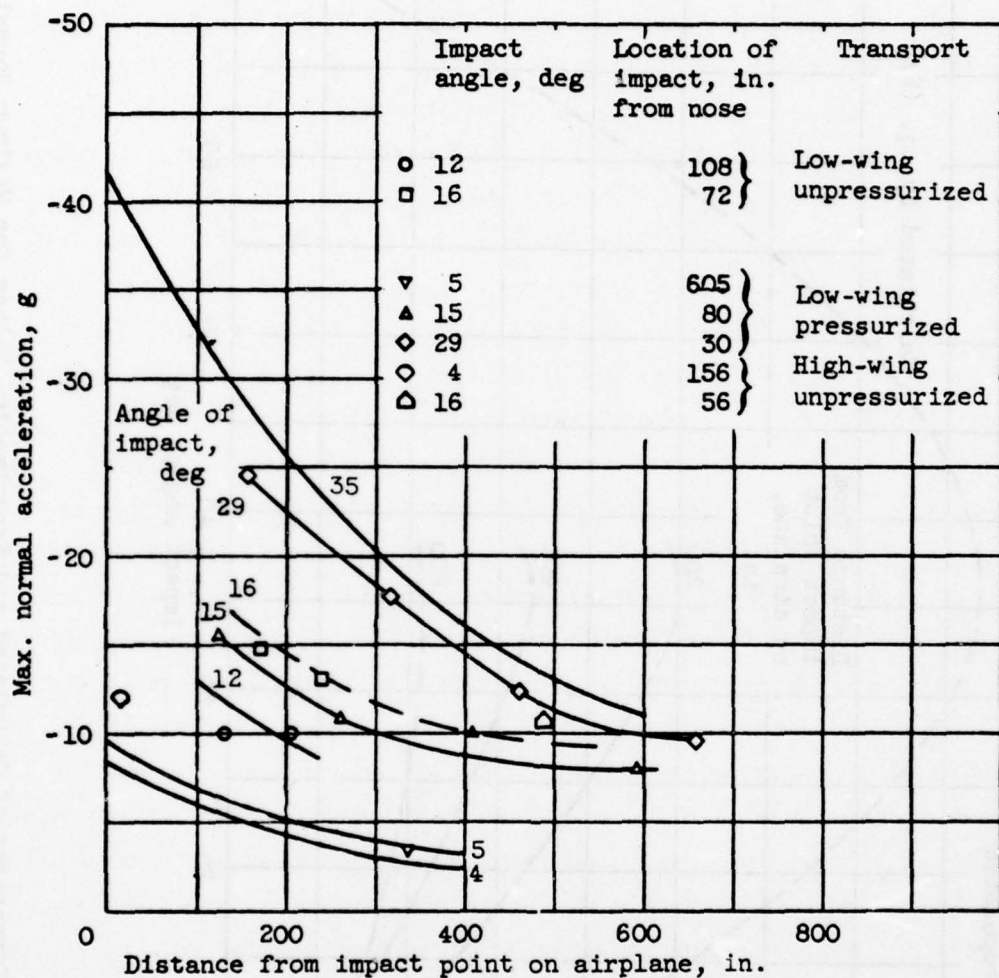


Figure B-9. Effect of Position in Airplane and Airplane Configuration on Maximum Normal Accelerations During Unflared Landing Crashes (Impact Velocity Corrected to 95 mph) (Reference 22)

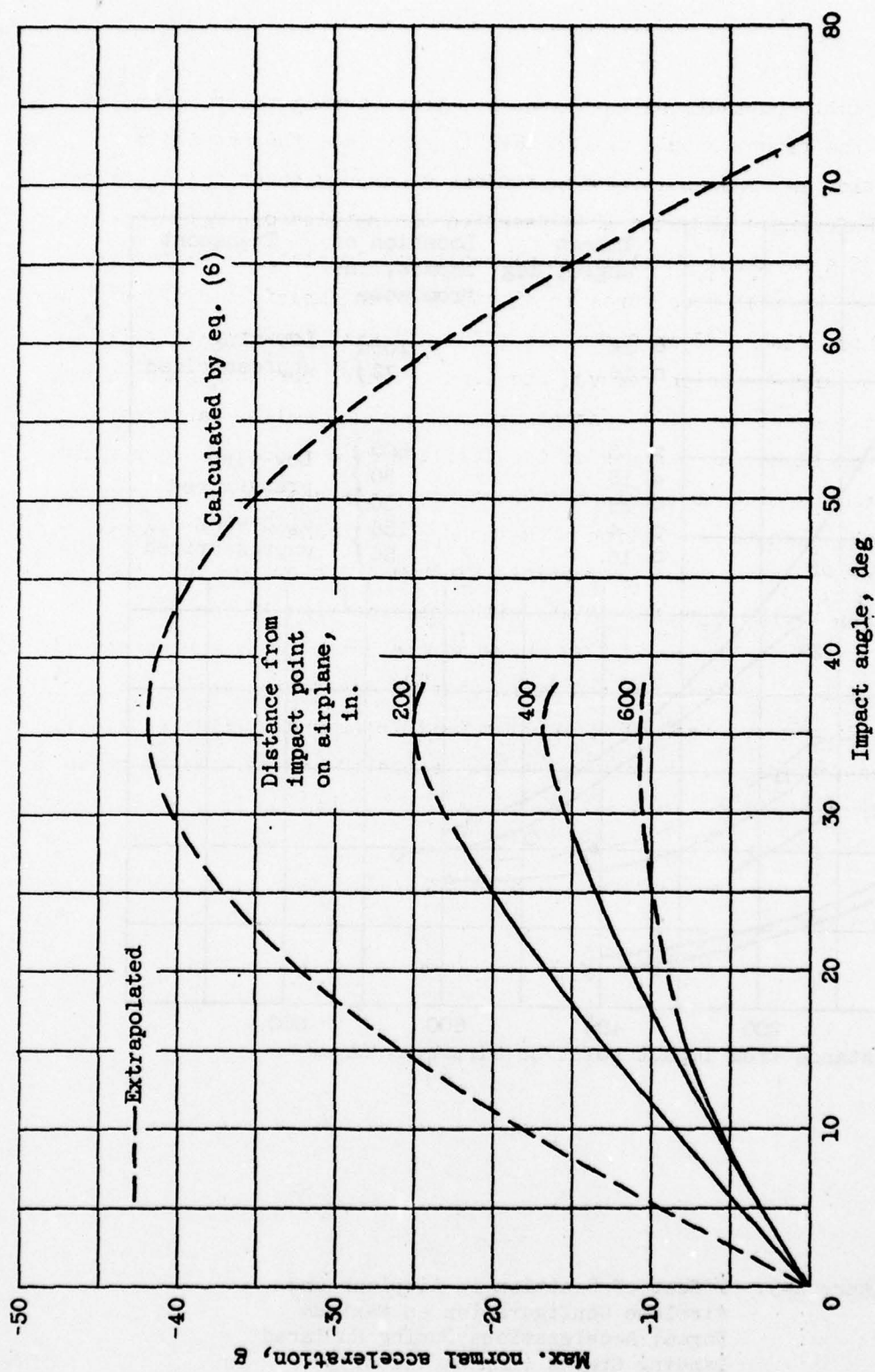


Figure B-10. Comparison of Calculated and Experimental Values for Maximum Normal Acceleration at Various Impact Angles (Impact Speed Corrected to 95 mph). (Reference 22)

ever, it is cautioned that the equations developed during the program and presented in the report should not be used to calculate the magnitude of the acceleration in crashes involving different circumstances and different airplanes. References (23) and (24) describe the results of full scale crash tests of a Lockheed Model 1649A aircraft and Douglas DC-7 aircraft, respectively. The test procedures to obtain desired impact conditions were similar to those described in Reference (22). Initial impact was at 112 knots against barriers which removed the landing gear, permitting the airplane to become airborne until contact with wing and fuselage barriers. The terrain was sloped 20 degrees at the fuselage impact point. No attempt in the program was made to relate responses to the type of flexible ground that was used. With the exception of Reference (22) none of the reports referenced herein discuss the properties of the terrain or the influence it may have had on the results. Also, with the exception of the brief analysis described in Reference (22), none of the crash tests are supported by analysis of the results from the standpoint of developing analytical models to predict responses, even on an inflexible ground. In general, the responses recorded during the tests are tabulated and related to human tolerance curves.

B.6 DESIGN PROCEDURES AND CRITERIA

There are many design procedures and computer programs available for assessing landing gear and aircraft performance during take-off and landing from various types of airfields. Computer programs are available for single wheel (References (3) and (10)) and multiple wheel (References (3), (11) and (15)) landing gears. In addition, design curves or nomographs are also available for single wheel (Reference (13)) and multiple wheel (References (8), (9) and (12)) configurations. Reference (4) contains a series of computer programs to help evaluate various aircraft operations, including airfield capability, landing impact with and without runout, taxi, take-off and turning. Reference (16) provides a digital computer program for use in predicting take-off performance on clay and sand airfields. The prediction of the dynamic response of lunar vehicles which traverse yielding and unyielding surfaces is available from an analogue computer program described in Reference (19). Reference (21) presents a digital computer program for predicting the rigid and flexible pavement responses due to moving loads as well as pavement design criteria and procedures. Reference (21) also contains a list of additional literature in its Appendix A (Literature Survey) which may provide additional useful information. Subjects which may be of interest include Airport Pavement Response (Static and Dynamic Analysis), Material Characterization, and Pavement Testing. Several references, including (4), (9), (10), and (13) provide criteria related to aircraft flotation and include the effects of soil interaction.

B.7 SUMMARY

The review of available literature attempts to encompass a wide cross section of areas. The emphasis in this literature evaluation is on airfield applications. The test data that are available are generally obtained for the purpose of supporting analyses or for the development of procedures and criteria to evaluate aircraft performance, and not for the

purpose of helping predict dynamic responses wherein large deformations occur. Even the full scale crash tests that have previously been performed on flexible ground surfaces have not addressed themselves to the significance of the terrain properties on structure and, ultimately, occupant response. For example, little or no measurements of ground flexibility, moisture, finish, or distribution as a function of depth or space have been made in any of the full scale crash tests reported herein. No measurements have been made to ascertain penetration by airframe or the relationship of penetration to airframe size or shape or to the impact velocities. While the penetration of ground by tires (sinkage) for the landing gear-ground interaction is available, these data do not relate easily to the impact velocity combinations and varied shapes that penetrate a flexible ground during a crash condition.

The research effort with regard to developing analytical models to describe landing gear-soil interaction and provide flotation criteria for aircraft operating from unpaved runways is substantial. A heavy reliance is placed on the use of the Mobility Number (Ω) = $\frac{CI(bd)}{F_t} \left(\frac{\delta_t}{h_t} \right)^{\frac{1}{2}}$ *

where CI = Cone Index
 bd = Tire Print Area
 F_t = Tire Force
 δ_t = Tire Deflection
 h_t = Height of Tire

However, the analytical techniques developed for landing gear-soil interaction use are not directly applicable to structural crashworthiness investigations. Modifications are needed which account for airframe shape, crash attitude, shear flow distribution, structure flexibility, and dynamic load effects.

The analysis of flexible ground-structure interaction during relatively high dynamic impact conditions would benefit from an orderly and concerted

*The above mobility number is for clay soil. Mobility numbers for other types of soil take other forms.

effort to accumulate data from typical airframe-terrain interaction tests and supportive laboratory soil tests. As a minimum, spatial and depthwise material properties (CBR, soil strength, moisture content), airframe response in the region of impact, airframe configuration (shape and size), post-impact terrain, penetration (size and depth) for a range of typical airplane impact velocities and attitudes, and soil configuration is needed. The data should be obtained for the purpose of developing curves which relate vertical force to sinkage as a function of CBR, soil shear strength to CBR, and horizontal force to frontal area as a function of shear strength.

B.8 LITERATURE MATRIX CATEGORIZATION

Table B-1 presents a literature matrix categorization which cross indexes subject matter and references. Table B-2 provides a summary by report number of applicable test data.

TABLE B-1. LITERATURE MATRIX CATEGORIZATION

REFERENCE NO.	1	2	3	4	5	6	7	8	9	10	11	12	13	14
ANALYSIS														
Analytical Model														
Surface														
Tire/Wheel/Gear														
Interaction														
Data Correlation														
Parametric Study														
LANDING SURFACE CHAR.														
Material Prop.														
Roughness Prop.														
Performance Char.														
LANDING SURFACE/ GEAR INTERACTION TESTS														
Test Procedures														
Data Analysis														
CRASH TESTS														
Test Procedures														
Data Analysis														
Empirical Criteria														
DESIGN														
Procedures														
Criteria														
Design Tools														
Nomographs														
Computer Prog.														

Specific Contents and Areas of Applicability

TABLE B-1. LITERATURE MATRIX CATEGORIZATION (Continued)

REFERENCE NO.	15	16	17	18	19	20	21	22	23	24	25	26
ANALYSIS												
Analytical Model												
Surface												
Tire/Wheel/Gear												
Interaction												
Data Correlation												
Parametric Study												
LANDING SURFACE CHAR.												
Material Prop.												
Roughness Prop.												
Performance Char.												
LANDING SURFACE/ GEAR INTERACTION TESTS												
Test Procedures												
Data Analysis												
CRASH TESTS												
Test Procedures												
Data Analysis												
Empirical Criteria												
DESIGN												
Procedures												
Criteria												
Design Tools												
Nomographs												
Computer Prog.												
Specific Contents and Areas of Applicability												

TABLE B-2. SOIL/INTERACTION TEST PARAMETER INDEX

REFERENCE NO.	1	2	3	4	5	6	7	8
LANDING SUR./SOIL								
Type	Clay	Clay	-	-	Clay/Sand	Clay/Sand	Sand	-
% Water Content	30.1-34.5	-	-	-	-	8	1	-
Density (lb/ft ³)	88.5-92.3	-	-	-	-	-	90-103	-
CBR (CI) [CPR]	-	-	-	-	1.5-4.4	(15-47)	(7-90)	-
Others	-	Hardness	-	-	-	-	-	-
TIRE/WHEEL								
Size (a)	-	29x11-10, 8PR 7.5x10, 8PR	-	-	29x10-11, 8PR	11x20, 12PR	*	-
Pressure (lb/in ²)	-	-	-	-	30-70	15-60	2-48	-
Number Per Gear	-	1	-	-	-	1	1	-
VEHICLE								
Type	-	Airplane	-	-	Cart	Cart	Cart	-
Load (lb)	-	9755-10547	-	-	2600-5300	3000	100-7760	-
Sink Speed (ft/sec)	-	6.6-34.7	-	-	0	0	-	-
Long. Speed (ft/sec)	-	90.2-145.2	-	-	0-169	1	-	-
Pitch Angle	-	(-6.5)-7.0	-	-	0	0	0	-
Yaw Angle	-	.1-4.0	-	-	0	0	0	-
REFERENCED DATA (b)	5	-	5,17	5,17	-	-	-	6,13,15
							* 4x7, 2PR 4x20, 2PR 6x16, 2PR 9x14, 2PR 16x15-6, 2PR 11x20, 12PR 1.75x26, 2PR 9x14, 2PR 4.5x18, 4PR	

TABLE B-2. SOIL/INTERACTION TEST PARAMETER INDEX (Continued)

REFERENCE NO.	9	10	11	11	11	12	13	14	15
LANDING SUR./SOIL									
Type	-	Clay/Sand	Clay/Sand	Clay/Sand	Clay/Sand	-	Clay	Clay/Sand	Clay/Sand
% Water Content	-	2.5-42.2	1.5-29.3	1-42	6-35.4	-	16.2-24.8	6-35.4	.8-29.6
Density (lb/ft ³)	-	75.1-99.5	75.5-97.4	75-102	83.6-104	-	93.9-101.8	83.6-104	77.2-120.8
CBR (CI) [CPR]	-	0.7-1.4	[8-35.7]	(20-45)	1-2.3	-	7-17	1-2.3	.8-64
Others	-	-	-	-	-	-	-	-	-
TIRE/WHEEL									
Size (a)	-	7.00x6,6PR 8,50x10,8PR	-	-	7.00x6,6PR	-	*	29x11-10,8PR	46x16,26PR 32x11.5-15,12PR
Pressure (lb/in ²)	-	-	-	-	2.2-12.5	-	-	30-70	30
Number Per Gear	-	1	-	-	2	-	1,2,3,12	1,2	8
VEHICLE									
Type	-	Cart	Flat Plate	Cart	Cart	-	Cart	Cart	Airplane
Load (lb)	-	300-2000	-	800-1400	2600-5200	-	1000-273,000	2600-5200	156,500
Sink Speed (ft/sec)	-	0	-	0	0	-	0	0	0
Long. Speed (ft/sec)	-	20	-	10	10-147	-	0.5-25.3	10-147	<10
Pitch Angle	-	0	-	0	0	-	0	0	-
Yaw Angle	-	0	-	0	0	-	0	0-6	-
REFERENCED DATA (b)	-	5,6,13,8	13,6,15	13,6,15	13,6,15	-	-	-	-
							* 9.00x14,8PR 34x9.9,14PR 20.00x20,22PR 25.00x28,30PR 56x16,24PR 17.00x16,12PR 30x11.5,24PR 56x16,32PR 56x16,38PR		

(a) Tire Size: Diameter x Width, PR = ply rating

(b) Report Number in the Literature Survey

TABLE B-2. SOIL/INTERACTION TEST PARAMETER INDEX (Continued)

REFERENCE NO.	15	16	17	18	19	20	21	22	23	24	25	26
LANDING SUR./SOIL												
Type	Sand	-	Clay	Sand	-	-	Soil	-	-	-	-	Sand
% Water Content	-	-	31.7-33.4	.2-.5	-	-	30,20	-	-	-	-	46-56
Density (lb/ft ³)	-	-	84.6-86.1	90.3-104.6	-	-	91.2,107.9	-	-	-	-	-
CBR (CI) [CPR]	2.5-5.5	-	1.3-2.8	(3.75-54)	-	-	2.10	-	-	-	-	-
Others							-					
TIRE/WHEEL												
Size	46x16,26PR 32x11.5-15,12PR	-		*	-	-	-	-	-	-	-	-
Pressure (lb/in ²)	30,36	-	70	-	-	-	50-100	-	-	-	-	-
Number Per Gear	4,8	-	1,2	1	-	-	1	-	-	-	-	-
VEHICLE												
Type	Airplane	-	Cart	Cart	-	-	Cart	-	-	-	-	-
Load (lb)	138,000- 180,000	-	-	465-4500	-	-	2000-3000	-	-	-	-	-
Sink Speed (ft/sec)	2-4	-	-	0	-	-	0	-	-	-	-	-
Long. Speed (ft/sec)	RTO	-	12-147	.5-18	-	-	0-66	-	-	-	-	-
Pitch Angle	-	-	0	0	-	-	0	-	-	-	-	-
Yaw Angle	-	-	0	0	-	-	0	-	-	-	-	-
REFERENCED DATA (a)	15	15	5,26	* 6.00x16,4PR 4.15x18,4PR 9.00x14,2PR 11.00x20,12PR 9.00x14,8PR 6.00x16,2PR								

(a) Tire Size: Diameter x Width, PR = ply rating

(b) Report Number in the Literature Survey

B.9 ABSTRACTS

1. Cheng, Robert Y.K.; EFFECT OF SHEARING STRAIN-RATE ON THE ULTIMATE SHEARING RESISTANCE OF CLAY; NASA CR-2634; February 1976

This report describes laboratory tests performed to determine the shearing resistance of cohesive soils subjected to strain rates between 1 and 14 rad/sec. A fast step-loading torque apparatus was used to induce a state of pure shear in a hollow cylindrical soil specimen. The relationship between shearing resistance and rate of shear deformation was established for various soil densities expressed in terms of initial water content.

The results of the tests described in this report show that the shearing resistance increases initially with shearing velocity, but subsequently reaches a terminal value as the shearing velocity increases. The terminal shearing resistance was found to increase as the density of the soil increases.

Mississippi Buckshot Clay was used in all the tests described in this report. This is the same type of clay used in the test beds at the NASA-Langley facility for the measurement of drag loads on aircraft tires during high-speed operations in clay soil.

2. Cook, C.E. and Gargiulo, J.D.; AN INVESTIGATION OF LANDING GEAR-SOFT SOIL INTERACTION UTILIZING THE OV-10A AIRCRAFT; North American Aviation/Columbus, North American Rockwell; NR 70H-570; January 1971.

This report presents the results of a study to investigate the interaction between the landing gear of the OV-10A airplane and soft soil. Sixteen landing and takeoffs were made by the OV-10A on soft unprepared terrain. Two fifty-channel oscillographs were used to measure time histories of airplane response. Measurements were also taken

of the terrain contour and static and dynamic strengths of the soil. Landings were successfully performed with soil penetrometer (static strength) readings as low as 40 (static load of 20 psi) for sink speeds as great as 16 feet per second.

An analytical model of soil is developed by assuming that the static and dynamic strength properties of soil may be represented by a second order differential equation with variable stiffness and damping coefficients. These are determined from experimental data from penetrometer and a specially constructed cylinder drop test vehicle.

An analytical model of a pneumatic tire on soft soil is also developed. The primary inputs to the model are the vertical and drag forces generated by the soil model.

Equations of motion are presented for a mathematical model of the OV-10A landing and taking off from yieldable uneven terrain. This model simulates the soil-tire interactions, landing gear-airplane interactions, and airplane dynamic response. A system of 20 non-linear, coupled second order differential equations are used. Analytical determination of landing gear loads for correlation with experimental data was included in the work to be performed under this contract. However, this task could not be accomplished within the allocated funds.

3. Cranshaw, B.M.; AIRCRAFT LANDING GEAR DYNAMIC LOADS INDUCED BY SOIL LANDING FIELDS, VOL. I: PREDICTION MODEL AND WHEEL LOADS; Flight Dynamics Laboratory, Wright-Patterson Air Force Base; AFFDL-TR-70-169, Vol. I; June 1972.

This report presents the results of a study to develop a mathematical model to predict sinkage and the resulting loads for aircraft wheels operating on bare soil together with experimental results

using a 29x11 10PR Type III tire. Four primary factors which determine soil rutting and drag have been identified. They consist of the tire spring rate, the soil load deflection relation, a drag inertia force, and a lift inertia force. Soil load deflections are based on the mobility number concept developed by the U.S. Army Corps of Engineers Waterways Experiment Station (WES). Empirical constants obtained from tests conducted at the NASA-Langley Landing Loads Track were used to compute the inertia forces. Comparisons of predicted and measured rut depths and drag loads are made for a clay soil with CBR's ranging from 1.5 to 2.3 and speeds from 0 to 90 knots for tire inflation pressures of 30, 45, and 70 psi. Similar comparisons are made for sand having a surface strength of CBR 1.5. The experimental program included 173 tests with a single wheel and 39 tests with two wheels in tandem on buckshot clay and 24 single wheel tests on sand. Overall average differences between predictions and test data for rut depths were the following: 11% on CBR 1.5, less than 1% on CBR 2.3, and 1.5% on sand. Overall average differences for drag loads were the following: 6% on CBR 1.5, 9% on CBR 2.3, and 12% on sand. Average positive and negative differences were somewhat higher and were between 11% and 36%. An alternate computation using a spring-mass-damper model as used in vibrating foundation studies is also included. This alternate model is not recommended as it does not account for drag load interaction and thus is not representative of the physical system. Methods for improvement of the alternate model are discussed. A computer program is described which incorporates the soil/wheel interaction model with a simulation of the C-130 aircraft during taxi and take-off. Analyses with this program show that moderate roughness has negligible effect on take-off distance for either soft fields or hard surfaces.

4. Crenshaw, B.M.; DEVELOPMENT OF AN ANALYTICAL TECHNIQUE TO PREDICT AIRCRAFT LANDING GEAR/SOIL INTERACTION; Flight Dynamics Laboratory, Wright-Patterson Air Force Base; AFFDL-TR-74-115, Vol. I and II; January 1975.

This report describes methods and evaluating techniques for determining aircraft takeoff performance, loads, and capabilities for operation on soil surface airfields. In addition to take-off and landing distance evaluations, considerations have also been given to ground operations such as landing impact, taxi, and turning. Calculation procedures have been developed and criteria recommendations made.

A revised soil model has been developed to incorporate soil load deflection curves and to allow for a more meaningful physical representation of the soil response available at the time (1974). The new model includes the horizontal shear effects resulting from "skid sinkage".

A series of computer programs were developed during the course of this program for calculating aircraft loads and dynamic response on unpaved surfaces. For given soil strength and surface roughness, these programs compute rut depth, soil drag loads, aircraft gear loads, and structural accelerations as functions of time and include the dynamic interaction between the aircraft and the flexible soil surface.

5. Crenshaw, B.M., Butterworth, C.K., and Truesdale, W.B.; AIRCRAFT LANDING GEAR DYNAMIC LOADS FROM OPERATION ON CLAY AND SANDY SOIL; Flight Dynamics Laboratory, Wright-Patterson Air Force Base; AFFDL-TR-69-51; February 1971.

This report presents results of tests to obtain experimental data on wheel performance on soil over a speed range of 0 to 100 knots. The tests were conducted on three soil strengths, CBR 1.5, 2.3 and 4.4 for buckshot clay and CBR 1.5 for sand. The configuration tested was a single 29 x 11-10 8PR tire loaded by 5000 pounds ballast weight. In addition to soil type and strength variations, the test variables were tire pressure and speed. Loads and rut depths were obtained for both free rolling and braking conditions. Free rolling drag ratios (μ) as high as 0.45 were obtained for soils with a CBR of 1.5. The drag ratio for free rolling decreased with increasing soil strengths. During braking, drag ratios as high as 1.0 were obtained for soft soils but approached more conventional values with increasing soil strength. The rut depth was a maximum at zero forward velocity and decreased with increasing forward velocity but reached another maxima in the 30 to 50 knot speed range and then decreased for the higher speeds. Rut depths of about 2.2 inches were obtained on CBR 1.5 and 1.2 inches for CBR 2.3 for speeds greater than zero. Rut depths for static conditions were considerably greater. Similar responses were obtained on the sand surfaces. This program has established that there is a pronounced high speed interaction between a wheel and a soft surface. This interaction is most pronounced for soft surfaces and high tire pressures; it is reduced if either the tire pressure is reduced or if the soil strength is increased. An analog computer program of the C-130 airplane was developed to incorporate the high speed effects found during the tests into a soil-gear interaction model. Results from this computer program compared loads from paved and

soft soil runways. Where soil surfaces were considered in the simulation, wing shear loads are smaller because gear vertical loads are attenuated by an effective reduction in profile amplitudes on the yielding surface. This testing has generally verified empirical prediction methods for drag ratios for low speeds but does not agree well for the higher speeds. Wheel drag loads were found to vary linearly with rut depth.

6. Freitag, D.R., Green, A.J., and Murphy, Jr., N.R.; NORMAL STRESSES AT THE TIRE-SOIL INTERFACE IN YIELDING SOILS; U.S. Army Engineer Waterways Experiment Station, Corps of Engineers; Misc. Paper No. 4-629; February 1964.

This paper describes the results of tests made to measure the distribution of stresses at the tire-soil interface under some representative test conditions. Two soils, a sand and a clay, carefully placed in a test pit, were used in the program. Each soil was tested at three different levels of strength. A single 11.00x20 12PR military tire at one test load was employed. Stresses, however, were measured at several different inflation pressures. Tests were performed with the wheel powered and with it towed at a constant speed of approximately .7 mph.

The results of the test performed indicate that the resultant of the normal stress field at the tire-surface interface passes through the center line of the wheel axle for both towed and powered wheels. These results are restricted to very slow moving vehicles, however.

7. Green, A.J.; PERFORMANCE OF SOILS UNDER TIRE LOADS, REPORT 5:
DEVELOPMENT OF MOBILITY NUMBERS FOR COARSE-GRAINED SOILS;
Army Engineer Waterways Experimental Station, Corp of
Engineers; Technical Report No. 3-666; July 1967.

This report describes the results of a study to examine the effects of tire deflection, tire geometry, wheel load, and soil strength on the performance of coarse-grained soils subject to moving tire loads. Empirical criteria were developed based on analysis of test results that combine the independent parameters of the soil-vehicle system and relate them to dependent performance characteristics such as sinkage, towed force, etc. A combination of independent parameters called mobility numbers were developed which account for the combined effects of soil strength, tire section width and diameter, wheel load, and tire deflection on wheel performance as measured by performance coefficients. The mobility numbers developed in this study are applicable to single wheels operating on sand at speeds common to surface vehicles.

A multiple-pass analysis was conducted to illustrate that performance on the second and third passes also can be related to the sand mobility number, although the relation was not the same as that for the first pass. It is shown in a similar fashion that the performance of vehicles on coarse-grained sand can be predicted using a relation based on the sand mobility number.

8. Kraft, D.C.; ANALYTICAL LANDING GEAR-SOIL INTERACTION-PHASE I;
Flight Dynamics Laboratory, Wright-Patterson Air Force Base;
AFFDL-TR-68-88; August 1968.

This report describes the results of a study to determine the variables which significantly influence aircraft performance when operating on soil runways.

Analysis of available experimental drag-sinkage-velocity data led to the defining of at least three distinct regions for which the sinkage ratio-velocity relationship shows a distinct response. These velocity regions are 0-5 knots, 5-50 knots, and velocities greater than 50 knots. A drag ratio-sinkage ratio least square fit was developed for use in the second of these velocity regions. The effects of twin wheel arrangements were analyzed on a preliminary basis. The results of a sinkage study using available (1968) prediction methods indicates that present sinkage analysis accuracy is in the range of $\pm 50\%$ to $\pm 100\%$.

In order to develop a suitable flotation criteria, an investigation was conducted into a dynamic landing gear contacting element-soil interaction response model, utilizing elastic theory. These results led to the development of a flotation parameter (related to sinkage) and a flotation index (related to drag) in nomographic form, which permits comparative flotation analysis of landing gear systems.

9. Kraft, D.C., Hoppenjans, J.R., and Edelen, Jr., W.F.; DESIGN PROCEDURE FOR ESTIMATING AIRCRAFT CAPABILITY TO OPERATE ON SOIL SURFACES; Flight Dynamics Laboratory, Wright-Patterson Air Force Base; AFFDL-TR-72-129; December 1972.

This report describes a systematic design procedure for establishing various landing gear combinations of tire size, spacing, and configuration which will minimize rolling drag and satisfy the

criteria of 200 non-braking passes for aircraft having take-off/landing weights of 150,000 to 250,000 lbs. and low horizontal speeds (close to or less than 40 knots), operating on a standardized CBR 6 (or equivalent) soil surface. The design procedure presented combines the latest results (1972) of Air Force sponsored landing gear/soil interaction research with previously developed Army Corps of Engineers Waterways Experiment Station (WES) coverage technique.

The procedure is a first attempt to make the research results of existing Air Force Flight Dynamics Laboratory programs available toward the improvement of flotation design capability. The design procedure, subject to certain stated limitations, includes techniques for (1) predicting rolling and braking drags and drag ratios, (2) incorporating multiwheel influences on drag and sinkage, and (3) determining allowable aircraft passes. Additionally, the design procedure has been incorporated in a computer program format for utilization on the CDC 6600 located at Wright-Patterson Air Force Base. The computer program is restricted to aircraft with tricycle type landing gear systems.

10. Kraft, D.C., Luning, H., Hoppenjans, J.R.; AIRCRAFT LANDING GEAR-SOILS INTERACTION AND FLOTATION CRITERIA, PHASE II: Flight Dynamics Laboratory, Wright-Patterson Air Force Base; AFFDL-TR-69-76; November 1969.

This report describes the results of an investigation directed at defining landing gear-soil interaction and developing flotation criteria to permit comparative evaluation of the relative merits of various landing gear configurations.

A basic aircraft tire-soil interaction equation relating the drag ratio (R/P) to sinkage ratio (Z/D) was developed for the velocity range 5 knots to 40 knots. The influence of high velocity and mul-

tiple wheel configurations on flotation performance was determined on a preliminary basis. Empirical sinkage prediction equations were developed for predicting the sinkage of aircraft type tires on cohesive and cohesionless soils with an estimated accuracy of $\pm 40\%$ within the 90% confidence limits. The results of the Single Wheel Verification Tests are reported and used to verify the developed flotation analysis equations.

An analytical approach to sinkage prediction using finite element techniques was developed to give a more rational approach to sinkage analysis. The soil was assumed to be an elastic-perfectly plastic medium. The results of this analytical approach as given by the computer program developed during this study and the results of a test case evaluation are described in detail.

A preliminary Single Wheel Relative Merit Index (RMI) was developed for permitting a comparative evaluation of the flotation characteristics of aircraft tires on soil. The RMI was used to rate the flotation capacity of aircraft tires currently used on cargo, bomber, and fighter aircraft.

11. Kraft, D.C., Luming, H., and Hoppenjans, J.R.; MULTIWHEEL LANDING GEAR-SOILS INTERACTION AND FLOTATION CRITERIA-PHASE III; Flight Dynamics Laboratory, Wright-Patterson Air Force Base; AFFDL-TR-71-12; May 1971.

This report describes the results of the third phase of a study to analytically define landing gear-soil interaction and to develop a system for rating the relative flotation capacity of landing gear contact elements and landing gear systems during aircraft operation on semi and unprepared soil runways. During this phase, existing data relating drag ratio to multiwheel geometry parameters were collected and summarized. Also, twin plate vertical load tests were

performed to determine the sinkage interaction effects produced by adjacent dynamic plate loads as compared to a single isolated plate load under similar test conditions.

A computer program has been developed to study the effects of multi-wheel landing gears on the sinkage of tires into soil. The trends shown in these results were consistent with those observed in the twin plate vertical load test.

Based on the results of this study, multiwheel criteria were developed which permit the evaluation of aircraft flotation performance. The criteria also permits aircraft designers to determine optimum landing gear configuration for aircraft leading to drag minimization. Available and proposed flotation/operation criteria are outlined.

12. Ladd, D.W.; GROUND FLOTATION REQUIREMENTS FOR AIRCRAFT LANDING GEAR; Army Engineer Waterways Experiment Station, Corps of Engineers; Miscellaneous Paper No. 4-459; July 1965.

This paper presents a set of design curves which can be used to assist the aircraft designer in designing a landing gear that will support a given aircraft load without overloading an airfield of stated strength. Seven classes of Zone-of-Interior and Theater-of-Operation airfields are defined to which the design curves presented specifically apply. The landing gear design parameters included are number of wheels, spacing of wheels, tire contact area, gear type, and load range.

13. Ladd, D., Ulery, Jr., H., et al; AIRCRAFT GROUND-FLOTATION INVESTIGATION, Parts I-XIX; Flight Dynamics Laboratory, Wright-Patterson Air Force Base; AFFDL-TDR-66-43, Parts I-XIX; August 1967.

This report summarizes results of an extensive study to develop a

method for designing an efficient landing gear configuration for aircraft required to operate on Theater-Of-Operation class airfields. The method was developed from a series of ground-flotation tests conducted on mat-surfaced subgrades and unsurfaced subgrades. Also presented is a discussion of the testing procedures and techniques and of the analysis of all tests conducted in conjunction with the ground flotation investigation, including tracking, drag, and speed tests.

To develop criteria for the efficient design of aircraft landing gears, a series of traffic tests were conducted with numerous wheel configurations, loads, and tire pressures. The configurations varied from a single wheel up to 12 wheels; loading weights varied from 1000 to 273000 pounds; tire pressure ranged from 10 to 250 psi; and wheel spacing varied from 2.0 radii up to 6.8 radii. From data developed from these tests, a generalized single wheel criteria was developed. Speed versus drag relations were obtained from scale model tests in which various speeds, loads, tire pressures and tire sizes were investigated.

14. Leland, T.J.W. and Smith, E.G.; AIRCRAFT TIRE BEHAVIOR DURING HIGH-SPEED OPERATIONS IN SOIL: NASA TN D-6813; August 1972.

An investigation to determine aircraft tire behavior and operating problems in soil of different characteristics was conducted at the Langley landing-loads track using a 29 x 11.0-10 8PR Type III tire. Four clay test beds of different moisture content and one sand test bed were used to explore the effects on axle drag loads developed during operation at different tire inflation pressures in free rolling, locked-wheel braking, and yawed (cornering) modes, all at forward speeds up to 95 knots.

The test results indicate that, in general, axle drag loads are

highly dependent on forward velocity, with loads initially decreasing from static or low speed and then rising sharply with increasing forward speed to a peak in the velocity range of 40 knots for the configurations tested. Further increases in speed bring about a reduction in drag load by a phenomena not presently understood. In addition, for a given soil strength, the magnitude of the axle drag load is strongly a function of tire inflation pressure with higher inflation pressures resulting in higher axle drag coefficients.

15. Richmond, L.D.; Brueske, N.W.; DeBord, K.J.; et al; AIRCRAFT DYNAMIC LOADS FROM SUBSTANDARD LANDING SITES: Flight Dynamics Laboratory, Wright-Patterson Air Force Base; AFDL-TR-67-145, Parts I-V, September 1968.

This report describes the results of a detailed study of ground-induced dynamic loads resulting from operations on substandard airfields. The study was divided into 5 phases. A mathematical model to study tire-soil interaction effects was developed in Phase I. Phase II was a site selection and field measurement program to obtain field roughness profiles and soil strength information from fields typical of those expected to be found in remote theaters of operations. The information from Phases I and II was used in Phase III to conduct comprehensive airplane ground-load dynamic analyses and to formulate airplane design loads and criteria. The development of the tire-soil model was based on the results of a literature survey and experimental data collected from the 367-80 airplane (707/KC-133 prototype) during high-flotation taxi tests conducted by The Boeing Company at Harper Lake, California, in September 1964. The development resulted in empirical expressions that related soil sinkage and rolling resistance to soil strength, tire vertical force, tire characteristics, and taxi velocity. The original development of the empirical non-dimensional expressions was accomplished by the U.S. Army Corps Engineer Waterways Experiment

Station (WES). The results of the literature survey and the tire-soil model development obtained during the phase I study are presented in Part II. A total of 9 substandard sites were selected for field measurements from approximately 27 sites visited. These sites, located throughout the United States were selected on the basis of their availability to the field survey team and their suitability as a forward-area airfield. The profiles on these sites represented various degrees of preparation, from semi-prepared to unprepared, and included a variety of soil types. Soil strength measurements and soil samples were collected at each site and the profile roughness was measured. These measurements are presented in Parts III and IV. Phase III was an analytical study to determine the dynamic loads and degradation in takeoff performance of airplanes operating from substandard airfields. Digital and analog computer models simulating the 367-80 airplane in a high flotation configuration were used to conduct the landing impact, taxi, and landing-and-takeoff-distance analysis. The effects of soil strength and profile roughness were included. Parametric variations of tire pressure, gross weight, and taxi velocity were also examined. Prior to the dynamic analysis, a statistical analysis of the profile data was performed. From these data, artificial profiles and sets of discrete one-minus-cosine bumps representative of one of the measured profiles were generated. The dynamic loads resulting from excitation due to the artificial profile and the discrete bumps were compared to the loads from the actual profile. The landing impact analysis was performed using a model similar to the taxi-analysis model except that soil flexibility was not included. A smooth, rigid surface was used in determining the maximum gear and airplane loads developed during landing impact. The takeoff-and-landing-distance performance analysis was performed using a structurally rigid model operating on a smooth, soft soil surface. The effects of changes in the soil strength,

tire inflation pressure, and gross weight on takeoff distances were examined. The variation in landing distance with braking coefficient was investigated.

From the results of this study, it was concluded that the simplified soil representation was satisfactory for the taxi analysis because of the relatively small influence that the soil strength has on dynamic loads. The effects of surface roughness were most pronounced on the dynamic loads. For analysis purposes, the discrete excitation will give peak loads that are conservative, while the artificial runways will give results that are unconservative. The results indicate that this class of airplane could successfully operate from semi-prepared sites with only minor modifications to current criteria and operating procedures. It does not seem feasible to operate this class of airplane from the unprepared sites examined in this study.

16. Sharp, A.L.; COMPUTER PROGRAMS FOR THE PREDICTION OF AIRCRAFT TAKEOFF PERFORMANCE ON CLAY AND SAND AIRFIELDS; Flight Dynamics Laboratory, Wright-Patterson Air Force Base; AFFDL-TR-68-115; April 1969.

This report describes a prediction method for estimating wheel sinkage, landing gear drag, and aircraft take-off performance on clay and sand airfields of various bearing strengths. The method is based on a method developed by Boeing (AFFDL-TR-67-145) which uses modified Mobility Numbers developed by the Army Waterways Experiment Station (WES). Estimates of take-off distance, wheel drag to vertical force ratios for the full ground velocity range, and the wheel sinkage into the soils are prepared for the C-5 and C-141 aircraft.

Three FORTRAN IV computer programs were developed based on the

methods generated by Boeing and WES. The first of these is used to calculate drag and sinkage for wheels attached to one strut while taxiing at constant speed. The second considers the complete aircraft taxiing at constant velocity and the third calculates takeoff performance of a complete aircraft on hard surface (paved runways) and on clay and sandy soils. The computer programs were tested for accuracy by analyzing conditions which were identical to those used by Boeing and comparing the results with Boeing's full scale airplane tests.

17. Truesdale, W.B. and Nelson, R.D.; AIRCRAFT LANDING GEAR DYNAMIC LOADS INDUCED BY SOIL LANDING FIELDS, VOL. II: SOIL TESTS AND SOIL RESPONSE STUDIES: Flight Dynamics Laboratory, Wright-Patterson Air Force Base; AFFDL-TR-70-169, Vol. II; June 1972.

This report contains a description of the construction and maintenance of the buckshot clay test bed used for tandem and single wheel high speed landing gear tests conducted at the NASA Langley Landing Loads Track. The test bed was constructed to a CBR strength of 2.7, moisture content of 32.5 percent, dry density of 86.0 pcf, degree of saturation of 91.7 percent, and airfield penetration resistance of 1.7 to 1.8. Analysis of dynamic soil behavior indicated that wave propagation velocities in the soil and soil inertia effects become significant at forward velocities greater than 60 knots. Strain-rate effects are significant at all velocities for buckshot clay and cause 50 to 60 percent increases of shear strength at a forward velocity of 50 knots. Strain-rate effects on sand are insignificant except when pore pressures are developed. The wheel will "outrun" the bow wave or shear wave propagating ahead of the wheel at forward velocities greater than the 150 to 250 knot velocity of the soil shear wave. A series of

dynamic plate bearing tests conducted with a controlled rate of loading have shown that the response of a rolling wheel can be duplicated in a dynamic plate test. These tests showed a decrease in soil stiffness in the same velocity range in which increased drag and sinkage were observed to occur in the field tests. The increase in sinkage and drag loads that occurred when brakes were applied can be accounted for by the passive earth pressure theories and the change in stress distribution on the soil-wheel interface.

18. Turnage, G.W., and Green, Jr., A.J.; PERFORMANCE OF SOILS UNDER TIRE LOADS. ANALYSIS OF TESTS IN SAND FROM SEPTEMBER 1962 THROUGH NOVEMBER 1963; U.S. Army Engineer Waterways Experiment Station, Corps of Engineers; Technical Report No. 3-666, Report 4; February 1966.

This report examines the effects of tire deflection, tread, carcass stiffness, construction, speed, and slip on tire performance in a dry sand. Tests were performed using both Yuma (desert) and mortar sand. Test speeds varied from approximately .3 mph to 12 mph.

The test results indicate that for best performance in a dry sand, a tire should be highly deflected, smooth, and of diagonal-ply construction. Variations in carcass stiffness have negligible effects on tire performance when comparisons are made at equal loads and deflections. Performance of pneumatic tires in sand is affected by speed; however, the extent of this influence was not wholly determined.

19. Van Deusen, B.D.; A STATISTICAL TECHNIQUE FOR THE DYNAMIC ANALYSIS OF VEHICLES TRAVERSING ROUGH YIELDING AND NON-YIELDING SURFACES: NASA CR-659; March 1967.

This report describes a statistical analysis technique for the classification of virgin terrestrial and extraterrestrial surfaces. A method is devised whereby a single parameter is used to completely specify the surface roughness in a statistical sense.

A dynamic nonlinear yielding surface model was developed from existing information of soil mechanics. The model includes hysteresis due to initial soil compaction and effects of vehicle speed and loading area.

An analogue computer program, capable of predicting the dynamic response of typical lunar vehicles traversing yielding and non-yielding surfaces, was developed. A technique is included which allows a random surface profile to be introduced between the vehicle model and the yielding surface model and allows vehicle-surface separation.

20. Eiband, A.M., Simpkinson, S.H., Black, D.O.; ACCELERATIONS AND PASSENGER HARNESS LOADS MEASURED IN FULL-SCALE, LIGHT-AIRPLANE CRASHES: NACA TN 2991; August 1953.

Full-scale, light-airplane crashes simulating stall-spin accidents were conducted to determine the decelerations to which occupants are exposed and the resulting harness forces encountered in this type of accident. Crashes at impact speeds from 42 to 60 miles per hour were studied. The airplanes used were of the familiar steel-tube, fabric-covered, tandem, two-seat type.

In crashes up to an impact speed of 60 miles per hour, crumpling of the forward fuselage structure prevented the maximum decelera-

tion at the rear-seat location from exceeding 26 to 33g. This maximum g value appeared independent of the impact speed. Restraining forces in the seat-belt/shoulder-harness combination reached 5800 pounds. The rear-seat occupant can survive crashes of the type studied at impact speeds up to 60 miles per hour, if body movement is restrained by an adequate seat-belt/shoulder-harness combination so as to prevent injurious contact with obstacles normally present in the cabin. Inwardly collapsing cabin structure, however, is a potential hazard in the higher-speed crashes.

21. Wignot, J.E., et al; AIRCRAFT DYNAMIC WHEEL LOAD EFFECTS ON AIRPORT PAVEMENTS; Lockheed-California Company; Federal Aviation Administration; FAA-RD-70-19, May 1970.

This report describes the results of a program which included scaled pavement tests, analysis to determine airplane imposed loads on pavement and pavement response, correlation between empirical data and analyses and a literature review. Based on the results of the program, it was concluded that airplane dynamic wheel loads have significant effects on portions of airport pavement.

The results of the investigation indicate that the two distinguishable effects that influence the stress the pavement experiences are (1) airplane induced loads and (2) moving load phenomenon. For a given level of runway unevenness, the loads that will be imposed on the pavement can be accurately defined for various ground operations performed. However, the pavement response to a moving load can vary substantially depending upon the kinds of materials and types of construction used. To obtain proper assessment of moving load effects, full scale pavement tests are considered necessary

to provide needed data.

Two test plans are presented. One approach involves "Operational Statistical Tests" and depends upon a heavy statistical sample of data. The alternate approach involves "Moving Load Track Tests" and provides data for point-by-point correlation using analytical data under carefully controlled conditions and configurations.

22. Preston, G.M. and Pesman, G.J.; ACCELERATIONS IN TRANSPORT-AIRPLANE CRASHES: NACA TN 4158; February 1958.

Full-scale transport airplanes were crashed experimentally to determine the crash loads that result from a variety of crash events. It was concluded that pressurized transport airplanes can withstand high-impact-angle crashes and still maintain survivable areas within the fuselage. During unflared-landing crashes, greater fuselage crushing occurred with high-wing than with low-wing airplanes. Airplanes with strong fuselage structures that do not deform and produce sharp, well-supported plowing edges will have relatively low longitudinal acceleration during crashes similar to those studied. Normal accelerations exceeding human tolerance can occur in crashes in which modest fuselage damage occurs. Within the structural range represented by the airplanes crashed, the configuration of the airplane had little effect on the normal acceleration.

23. Reed, W.H., Robertson, S.H., Weinberg, L.W.T., Tyndall, L.H.; FULL-SCALE DYNAMIC CRASH TEST OF A LOCKHEED CONSTELLATION MODEL 1649 AIRCRAFT; Aviation Safety Engineering and Research, Federal Aviation Agency; FAA-ADS-38; October 1965.

This report provides the details of a full-scale crash test of a large transport aircraft. The purpose of the test was to obtain

crash environment data of the test aircraft and the various experiments installed aboard the aircraft.

The Federal Aviation Agency sponsored the test program with the participation of several other organizations who provided data recording equipment and special experiments onboard the test aircraft. The participating organizations included the U.S. Navy, the U.S. Army, the U.S. Air Force, the Society of Automotive Engineers and the Flight Safety Foundation which conducted the test under contract to and with the guidance of the FAA. The special experiments consisted of military crew and commercial passenger seats, cargo restraint systems, postcrash locator beacons, baby and child restraint systems, radioactive material containers, a military litter system, and provisions for emergency lighting.

The test involved a Lockheed Constellation Model 1649A aircraft, which was guided into a series of crash barriers with a monorail nose gear guidance system. The aircraft was accelerated under its own power by remote control for a distance of 4,000 feet, reaching a velocity of 112 knots. Initial impact occurred against barriers which removed the landing gear, permitting the airplane to become airborne until the moment of impact with the wing and fuselage crash barriers.

The wing fuel tanks were ripped open by the wing barriers, allowing simulated fuel to spill out in a heavy mist during the crash sequence. The fuselage was broken in two places during the crash, just aft of the cockpit between fuselage stations 370 and 380 and just aft of the galley between fuselage stations 1020 and 1030. Peak longitudinal accelerations on the order of 25G's were measured at the cockpit floor when the aircraft impacted the 20 degree slope. Most of the onboard experiments remained in their relative locations throughout the test.

24. Reed, W.H., et al; FULL SCALE DYNAMIC CRASH TEST OF A DOUGLAS DC-7 AIRCRAFT, Aviation Safety Engineering and Research; FAA Technical Report ADS-37, Federal Aviation Administration, Washington, D.C., April 1965, AD 624051.

This report describes a test program designed to obtain crash environment data regarding fuel containment and to collect data on the behavior of various components and equipment aboard the aircraft, using a DC-7 as the test vehicle.

The test involved a DC-7 aircraft which was guided into a series of crash barriers with a monorail nose gear guidance system. The aircraft was accelerated under its own power by remote control for a distance of 4000 feet, reaching a velocity of 110 knots. At the end of this acceleration run, the aircraft impacted against a specially designed barrier which removed the landing gear, permitting the aircraft to become airborne until the moment of impact with wing and fuselage crash barriers.

The wing and fuselage barriers were designed to provide the following crash sequence: The left wing was to impact against an earthen mound shaped to produce a simulated wing-low accident. Simultaneously, the right wing was to impact telephone poles implanted vertically to simulate trees. Next, the main fuselage was to impact against an 8-degree slope. The slope was designed so that the aircraft could become airborne after sliding a short distance along the ground. Finally, the aircraft was to impact against a 20-degree slope to simulate a crash with a steeper angle of impact.

The test occurred as planned except that the aircraft, instead of coming to rest on the 20-degree slope, bounced over the hill on which the slope was formed and landed at the base of the backside of the hill. A failure of the voltage control regulator, in the

data recording system, prevented the program from reaching all its objectives.

25. Sela, A.D., and Ehrlich, I.R.; LOAD SUPPORT CAPACITY OF FLAT PLATES OF VARIOUS SHAPES IN SOIL; Automotive Engineering Congress, Society of Automotive Engineers; Paper No. 710178; January 1971.

This paper reports the results of a study to develop a general theory of plate sinkage which is applicable to a wide variety of soils, sinkages, plate sizes, and plate shapes.

The plate sinkage model developed in this study was verified, using available soil test results. The soils considered in these tests were air dry mason sand, buckshot clay, very fine grained Yuma sand, Michigan loam, and Ohio sand. No CBR numbers were given for these soils. The analytical model was found to correlate with all the experimental results included in the paper. The model has two regions of application--a "transition" region which is between 0 and 1 inch of sinkage and the region greater than 1" sinkage.

26. Whitman, R.V., and Healy, K.A.; SHEAR STRENGTH OF SANDS DURING RAPID LOADINGS, Journal of the Soil Mechanics and Foundations Division, Proceedings of the American Society of Civil Engineers; April 1962.

Triaxial tests with times-to-failure from 5 min. to 5 milliseconds have been used to investigate the effect of strain-rate on the strength of dry and saturated sands. New techniques were developed for applying strains rapidly, and for measuring the resultant stresses and pore pressures. It was necessary to give careful attention to the possible influence of testing errors, of inertia forces, and of the membrane effect.

The peak friction angles of the sands that were tested were substantially independent of failure-time. However, the excess pore pressures generated within saturated loose sands, did, for certain conditions, vary with failure-time. For these conditions the compressive strengths were correspondingly time-dependent. A tentative hypothesis has been advanced to explain this behavior. One loose saturated sand exhibited a pronounced yield point at low strains, and the yield point stress decreased as the rapidity of load application increased.

APPENDIX C

MEASURED RESPONSE TIME HISTORIES

TESTS 1 THROUGH 4

A detailed discussion describing the instrumentation used in tests 1 through 4 can be found in Section 2.6. As a convenience to the reader, Tables 2-6 through 2-9 and Table 2-11 are reprinted in this appendix as Tables C-2 through C-6. These tables identify the accelerometers, load cells and transducers as to location, type sensitivity and polarity.

Figures C1 through C-48 depict the 100 Hz low-pass filtered response level time histories measured during the four tests. The histories measured during test 1 are shown in Figures C-1 through C-12, test 2 histories in Figures C-13 through C-24, test 3 histories in Figures C-25 through C-36, and test 4 histories in Figures C-37 through C-48. A description of the filtering technique used in generating these time histories is presented in Section 2.8.

The ordinate of each plot history is identified as to transducer number and scale factor. The abscissa of all plots is time measured in seconds. The origin of the time scale ($t = 0.0$) for the plots associated with each test is somewhat arbitrary in that the time trace begins sometime during the free swing descent of the test airplane. The time at which impact occurred is identified on each plot and also summarized below in Table C-1.

TABLE C-1. IMPACT TIME SUMMARY

TEST NO.	TIME AT IMPACT (sec)
1	0.185
2	1.063
3	1.007
4	0.605

BEST AVAILABLE COPY

TABLE C-2. ACCELEROMETER LOCATIONS AND RESPONSE SETTING FOR TEST 1

Accel. No.	Location	F.S.	W.L.	B.L.	Accel. Type	Axis	Peak Response (G)	Polarity	Tape Channel
VP1	Pilot Pelvis	44	+4.5	L10	ENDEVCO 2260CA	Vertical	100	+	A2
HPA2	Pilot Pelvis	44	+4.5	L10	2260CA	Horizontal	100	-	A8
HPA3	Pilot Head	49	+30	L10	2260CA	Vertical	100	+	A3
HPA4	Pilot Head	49	+30	L10	2260CA	Horizontal	100	-	A4
VCA5	Co-Pilot Pelvis	42	+4.5	R10	2260CA	Vertical	100	+	A6
HCA6	Co-Pilot Pelvis	42	+4.5	R10	2260CA	Horizontal	150	-	A9
VCA7	Co-Pilot Head	47	30	R10	2260CA	Vertical	100	+	A7
HCA8	Co-Pilot Head	47	30	R10	2260CA	Horizontal	100	-	A1
VSA9	Pilot Seat Leg	40	-1	L10	2260CA	Vertical	100	-	A5
HSAL0	Pilot Seat Leg	40	-1	L10	2260CA	Horizontal	150	+	A10
VEB1	Engine	-18	+10	0	Kistler 818	Vertical	150	+	C1
HEB2	Engine	-18	+10	0	818	Horizontal	150	+	C2
VTB3	Tail Unit	228	+10	0	818	Vertical	50	-	C3
HTB4	Tail Unit	228	+10	0	818	Horizontal	50	+	C4
VCB5	Rear Cabin	108	-6	L14	818	Vertical	200	+	C5
HCB6	Rear Cabin	108	-6	L14	818	Horizontal	200	-	C6
VCB7	Cabin Cargo Bulkhead	90	-10	L8	818	Vertical	200	+	C7
HCB8	Cabin Cargo Bulkhead	90	-10	L8	818	Horizontal	200	-	C8
VCB9	Top Cabin	34	+32	R21	818	Vertical	150	-	C9
HCB10	Top Cabin	34	+32	R21	818	Horizontal	150	+	C10
VCB11	Top Cabin	65	+32	R15	818	Vertical	150	-	C11
HCB12	Top Cabin	65	+32	R15	818	Horizontal	150	+	C12
VB13	Wing	34	+32	R98	818	Vertical	50	+	C13
HVB14	Wing	34	+32	R98	818	Horizontal	50	+	D1
VB15	Wing	34	+32	L98	818	Vertical	50	+	D2
HVB16	Wing	34	+32	L98	818	Horizontal	50	+	D3
VCB17	Cabin Floor	44	-13	L8	818	Vertical	250	+	D4
HCB18	Cabin Floor	44	-13	L8	818	Horizontal	250	+	D5
VFC1	Firewall	+8	+5	L22	ENDEVCO	Vertical	250	-	A11
HFC2	Firewall	+8	+5	L22	7232C-570S	Horizontal	250	+	A12
VFC3	Firewall	0	-16.80	L14	7232C-570S	Vertical	350	+	A13
HFC4	Firewall	0	-16.80	L14	7232C-570S	Horizontal	350	+	B1
VCC5	Cabin floor	27	-15	L13.5	7232C-570S	Vertical	300	+	B2
HCC6	Cabin floor	27	-15	L13.5	7232C-570S	Horizontal	300	+	B3
VCC7	Cabin floor	27	-15	0	7232C-570S	Vertical	300	+	B4
HCC8	Cabin floor	27	-15	0	7232C-570S	Horizontal	300	+	B5
VCC9	Cabin floor	27	-15	R13.5	7232C-570S	Vertical	300	+	B6
HCC10	Cabin floor	27	-15	R13.5	7232C-570S	Horizontal	300	+	B7
VCC11	Cabin floor	60	-12	L14	7232C-570S	Vertical	250	+	B8
HCC12	Cabin floor	60	-12	L14	7232C-570S	Horizontal	250	+	B9
VCC13	Cabin floor	60	-12	0	7232C-570S	Vertical	250	+	B10
HCC14	Cabin floor	60	-12	0	7232C-570S	Horizontal	250	+	B11
VCC15	Cabin floor	60	-12	R14	7232C-570S	Vertical	250	+	B12
HCC16	Cabin floor	60	-12	R14	7232C-570S	Horizontal	250	+	B13

BEST AVAILABLE COPY

TABLE C-3. ACCELEROMETER LOCATIONS AND RESPONSE SETTING FOR TEST 2

Accel. No.	Location	F.S.	W.L.	B.L.	Accel. Type	Axis	Peak Response (G)	Polarity	Tape Channel
VPA1	Pilot Pelvis	44	+4.5	L10	ENDEVCO 2260CA	Vertical	100	+	A2
HPA2	Pilot Pelvis	44	+4.5	L10	2260CA	Horizontal	100	-	A8
VPA3	Pilot Head	49	+30	L10	2260CA	Vertical	100	+	A3
HPA4	Pilot Head	49	+30	L10	2260CA	Horizontal	100	-	A4
VCA5	Co-Pilot Pelvis	42	+4.5	R10	2260CA	Vertical	100	+	A6
HCA6	Co-Pilot Pelvis	42	+4.5	R10	2260CA	Horizontal	100	-	A9
VCA7	Co-Pilot Head	47	30	R10	2260CA	Vertical	100	+	A7
HCA8	Co-Pilot Head	47	30	R10	2260CA	Horizontal	100	-	A1
VSA9	Pilot Seat Leg	40	-1	L10	2260CA	Vertical	150	-	A5
HSAL0	Pilot Seat Leg	40	-1	L10	2260CA	Horizontal	150	+	A10
VEB1	Engine	-18	+10	0	Kistler 818	Vertical	150	+	C1
HEB2	Engine	-18	+10	0	818	Horizontal	150	+	C2
VTB3	Tail Unit	228	+10	0	818	Vertical	75	-	C3
HTB4	Tail Unit	228	+10	0	818	Horizontal	75	+	C4
VCB5	Rear Cabin	108	-6	L14	818	Vertical	250	+	C5
HCB6	Rear Cabin	108	-6	L14	818	Horizontal	250	-	C6
VCB7	Cabin Cargo Bulkhead	90	-10	L8	818	Vertical	250	+	C7
HCB8	Cabin Cargo Bulkhead	90	-10	L8	818	Horizontal	250	-	C8
VCB9	Top Cabin	34	+32	R21	818	Vertical	200	-	C9
HCB10	Top Cabin	34	+32	R21	818	Horizontal	200	+	C10
VCB11	Top Cabin	65	+32	R15	818	Vertical	200	-	C11
HCB12	Top Cabin	65	+32	R15	818	Horizontal	200	+	C12
VWB13	Wing	34	+32	R98	818	Vertical	100	+	C13
HWB14	Wing	34	+32	R98	818	Horizontal	100	+	D1
VWB15	Wing	34	+32	L98	818	Vertical	100	+	D2
HWB16	Wing	34	+32	L98	818	Horizontal	100	+	D3
VCB17	Cabin Floor	44	-13	L8	818	Vertical	350	+	D4
HCB18	Cabin Floor	44	-13	L8	818	Horizontal	350	+	D5
VFC1	Firewall	+8	+5	L22	ENDEVCO 7232C-570S	Vertical	250	-	A11
HFC2	Firewall	+8	+5	L22	7232C-570S	Horizontal	250	+	A12
VFC3	Firewall	0	-16.80	L14	7232C-570S	Vertical	350	+	A13
HFC4	Firewall	0	-16.80	L14	7232C-570S	Horizontal	350	+	B1
VCC5	Cabin floor	27	-15	L13.5	7232C-570S	Vertical	350	+	B2
HCC6	Cabin floor	27	-15	L13.5	7232C-570S	Horizontal	350	+	B3
VCC7	Cabin floor	27	-15	0	7232C-570S	Vertical	350	+	B4
HCC8	Cabin floor	27	-15	0	7232C-570S	Horizontal	350	+	B5
VCC9	Cabin floor	27	-15	R13.5	7232C-570S	Vertical	350	+	B6
HCC10	Cabin floor	27	-15	R13.5	7232C-570S	Horizontal	350	+	B7
VCC11	Cabin floor	60	-12	L14	7232C-570S	Vertical	350	+	B8
HCC12	Cabin floor	60	-12	L14	7232C-570S	Horizontal	350	+	B9
VCC13	Cabin floor	60	-12	0	7232C-570S	Vertical	350	+	B10
HCC14	Cabin floor	60	-12	0	7232C-570S	Horizontal	350	+	B11
VCC15	Cabin floor	60	-12	R14	7232C-570S	Vertical	350	+	B12
HCC16	Cabin floor	60	-12	R14	7232C-570S	Horizontal	350	+	B13

BEST AVAILABLE COPY

TABLE C-4. ACCELEROMETER LOCATIONS AND RESPONSE SETTING FOR TEST 3

Accel. No.	Location	F.S.	W.L.	B.L.	Accel. Type	Axis	Peak Response (G)	Polarity	Tape Channel
HPA1	Pilot Pelvis	44	+4.5	L10	ENDEVCO	2260CA Vertical	100	+	A1
HPA2	Pilot Pelvis	44	+4.5	L10	ENDEVCO	2260CA Horizontal	100	-	A2
HPA3	Pilot Pelvis	44	+4.5	L10	ENDEVCO	2260CA Lateral	100	-	A3
HPA4	Pilot Head	49	+30	L10	ENDEVCO	2260CA Vertical	100	+	A4
HPA5	Pilot Head	49	+30	L10	ENDEVCO	2260CA Horizontal	100	+	A5
HPA6	Pilot Head	49	+30	L10	ENDEVCO	2260CA Lateral	100	+	A6
VCA7	Co-pilot Pelvis	42	+4.5	R10	ENDEVCO	2260CA Vertical	100	+	A7
HCA8	Co-pilot Pelvis	42	+4.5	R10	ENDEVCO	2260CA Horizontal	100	-	A8
LCA9	Co-pilot Pelvis	42	+4.5	R10	ENDEVCO	2260CA Lateral	100	-	A9
VCA10	Pilot seat leg	40	-1	L10	ENDEVCO	7232C-750S Vertical	150	-	A10
VEB1	Engine	-18	+10	0	Kistler	818 Vertical	150	+	C1
HEB2	Engine	-18	+10	0	Kistler	818 Horizontal	150	+	C2
LEB3	Engine	-18	+10	0	Kistler	818 Lateral	150	+	C3
VTB4	Tail Unit	228	+10	0	Kistler	818 Vertical	100	-	C4
HTB5	Tail Unit	228	+10	0	Kistler	818 Horizontal	100	+	C5
LTB6	Tail Unit	228	+10	0	Kistler	818 Lateral	100	+	C6
VCB7	Rear Cabin	108	-6	L14	Kistler	818 Vertical	250	+	C7
VCB8	Rear Cabin	108	-6	L14	Kistler	818 Horizontal	250	-	C8
VCB9	Cabin Cargo Bulkhead	90	-10	L8	Kistler	818 Vertical	250	+	C9
HCB10	Cabin Cargo Bulkhead	90	-10	L8	Kistler	818 Horizontal	250	+	C10
LCB11	Cabin Cargo Bulkhead	90	-10	L8	Kistler	818 Lateral	250	+	C11
VCB12	Top Cabin Fwd.	34	+32	R21	Kistler	818 Vertical	200	+	C12
HCB13	Top Cabin Fwd.	34	+32	R21	Kistler	818 Horizontal	200	+	C13
VCB14	Top Cabin Rear	65	+32	R15	Kistler	818 Vertical	200	-	D1
HCB15	Top Cabin Rear	65	+32	R15	Kistler	818 Horizontal	150	+	D2
VCB16	Wing Right	34	+32	R98	Kistler	818 Vertical	100	+	D3
HCB17	Wing Right	34	+32	R98	Kistler	818 Horizontal	100	+	D4
VCB18	Wing Right	34	+32	R98	Kistler	818 Lateral	100	+	D5
VCB19	Wing, left	34	+32	L98	Kistler	818 Vertical	100	+	D6
HCB20	Wing, left	34	+32	L98	Kistler	818 Horizontal	100	+	D7
VFC1	Firewall	0	-16.8	L14	ENDEVCO	7232C-750S Vertical	350	+	A11
HFC2	Firewall	0	-16.8	L14	ENDEVCO	7232C-750S Horizontal	350	+	A12
VCC3	Cabin Floor	27	-15	R13.5	ENDEVCO	7232C-750S Vertical	350	+	A13
HCC4	Cabin Floor	27	-15	R13.5	ENDEVCO	7232C-750S Horizontal	350	+	B1
LCC5	Cabin Floor	27	-15	R13.5	ENDEVCO	7232C-750S Lateral	350	+	B2
VCC6	Cabin Floor	44	-13	R8	ENDEVCO	7232C-750S Vertical	350	+	B3
HCC7	Cabin Floor	44	-13	R8	ENDEVCO	7232C-750S Horizontal	350	+	B4
VCC8	Cabin Floor	44	-13	R8	ENDEVCO	7232C-750S Lateral	350	+	B5
LCC9	Cabin Floor	60	-12	L14	ENDEVCO	7232C-750S Vertical	300	+	B6
HCC10	Cabin Floor	60	-12	L14	ENDEVCO	7232C-750S Horizontal	300	+	B7
VCC11	Cabin Floor	60	-12	L14	ENDEVCO	7232C-750S Lateral	300	+	B8
LCC12	Cabin Floor	60	-12	R14	ENDEVCO	7232C-750S Vertical	350	+	B9
HCC13	Cabin Floor	60	-12	R14	ENDEVCO	7232C-750S Horizontal	350	+	B10
LCC14	Cabin Floor	60	-12	R14	ENDEVCO	7232C-750S Lateral	350	+	B11
HCC15	Co-Pilot Head	47	30	R10	ENDEVCO	7232C-750S Vertical	100	+	B12
LCC16	Co-Pilot Head	47	30	R10	ENDEVCO	7232C-750S Horizontal	100	+	B13
HCC17	Pilot Seat Leg	40	-1	L10	ENDEVCO	7232C-750S Lateral	150	+	D8
***	Elt Bracket	115	+10	R14	ENDEVCO	2260C Horizontal	100	-	

***This accelerometer was added at the request of the FAA and the output was recorded on an oscillograph through J-Box channel 32

BEST AVAILABLE COPY

TABLE C-5. ACCELEROMETER LOCATIONS AND RESPONSE SETTING FOR TEST 4

Accel. No.	Location	F.S.	W.L.	B.L.	Accel. Type	Axis	Peak Response(G)	Polarity	Tape Channel
VPAL	Pilot Pelvis	44	+4.5	L10	ENDEVCO	Vertical	100	+	A1
HPA2	Pilot Pelvis	44	+4.5	L10	ENDEVCO	Horizontal	100	-	A2
VPA3	Pilot Head	49	+30	L10	2260CA	Vertical	100	-	A3
HPA4	Pilot Head	49	+30	L10	2260CA	Horizontal	100	-	A4
VCA5	Co-pilot Pelvis	42	+4.5	R10	2260CA	Vertical	100	+	A5
HCA6	Co-pilot Pelvis	42	+4.5	R10	2260CA	Horizontal	100	-	A6
VCA7 *	Co-pilot Head	47	30	R10	2260C	Vertical	100	+	A7
HCA8	Co-pilot Head	47	30	R10	2260C	Horizontal	100	-	A8
VSA9	Pilot Seat Leg	40	-1	L10	2260CA	Vertical	150	-	A9
HSAL0	Pilot Seat Leg	40	-1	L10	2260CA	Horizontal	150	+	A10
VEB1	Engine	-18	+10	0	Kistler	Vertical	150	+	C1
HEB2	Engine	-18	+10	0	Kistler	Horizontal	150	+	C2
VTB3	Tail Unit	228	+10	0	818	Vertical	75	-	C3
VNG4	Nose Gear	-6.7	-36.5	0	818	Vertical	75	+	C4
VCB5	Rear Cabin	108	-6	L14	818	Vertical	250	+	C5
HCB6	Rear Cabin	108	-6	L14	818	Horizontal	250	-	C6
VCB7	Cabin Cargo Bulkhead	90	-10	L8	818	Vertical	250	+	C7
HCB8	Cabin Cargo Bulkhead	90	-10	L8	818	Horizontal	250	-	C8
VCB9	Top Cabin	34	+32	R21	818	Vertical	200	-	C9
HCB10	Top Cabin	34	+32	R21	818	Horizontal	200	+	C10
VCB11	Top Cabin	65	+32	R15	818	Vertical	200	-	C11
HCB12	Top Cabin	65	+32	R15	818	Horizontal	200	+	C12
VWB13	Wing	34	+32	R98	818	Vertical	100	+	C13
HWB14	Wing	34	+32	R98	818	Horizontal	100	+	D1
VWB15	Wing	34	+32	L98	818	Vertical	100	+	D2
HWB16	Wing	34	+32	L98	818	Horizontal	100	+	D3
VCB17	Right Main Gear	60	-31.7	R48.8	818	Vertical	100	+	D4
HCB18	Cabin Floor	44	-13	L8	818	Horizontal	350	+	D5
VWB19	Cabin Floor	44	-13	L8	818	Vertical	350	+	D6
HWB20	Right Main Gear	60	-31.7	R48.8	818	Horizontal	50	+	D7
VFC1	Elc Bracket	115	+10	R14	818	Vertical	100	-	A11
FWC2	Firewall	+3	+5	L22	ENDEVCO	Vertical	250	-	A12
VFC3	Firewall	+3	+5	L22	ENDEVCO	Horizontal	250	+	A13
FWC4	Firewall	0	-16.80	L14	7232C-750S	Vertical	350	+	B1
VCC5	Cabin Floor	27	-15	L13.5	7232C-750S	Horizontal	450	+	B2
HCC6	Cabin Floor	27	-15	L13.5	7232C-750S	Vertical	350	+	B3
VCC7	Cabin Floor	27	-15	0	7232C-750S	Horizontal	400	+	B4
HCC8	Cabin Floor	27	-15	0	7232C-750S	Vertical	350	+	B5
VCC9	Cabin Floor	27	-15	0	7232C-750S	Horizontal	400	+	B6
HCC10	Cabin Floor	27	-15	R13.5	7232C-750S	Vertical	350	+	B7
VCC11	Cabin Floor	60	-12	L14	7232C-750S	Horizontal	350	+	B8
HCC12	Cabin Floor	60	-12	L14	7232C-750S	Vertical	350	+	B9
VCC13	Cabin Floor	60	-12	0	7232C-750S	Horizontal	350	+	B10
HCC14	Cabin Floor	60	-12	0	7232C-750S	Vertical	350	+	B11
VCC15	Cabin Floor	60	-12	R14	7232C-750S	Horizontal	350	+	B12
HCC16	Cabin Floor	60	-12	R14	7232C-750S	Vertical	350	+	B13

*An Endevco 2260C Accelerometer was substituted from NASA stock.

TABLE C-6. LOAD CELL AND DISPLACEMENT MEASUREMENT INSTALLATIONS FOR TESTS 1, 2, 3, AND 4

Data Channel	Location	Peak Setting	Polarity	Tape and Channel			
				Test 1	Test 2	Test 3	Test 4
PS1	Pilot Shoulder Strap	+1150 (a)	+ Tension	D-6	D-6	D-9	D-9
CPS1	Copilot Shoulder Strap	+1150 (a)	+ Tension	D-7	D-7	D-10	D-10
PL1	Pilot Lap Belt	+1150 (a)	+ Tension	D-8	D-8	D-11	D-11
CPL1	Copilot Lap Belt	+1113 (a)	+ Tension	D-9	D-9	D-12	D-12
PCD1	Pilot Chest Deflection	+2.5 (b)	+ Tension	D-12	D-12	(c)	D-8
CLD1	Cabin Longitudinal Displacement	+3 (b)	+ Tension	D-10	D-10	(c)	(c)
CVD1	Cabin Vertical Displacement	+3 (b)	+ Tension	D-11	D-11	(c)	(c)
(a) Force in Pounds (b) Deflection in Inches (c) Not Installed							

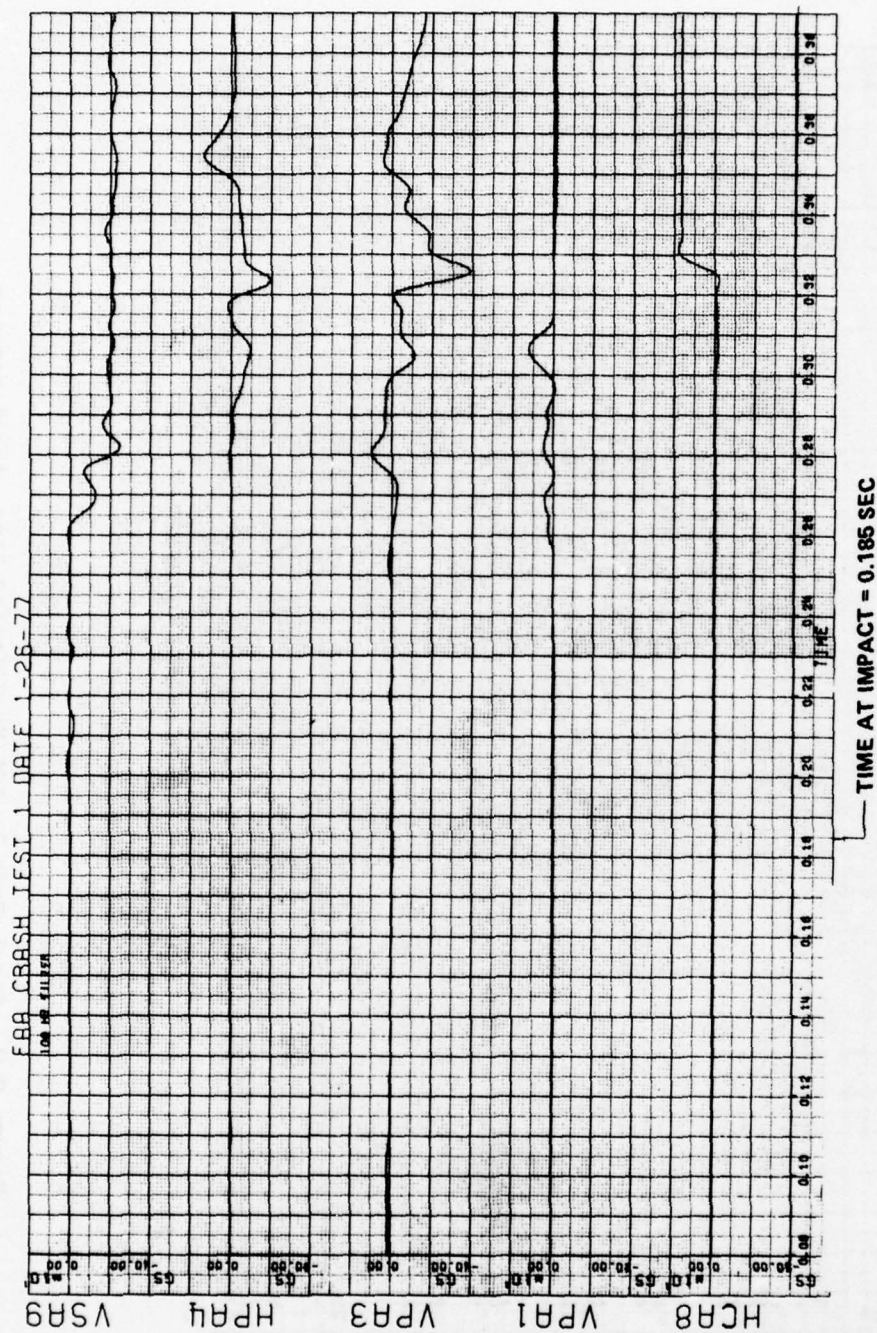


Figure C-1. Crash Test 1, 100 Hz Filtered Data, Accelerometer Numbers HCA8, VPA1, VPA3, HPA4, VSA9

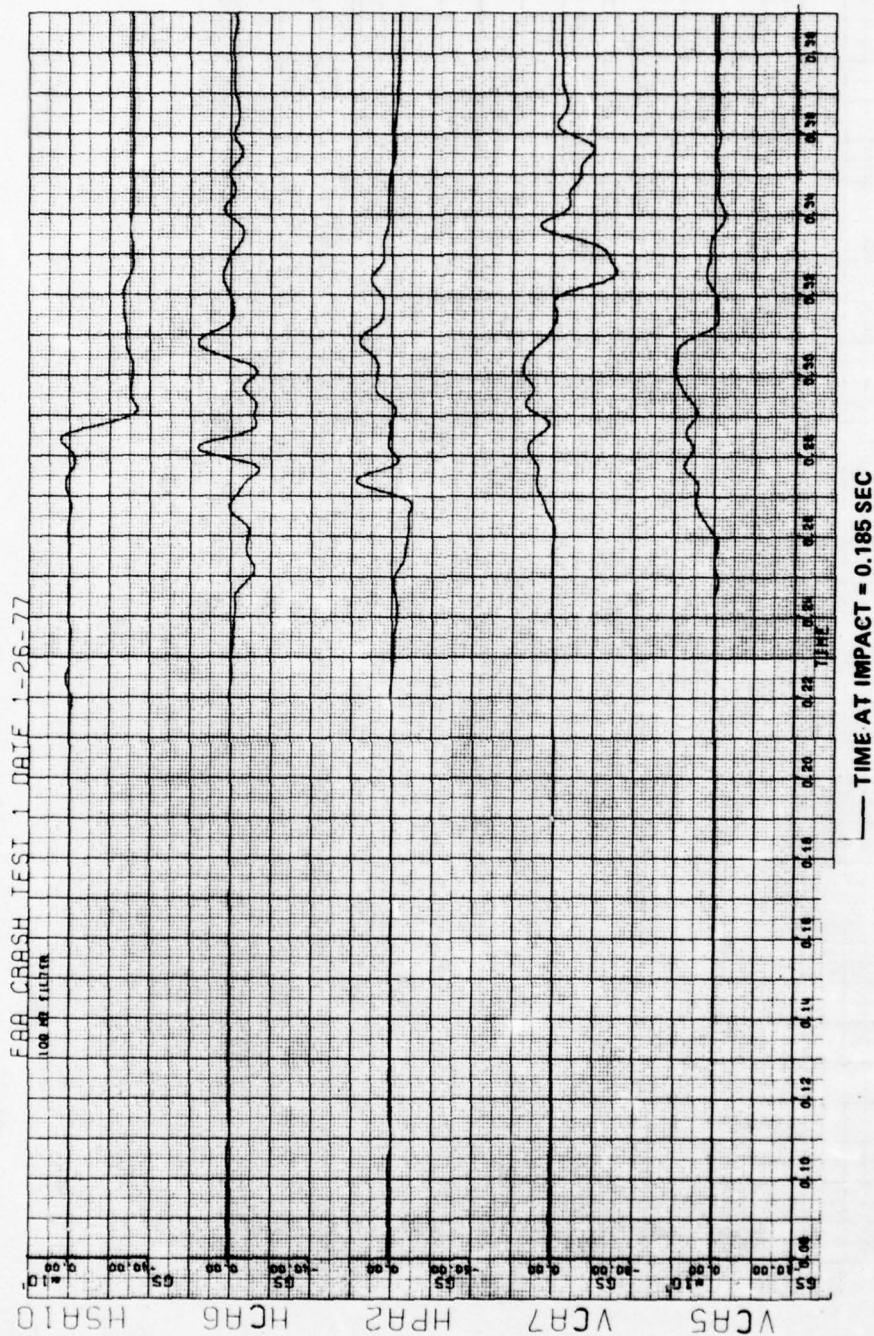


Figure C-2. Crash Test 1, 100 Hz Filtered Data, Accelerometer Numbers VCA5, VCA7, HPA2, HCA6, HSA10

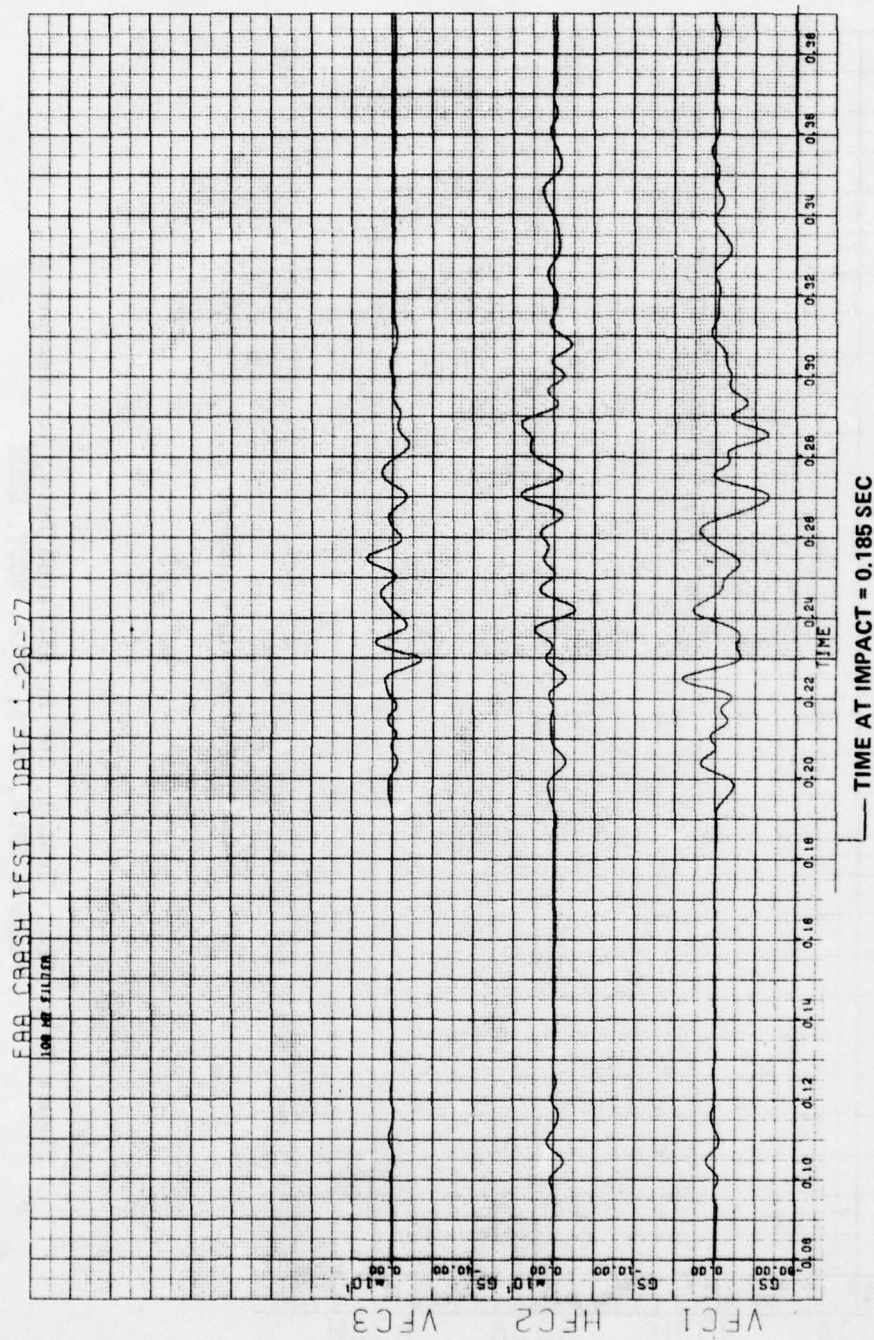


Figure C-3. Crash Test 1, 100 Hz Filtered Data, Accelerometer Numbers VFC1, HFC2, VFC3

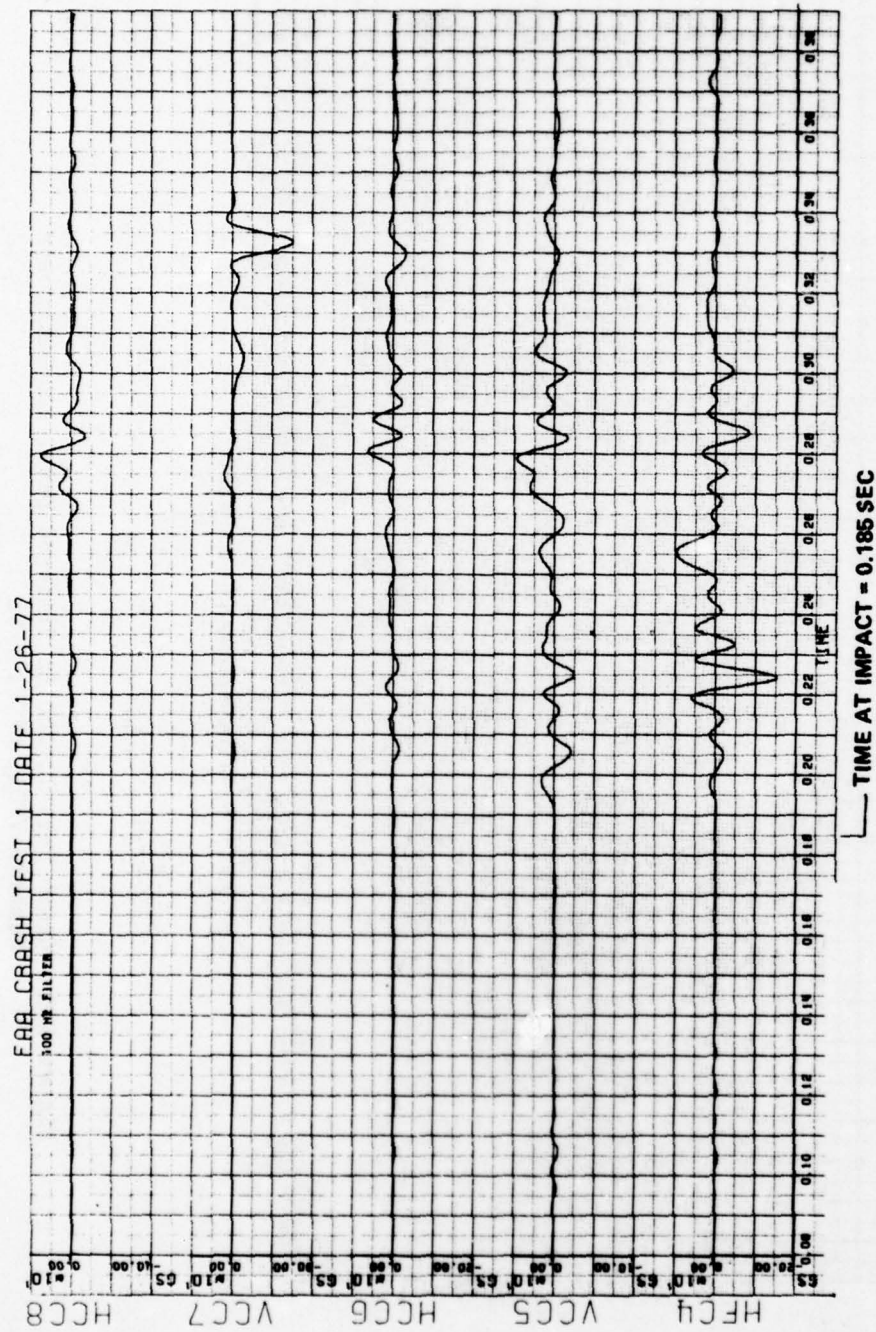


Figure C-4. Crash Test 1, 100 Hz Filtered Data, Accelerometer Numbers HFC4, VCC5, HCC6, VCC7, HCC8

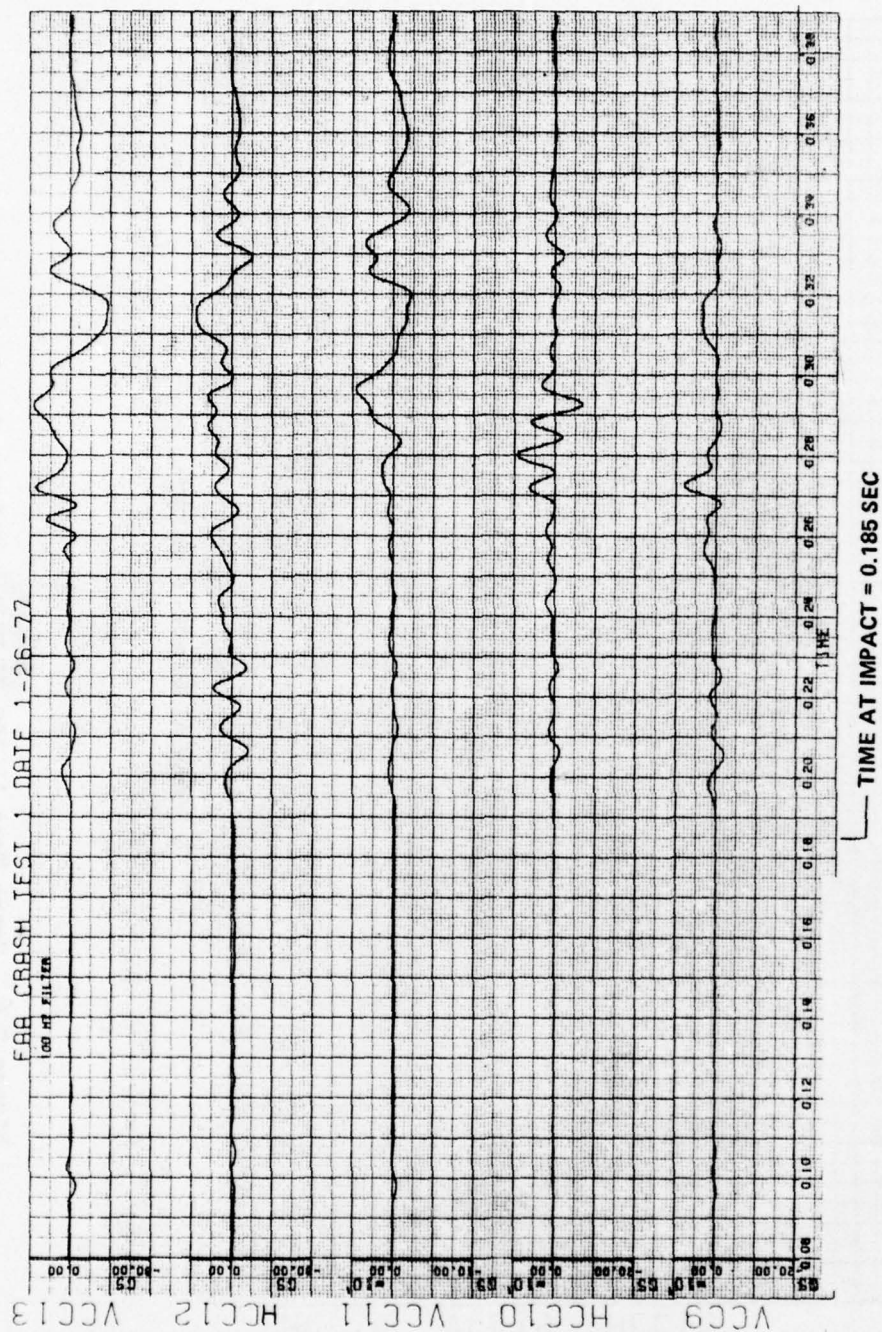


Figure C-5. Crash Test 1, 100 Hz Filtered Data, Accelerometer Numbers VCC9, VCC10, VCC11, VCC12, VCC13

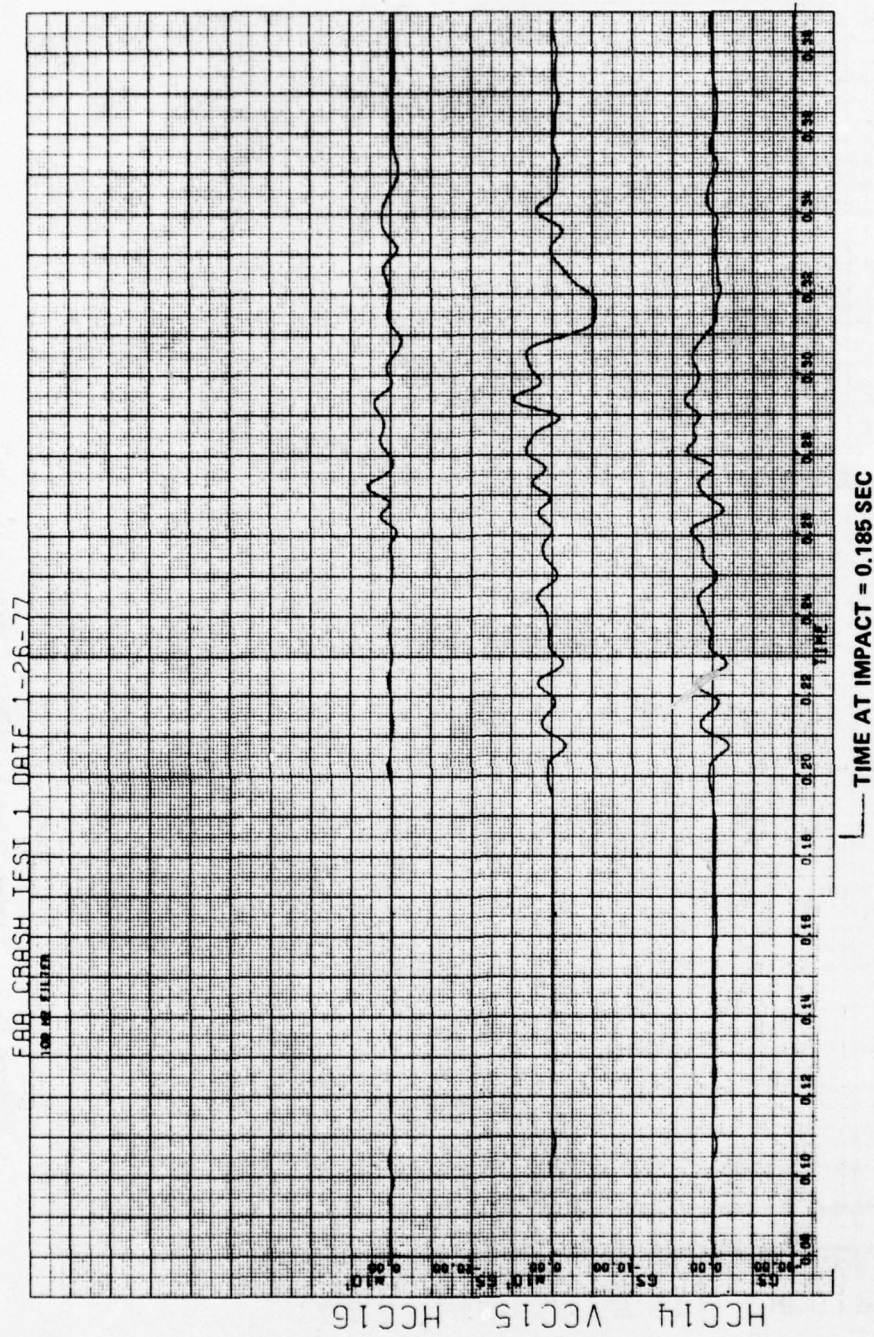


Figure C-6. Crash Test 1, 100 Hz Filtered Data, Accelerometer Numbers HCC14, VCC15, VCC16

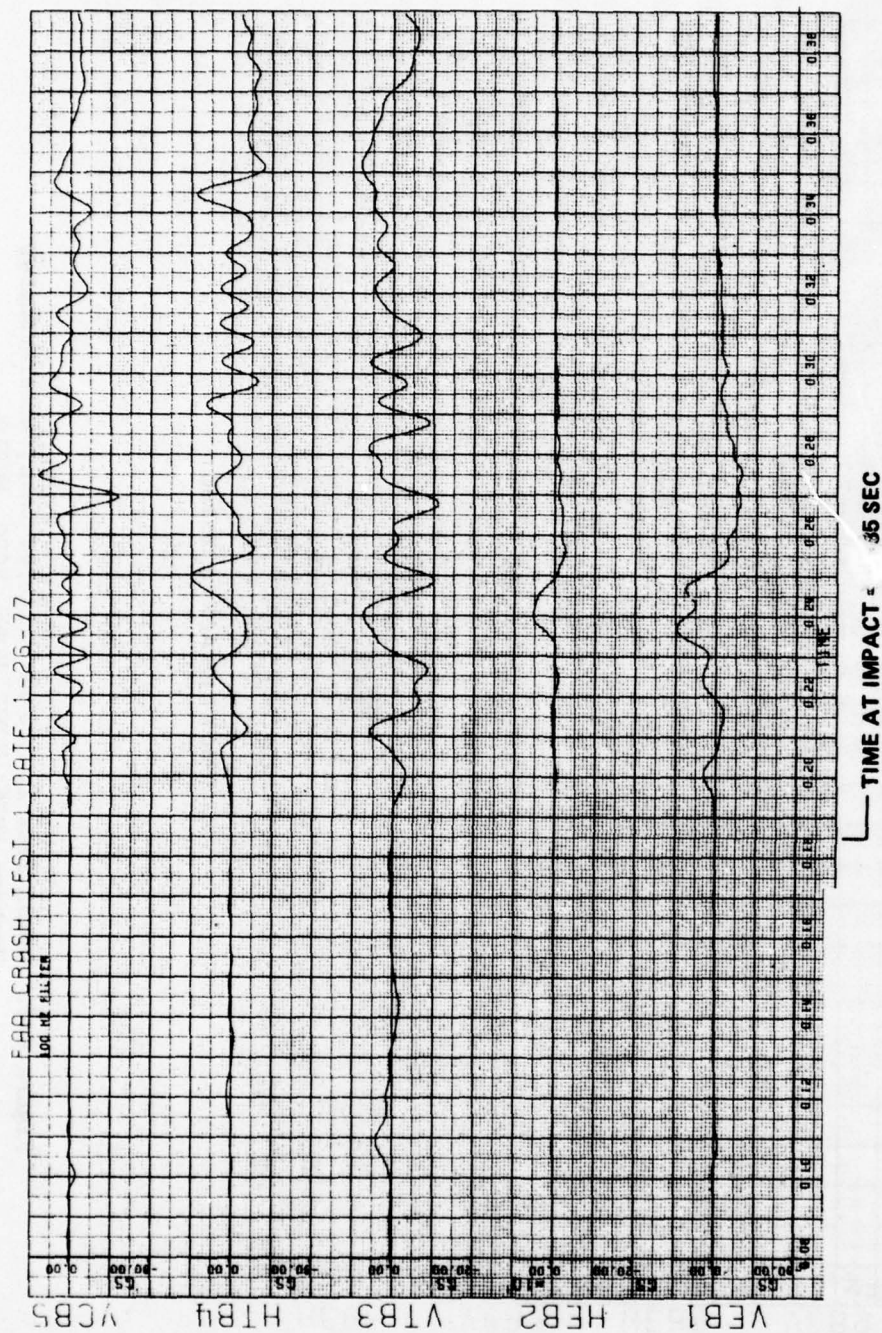


Figure C-7. Crash Test 1, 100 Hz Filtered Data, Accelerometer Numbers VEB1, HEB2, VTB3, HTB4, VCB5

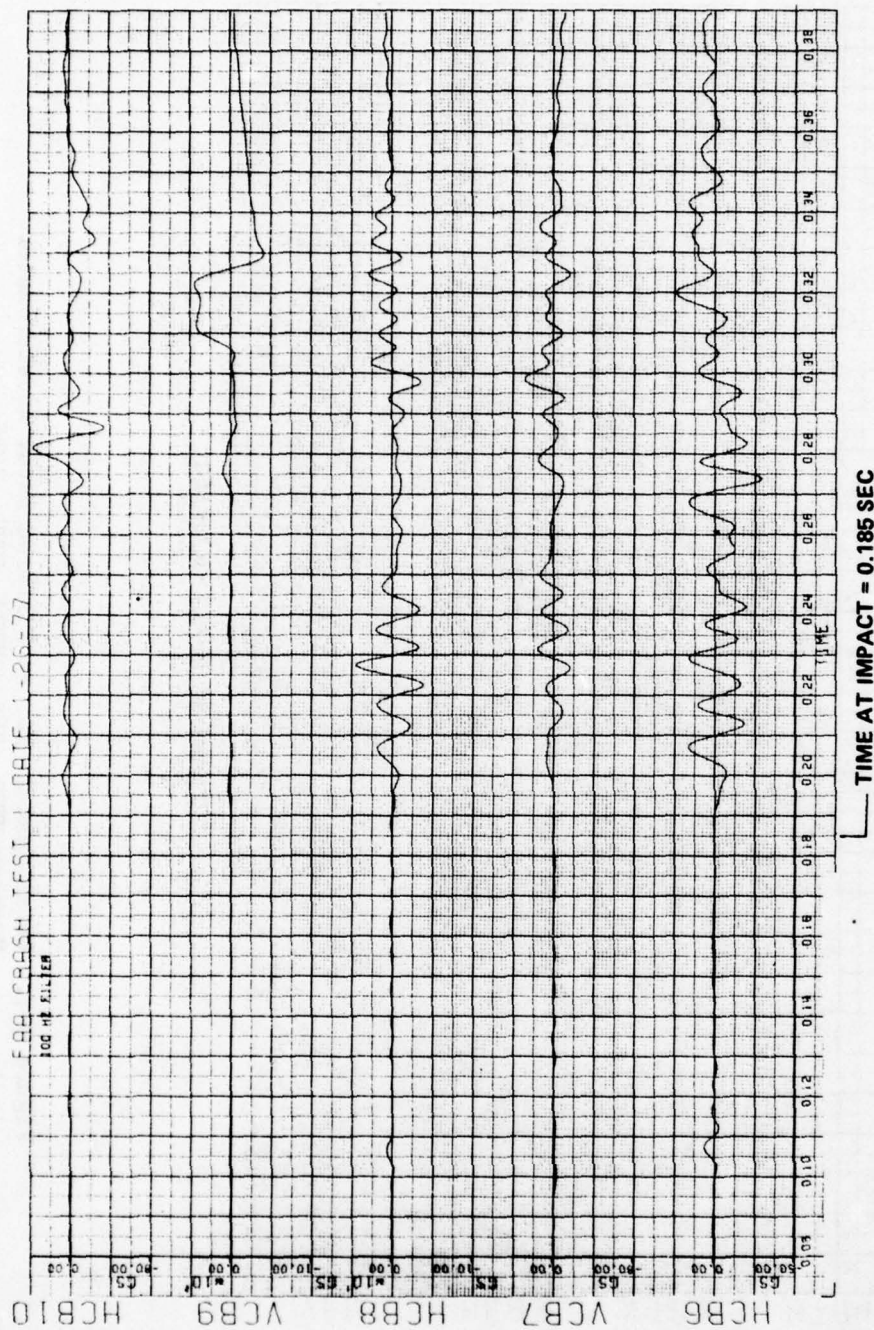


Figure C-8. Crash Test 1, 100 Hz Filtered Data, Accelerometer Numbers HCB6, VCB7, HCB8, VCB9, HCB10

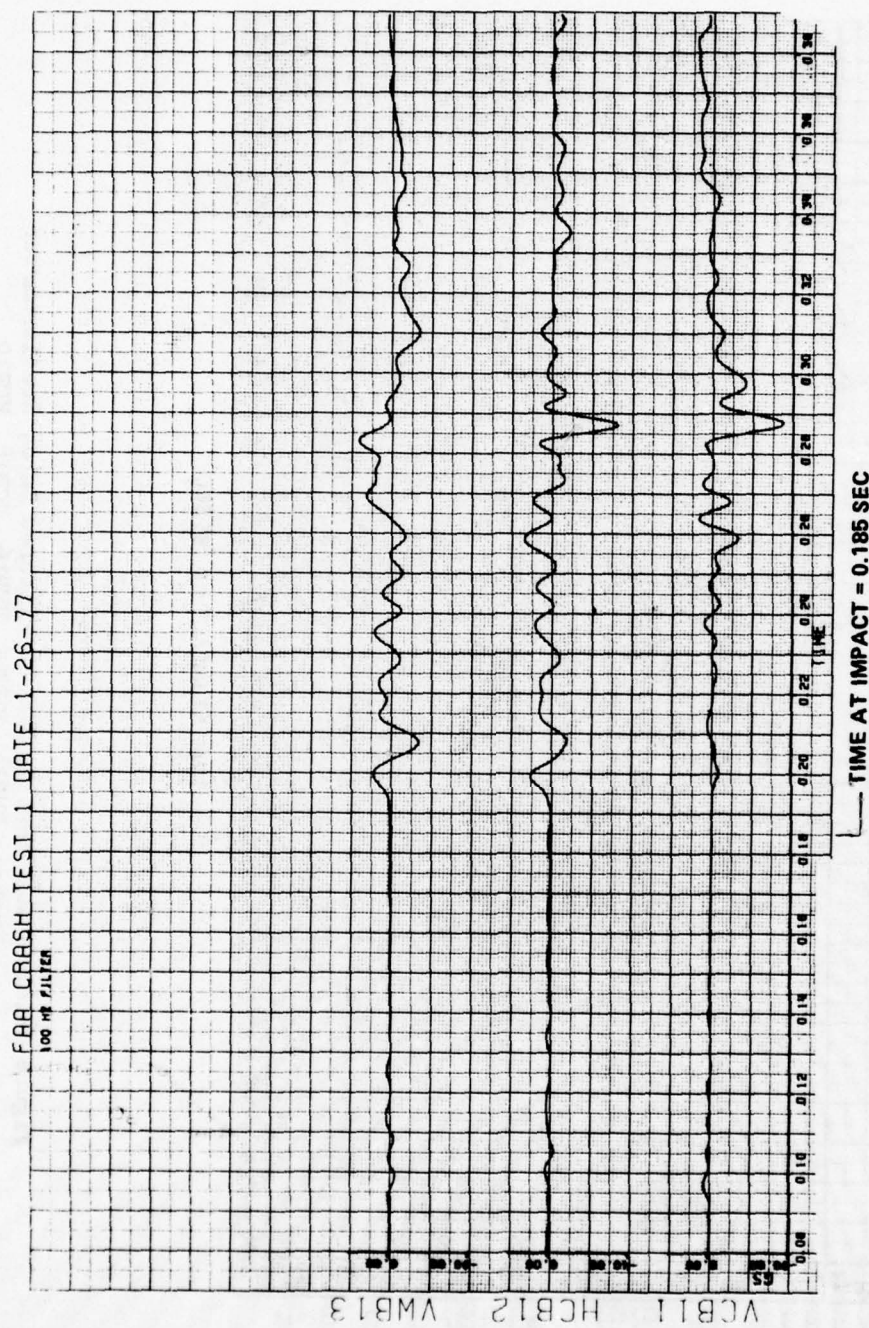


Figure C-9. Crash Test 1, 100 Hz Filtered Data, Accelerometer Numbers VCB11, HCB12, VWB13

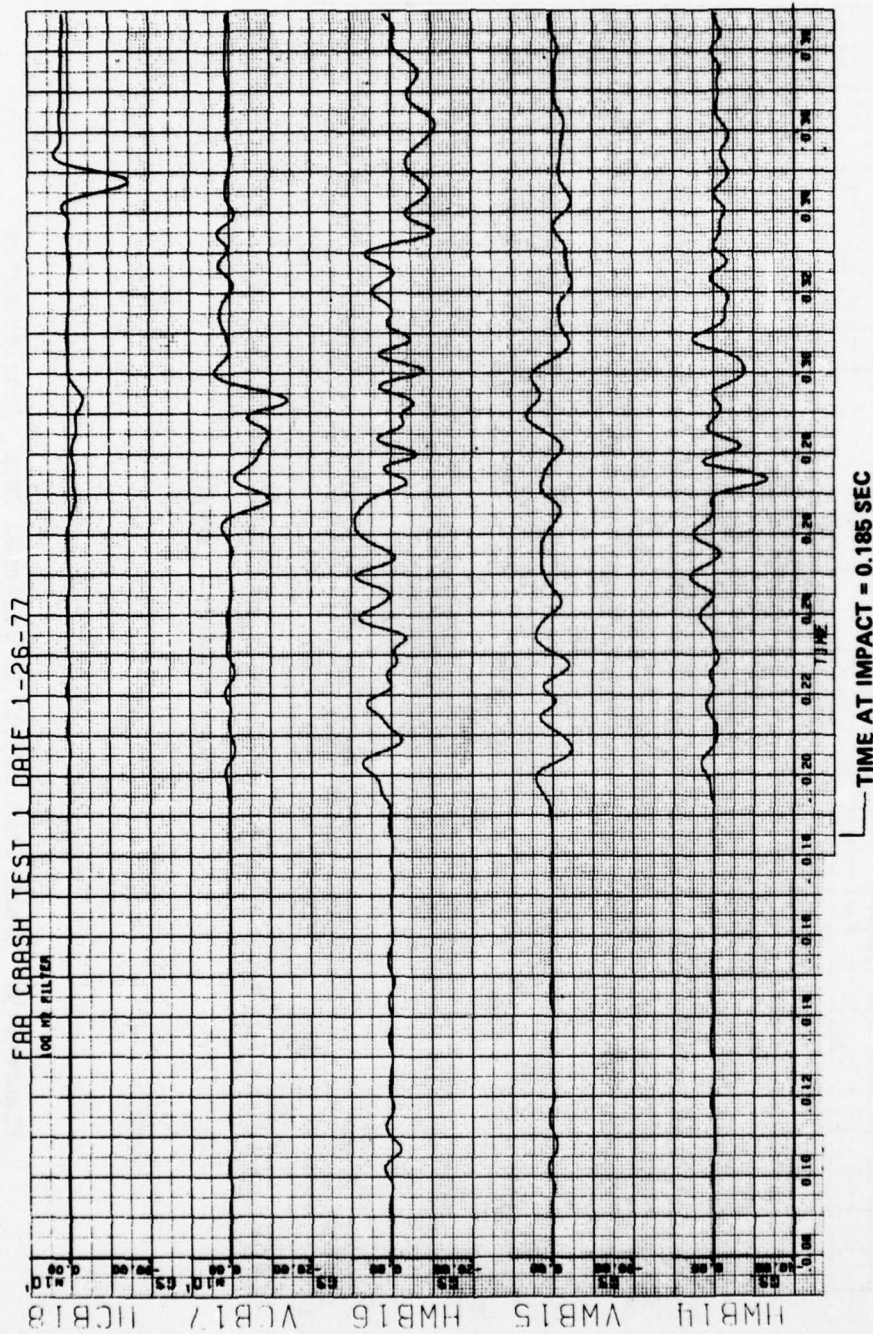


Figure C-10. Crash Test 1, 100 Hz Filtered Data, Accelerometer Numbers HCB14, VMB15, VMB16, VCB18, HCB19

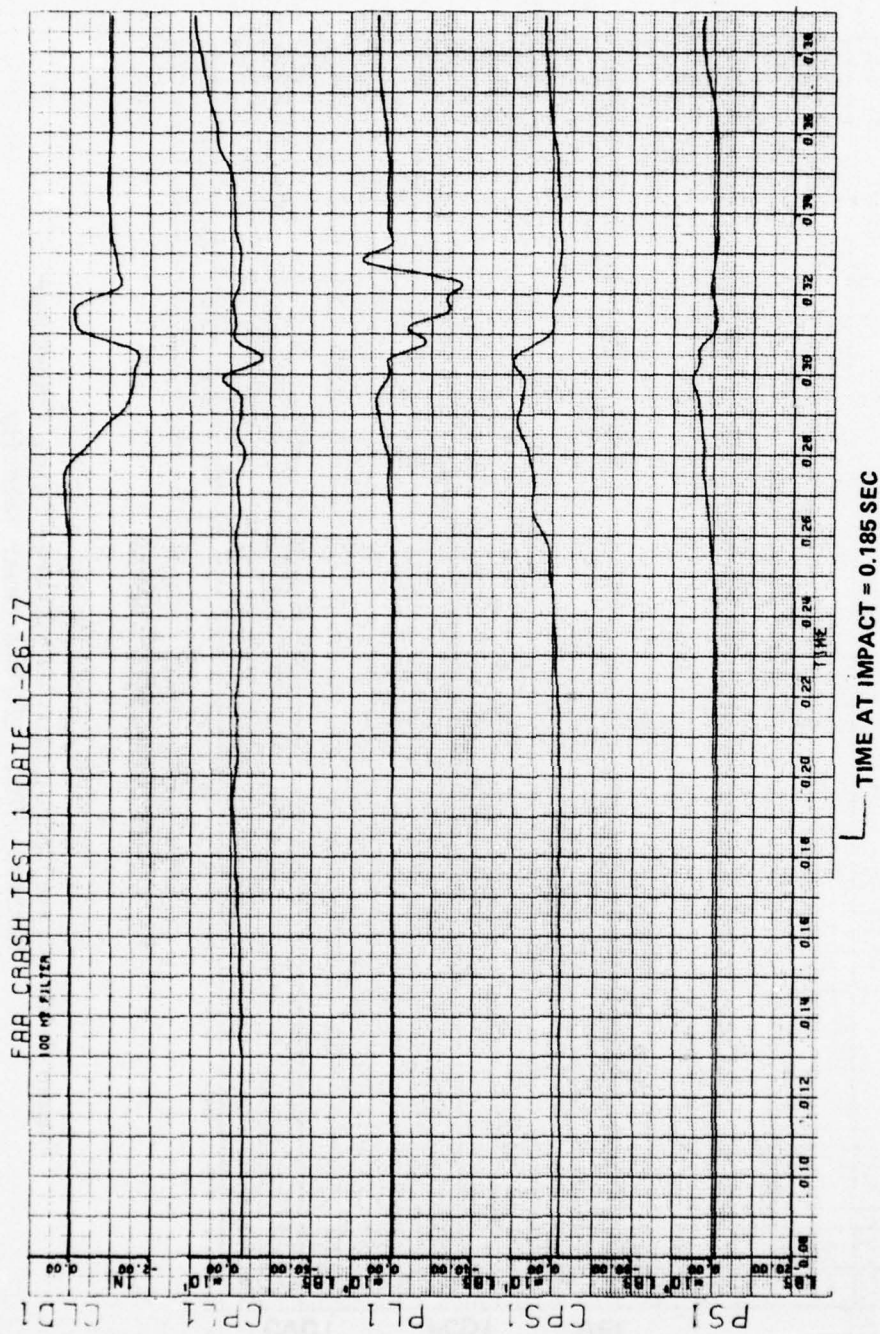


Figure C-11. Crash Test 1, 100 Hz Filtered Data, Transducer Numbers PSL, CPS1, PLL, CPL1, CLD1

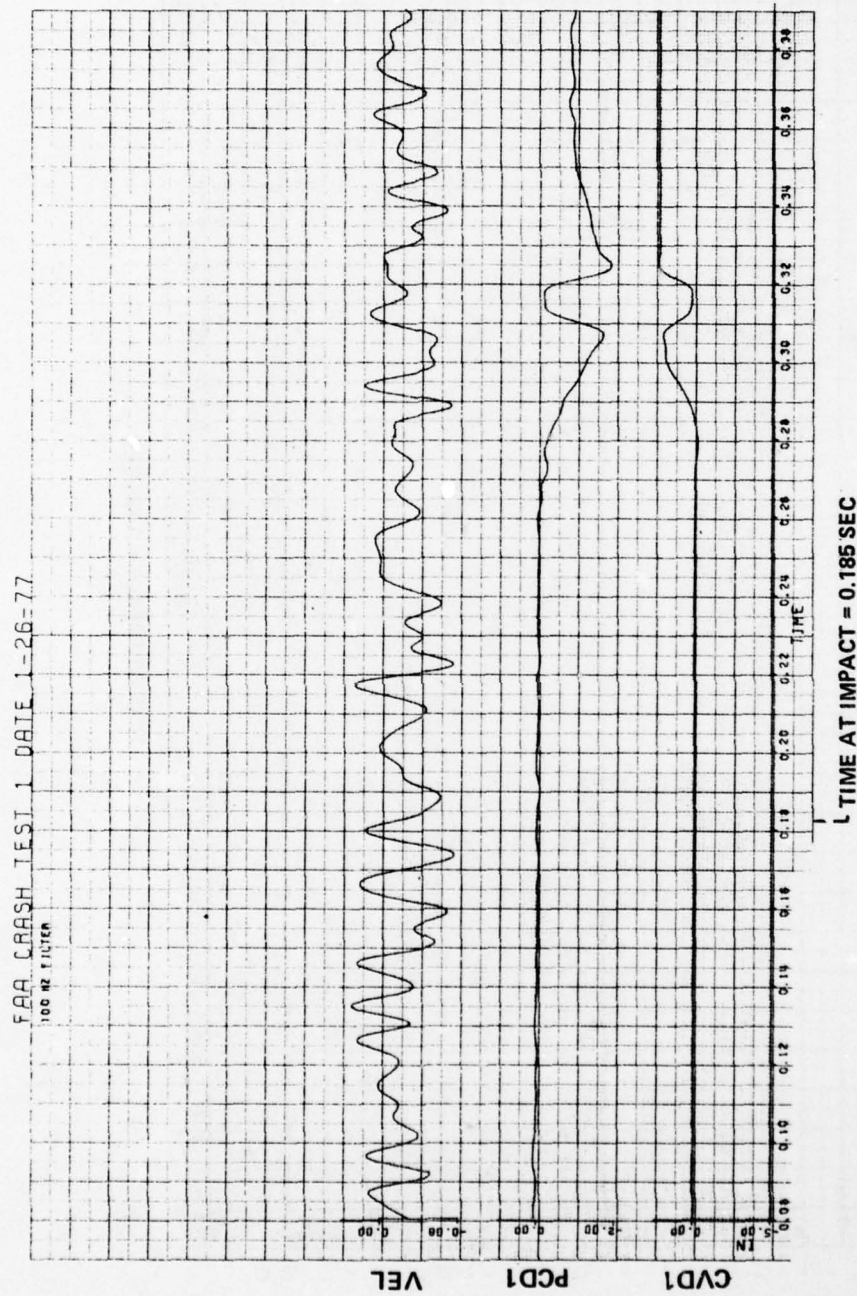


Figure C-12. Crash Test 1, 100 Hz Filtered Data, Transducer Numbers CVD1, PCD1 and Radar Velocity

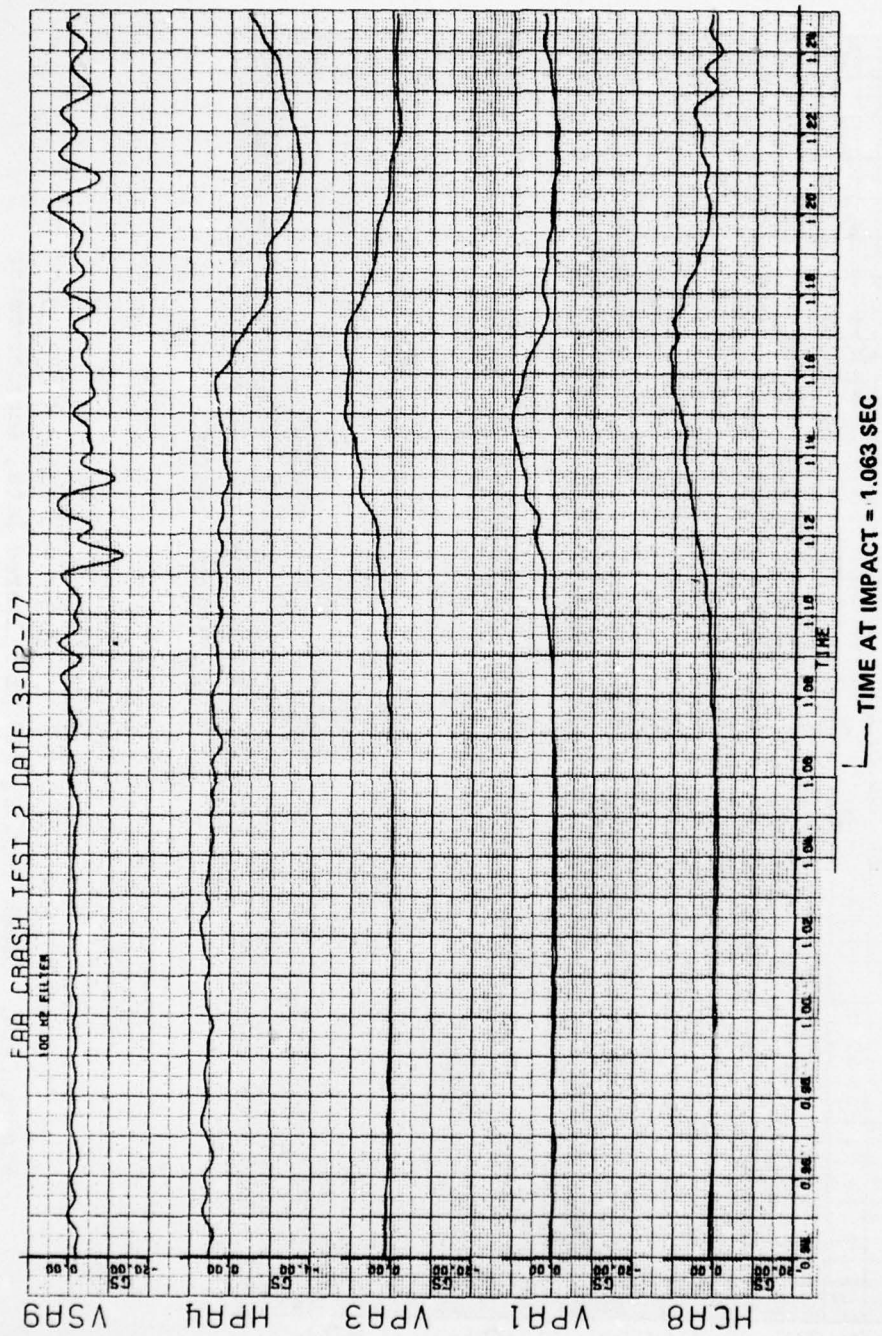


Figure C-13. Crash Test 2, 100 Hz Filtered Data, Accelerometer Numbers HCA8, VPA1, VPA3, HPA4, VSA9

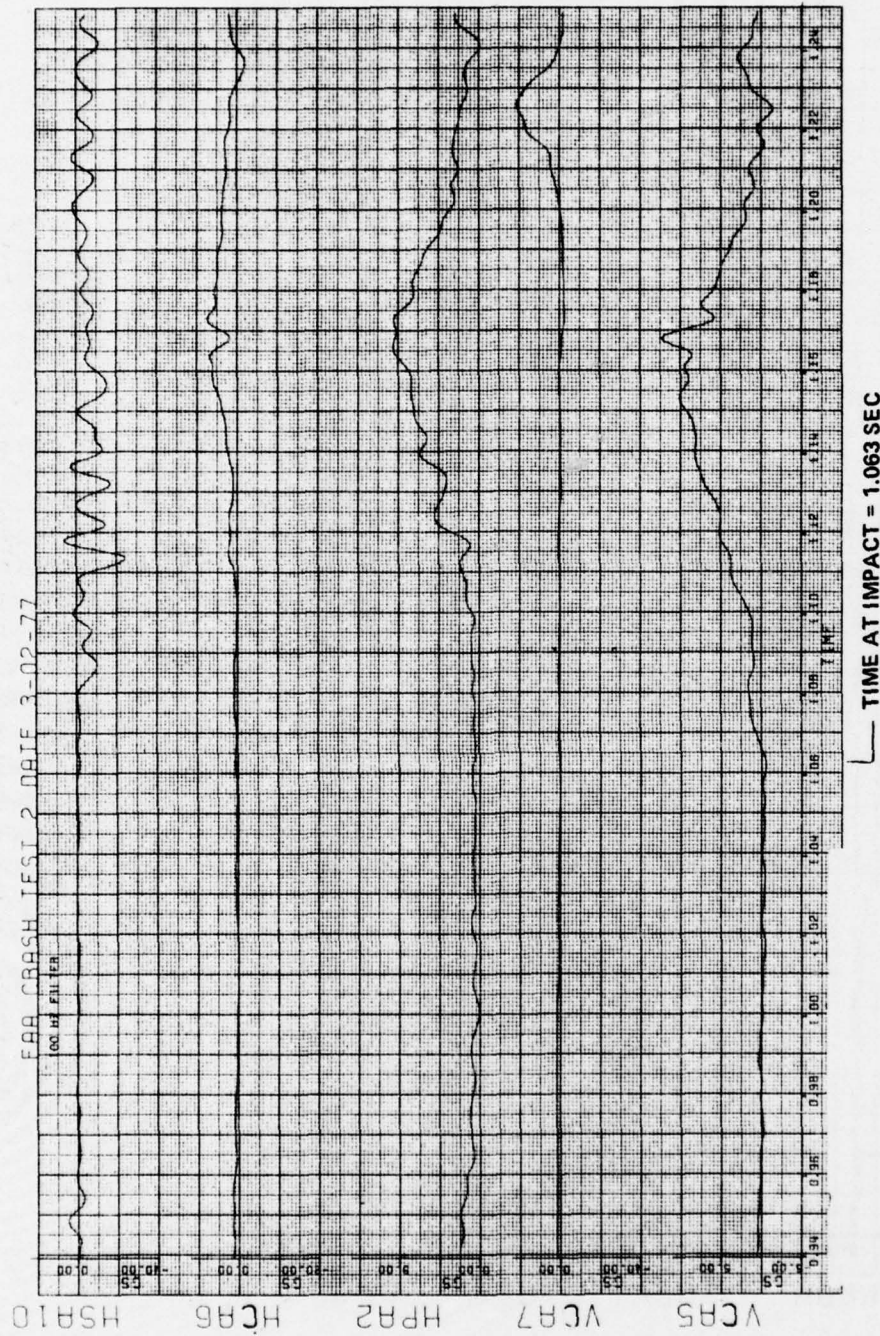


Figure C-14. Crash Test 2, 100 Hz Filtered Data, Accelerometer
Numbers VCA8, VCA7, HPA2, HCA6, HSA10

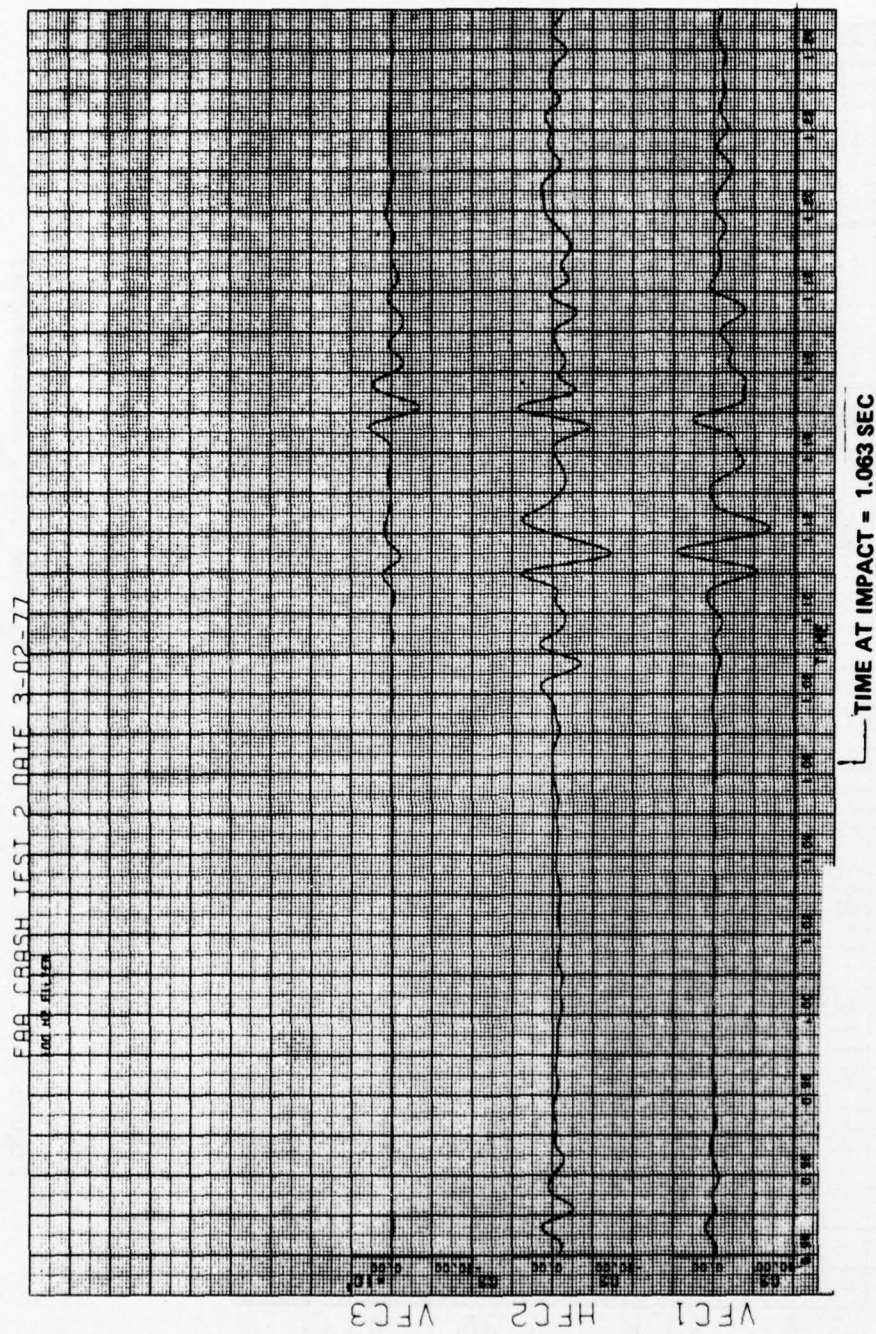


Figure C-15. Crash Test 2, 100 Hz Filtered Data, Accelerometer Numbers VFC1, HFC2, VFC3

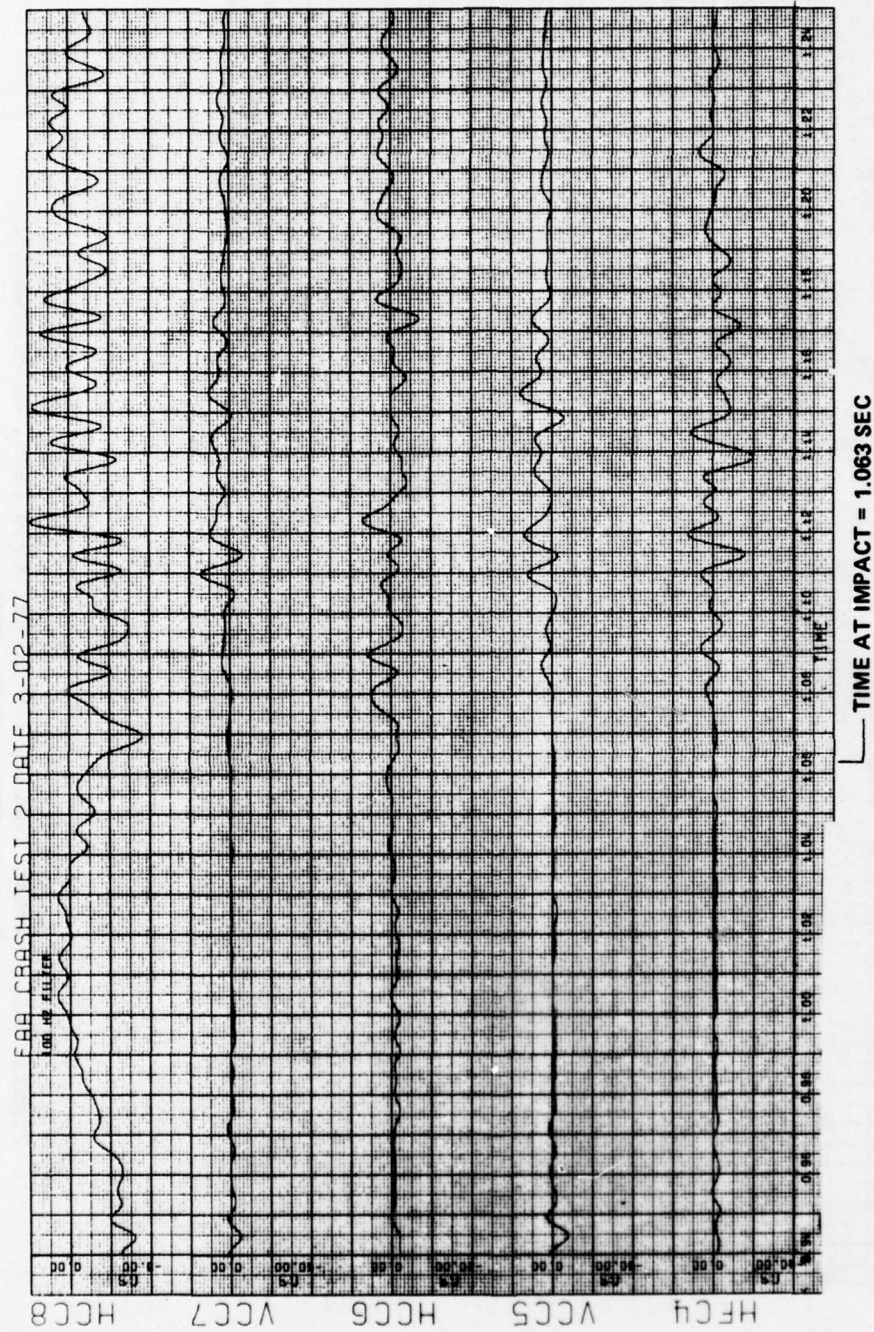


Figure C-16. Crash Test 2, 100 Hz Filtered Data, Accelerometer Numbers HFC4, VCC5, HCC6, VCC7, HCC8

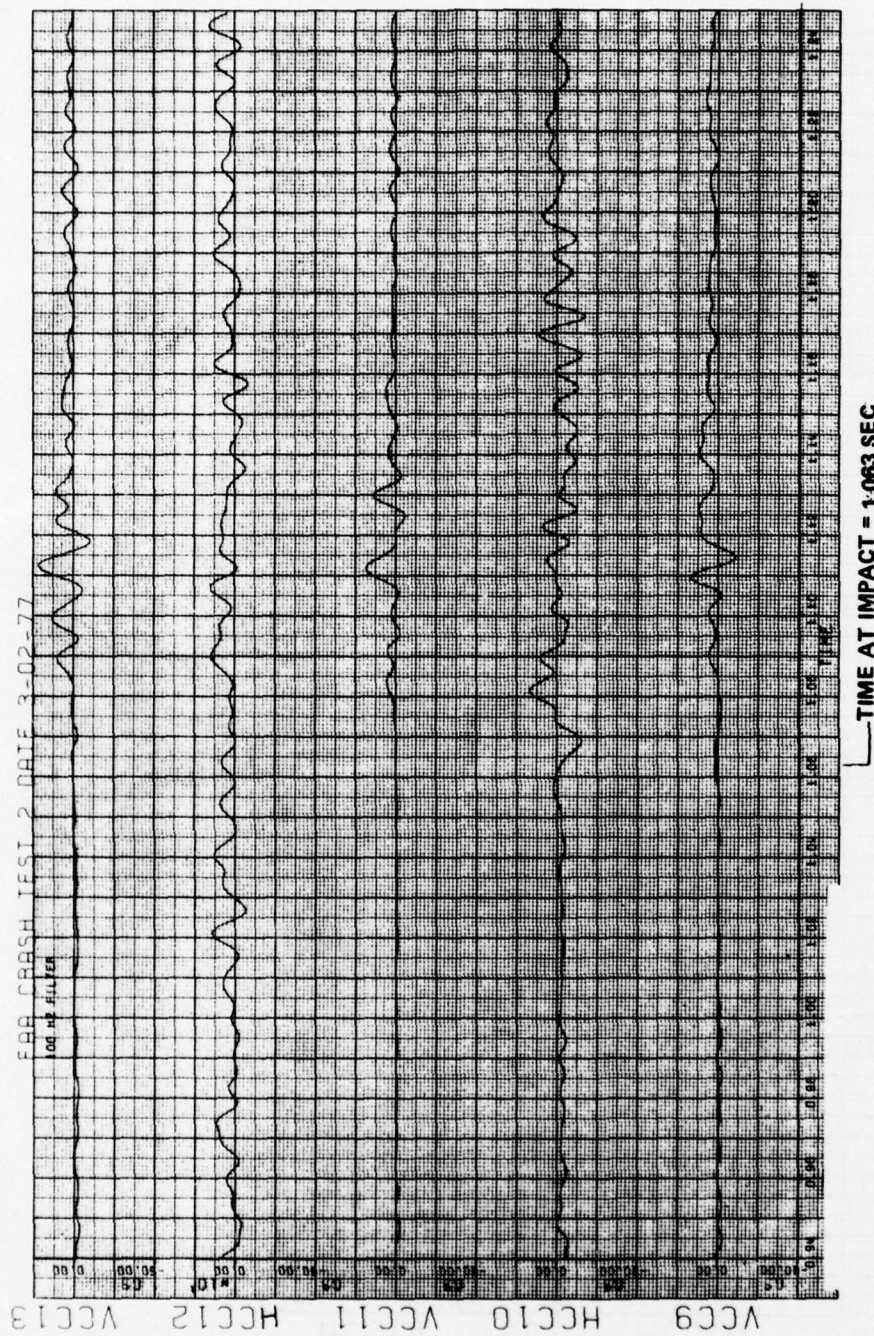


Figure C-17. Crash Test 2, 100 Hz Filtered Data, Accelerometer Numbers VCC9, HCC10, VCC11, HCC12, VCC13

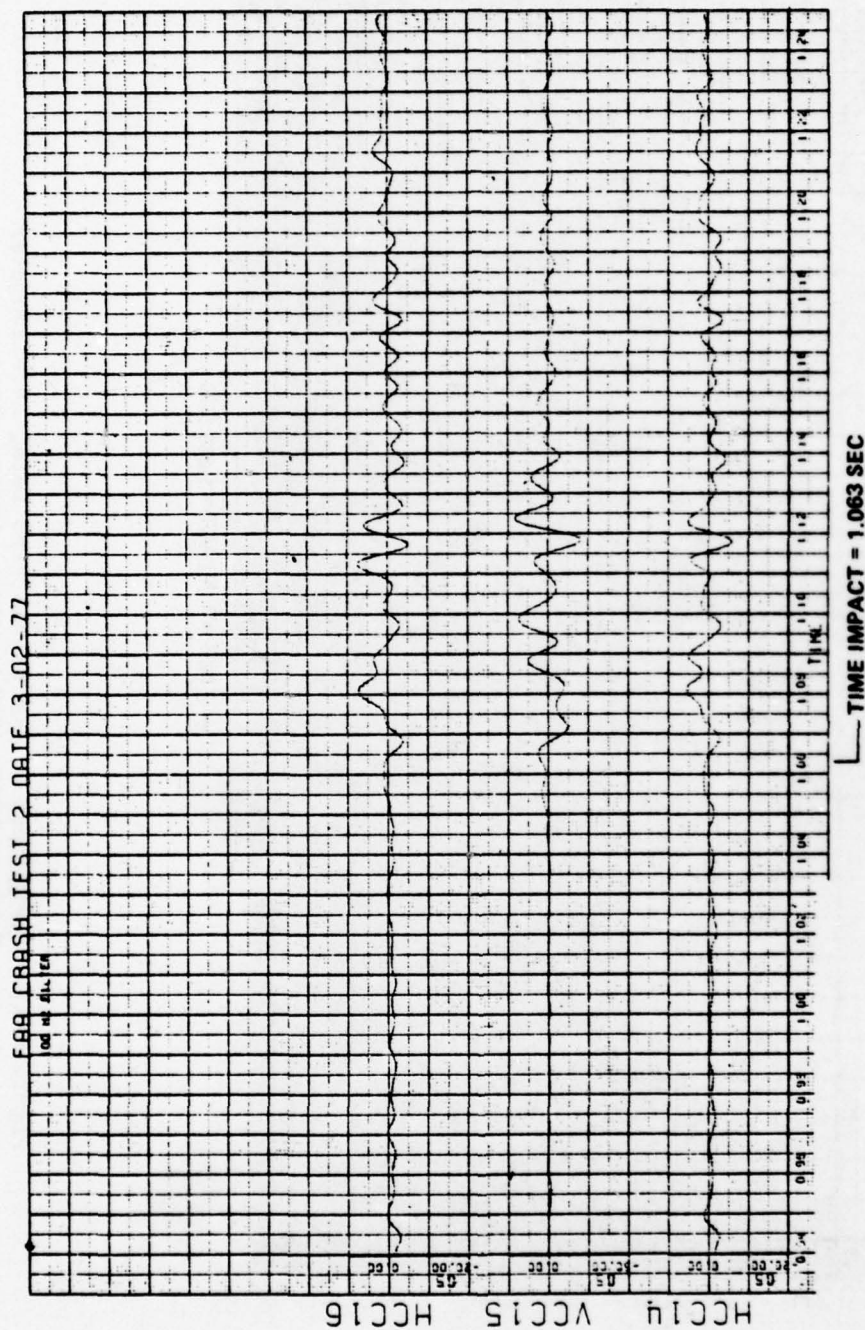


Figure C-18. Crash Test 2, 100 Hz Filtered Data, Accelerometer Numbers HCC14, VCC15, HCC16

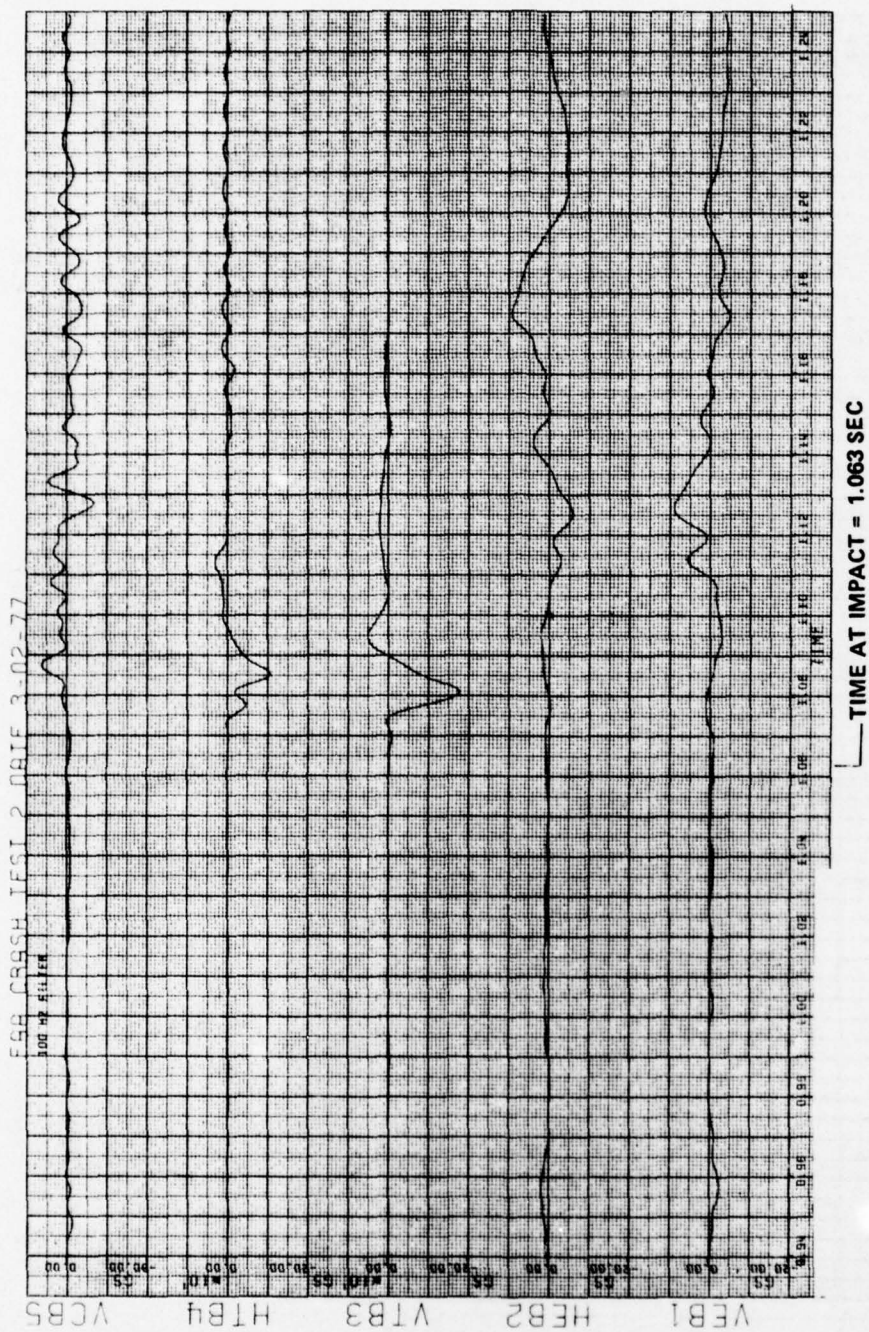


Figure C-19. Crash Test 2, 100 Hz Filtered Data, Accelerometer Numbers VEB1, HEB2, VTB3, HTB4, VCB5

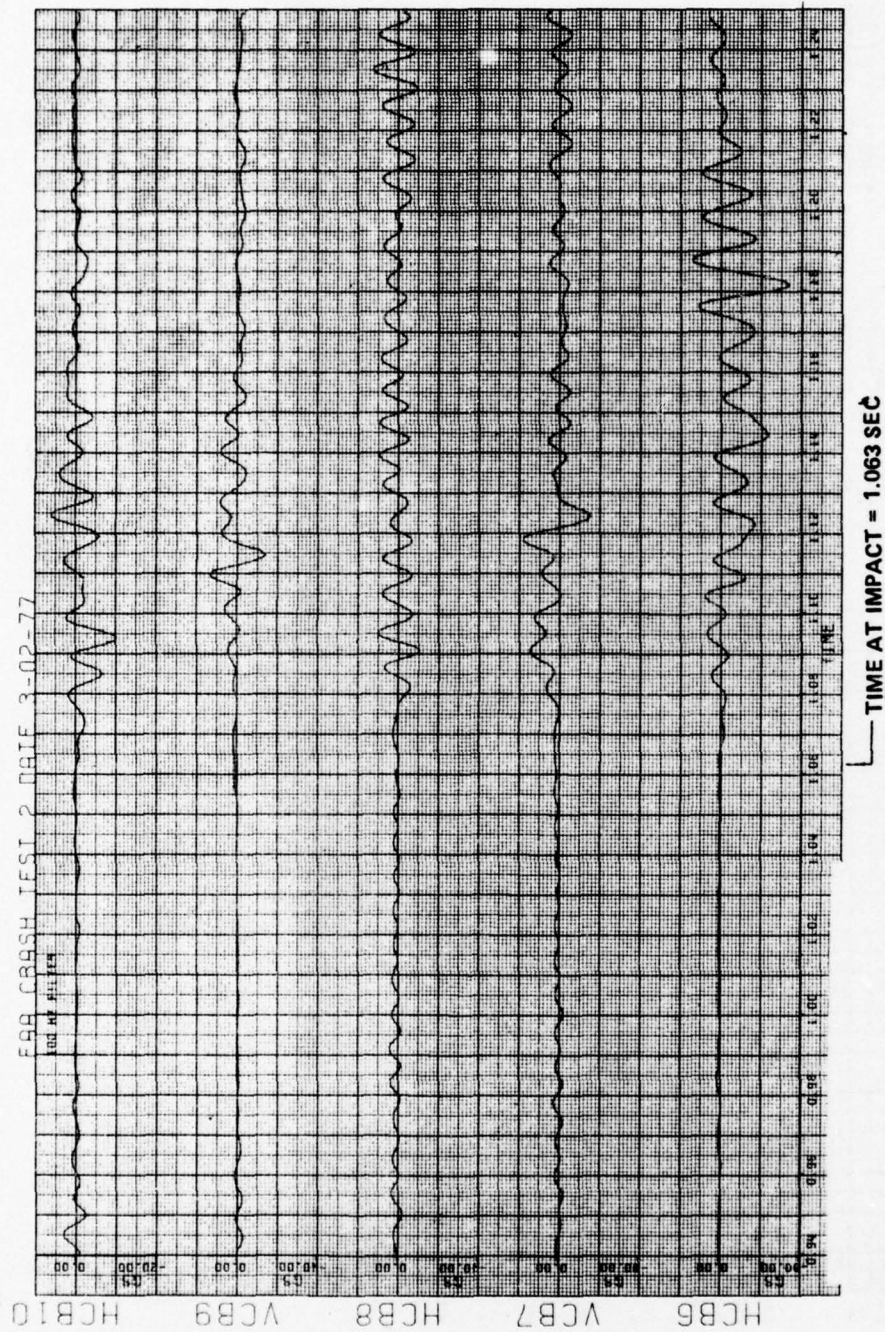


Figure C-20. Crash Test 2, 100 Hz Filtered Data, Accelerometer Numbers HCB6, VCB7, HCB8, VCB9, HCB10

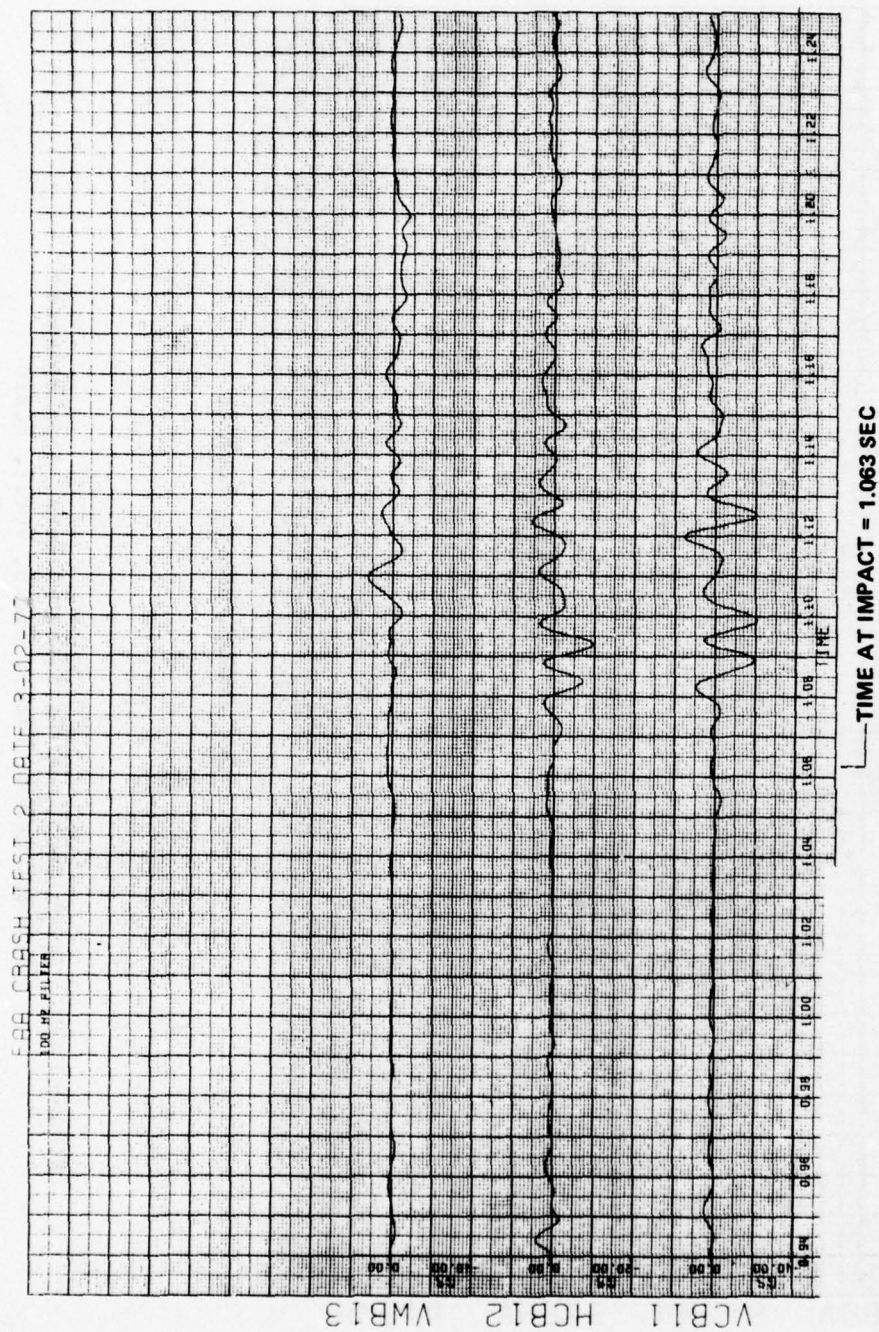


Figure C-21. Crash Test 2, 100 Hz Filtered Data, Accelerometer Numbers VCB11, HCB12, VWB13

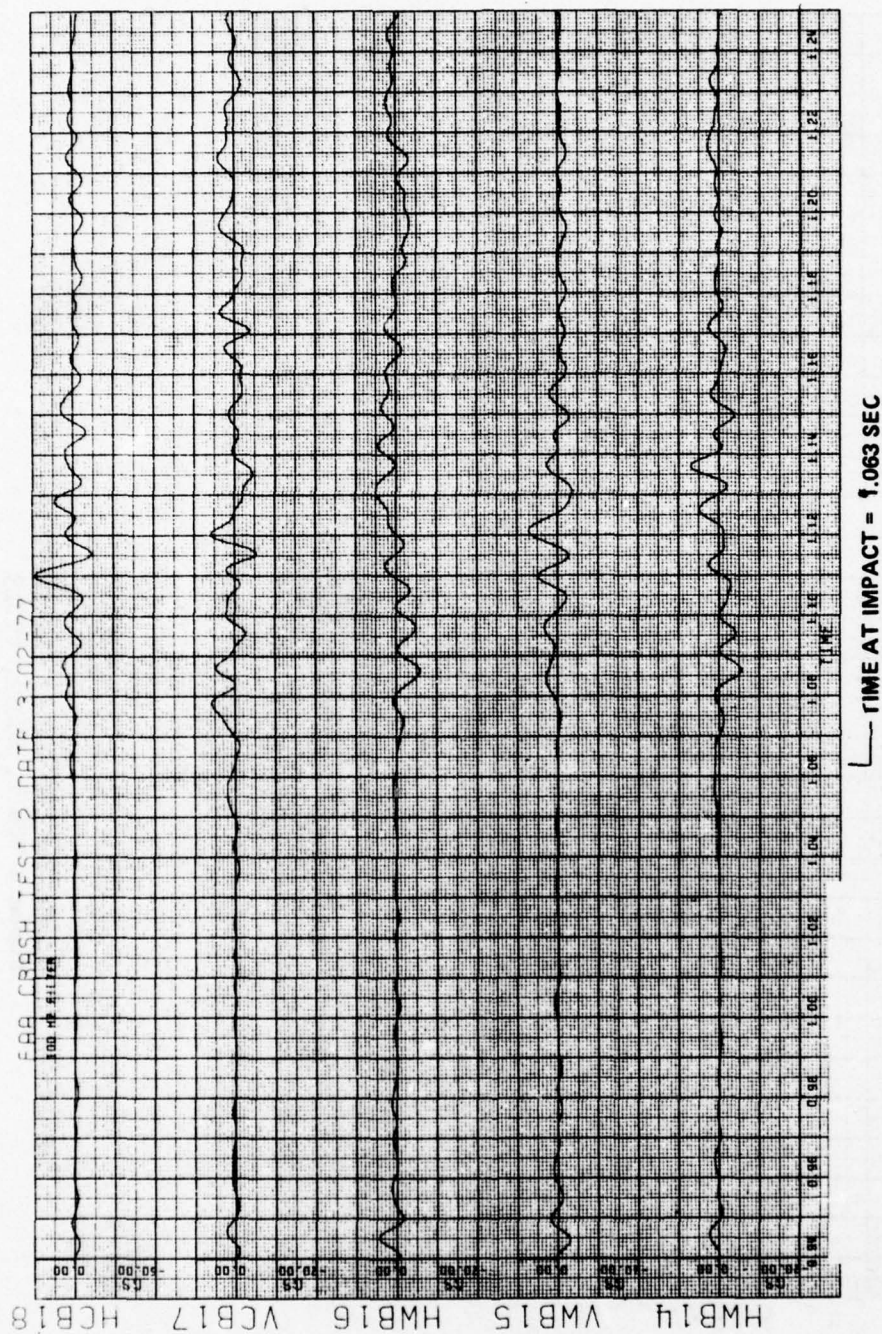


Figure C-22. Crash Test, 100 Hz Filtered Data, Accelerometer Numbers HMB14, VMB15, HMB16, VCB17, HCB18

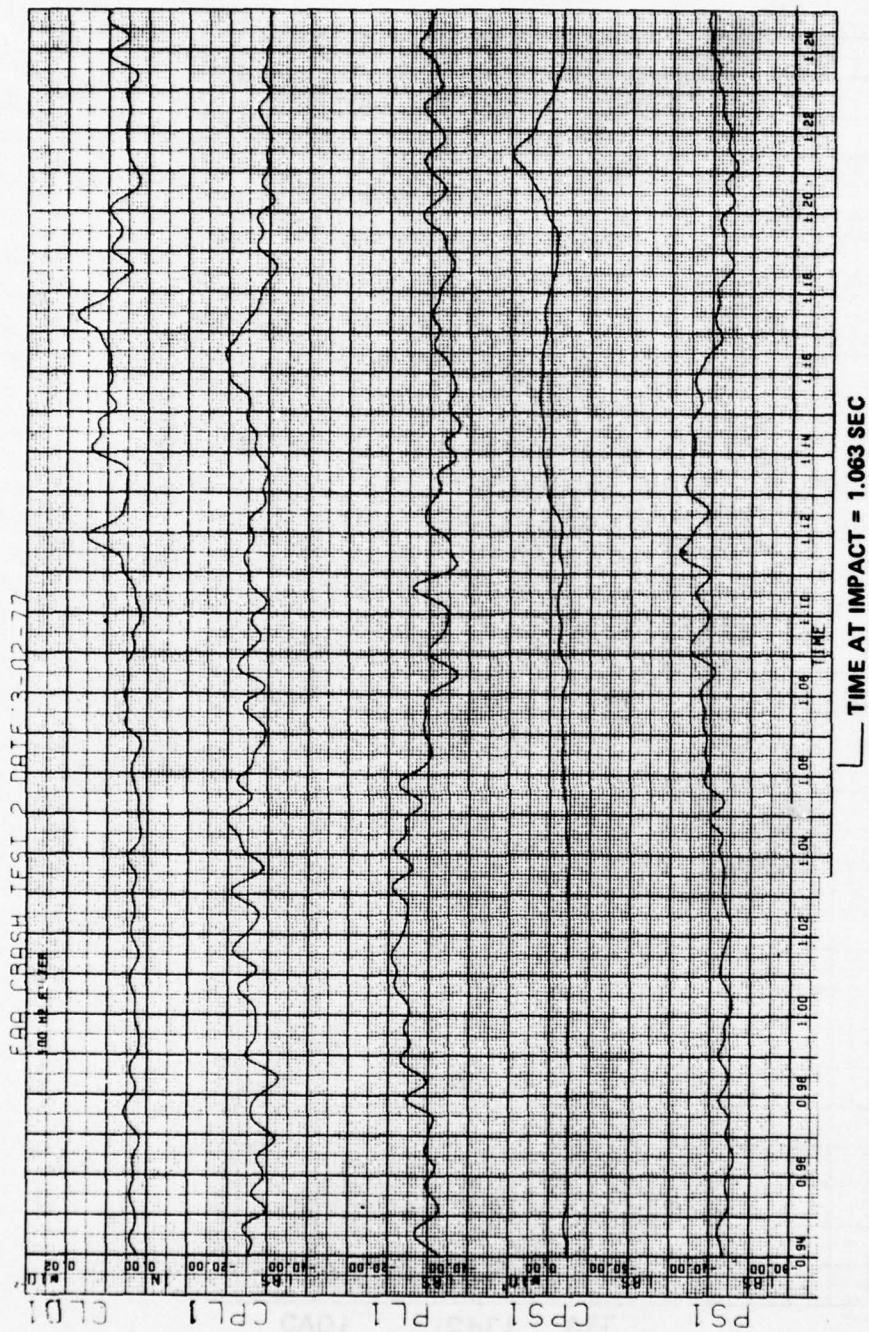


Figure C-23. Crash Test 2, 100 Hz Filtered Data, Transducer Numbers PS1, CPS1, PL1, CPL1, CLD1

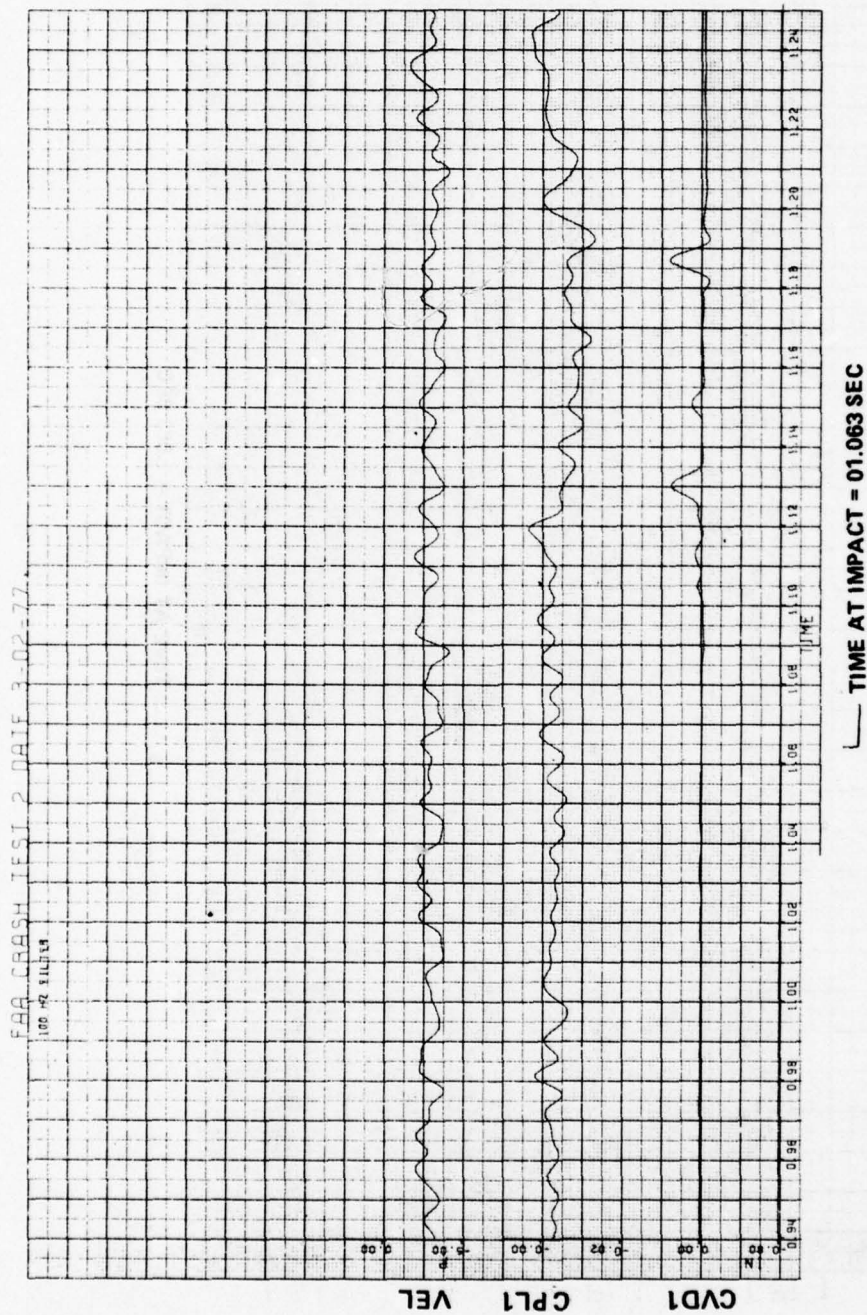


Figure C-24. Crash Test 2, 100 Hz Filtered Data, Transducer Numbers CVD1, CPL1, and Radar Velocity

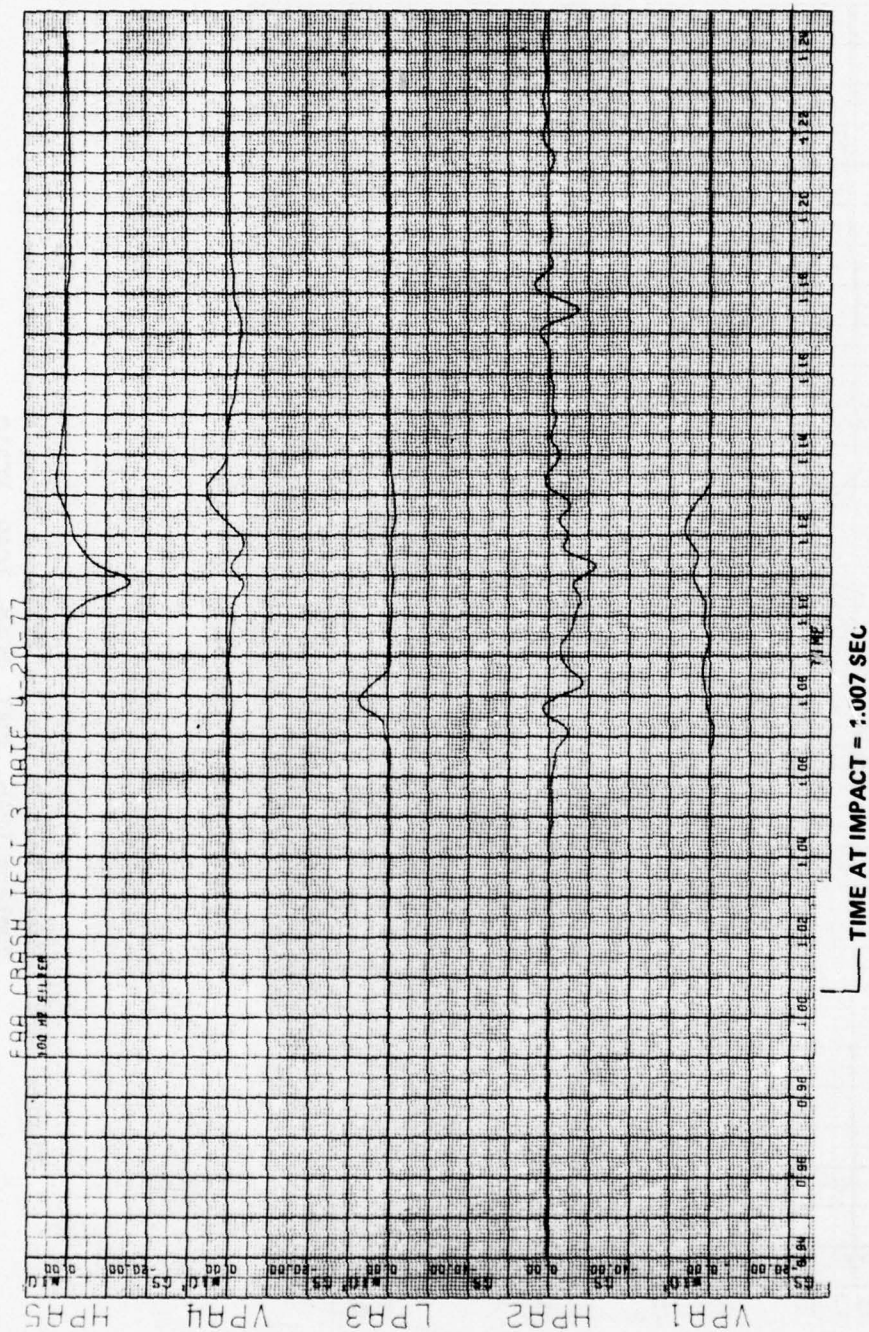


Figure C-25. Crash Test 3, 100 Hz Filtered Data, Accelerometer Numbers VPA1, HPA2, LPA3, VPA4, HPA5

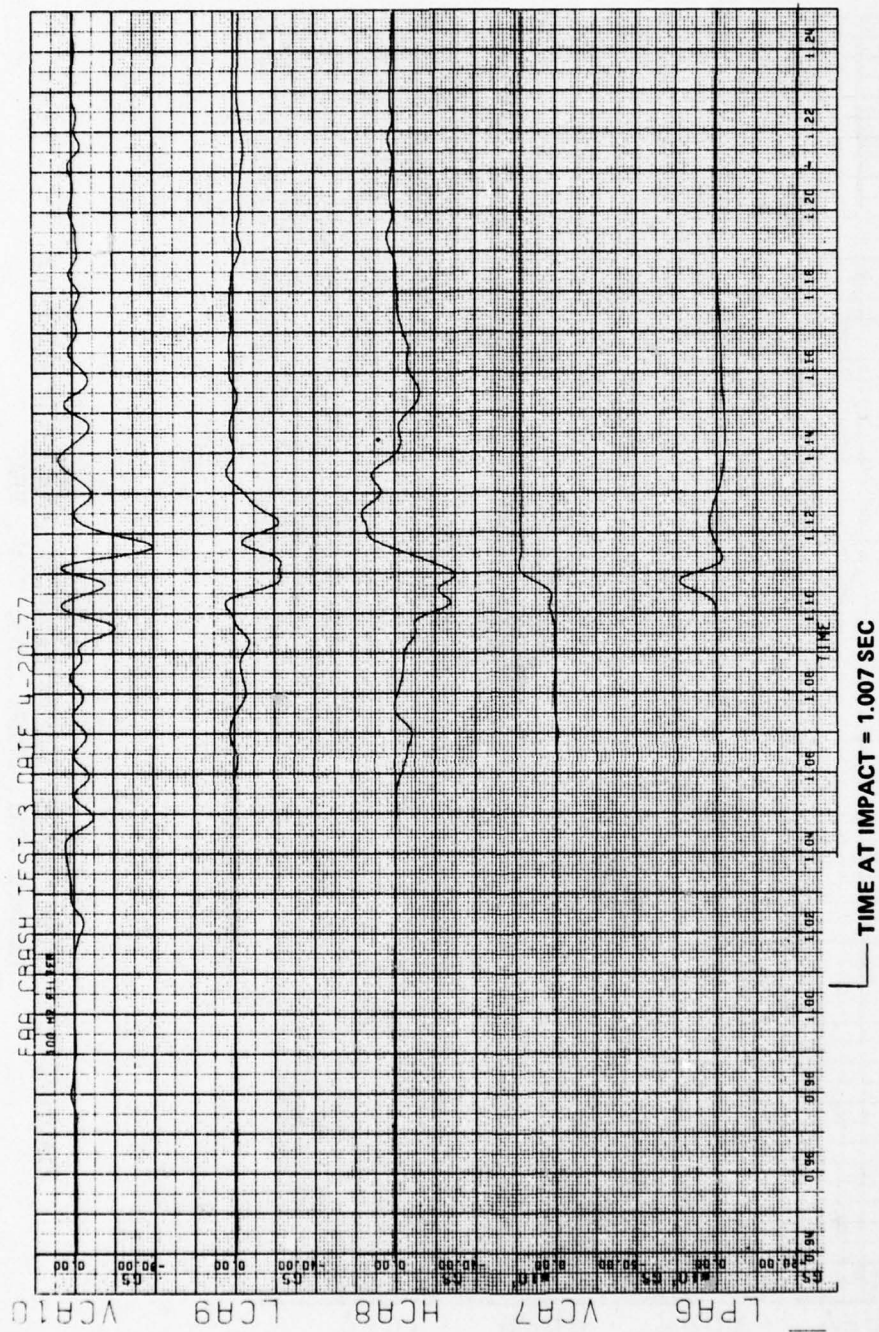


Figure C-26. Crash Test 3, 100 Hz Filtered Data, Accelerometer Numbers LPA6, VCA7, HCA8, LCA9, VCA10

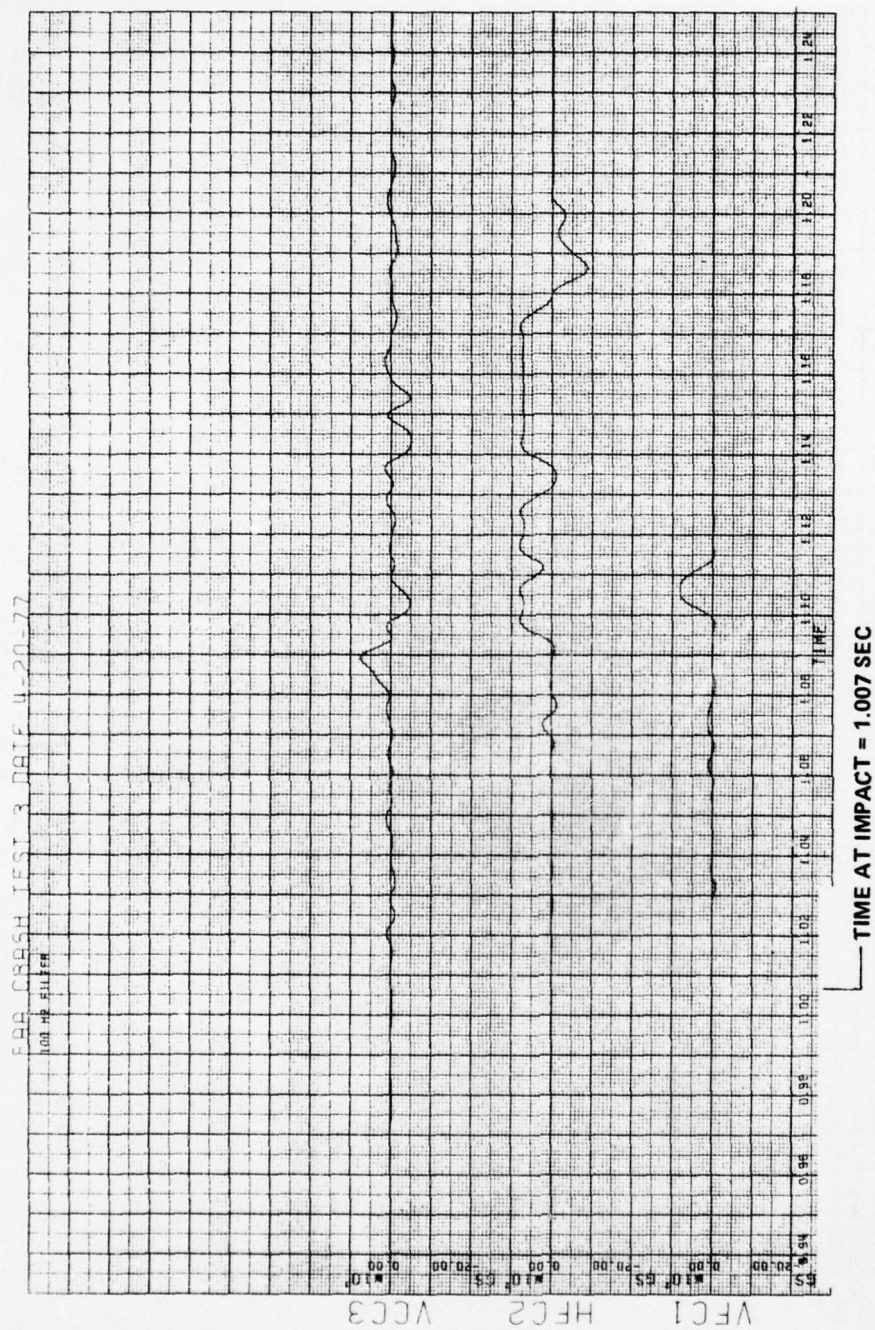


Figure C-27. Crash Test 3, 100 Hz Filtered Data, Accelerometer
 Numbers VFC1, HFC2, VCC3

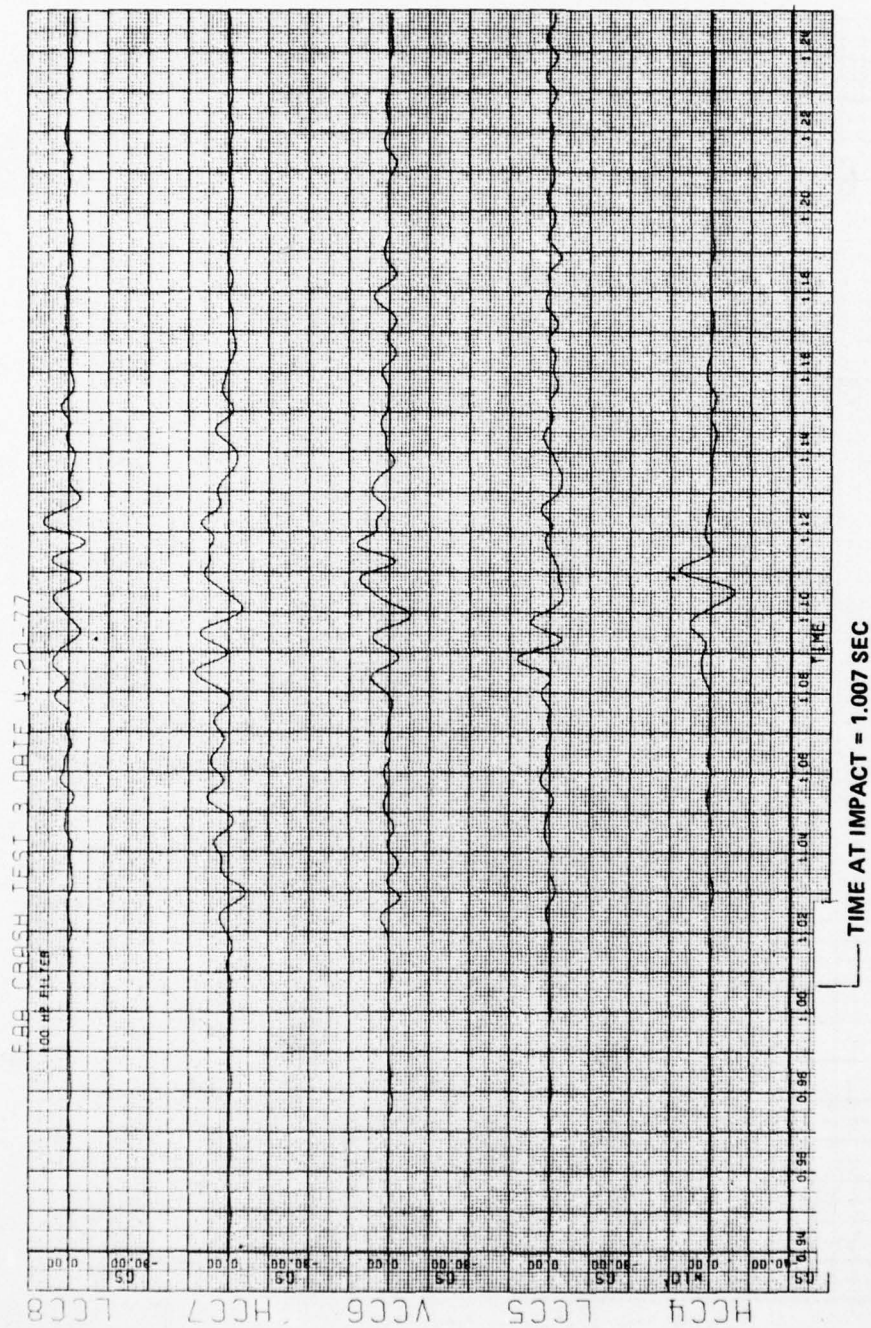


Figure C-28. Crash Test 3, 100 Hz Filtered Data, Accelerometer Numbers HCC4, LCC5, VCC6, HCC7, LCC8

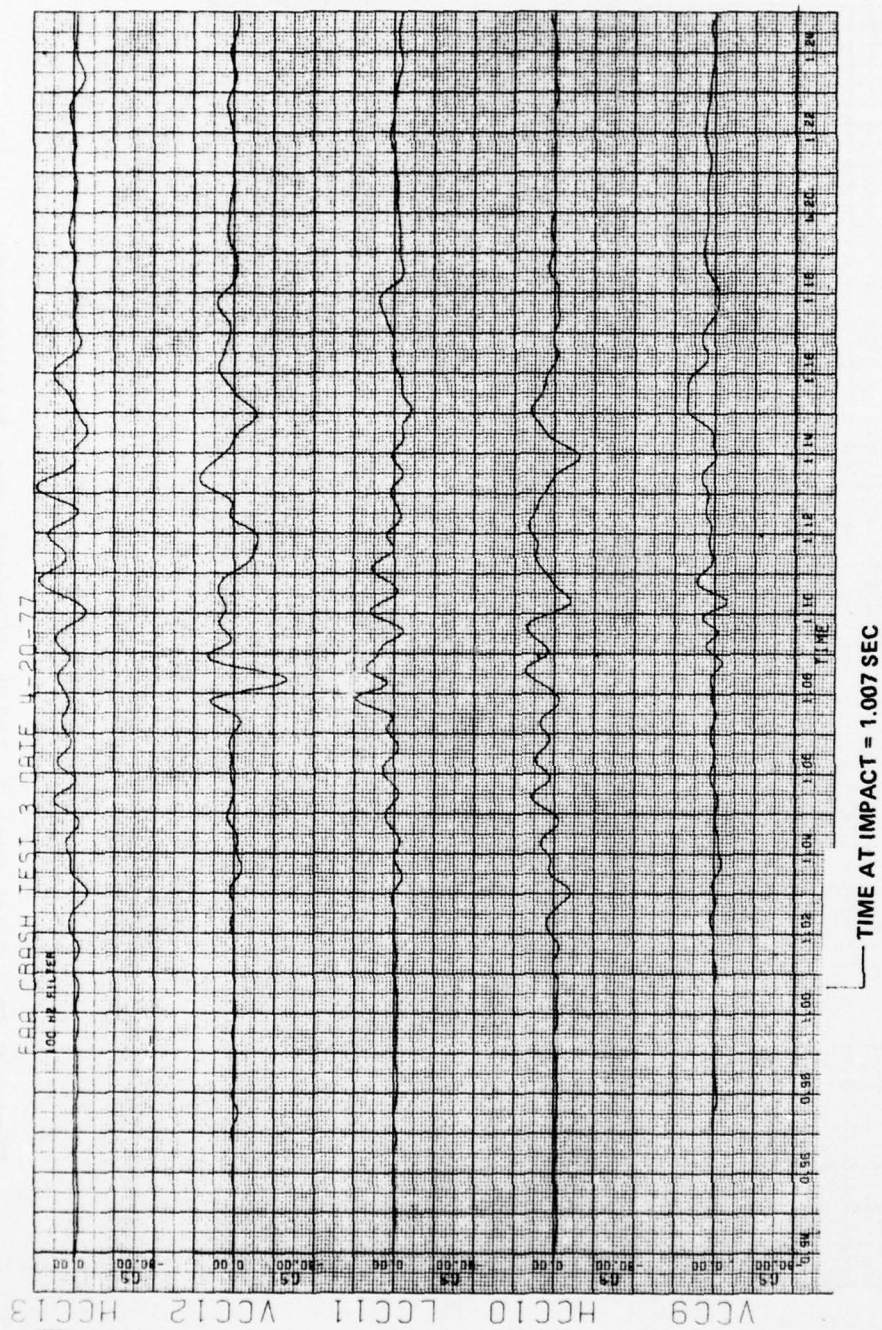


Figure C-29. Crash Test 3, 100 Hz Filtered Data, Accelerometer Numbers VCC9, VCC10, LCC11, VCC12, HCC13

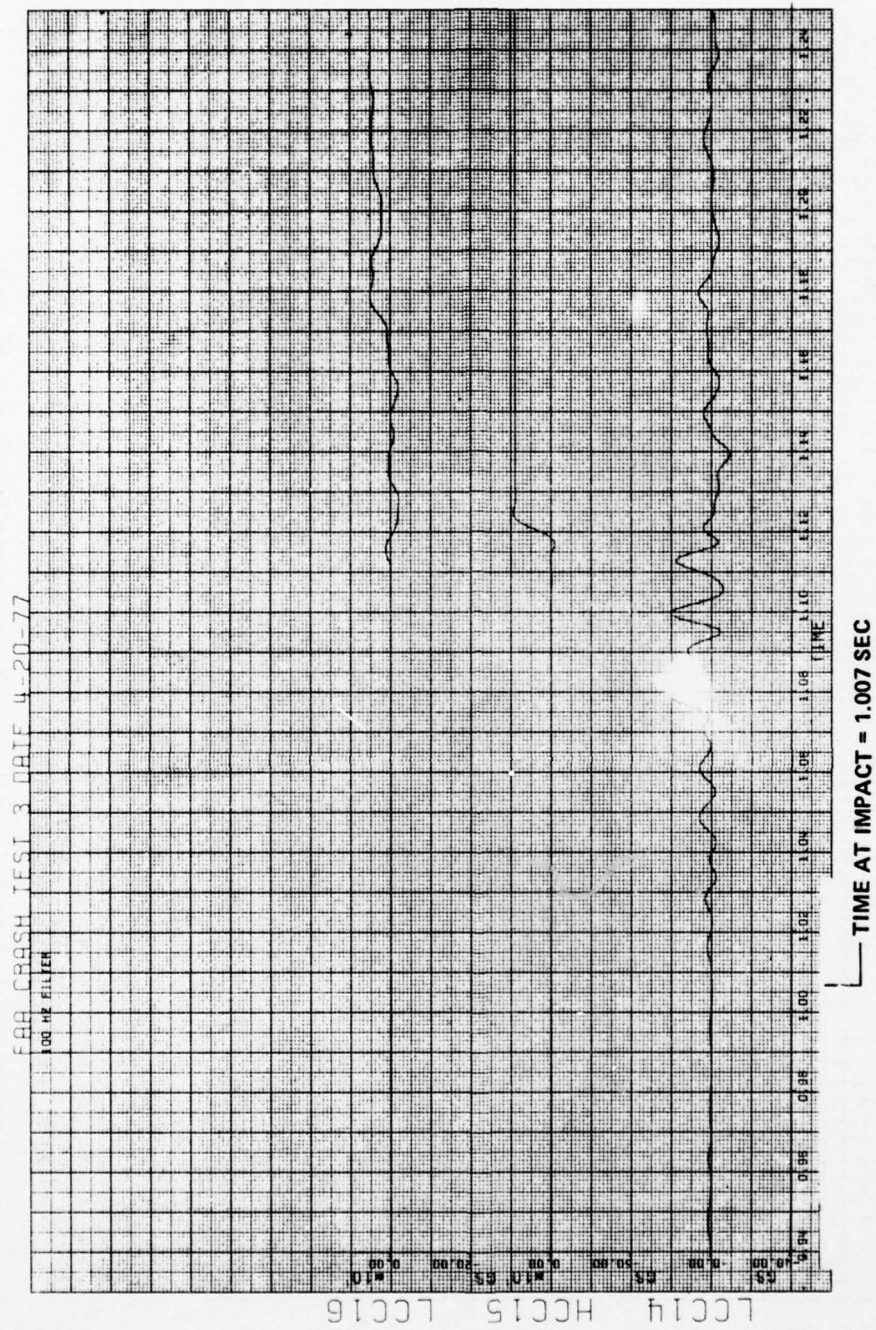


Figure C-30. Crash Test 3, 100 Hz Filtered Data, Accelerometer Numbers LCC14, HCC15, LCC16

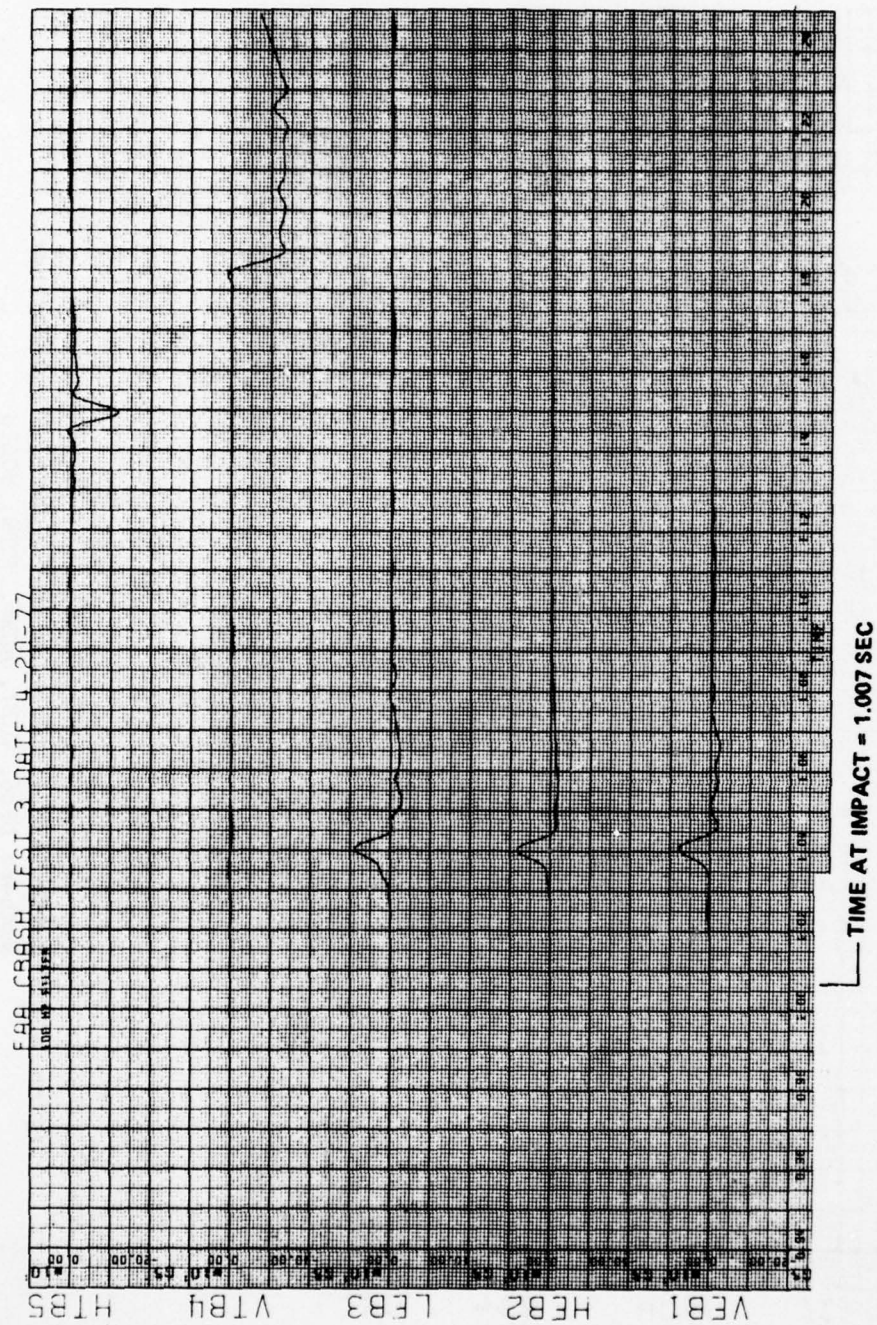


Figure C-31. Crash Test 3, 100 Hz Filtered Data, Accelerometer Numbers VEB1, HEB2, LEB3, VTB4, HTB5

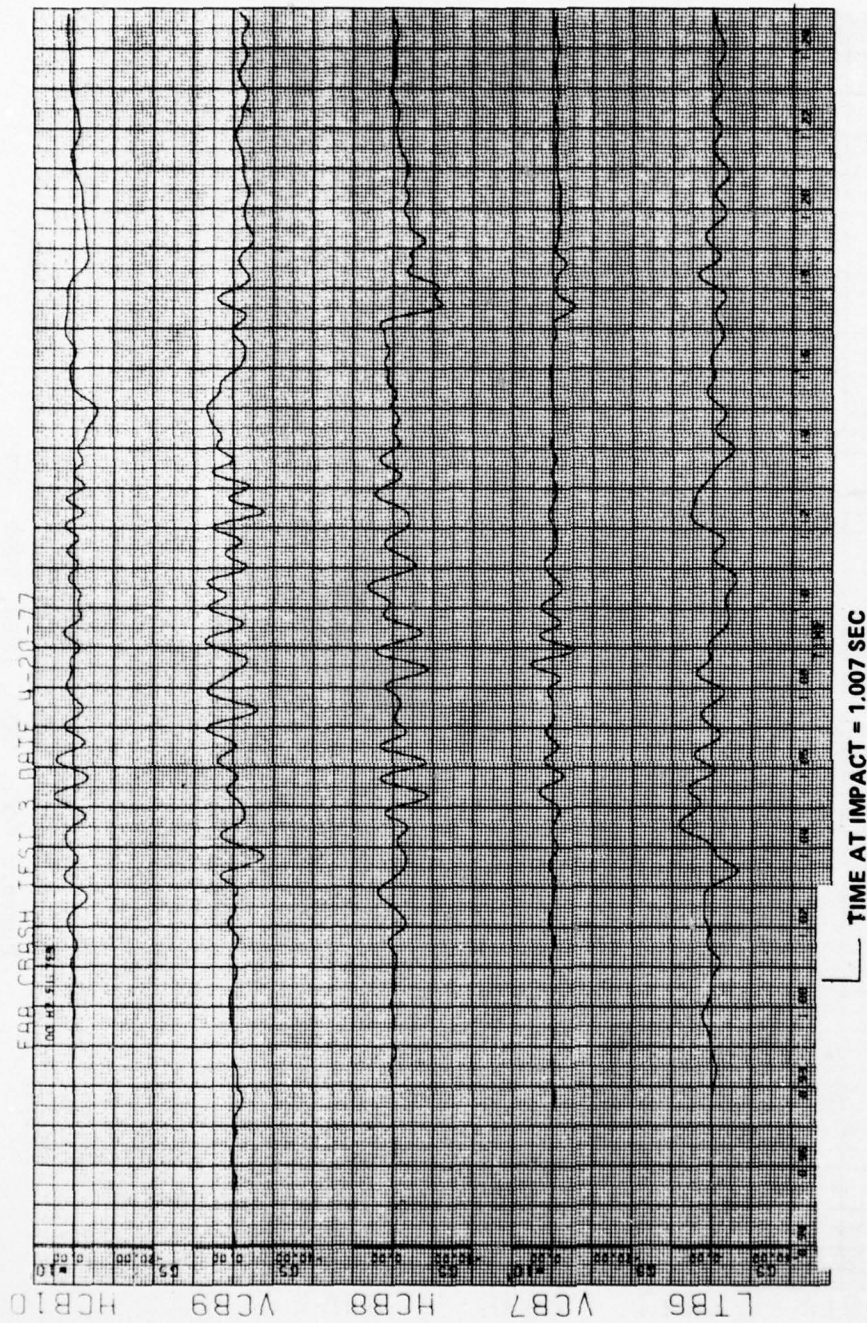


Figure C-32. Crash Test 3, 100 Hz Filtered Data, Accelerometer Numbers LTB6, VCB7, HCB8, VCB9, HCB10

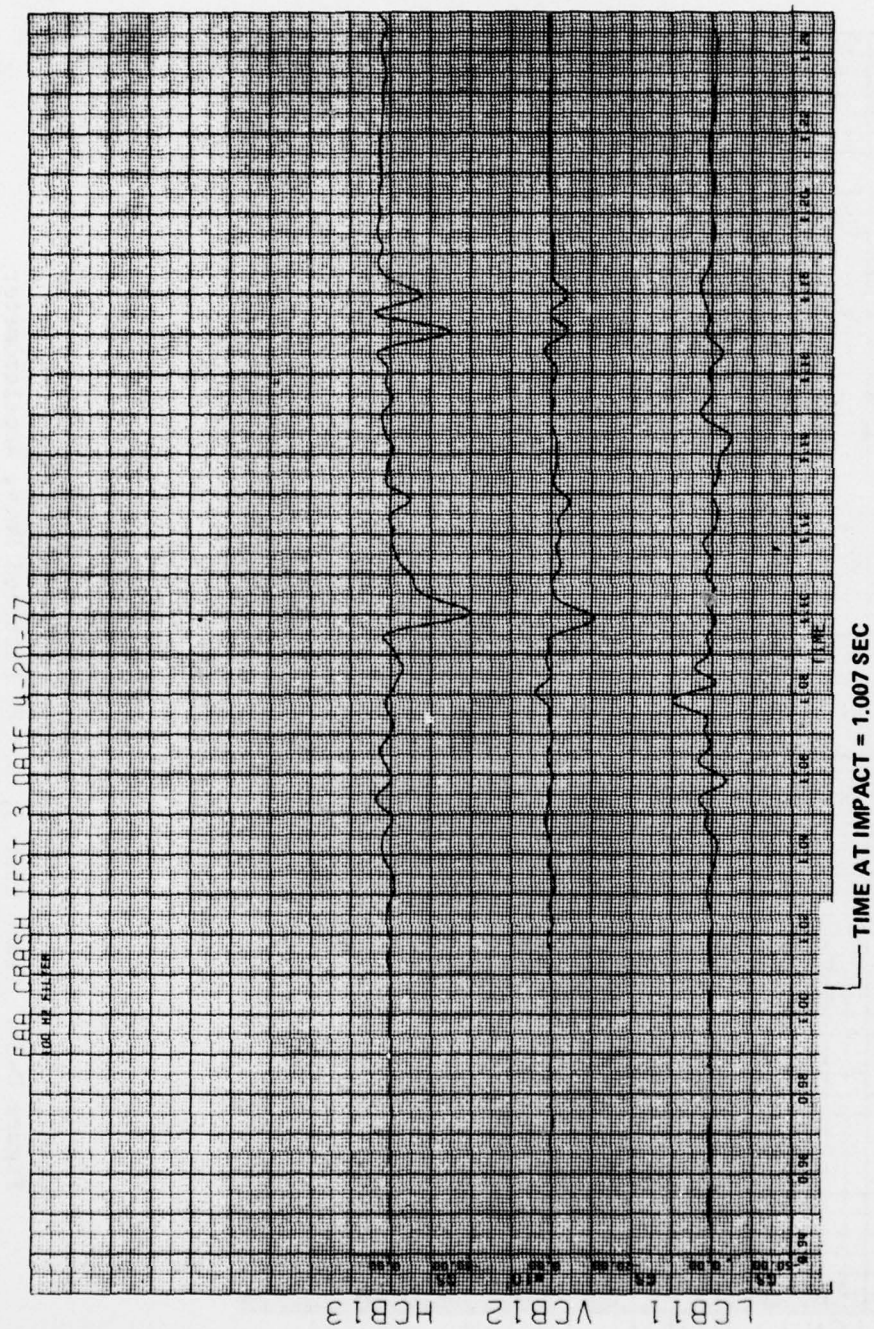


Figure C-33. Crash Test 3, 100 Hz Filtered Data, Accelerometer Numbers LCB11, VCB12, HCB13

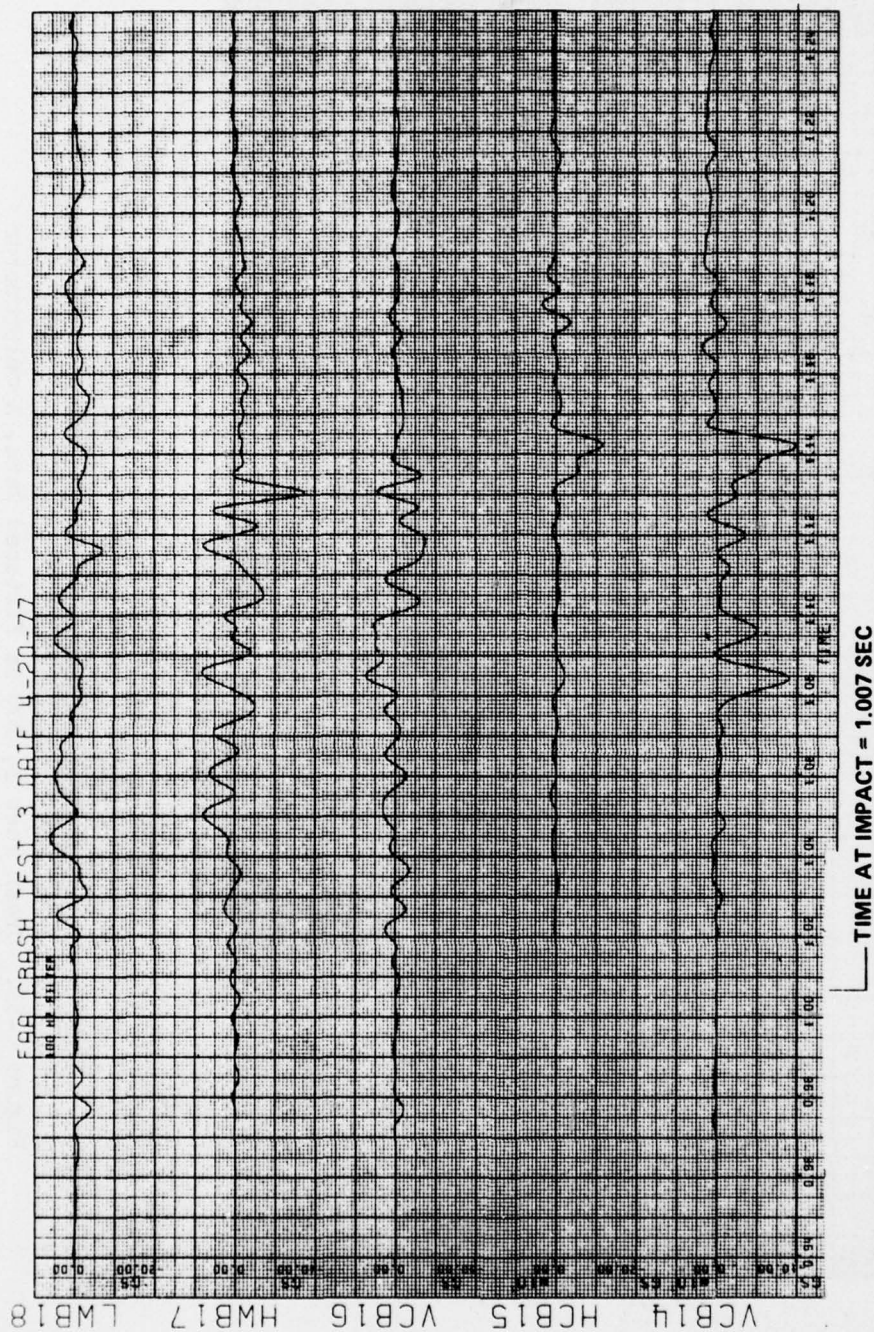


Figure C-34. Crash Test 3, 100 Hz Filtered Data, Accelerometer Numbers VCB14, HCB15, VCB16, HMB17, LWB18

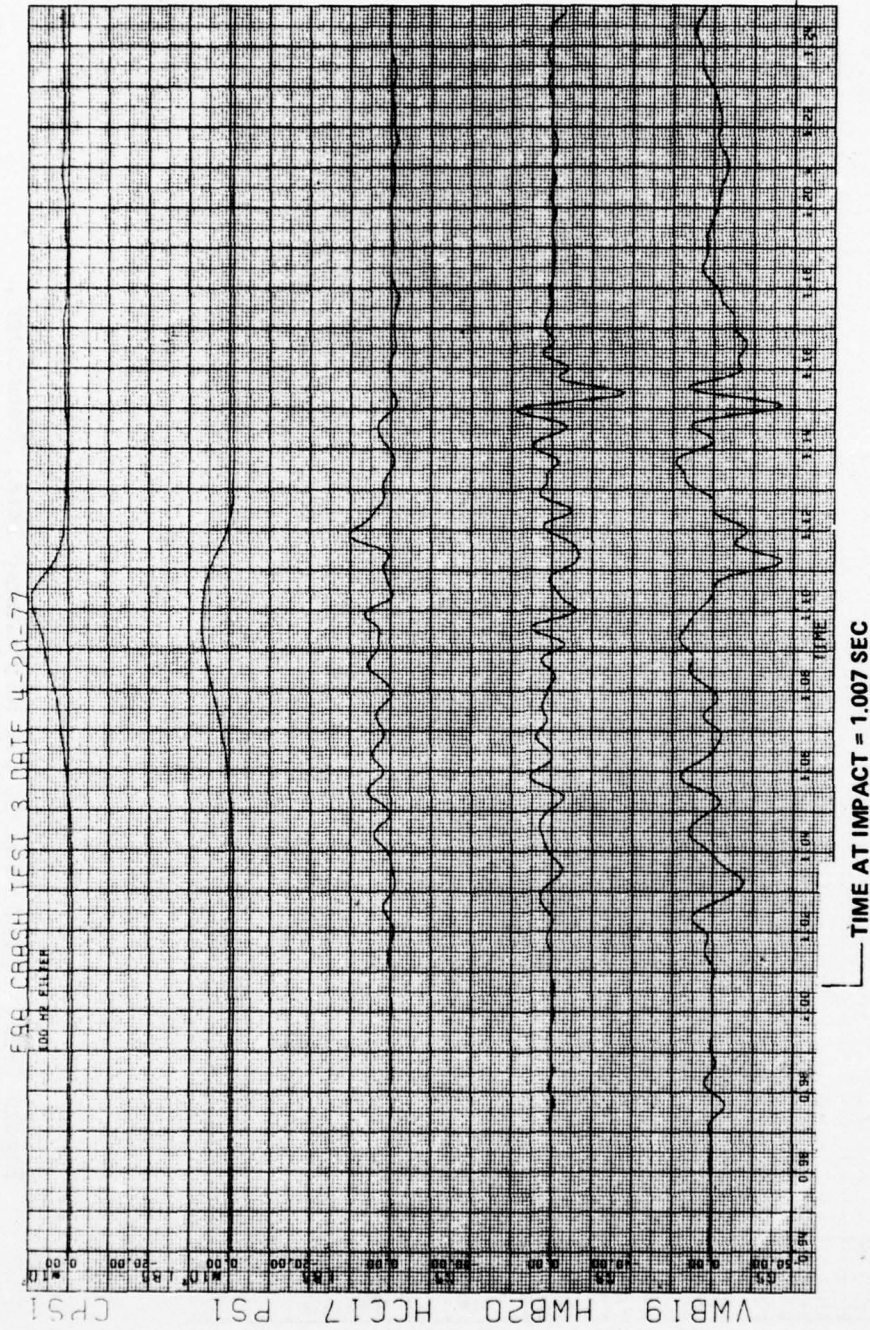


Figure C-35. Crash Test 3, 100 Hz Filtered Data, Accelerometer Numbers VWB19, HMB20, HCC17, Transducer Numbers PS1, CPS1

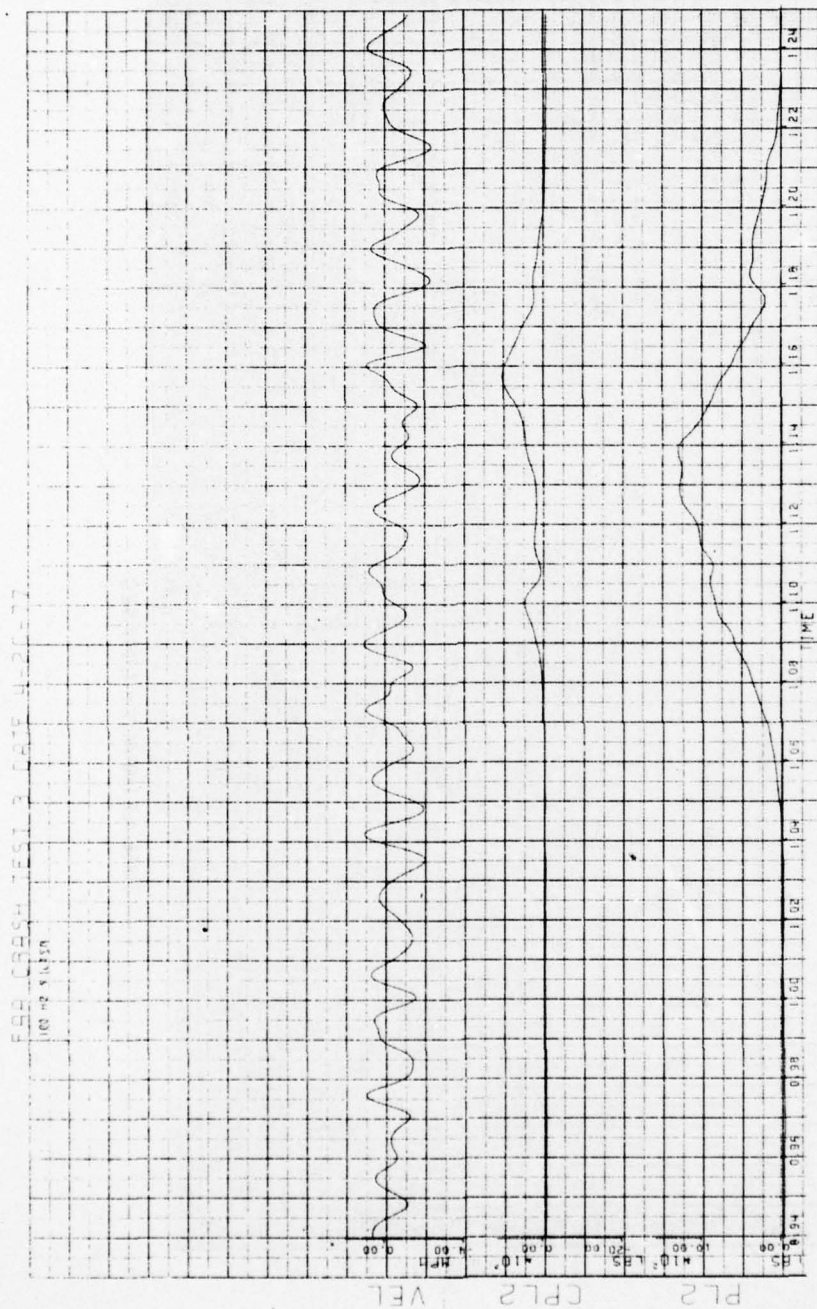


Figure C-36. Crash Test 3, 100 Hz Filtered Data, Transducer Numbers PL2, CPL2 and Radar Velocity

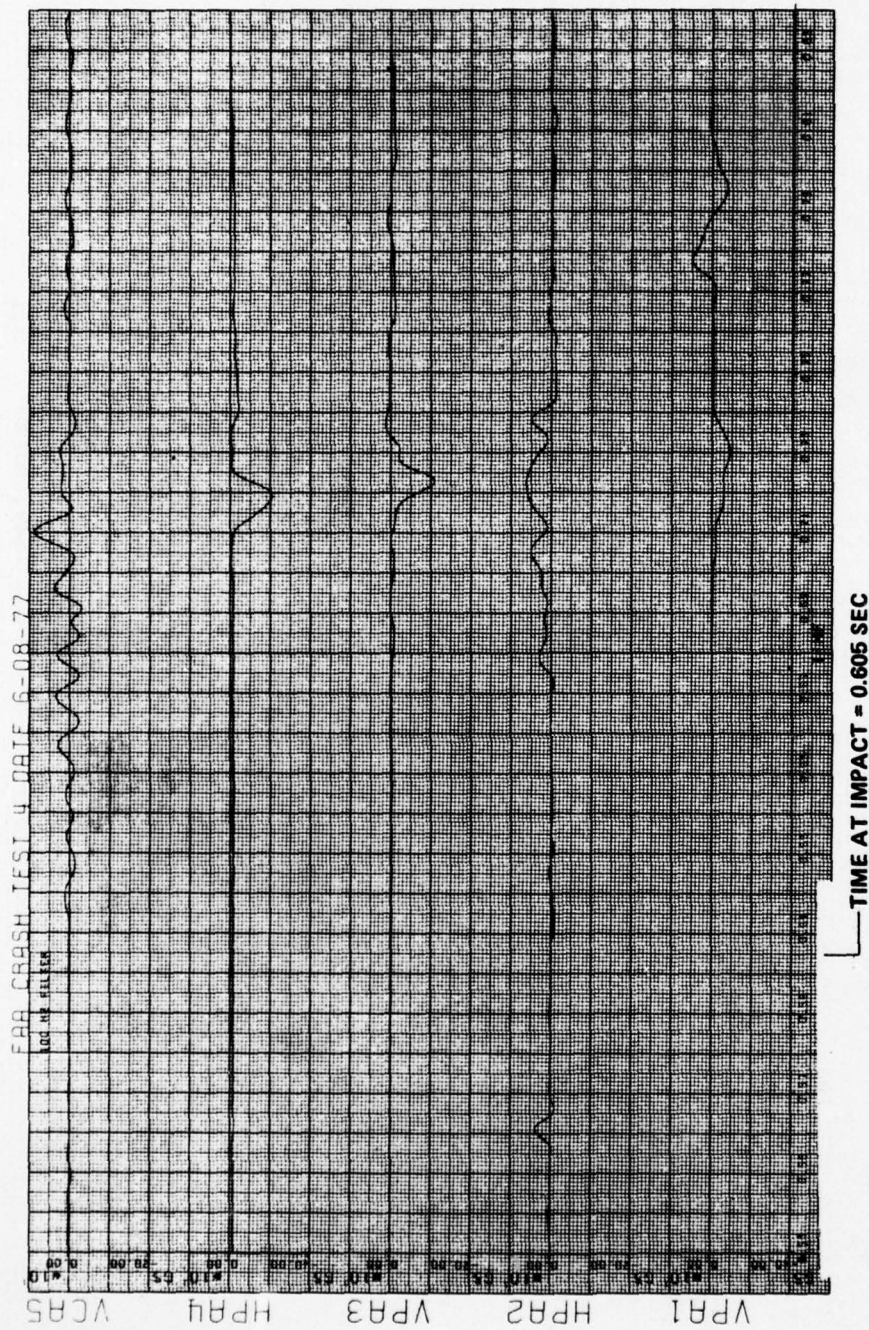


Figure C-37. Crash Test 4, 100 Hz Filtered Data, Accelerometer Numbers VPA1, HPA2, VPA3, HPA4, VCA5

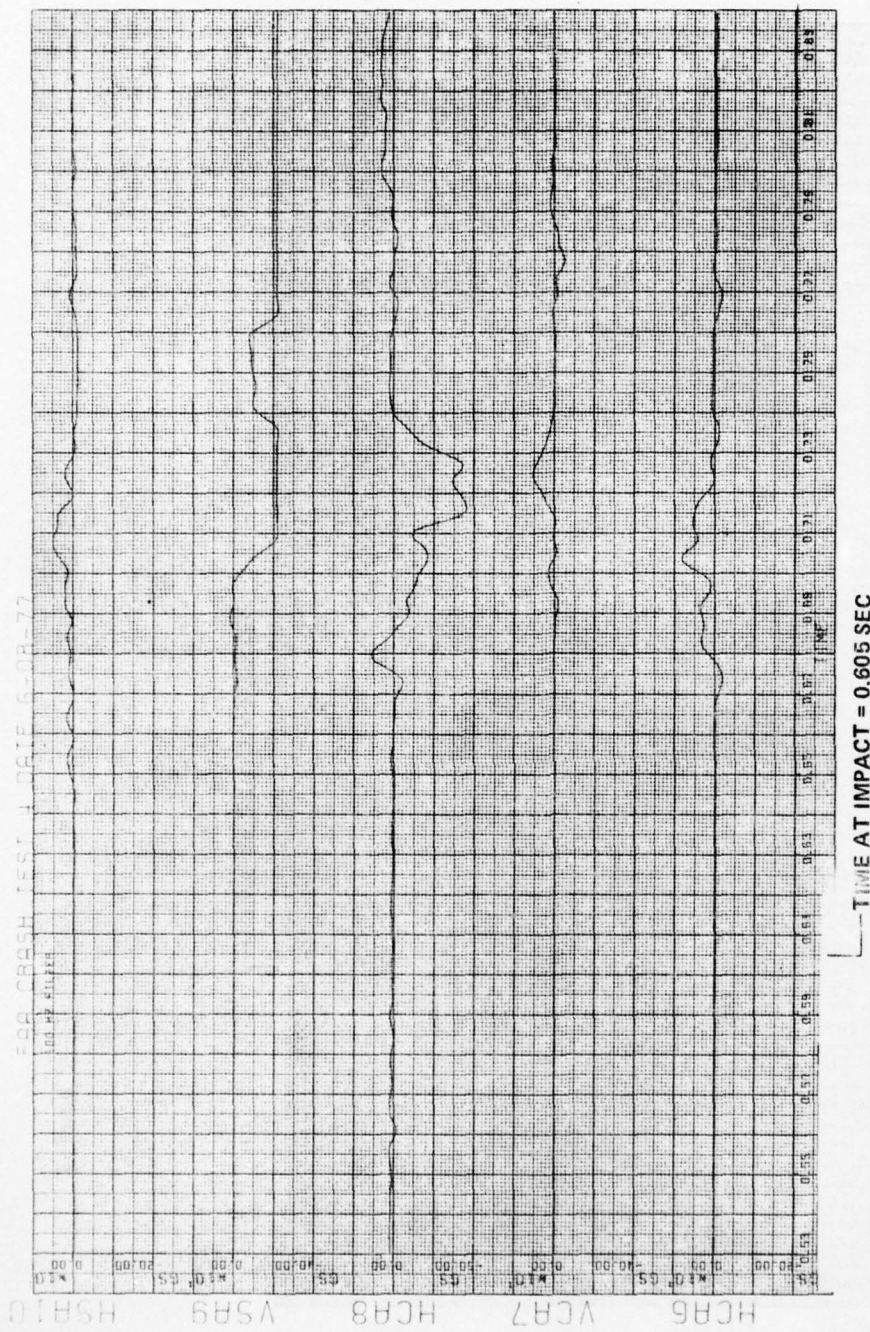


Figure C-38. Crash Test 4, 100 Hz Filtered Data, Accelerometer Numbers HCA6, VCA7, HCA8, VSA9, HSA10

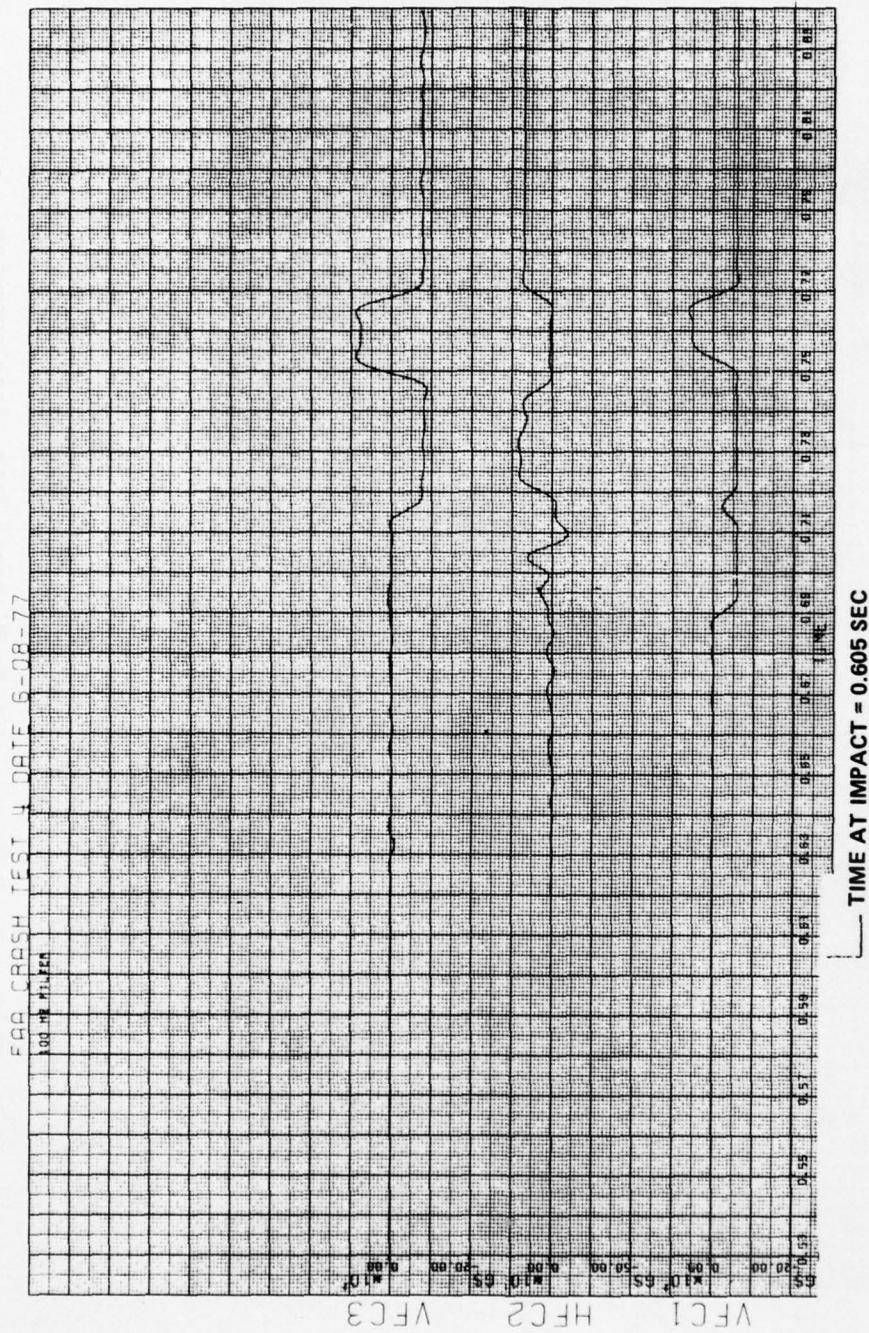


Figure C-39. Crash Test 4, 100 Hz Filtered Data, Accelerometer Numbers VFC1, HFC2, VFC3

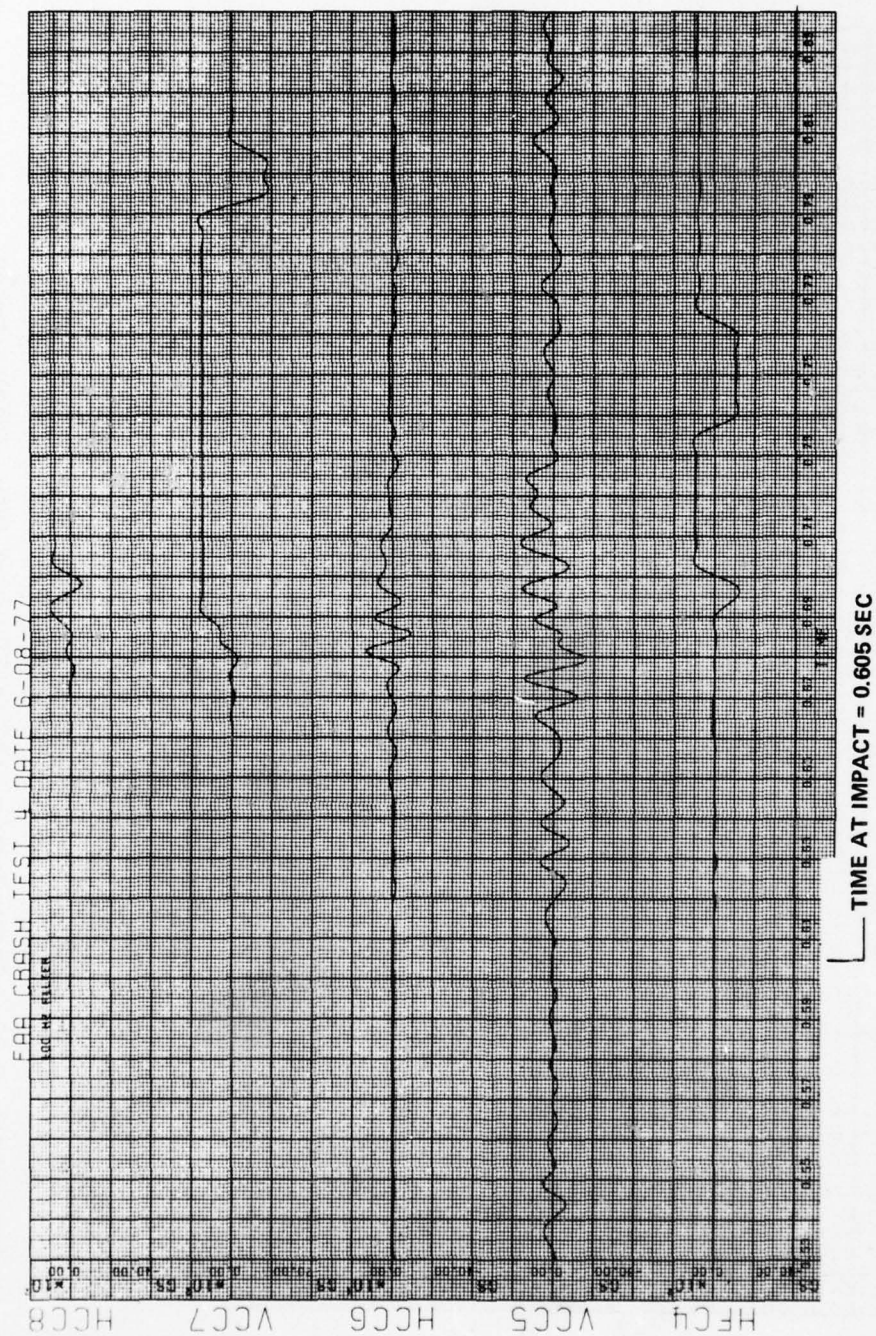


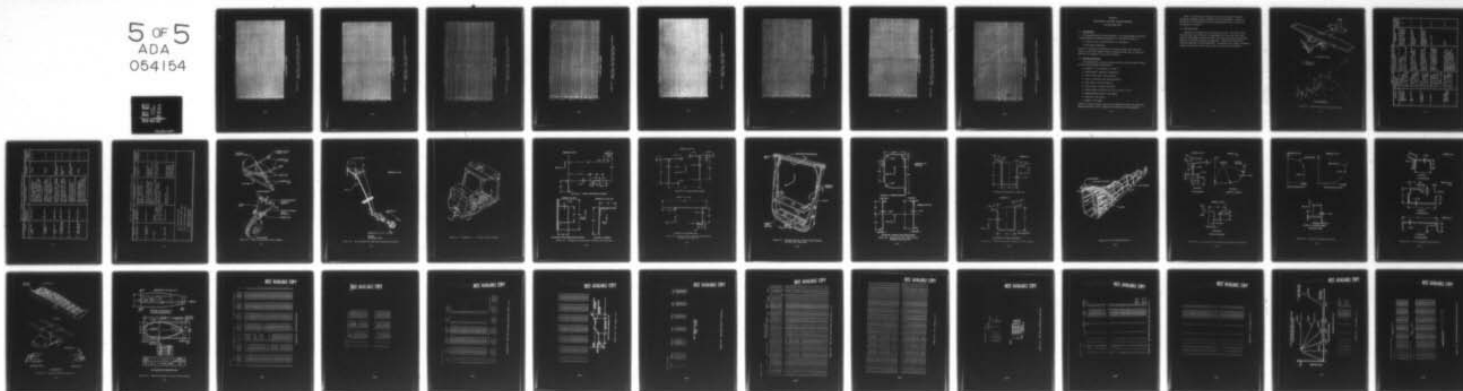
Figure C-40. Crash Test 4, 100 Hz Filtered Data, Accelerometer Numbers HFC4, VCC5, HCC6, VCC7, HCC8

AD-A054 154

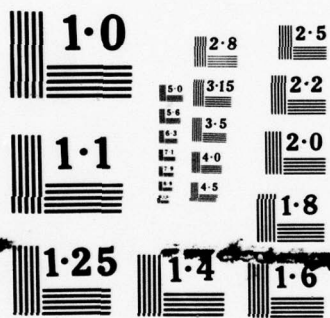
LOCKHEED-CALIFORNIA CO BURBANK
FULL SCALE CRASH TEST EXPERIMENTAL VERIFICATION OF A METHOD OF --ETC(U)
FEB 78 G WITTLIN, M A GAMON, W L LABARGE DOT-FA75WA-3707
LR-28306 FAA-RD-77-188 NL

UNCLASSIFIED

5 OF 5
ADA
054154



END
DATE
FILMED
7-78
DDC



NATIONAL BUREAU OF STANDARDS
MICROCOPY RESOLUTION TEST CHART

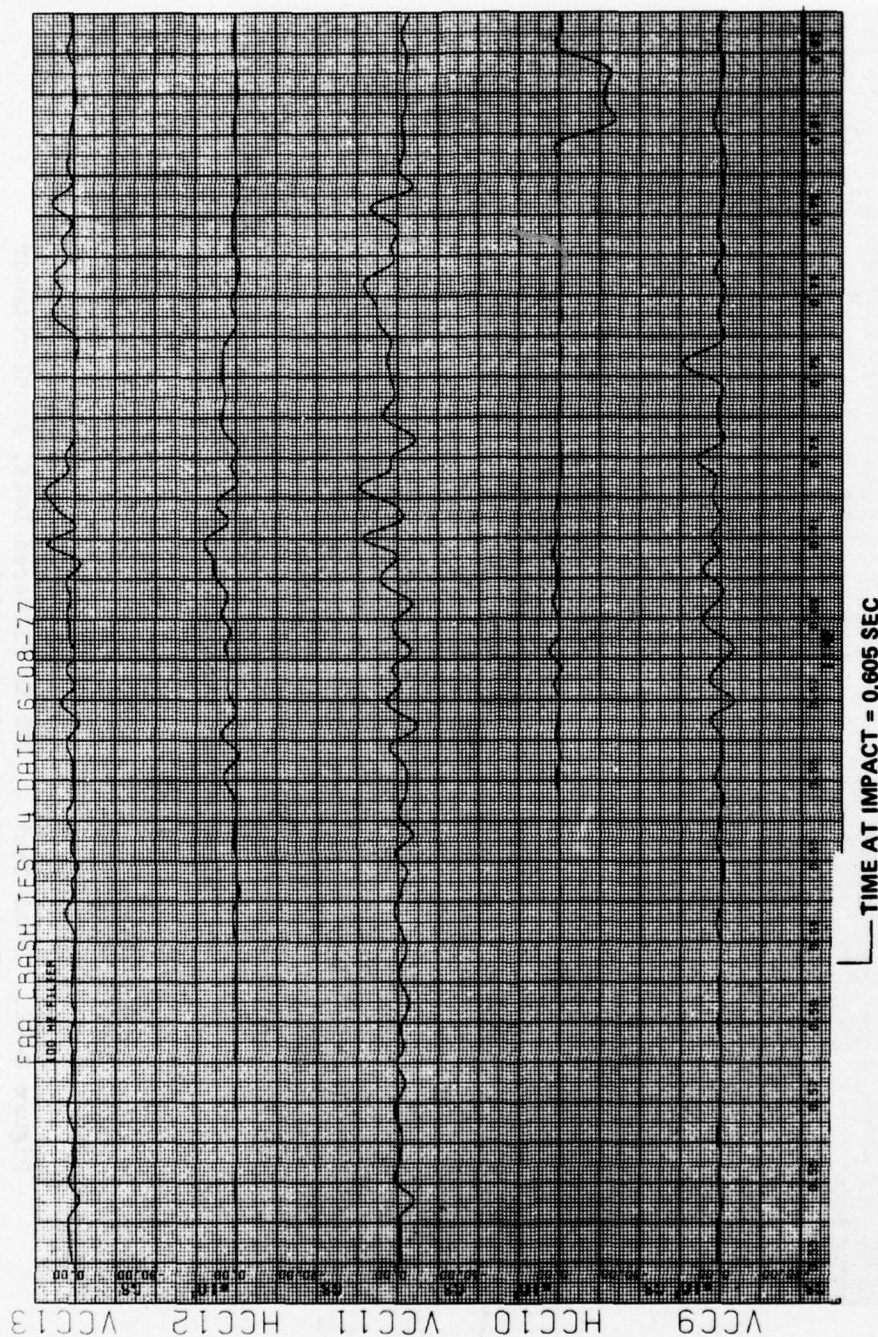


Figure C-41. Crash Test 4, 100 Hz Filtered Data, Accelerometer Numbers VCC9, HCC10, VCC11, HCC12, VCC13

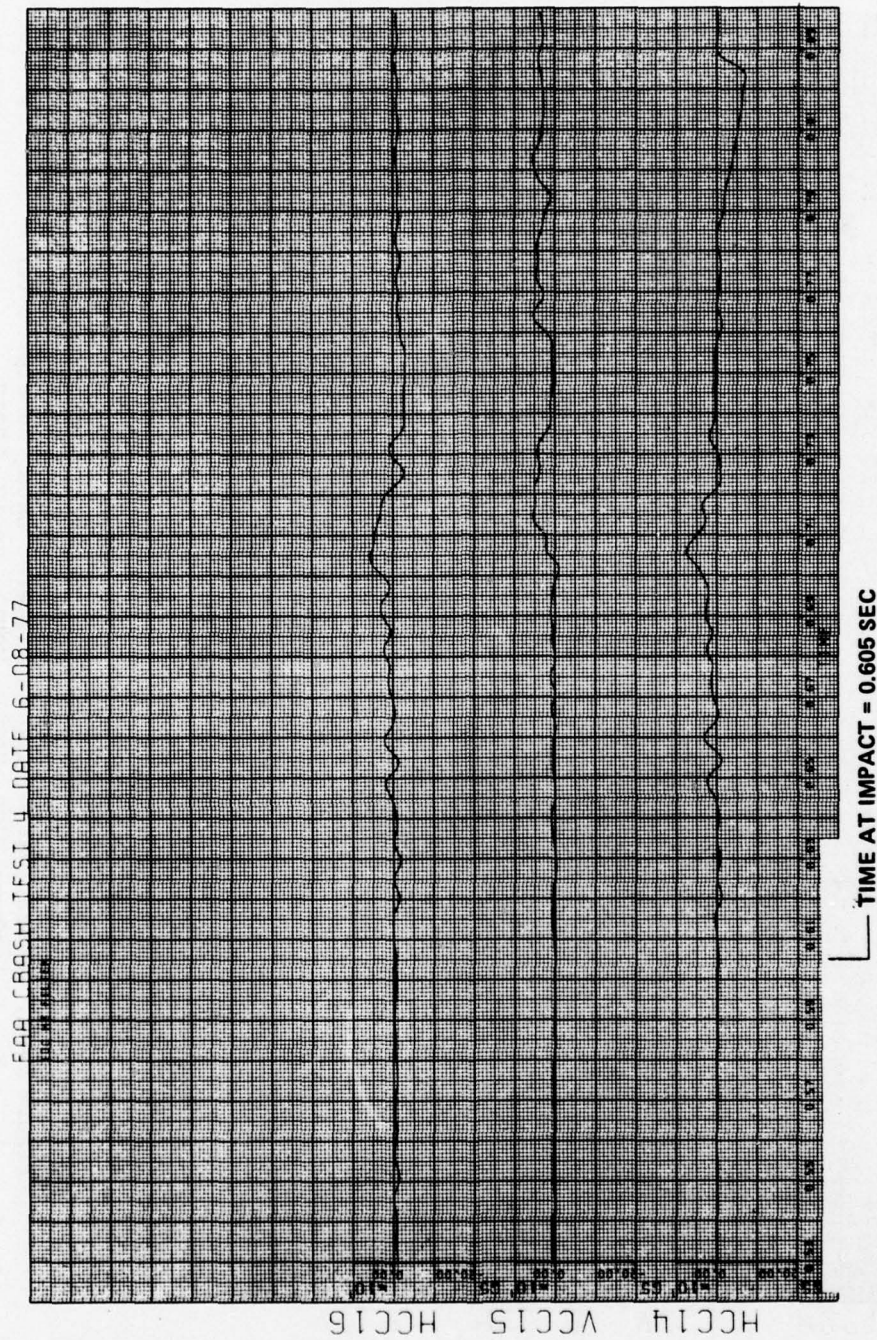


Figure C-42. Crash Test 4, 100 Hz Filtered Data, Accelerometer Numbers HCC14, VCC15, HCC16

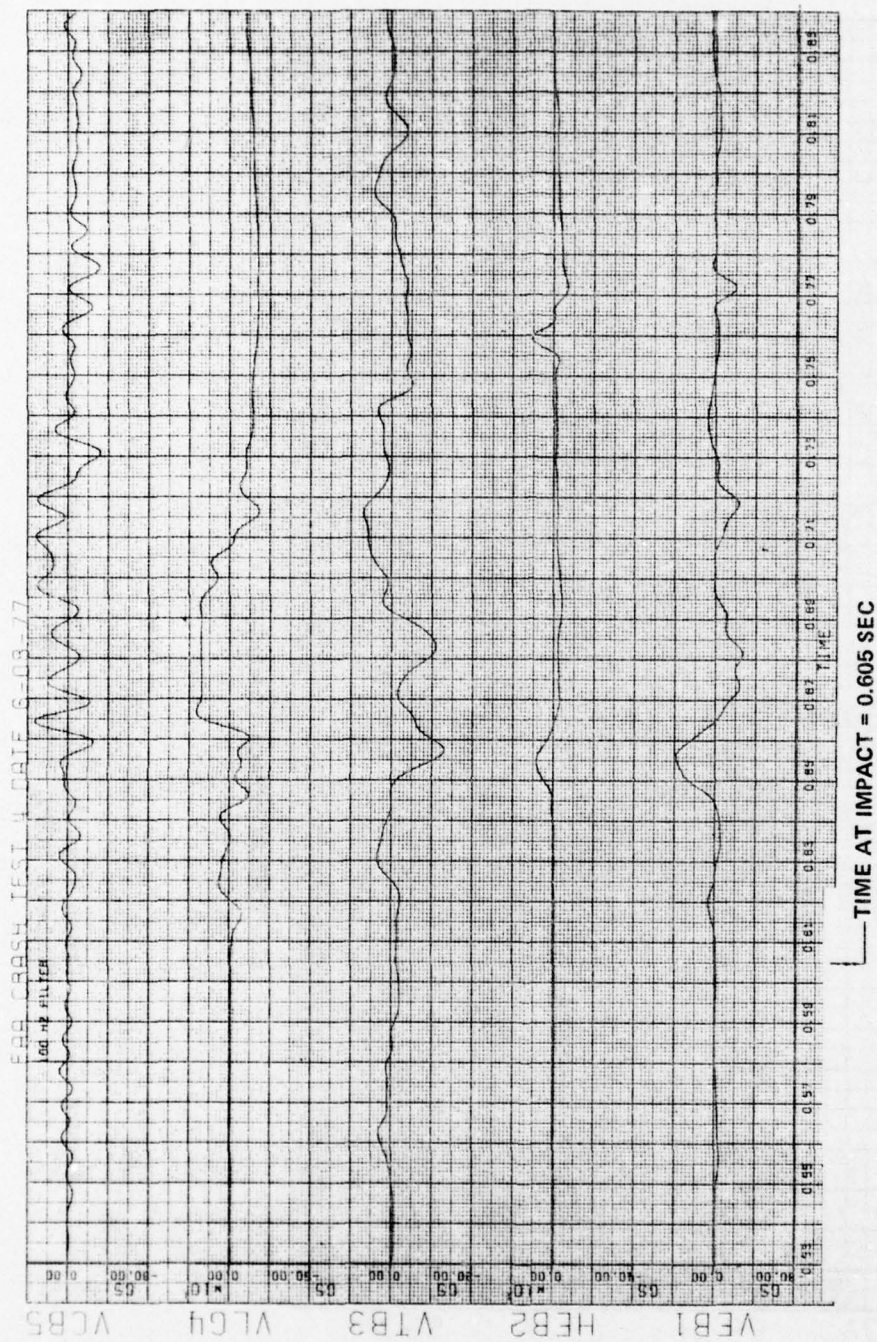


Figure C-43. Crash Test 4, 100 Hz Filtered Data, Accelerometer Numbers VEB1, HEB2, VTB3, VLG4, VCB5

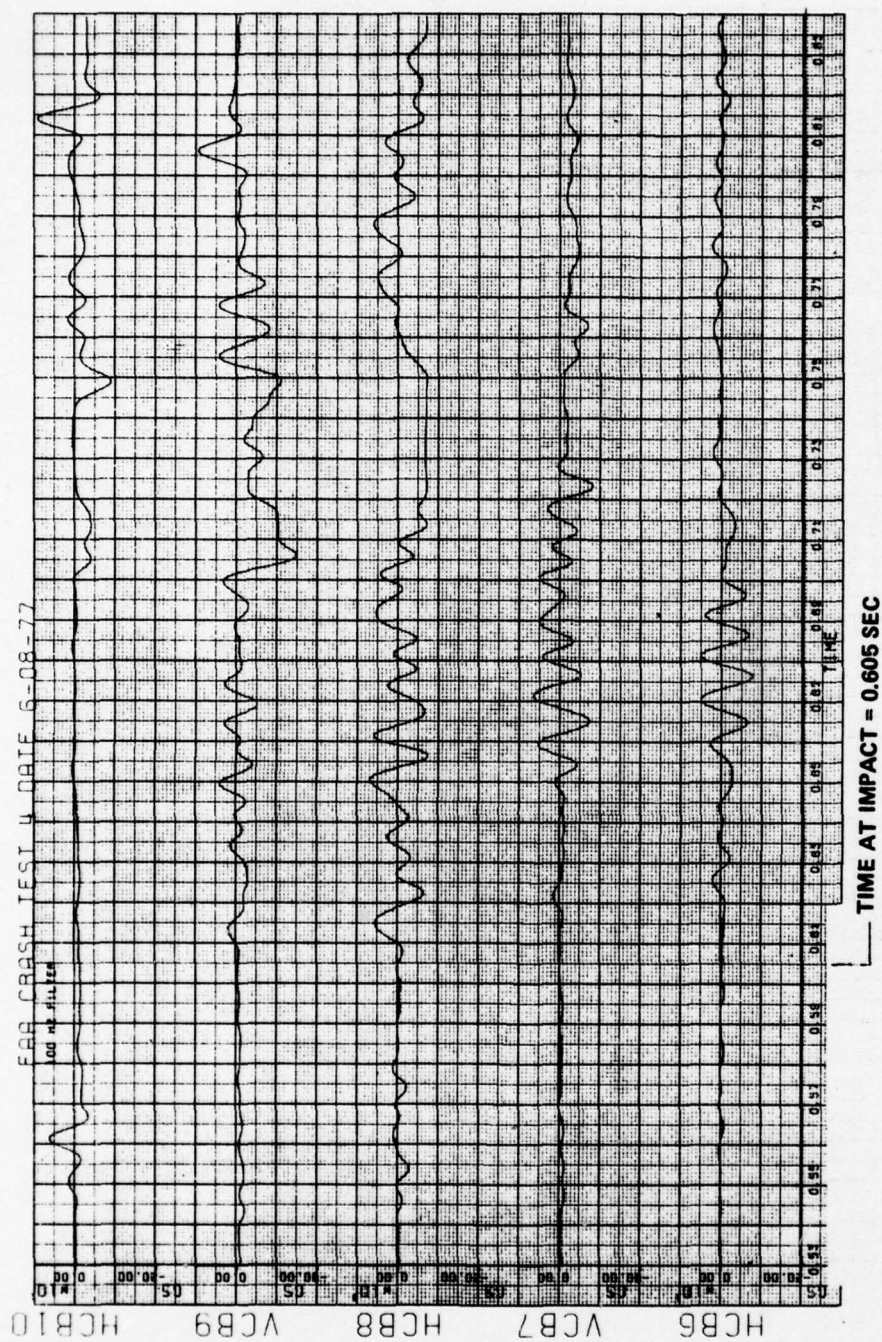


Figure C-44. Crash Test 4, 100 Hz Filtered Data, Accelerometer Numbers HCB6, VCB7, HCB8, VCB9, HCB10

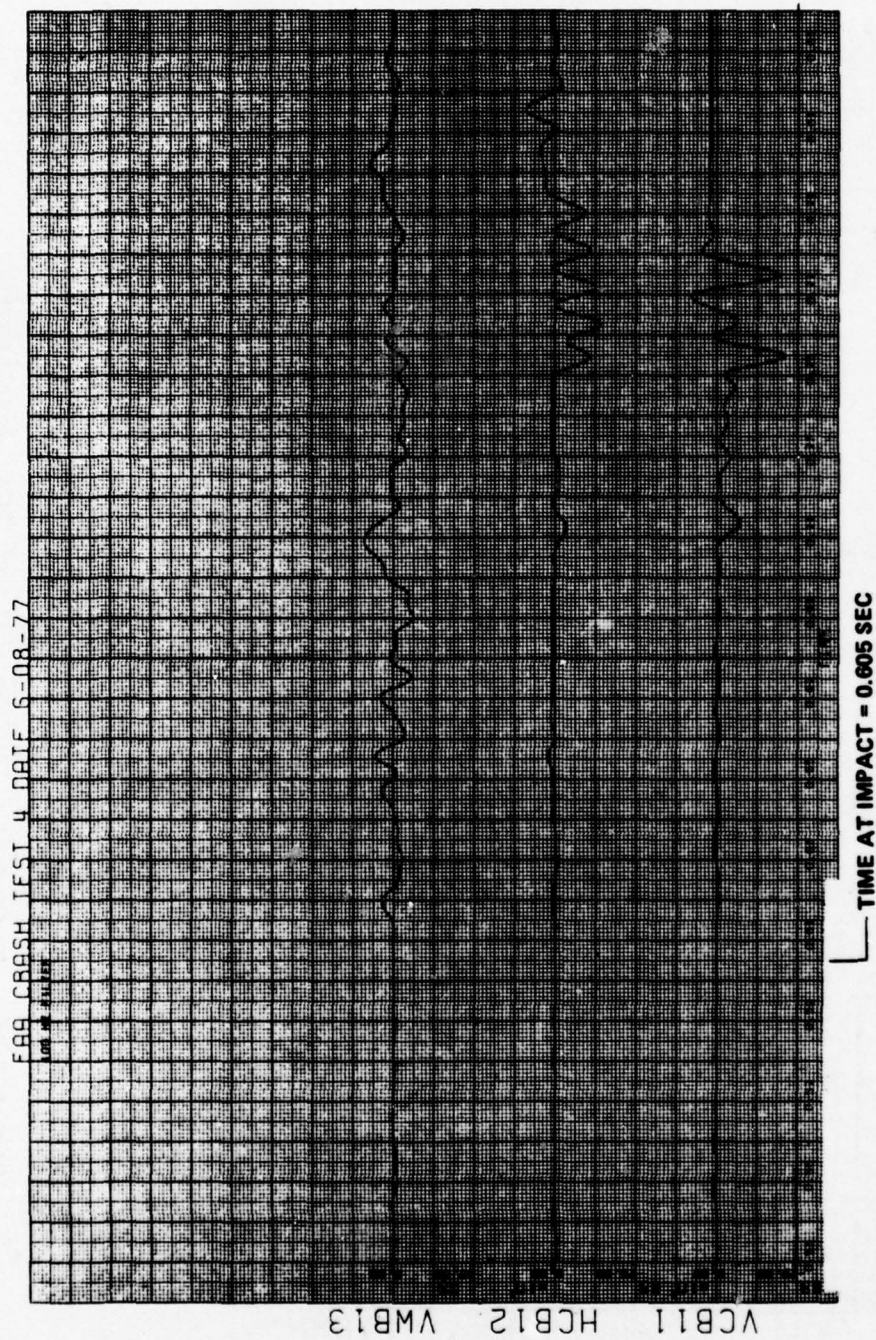


Figure C-45. Crash Test 4, 100 Hz Filtered Data, Accelerometer Numbers VCB11, HCB12, VWB13

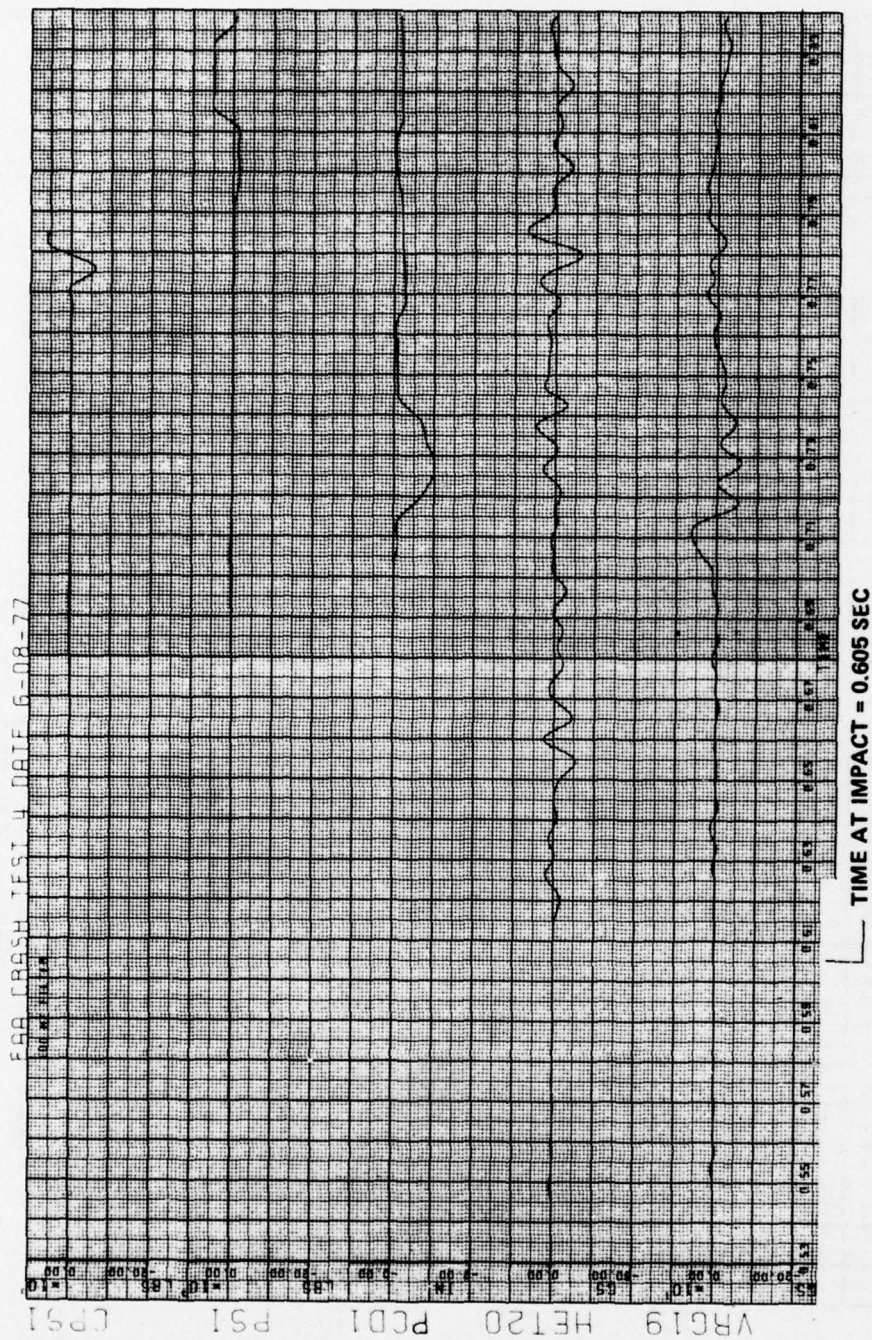


Figure C-47. Crash Test 4, 100 Hz Filtered Data, Accelerometer Numbers VRG19, HET20, Transducer Numbers PCD1, PS1, CPS1

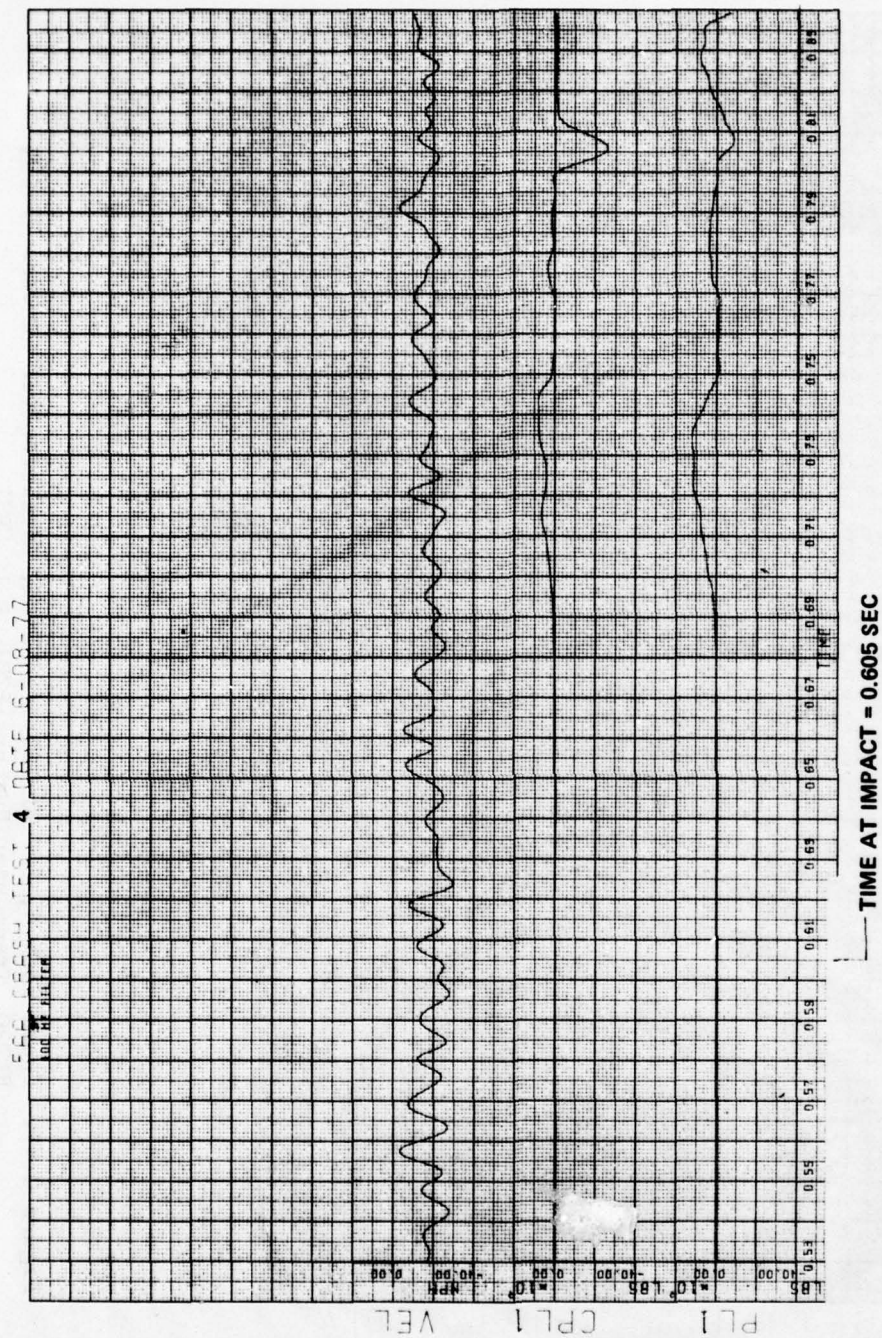


Figure C-48. Crash Test 4, 100 Hz Filtered Data, Transducer Numbers PL1, CPL1, VEL

APPENDIX D
SINGLE-ENGINE, HIGH-WING AIRPLANE STRUCTURE
AND MATH MODEL DATA

D.1 INTRODUCTION

This appendix presents data applicable to the single-engine, high-wing airplane tested and analyzed during Task II. The data consists of:

- Structure that is representative of the airplane
- Math model information

Section D.2 describes the airplane and provides typical cross sections. Section D.3 provides computer printout showing the data that is input into KRASH for the analysis of the crash conditions.

D.2 AIRPLANE DESCRIPTION

The single-engine, high-wing airplane modeled during the Task II effort has the following general description:

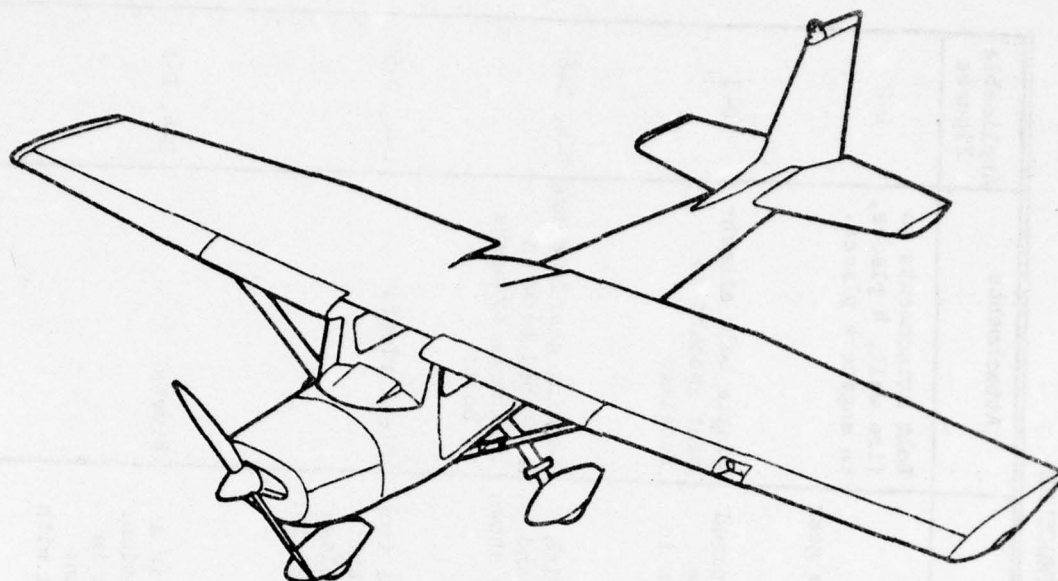
- Category I type (Reference 1, Table 4)
- Single-engine, high-wing configuration
- Side by side seats (four occupants)
- Used for training, and business purposes
- Stall speed ≤ 57 mph (flaps up)
- Cruise speed ≤ 121 mph (75% power)
- Flight design load factor of; $+3.8$ g's and -1.52 g's
- Maximum takeoff weight = 2300 pounds
- Wing span = 434 inches
- Length - 323 inches

Figure D-1 shows an overall view of the airplane and Figure D-1b shows the mathematical model used to represent the structure for crash analysis.

Table D-1 describes the airplane structure with regard to material properties, strength, design, concepts, size and attachments. Figures D-2 through D-15 show different structures and approximate cross sections for the respective structure.

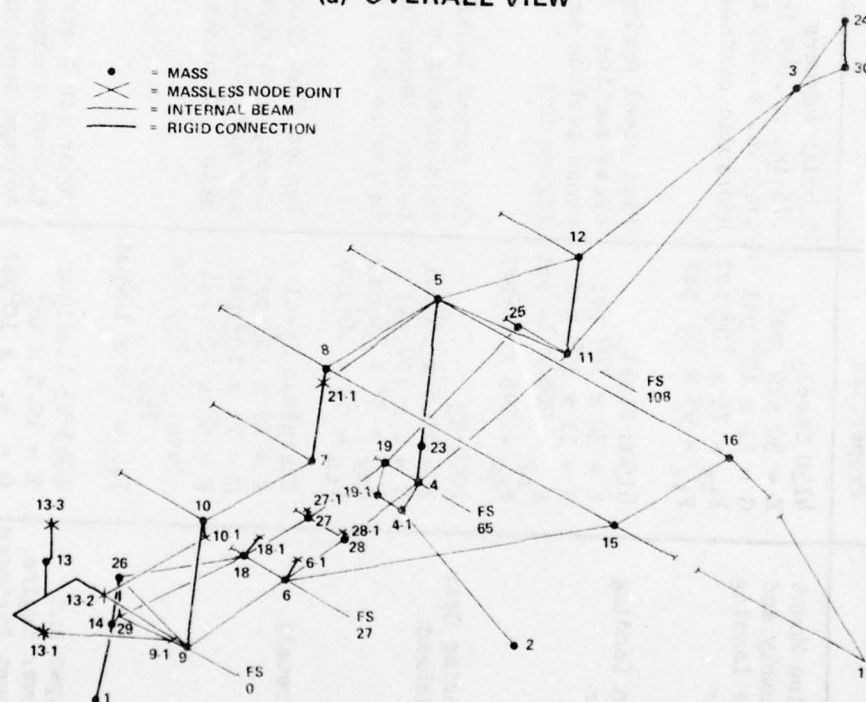
D.3 MATH MODEL DATA

Figures D-16 through D-24 provide math model data. The data is taken from the crash test 3 model but is representative of all four crash tests. Figures D-16 through D-18 show the mass, node point and external spring data. Figure D-19 provides the material properties. Figures D-20 through D-23 shows the beam data including properties, nonlinearities and rupture allowables. Figure D-24 shows the vehicle model weight, cg and inertia properties.



(a) OVERALL VIEW

- = MASS
- × = MASSLESS NODE POINT
- = INTERNAL BEAM
- = RIGID CONNECTION



(b) MATH MODEL

Figure D-1. Airplane Overall View and Math Model

TABLE D-1. DESCRIPTION OF AIRPLANE STRUCTURE

Structure	Materials and Properties	Concepts and Size	Attachments	Applicable Figures
1. Engine Mount Assembly and Nose Landing Gear	4130 Steel ₆ E = 30×10^6 psi G = 11×10^6 psi F _{ty} = 75×10^3 psi F _{tu} = 95×10^3 psi	Tubular members .75 in. x .049 in. .625 in. x .049 in. Hydraulic cylinder nose gear	Bolt attachments to fire wall, 4 places, to engine 4 places.	D-2
2. Main Landing Gear	6150H Steel ₆ E = 30×10^6 psi G = 11×10^6 psi F _{ty} = 205×10^3 psi F _{tu} = 245×10^3 psi	Flat steel spring. Tapered cross section. Average cross section are shown in Figure B-3	Single bolt attachment inboard to fuselage	D-3
3. Landing Gear Bulkhead	2024-T3 E = 10.5×10^6 psi G = 4×10^6 psi F _{ty} = 37×10^3 psi F _{tu} = 63×10^3 psi	Two formed bulkheads with skin attachment above and below. Dimensions are shown in Figure B-5	Landing gear forgings attached between bulkheads by means of bolts	D-4, D-6
4. Firewall	Stainless Steel E = 27×10^6 psi G = 11×10^3 psi F = 58×10^3 psi (avg. of F _{ty} and F _{tc}) F _{tu} = 124×10^3 psi	Beaded flat aluminized iron sheet, a peripheral stiffener and attaching fuselage skin. Thickness = .025 in.	Steel rivets	D-4, D-5
5. Upper and Lower Engine Mount Stringer	2043-T3 Aluminum E = 10.5×10^6 psi G = 4×10^6 psi F _{ty} = 37×10^3 psi F _{tu} = 63×10^3 psi	Upper mount stringer is a tapered U channel section. Average section shown in Figure B-5, Lower Mount Stringer is a Channel with J edges, as shown in Figure B-5	Rivets	D-4, D-5

TABLE D-1. DESCRIPTION OF AIRPLANE STRUCTURE (Cont'd)

Structure	Materials and Properties	Concepts and Size	Attachments	Applicable Figures
6. Upper Cabin Area	Same as No. 5	This area is comprised of a root rib-upper door jam, cabin top skin and two stringers. It extends from the forward door post to aft door post. Dimensions are shown in Figure B-5.	Rivets	D-4, D-6
7. Forward Floor Bulkhead	Same as No. 5	Consists of formed bulkhead stiffener on aft side, floor-board on top and skin on bottom. Average cross section, as shown in Figure B-7.	Rivets	D-7, D-8
8. Forward Door Post	Same as No. 5	Assemblage of three pieces, as shown in Figure B-7. Maximum cross-section is shown.	Rivets, screws and bolts	D-7, D-8
9. Fuselage Carry thru Structure	Same as No. 5	Formed channels, same dimension front and rear. Approximate dimensions are shown in Figure B-7	Rivets and bolts	D-7, D-9
10. Rear Door Post	Same as No. 5	Assemblage of three pieces, doorpost, jam and skin. Dimensions along uniform length are shown in Figure B-9.	Rivets, screws and bolts	D-10, D-11
11. Upper and Lower Aft Fuselage	Same as No. 5	Upper sections consists of skin-stringer arrangement. Lower section is a semi-monocoque structure. Approximate dimensions are shown in Figure B-9	Rivets	D-10, D-11

TABLE D-1. DESCRIPTION OF AIRPLANE STRUCTURE (Cont'd)

Structure	Materials and Properties	Concepts and Size	Attachments	Applicable Figures
12. Tail Cone	Same as No. 5	Tapered semi-monocoque section. Approximate average section is shown in Figure B-10	Rivets	D-11, D-12
13. Bulkhead at F.S. 108	Same as No. 5	Formed one piece sheet metal Bulb angle reinforce lower section. Approximate cross-section is shown in Figure B-10.	Bolts at wing attachment. Rivets at forward section.	D-10, D-13
14. Wing	6061-T6 E = 10.5×10^6 psi G = 4×10^6 psi F _{ty} = 32×10^3 psi F _{tu} = 38×10^3 psi	Two spar arrangement. Average cross section at constant chord line and for tapered expanse is used.	Bolted to strut and fuselage top	D-14, D-15
15. Wing Strut	Same as No. 14	Extruded tube Uniform cross section	Forged attachment fittings single bolted at each end of strut extrusion	D-14, D-15
<p>F_{ty} = Tensile yield stress F_{cy} = Compressive yield stress F_{tu} = Tensile ultimate stress E = Modulus of Elasticity G = Modulus of Rigidity</p>				

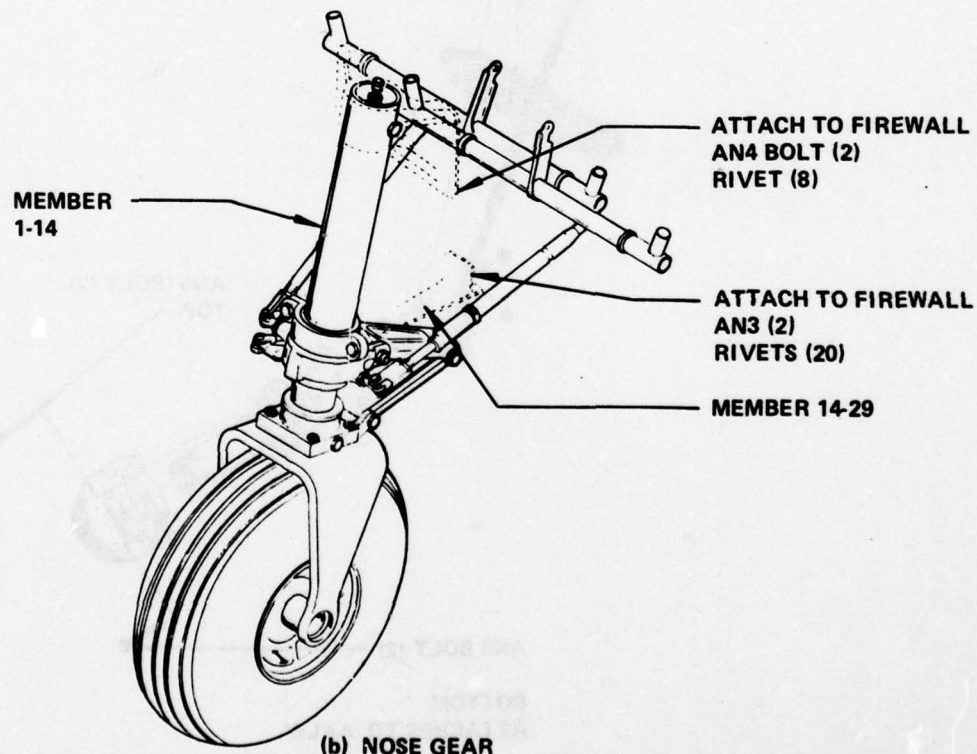
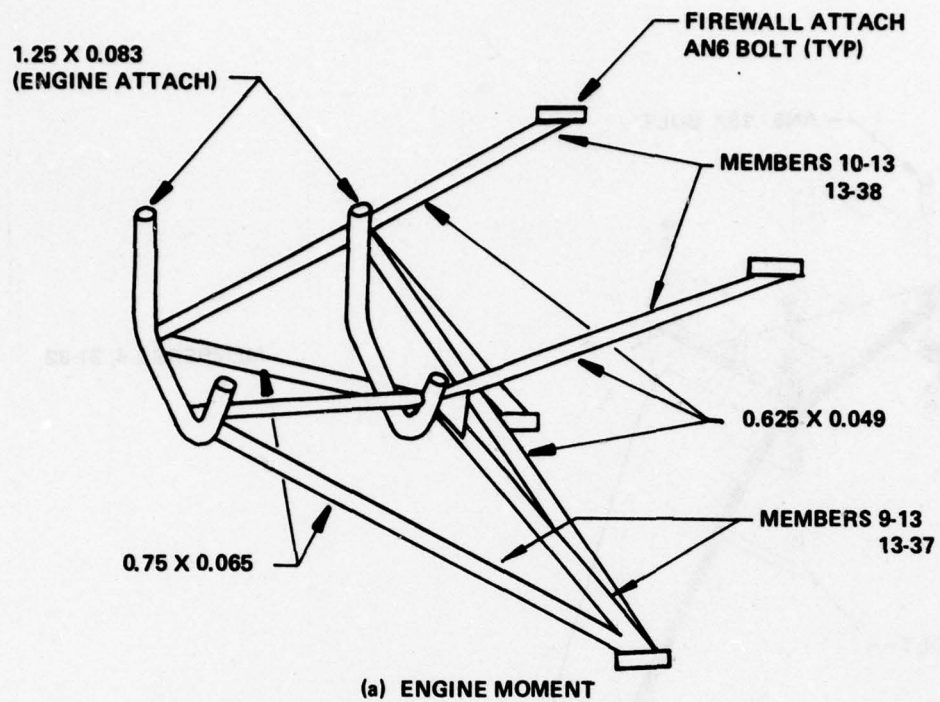


Figure D-2. Engine Mount and Nose Gear Assembly

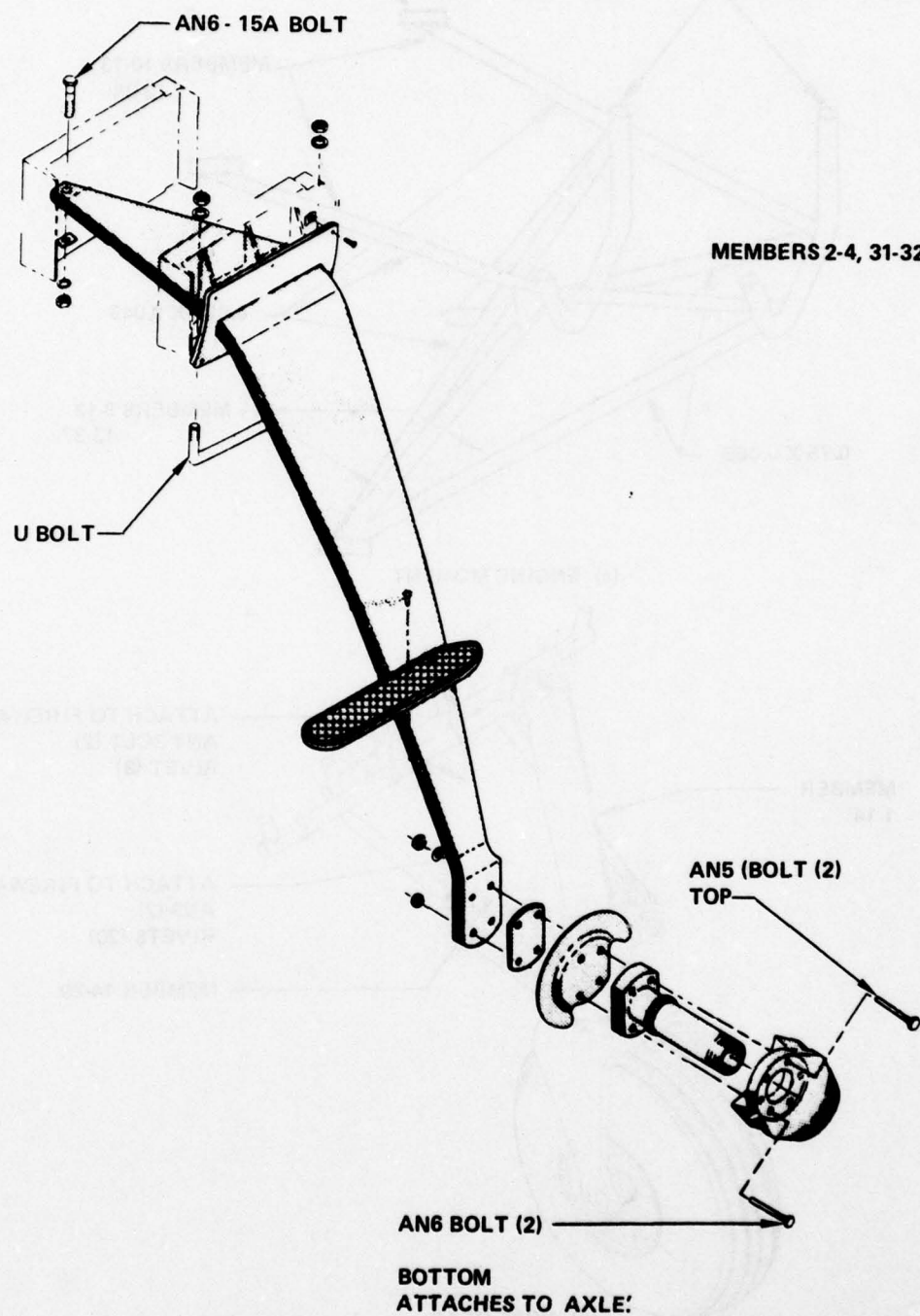


Figure D-3. Main Landing Gear Cantilever Spring Cross Section

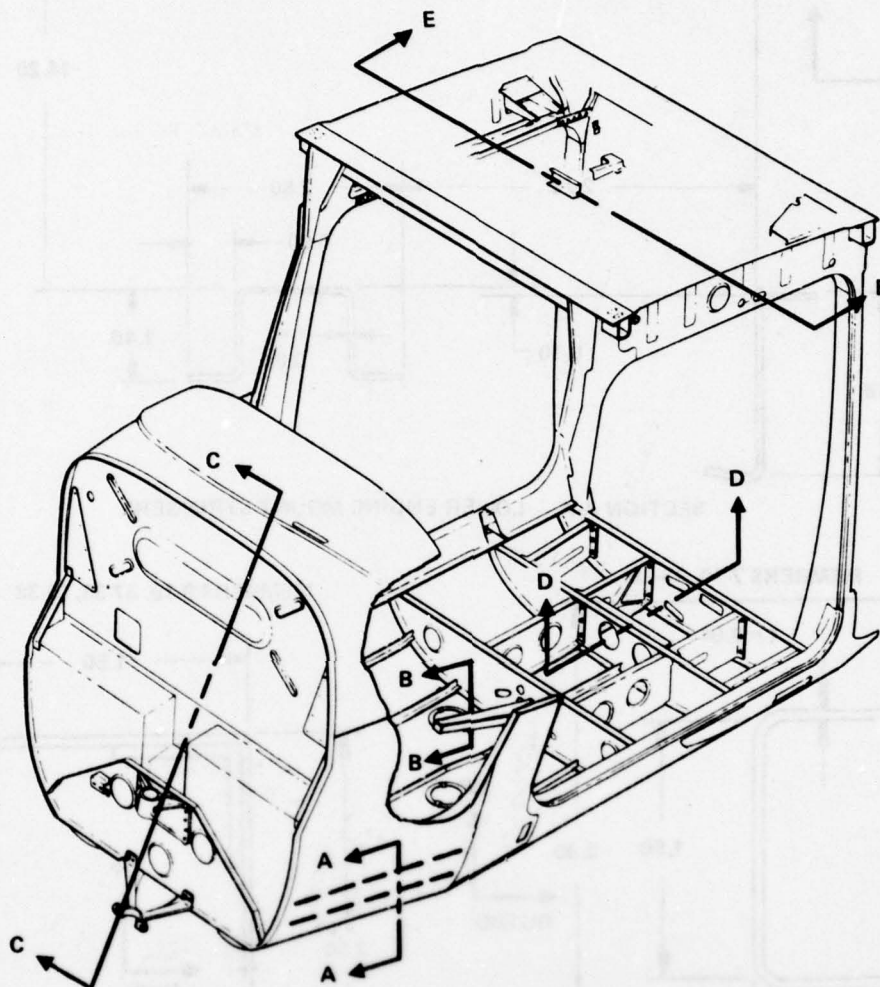
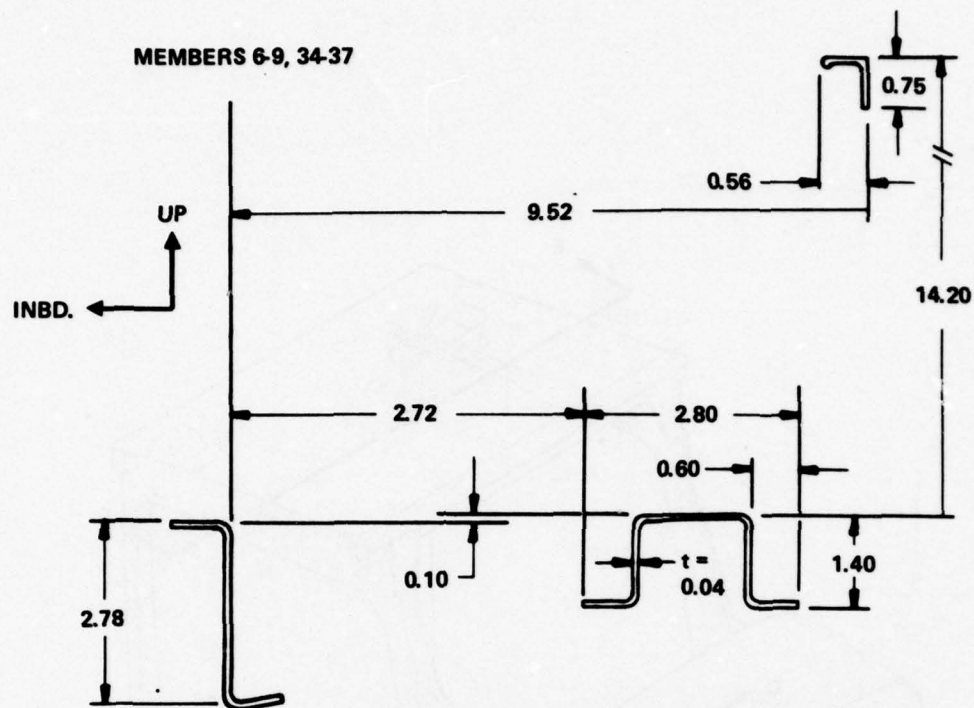
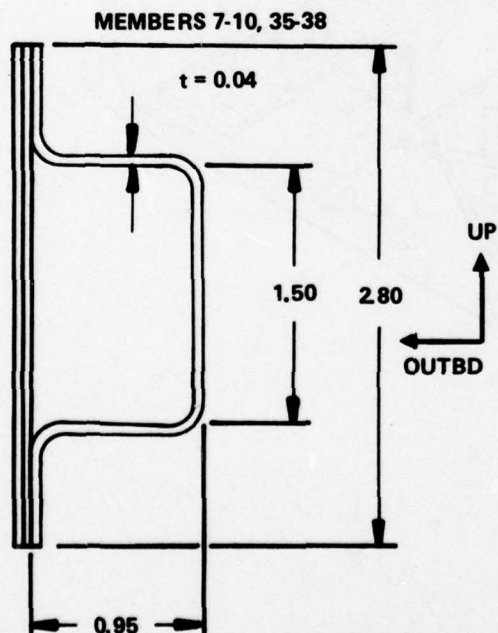


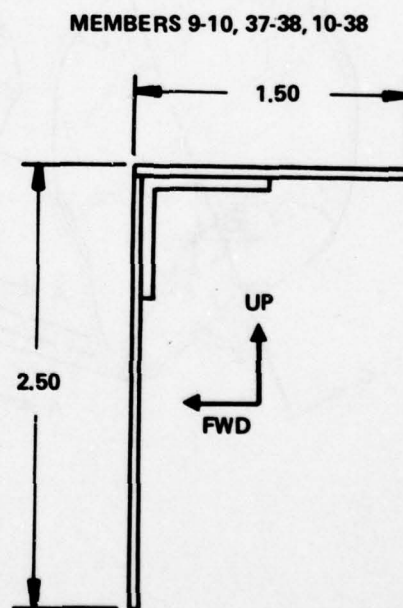
Figure D-4. Fuselage Front and Center Section Assembly



SECTION A-A. LOWER ENGINE MOUNT STRINGERS



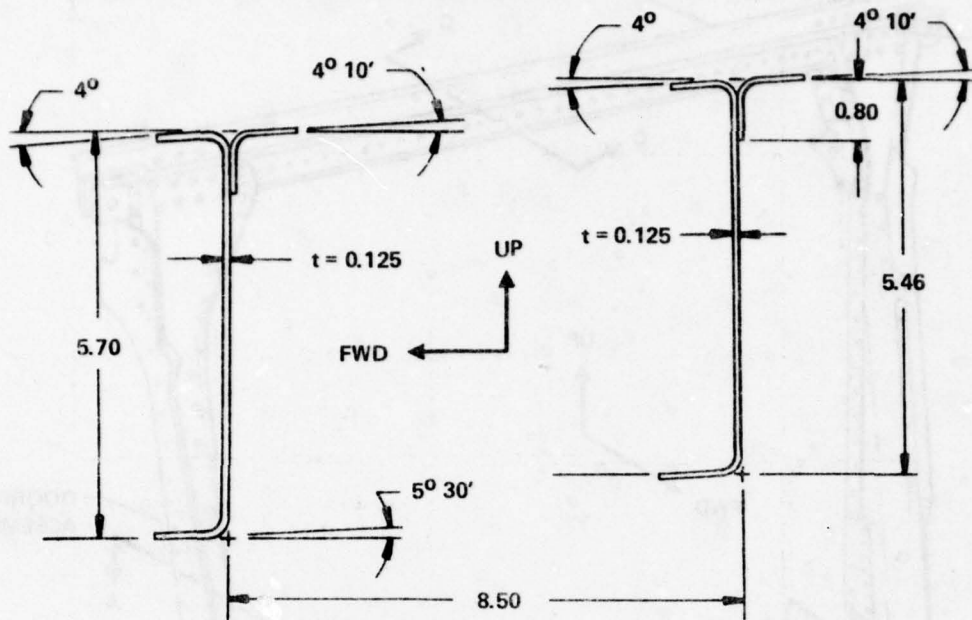
SECTION B-B. UPPER ENGINE MOUNT STRINGER



SECTION C-C. FIREWALL

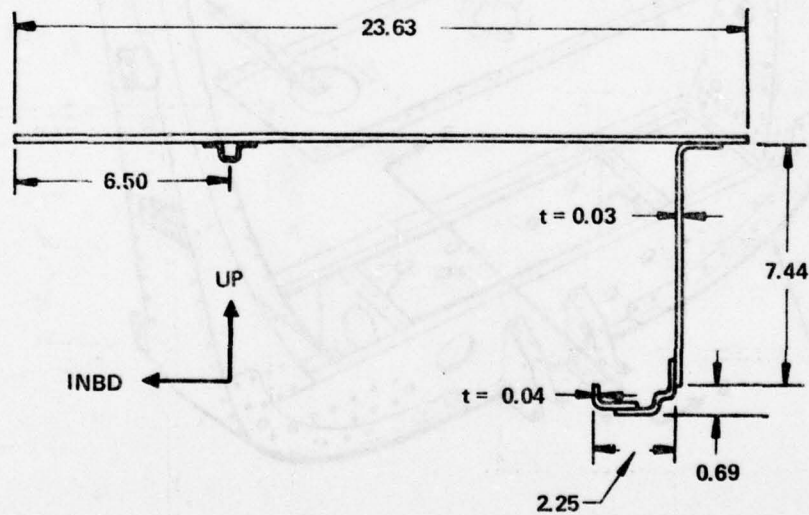
Figure D-5. Fuselage Front and Center Structure Cross Sections

MEMBERS 4-23, 31-47



SECTION D-D. LANDING GEAR BULKHEAD

MEMBERS: 5-8, 33-36



SECTION E-E. UPPER CABIN AREA

Figure D-6. Fuselage Upper Cabin and Landing Gear Bulkhead Cross Sections

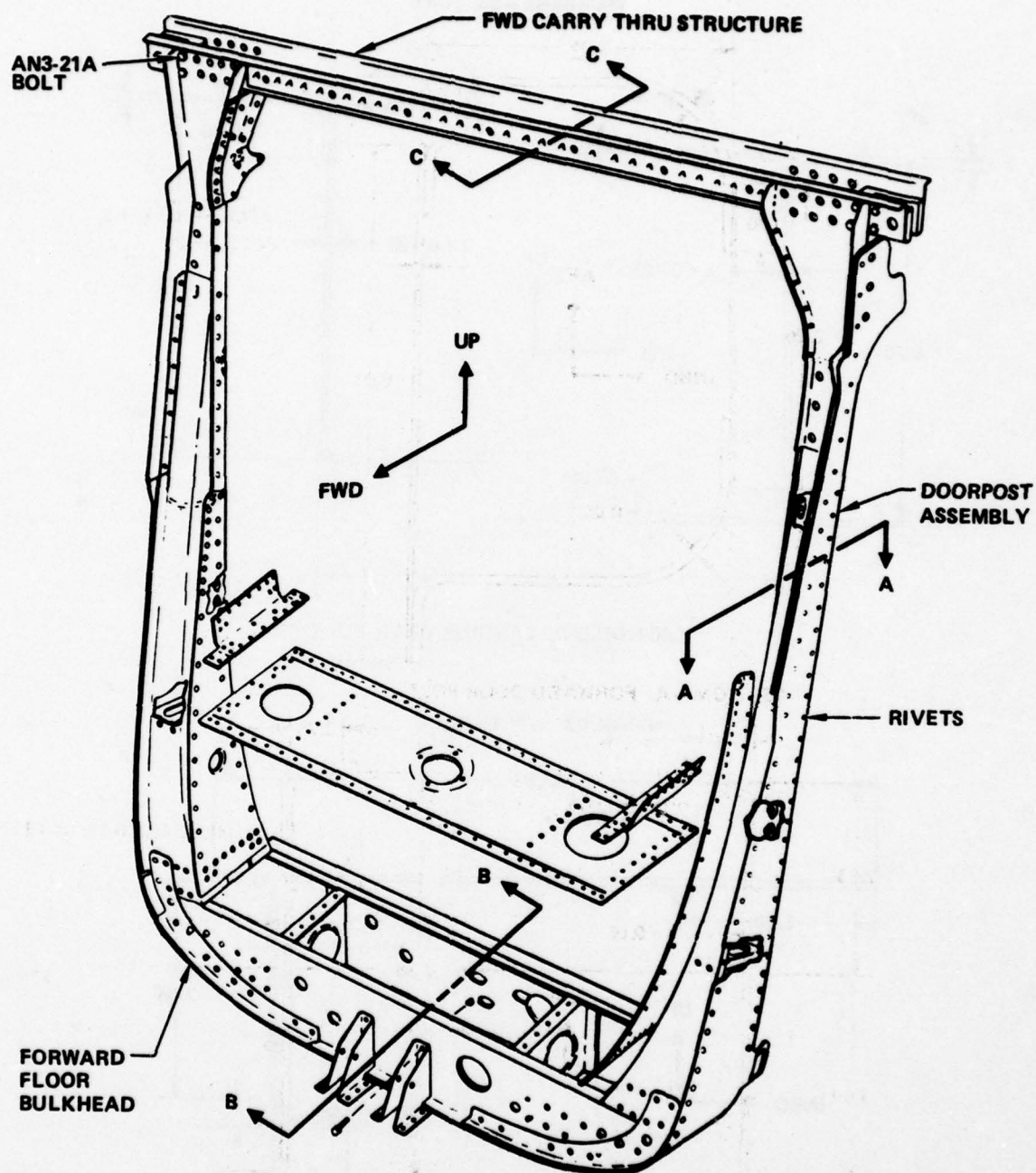
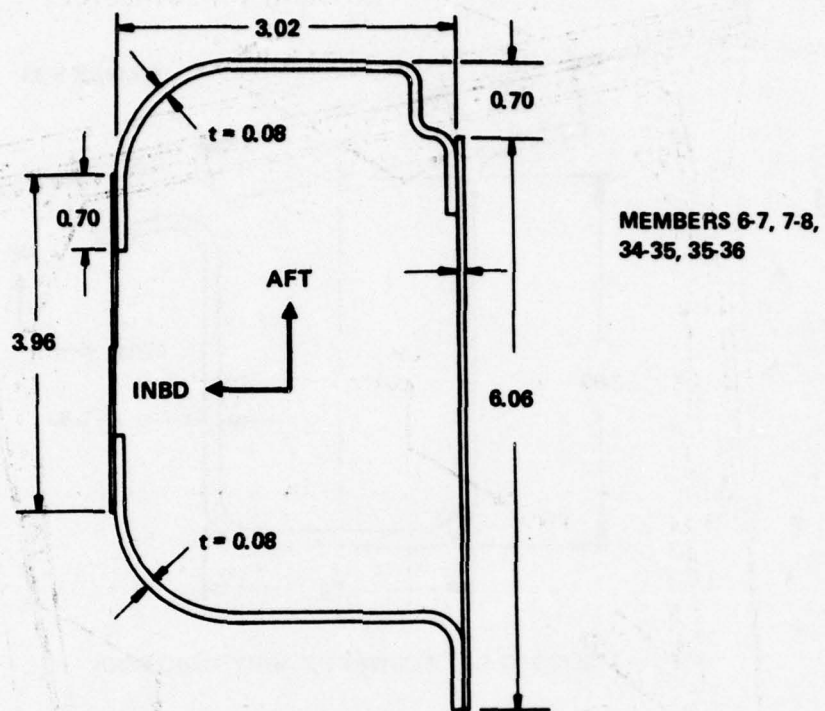
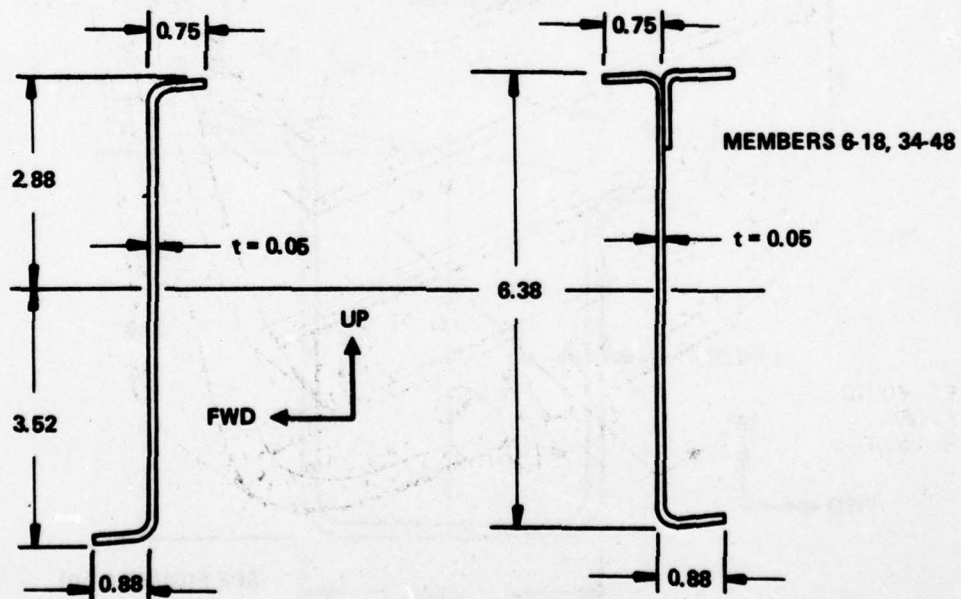


Figure D-7. Forward Door Post, Forward Floor Bulkhead, and Carry Thru Structure

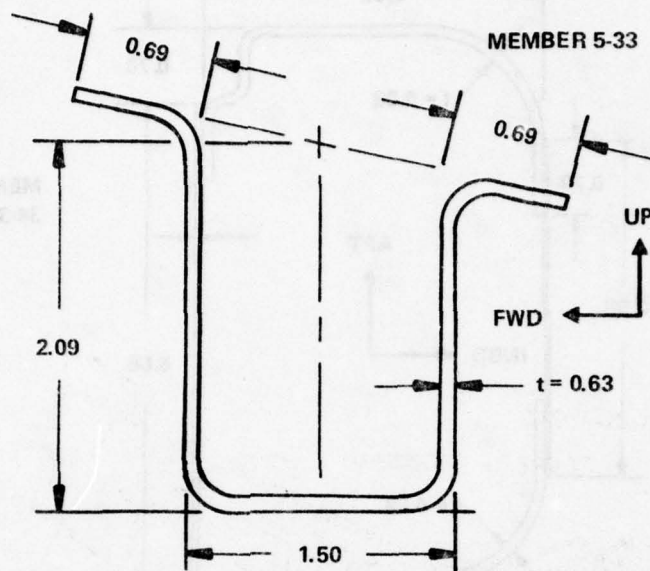


SECTION A-A. FORWARD DOOR POST

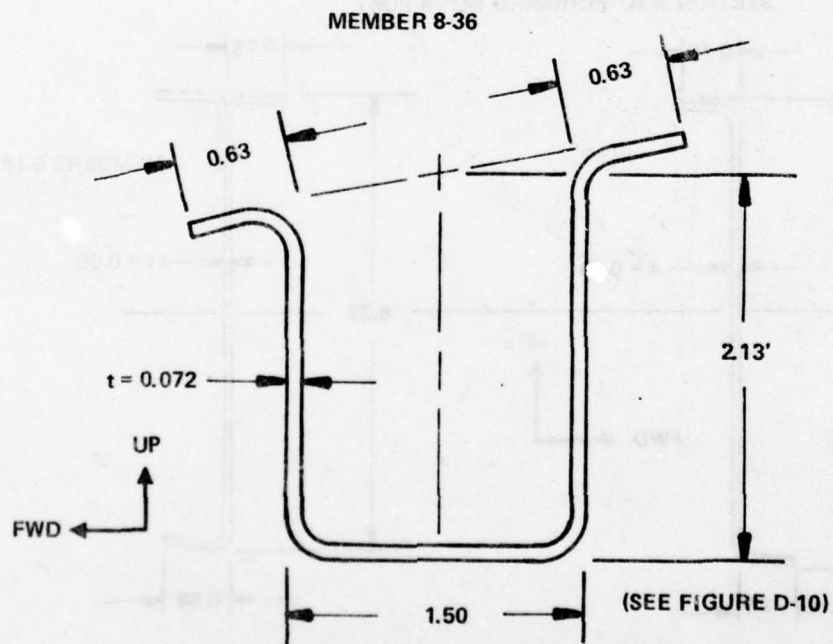


SECTION B-B. FORWARD FLOOR AND BULKHEAD

Figure D-8. Forward Door Post, Forward Floor
Bulkhead Cross Sections



SECTION C-C. FORWARD CARRY THRU SPAR



SECTION D-D. AFT CARRY THRU SPAR

Figure D-9. Forward and Aft Carry Thru Spar Cross Sections

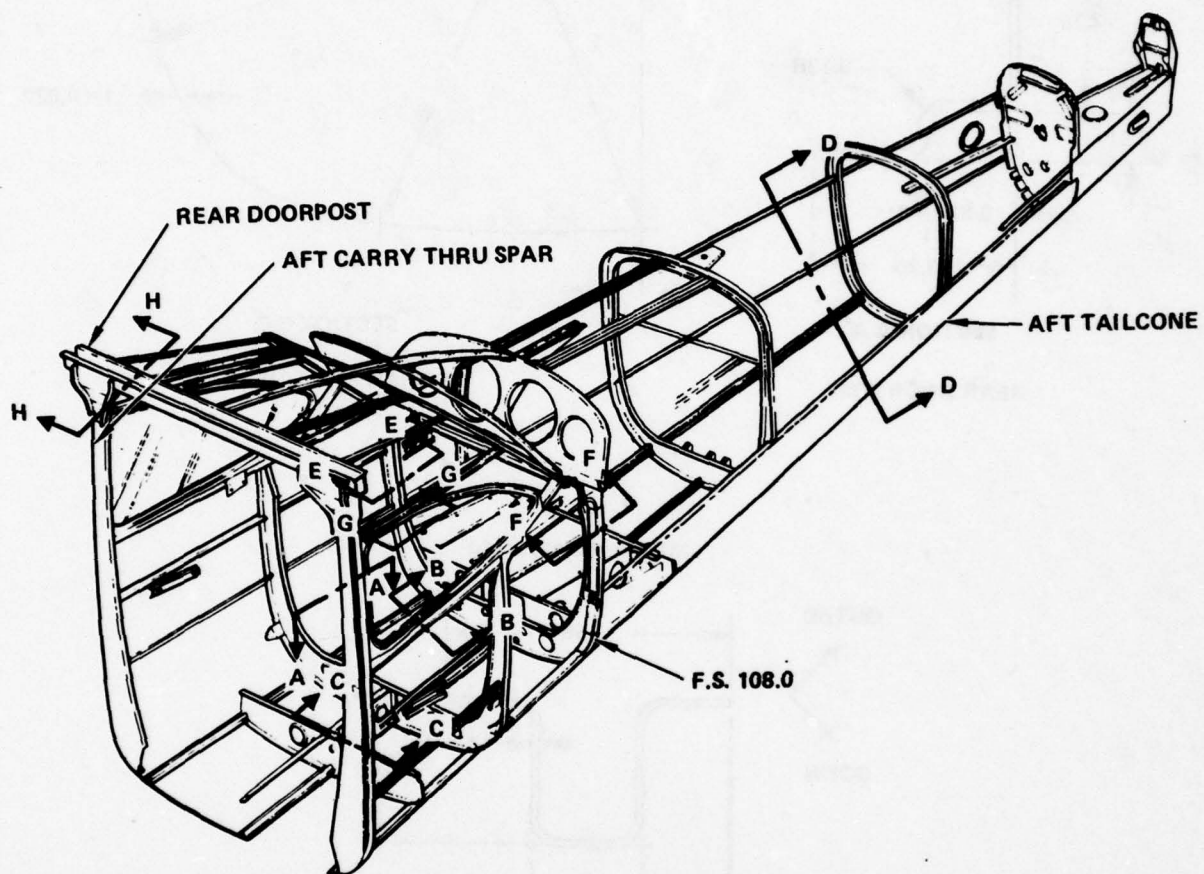


Figure D-10. Aft Fuselage Structure

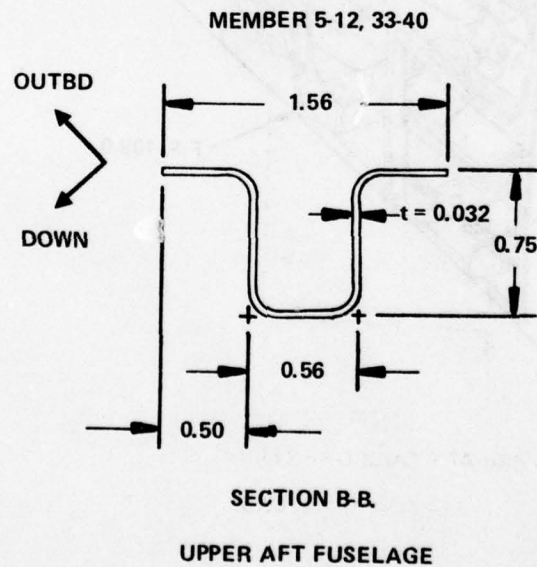
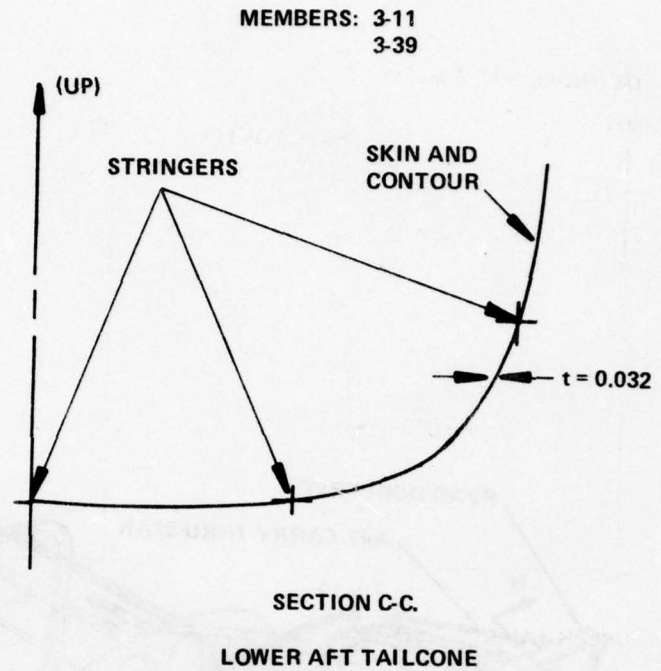
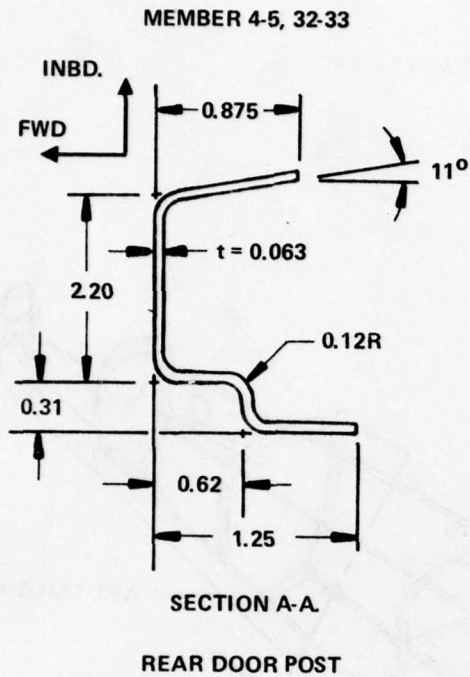
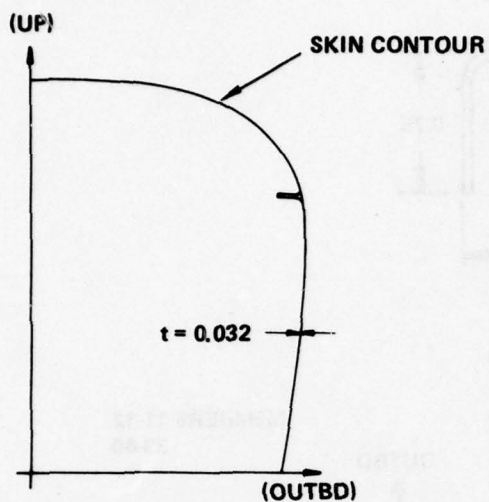


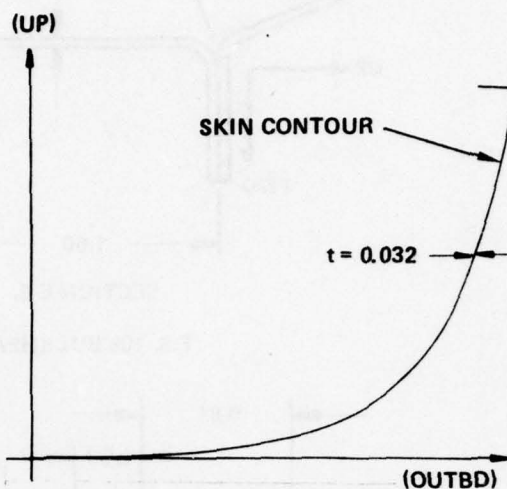
Figure D-11. Rear Door Post and Upper Aft Fuselage Cross Sections

MEMBERS 3-12, 3-40

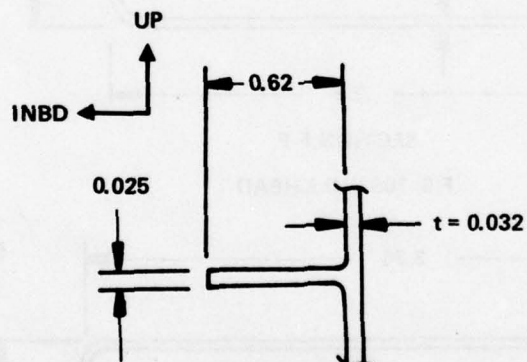


UPPER TAILCONE SECTION

MEMBERS 3-11, 3-39



LOWER TAILCONE SECTION

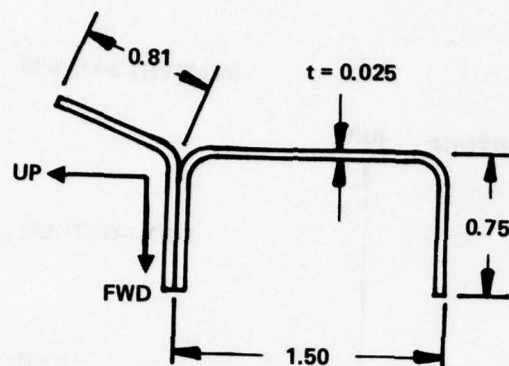


MEMBER 3-12, 3-36, 3-40

UPPER AFT TAILCONE STRINGER

SECTION D-D VIEWS

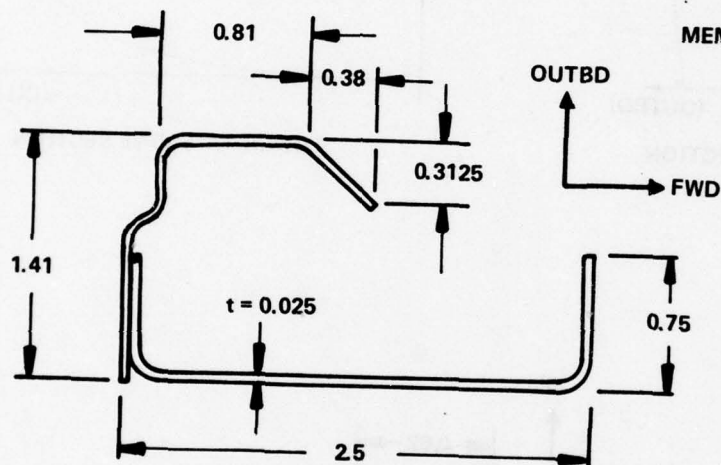
Figure D-12. Tailcone Contours and Stringer



MEMBERS 12-40

SECTION E-E.

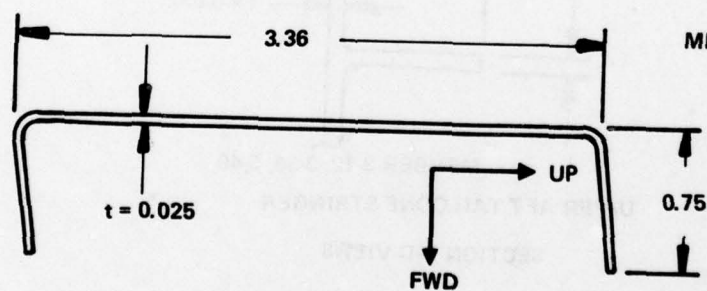
F.S. 108 BULKHEAD



MEMBERS 11-12,
39-40

SECTION F-F.

F.S. 108 BULKHEAD

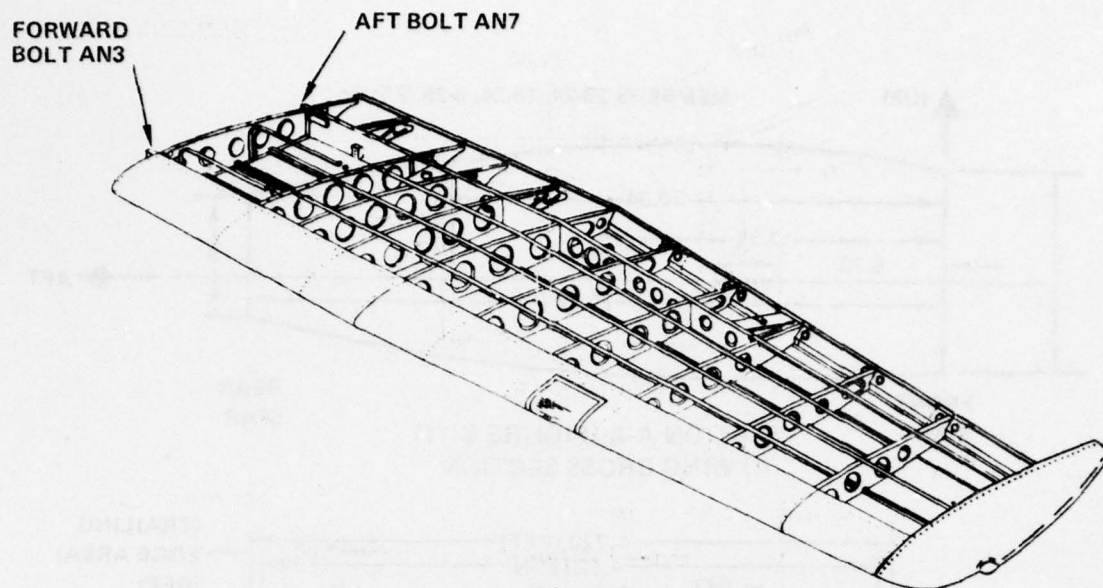


MEMBER 11-39

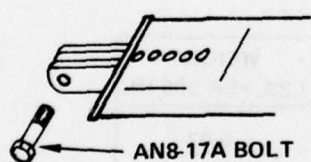
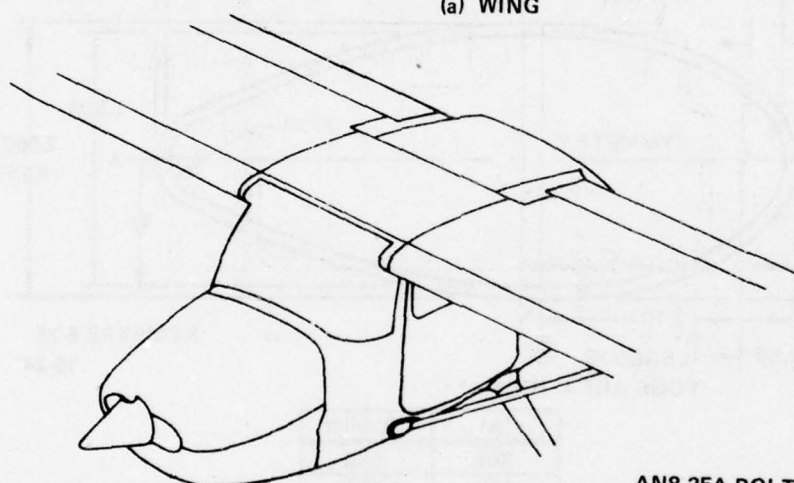
SECTION G-G.

F.S. 108 BULKHEAD

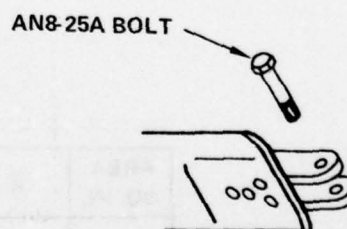
Figure D-13. F.S. 108 Bulkhead Cross-Sections



(a) WING



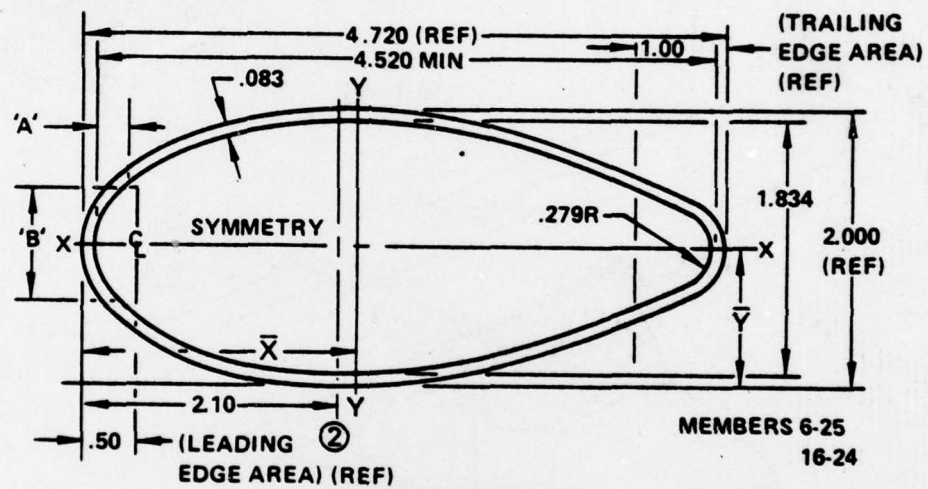
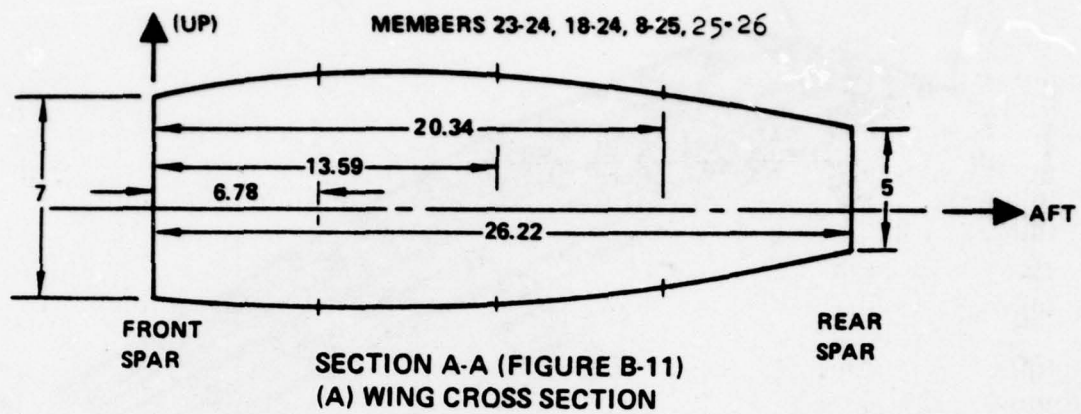
FUSELAGE ATTACH



WING ATTACH

(b) WING STRUT

Figure D-14. Wing and Wing Strut Structure



'A'	'B' MIN
.255	.955
.825	1.565
3.040	1.470
3.755	1.070

AREA SQ. IN.	\bar{X}	\bar{Y}	I'_{XX}	I'_{YY}	WEIGHT LBS. PER 100 IN.
.897	2.27	1.0	.4645	1.8686	8.97

(B) WING STRUT CROSS SECTION

Figure D-15. Wing and Wing Strut Structure Cross Sections

BEST AVAILABLE COPY

MASS DATA										MASS MOMENTS OF INERTIA (LB-IN-SEC**2)									
MASS COORDINATES P.C.S.S.L.M.L.																			
WEIGHTS																			
I	W	X**	Y**	Z**	IX	IV	IY	IY	IY	I	W	X**	Y**	Z**	IX	IV	IY	IY	IY
1	2.116000 01	-7.500000 00	0.00	-4.110000 01	0.000000 00	1.134100 00	1.134100 00	1.134100 00	1.134100 00	1	W	X**	Y**	Z**	IX	IV	IY	IY	IY
2	3.600000 01	5.795000 01	4.500000 01	-3.300000 01	2.000000 00	6.530000 00	6.530000 00	6.530000 00	6.530000 00	2	W	X**	Y**	Z**	IX	IV	IY	IY	IY
3	1.000000 01	2.000000 01	0.00	1.000000 01	0.00	3.172000 01	3.172000 01	3.172000 01	3.172000 01	3	W	X**	Y**	Z**	IX	IV	IY	IY	IY
4	3.557000 01	6.530000 01	1.000000 01	-1.000000 01	0.00	9.950000 00	9.950000 00	9.950000 00	9.950000 00	4	W	X**	Y**	Z**	IX	IV	IY	IY	IY
5	1.000000 01	0.00	0.00	0.00	0.00	0.00	0.00	0.00	0.00	5	W	X**	Y**	Z**	IX	IV	IY	IY	IY
6	1.000000 01	0.00	0.00	0.00	0.00	0.00	0.00	0.00	0.00	6	W	X**	Y**	Z**	IX	IV	IY	IY	IY
7	1.000000 01	0.00	0.00	0.00	0.00	0.00	0.00	0.00	0.00	7	W	X**	Y**	Z**	IX	IV	IY	IY	IY
8	1.000000 01	0.00	0.00	0.00	0.00	0.00	0.00	0.00	0.00	8	W	X**	Y**	Z**	IX	IV	IY	IY	IY
9	1.000000 01	0.00	0.00	0.00	0.00	0.00	0.00	0.00	0.00	9	W	X**	Y**	Z**	IX	IV	IY	IY	IY
10	1.000000 01	0.00	0.00	0.00	0.00	0.00	0.00	0.00	0.00	10	W	X**	Y**	Z**	IX	IV	IY	IY	IY
11	1.000000 01	0.00	0.00	0.00	0.00	0.00	0.00	0.00	0.00	11	W	X**	Y**	Z**	IX	IV	IY	IY	IY
12	1.000000 01	0.00	0.00	0.00	0.00	0.00	0.00	0.00	0.00	12	W	X**	Y**	Z**	IX	IV	IY	IY	IY
13	1.000000 01	0.00	0.00	0.00	0.00	0.00	0.00	0.00	0.00	13	W	X**	Y**	Z**	IX	IV	IY	IY	IY
14	1.000000 01	0.00	0.00	0.00	0.00	0.00	0.00	0.00	0.00	14	W	X**	Y**	Z**	IX	IV	IY	IY	IY
15	1.000000 01	0.00	0.00	0.00	0.00	0.00	0.00	0.00	0.00	15	W	X**	Y**	Z**	IX	IV	IY	IY	IY
16	1.000000 01	0.00	0.00	0.00	0.00	0.00	0.00	0.00	0.00	16	W	X**	Y**	Z**	IX	IV	IY	IY	IY
17	1.000000 01	0.00	0.00	0.00	0.00	0.00	0.00	0.00	0.00	17	W	X**	Y**	Z**	IX	IV	IY	IY	IY
18	1.000000 01	0.00	0.00	0.00	0.00	0.00	0.00	0.00	0.00	18	W	X**	Y**	Z**	IX	IV	IY	IY	IY
19	1.000000 01	0.00	0.00	0.00	0.00	0.00	0.00	0.00	0.00	19	W	X**	Y**	Z**	IX	IV	IY	IY	IY
20	1.000000 01	0.00	0.00	0.00	0.00	0.00	0.00	0.00	0.00	20	W	X**	Y**	Z**	IX	IV	IY	IY	IY
21	1.000000 01	0.00	0.00	0.00	0.00	0.00	0.00	0.00	0.00	21	W	X**	Y**	Z**	IX	IV	IY	IY	IY
22	1.000000 01	0.00	0.00	0.00	0.00	0.00	0.00	0.00	0.00	22	W	X**	Y**	Z**	IX	IV	IY	IY	IY
23	1.000000 01	0.00	0.00	0.00	0.00	0.00	0.00	0.00	0.00	23	W	X**	Y**	Z**	IX	IV	IY	IY	IY
24	1.000000 01	0.00	0.00	0.00	0.00	0.00	0.00	0.00	0.00	24	W	X**	Y**	Z**	IX	IV	IY	IY	IY
25	1.000000 01	0.00	0.00	0.00	0.00	0.00	0.00	0.00	0.00	25	W	X**	Y**	Z**	IX	IV	IY	IY	IY
26	1.000000 01	0.00	0.00	0.00	0.00	0.00	0.00	0.00	0.00	26	W	X**	Y**	Z**	IX	IV	IY	IY	IY
27	1.000000 01	0.00	0.00	0.00	0.00	0.00	0.00	0.00	0.00	27	W	X**	Y**	Z**	IX	IV	IY	IY	IY
28	1.000000 01	0.00	0.00	0.00	0.00	0.00	0.00	0.00	0.00	28	W	X**	Y**	Z**	IX	IV	IY	IY	IY
29	1.000000 01	0.00	0.00	0.00	0.00	0.00	0.00	0.00	0.00	29	W	X**	Y**	Z**	IX	IV	IY	IY	IY
30	1.000000 01	0.00	0.00	0.00	0.00	0.00	0.00	0.00	0.00	30	W	X**	Y**	Z**	IX	IV	IY	IY	IY
31	1.000000 01	0.00	0.00	0.00	0.00	0.00	0.00	0.00	0.00	31	W	X**	Y**	Z**	IX	IV	IY	IY	IY
32	1.000000 01	0.00	0.00	0.00	0.00	0.00	0.00	0.00	0.00	32	W	X**	Y**	Z**	IX	IV	IY	IY	IY
33	1.000000 01	0.00	0.00	0.00	0.00	0.00	0.00	0.00	0.00	33	W	X**	Y**	Z**	IX	IV	IY	IY	IY
34	1.000000 01	0.00	0.00	0.00	0.00	0.00	0.00	0.00	0.00	34	W	X**	Y**	Z**	IX	IV	IY	IY	IY
35	1.000000 01	0.00	0.00	0.00	0.00	0.00	0.00	0.00	0.00	35	W	X**	Y**	Z**	IX	IV	IY	IY	IY
36	1.000000 01	0.00	0.00	0.00	0.00	0.00	0.00	0.00	0.00	36	W	X**	Y**	Z**	IX	IV	IY	IY	IY
37	1.000000 01	0.00	0.00	0.00	0.00	0.00	0.00	0.00	0.00	37	W	X**	Y**	Z**	IX	IV	IY	IY	IY
38	1.000000 01	0.00	0.00	0.00	0.00	0.00	0.00	0.00	0.00	38	W	X**	Y**	Z**	IX	IV	IY	IY	IY
39	1.000000 01	0.00	0.00	0.00	0.00	0.00	0.00	0.00	0.00	39	W	X**	Y**	Z**	IX	IV	IY	IY	IY
40	1.000000 01	0.00	0.00	0.00	0.00	0.00	0.00	0.00	0.00	40	W	X**	Y**	Z**	IX	IV	IY	IY	IY
41	1.000000 01	0.00	0.00	0.00	0.00	0.00	0.00	0.00	0.00	41	W	X**	Y**	Z**	IX	IV	IY	IY	IY
42	1.000000 01	0.00	0.00	0.00	0.00	0.00	0.00	0.00	0.00	42	W	X**	Y**	Z**	IX	IV	IY	IY	IY
43	1.000000 01	0.00	0.00	0.00	0.00	0.00	0.00	0.00	0.00	43	W	X**	Y**	Z**	IX	IV	IY	IY	IY
44	1.000000 01	0.00	0.00	0.00	0.00	0.00	0.00	0.00	0.00	44	W	X**	Y**	Z**	IX	IV	IY	IY	IY
45	1.000000 01	0.00	0.00	0.00	0.00	0.00	0.00	0.00	0.00	45	W	X**	Y**	Z**	IX	IV	IY	IY	IY
46	1.000000 01	0.00	0.00	0.00	0.00	0.00	0.00	0.00	0.00	46	W	X**	Y**	Z**	IX	IV	IY	IY	IY
47	1.000000 01	0.00	0.00	0.00	0.00	0.00	0.00	0.00	0.00	47	W	X**	Y**	Z**	IX	IV	IY	IY	IY
48	1.000000 01	0.00	0.00	0.00	0.00	0.00	0.00	0.00	0.00	48	W	X**	Y**	Z**	IX	IV	IY	IY	IY

Figure D-16. Math Model Mass Data

BEST AVAILABLE COPY

NETS POINT DATA

STATION	N.O.	DATE	TIME	COORDINATES	E.S.	R.L.	M.L.
1	4	1	5.100000	01	1.500000	01	-1.550000
2	1	1	3.300000	01	1.500000	01	-1.550000
3	1	1	0.0	01	1.461000	01	-1.825000
4	1	1	3.400000	01	1.956000	01	5.590000
5	1	1	-2.970000	01	9.070000	00	-5.310000
6	1	1	-1.260000	01	3.070000	00	-5.310000
7	1	1	-1.300000	01	0.0	01	1.300000
8	1	1	-2.160000	01	0.0	01	-8.440000
9	1	1	3.300000	01	5.000000	00	-1.550000
10	1	1	6.100000	01	8.000000	00	-1.550000
11	1	1	4.600000	01	1.500000	01	-9.400000
12	2	2	4.600000	01	5.000000	00	-8.400000
13	3	3	3.400000	01	1.500000	01	-9.400000
14	4	4	3.400000	01	5.000000	00	-9.400000
15	1	1	3.300000	01	1.500000	01	-1.550000
16	1	1	4.500000	01	5.000000	01	-1.550000
17	1	1	4.500000	01	5.000000	01	-1.550000
18	1	1	4.500000	01	5.000000	01	-1.550000
19	1	1	4.500000	01	5.000000	01	-1.550000
20	1	1	4.500000	01	5.000000	01	-1.550000
21	1	1	4.500000	01	5.000000	01	-1.550000
22	1	1	4.500000	01	5.000000	01	-1.550000
23	1	1	4.500000	01	5.000000	01	-1.550000
24	1	1	4.500000	01	5.000000	01	-1.550000
25	1	1	4.500000	01	5.000000	01	-1.550000
26	1	1	4.500000	01	5.000000	01	-1.550000
27	1	1	4.500000	01	5.000000	01	-1.550000
28	1	1	4.500000	01	5.000000	01	-1.550000
29	1	1	4.500000	01	5.000000	01	-1.550000
30	1	1	4.500000	01	5.000000	01	-1.550000
31	1	1	4.500000	01	5.000000	01	-1.550000
32	1	1	4.500000	01	5.000000	01	-1.550000
33	1	1	4.500000	01	5.000000	01	-1.550000
34	1	1	4.500000	01	5.000000	01	-1.550000
35	1	1	4.500000	01	5.000000	01	-1.550000
36	1	1	4.500000	01	5.000000	01	-1.550000
37	1	1	4.500000	01	5.000000	01	-1.550000
38	1	1	4.500000	01	5.000000	01	-1.550000
39	1	1	4.500000	01	5.000000	01	-1.550000
40	1	1	4.500000	01	5.000000	01	-1.550000
41	1	1	4.500000	01	5.000000	01	-1.550000
42	1	1	4.500000	01	5.000000	01	-1.550000
43	1	1	4.500000	01	5.000000	01	-1.550000
44	1	1	4.500000	01	5.000000	01	-1.550000
45	1	1	4.500000	01	5.000000	01	-1.550000
46	1	1	4.500000	01	5.000000	01	-1.550000
47	1	1	4.500000	01	5.000000	01	-1.550000
48	1	1	4.500000	01	5.000000	01	-1.550000
49	1	1	4.500000	01	5.000000	01	-1.550000
50	1	1	4.500000	01	5.000000	01	-1.550000

EXTERNAL SPRING DATA

SPRING	FREE LENGTH	FRICTION COEFFICIENT	AUTOMATIC SPRING	PLOTTING FORCE	GROUND FLEXIBILITY
1 4 1	1.000000	0.0	1.000000	0.0	0.0
1 1 1	7.000000	4.000000	1.000000	0.0	0.0
1 3 0	7.000000	4.000000	1.000000	0.0	0.0
2 1 0	8.000000	4.000000	1.000000	0.0	0.0
2 3 0	8.000000	4.000000	1.000000	0.0	0.0
3 1 0	1.000000	4.000000	1.000000	0.0	0.0
4 3 0	4.000000	4.000000	1.000000	0.0	0.0
6 3 0	6.000000	4.000000	1.000000	0.0	0.0
9 1 0	1.000000	4.000000	1.000000	0.0	0.0
9 3 0	2.000000	4.000000	1.000000	0.0	0.0
11 3 0	2.000000	4.000000	1.000000	0.0	0.0
13 1 0	2.000000	4.000000	1.000000	0.0	0.0
13 3 0	1.500000	4.000000	1.000000	0.0	0.0
17 1 0	1.000000	4.000000	1.000000	0.0	0.0
17 3 0	1.000000	4.000000	1.000000	0.0	0.0
18 3 0	1.000000	4.000000	1.000000	0.0	0.0
19 3 0	1.000000	4.000000	1.000000	0.0	0.0
25 1 0	2.000000	4.000000	1.000000	0.0	0.0
27 3 0	4.000000	4.000000	1.000000	0.0	0.0
28 3 0	4.000000	4.000000	1.000000	0.0	0.0
29 1 0	1.000000	4.000000	1.000000	0.0	0.0
29 3 0	5.000000	4.000000	1.000000	0.0	0.0
30 3 0	1.000000	4.000000	1.000000	0.0	0.0
31 1 0	8.000000	4.000000	1.000000	0.0	0.0
31 3 0	9.000000	4.000000	1.000000	0.0	0.0
33 3 0	4.000000	4.000000	1.000000	0.0	0.0
34 3 0	5.000000	4.000000	1.000000	0.0	0.0
37 1 0	1.000000	4.000000	1.000000	0.0	0.0
37 3 0	3.000000	4.000000	1.000000	0.0	0.0
39 3 0	2.000000	4.000000	1.000000	0.0	0.0
43 1 0	1.000000	4.000000	1.000000	0.0	0.0
43 3 0	1.000000	4.000000	1.000000	0.0	0.0

SPRING	DEFLECTION COORDINATES	SPRING AXIAL FORCES
1 4 1	5.000000	5.000000
1 1 1	1.000000	1.000000
1 3 0	1.000000	1.000000
2 1 0	1.000000	1.000000
2 3 0	1.000000	1.000000
3 1 0	1.000000	1.000000
4 3 0	1.000000	1.000000
6 3 0	1.000000	1.000000
9 1 0	1.000000	1.000000
9 3 0	1.000000	1.000000
11 3 0	1.000000	1.000000
13 1 0	1.000000	1.000000
13 3 0	1.000000	1.000000
17 1 0	1.000000	1.000000
17 3 0	1.000000	1.000000
18 3 0	1.000000	1.000000
19 3 0	1.000000	1.000000
25 1 0	1.000000	1.000000
27 3 0	1.000000	1.000000
28 3 0	1.000000	1.000000
29 1 0	1.000000	1.000000
29 3 0	1.000000	1.000000
30 3 0	1.000000	1.000000
31 1 0	1.000000	1.000000
31 3 0	1.000000	1.000000
33 3 0	1.000000	1.000000
34 3 0	1.000000	1.000000
37 1 0	1.000000	1.000000
37 3 0	1.000000	1.000000
39 3 0	1.000000	1.000000
43 1 0	1.000000	1.000000
43 3 0	1.000000	1.000000

Figure D-18. Math Model External Spring Data (Sheet 1 of 2)

BEST AVAILABLE COPY

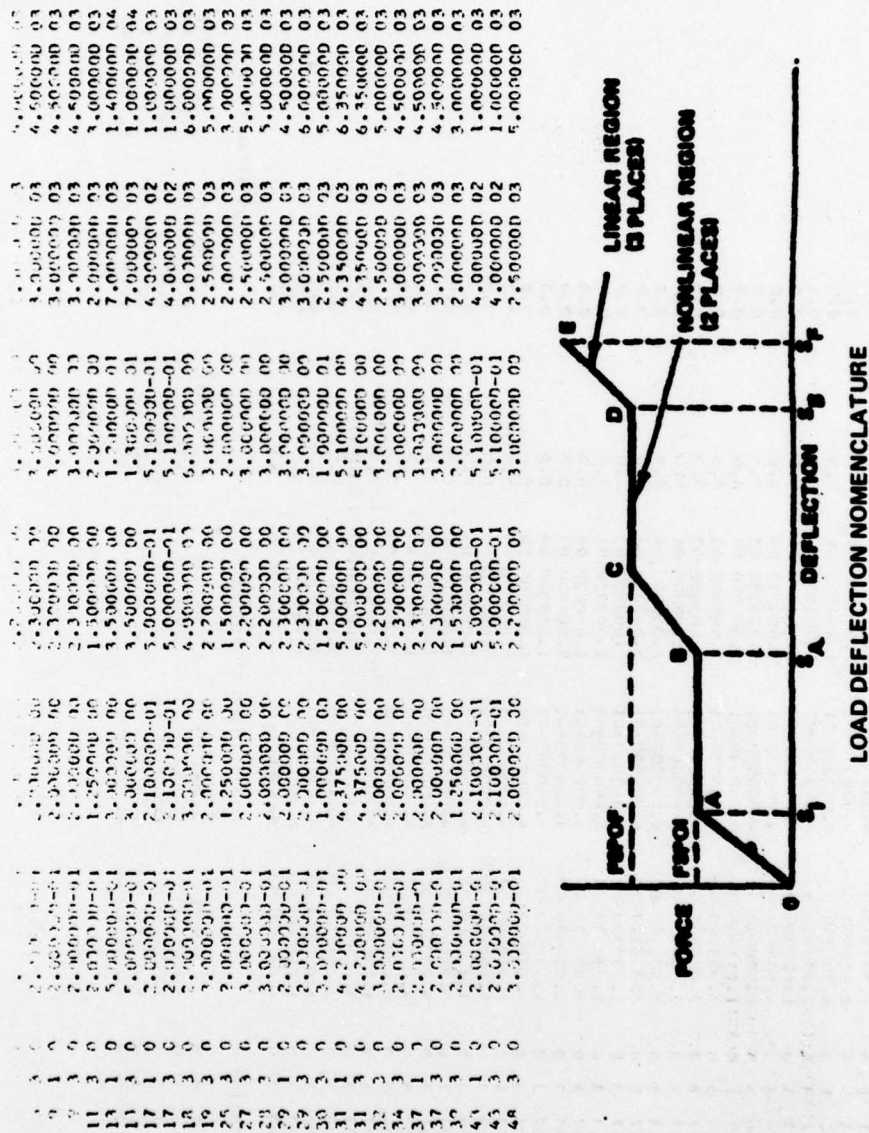


Figure D-18. Con't (Sheet 2 of 2)

BEST AVAILABLE COPY

MATERIAL PROPERTIES					
MATERIAL ID.	MODULUS OF ELASTICITY	MODULUS OF RIGIDITY	TENSION STRESS	COMPRESS. STRESS	SHEAR STRESS
1	3.00000 07	1.10000 07	75000.	75000.	37500.
2	3.00000 07	1.10000 07	205000.	205000.	102500.
3	3.00000 07	1.25000 07	70000.	46000.	35000.
4	1.00000 07	4.00000 06	47000.	39000.	22000.
5	1.00000 07	3.00000 06	35000.	34000.	17000.
6	1.00000 07	3.00000 06	15000.	16000.	7500.
7	1.00000 06	3.00000 05	15000.	16000.	7500.
8	1.00000 06	0.0	15000.	16000.	7500.
9	1.00000 06	3.00000 05	15000.	16000.	7500.
10	1.00000 06	3.00000 05	15000.	16000.	7500.

NOTE: MODULUS IN LB/IN²
STRESS IN LB/IN²

Figure D-19. Math Model Material Properties

D-26

Figure D-20. Math Model Internal Beam Data (Sheet 1 of 2)

BEST AVAILABLE COPY

[illegible]

Figure D-20. Con't (Sheet 2 of 2)

BEST AVAILABLE COPY

UNSYMMETRICAL BEAM DATA

BEAM	COMPRESSION FLAG	DEADEND
1J 1 J 4 5	1.000	0.0
15 5 21 0 1	1	0.0
25 7 9 2 0	1	0.0
50 5 10 0 0	1	0.0
59 1 13 0 4	-1	1.2000 01
70 33 45 0 1	1	0.0
90 35 37 0 0	1	0.0
95 34 38 0 0	1	0.0

NOTE:

- IJ = BEAM NUMBER
- I = MASS POINT, i^{th} END
- J = MASS POINT, j^{th} END
- M = NODE POINT, i^{th} END
- N = NODE POINT, j^{th} END
- IJUB = +1 TENSION
- IJUB = -1 COMPRESSION

Figure D-21. Math Model Unsymmetrical Beam Data

BEST AVAILABLE COPY

NONLINEAR BEAM DATA

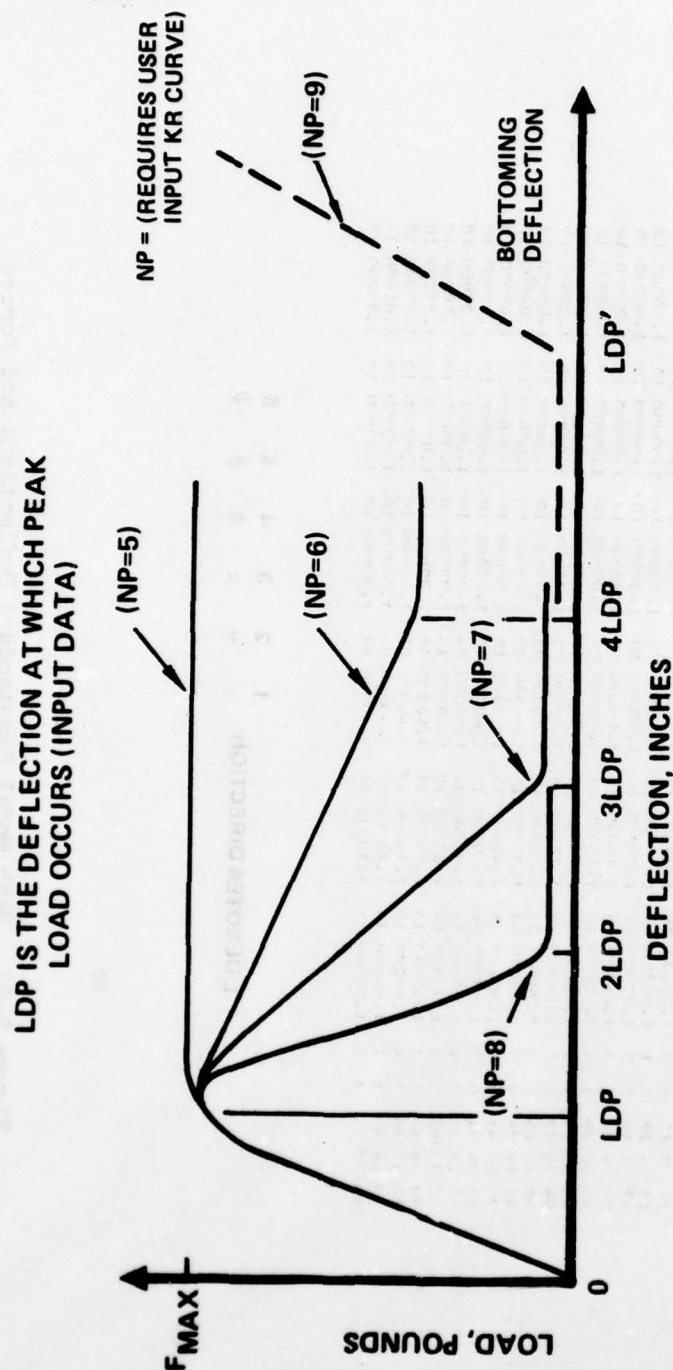
LINE	ITEM	SECTION	STANDARD TABLE NO.	LINEAR DEFLECTION	NONLINEAR DEFLECTION
1	1	1	10	0.0	0.0
1	1	1	10	1.5000E-01	0.0
1	1	1	10	5.0000E-01	0.0
1	1	1	10	2.5000E-01	0.0
1	1	1	10	5.5000E-01	0.0
1	1	1	10	1.0000E-01	0.0
1	1	1	10	1.0000E-02	0.0
1	1	1	10	1.0000E-03	0.0
1	1	1	10	1.0000E-04	0.0
1	1	1	10	1.0000E-05	0.0
1	1	1	10	1.0000E-06	0.0
1	1	1	10	1.0000E-07	0.0
1	1	1	10	1.0000E-08	0.0
1	1	1	10	1.0000E-09	0.0
1	1	1	10	1.0000E-10	0.0
1	1	1	10	1.0000E-11	0.0
1	1	1	10	1.0000E-12	0.0
1	1	1	10	1.0000E-13	0.0
1	1	1	10	1.0000E-14	0.0
1	1	1	10	1.0000E-15	0.0
1	1	1	10	1.0000E-16	0.0
1	1	1	10	1.0000E-17	0.0
1	1	1	10	1.0000E-18	0.0
1	1	1	10	1.0000E-19	0.0
1	1	1	10	1.0000E-20	0.0
1	1	1	10	1.0000E-21	0.0
1	1	1	10	1.0000E-22	0.0
1	1	1	10	1.0000E-23	0.0
1	1	1	10	1.0000E-24	0.0
1	1	1	10	1.0000E-25	0.0
1	1	1	10	1.0000E-26	0.0
1	1	1	10	1.0000E-27	0.0
1	1	1	10	1.0000E-28	0.0
1	1	1	10	1.0000E-29	0.0
1	1	1	10	1.0000E-30	0.0
1	1	1	10	1.0000E-31	0.0
1	1	1	10	1.0000E-32	0.0
1	1	1	10	1.0000E-33	0.0
1	1	1	10	1.0000E-34	0.0
1	1	1	10	1.0000E-35	0.0
1	1	1	10	1.0000E-36	0.0
1	1	1	10	1.0000E-37	0.0
1	1	1	10	1.0000E-38	0.0
1	1	1	10	1.0000E-39	0.0
1	1	1	10	1.0000E-40	0.0
1	1	1	10	1.0000E-41	0.0
1	1	1	10	1.0000E-42	0.0
1	1	1	10	1.0000E-43	0.0
1	1	1	10	1.0000E-44	0.0
1	1	1	10	1.0000E-45	0.0
1	1	1	10	1.0000E-46	0.0
1	1	1	10	1.0000E-47	0.0
1	1	1	10	1.0000E-48	0.0
1	1	1	10	1.0000E-49	0.0
1	1	1	10	1.0000E-50	0.0
1	1	1	10	1.0000E-51	0.0
1	1	1	10	1.0000E-52	0.0
1	1	1	10	1.0000E-53	0.0
1	1	1	10	1.0000E-54	0.0
1	1	1	10	1.0000E-55	0.0
1	1	1	10	1.0000E-56	0.0
1	1	1	10	1.0000E-57	0.0
1	1	1	10	1.0000E-58	0.0
1	1	1	10	1.0000E-59	0.0
1	1	1	10	1.0000E-60	0.0
1	1	1	10	1.0000E-61	0.0
1	1	1	10	1.0000E-62	0.0
1	1	1	10	1.0000E-63	0.0
1	1	1	10	1.0000E-64	0.0
1	1	1	10	1.0000E-65	0.0
1	1	1	10	1.0000E-66	0.0
1	1	1	10	1.0000E-67	0.0
1	1	1	10	1.0000E-68	0.0
1	1	1	10	1.0000E-69	0.0
1	1	1	10	1.0000E-70	0.0
1	1	1	10	1.0000E-71	0.0
1	1	1	10	1.0000E-72	0.0
1	1	1	10	1.0000E-73	0.0
1	1	1	10	1.0000E-74	0.0
1	1	1	10	1.0000E-75	0.0
1	1	1	10	1.0000E-76	0.0
1	1	1	10	1.0000E-77	0.0
1	1	1	10	1.0000E-78	0.0
1	1	1	10	1.0000E-79	0.0
1	1	1	10	1.0000E-80	0.0
1	1	1	10	1.0000E-81	0.0
1	1	1	10	1.0000E-82	0.0
1	1	1	10	1.0000E-83	0.0
1	1	1	10	1.0000E-84	0.0
1	1	1	10	1.0000E-85	0.0
1	1	1	10	1.0000E-86	0.0
1	1	1	10	1.0000E-87	0.0
1	1	1	10	1.0000E-88	0.0
1	1	1	10	1.0000E-89	0.0
1	1	1	10	1.0000E-90	0.0
1	1	1	10	1.0000E-91	0.0
1	1	1	10	1.0000E-92	0.0
1	1	1	10	1.0000E-93	0.0
1	1	1	10	1.0000E-94	0.0
1	1	1	10	1.0000E-95	0.0
1	1	1	10	1.0000E-96	0.0
1	1	1	10	1.0000E-97	0.0
1	1	1	10	1.0000E-98	0.0
1	1	1	10	1.0000E-99	0.0
1	1	1	10	1.0000E-100	0.0

Figure D-22. Math Model Nonlinear Beam Data (Sheet 1 of 3)

BEST AVAILABLE COPY

40	14	26	0	0	1	3	1.73000E-01	0.0
41	14	26	0	0	3	8	1.33300E-00	0.0
42	14	26	0	0	3	8	1.70000E-01	0.0
43	15	17	0	0	3	5	1.30000E-01	0.0
44	16	17	0	0	3	5	1.50000E-01	0.0
45	17	26	0	0	1	5	1.00000E-01	0.0
46	17	26	0	0	1	5	9.00000E-02	0.0
47	18	27	0	0	3	5	2.00000E-00	0.0
48	18	27	0	0	5	5	1.00000E-01	0.0
49	19	26	0	0	1	5	1.00000E-01	0.0
50	19	26	0	0	3	5	6.80000E-01	0.0
51	19	27	0	0	5	5	4.60000E-02	0.0
52	19	27	0	0	1	5	8.00000E-02	0.0
53	19	27	0	0	3	5	4.00000E-00	0.0
54	19	27	0	0	5	5	2.00000E-01	0.0
55	20	26	0	0	1	5	1.00000E-01	0.0
56	20	26	0	0	3	5	1.00000E-00	0.0
57	20	26	0	0	5	5	1.00000E-00	0.0
58	20	26	0	0	1	5	1.00000E-01	0.0
59	20	26	0	0	3	5	1.00000E-01	0.0
60	20	26	0	0	5	5	1.00000E-01	0.0
61	20	26	0	0	1	5	1.00000E-01	0.0
62	20	26	0	0	3	5	1.00000E-01	0.0
63	20	26	0	0	5	5	1.00000E-01	0.0
64	20	26	0	0	1	5	1.00000E-01	0.0
65	20	26	0	0	3	5	1.00000E-01	0.0
66	20	26	0	0	5	5	1.00000E-01	0.0
67	20	26	0	0	1	5	1.00000E-01	0.0
68	20	26	0	0	3	5	1.00000E-01	0.0
69	20	26	0	0	5	5	1.00000E-01	0.0
70	20	26	0	0	1	5	1.00000E-01	0.0
71	20	26	0	0	3	5	1.00000E-01	0.0
72	20	26	0	0	5	5	1.00000E-01	0.0
73	20	26	0	0	1	5	1.00000E-01	0.0
74	20	26	0	0	3	5	1.00000E-01	0.0
75	20	26	0	0	5	5	1.00000E-01	0.0
76	20	26	0	0	1	5	1.00000E-01	0.0
77	20	26	0	0	3	5	1.00000E-01	0.0
78	20	26	0	0	5	5	1.00000E-01	0.0

Figure D-22. Con't (Sheet 2 of 3)



STANDARD KR CURVE DATA

13	35	37	0	0	1	1	1.00000E-01	0.00000E+00
36	39	0	0	0	9	9	1.00000E-01	0.00000E+00
31	36	0	0	0	1	1	1.00000E-01	0.00000E+00
67	37	36	0	0	1	1	4.00000E-02	0.0
35	37	37	0	0	5	5	1.00000E-00	0.0
33	37	36	0	0	5	5	1.00000E-01	0.0
58	13	37	5	1	1	9	1.00000E-01	0.0
75	13	37	6	1	1	9	1.00000E-01	0.00000E+00
37	37	0	0	0	1	9	1.00000E-01	0.00000E+00
50	37	0	0	0	1	1	1.00000E-01	0.0
13	38	6	1	1	13	48	1.00000E-01	0.00000E+00
97	41	43	0	1	1	5	1.50000E-01	0.0
62	43	43	0	0	5	5	1.50000E-01	0.0

Figure D-22. Con't (Sheet 3 of 3)

BEST AVAILABLE COPY

[illegible]

Figure D-23. Math Model Nonstandard Deflections and Forces

BEST AVAILABLE COPY

VEHICLE PARAMETERS
VEHICLE WT = 2.3713200 03
VEHICLE CG POSITION
X (CM) = 6.51420 01
Y (CM) = -2.16690-15
Z (CM) = 6.39760 00
VEHICLE INITIAL COORDINATES
X(0) = 1.5670 00
Y(0) = 1.77020 06
Z(0) = 2.06333 06
VEHICLE INITIAL COORDINATES
XCG IS THE DISTANCE FROM GROUND INTERSECTION TO VEHICLE CG, FORWARD
YCG IS THE DISTANCE FROM GROUND PLANE TO VEHICLE CG, DOWN
XCG = 0.0
YCG = -7.47050 01

Figure D-24. Math Model Parameter Data